METHODS OF REMEDIAL TREATMENT FOR CARBONATION-INDUCED CORROSION OF REINFORCED CONCRETE

JUNICHIRO KUBO

Submitted in accordance with the requirements for the degree of Ph.D.

University of Leeds
School of Civil Engineering
March 2007

ACKNOWLEDGEMENTS

I am deeply indebted to Professor C. L. Page, my supervisor over the whole duration of this research. His knowledge and expertise, guidance, advice, encouragement and all the support could not have been appreciated more greatly. I am also grateful to Dr. M. M. Page, my co-supervisor, for advice on the experimental work, mathematical modelling, and statistical analysis as well as for her patience in reading through this thesis. I should like to express my appreciation to Dr. L. Y. Li for helpful discussion on mathematical modelling. I also wish to thank Professor A. Neville and Dr. X. Hu for the kind guidance on EIS measurements.

I am very grateful to the Central Japan Railway Company, for providing funds to support this research. Dr. M. Seki and Dr. Y. Ito are in particular immensely appreciated for the precious discussions on the significance of my research. I should like to thank Dr. H. Tanaka, Dr. T. Noda, Mr. K. Kondo, Mr. T. Mizuno, Mr. K. Ichikawa, Mr. M. Hasegawa, and Dr. H. Inaguma, whose support and encouragement were greatly appreciated.

I should like particularly to thank Dr. S. Sawada for the work he has done in collaboration with me, as reported in Part 1 of Chapter 4 in my thesis. His help on the experimental work and useful discussion were invaluable.

The entire technical staff of the School of Civil Engineering, in particular Mr. S. Shaw and Ms. K. Stevens, are thanked for their help and assistance in the laboratory work.

I am also grateful to Mr. K. Tagawa and Mr. T. Inaguma for the preparation of equipment when I needed to conduct experiments in Japan during this project. I also should like to thank Dr. T. Shichi, Dr. C. Terashima, Dr. K. Arihara and Dr. T. Numata for their help and useful discussion on chemistry.

I should like to thank my brother-in-law, Mr. T. W. Cann, for reading through Chapters 4-6 and for polishing the English statements involved there.

Finally I am grateful to my wife, Yuki, as well as to my parents, parents-in-law, sisters, and grandmother, for their love, understanding and encouragement. I should like to thank my son and daughter, Tomas and Eileen, for charming me anytime with their sweetest smiles.

THE UNIVERSITY OF LEEDS

METHODS OF REMEDIAL TREATMENT FOR CARBONATION-INDUCED CORROSION OF REINFORCED CONCRETE

Junichiro KUBO **Doctor of Philosophy March 2007**

ABSTRACT

The importance of carbonation-induced corrosion has grown in recent years owing to the increasing age of reinforced concrete structures. Among the various remedial treatments for the alleviation of the deterioration process, applications of corrosion inhibitors and surface coatings are highlighted in this thesis owing to their ease of practical application to such structures as railway viaducts. The factors that may enhance the effectiveness of the above two methods in terms of retardation of embedded steel corrosion have investigated as follows: (1) Electrochemical injection of corrosion inhibitors into concrete and (2) Fatigue resistance of surface coatings.

(1) After the concentration threshold of electrolytes of three organic base corrosion inhibitors, namely ethanolamine, guanidine, and arginine, required for steel passivation had been investigated by steel immersion tests, the inhibitors were injected into fully/partially carbonated cement-based materials from external electrolytes under the influence of an electrical field. The penetrations of the three inhibitors into the embedded steel cathode were satisfactory in terms of steel inhibition. The field-induced penetration was markedly affected by the pK_a values of the inhibitors and the pore solution pH. When the electrochemical treatment was applied to partially carbonated cementitious materials, adequate accumulation of the inhibitors was also attained at the cathode for steel passivation; however, the migration of cationic inhibitors was found to be discouraged in the carbonated region by the lowered current densities effectively applied to this region owing to its large resistivity. Mathematical modelling was performed for simulation of the proposed electrochemical inhibitor injection. A model based on the Nernst-Planck equation, taking account of dissociation equilibria and solubility products of the relevant species, and activity coefficient of molecules, yielded a reasonable agreement with the experimental data. In the application of this model to the 2-D cases, representing the domain with a resistor network that could simulate the current distribution within the material resulted in good prediction of concentrations of the species observed in the experiments. The long-term effectiveness of the electrochemical inhibitor injection was monitored for a reasonably long period, whilst the treated concrete specimens were exposed to cyclic wet/dry conditions. As a result, the injected corrosion inhibitors were found to be effective in promoting steel passivation, and ethanolamine showed the best performance with the smallest steel corrosion rates observed during the experiment.

(2) For the investigation of properties of surface coatings affecting their long-term fatigue resistance, fatigue tests with a total of 18 million cycles were carried out under varied temperatures for several coatings bridging a substrate crack whose properties (width and dynamic amplitude) were determined by on-site survey methods. It was found that the thickness and the composition are two important properties of surface coatings that significantly influenced their long-term durability when they were exposed to varied environmental temperatures.

KEY WORDS: Carbonation, Corrosion, Organic corrosion inhibitor, Surface coating, Electrochemical treatment, Mathematical modelling, Electrochemical monitoring, Durability, Ionic migration, Dissociation constant, Activity coefficient, Current distribution, Fatigue resistance

TABLE OF CONTENTS

ABBREVIATIONS AND FREQUENTLY USED SYMBOL

Abbreviations

ACN	Acetonitrile
AFm	Mono-ferro-aluminate
ASR	Alkali-silica reaction
CBA	Crack-bridging ability
CP	Cathodic protection
CPE	Constant phase element
C-S-H	Calcium silicate hydrate ($CaO.SiO_2.H_2O$)
DMEA	Dimethylethanolamine
DOD	Degree of drying
EC	Equivalent circuit
EI	Electrochemical interface
ECR	Electrochemical chloride removal
EIS	Electrochemical impedance spectroscopy
FRA	Frequency response analyser
KCL	Kirchhoff's current law
KVL	Kirchhoff's voltage law
LOI	Loss on ignition
MCI	(Commercial) Migratory corrosion inhibitors
MFP	Monofluorophosphate
MSA	Methanesulfonic acid
N/D	Not detectable
OPC	Ordinary Portland cement
PCM	Polymer cement mortar
ppm	Parts per million
PTFE	Polyterafluoroethylene
PVC	Polyvinyl chloride
RC	Reinforced concrete
RH	Relative humidity
rpm	Revolution per minute
$scCO_2$	Super-critical carbon dioxide
SCE	Saturated calomel electrode
UV	Ultraviolet

Symbol

α	Significance level
α	Assumed molar conductivity for hydroxyl ions ($S \cdot m^2/mol$)
β	Assumed molar conductivity for anions except hydroxyl ions ($S \cdot m^2/mol$)
γ	Activity coefficient
γ_m	Molecular activity coefficient
δ	Thickness of diffusion layer (m)
ε	Porosity
κ	Conductivity (S/m or $\Omega^{-1}m^{-1}$)
Λ	Molar conductivity or equivalent conductivity ($S \cdot cm^2/mol$)
Λ_0	Molar conductivity at infinite dilution ($S \cdot cm^2/mol$)
λ_{ij}	Binary interaction parameter
μ	Diffusion resistance coefficient
ρ	Density (g/cm^3)
σ^2	Variance of samples
τ	Tortuosity
τ_D	Time constant (s)
φ	Electrostatic potential (V)
ω	Angular frequency (rad/s)
A	Cross section area (m^2 or cm^2)
B	Stern-Geary constant (mV)
b_a	Anodic Tafel slope (mV)
b_c	Cathodic Tafel slope (mV)
C	Concentration of species in liquid phase (mol/l or mol/m^3 or mol/cm^3)
C_0	Pure capacitance (F/cm^2)
C_c	Concrete Matrix capacitance (F/cm^2)
C_{dl}	Double layer capacitance (F/cm^2)
C_f	Film capacitance (F/cm^2)
D	Diffusion coefficient (m^2/s)
D_{eff}	Effective diffusion coefficient (m^2/s)
E	Electric potential (V)
E_{corr}	Corrosion potential (mV)
F	Faraday constant (9.64846×10^4 C/mol)
f	Frequency (s^{-1})
H	Null hypothesis

I	Ionic strength (mol/l)
I_{corr}	Corrosion current (A/cm^2)
I_{app}	Instantaneous current step (A/m^2)
i	Applied current density (A/m^2)
J	Flux ($mol/m^3/s$)
j	Imaginary unit (square root of -1)
J_{DISS}	Dissolution flux ($mol/m^3/s$)
K	Equivalent constant or solubility product
k	Kohlrausch's constant
K'	Apparent equivalent constant or apparent equivalent constant
K_a	Acid dissociation constant
K_a'	Apparent dissociation constant
k_l	Dissolution rate constant (s^{-1})
K_H	Henry's constant ($10^{-1.42}$ M/atm at 25°C)
L	Length of specimen (m)
M	Molarity (mol/l)
M_{Fe}	Molar weight of Fe (56g/mol)
m_I	Number of moles of inhibitor ions (mol)
m_M	Number of moles of inhibitor molecules (mol)
N	Normal concentration (mol/l)
N	Number of samples
n	Number of cycles
p	Degree of dispersion
P_{CO2}	Partial pressure of carbon dioxide gas (atm)
pH	Negative logarithm of concentration of hydrogen ion
pK	Negative logarithm of the dissociation constant
pK_a	Negative logarithm of the acid dissociation constant
pK_a'	Negative logarithm of the apparent acid dissociation constant
R	Gas constant (8.3143 J/mol K)
R	Reaction rate ($mol/m^3/s$)
R	Element resistance (Ω)
R	Air layer thickness (m)
R_0	Solution resistance ($\Omega \cdot cm^2$)
R_c	Concrete matrix resistance ($\Omega \cdot cm^2$)
R_{ct}	Charge transfer resistance ($\Omega \cdot cm^2$)

R_f	Film resistance ($\Omega \cdot cm^2$)
R_s	Solution resistance ($\Omega \cdot cm^2$)
R_Ω	Ohmic resistance ($\Omega \cdot cm^2$)
RNH_2	Organic base
RNH_3^+	Conjugate acid of organic base
$R(NH_3^+)_2$	Double conjugate acid of organic base (for arginine only)
$RNHCOO^-$	Carbonate form of organic base
RNH_2COO^-	Carboxyl form of organic base
R_p	Polarisation resistance ($\Omega \cdot cm^2$)
R_w	Diffusion resistance ($\Omega \cdot cm^2$)
S	Amount of ions in solid phase (mmol/g)
S	Thickness of coating (μm)
T	Absolute temperature (K)
t	Time (s)
t	Thickness (mm or μm)
t	t-statistic value
u	Mobility of ion ($S \cdot m^2/C$)
V	Volume of solution (l)
V_t	Potential at a given time (V)
W	Weight of sample (g)
W	Warburg impedance
w	Water content (g/g dry sample)
W_o	Maximum crack width (mm)
W_u	Minimum crack width (mm)
w/c	Water cement ratio
W_{loss}	Weight loss (mg)
$\overline{X}$	Mean of samples
x_a	Length of anolyte for 1D analysis (m)
Z	Impedance ($\Omega \cdot cm^2$)
Z'	Real components of impedance ($\Omega \cdot cm^2$)
Z''	Imaginary components of impedance ($\Omega \cdot cm^2$)
z	Electric charge number
z_a	Length of anolyte for 2D analysis (m)

LIST OF TABLES

LIST OF FIGURES

CHAPTER 1

INTRODUCTION

1.1 FIELD OF STUDY

In recent years a number of reinforced concrete structures have been reported to experience carbonation-induced deterioration associated with reinforcement corrosion, owing to the increasing age, which may affect their service life (Parrott 1990, Glass et al. 1991, Tsiatas and Robinson 2002). It is widely known that corrosion of steel reinforcement is normally inhibited in an alkaline environment within concrete (pH 13-14) with a chemically stable thin oxide film (γ-Fe_2O_3) protecting the steel surface from contact with moisture and oxygen (Parrott 1987). Carbonation involves a gradual interaction between acidic carbon dioxide gas from the air and the alkaline solid cement hydration products (calcium hydroxide and, to a lesser extent, calcium silicate hydrate (C-S-H)) to form calcium carbonate by the following simplified reactions, which consequently results in depression of the pore solution pH to a value below 10.

$$Ca(OH)_2 + CO_2 \Rightarrow CaCO_3 + H_2O \quad (1\text{-A})$$

$$C\text{-}S\text{-}H + CO_2 \Rightarrow CaCO_3 + SiO_2 + H_2O \quad (1\text{-B})$$

The kinetics of carbonation are diffusion-controlled and this results in approximately parabolic relationships between the average carbonation depth (x), estimated, for example, by the simple phenolphthalein test, and the time of exposure (t) ($x=k\ t^{1/2}$) (Tuutti 1982). A large number of factors affect the magnitude of the proportionality constant (k) in the above equation. These include exposure conditions (relative humidity, temperature, and carbon dioxide concentration), mix composition (water/cement ratio, cement type, aggregate porosity and content) and manufacturing variables (compaction and curing). As the carbonation front slowly approaches the steel reinforcement, depassivation starts to occur, sometimes leading to the initiation of corrosion, whilst corrosion is observed to be mainly controlled by the "un-neutralised remainder" (cover depth minus carbonation depth) (Parrott 1994). A secondary effect of carbonation is that it may cause the release of bound chloride ions into the pore solution phase of concrete that contains a modest level of chloride salts (see subsection 5.4.3.1), which worsens the corrosive environment (Tuutti 1982).

Carbonation and chloride ions are known to be the two major factors responsible for the corrosion of steel reinforcement in concrete; however, the former is generally considered to be less damaging and the carbonation-induced corrosion problems that arise are often slow to develop to a stage where remedial treatment becomes necessary. This is because the climatic conditions that tend to favour rapid carbonation (RH range 50%-70%) are not ones that give rise to substantial rates of corrosion of steel embedded in carbonated concrete and carbonation-induced corrosion is normally associated with uniform attack rather than pitting, as pointed out in several reports (Tuutti 1980, González et al. 1980, Parrott 1987, Glass et al. 1991). Corrosion can then manifest itself only if the moisture content of the concrete is sufficiently high to maintain an electrolyte phase of fairly high conductivity within the pores. However, since real structures may be subject to wet and dry periods characterised by seasonal variations of climate as observed in many countries, corrosion is likely to proceed due to carbonation. Corrosion of reinforcing bars may affect the durability of the structures. As the steel corrodes, the rust occupies a volume from two to four times greater than the parent steel (Bertolini et al. 2004), resulting in bursting stress which ultimately cracks and spalls the cover concrete. In addition, the contribution of the reinforcement to the strength of the structure may be reduced.

The increasing number of reinforced concrete structures affected by reinforcement corrosion due to carbonation has led to the development of protective methods in order to improve the durability of such structures. For remedial treatment, several techniques have widely and practically been used. The classic method of partial replacement by chipping out the carbonated concrete from around the bars, cleaning the exposed steel, reinstating the patch with an appropriate cementitious mortar or concrete, with or without corrosion inhibitors, and sometimes applying a coating for better resistance to further carbonation in addition to a better visual appearance has normally proved to be effective. However the disadvantage of this treatment is that it involves noise, dust and general disruption whilst repairs are being undertaken, and that it is time-consuming and expensive. There are several more recent approaches devised to reduce such undesirable effects.

Corrosion inhibitors have been used as admixtures in concrete for new structures as a preventive measure. As a remedial treatment to alleviate corrosion of the embedded steel, corrosion inhibitors are mostly applied to the concrete by spraying or flooding on to surface so that they can penetrate through the concrete pores towards the reinforcing bars by absorption and diffusion. It is expected that these inhibitors are capable of repassivating the

steel if maintained at an appropriate concentration in the vicinity of the bars. The expected advantages of this remedial method are the ease of application, and low cost. However the use of corrosion inhibitors in reinforced concrete repair systems is a relatively new field and far less well established than some other applications of inhibitors (Page et al. 2000, Elsener 2001). The main issues are concerned with the desirable concentration, the degree of penetration, and the long-term inhibitive performance.

Another approach may be application of surface coatings, which prevents carbon dioxide ingress into concrete and retards the process of further carbonation. Simultaneously they may play an important role in a protection from water and oxygen ingress that subsequently leads to corrosion of the reinforcing bars. They can provide effective protection to both concrete and the embedded reinforcing steel for rehabilitation of deteriorated concrete, and can enhance the durability of the structure. They are easy to apply and some are low in cost. A wide variety of coatings have been used depending on the characteristics of the structure or the state of the deterioration, and their performance in alleviating corrosion of embedded steel or retarding further penetration of carbonation has been investigated (Seneviratne et al. 2000).

Since corrosion reactions are electrochemical processes, various electrochemical techniques have recently been developed for the protection and repair of reinforced concrete structures with corrosion problems resulting from carbonation (Mietz 1998, Page 2002).

• Electrochemical re-alkalisation is one example. This technology involves a current density of approximately 1-2A/m^2 passed from an externally installed anode mesh through concrete to the embedded reinforcing bars for a limited period of time (up to a few weeks) and restores the pH value in the vicinity of the reinforcing bars to a level high enough to passivate the steel again. In addition, the presence of alkaline electrolyte in the concrete pores acts as a carbon dioxide trap when exposed to the air after the treatment. This method has been developed as a rehabilitation treatment since the mid-1980s. However there are still some unsolved issues concerned with the criteria by which the completion of a successful treatment is determined and also the long-term durability of this remedial method. Presently CEN is working on a European standard for re-alkalisation of concrete.

• Cathodic protection (CP) with impressed current is another example. This technique, more often applied for the alleviation of chloride-induced corrosion, has also been proved to be effective in repassivating steel in carbonated concrete. During this electrochemical treatment, the steel is subjected to cathodic polarisation, i.e. its potential is driven to values more

negative than the free corrosion value, so that the corrosion rate is reduced. An accompanying advantage is that the pH of the concrete is raised owing to the electrode reactions and electro-migration processes (Page 1997). One drawback of impressed current CP may be that, once applied, the protection may need to be operated for the remaining service life of the structure, which requires long-term monitoring and periodic adjustment of the electrical installation.

The author's company (Central Japan Railway Company) possesses quite a large amount of reinforced concrete viaducts (around 75miles/120km in length), which were constructed in early 1960s prior to the commencement of operation of the so called "Bullet train" in 1964. Taking into account the fact that chloride-contaminated or ASR (alkali-silica reaction) susceptible aggregate was fortunately not used for the construction of the structures and that the viaducts are not located at such severe environments as coastal sites where chloride-induced corrosion can become a problem, it has been believed that carbonation would be a significantly important factor that may deteriorate structures aged over 40 years. Among the aforementioned remedial treatment methods for carbonation-induced corrosion of reinforced concrete, simple and easy ones are desirable that would minimise the disruption of the operation of trains, when it comes to their application to railway structures. Therefore, the applications of corrosion inhibitors and surface coatings are highlighted in this thesis, where the potential of the two methods that may prolong the service life of the structures is discussed.

1.2 SCOPE OF STUDY

This research is concerned with remedial treatment for carbonation-induced corrosion of reinforcing steel embedded in concrete. The aim of this research is to provide a better understanding of the issues underlying the remedial treatment of carbonation-induced corrosion of steel in concrete and to improve the application of such treatments intended to alleviate carbonation-induced corrosion as surface-applied corrosion inhibitors and surface coatings. There are two major research areas as described below.

(A) Electrochemical injection of corrosion inhibitors into concrete

The use of corrosion inhibitors as a remedial treatment is very simple in principle. However, it has been reported that the concentration of corrosion inhibitors reaching the reinforcing

bars by just spraying or ponding these materials on to the concrete surface may be insufficient for the steel to be repassivated in a short time (Page et al. 2000).

If an electrolyte is attached on the surface of the concrete and an electrical field is applied between an anode placed in the electrolyte and embedded reinforcing steel acting as a cathode similarly as in the case of electrochemical re-alkalisation, positive ions may penetrate through the concrete pores towards the steel bars acting as cathode. Some organic corrosion inhibitors form positive ions when they dissolve in water. When these inhibitors are used for the anolyte solutions, under an external current, substantial amount of inhibitors are expected to reach the vicinity of the steel rather quickly, which may subsequently contribute to the retardation of the corrosion process after the treatment.

Organic base corrosion inhibitors are not fully ionised in the pore solution following the reaction below; the ratio of the concentration of the ion to the molecule of an inhibitor in the electrolyte is determined by its dissociation constant (K_a) and the pH of the environment (see Chapter 4).

$$RNH_3^+ \Leftrightarrow RNH_2 + H^+ \qquad (1\text{-}C)$$

It follows that a larger proportion of ionised species is found in a neutralised solution than in an alkaline solution when organic corrosion inhibitors are dissolved. Since field-induced migration of organic base corrosion inhibitors occurs only when they are ionic, the application of this treatment to carbonated concrete (of near-neutral pH) is expected to be effective. There are a number of issues to be addressed when surface-applied corrosion inhibitors are to be applied to concrete (Page et al. 2000), namely:

(1) The evidence that inhibitors can stop or at least reduce corrosion rates of the steel in concrete that suffers from carbonation
(2) The level of concentration of inhibitors required at the reinforcing steel to passivate it
(3) The method that secures the required concentration of corrosion inhibitors at the reinforcing steel when employed
(4) The deleterious side effects that might arise as a result of the application of corrosion inhibitors
(5) The longevity of the method, that is, the period during which the corrosion inhibitors are likely to remain in an adequate concentration at the steel to keep it passivated

Using experimental and mathematical modelling approaches, the above issues are discussed in this thesis with reference to the electrochemical injection of organic base corrosion inhibitors into carbonated concrete. The profiles of carbonation depth in real concrete are usually not uniform (see section 4.8), thus the effectiveness of the inhibitor injection into partially carbonated material is also investigated.

(B) Durability of surface coatings against fatigue

In general, the fundamental properties required for surface coatings applied on concrete as an anti-carbonation measure are a high resistance against carbon dioxide diffusion, prevention of water ingress, weather resistance, and adhesion. In addition to these requirements, the long-term stability of the coatings has recently been questioned (Swamy and Tanikawa, 1993, Delucchi et al. 2004) due to the increasing use of coatings in aggressive environments. Among the properties concerned with long-term durability of coatings, crack-bridging ability, which is indicated as ability to accommodate the movement of the substrate beneath the coatings and is usually measured by a single tensile test, can be an important factor when a coating is applied over cracks existing on the concrete surface that are expected to move. Coatings with excellent crack-bridging ability are often used on the bottom surface of motorway bridges or railway viaducts, where the cracks may move due to the applications of dynamic active loads generated by passage of vehicles. If a coating is broken, it will be a problem because a degraded coating will eventually lose its barrier properties and become less effective in retarding the progress of carbonation and in protecting the steel from corrosion. The investigations carried out by the Central Japan Railway Company (Seki et al. 2001), however, showed the generation of cracks on coatings just along the line of the original concrete cracks in the railway viaducts several years after their application. This indicated that highlighting fatigue resistance in addition to crack-bridging ability may be important for the long-term durability of coatings applied on our structures. In this study, fatigue resistance is defined according to the bridging performance under cyclic tensile conditions. The property will be discussed based on the evidence obtained from fatigue tests of millions of cycles conducted at widely different temperatures using several coatings of different materials with varied thickness applied to carbonated concrete specimens.

1.3 OUTLINE OF THESIS

The thesis is divided into eight chapters. The chapters that follow this introductory chapter (Chapter 1) are outlined as follows:

Chapter 2 describes the overall experimental programme undertaken, giving details of materials, preparation of specimens and experimental techniques employed in this study.

Among the five uncertainties listed above in section 1.2 (A), the issue (2) is discussed in Chapter 3. The inhibitive ability of three organic corrosion inhibitors is investigated by immersing steel bars in different concentrations of basic or neutralised model electrolytes of the inhibitors concerned at controlled pH values, which are intended to simulate the pore solution phase present within carbonated concrete. The mechanism of the inhibition and the concentrations of the targeted inhibitors required for passivation of steel are described in this Chapter.

Two of the remaining uncertainties, listed as (3) and (4) above in section 1.2(A), are discussed in Chapters 4 and 5.

Chapter 4 is an experimental chapter, where the two issues are studied with reference to the introduction of a novel proposed electrochemical method of inhibitor injection into carbonated concrete. The migration of the studied corrosion inhibitors towards the embedded steel cathode is elucidated, mainly highlighting the effect of their dissociation constant values (K_a). Part 1 of this Chapter describes a one-dimensional approach and deals with fully carbonated cementitious material; this is then developed to a two-dimensional approach in Part 2 of this Chapter that deals with partially carbonated cementitious material.

Chapter 5 is a mathematical modelling Chapter for the simulation of changes in the pore solution phase chemistry during the electrochemical injection of the corrosion inhibitors described in Chapter 4. The model is based on the Nernst-Planck equations, where acid/base dissociation equilibria and solubility products of relevant species are taken into account. The predictions made for a fully or partially carbonated cementitious material by means of a one-dimensional or two-dimensional model are compared with the experimental results obtained in Chapter 4.

Chapter 6 describes experiments aimed at elucidating the long-term effectiveness of the proposed inhibitor injection method, which is the final issue listed above as (5) in section 1.2(A). The effectiveness of the inhibitors on the retardation of carbonation-induced steel corrosion in concrete (issue (1)) is also discussed in this Chapter. The states of the steel embedded in concrete specimens after the treatments with three inhibitors are electrochemically monitored for a period of several months. The effect of injected inhibitors

is also compared to that of electrochemical re-alkalisation. The concentration profile evolution of injected inhibitors with respect to time is investigated by both experimental and modelling approaches. In this Chapter, the possible application of an application of anodic polarisation for instant passivation determination or long-term passivation of embedded steel is also discussed.

Chapter 7 examines long-term durability of surface coatings in terms of fatigue resistance. Based on the on-site investigation of coating and substrate performances on railway RC viaducts, fatigue tests of millions of cycles have been devised and carried out at different temperatures for various coatings applied to carbonated concrete. The properties of coatings that may affect the long-term fatigue resistance are discussed.

Chapter 8 summarises the general conclusions and describes recommendations for future investigations.

CHAPTER 2

MATERIALS AND EXPERIMENTAL TECHNIQUES

2.1 MATEIRALS

2.1.1 Cements

Ordinary Portland Cement (OPC) was used to manufacture cement paste and concrete specimens. The chemical analyses of cements are shown in Table 2.1. Two different batches of OPC were used for the work described in this thesis. OPC 1 was used for experimental work presented in Chapters 4 and 6, whilst OPC 2 was used for the work described in Chapter 7.

Table 2.1 Chemical analyses of OPC (% by mass)

Cement type	OPC 1	OPC 2
CaO	63.76	63.66
SiO_2	20.69	20.56
Al_2O_3	4.72	5.20
Fe_2O_3	3.06	2.62
SO_3	2.92	2.39
MgO	2.08	0.73
Na_2O	0.26	0.29
K_2O	0.61	0.36
Cl	0.04	0.02
LOI	0.87	2.65

2.1.2 Water

18 MΩ deionised water, which was produced by an Elga UHQ water purifier, was used to dilute the samples in the ion chromatographic analysis (see section 2.4). For other purposes distilled water was used throughout the experiments presented in this thesis.

2.1.3 Aggregate

The fine aggregate used to prepare concrete specimens described in Chapters 6 and 7 was quartzitic sand and the coarse aggregate used was uncrushed quartzitic gravel. Two different batches of fine and coarse aggregate were used for this thesis. The fine aggregate 1 and the

coarse aggregate 1 with a maximum size of 10mm were used for experimental work presented in Chapter 6, and the fine aggregate 2 and the coarse aggregate 2 with a maximum size of 15mm were used in Chapter 7 respectively. The results of sieve analysis, which was performed according to BS 812-103.1 (1985) for aggregate 1 and JIS A 5005 (1993) for aggregate 2, are shown in Tables 2.2 and 2.3, together with limits specified in BS 882 (1992) for aggregate 1 and JIS A 5005 (1993) and JIS A 5308 (1998) for aggregate 2.

Table 2.2 Sieve analysis of fine aggregate

Fine aggregate 1			Fine aggregate 2		
Sieve size (mm)	Percentage by mass passing through sieve		Sieve size (mm)	Percentage by mass passing through sieve	
	Limits*	Results		Limits	Results
-	-	-	10	100	100
-	-	-	5	90-100	100
2.36	65-100	84	2.5	80-100	87
1.18	45-100	78	1.2	50-90	65
0.6	25-80	71	0.6	25-65	47
0.3	5-48	19	0.3	10-35	25

* For grade M (medium)

Table 2.3 Sieve analysis of coarse aggregate

Coarse aggregate 1			Coarse aggregate 2		
Sieve size (mm)	Percentage by mass passing through sieve		Sieve size (mm)	Percentage by mass passing through sieve	
	Limits	Results		Limits	Results
-	-	-	20	100	100
14	100	100	15	90-100	100
10	85-100	97	10	40-70	65
5	0-25	0.7	5	0-15	13
2.36	0-5	0.1	2.5	0-5	1

2.1.4 Electrodes

Type 316 stainless steel mesh was used as the cathode for the experiments presented in Chapters 4 and 6. The same type of steel mesh was used as a counter electrode for the measurement of the electrochemical characteristics of embedded steel in concrete by electrochemical impedance spectroscopy, as detailed in Chapter 6. Mild steel bars with a diameter of 6.35mm were used as working electrodes in the immersion tests presented in Chapter 3. Mild steel bars with the same chemical composition but with a diameter of 8mm were used as the embedded steel reinforcements in Chapter 6, which acted as cathodes while constant current density was externally applied for the inhibitor injection treatments. The chemical analysis of the steel used is shown in Table 2.4. Carbon rods with a diameter of

5mm and a length of 100mm were used as the anode for the experiments presented in Chapters 4 and 6.

Table 2.4 Chemical composition of mild steel bars (% by weight)

Al	Si	Ti	V	Cr	Mn	Fe	Co	Ni
0.05	0.21	<0.05	<0.05	0.30	1.01	97.11	<0.05	<0.05
Cu	Nb	Mo	Sn	W	P	C	S	
<0.05	<0.05	<0.05	<0.05	<0.05	0.01	0.23	0.01	

2.1.5 Chemicals

All chemicals used for preparing electrolytes in the experimental work presented in this thesis are listed in Table 2.5, together with their grades and suppliers. The chemicals (a) in the table were used for experimental work presented in Chapters 3, 4, 5 or a part of Chapter 6 carried out in Leeds University, whilst the chemicals (b) were used for experimental work in the rest of Chapter 6 and Chapter 7 that was carried out at the Research Institute of Central Japan Railway Company in Nagoya, Japan.

Table 2.5 List of chemicals

Chemical	Grade	Supplier
Ethanolamine	(a) Analytical reagent (b) 99.0%+	(a) Fisher Scientific UK Ltd. (b) Wako Pure Chemical Industries Ltd.
Guanidine carbonate	(a) 98.0%+ (b) 98.0%+	(a) Avocado Research Chemicals. (b) Wako Pure Chemical Industries Ltd.
L-Arginine	(a) Analytical reagent (b) 99.0%+	(a) Avocado Research Chemicals. (b) Wako Pure Chemical Industries Ltd.
Nitric acid	(a) Analytical reagent (b) Analytical reagent	(a) Fisher Scientific UK Ltd. (b) Wako Pure Chemical Industries Ltd.
Sodium chloride	(a) Analytical reagent	(a) Fisher Scientific UK Ltd.
Sodium carbonate	(b) 99.5%+	(b) Wako Pure Chemical Industries Ltd.
Potassium nitrate	(a) Analytical reagent (b) 99.5%+	(a) Fisher Scientific UK Ltd. (b) Wako Pure Chemical Industries Ltd.
Sodium sulphate	(a) Analytical reagent	(a) Fisher Scientific UK Ltd.
Magnesium chloride $+ 6H_2O$	(a) Analytical reagent	(a) Fisher Scientific UK Ltd.
Diammonium hydrogen citrate	(b) 99.0%+	(b) Wako Pure Chemical Industries Ltd.
2-Mercapto-benzothiazole	(b) 95.0%+	(b) Tokyo Kasei Kogyo Ltd.

Purchased and used in (a) Leeds, UK, (b) Nagoya, Japan.

2.2 CARBONATION

2.2.1 Accelerated carbonation

In order to shorten the period required for the carbonation of cement-based materials, accelerated carbonation was employed to produce carbonated specimens presented in Chapters 4, 6, and 7. While being carbonated, the samples were exposed to high concentrations of carbon dioxide gas at a suitable relative humidity (RH). The set-up for the production of the carbonated specimens appearing in Chapters 4 and 6 is shown in Figure 2.1, where the specimens were placed upright over saturated sodium chloride solution in a sealed tank, where the atmosphere was maintained at approximately 75% RH. This is because carbonation rates are highest in atmospheres of RH in the range of 50-75% (Richardson 2002). 100% carbon dioxide gas was supplied from a compression cylinder and enclosed in the tank for about half an hour, twice every day at a room temperature. For the confirmation of the carbonation depth, some of the specimens were broken into pieces and then sprayed with phenolphthalein indicator solution, the colour of which changes from colourless below a pH value of about 9.2 to red-pink above that value. For the rapid carbonation of the concrete specimens presented in Chapter 7, an automated rapid carbonation chamber (Asahi neutralised test chamber manufactured by Asahi Kagaku Co. Ltd., Tokyo, Japan) was used, in which the temperature, carbon dioxide concentration, and RH were automatically maintained at 20°C, 5% and 60% respectively.

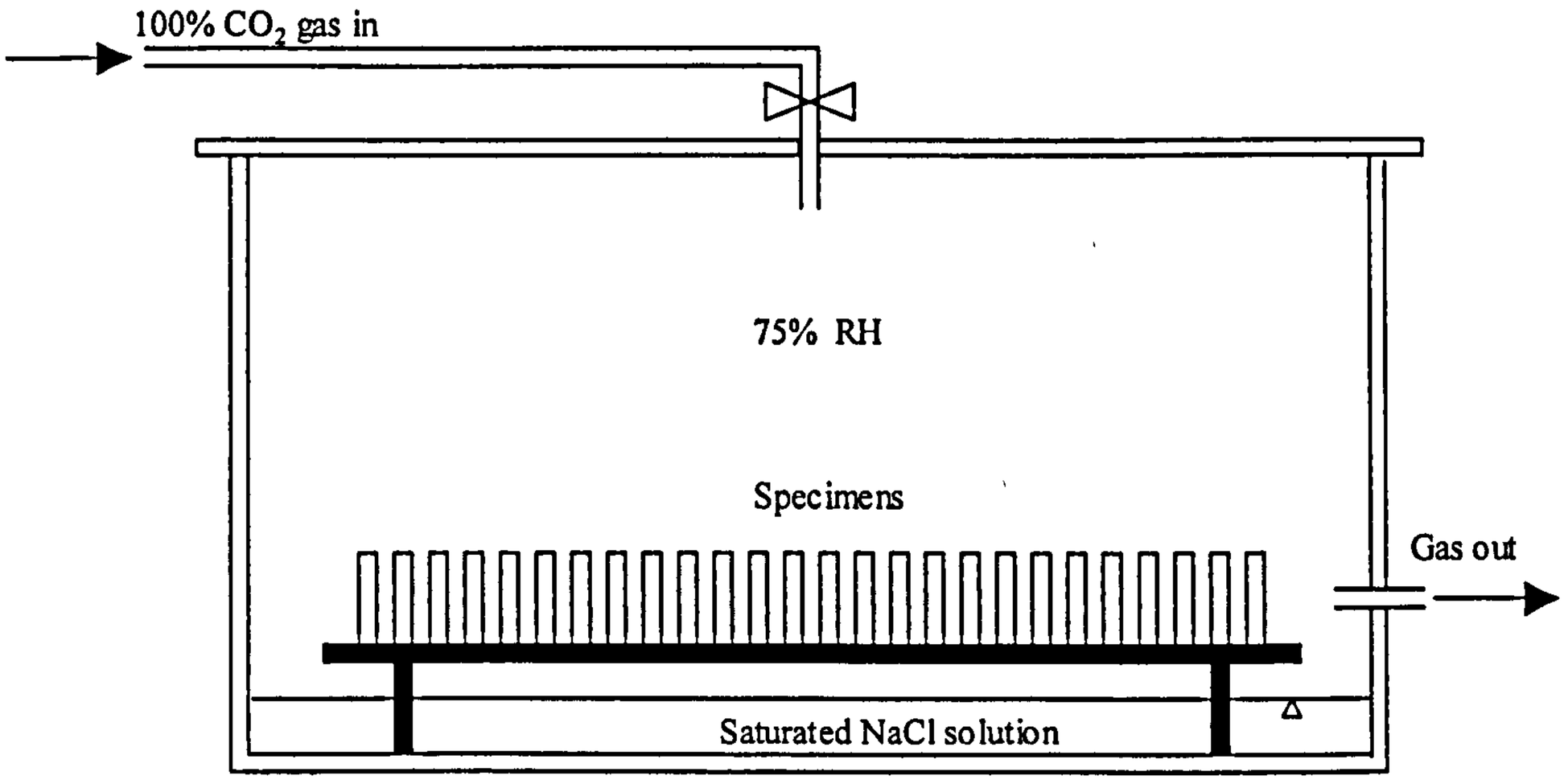

Figure 2.1 Set-up for accelerated carbonation of specimens

2.2.2 Super critical carbonation

For the production of carbonated cement paste discs with stainless electrodes embedded in the middle in Chapter 4 Part 1, a technique utilising super-critical carbonation was employed. Super-critical carbon dioxide (hereafter abbreviated as $scCO_2$) is a fluid under super-critical conditions in which both temperature and pressure are above the critical values, so that the liquid and gas phases both have the same density (Cansell et al. 1998). Owing to its liquid-like density but gas-like diffusivity and viscosity which allow it to penetrate into fine pores rapidly (Purnell et al. 2001), the period required to obtain full carbonation of cement-based materials is reduced from months to hours. In addition, compared with other super-critical fluids, $scCO_2$ is easier to produce because of its low critical temperature (31°C) and pressure (71 bar), which is why the application of $scCO_2$ has been recently studied for the rapid production of carbonated cement materials (Jones 1998; Jones and Tingley 1999; Short et al. 2001; Purnell et al. 2001; Shaw 2002).

The super-critical carbonation unit used to produce super-critically carbonated cement paste discs in Chapter 4 Part 1 is shown in Figure 2.2. This equipment was supplied by Critical Processes Ltd. This apparatus consists of a pressure vessel and an oven with pump and cooling. The stainless steel pressure vessel was placed inside the oven and heated until the required temperature was obtained in order to achieve the super-critical condition quickly. The cement paste discs detailed in subsection 4.4.1.2 were stacked in a stainless steel sample holder and then inserted into the pressure vessel. After the inlet and outlet pipes for the flow of liquid carbon dioxide were attached to the vessel, the liquid was introduced from a CO_2 gas cylinder. The completion of carbonation of the specimens was confirmed by the phenolphthalein test described in the previous subsection.

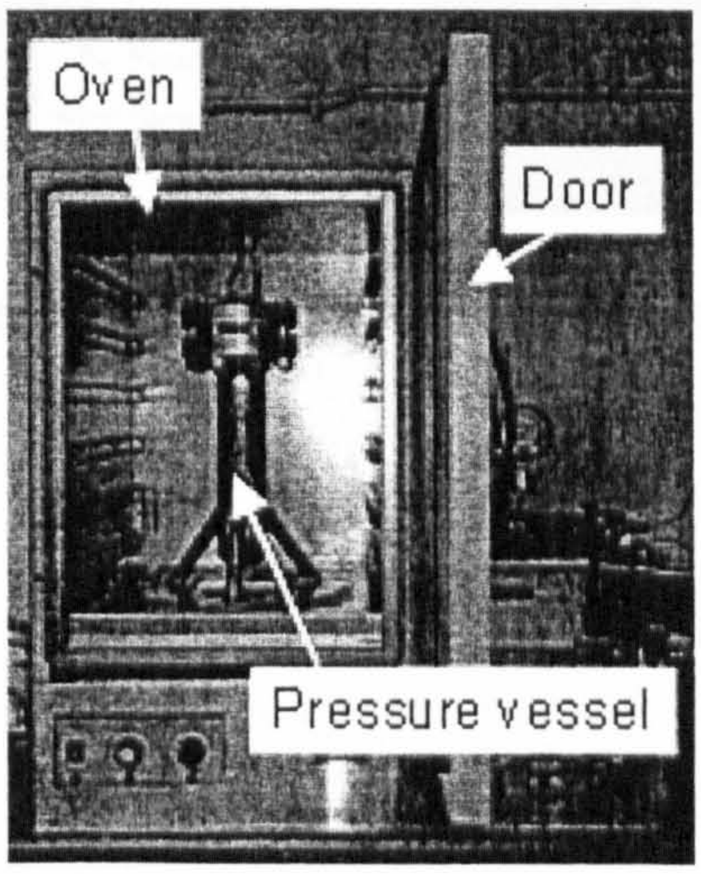

Figure 2.2 Super-critical carbonation unit

2.3 EXPRESSION OF PORE SOLUTION

In order to determine the ionic constituents of the pore solution in cement pastes, a method of extracting capillary pore solutions under pressure was employed in Chapter 4. This technique was first used by Longuet et al. (1973) and subsequently developed by Barneyback and Diamond (1981) and Page and Vennesland (1983). As illustrated in Figure 2.3, the pore expression device consists of a support cylinder, platen, die body and piston assembly. After all the parts except the piston were assembled, the specimen was dropped into the bore of the die body. A Teflon disc was then inserted between the specimen and the piston, completely covering the entire diameter of the hole in order to prevent the expressed liquid from leaking upward. Plastic tubing was fitted into the fluid drain channel and a plastic vial was placed under the open end of the tubing. The piston was then loaded and a pressure was slowly applied until the maximum load value reached 600kN. The extracted solution was drawn through the tubing and stored in the sealed plastic vial to prevent exposure to air. After each run, the parts were cleaned with distilled water and acetone, and the surfaces were sprayed with PTFE non-stick spray for lubrication.

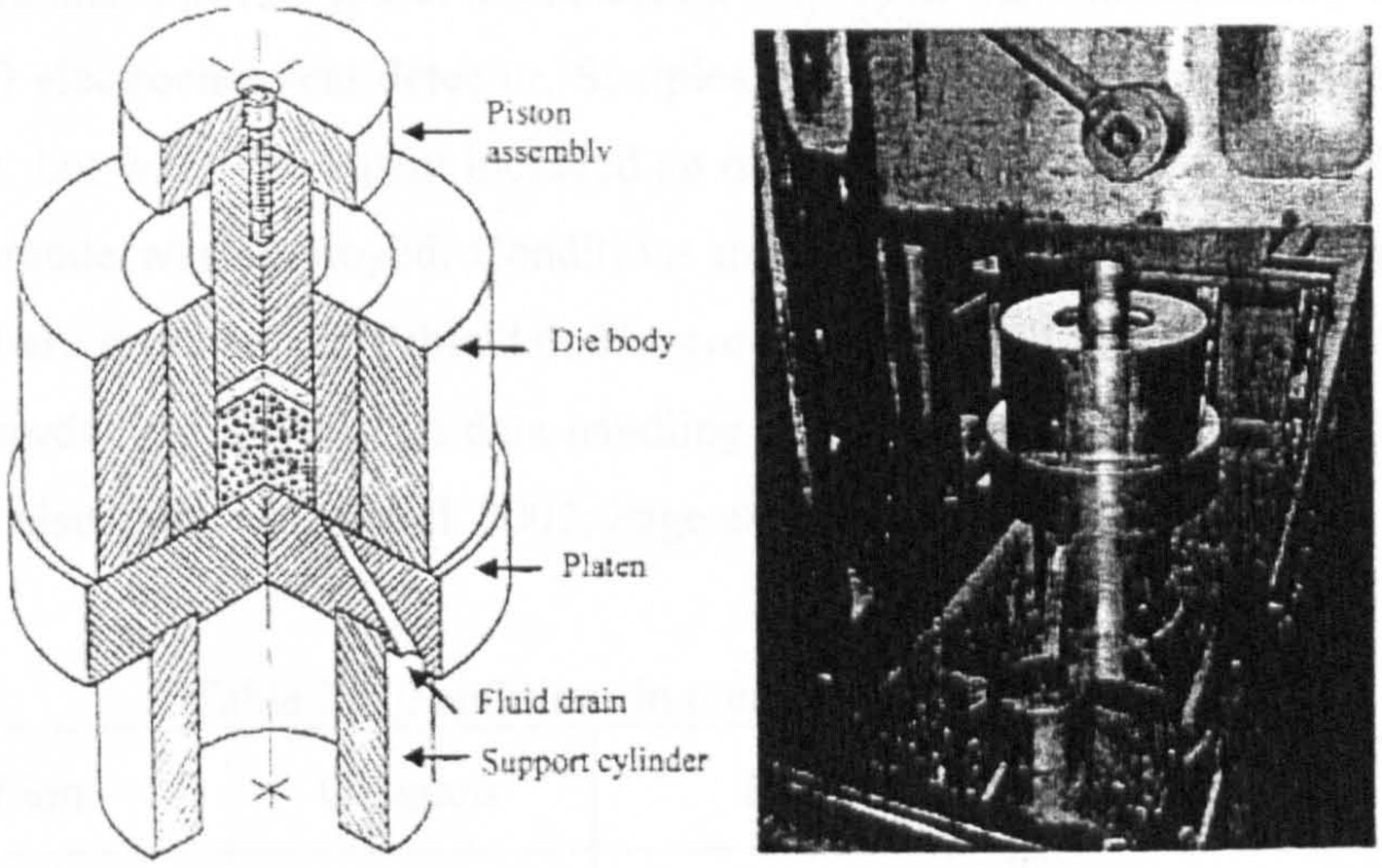

Figure 2.3 Pore expression device (left: Barneyback and Diamond 1981)

2.4 ANALYSIS OF IONIC CONCENTRATIONS

Ionic concentrations presented in Chapters 4 and 6 were determined by means of ion chromatography. In this technique, samples are passed through a column containing an ion exchange resin that strips out the ions. The column is then washed with an eluent solution, which removes different ions from the column at different rates. The rate depends on the balance between affinities of particular ions for the column and the eluent. The conductivity of the eluent which is contaminated with particular ions at different times is measured and the values are plotted against time. A number of peaks are produced and each peak's time corresponds to a different ion. Concentration of ions (ppm) in the same sample solutions are estimated by comparing with the corresponding time and peak areas of standard solutions containing known amounts of targeted ions.

Analysis was performed using a Dionex DX500 ion chromatography system equipped with a GP50 gradient pump. Samples were diluted with deionised water in the appropriate ratio and then filtered through 0.22 μm Millex-GX filter units (Millipore) before being injected into the ion chromatograph. Filtered samples were passed through appropriate Dionex analytical and guard columns. The method of ion detection employed was conductimetry by means of a Dionex ED40 electrochemical detector. Samples were usually analysed in auto-suppression recycle mode, but when the eluent included an organic solvent, acetonitrile (ACN), external regeneration mode was employed. Conditions used for the ion chromatograph detection of different ions are presented in Table 2.6. The conductivity profiles and concentrations of the ions were recorded using PeakNet data handling software. Further details of the procedures are presented elsewhere (Page et al. 2002; Page et al. 2005; Sawada 2005).

Table 2.6 Conditions in methods of ion detection

Type of ion	Columns	Eluent	Flow rate	Regeneration system
Standard cations (Na^+, K^+, Mg^{2+}, Ca^{2+})	CS14 & CG14	6mM H_2SO_4	1ml/min	Recycle
Ethanolamine	CS14 & CG14	6mM H_2SO_4	1ml/min	Recycle
Guanidine	CS14 & CG14	10mM MSA + 15% ACN	1ml/min	External regeneration
Arginine	CS14 & CG14	6mM H_2SO_4	1ml/min	Recycle
Standard anions (Cl^-, NO_3^-, SO_4^{2-})	AS14 & AG14	2mM Na_2CO_3+ 2.5mM $NaHCO_3$	2ml/min	Recycle

MSA: methanesulfonic acid, ACN: acetonitrile

Typical conductivity peaks of organic corrosion inhibitors, ethanolamine, guanidine and arginine are shown in Fig. 2.4 together with standard cations, namely sodium, potassium, magnesium, and calcium ions. Among the organic inhibitors investigated in Chapters 3-6, ethanolamine and arginine were readily detectable by the same conditions as standard cations; however, as pointed out by Page et al. (2005), the determination of guanidine in mixtures of ions caused a problem, similar co-elution between guanidine and potassium ions being observed. This problem was solved by using 15% ACN in 10mM methanesulfonic acid (MSA) eluent as described by Page et al. (2005).

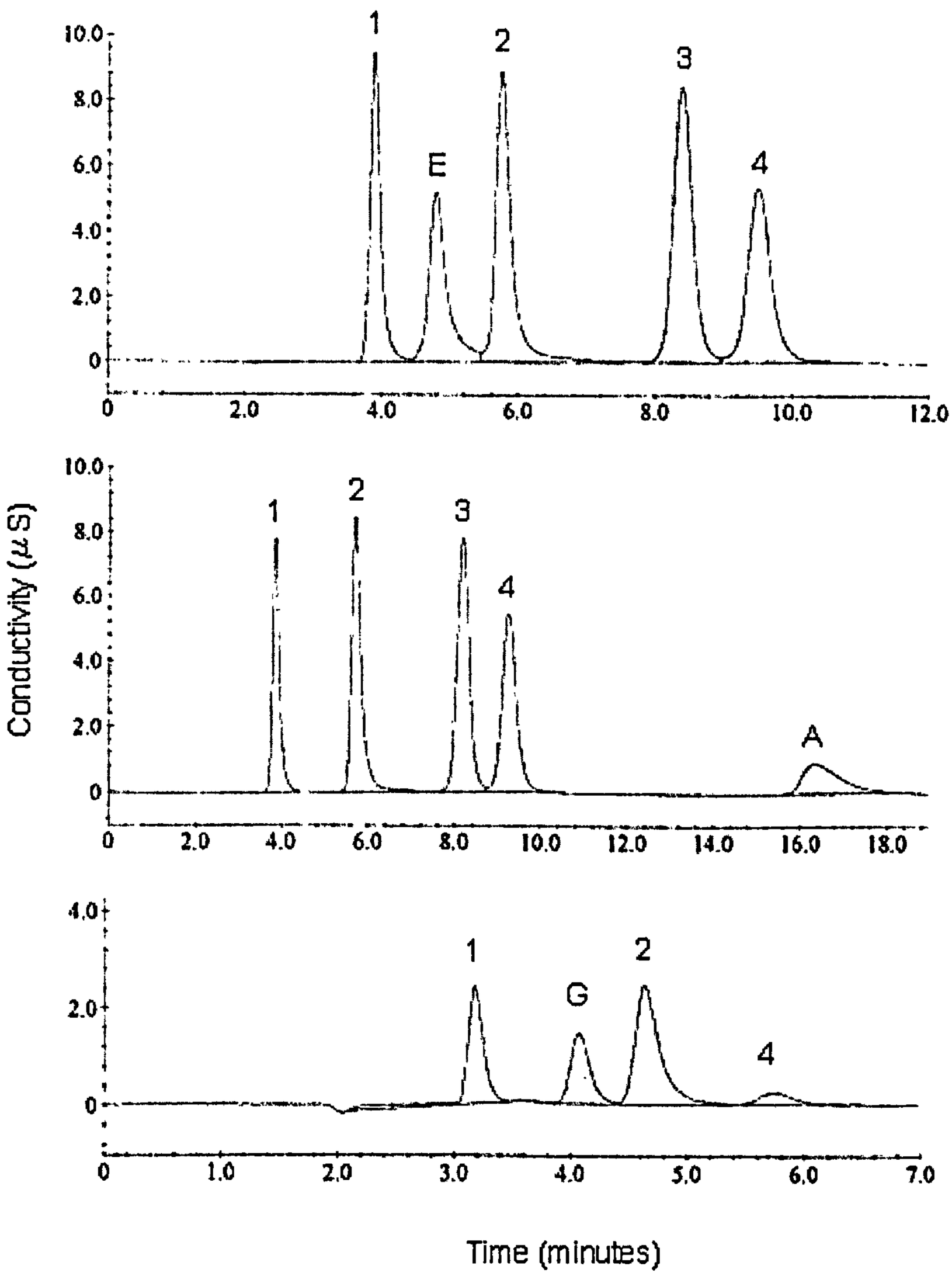

Figure 2.4 Typical conductivity peaks of corrosion inhibitors (Standard cations: 1=Na^+, 2=K^+, 3=Mg^{2+}, 4=Ca^{2+}, E=ethanolamine, A=arginine, G=guanidine)

2.5 MEASUREMENT OF POTENTIAL AND PH

A saturated calomel electrode (SCE) was used to measure the potentials of steel bars in electrolytes or concrete, as described in Chapters 3 and 6. While not in use, the electrode was kept in a saturated potassium nitrate solution.

In the experimental work presented in Chapters 3 and 4, the pH values of electrolytes were measured by means of a digital pH meter, "AR15" (Accumet Reseach 15) with a glass bodied combination electrode manufactured by Fischer Scientific Company. The pH meter was calibrated with buffers at pH 4.0, 7.0, and 9.2 before the measurements were taken. In the work presented in Chapter 5, 6, the pH values were measured by means of a different digital pH meter, "pH/DO Meter D-55" manufactured by Horiba Instruments, which was calibrated with buffers at pH 4.0, 7.4, and 10.0 before the measurement.

2.6 PRECISION WIRE ERROSION METHOD

Precision wire errosion was employed for cutting steel bars into sections with a required length as described in Chapter 6, ensuring that minimal loss of metal was incurred. Ngala et al. (2004) were the first group to apply this technique for cutting cleaned steel bars by means of a precision wire with a diameter of 0.25mm for gravimetric analysis of the bars removed from laboratory concrete specimens whose surface had been treated with an ethanolamine-based corrosion inhibitor. In this thesis, precision wire erosion instrument, "AQ325L" manufactured by Sodick, was used for cutting steel bars by means of a precision wire with a diameter of 0.2mm. When the cut was in progress, special attention was paid to make sure that each cut was exactly perpendicular to the axis of bar.

2.7 DETERMINATION OF BULK DENSITY AND POROSITY

Bulk density measurements were conducted for cement paste discs in Chapter 4. The procedures for measurement are described below where a balance (OHAUS Explorer) measuring to 0.0001g was used. The weight of saturated specimen immersed in water was measured and recorded (W_1). The specimen was then removed from the water and lightly wiped with a lens tissue. The specimen was reweighed in air, and the saturated surface dry weight (W_2) was recorded. The bulk density, ρ (g/cm^3) was determined according to Archimedes' principle as the ratio of weight in air to loss of weight in water:

$$\rho = \frac{W_2}{W_2 - W_1}\rho_w \tag{2-1}$$

where ρ_w is density of water, which is assumed to be 1.0 in this thesis. For the purpose of obtaining the total porosity, the saturated surface-dry specimen was placed in an oven at 105±5°C for 24 hours and then its weight (W_3) was measured and recorded. Then the total porosity, ε is given by:

$$\varepsilon = \frac{W_2 - W_3}{W_2 - W_1}\rho_w \tag{2-2}$$

CHAPTER 3

ACTIONS OF ORGANIC CORROSION INHIBITORS IN MODEL ELECTROLYTES

3.1 INTRODUCTION

3.1.1 Scope of the study

Corrosion inhibitors (as the term is used in this thesis) are chemicals that cause changes at the steel/concrete interface which can result in a reduction of the overall corrosion rate of steel in concrete. Corrosion inhibitors have been used as admixtures for new structures as a preventive measure since the 1970s. They have recently been developed to be applied on the concrete surface for the rehabilitation of reinforcing steel bars embedded in the existing structures. In recent years, several amine/alkanolamine based corrosion inhibitors have been applied for rehabilitation of reinforced concrete structures suffering from corrosion. One of the claimed advantages of these types of inhibitors is their ability to diffuse considerable distances into concrete owing to their high vapour pressure (Maeder 1994) as well as their economic availability and ease of application. They are supposed to be simple alternatives to other available rehabilitation methods such as patch repair or impressed current cathodic protection, but there are still several aspects to be clarified concerned with the effectiveness of surface-applied corrosion inhibitors (Page et al. 2000) as mentioned in Chapter 1 (see section 1.2).

Among the uncertainties listed in section 1.2, the issue (2) is discussed in this chapter with reference to investigations of the behaviour of the amine/alkanolamine corrosion inhibitors, namely ethanolamine, guanidine, and arginine, in model electrolytes which were intended to simulate the pore solution phase present within carbonated concrete. The steel is maintained in a passive condition before immersion in the electrolytes with variously controlled concentrations and pH values. There were two objectives: (A) investigations on the mechanism of corrosion inhibition of the steel in air-saturated neutral or alkaline electrolytes, and (B) knowledge acquisition on the concentrations of the inhibitors required for the inhibition of corrosion of the steel in the electrolytes. These matters were experimentally studied by immersing mild steel bars in air-saturated model electrolytes of

amine/alkanolamine corrosion inhibitors for 35-42 days, during which the potential and corrosion rates were monitored at regular intervals.

3.1.2 Mechanism of steel corrosion

The understanding of metallic corrosion processes is based on the realisation that their mechanism is electrochemical in nature. Metal surfaces act as the sites for electrode reactions, termed anodic and cathodic processes, which are coupled together to form corrosion cells (Bentur et al. 1997).

$$\text{Anodic reaction: } 2Fe + 4e^- \Rightarrow 2\,Fe^{2+} \qquad (3\text{-A})$$

$$\text{Cathodic reaction: } O_2 + 2H_2O + 4e^- \Rightarrow 4OH^- \qquad (3\text{-B})$$

This mechanism is illustrated in Figure 3.1 for the particular case of iron corroding in oxygenated water to form rust. The removal of iron is an electrochemical reaction that causes the iron to appear in the surrounding water solution as ferrous (Fe^{2+}) ions. The dissolution of iron occurs within a limited volume of water present in the pores of concrete surrounding the steel. As a result of this dissolution, the steel mass and its cross-sectional area are reduced. With the ferrous ions in solution, reactions between ferrous ions, hydroxyl ions and dissolved oxygen molecules can occur within the pore water. The product of these reactions is one of the varieties of rust (hydrated iron oxide) which precipitates out of the pore water and deposits itself in the restricted space in the concrete around the steel. The formation of rust in a confined space sets up expansive stresses which may crack the concrete cover. This causes visual or structural problems and allows greater oxygen and water access to the steel. The formation of rust proceeds according to the following reactions, where ferric oxide is more stable and the conversion of ferrous oxide to ferric oxide usually occurs:

$$Fe^{2+} + 2OH^- \Rightarrow Fe(OH)_2 \text{ (Ferrous oxide)} \qquad (3\text{-C})$$

$$Fe(OH)_2 + O_2 \Rightarrow FeOOH + H_2O \text{ (Hydrated ferric oxide)} \qquad (3\text{-D})$$

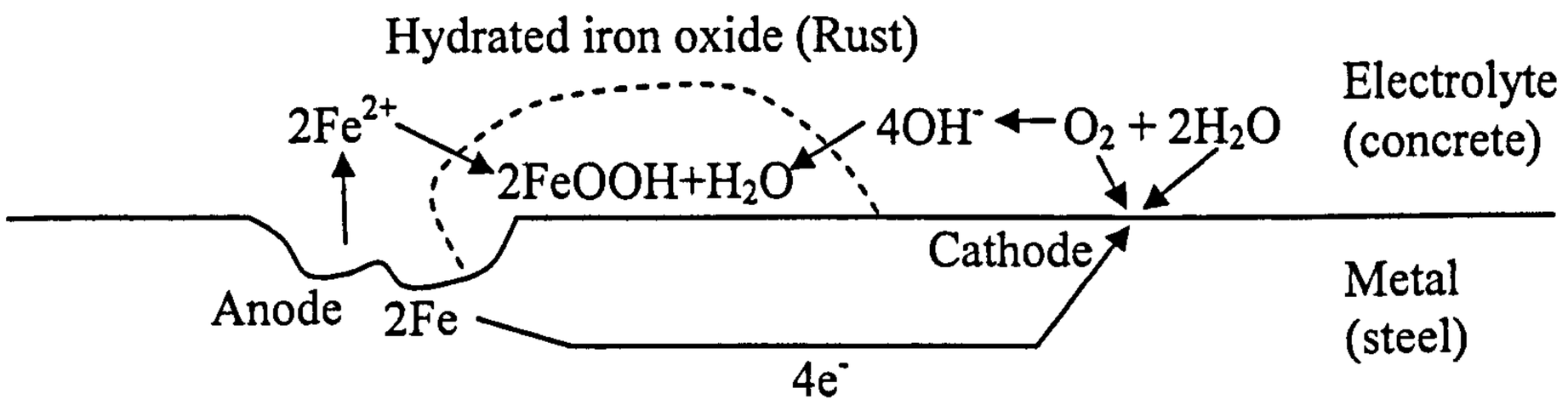

Figure 3.1 Mechanism of steel corrosion

3.2 LITERATURE REVIEW

Corrosion inhibitors can be classified into three main categories: anodic, cathodic and mixed. Anodic inhibitors, whose inhibitive action depends on the anion, suppress the anodic reaction by the formation of a protective film on the anode, resulting in the shift of corrosion potential of the metal to a noble value with time. For example, nitrite is identified as an anodic inhibitor since it functions at the anode, quickly oxidising ferrous ions to ferric ions, formed anodically at defects in the passive film by the following reaction (Gaidis and Rosenberg 1979):

$$2Fe^{2+} + 2OH^{-} + 2NO_2^{-} \Rightarrow 2NO + Fe_2O_3 + H_2O \qquad (3\text{-E})$$

Cathodic inhibitors, whose inhibitive action depends on the cation that forms insoluble deposits with hydroxyl ions, suppress the cathodic reaction by retarding oxygen reduction or hydrogen evolution, resulting in a shift of the potential towards a negative value with time. The salts of magnesium and zinc are the examples of cathodic inhibitors, reacting with the hydroxyl ions present at the cathode, forming insoluble magnesium and zinc hydroxides which precipitate on to the cathode and reduce oxygen diffusion through to the steel and the conduction of electrons.

Mixed inhibitors retard both the anodic and the cathodic reactions to a certain degree.

Anstice (2000) investigated the behaviour of the various inhibitors in model electrolytes at alkaline or neutral pH values, with or without chloride addition, namely nitrite ions (in the form of sodium nitrite), sodium monofluorophosphate (Na_2PO_3F) and a proprietary alkanolamine-based inhibitor that contains ethanolamine as a major constituent. After immersing mild steel bars in air-saturated aqueous electrolytes for six weeks, he concluded that all of the three inhibitors examined behaved as passivating anodic inhibitors since the corrosion potential was observed to shift in the more positive direction as the corrosion rate was reduced to very low values.

There are several hypotheses (Page 1970) by which anionic corrosion inhibitors could exert inhibitive performance described as follows. These hypotheses may also apply to the elucidation of the effectiveness of organic cation based corrosion inhibitors such as amine/alkanolamine inhibitors on the passivation of steel, whilst the mechanism of the passivation has not been fully understood yet:

(1) Buffering hypothesis

The mechanism leading to the onset of corrosion starts at certain locations on the reinforcing steel where ruptures in the passive layer occur leading to iron dissolution and hydrolysis that produces $FeOH^+$ and H^+, creating an acidic environment. This causes the breakdown of the oxide film by a reductive dissolution process forming ferrous ions as follows:

$$Fe_2O_3 + 6H^+ + 2e^- \Leftrightarrow 2Fe^{2+} + 3H_2O \qquad (3\text{-F})$$

Gilroy and Mayne (1965) experimentally showed that anions that buffer at moderately alkaline pH, such as borate, have the ability to promote anodic passivation of iron due to their buffering action. It might be expected that amine/alkanolamine corrosion inhibitors could retard the breakdown process (reaction (3-F)) by functioning as buffers according to their dissociation constants (pKa) by the following equilibrium:

$$R\text{-}NH_2 + H^+ \Leftrightarrow RNH_3^+ \qquad (3\text{-G})$$

(2) Adsorption/ Ion incorporation hypothesis

Brasher (1969) proposed that the primary inhibitive function relies upon adsorption of the anion on to the metal surface at points of breakdown of the oxide film, retarding the dissolution of ferrous ions. In the case of cations of organic corrosion inhibitors in neutral solutions, it has been claimed by some researchers that the inhibiting effects are attributed to their adsorption on the metal surfaces that prevents further dissolution of metal. (Maitra et al. 1983 and 1984, Aramaki et al. 1994). From the fact that the presence of nitrogen atoms at the film surface, Aramaki et al. (1994) confirmed by means of X-ray photo-electron spectra that the organic inhibitor cations, namely alkyltrimethylammonium ions, were adsorbed on the passive film. Maitra et al. (1984) demonstrated using guanidine derivatives as organic corrosion inhibitors that the adsorption takes place on iron depends directly on their concentration in the solution, following Langmuir adsorption isotherm described as follows:

$$\theta/(1-\theta) = A \cdot C \cdot e^{-Q/RT} \qquad (3\text{-}1)$$

where θ is the fraction of the metal surface covered by the adsorbed species, A is a constant characteristic of the adsorption nature, C is the concentration of the material to be adsorbed, Q is the heat of adsorption, R is the gas constant, and T is the temperature. The adsorption is believed to block either cathodic or anodic reactions or both. However Page and Mayne (1972) found that air-saturated solutions of sodium benzoate completely inhibit the corrosion of iron only in when the salt is present at intermediate concentration, and claimed that the obtained results cannot be satisfactorily explained by concentration-dependent adsorption

hypothesis as indicated by Eq. (3-1). In this way, the inhibition mechanism based on the adsorption hypothesis cannot always elucidate the effectiveness of corrosion inhibitors on steel passivation.

Since the adsorption of anions on the film surface is associated with the breakdown of passive film, a cation inhibitor, which can restrict the aggressive action of the anion to the film via "electrostatic interaction" between both ions, may suppress the breakdown of passive film. It was reported by Aramaki et al. (1991) that the pitting potential of steel in an aqueous solution containing chloride ions is raised by addition of ammonium compounds.

(3) Insoluble product hypothesis

Hoar (1937) showed that salts that give a stable precipitate on being mixed with stannous chloride were inhibitive towards metallic tin, although those that gave precipitate were corrosive. This might be interpreted as implying that the precipitation acted as an insoluble barrier at anodic sites, resulting in the prevention of metal dissolution. Mayne and Page (1974) investigated the uptake of benzoate and acetate ions from aqueous non-buffered solutions into the air-formed oxide film on mild steel in the range pH 6 to pH 12 by means of radioactive tracers, and concluded that the inhibitive function of the ions depended on their ability to deposit adherent, insoluble basic ferric salts when anodic acidity developed at sites of breakdown of the air-formed oxide film, arresting reductive dissolution of the film. Other evidence is that carboxylates, which form iron carboxylate complexes on the metal surface, inhibit corrosion in neutral and slightly alkaline oxidising environments (Granata et al. 1986).

As regards to the required concentration of corrosion inhibitors that is able to maintain the steel in a passive condition, it is believed that, in many cases, change from aggressive action to passivation occurs at a certain critical concentration specific to each anion involved (Brasher 1969). Maitra et al. (1984) investigated corrosion of pure iron in neutral aqueous solutions of guanidine derivatives, and concluded that corrosion reaction decreases with increasing inhibitor concentrations. Anstice (2000) concluded from his investigations mentioned previously that sodium nitrite was the most effective inhibitor of those he studies in neutralised solutions, inhibitor concentrations of 0.01M reducing the corrosion rate in the case of no chloride addition and 1M in the case of 1.0M chloride addition. In the neutralised solutions of ethanolamine, the inhibiting threshold of the inhibitor concentrations was found to lie between 0.1M and 1.0M in the absence of chloride and 1M in the presence of only 0.01M chloride. Jamil et al. (2003) investigated the effectiveness of amino alcohol-based inhibitor by mixing it with electrolytes simulating the concrete pore solutions in the presence

of chloride ions (2g/l NaCl), and found that the threshold of inhibitor concentration was between 0.5-1.0% (vol/vol).

3.3 MATERIALS AND EXPERIMENTAL TECHNIQUES

3.3.1 Preparation of model electrolytes

Aqueous solutions of amine or alkanolamine based inhibitors, namely ethanolamine, guanidine, and arginine with a wide range of pKa values, as shown in Table 3.1 below, were made at three different pH values, approximately 11.0, 9.0, and 7.0, simulating the carbonated pore solutions containing the inhibitor at two different concentrations, 0.1M and 0.01M without chloride. L-arginine was used for the preparation of arginine aqueous solutions. The control solution was de-ionised water. The specimens were prepared in triplicate for each condition.

After the solutions were made, their natural pH values were recorded as shown in Table 3.2 by means of a digital pH meter, "AR15" (Accumet Reseach 15) by Fischer Scientific Company introduced in the previous chapter.

In order to prepare the solutions with a reduced pH of 9.0 and 7.0, carbon dioxide was bubbled through them from a carbon dioxide cylinder through plastic tubes to lower the pH to below 7.0. Then the solutions with a pH of 9.0 and 7.0 were obtained by carefully titrating the natural solutions with the carbonated solutions.

Table 3.1 Chemicals used as inhibitors (Lide 2006)

Species	pKa
Ethanolamine ($OH\text{-}CH_2\text{-}CH_2\text{-}NH_2$)	9.5
Guanidine ($NH{=}C\text{-}(NH_2)_2$)	13.6
Arginine ($NH{=}C(NH_2)\text{-}NH\text{-}(CH_2)_3\text{-}CH(NH_2)\text{-}COOH$)	1.82, 8.99, 12.50

Table 3.2 Natural pH values of the solutions

C	E1	E2	G1	G2	A1	A2
5.90	10.52	11.21	11.11	11.38	10.70	11.30

Key C = Control solution (de-ionised water and no inhibitor addition)
E1 = 0.01M ethanolamine
E2 = 0.1M ethanolamine
G1 = 0.01M guanidine
G2 = 0.1M guanidine
A1 = 0.01M arginine
A2 = 0.1M arginine

3.3.2 Preparation of mild steel bars

Bright drawn mild steel bars with a diameter of 6.35mm whose chemical composition is described in Table 2.4 (shown in the section 2.1.4) were used for the experiment. The bars were cut into 100mm lengths and each of the ends was squared off in a lathe. The steel bars were then degreased by cleaning the surface using acetone and ethanol after the surface had been cleaned with P1000 grade emery paper to remove any surface debris. The top halves of the bars were masked with shrink fit tubing. Areas of approximately 5 mm in length at both ends of the unmasked bottom halves of the bars were covered by applying Fortolac (a proprietary stopping off lacquer supplied by Mac Dermid Canning plc) in order to allow a known surface area to be exposed to the test solution. A wire was then soldered to the top of the bar and the interface was again completely sealed with Fortolac. Finally the bars were left in a desiccator for a period of one week to allow an oxide layer to form on the exposed surface. A total area of 8.89cm^2 of steel was left exposed for testing.

3.3.3 Gel bridge construction

Gel bridges were constructed to connect all the test cells to one common reference electrode (a saturated calomel electrode). A solution containing 3.5% agar and 15% potassium nitrate by weight was heated and stirred until the agar went into solution and a viscous liquid formed. This was then injected into plastic tubes, using a syringe, before it cooled and formed a gel. Once the bridges had cooled, they were kept in water to prevent the gel from drying out.

3.3.4 Cell assembly

Each solution was poured into 200ml beakers on which a PVC lid was put to keep the bars upright and fixed in place with PTFE tape. The PVC lid had been drilled so that the bars, stainless counter electrode, and the gel bridges could be fixed. It was then confirmed that the bars were not touching the glass container and the exposed steel area was fully submerged in the test solution. A diagram of the cell assembly is shown in Figure 3.2.

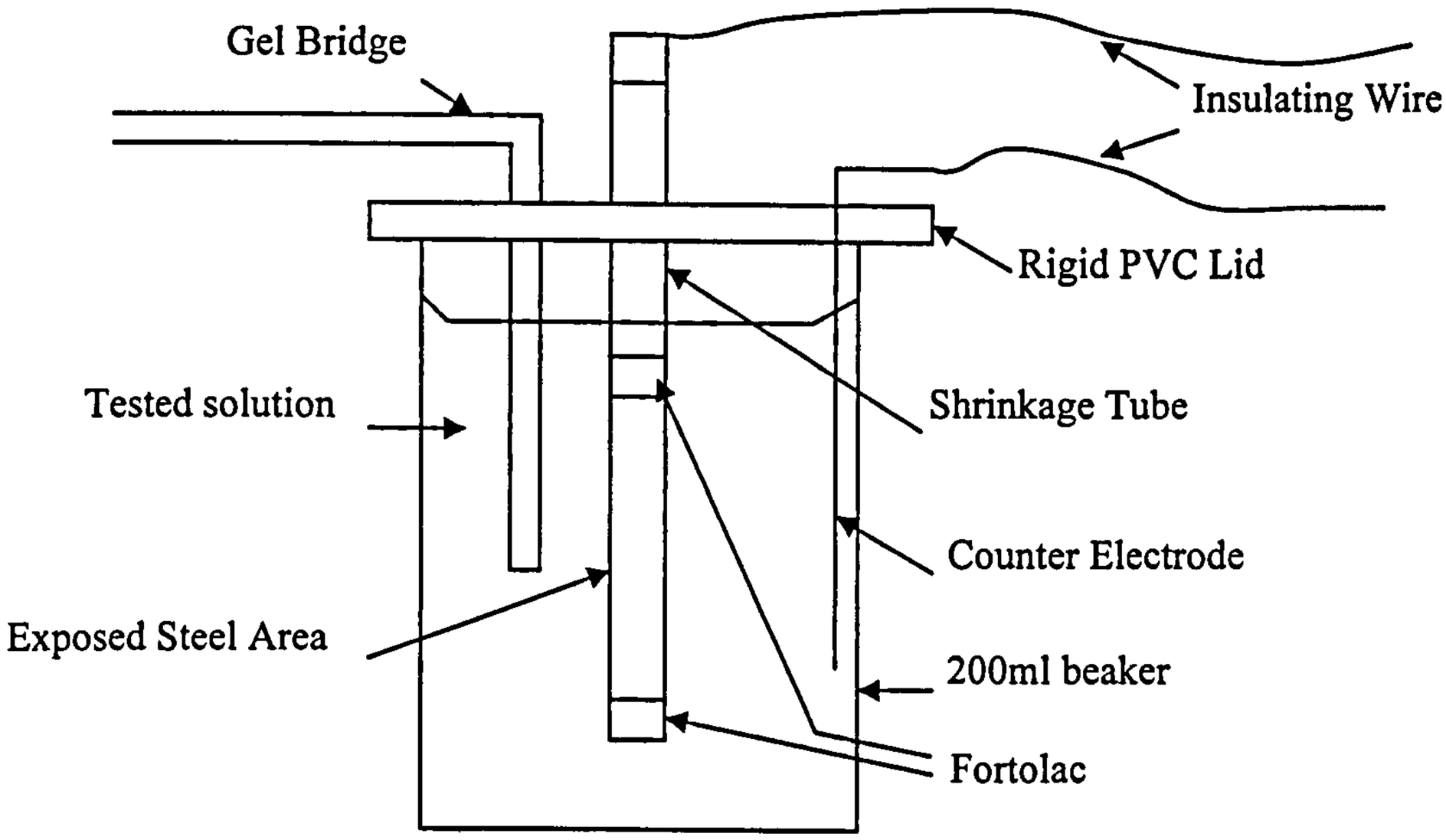

Figure 3.2 Schematic diagram of the cell assembly

3.3.5 Final set-up

A clear box with an internal dimension 500mm long, 300mm wide, and 200mm high was filled to a depth of approximately 20mm with de-ionised water, which maintained the relative humidity inside the box at around 100% to prevent the solutions from evaporating. Then the beakers of each solution were arranged in groups connecting to a solution of 2M potassium nitrate in a beaker with gel bridges. Also each of the potassium nitrate beakers within the groups was connected to a central beaker of 2M potassium nitrate, where a saturated calomel reference electrode was contained for measurement of corrosion potentials and currents. Solid potassium hydroxide pellets were placed on small trays inside the box to absorb carbon dioxide in the air and thus to prevent the pH of the solutions from changing rapidly. The final set-up is shown in Figure 3.3.

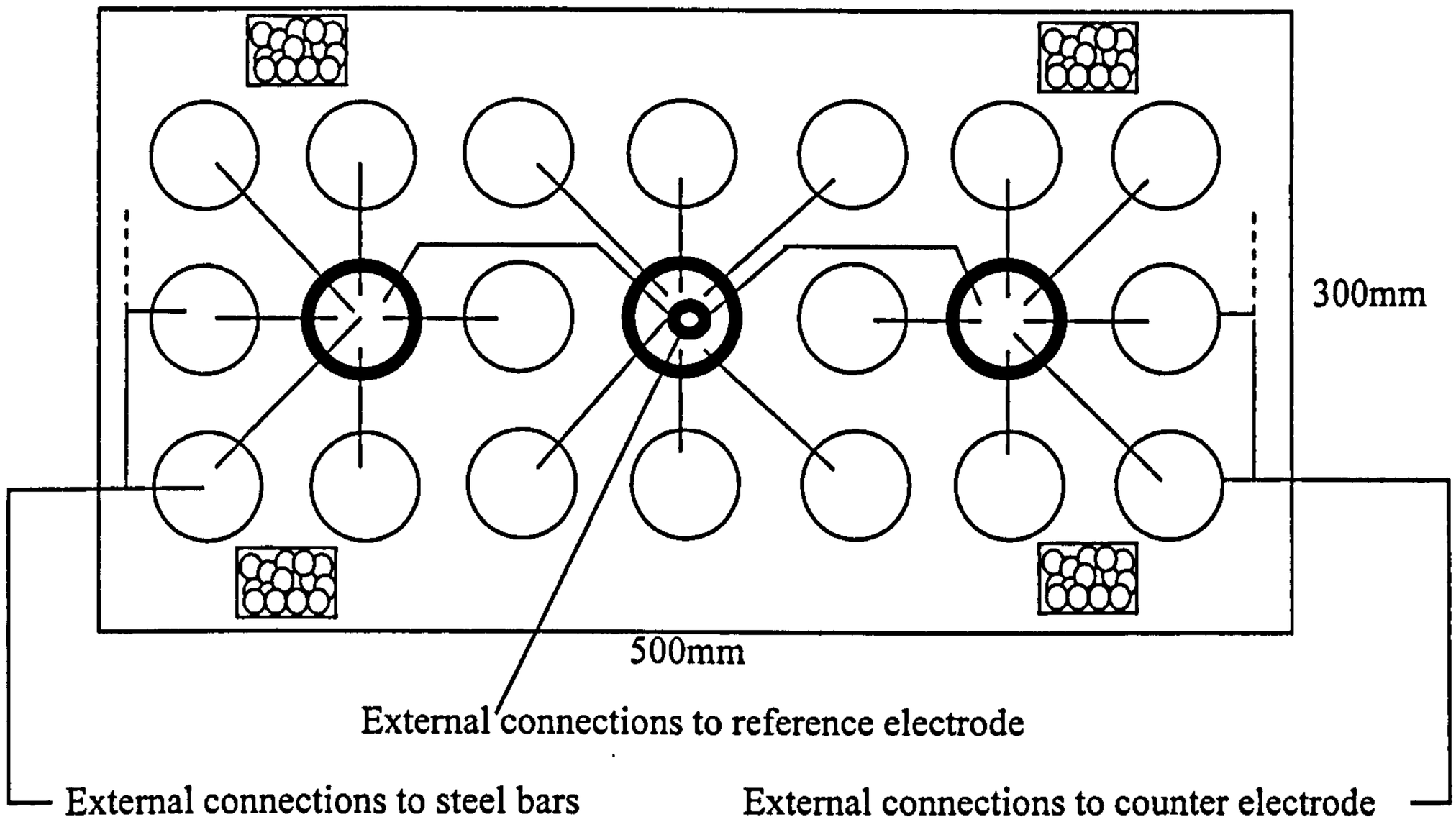

Figure 3.3 Schematic plan of experimental set-up for the immersion tests

3.3.6 Electrochemical monitoring

Corrosion potentials and corrosion rates were measured for steel immersed in aqueous solutions in order to determine their corrosion behaviour. The electrochemical monitoring was carried out by means of a potentiostat/galvanostat, Gill AC serial no. 685, manufactured by ACM Instruments after 1, 3, 7, 14, 21, 28, and 35 or 42 days of immersion of the steel bars. The corrosion potential (Ecorr) was first measured with respect to a stable calomel reference electrode, and then ΔE-ΔI profile near the steel potential (Ecorr) was obtained by the linear polarisation technique with a potential shift range of ±10mV and a scan rate of

10mV/min. This is because it has been demonstrated that the current-potential curve of the steel reinforcing bars embedded in concrete has a linear relationship for potential range around 20-30mV of Ecorr (even high in the case of very high corrosion rates and may be smaller than 20mV in some conditions of extremely low corrosion rates), and that the optimum scan rate that gives accurate measurement without affecting the transient properties of steel passive films lies between 2.5-10mV/min (González et al. 1985).

Finally the polarisation resistance (Rp) was calculated by

$$R_p = \frac{\Delta E}{\Delta I} \tag{3-2}$$

The overall corrosion current I_{corr}, flowing between anodic and cathodic regions of the reinforcing steel is given by the Stern-Geary equation (Stern and Geary 1957) given below

$$I_{corr} = B / R_P \tag{3-3}$$

$$B = \frac{b_a b_c}{2.303(b_a + b_c)} \tag{3-4}$$

where b_a and b_c are anodic and cathodic Tafel slopes respectively, and the value of B is assumed to be 26mV for active corrosion (Andrade and González 1978), which was derived from calibrating polarization resistance measurements with gravimetric measurements.

The corrosion rate i_{corr} is therefore:

$$i_{corr} = I_{corr} / A \tag{3-5}$$

where A is the corroding area.

The criteria for evaluating the severity of corrosion from i_{corr} values were proposed by Andrade et al. (1990), where corrosion is negligible for the corrosion rate below 0.1μA/cm^2, active for the rate greater than 0.1-0.2μA/cm^2, and significant for the rate greater than 1μA/cm^2.

3.4 RESULTS AND DISCUSSION

Figures 3.4 to 3.15 show the results of the electrochemical monitoring of the mild steel bars immersed in the model electrolytes with various pH values. Corrosion potential measurements (Ecorr) were carried out alongside the Icorr measurements. The Ecorr values mentioned here correspond to ones versus a saturated calomel electrode (SCE scale).

Figures 3.4 and 3.5 show the evolutions of Icorr and Ecorr respectively with respect to time for the steel bars immersed in 0.1M ethanolamine solutions with pH values of 7.0, 9.0 and their natural value, together with the results of the control specimens immersed in distilled water. It can be seen that 0.1M ethanolamine solutions at all three pH values were effective in keeping the steel bars passivated during the experiment period, where the measured Icorr values were below 0.1$\mu A/cm^2$ and Ecorr values were over -250mV. However, as can be seen in Figures 3.10 and 3.11, in the case of 0.01M ethanolamine solutions, at all pH values the bars started to corrode. Even the solutions at a natural value (pH 10.52) were found to be still corrosive 10 days after the immersion had been started. This may imply that the threshold concentration at which an ethanolamine solution with a pH range of 7-10 is inhibitive or corrosive lies between 0.01M and 0.1M. It can be seen that as the corrosion rate is reduced the corrosion potential shifts towards the more positive value, indicating that ethanolamine behaves as a passivating anodic inhibitor of steel corrosion in air-saturated aqueous solutions at alkaline and neutral pH values. These results concerned with the passivating inhibitor concentrations of ethanolamine electrolytes correspond to those demonstrated by Anstice (2000).

Figures 3.6 and 3.7 show the evolution of Icorr and Ecorr in the case of 0.1M guanidine solutions at different pH values, and Figures 3.12 and 3.13 in the case of 0.01M solutions. The results show that guanidine at both concentrations has an inhibitive effect on steel bars except for solutions at a concentration of 0.01M with a pH of 7.00. The pH of the pore solutions of carbonated cement pastes is in general close to 9, thus it might be expected that 0.01M guanidine solutions are effective in terms of steel passivation. It can also be seen that as the corrosion rate is reduced the corrosion potential shifts towards the more positive value, indicating that guanidine behaves as a passivating anodic inhibitor of steel corrosion in air-saturated aqueous solutions at alkaline and neutral pH values.

Figures 3.8 and 3.9 show the evolutions of Icorr and Ecorr in the case of 0.1M arginine solutions at different pH values, and Figures 3.14 and 3.15 in the case of 0.01M solutions. It

can be deduced from these results that arginine solutions at a concentration of 0.1M are effective in maintaining the steel bars passivated, whilst the solutions at a concentration of 0.01M lack the ability to keep the steel passivated except those at natural pH. As in the case of ethanolamine, these results indicate that the threshold concentration at which an arginine solution inhibits lies between 0.01M and 0.1M. It can also be seen that as the corrosion rate is reduced the corrosion potential shifts towards the more positive value, indicating that arginine behaves as a passivating anodic inhibitor of steel corrosion in air-saturated aqueous solutions at alkaline and neutral pH values.

3.5 CONCLUSIONS

(1) The three amine/alkanolamine based corrosion inhibitors studied in this chapter, namely ethanolamine, guanidine, and arginine, all behave as passivating anodic inhibitors of steel corrosion in air-saturated aqueous solutions at alkaline and neutral pH values, since the corrosion potential shifts towards the more positive value as the corrosion rate is reduced.

(2) The solutions at a concentration of 1.0M of all of the above three inhibitors are inhibitive at neutral pH values. The threshold concentration at which each inhibitor is inhibitive or corrosive in neutralised solutions that simulate the pore solutions of carbonated cement pastes lies between 0.01M and 0.1M for ethanolamine and arginine, whilst it lies below 0.01M for guanidine except at a considerably reduced pH value of 7.0.

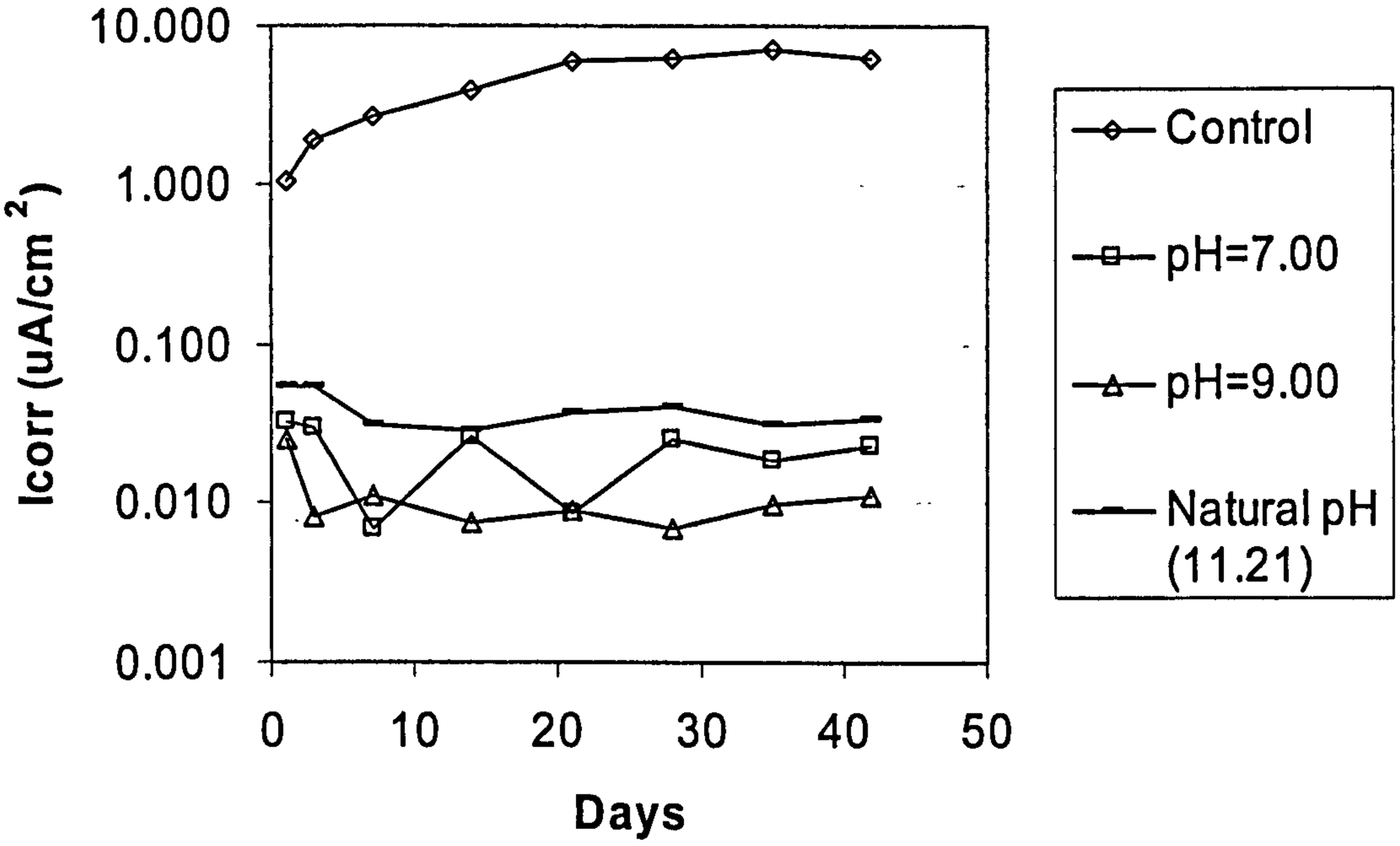

Figure 3.4 Icorr versus time of mild steel bars immersed in 0.1M ethanolamine solutions with various pH values for 42 days

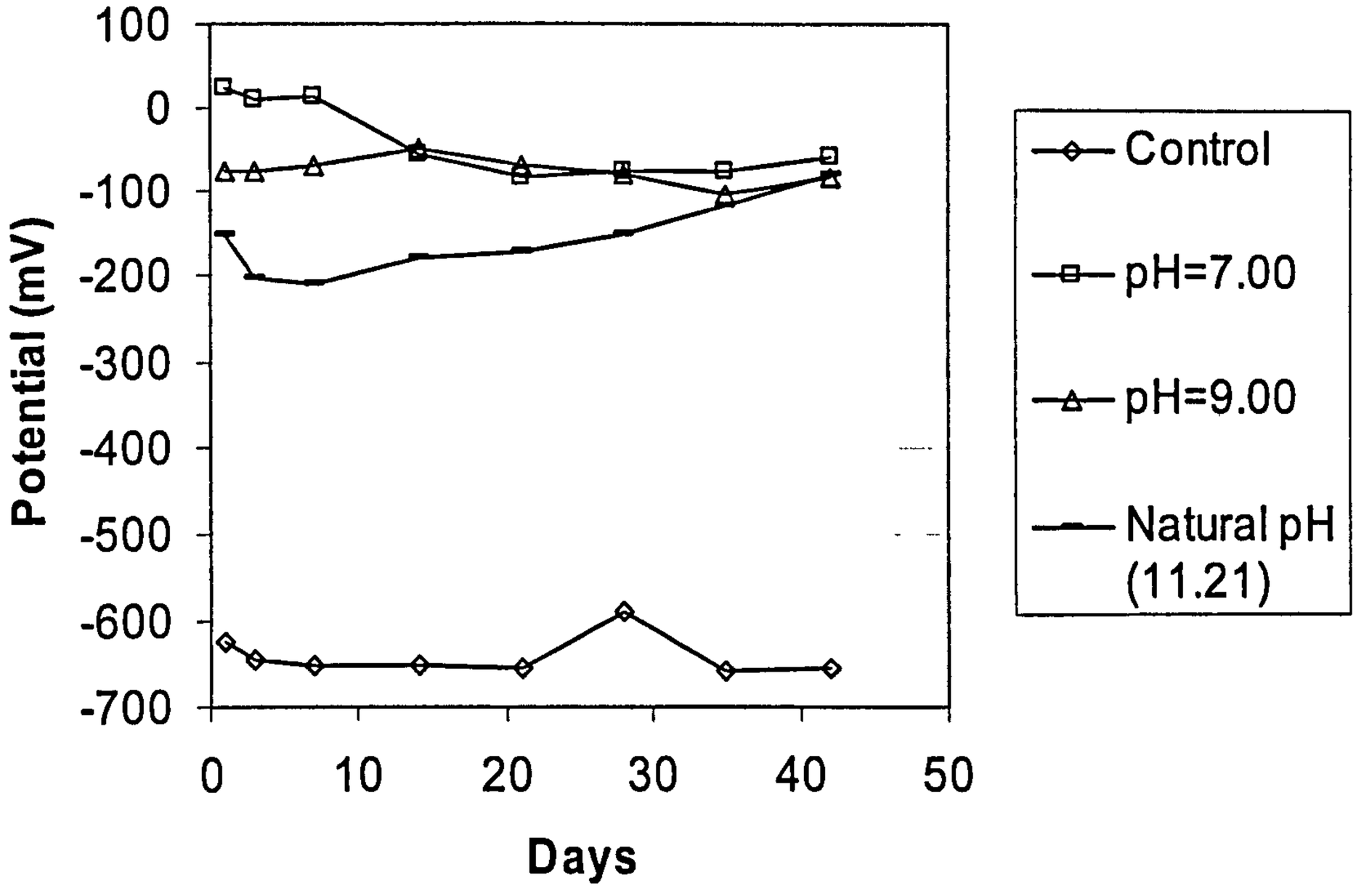

Figure 3.5 Ecorr versus time of mild steel bars immersed in 0.1M ethanolamine solutions with various pH values for 42 days

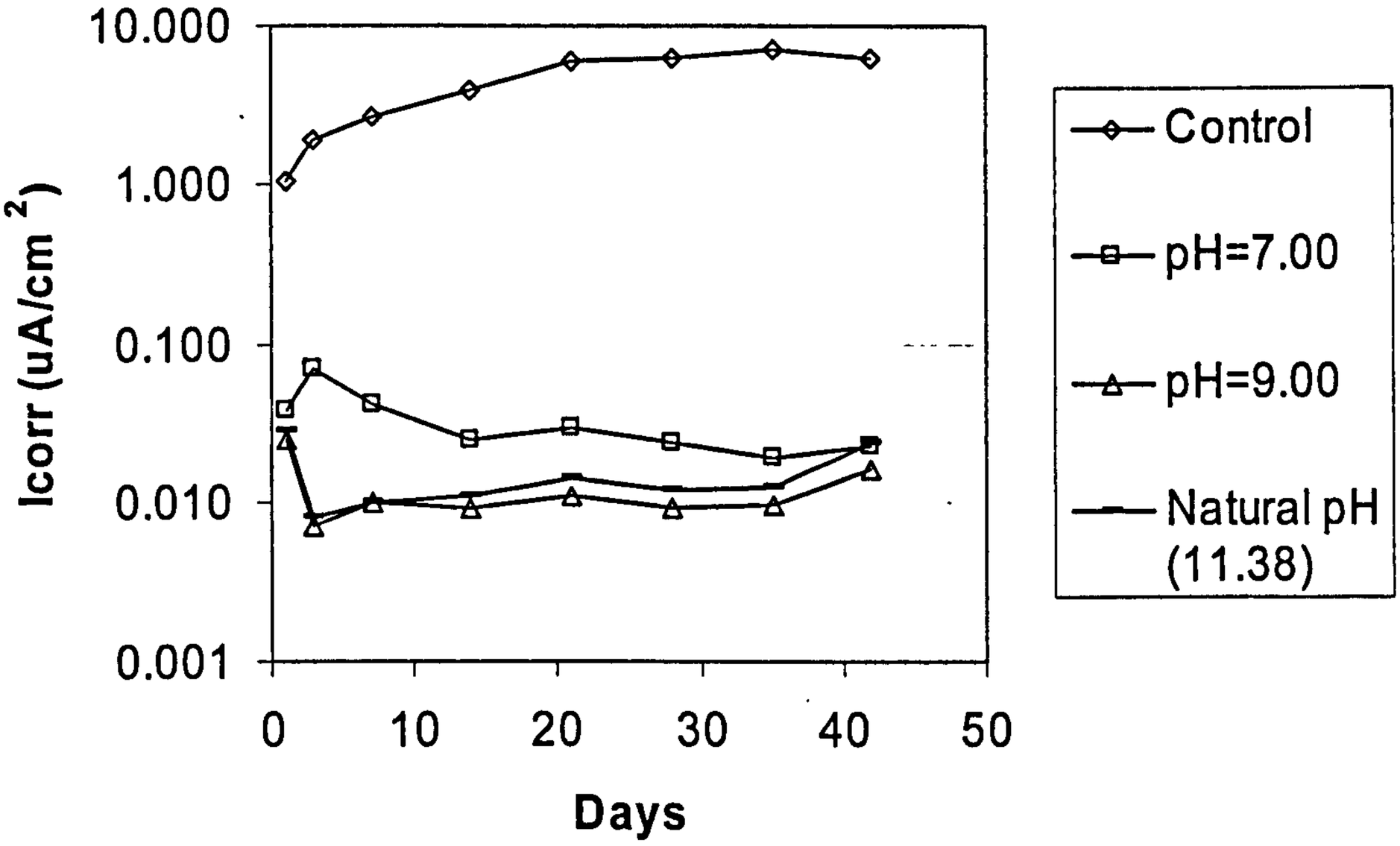

Figure 3.6 Icorr versus time of mild steel bars immersed in 0.1M guanidine solutions with various pH values for 42 days

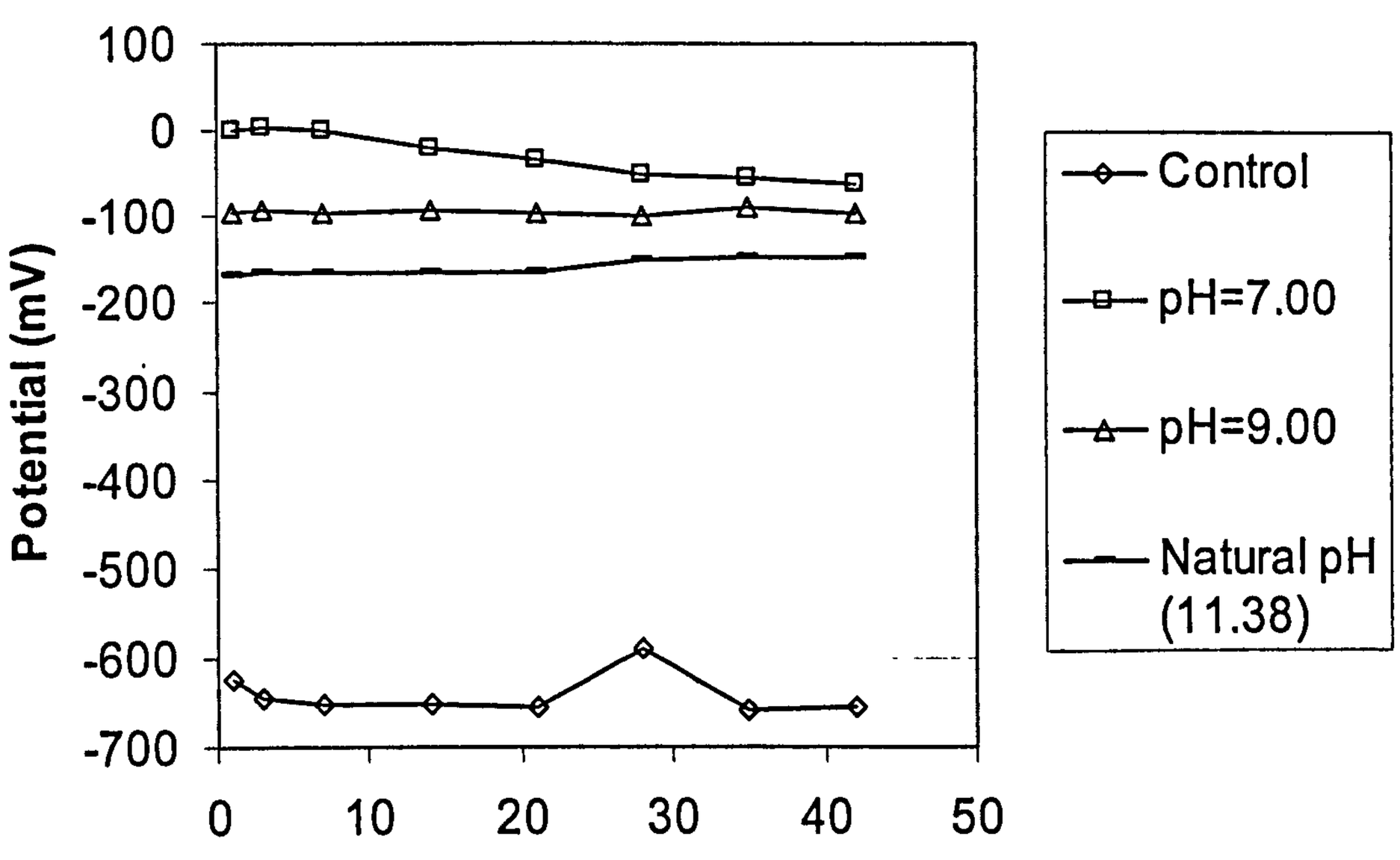

Figure 3.7 Ecorr versus time of mild steel bars immersed in 0.1M guanidine solutions with various pH values for 42 days

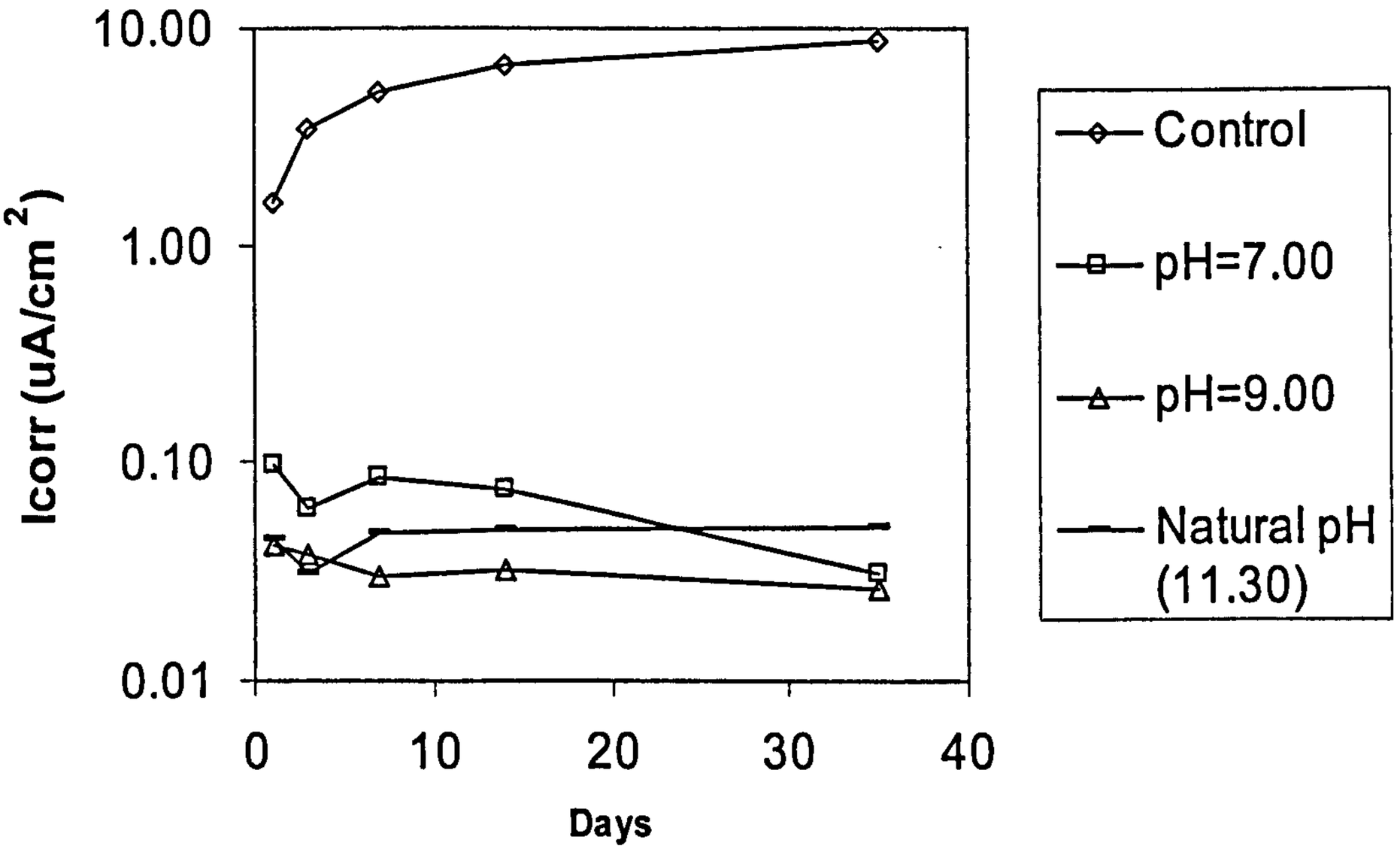

Figure 3.8 Icorr versus time of mild steel bars immersed in 0.1M arginine solutions with various pH values for 35 days

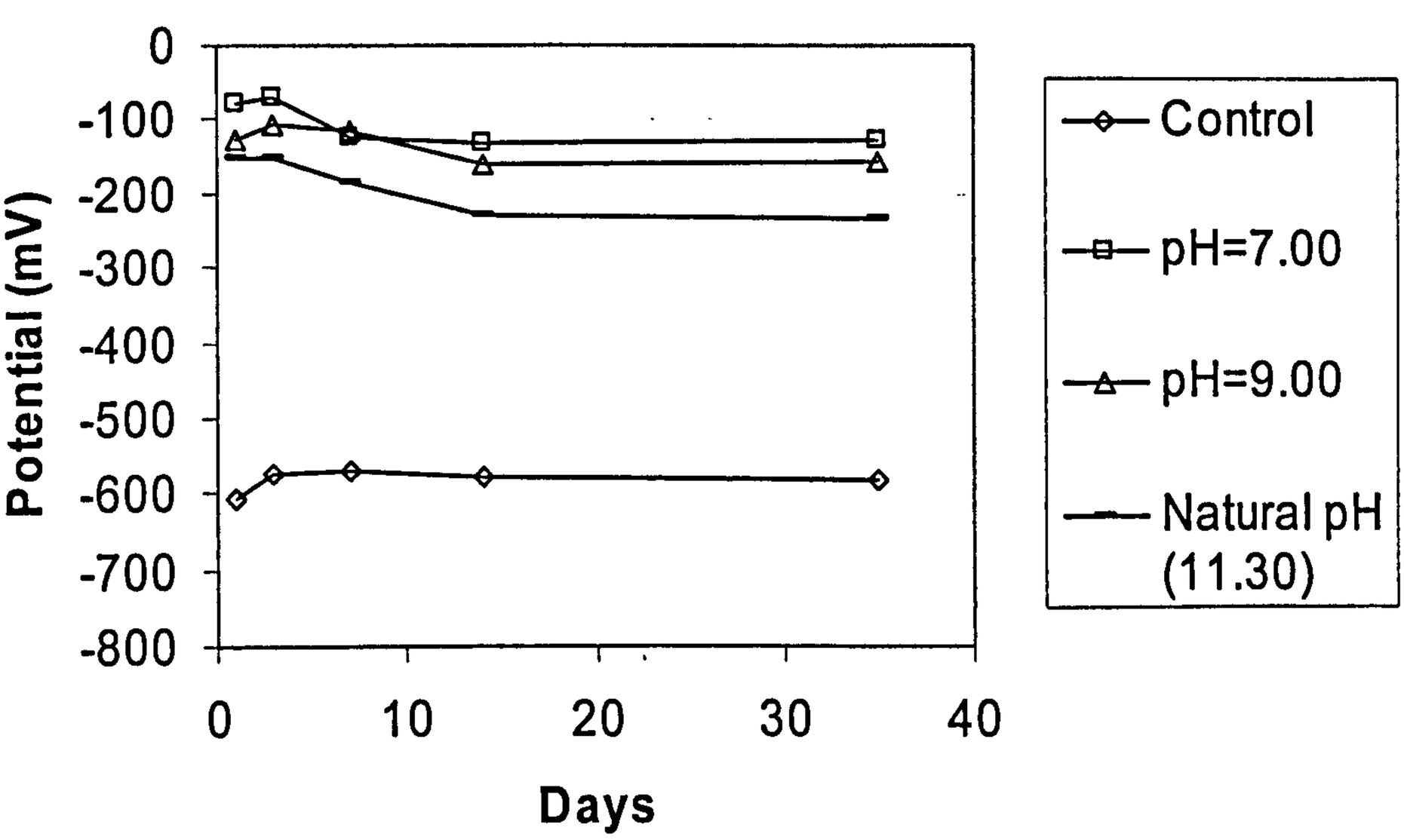

Figure 3.9 Ecorr versus time of mild steel bars immersed in 0.1M arginine solutions with various pH values for 35 days

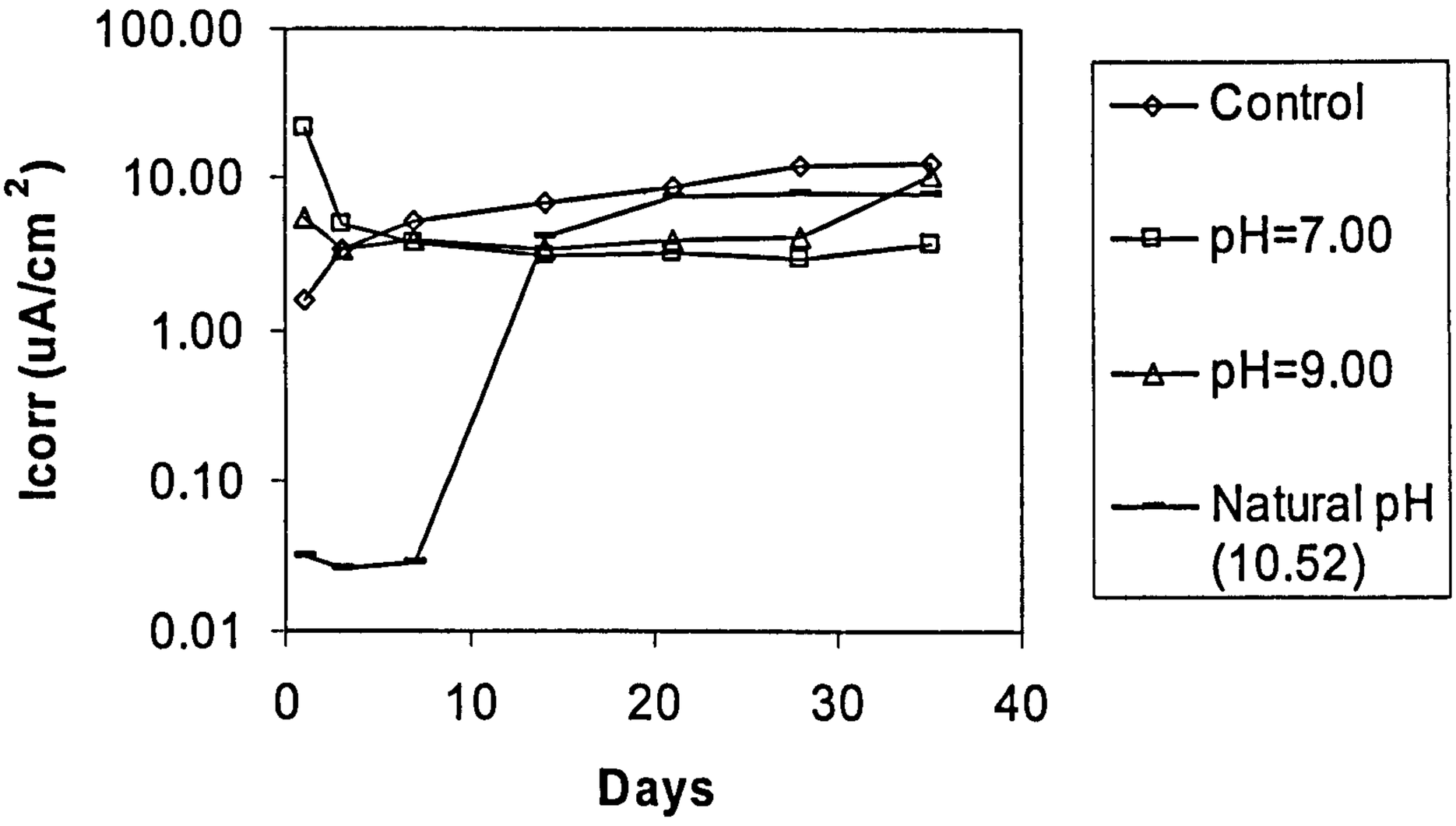

Figure 3.10 Icorr versus time of mild steel bars immersed in 0.01M ethanolamine with various pH values for 35 days

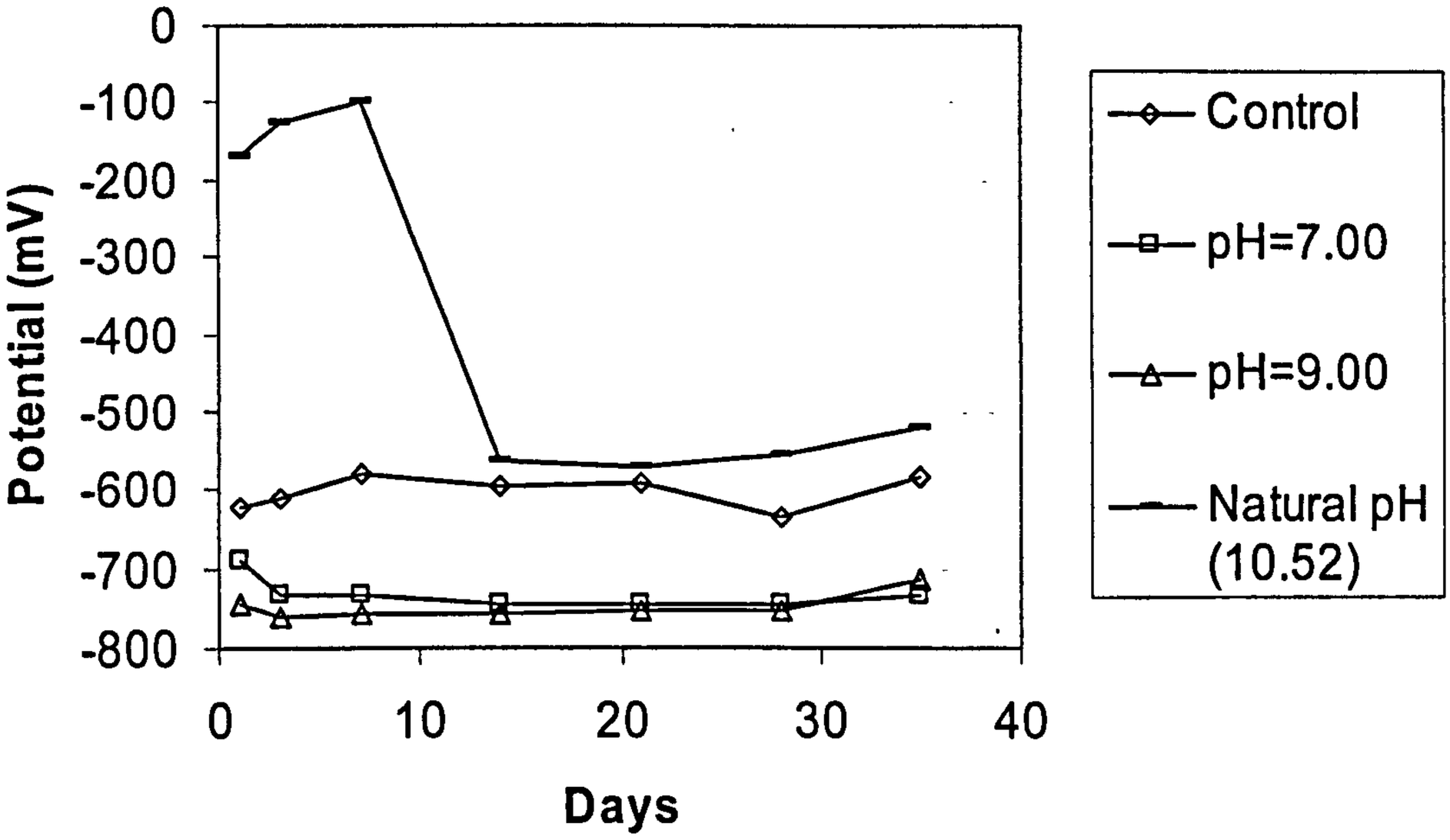

Figure 3.11 Ecorr versus time of mild steel bars immersed in 0.01M ethanolamine solutions with various pH values for 35 days

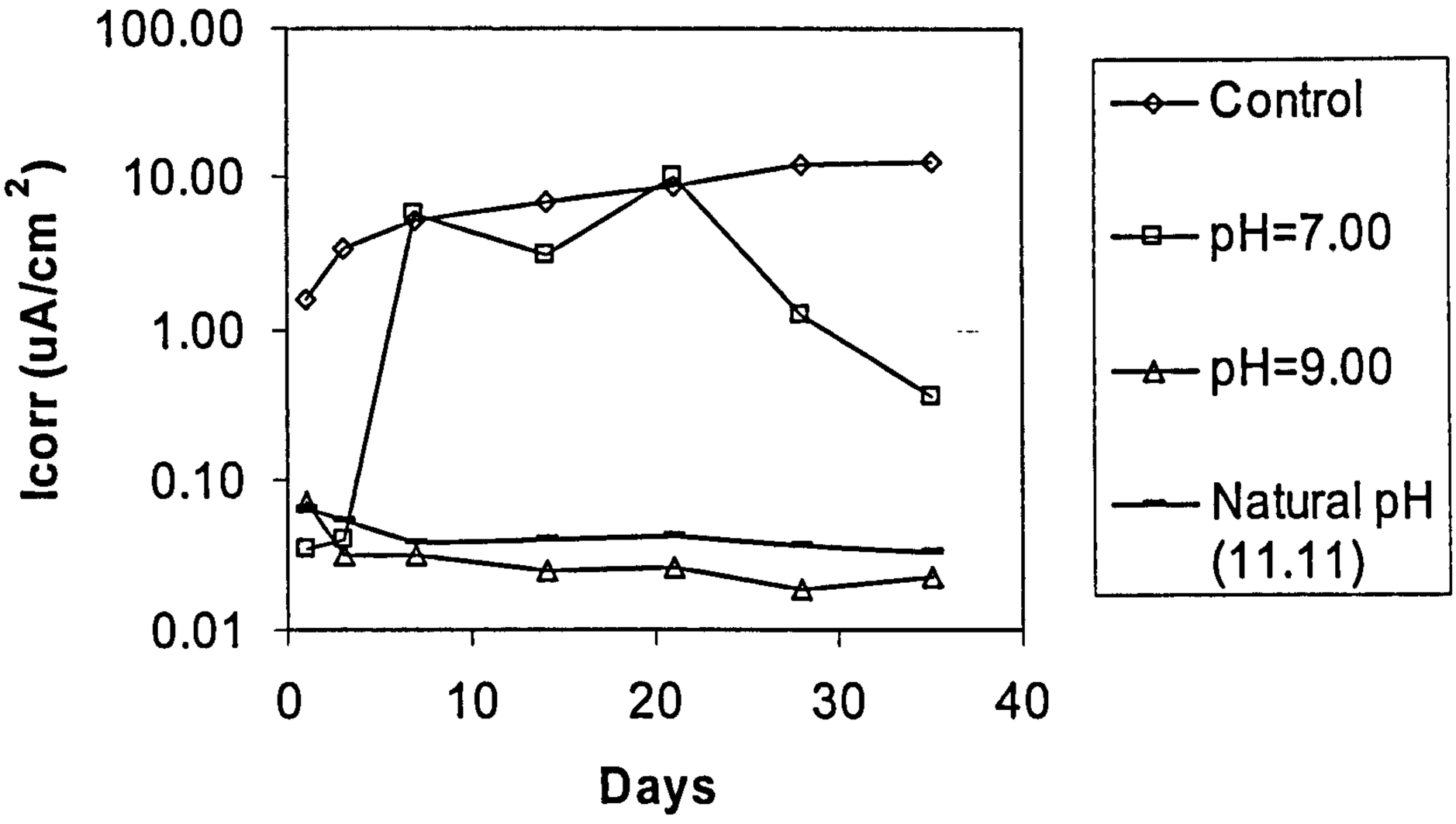

Figure 3.12 Icorr versus time of mild steel bars immersed in 0.01M guanidine solutions with various pH values for 35 days

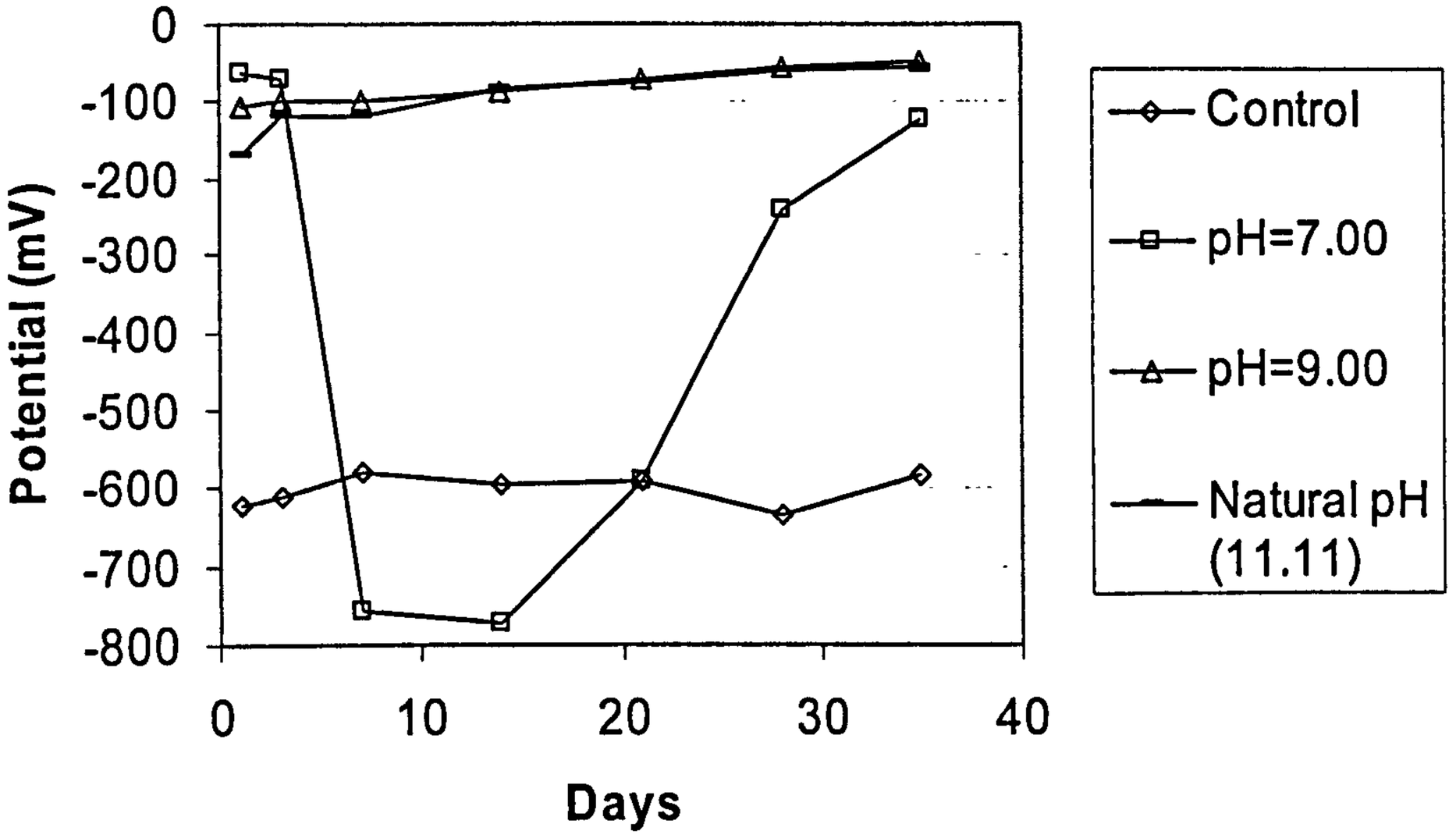

Figure 3.13 Ecorr versus time of mild steel bars immersed in 0.01M guanidine solutions with various pH values for 35 days

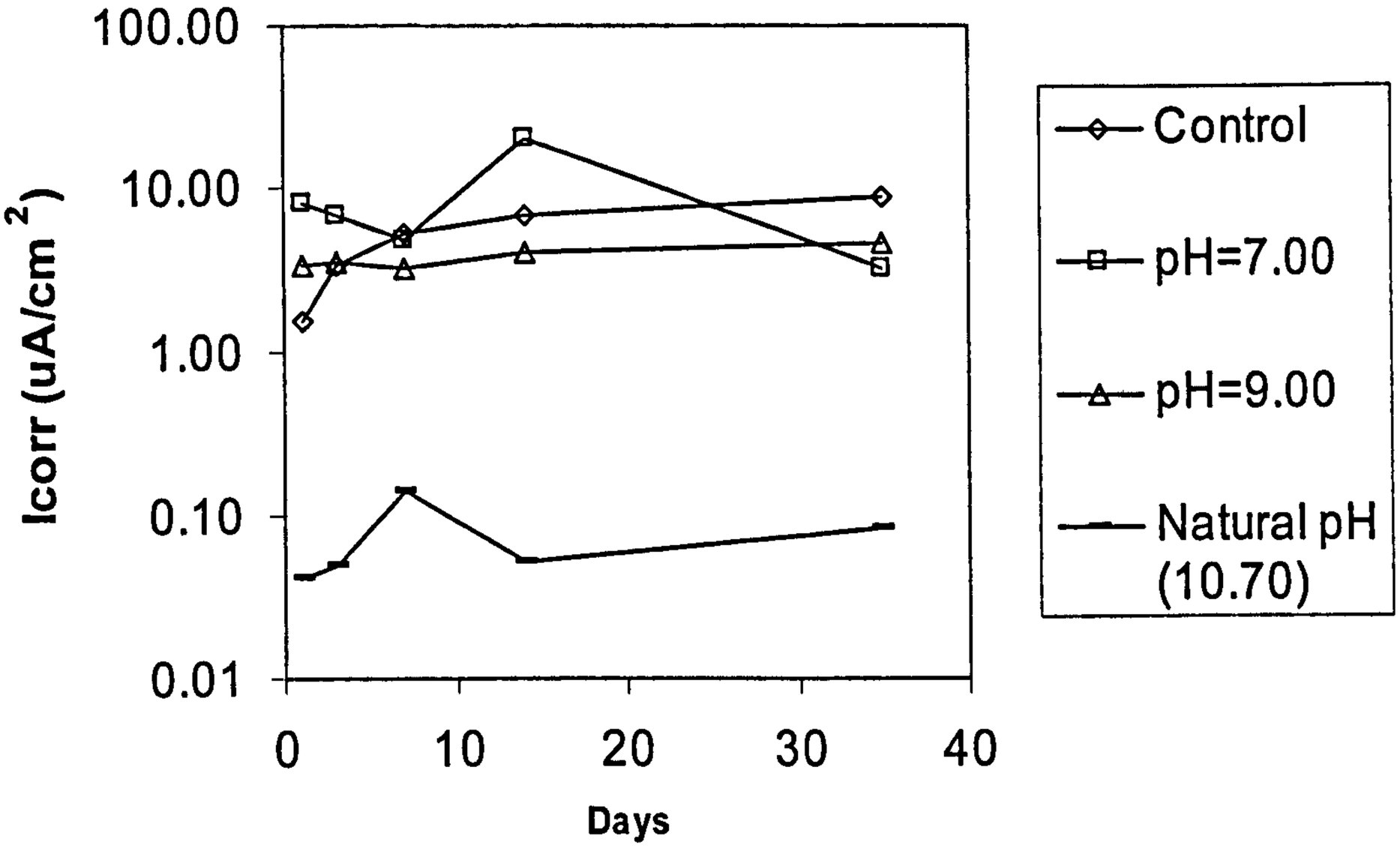

Figure 3.14 Icorr versus time of mild steel bars immersed in 0.01M arginine solutions with various pH values for 35 days

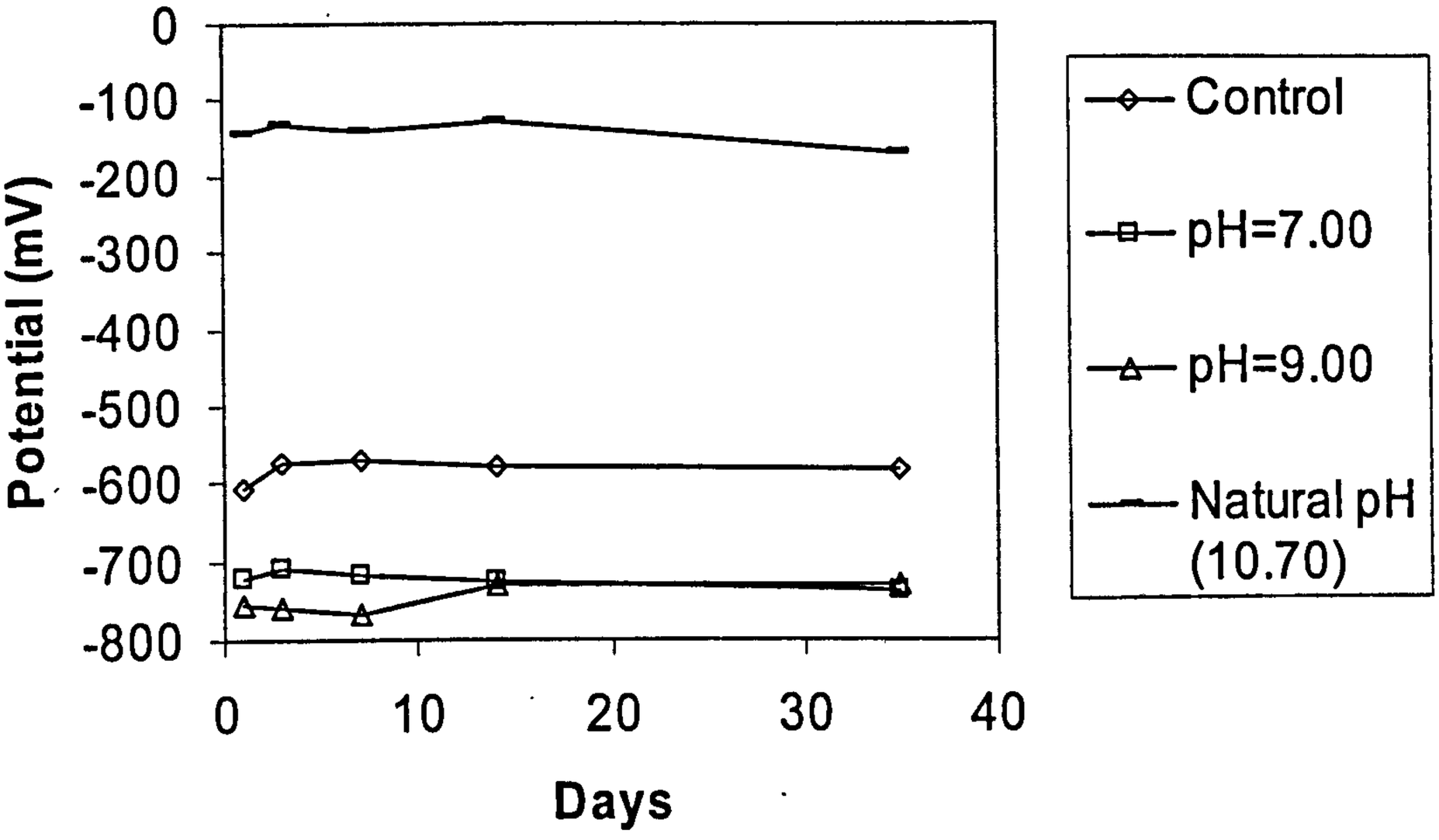

Figure 3.15 Ecorr versus time of mild steel bars immersed in 0.01M arginine solutions with various pH values for 35 days

CHAPTER 4

ELECTROCHEMICAL INJECTION OF ORGANIC CORROSION INHIBITORS INTO CARBONATED CEMENT PASTES

4.1 INTRODUCTION

4.1.1. Scope of this study

In the previous Chapter, it was found that, with a certain level of concentration, the neutralised solutions of inhibitors studied in this thesis, namely ethanolamine, guanidine, and arginine, could reduce corrosion rates of steel. In this Chapter a method which introduces the corrosion inhibitors at the concentrations required for passivation of steel in the vicinity of the reinforcing bars embedded in concrete is discussed.

Among the methods using corrosion inhibitors that are applied to existing concrete structures for restorative purposes, the simplest and the most economical would seem to be ponding the inhibitor solutions on to the concrete surface, expecting the required concentrations of the inhibitors to penetrate the material by diffusion and absorption. This surface application of inhibitors as a rehabilitation method requires the substantial transport of the substance to the reinforcing bar where it has to reach a sufficient concentration in order to protect the steel against corrosion or reduce the rate of the ongoing corrosion. Recently several researchers have investigated the effectiveness of surface-applied corrosion inhibitors for restorative applications, focusing on the ability of penetration or passivation for reinforcement (Bjegovic 1994, Alonso 1996, Phanasgaonkar et al. 1996 and 1997, Haynes et al. 1997, Elsener et al. 2000, Page et al. 2000, Elsener 2001, Tritthart 2003, Wombacher 2004, Ngala et al. 2004). However, the results have been inconsistent. One of the reasons for this is that, since cover depth and permeability of concrete vary, the maximum penetration depth of the inhibitor and the period required for it to reach the reinforcing bars may also vary greatly (Elsener 2001). For example, Alonso et al. (1996) suggested that monofluorophosphate (MFP) might be used as a corrosion inhibitor to reduce the corrosion rate of steel in carbonated concrete, whilst the period required for this penetration was unclear. However, Ngala et al. (2003) demonstrated that little penetration of MFP and no significant reduction in the corrosion rate of the embedded steel was observed in carbonated specimens. Ngala et

al. (2002) had shown that nitrite was effective as repair ponding material only in the case of non-carbonated concrete with relatively low level of chloride or carbonated concrete with very low chloride. The inhibitors based on amines and alkanolamines have relatively high vapour pressures and are claimed to be able to diffuse considerable distances through concrete pores (Maeder, 1994). However, Ngala et al. (2004) found that no inhibitory effect on the corrosion rate of the steel was observed in carbonated specimens mainly due to poor penetration of the substance. It can be concluded that corrosion inhibitors are not always capable of reliably restoring the passivasion of reinforcement bars in concrete by merely ponding them on the surface. In order to secure sufficient concentration of corrosion inhibitors on the reinforcing bars, their penetration in concrete may need to be induced by other mechanisms.

Most amine and alkanolamine-based corrosion inhibitors are dissolved in aqueous solutions, and are protonated according to their dissociation constants (K_a) and the solution pH. Cationic species in aqueous solution are driven to move toward the negative electrode under an electrical field, and hence the migration of cationic corrosion inhibitors may be accelerated when the inhibitor solutions are applied to a concrete surface, and currents are passed between anodes placed within the inhibitor solutions and reinforcing steel cathodes embedded within the concrete. In addition to the accumulation of the inhibitor in the vicinity of the steel bars, additional advantages are expected, namely the partial removal of chloride ions from concrete and the production of hydroxyl ions around the steel cathode, generated by cathodic reduction of water. For carbonated concrete, a sufficient concentration of inhibitor was observed to be attained around the steel bars in a shorter time than that achieved by conventional surface-applied treatments (Sawada et al. 2005). However, the transport mechanism of inhibitors has not yet been understood, since their penetration into the material is expected to be influenced by other constituents in the pore solutions, such as hydroxyl ions.

The aim of the present investigation was to provide a deeper understanding of the phenomena underlying the migration of corrosion inhibitors in cement-based materials. This chapter will explore the effects of electrochemical injection of three organic corrosion inhibitors studied in this thesis, namely ethanolamine, guanidine, and arginine, on the pore solution constituents of carbonated cement-based materials which have been experimentally examined. The pore solutions were squeezed from carbonated cement matrix which was subjected to the inhibitor injection treatment and analysed to determine the concentration

profiles of various ions. It was necessary to devise a means of performing detailed pore solution analyses of material sampled at closely spaced intervals along the migration path between the anode and cathode. The use of concrete specimens with coarse aggregates was considered unsuitable for this purpose because of the spatial resolution limitations imposed by the presence of the aggregates on sampling and analysis of the pore solution. It was therefore decided to undertake the experiments to be described in this Chapter with laminated specimens of cement pastes.

Part 1 of this Chapter describes the fundamental electrochemical injection approach for fully carbonated material in which the penetration of the inhibitor and the migration of ionic species can be considered to be one-dimensional phenomena. The target area is then developed to a two-dimensional field in Part 2 of this Chapter, where the proposed injection treatment is applied to partially carbonated material that simulates real concrete with a carbonation depth profile which is not uniform in usual cases. In Part 2, not only the penetration of inhibitors, but also the interaction of the chemical phase of the pore solutions in carbonated and non-carbonated sections of the cementitious material, are investigated.

The risk of the deleterious side effects that might arise by the application of electrochemical injection of corrosion inhibitors are also discussed in this Chapter.

The work presented in Part 1 of this Chapter that is concerned with the electrochemical injection of two (namely, ethanolamine and guanidine) of the three inhibitors studied in this thesis was conducted in collaboration with Dr S. Sawada, which is covered in Appendix G (Sawada et al. 2007).

4.1.2. Ionisation of inhibitors

In order for the electrochemical injection treatment proposed in the previous subsection to be efficient, it is desirable that significant proportion of the corrosion inhibitors should be electrically charged, thus the degree of ionisation of inhibitors in concrete pore solutions may be crucial. The extent of ionisation is governed by the dissociation constants (K_a) of the organic corrosion inhibitors and the pore solution pH values of the concrete. The equilibrium constant of a reversible dissociation is represented by the pK_a value, which is defined as the negative logarithm of the dissociation constant (K_a) as follows. In the case of organic bases, values are presented as pK_a values of their conjugate acids for the reaction:

$$RNH_3^+ \Leftrightarrow RNH_2 + H^+ \quad (4\text{-A})$$

$$K_a = [H^+][RNH_2] / [RNH_3^+] \quad (4\text{-}1)$$

$$pK_a = -\log K_a \quad (4\text{-}2)$$

where $[RNH_2]$, $[RNH_3^+]$, and $[H^+]$ denote the concentrations of the molecular organic bases, their conjugate acid and hydrogen ions (mole/l) respectively.

Aqueous solutions of three organic bases, ethanolamine ($HO\text{-}CH_2\text{-}CH_2\text{-}NH_2$), guanidine ($HN{=}C(NH_2)_2$) and arginine ($NH{=}C(NH_2)\text{-}NH\text{-}(CH_2)_3\text{-}CH(NH_2)\text{-}COOH$), studied in the previous Chapter, were used for the electrochemical treatment in order to examine the effect of the dissociation constants of organic corrosion inhibitors. The dissociation constants (expressed as pK_a values) of ethanolamine and guanidine are 9.5 and 13.6 respectively, their partially converted cationic conjugate acids being in the form of $HO\text{-}CH_2\text{-}CH_2\text{-}NH_3^+$, and $(NH_2)_3C^+$. On the other hand, arginine has three dissociation constants: pK_{a1} 1.82, pK_{a2} (defined as pK_a value of arginine in this thesis) 8.99, pK_{a3} 12.50 (Lide 2006), and the scheme of ionisation is shown in Figure 4.1. The equilibrium speciation in aqueous solutions of varied pH values is illustrated in Figure 4.2. In aqueous solutions of pH < their respective pK_a values, the predominant form of the inhibitor is cationic, whereas in solutions of pH > their pK_a values, the predominant form is molecular (note that in solutions of pH > pK_{a3} value, the predominant form is anionic for arginine).

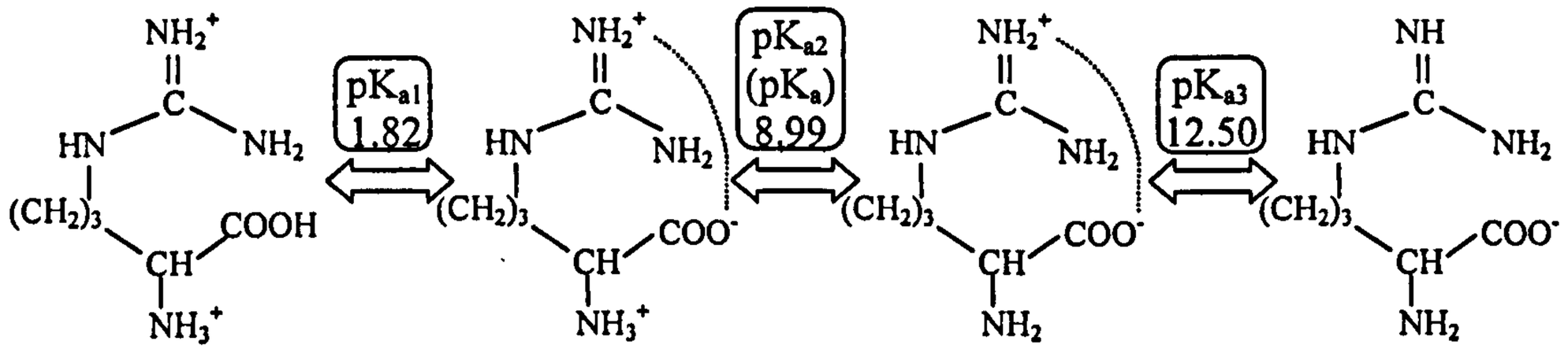

Figure 4.1 Scheme of ionisation of arginine

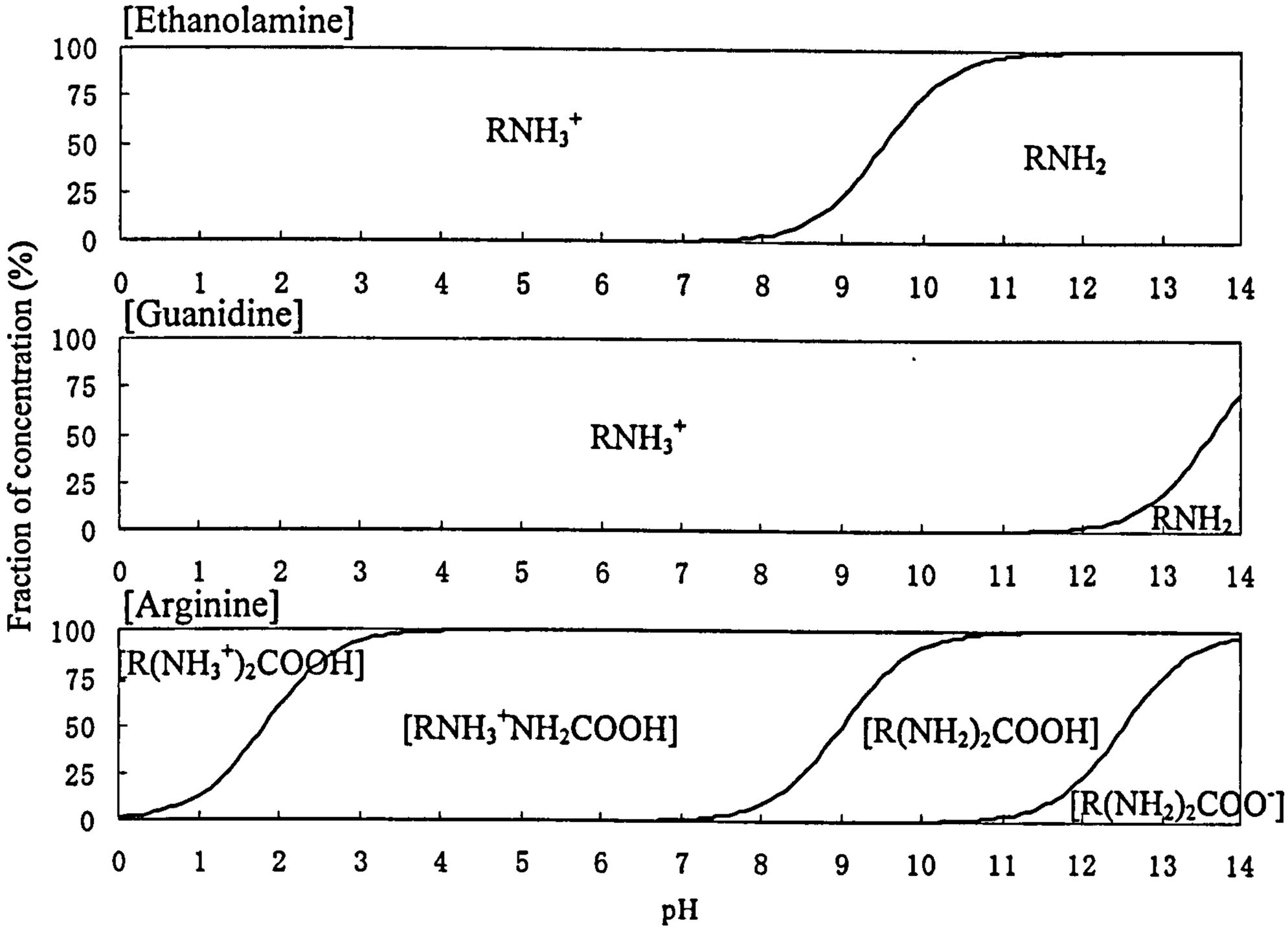

Figure 4.2 Speciation of the three inhibitors as a function of pH

The pore liquid in concrete produced from most common cements may be regarded as an alkaline solution and its pH values are normally in the range of 13-14 (Page and Vennesland 1983, Canham et al. 1987). Carbonation of concrete, however, reduces the pore solution pH from its initial high value to a near neutral value (around pH 9) (Anstice et al. 2005). As can be estimated from Figure 4.2, the predominant form of the three corrosion inhibitors in carbonated pore solutions is cationic, which is considered to be a beneficial factor in terms of injection efficiency in an electric field. On the contrary, as can be seen from Figure 4.2, the predominant form of the inhibitors in high pH solutions is different for the three species: molecular for ethanolamine, still cationic for guanidine, and anionic for arginine. Thus it is expected that, during the electrochemical treatment, since the pH in the material is raised by migration of hydroxyl ions that are cathodically generated by water electrolysis, the difference in the predominant form of the three inhibitors in such realkalised pore solutions might affect their penetration into the cement pastes.

4.2 LITERATURE REVIEW

The possibility of using electrochemical treatments of limited duration to promote the injection of certain types of corrosion inhibitor into reinforced concrete with the aim of controlling the corrosion rate of embedded steel reinforcement has been proposed by several researchers.

Asaro et al. (1990) were the first group to apply electric fields to cause migration of corrosion inhibitors, quaternary ammonium and quaternary phosphonium compounds, under the support of the Strategic Highway Research Program (SHRP) (Asaro et al. 1990, Hettiarachchi and Gaynor 1992). In their investigations, non-carbonated mortar or concrete columns (50.8mm in diameter and 203.2mm in height) with or without chlorides were subjected to electrolysis between an anode installed in a solution of saturated $Ca(OH)_2$ placed under the column and a cathode in saturated $Ca(OH)_2$ solution placed on the top of the column with or without tetra ethylphospohonium nitrite. The effectiveness of the electrochemically injected inhibitor in terms of corrosion prevention was investigated by monitoring the corrosion potential (E_{corr}) of the steel bars embedded in the columns that had been treated or not treated with inhibitors. In the case of mortar samples, the potential values of the steel embedded in the chloride-contaminated specimens treated with the inhibitor shifted to the positive direction and became equivalent to those obtained in the chloride-free specimens. In the case of concrete specimens; however, adequate potential enhancement was not observed within the experimental period. In this report, the concentration of inhibitors that accumulated in the vicinity of the steel by the help of the applied electric field was not presented, and is thus unknown. In addition, the current densities they recommended to achieve effective injection of inhibitor within a period of around 2 weeks were $10A/m^2$, which was believed to be higher than is normally applied for electrical treatment of concrete, as with electrochemical chloride extraction (Mietz 1998). According to Page et al. (2000), such high current density may lead to deleterious side effects such as ASR (alkali-silica reaction) or degradation of bond strength between the steel and concrete.

Phanasgaonkar et al. (2000) investigated inhibitor injection into chloride-contaminated non-carbonated concrete specimens under an electric field using dicyclohexylamine nitrite and a commercial migratory inhibitor. Currents were passed for two weeks between an anode placed in a piece of sponge soaked with saturated $Ca(OH)_2$ solution containing inhibitors and an embedded steel cathode. Linear polarisation resistance was measured for the assessment

of the inhibitive performance. In the case of the combined system of both applied electric field and inhibitors, a higher level of inhibition was observed than in the case of control specimens that were exposed to applied electric field only. The authors concluded that the electric field might enhance the transport of charged inhibitors, resulting in the higher inhibition of the embedded steel that had worked as cathode. However, the current density they applied was still high enough (7.73A/m^2) to cause possible side effects as mentioned in the previous case by Asaro et al. (1990). Furthermore, since the pK_a value of the inhibitor studied was 10.4, almost all of the inhibitor cations presumably converted to molecules in the pore solution whose pH value was enhanced by water electrolysis and hydroxyl migration. Thus it appears unlikely that the inhibitors were efficiently transferred by the migration under applied electrical field. The concentration of inhibitors that accumulated in the vicinity of the steel cathode was also unavailable in this report.

Holloway et al. (2004) carried out an electrochemical injection of MCI inhibitors (Migratory Corrosion Inhibitors) in a similar manner to Phanasgaonkar et al. (2000). After electrical treatment for 2 weeks, the concentration profiles of MCI were obtained from sectioned samples by means of an ammonium-sensing electrode which had been proven as an effective means for measuring amine concentration in $Ca(OH)_2$ solutions as part of diffusion cell experiments (Elsener et al. 2000). The results showed that when the electrochemically injected inhibitor concentrations were compared to those obtained in the case of surface application following the manufacturer's recommended dosage, the enhancement in inhibitor concentrations due to the electric field was indeed observed, but the degree was not significant throughout the sample. The reason for this could possible be that since the dissociation constants of the primary components of the MCI might not be high enough, the predominant form of the inhibitors was molecular with quite low mobility in the non-carbonated concrete specimens.

In their recent investigation, Sawada et al. (2005) conducted an electrochemical injection of organic base corrosion inhibitors with widely different pK_a values, namely ethanolamine (pK_a 9.5) and guanidine (pK_a 13.6), where constant current densities (in the range of 1-5 A/m^2) were applied to non-carbonated or carbonated concrete specimens between an embedded steel cathode and an external surface anode placed in an aqueous solution containing the relevant inhibitors for several days. The concentration profiles of electrochemically injected corrosion inhibitors within the concrete were analysed from sectioned samples by means of an ion chromatography technique as described in section 2.4,

which had been developed to evaluate features of the pore solution chemistry. It was shown that rates of injection into carbonated concrete of the organic base corrosion inhibitors, namely ethanolamine and guanidine, could be greatly enhanced. It was also shown that the migration of organic corrosion inhibitors into concrete was markedly affected by their acid dissociation constant (K_a) and the pore solution pH. The significant field-induced penetration of inhibitors into carbonated concrete was believed to be attributable to the near-neutral pH value of the carbonated pore solution. Although it was clear that the evolution of the pH profile within the pore solution and the magnitudes of the dissociation constants of the organic base inhibitors played a dominant role, several aspects of the inhibitor transport mechanism and its relationship to compositional features of the pore solution phase of the carbonated concrete remained unsolved. Since hydroxyl ions are generated by cathodic reduction of water and migrate from the cathode towards the anode through the pore solution phase in concrete, the carbonated pore solution would be re-alkalised during the electrochemical treatment. This pH rise would be expected to have some influence on the inward migration of corrosion inhibitors. The change of pH would also affect the solubility of substances containing calcium and magnesium ions in the pore solution. Furthermore, the application of electrochemical injection induces migration of other ionic species in the pore solution, such as sodium, potassium, chloride and sulphate ions. Ions cannot move independently in electrolytes since their transport is affected by other co-existing ions. It follows that the transport of inhibitors is influenced not only by hydroxyl ions but also by other major ions. It is thus important to characterise the distribution of the various ions in pore solution induced by the applied electrical fields.

No research or report has been found that deals with electrochemical injection of inhibitors applied to cementitious material specimens or real concrete in which the distribution of carbonation front is estimated to be non-uniform.

PART 1: MIRGARTION OF CORROSION INHIBITORS INJECTED INTO FULLY CARBONATED MEDIUM

4.3 INTRODUCTION

In Part 1 of this Chapter, the changes in the pore solution phase chemistry of carbonated hardened cement paste are experimentally studied, wherein aqueous solutions of three organic base corrosion inhibitors are applied to the surface of the material and constant current densities are passed between anodes placed within the inhibitor solutions and steel mesh cathodes embedded within the paste. The efficiency of injection of the inhibitors into fully carbonated hardened cementitious material at various current densities is investigated as a fundamental one-dimensional approach for elucidation of the phenomena underlying the transport of corrosion inhibitors. The concentrations of inhibitors that are attained in the vicinity of the steel cathode by means of this electrochemical method are examined in excess of the level, obtained in the previous Chapter, that is required for passivation of steel immersed in the equivalent solutions.

4.4 EXPERIMENTAL PROCEDURES

4.4.1. Specimen preparation

4.4.1.1 Carbonated cement paste

Ordinary Portland cement (OPC), whose chemical analysis is shown in Table 2.1, was used to produce cement paste specimens. After being sieved through a 150 μm mesh to remove coarse particles, the cement was then weighed and mixed with de-ionised water to produce paste of a water/cement ratio 0.6. The mixture was poured into cylindrical PVC containers with a diameter of 49mm and a height of 75mm after being thoroughly blended by hand for about 5 minutes. The containers were vibrated for approximately 2-4 minutes to get rid of any trapped air bubbles, and topped up with fresh paste. Cling film was placed on the surface of the paste before the containers were capped, and the cylinders were rotated at a speed of about 8 rpm for at least 24 hours in order to minimise segregation and bleeding. The specimens were then stored in a high humidity curing room at a temperature of 22±2°C. After 14 days the specimens were demoulded and immersed in a 35mM NaOH solution in order to minimise leaching of calcium hydroxide and any cement hydration products, and

then stored in another curing room at a temperature of 38±2°C for 8 weeks. When the cylindrical samples were fully cured, they were cut by means of a diamond saw lubricated with a small amount of distilled water into sliced discs with a thickness of approximately 5mm. The specimen surfaces were ground with grade 600 emery paper and rinsed with distilled water. The discs were carbonated in the manner described in subsection 2.2.1. Three months later, completion of carbonation was confirmed by spraying phenolphthalein on to the surfaces of broken specimens. Then the fully carbonated discs were kept at 75% RH in air over saturated NaCl solutions for a further period of 6-7 months until they were required for electrochemical treatment as described in subsection 4.4.3.

4.4.1.2 Super-critically carbonated cement paste

At the beginning stage of this project, the stainless steel mesh, serving as the cathode, was sandwiched between two sliced discs that had been made in the manner described above. However after the electrochemical injection treatment was finished and the cathode mesh was removed, it was quite difficult to measure the pH at the actual position of the cathode. In addition, it was also very hard to obtain the concentration of inhibitor at the cathode by analysing the fluid remaining on the steel mesh. It was then found to be desirable in the later stages of this project that the electrodes should be embedded in carbonated discs so that the pH and the inhibitor concentration at the cathode could be estimated by the analysis of the fluid after the pore expression of the discs. It was thus necessary to obtain such carbonated discs with embedded electrodes as soon as possible, which is why a rapid technique utilising super-critical carbon dioxide ($scCO_2$), detailed in subsection 2.2.2, was relied upon to produce carbonated cement paste discs.

Cement paste specimens with w/c of 0.6 were cast into specially prepared containers (49 mm in diameter and 8 mm in thickness) in which Type 316 stainless steel mesh was placed in the centre, as shown in Figure 4.3. The corners of the hexagonal shaped stainless steel mesh were buried in Plasticine so that electrical wire could be attached to the electrode after the disc was demoulded. The cement pastes were then vibrated for 1 minute to get rid of entrapped air bubbles. After the surface was flattened with a trowel, the discs were cured for one day in a sealed box in which the humidity was kept at about 100% RH. The discs were then demoulded and conditioned by placing them in an oven at 45°C until DOD (the degree of drying: defined by weight loss in an oven at 45°C divided by weight loss after 24 hours at 105°C) (Purnell et al. 2001) reached about 70%. The samples were exposed to water-

saturated scCO2 in a stainless steel pressure vessel for 12 hours at 71bar and 31°C, as shown in Figure 2.2. After removal from the vessel, the carbonation depths were measured by the phenolphthalein test and the fully carbonated discs were kept in air at 75% RH until they were required for the electrochemical treatment described in subsection 4.4.3.

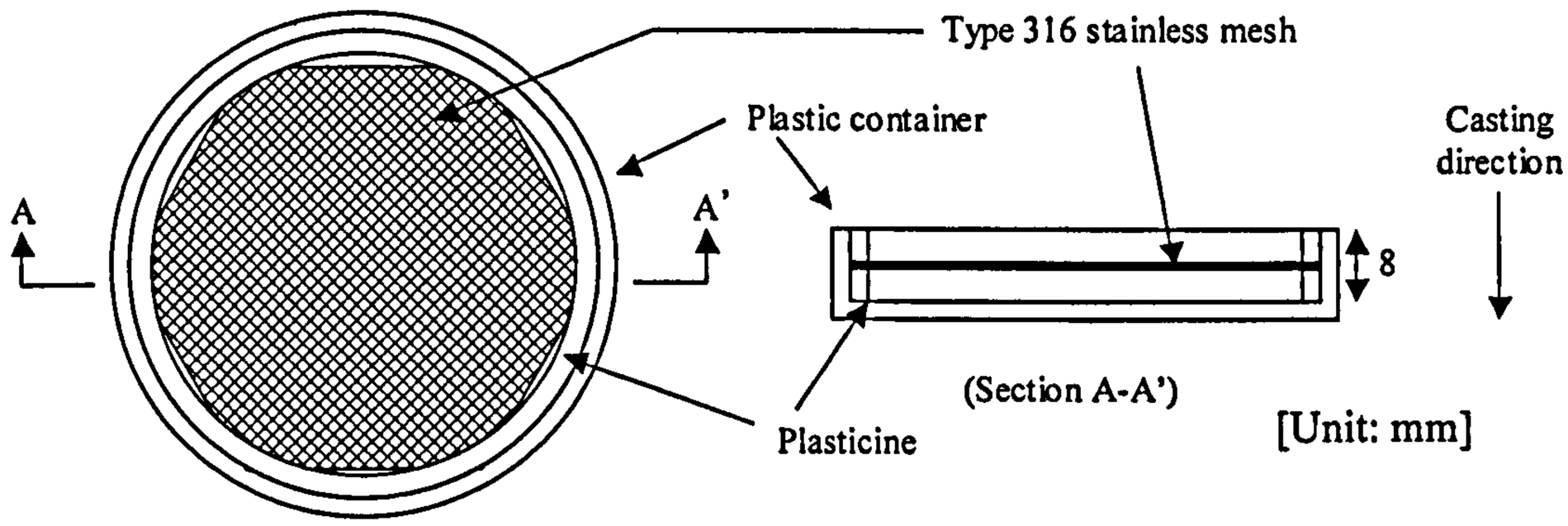

Figure 4.3 Container for producing carbonated cement paste discs with embedded stainless steel mesh

4.4.2. Organic corrosion inhibitors

The electrolyte solutions used for the electrochemical injection into the carbonated cement paste were 1M ethanolamine nitrate (mixture of 1M ethanolamine and 0.98M nitric acid: initial pH ~8.0), 0.5M guanidine carbonate (1M with respect to guanidine: initial pH ~11.9), and 0.5M arginine nitrate (mixture of 0.5M L-arginine and 0.48M nitric acid: initial pH ~8.0).

4.4.3. Treatment of specimens with corrosion inhibitors

For the electric current to be passed properly during the electrochemical treatment detailed later in this subsection, the carbonated cement paste discs needed to be fully saturated. Thus, the discs were converted to a saturated surface-dry condition according to the following procedures, by which the leaching of ions from the pore solutions was designed to be minimised. The discs were placed horizontally on glass plates, and distilled water was applied to each disc by means of soaked cotton wool until excess water was observed. The excess water was carefully removed by means of another piece of dry cotton wool, and the discs were placed in an upright position on platforms above distilled water in sealed tanks wherein humidity was kept at 100% RH. After being stored for 1 hour, the discs were removed from the tanks, and distilled water was added to the opposite side of each disc by

the same procedure. The discs were then put back into the tanks. After another hour, the weights of the discs were measured. These procedures were carried out once per day and were continued until the weights of the discs reached constant values and when a saturated-surface-dry condition was considered to be achieved. Some discs were then removed and used for measurement of bulk density and total porosity according to the procedure detailed in section 2.7. Other discs were stacked together with damp filter papers (Whatman No.145) placed between discs to ensure adequate contact, as is shown in Figure 4.4. Four specimens were set up for each test case and were subjected to electrolysis. Seven discs were stacked under the super-critically carbonated cement paste disc containing steel cathode mesh, the cover depth being assumed to be 34mm. For investigation of transport of species in the pore solutions behind the steel cathode, it was decided that three carbonated cement paste discs were to be placed on the cathode disc, referring to the results obtained by mathematical modelling described in the following Chapter, which demonstrates that the penetration of the inhibitors and the effect of water electrolysis taking place at the steel cathode were considered to be negligible approximately 20mm after the cathode (see Figure 5.5, 5.8, and 5.10 in Chapter 5).

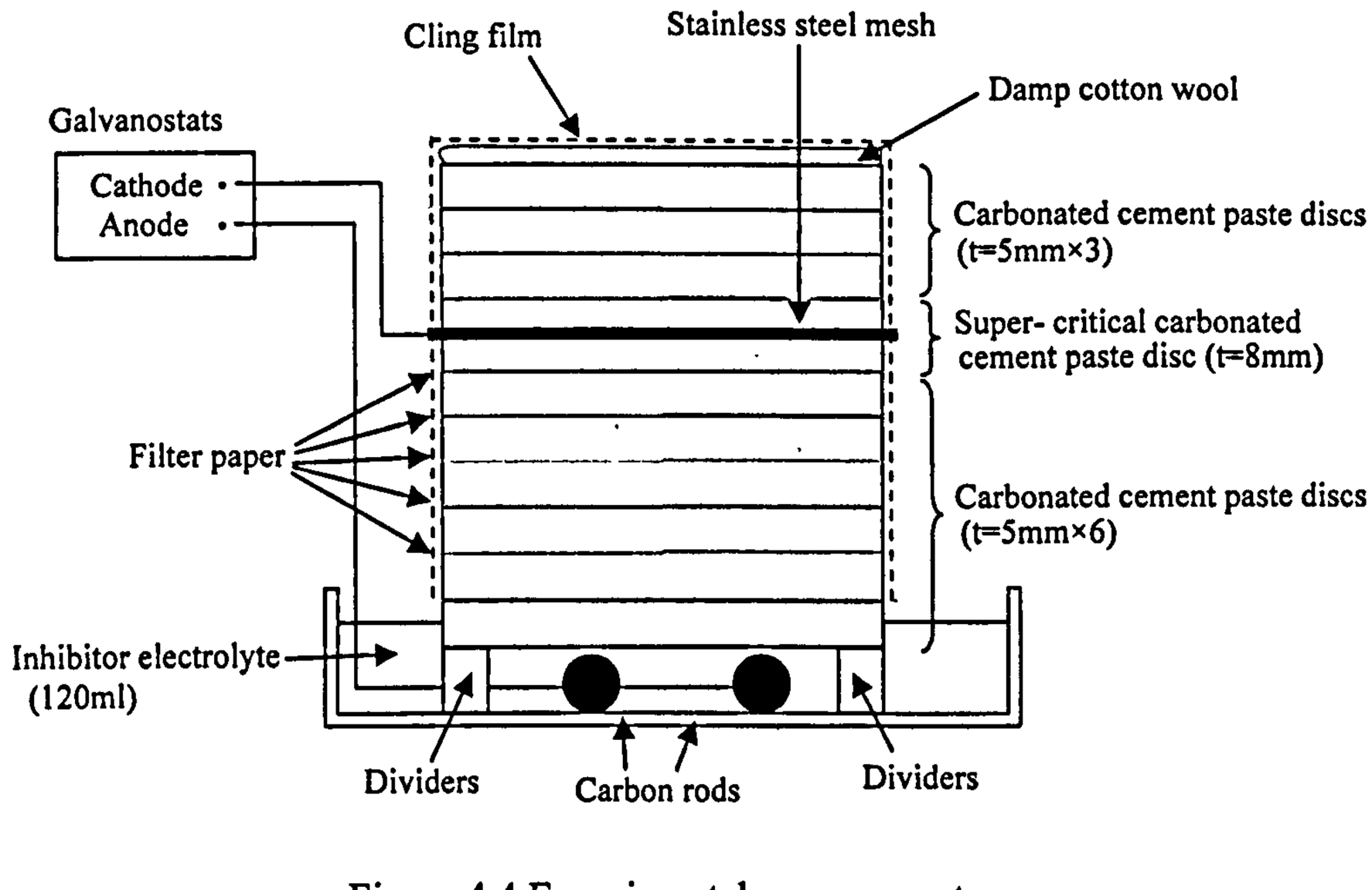

Figure 4.4 Experimental arrangement

Each treatment was performed in a container whose atmosphere was kept at about 100% RH. After each electrolyte solution of inhibitor described in subsection 4.4.2 was prepared, the concentration of inhibitors and associated anions, as well as the initial pH values, were measured. Two carbon rods serving as anodes were placed at the bottom of a shallow

container filled with 120 ml of one of the electrolytes. The stacked disc specimens were immersed in the electrolytes to a depth of 2 mm. The circuit was then completed and current densities were galvanostatically controlled at either 1 or 5 A/m^2 of the disc surface area for 7 days. Control specimens were also immersed for the same period to a depth of 2 mm in the above-mentioned three sorts of inhibitor electrolytes without application of a current. In this case, only one disc was placed on the cathode disc, since the diffusive penetration of the inhibitor towards the cathode was estimated to be slower than the migration in the electric field. The side surfaces of the piled discs were then wrapped with cling film, and damp cotton wool was placed on the top to restrict moisture loss caused by the temperature rise due to resistive heating during the electrochemical treatment.

4.4.4. Ionic distribution in pore solution

After the electrochemical treatment, four discs from the same layer were gathered and stored for one day in polythene bags inside a desiccator, at the bottom of which distilled water was placed. The four discs were used together as a specimen for pore solution expression, detailed as follows. For the determination of the ionic constituents of the pore solution in cement pastes, a method of extracting capillary pore solutions by pressure was employed, the procedure of which is detailed in section 2.3. In order to analyse initial pore solution constituents of the carbonated and the super-critically carbonated cement paste, the spare cement paste discs, which were not used for the electrochemical treatment, were also squeezed.

Within 30 minutes of collecting pore solutions, the pH was measured using a pH meter, as described in section 2.5, in order to determine the concentration of hydroxyl ions. After the measurement of pH values, titrations for carbonate and bicarbonate ions were conducted by means of the same electrode.

Concentrations of carbonate and bicarbonate ions were determined by monitoring pH during titration of a 1.0 ml sample of the pore solution against 10 mM nitric acid. For solutions containing ethanolamine or arginine, the titration of a pore solution with nitric acid was expected to result in three inflections, around pH 10.3, 9.5/9.0, and 6.4 respectively, each coinciding with the point of conversion of CO_3^{2-}/HCO_3^-, ethanolamine or arginine cation/molecule, and HCO_3^-/H_2CO_3 (Lide, 2006). For solutions containing guanidine, the titration was expected to result in only two inflections, around pH 10.3 and 6.4. In order to

estimate the concentration of the species converted in the inflections, the amounts of nitric acid required for reducing the pH down to pH 7.0 and 4.0 were recorded in the case of the solution containing ethanolamine or arginine, and pH 9.0 and 4.0 in the case of the solution containing guanidine. From the amounts of hydrogen ions consumed when the pH value was reduced from the former and the latter, and from published pK_a data for the system CO_3^{2-} /HCO_3^-/H_2CO_3 (Lide, 2006), the maximum amounts of carbonate and bicarbonate present in the pore solution were estimated. Detailed procedures of the calculation are shown in Appendix A.

Concentrations of corrosion inhibitors (ethanolamine, arginine, and guanidine), all other important cations (Na^+, K^+, Mg^{2+}, Ca^{2+}) and anions (Cl^-, SO_4^{2-}, NO_3^-) in the pore solution were determined by means of the ion chromatography system detailed in section 2.4.

The anolytes were collected immediately after the treatments were completed. The concentrations of major ions and pH values of the anolytes were also determined as above.

4.5 RESULTS

4.5.1 Initial pore solution constituents of carbonated cement paste

The ionic concentrations and pH values in the pore solution of cement paste after carbonation by two different procedures, namely accelerated carbonation and super-critical carbonation, are shown in Tables 4.1 and 4.2. The values of bulk density of the carbonated cement paste were 2.23 g/cm^3 for the accelerated procedure and 2.08 g/cm^3 for the super-critical procedure. Evaporable water contents, which were calculated from the loss of weight at 105 °C as described in section 2.7, were, respectively, 0.18 and 0.22 g/g dry weight of the samples from which the values of total porosity were determined to be 0.34 and 0.38. The pH values of hydrated cement pastes were effectively reduced by both carbonation procedures to around 9.0. The concentrations of other ions showed similar magnitudes to those reported by Anstice et al. (2005). As is the case with the data of super-critically carbonated cement pastes below, significant charge imbalances were found in some of the data of pore solution constituents presented in this thesis. This is mainly due to the analytical/experimental error generated during the titration of small amount of pore samples with nitric acid for the calculation of carbonate/bicarbonate ion concentrations (see subsection 4.4.4).

Table 4.1 Concentration of cations (mmol/l) in the pore solution of carbonated cement paste

Carbonation method	Na^+	K^+	Mg^{2+}	Ca^{2+}	Sum of charge
Accelerated	9.0	6.3	18.8	23.4	99.7
Super-critical	5.1	6.0	1.5	22.6	59.3

Table 4.2 Concentration of anions (mmol/l) in the pore solution of carbonated cement paste

Carbonation method	pH	OH^-	Cl^-	SO_4^{2-}	CO_3^{2-}	HCO_3^-	Sum of charge
Accelerated	9.0	1.07E-02	37.4	30.1	0.3	6.0	104.2
Super-critical	9.7	5.01E-02	33.1	17.4	1.0	4.4	74.5

4.5.2 Pore solution constituents after inhibitor injection treatment

Complete lists of data of pore solution constituents after inhibitor injection treatment are presented in Appendix B. The use of published thermodynamic data (pK_a values) and hydroxyl ion concentrations in pore solutions (without considering activity coefficients) for the calculations of the concentrations of inhibitors in cationic form led to apparent large charge imbalances, especially for some ethanolamine cases (Sawada et al. 2007). This may

be because the pK_a values of such species as organic corrosion inhibitors available in the literature were obtained in dilute solutions (Lide, 2006), and the values are no longer applicable to such concentrated electrolytes as pore solutions of the cement matrix after the electrochemical injection treatment. In order to take into account the interactions between inhibitor molecules and other species in the concentrated pore solutions, the apparent dissociation constant pK_a' values needed to be introduced (see subsection 5.4.4). For the calculation of ethanolamine and arginine cation concentrations, 9.75 and 9.30 were used as pK_a' values respectively, by which means most of the charge imbalances were minimised.

4.5.2.1 Organic corrosion inhibitors and associated anions

The concentration profiles of ethanolamine and nitrate ions in pore solutions are plotted in Figure 4.5. The penetration of ethanolamine into carbonated cement pastes was accelerated with increasing circulated charge passed during the electrochemical treatment. The concentrations of ethanolamine at the cathode were very small in the case of $0A/m^2$ for 7 days, however at the current density of $5A/m^2$ for the same period, significant amounts of ethanolamine (over 1.0mol/l) were observed to migrate and accumulate around the stainless steel cathode. As for nitrate ions, these penetrated into the medium faster than ethanolamine by the diffusion process only in the case of $0A/m^2$ and reached 40 mm from the treated surface. However, when the current densities were applied, the penetration of nitrate was restricted to within the first 20 mm because the ion is negatively charged.

The concentration profiles of guanidine and carbonate/bicarbonate ions in the pore solutions after the treatment with 0.5M guanidine carbonate are plotted in Figure 4.6. Guanidine progressively penetrated into the carbonated cement pastes with the increase in circulated charge. At the current density of $5A/m^2$ for 7 days, significant amounts of guanidine accumulated at the position of the stainless steel cathode, whereas no guanidine reached the cathode in the case of no applied current. The penetration depths of carbonate/bicarbonate ions were limited and smaller than that of guanidine except in the case of the applied current density of $5A/m^2$, at which a notable increase in concentration of carbonate ions at the cathode was clearly observed.

The concentration profiles of arginine and nitrate ions in pore solutions are plotted in Figure 4.7. Similar to the above two inhibitor cases, the penetration of arginine into carbonated cement pastes was enhanced with increasing circulated charge. The concentrations of

arginine at the cathode were very small in the case of $0A/m^2$ for 7 days. However, at the current density of $5A/m^2$, significant amounts of arginine (around 400mmol/l) were observed to accumulate near the stainless steel cathode. As for nitrate ions, these penetrated into the medium faster than arginine by diffusion in the case of $0A/m^2$ reaching 40mm from the treated surface. However, when the current densities were applied, as with the ethanolamine case, the penetration of nitrate was restricted to within the first 10 mm.

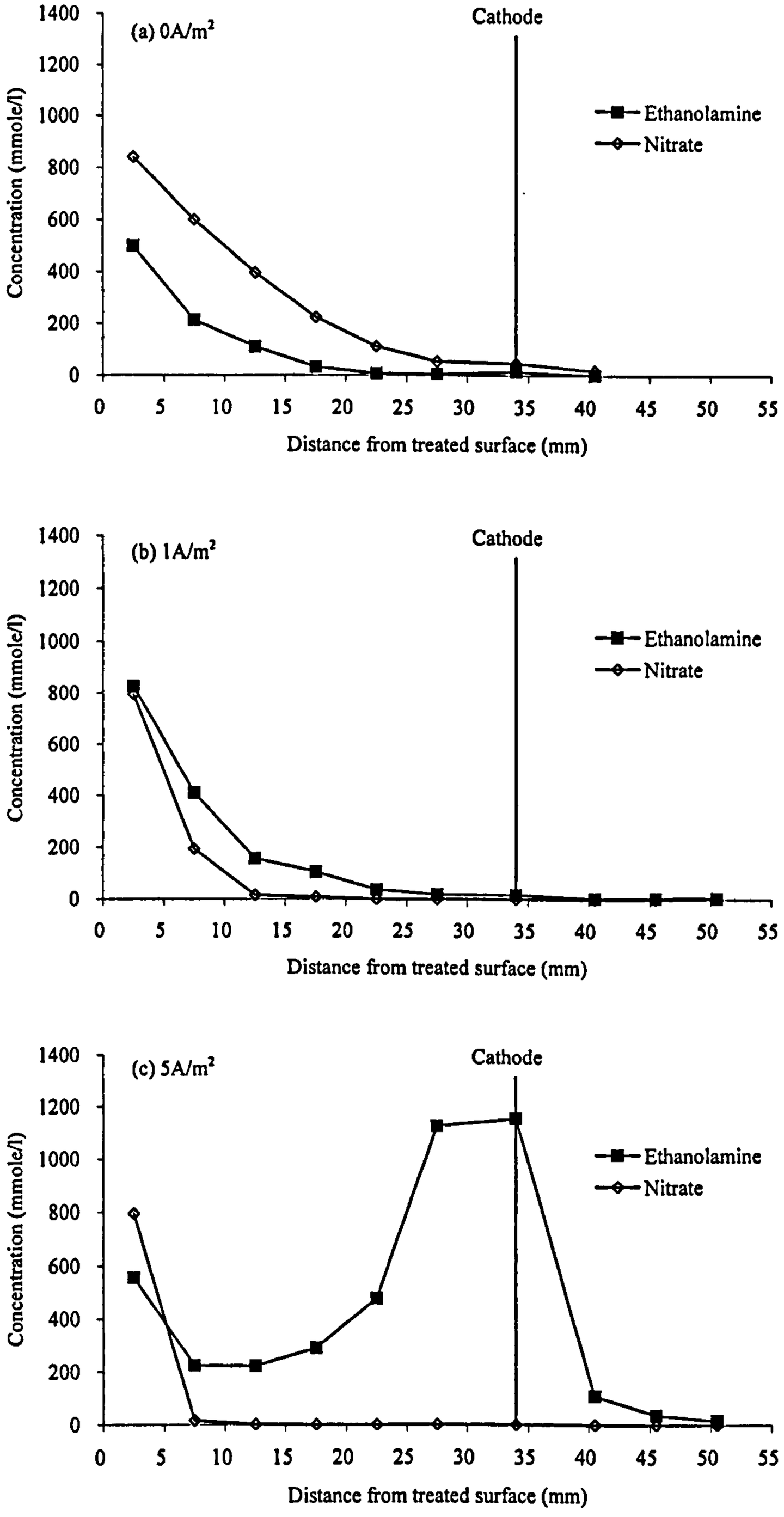

Figure 4.5 Concentration profiles of ethanolamine (applied as 1.0M ethanolamine nitrate) and nitrate ions in carbonated cement paste of w/c 0.6

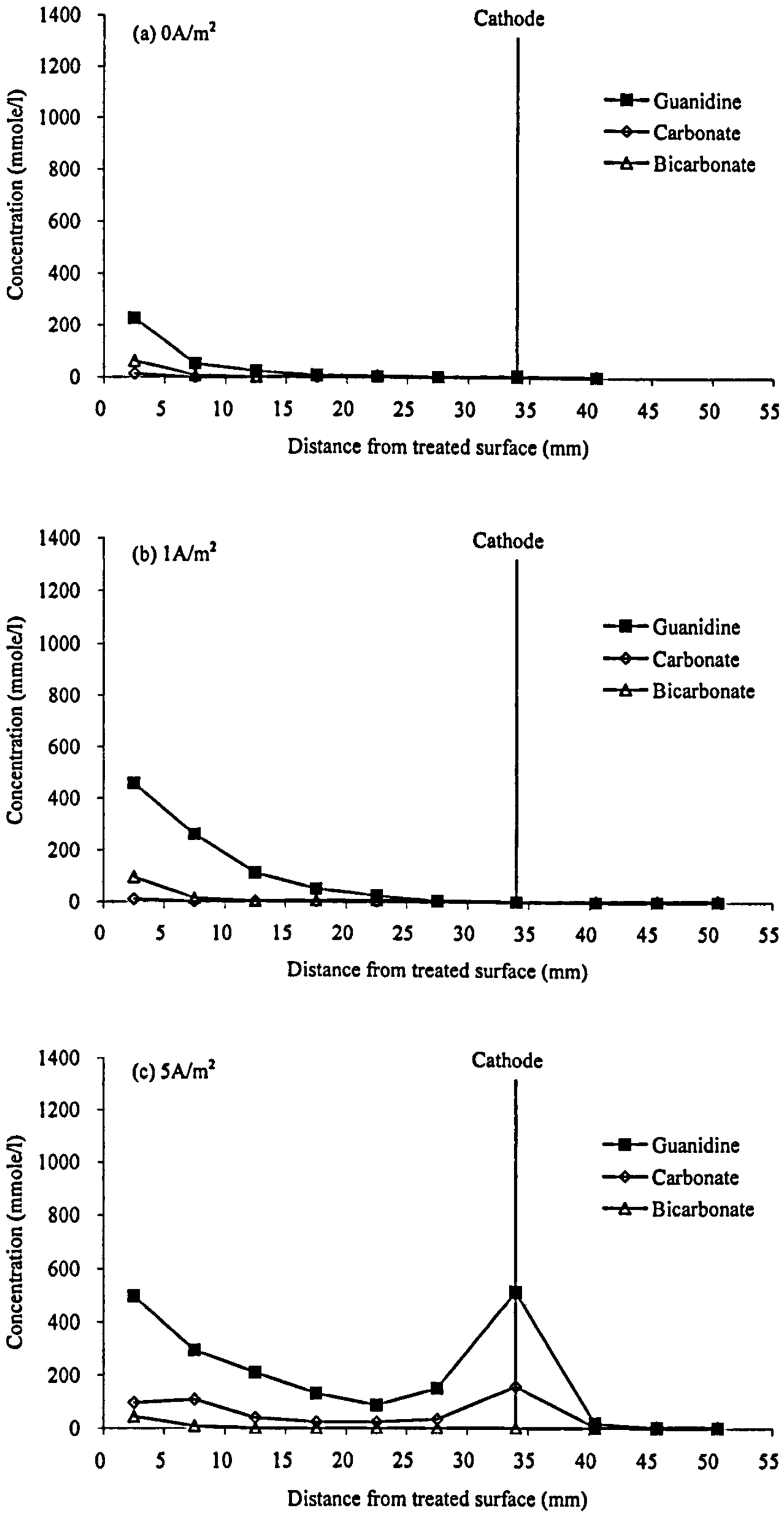

Figure 4.6 Concentration profiles of guanidine (applied as 0.5M guanidine carbonate) and carbonate/bicarbonate ions in carbonated cement paste of w/c 0.6

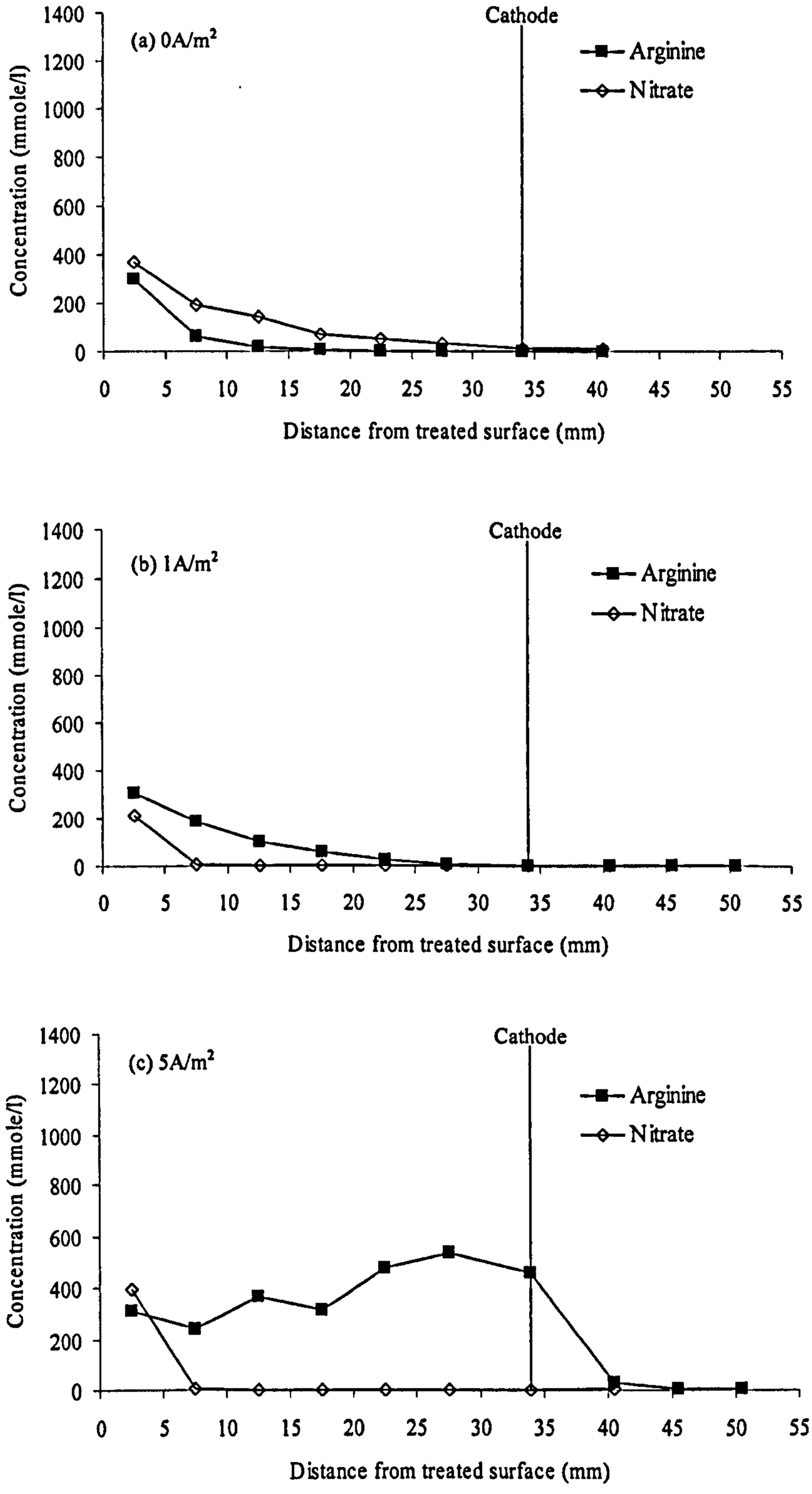

Figure 4.7 Concentration profiles of arginine (applied as 0.5M arginine nitrate) and nitrate ions in carbonated cement paste of w/c 0.6

4.5.2.2 Major cations

The concentration profiles of other major cations, Na^+, K^+, Mg^{2+} and Ca^{2+}, in the pore solutions after treatment with 1M ethanolamine nitrate and 0.5M arginine nitrate are plotted in Figure 4.8 and Figure 4.10. The variations of sodium and potassium concentrations with the applied current density were minor throughout the specimens. The concentrations of both positively charged alkali metal ions were found to slightly increase near the cathode when the current densities were applied. The concentrations of magnesium ions and calcium ions increased when ethanolamine nitrate was applied without current, but decreased with increase in the circulated charge, except for the calcium concentrations near the anode. The concentrations of calcium ions near the anode were found to have remained approximately the same as those for the diffusion case even after high current density was applied.

The concentration profiles of other major cations in the pore solutions, after treatment with 0.5M guanidine carbonate, are plotted in Figure 4.9. The concentrations of Na^+, K^+, Mg^{2+} and Ca^{2+} tended to decrease with increase in total charge passed through the specimens, but the variations were small. The sodium and potassium concentrations slightly increased near the cathode after treatment with $5A/m^2$ for 7 days, as can be seen in the ethanolamine and arginine cases.

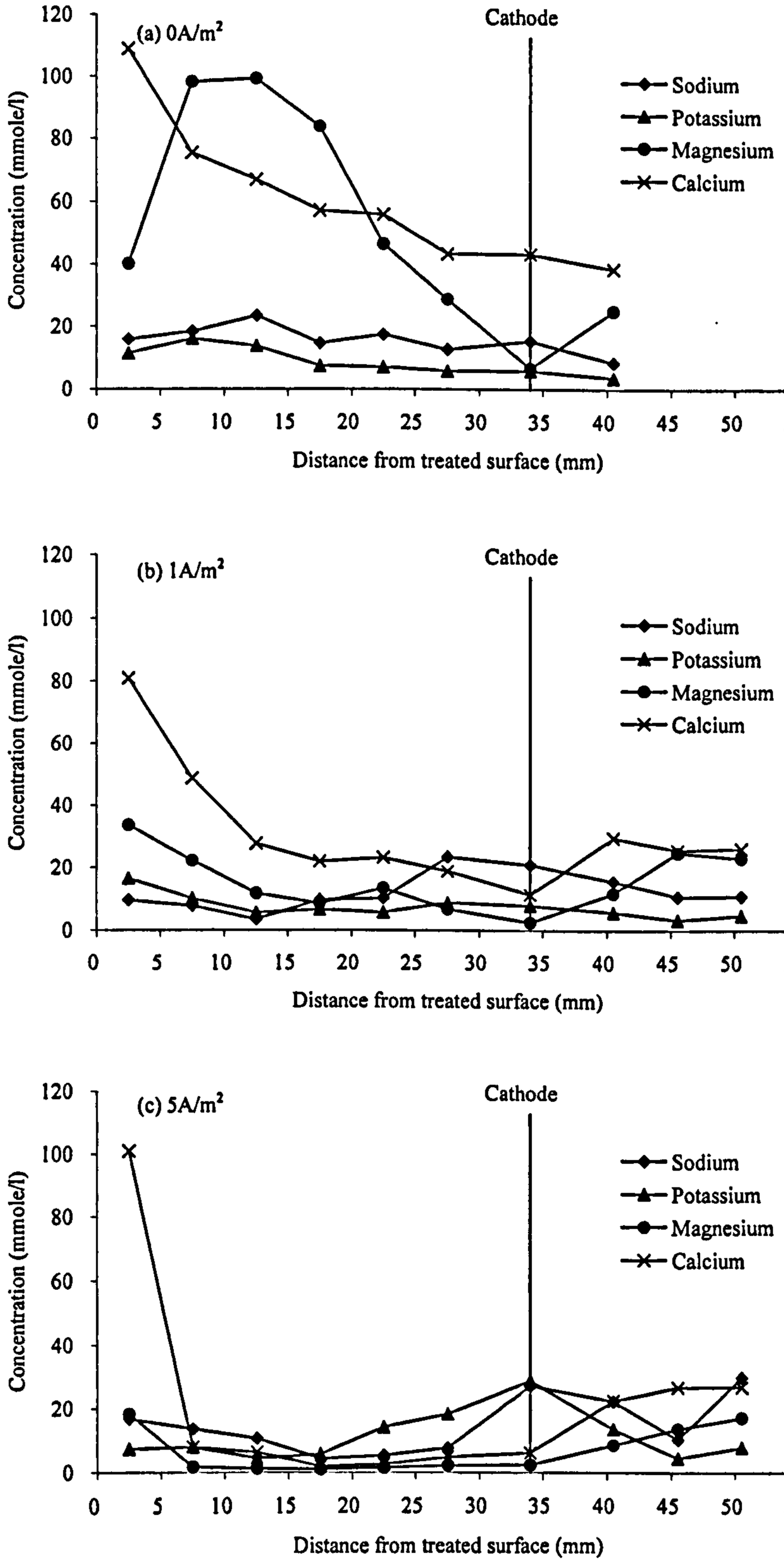

Figure 4.8 Concentration profiles of major cations (Na^+, K^+, Mg^{2+} and Ca^{2+}) in carbonated cement paste of w/c 0.6 treated with 1.0M ethanolamine nitrate

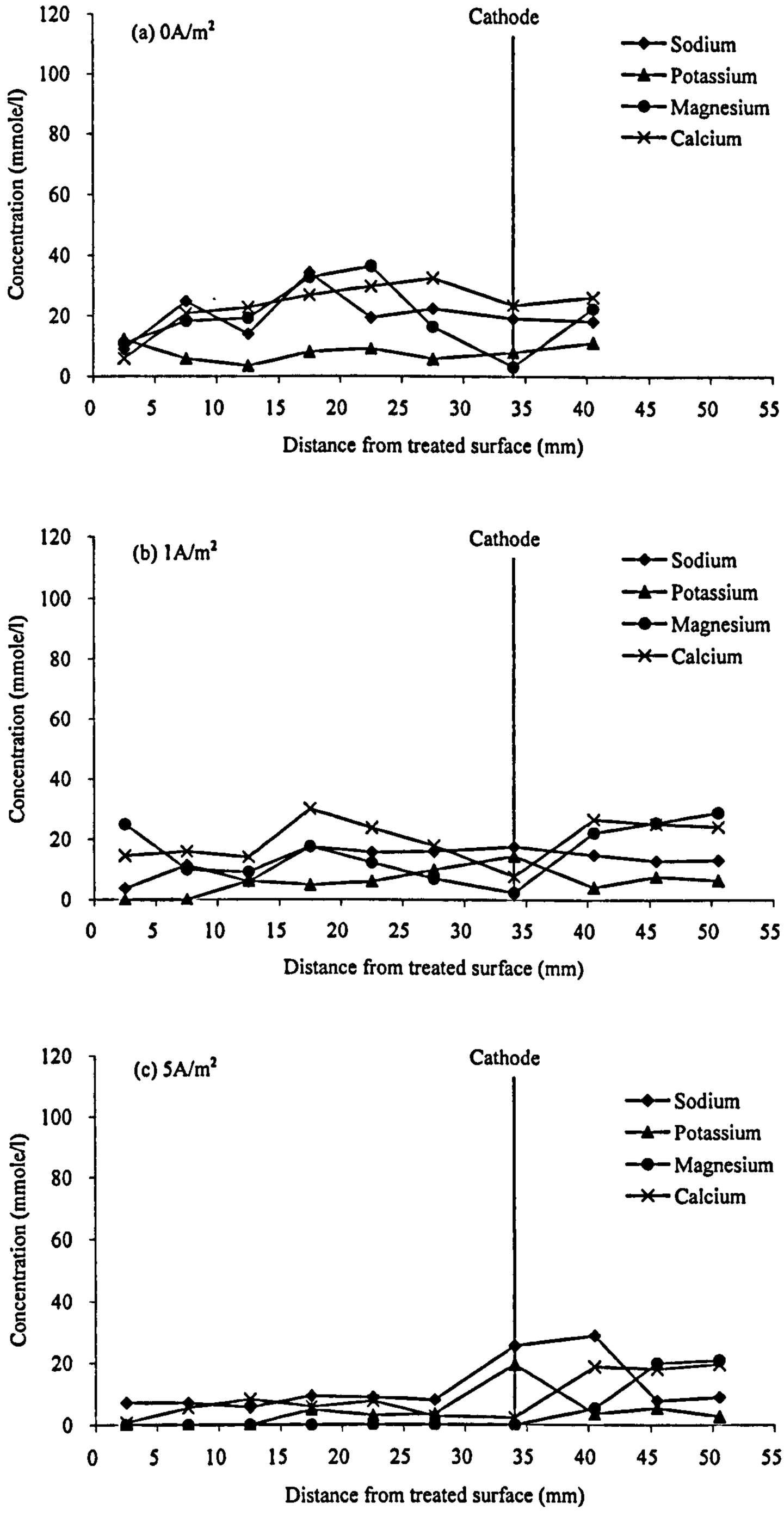

Figure 4.9 Concentration profiles of major cations (Na^+, K^+, Mg^{2+} and Ca^{2+}) in carbonated cement paste of w/c 0.6 treated with 0.5M guanidine carbonate

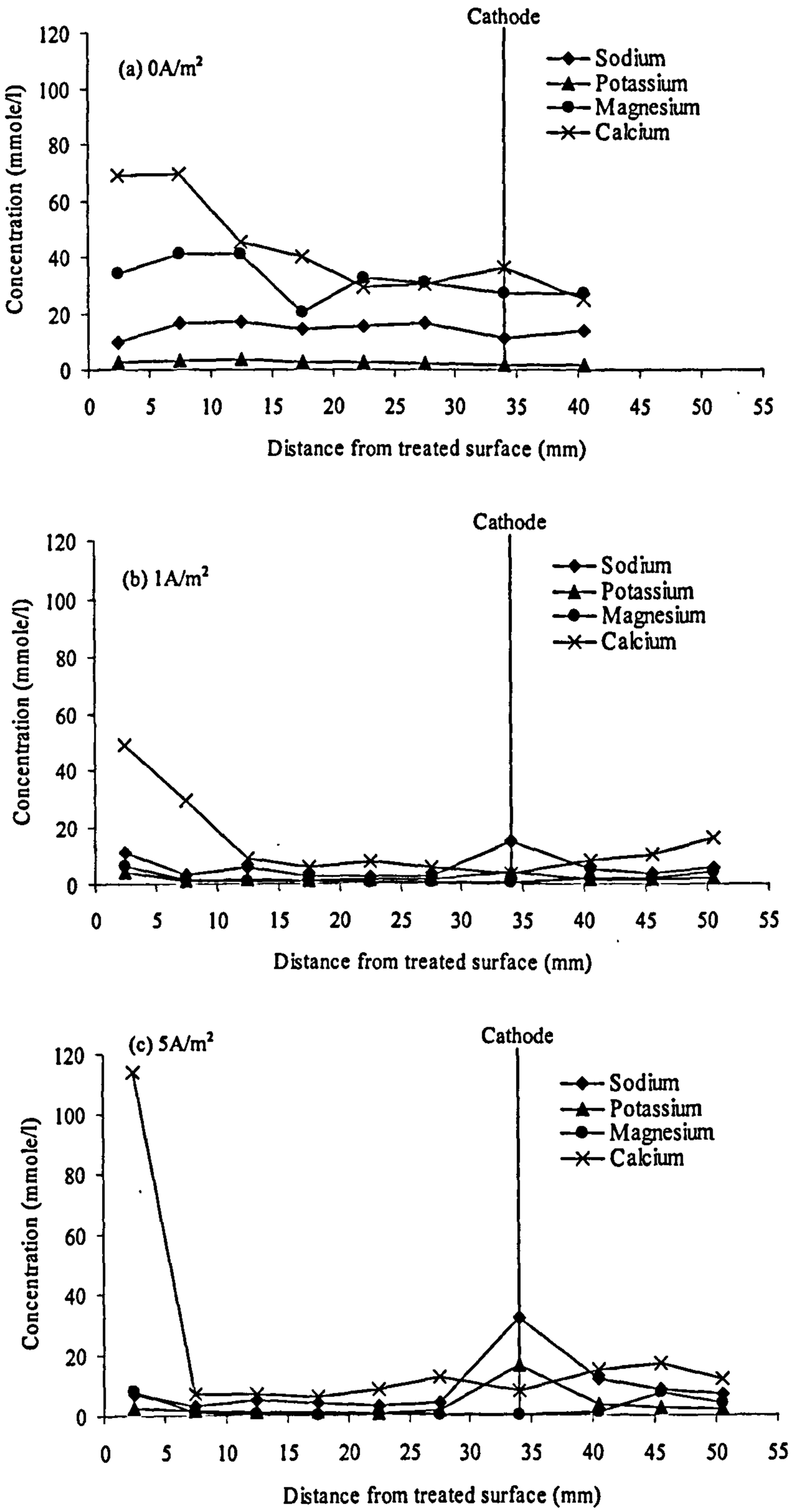

Figure 4.10 Concentration profiles of major cations (Na^+, K^+, Mg^{2+} and Ca^{2+}) in carbonated cement paste of w/c 0.6 treated with 0.5M arginine nitrate

4.5.2.3 Major anions

The concentration profiles of major anions, OH^-, Cl^-, SO_4^{2-}, CO_3^{2-} and HCO_3^-, in the pore solutions after treatment with 1M ethanolamine nitrate are plotted in Figure 4.11. The concentration of each anion showed little variation throughout the specimens in the case without current. At the current density of $1A/m^2$, the concentrations of all ions except sulfate ions decreased near the cathode. However, the concentrations of sulfate ions generally increased, especially near the anode. In the case of $5A/m^2$, the concentrations of most of the ions were reduced throughout the specimens compared with the case of $1A/m^2$, although a significant increase of carbonate ions was observed near the cathode. The concentrations of hydroxyl ions were negligible when compared to other anions even though a high current density was applied, upon which the pH observed at the cathode was 11.62 (4.2mmol/l).
In the case of the treatment with 0.5M arginine nitrate at each current density applied, a similar trend was observed in the profiles of the major anion concentrations, except for sulphate, which was found at high concentrations near the cathode at the current density of $1A/m^2$ and $5A/m^2$ as shown in Figure 4.13.

The concentration profiles of major anions in the pore solutions after treatment with 0.5M guanidine carbonate are plotted in Figure 4.12. In the case of no current density, chloride ions showed a similar profile to that found in the case of ethanolamine nitrate and arginine nitrate, though some increase was observed for sulfate ions. At the current density of $1A/m^2$, a significant increase in sulfate ion concentration was observed, especially near the anode, and the concentrations of chloride ions decreased progressively throughout the specimens. Polarization at the highest current density of $5A/m^2$ caused a significant increase in hydroxyl ion concentration at the position of the cathode, though contrastingly, the concentrations of sulfate ions were reduced.

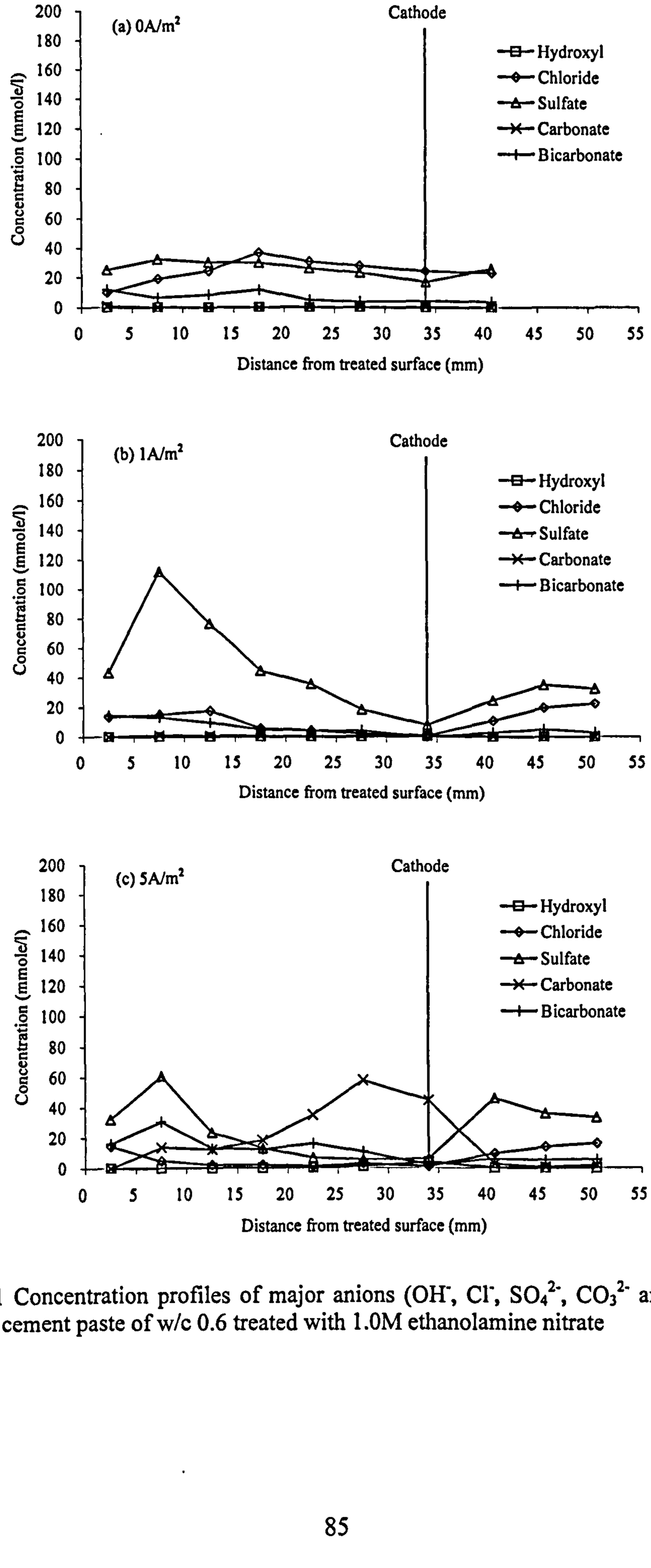

Figure 4.11 Concentration profiles of major anions (OH^-, Cl^-, SO_4^{2-}, CO_3^{2-} and HCO_3^-) in carbonated cement paste of w/c 0.6 treated with 1.0M ethanolamine nitrate

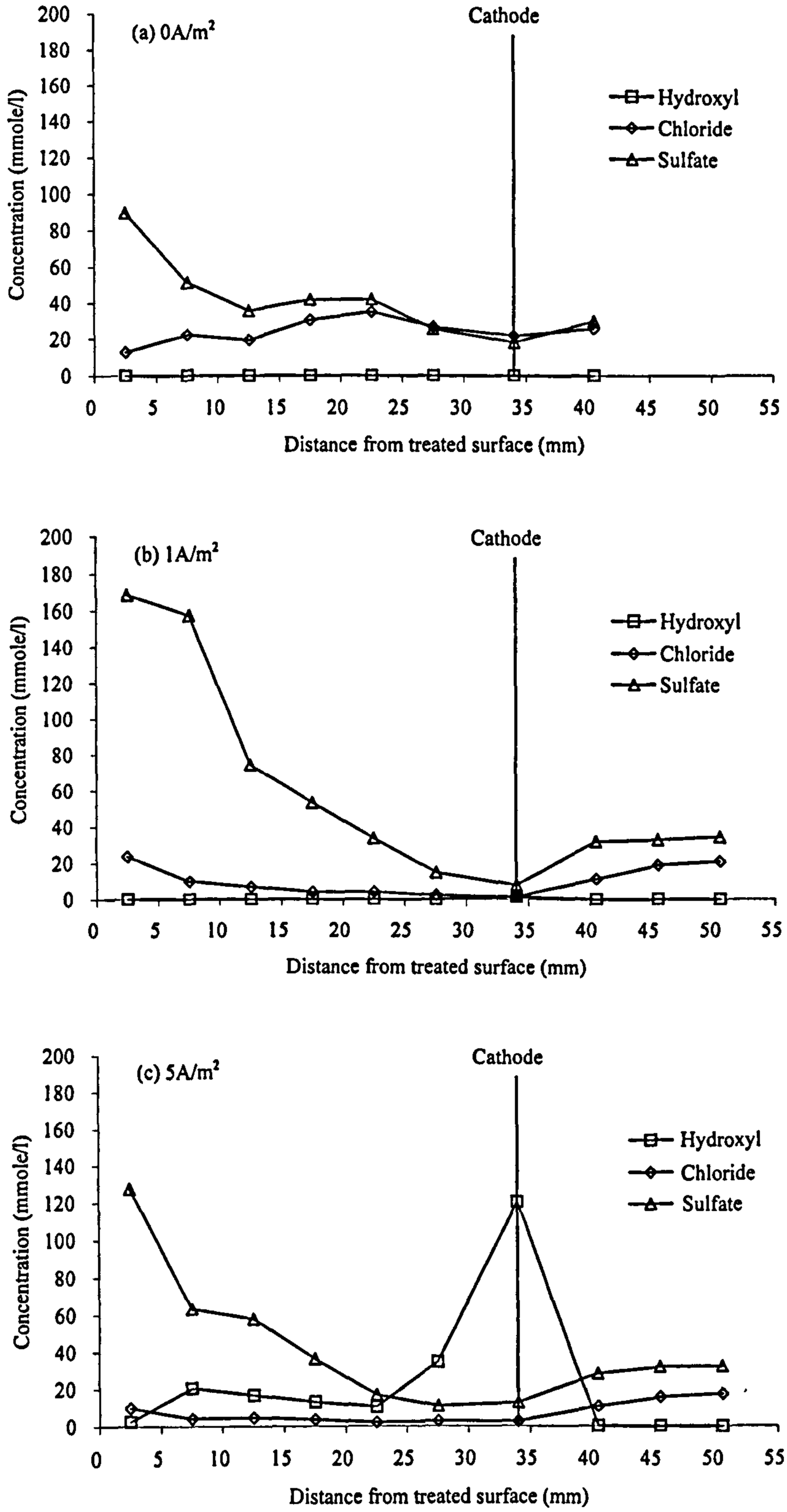

Figure 4.12 Concentration profiles of major anions (OH^-, Cl^-, SO_4^{2-}, CO_3^{2-} and HCO_3^-) in carbonated cement paste of w/c 0.6 treated with 0.5M guanidine carbonate

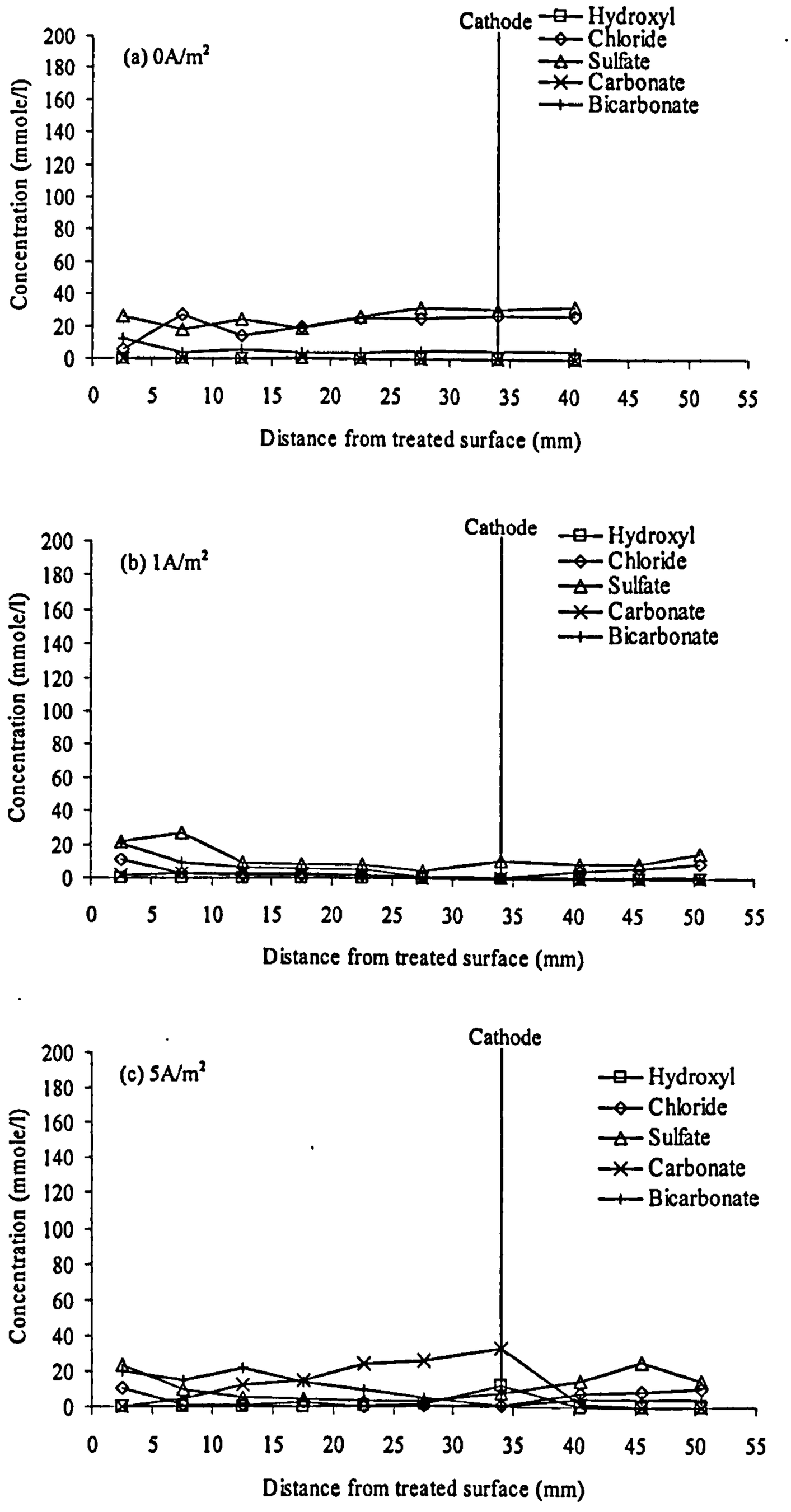

Figure 4.13 Concentration profiles of major anions (OH^-, Cl^-, SO_4^{2-}, CO_3^{2-} and HCO_3^-) in carbonated cement paste of w/c 0.6 treated with 0.5M arginine nitrate

4.5.3 Chemical compositions of the anolyte after inhibitor injection treatment

The pH values and chemical compositions of the anolyte after treatment are presented in Tables 4.3 and 4.4, together with initial values. The total charges for cations and anions detected in the anolyte showed reasonably similar values. The pH of ethanolamine nitrate and arginine nitrate solutions was found to have significantly decreased at the current density of $1A/m^2$ and $5A/m^2$, and the surface of the cement paste specimens immersed in these solutions was visibly deteriorated. The guanidine carbonate solution remained slightly alkaline (pH = about 9), even after the passage of $5A/m^2$ for 7 days.

Table 4.3 Concentrations of organic inhibitors and cations in the anolyte after treatment

Anolyte	Current Density (A/m^2)	Concentrations (mmol/l)							
		Organic inhibitors		Na^+	K^+	Mg^{2+}	Ca^{2+}	H^+	Sum of charge
		Total	Cationic						
1M ethanolamine nitrate	0	979.2	965.6	9.5	17.7	5.2	12.1	1.3E-05	1027.4
	1	970.8	970.8	2.1	N/D	5.7	38.5	9.5E+00	1071.0
	5	856.2	856.2	10.5	12.4	16.6	168.4	61.7	1310.7
	Initial	1090.1	1060.0	-	-	-	-	1.1E-05	1060.0
0.5M guanidine carbonate	0	954.9	954.6	8.9	N/D	2.7	2.8	1.1E-07	974.7
	1	912.1	912.0	3.8	N/D	3.0	2.5	2.0E-07	926.8
	5	651.1	651.1	5.0	N/D	0.0	1.5	1.6E-06	659.0
	Initial	985.3	968.7	-	-	-	-	1.6E-09	968.7
0.5M arginine nitrate	0	432.2	420.6	9.0	2.4	3.6	16.8	1.8E-05	472.9
	1	405.0	405.0*)	4.8	2.4	3.1	33.5	2.9E-01	493.2
	5	388.7	388.7**)	13.8	1.0	10.0	165.6	2.9E+00	819.8
	Initial	500.7	476.8	-	-	-	-	1.0E-05	476.8

N/D: Not detectable

*) includes $R(NH_3^+)_2$ type cations at 7.6mmol/l

**) includes $R(NH_3^+)_2$ type cations at 62.2mmol/l

Table 4.4 Concentrations of anions in the anolyte after treatment

Anolyte	Current Density (A/m^2)	pH	Concentrations (mmol/l)						
			OH^-	Cl^-	SO_4^{2-}	NO_3^-	CO_3^{2-}	HCO_3^-	Sum of charge
1M ethanolamine nitrate	0	7.9	7.9E-04	2.4	1.9	961.5	0.0	13.5	981.1
	1	2.0	1.0E-09	6.5	6.9	971.9	0.0	0.0	992.3
	5	1.2	1.6E-10	9.8	26.8	1092.7	0.0	0.0	1156.1
	Initial	8.0	8.9E-04	-	-	974.9	-	-	974.9
0.5M guanidine carbonate	0	9.9	8.7E-02	1.6	0.8	-	364.3	220.1	952.0
	1	9.7	5.0E-02	5.6	11.1	-	284.9	299.6	897.3
	5	8.8	6.3E-03	6.6	57.0	-	23.6	516.8	684.5
	Initial	11.8	6.3E+00	-	-	-	483.2	16.8	989.6
0.5M arginine nitrate	0	7.7	5.5E-04	3.0	0.6	452.0	0.0	16.5	472.7
	1	3.5	3.5E-08	4.5	5.8	453.7	0.0	0.0	469.7
	5	2.5	3.5E-09	26.5	27.6	598.6	0.0	0.0	680.3
	Initial	8.0	1.0E-3	-	-	491.8	-	-	491.8

N/D: Not detectable

4.6 DISCUSSION

The phenomena discussed here result from dynamic processes involving ions in the pore solution, which is a multi-component electrolyte, under the influence of an electrical field, wherein it is expected that concentrations of a combination of different ions/species may be governed by dissociation and/or solubility equilibria. The behaviour of the major species (organic corrosion inhibitors, hydroxyl ions, sulfate ions and carbonate/bicarbonate ions), which might be considered to have important roles by affecting other ions/species in the electrochemical injection approach for fully carbonated cement paste, is discussed in this section.

4.6.1 Organic corrosion inhibitors

Figures 4.5, 4.6, and 4,7 show the overall penetration profiles of ethanolamine, guanidine, and arginine, respectively, demonstrating that the injection of the inhibitors within the pore solution phase of the carbonated cement paste has been accelerated by the electrochemical treatment. At the current density of $5A/m^2$, the highest concentration of guanidine was observed at the position of the cathode, whereas the profiles for ethanolamine and arginine had plateaux of high concentrations in the region a few millimetres from the cathode. These differences may be explicable in terms of the different dissociation constants of ethanolamine (pK_a 9.5, pK_a' 9.75), guanidine (pK_a 13.6), and arginine (pK_{a2} 8.99, pK_{a2}' 9.30), resulting in different degrees of ionisation of the inhibitors in carbonated cement pastes. During electrochemical treatment, hydroxyl ions are generated around the steel cathode by electrolysis of water, and the cathodic region becomes highly alkaline. This re-alkalised region gradually moves towards the anode, driven by the migration of hydroxyl ions. When ethanolamine or arginine cations meet this highly alkaline environment, a significant proportion is deprotonated, and the further migration of the cations is prevented. It can be said that this is how ethanolamine or arginine accumulates in molecular form before reaching the cathode. This phenomenon may also explain why ethanolamine, which has a higher pK_a value than that of arginine, has a concentration peak that is closer (a few millimetres) to the cathode than arginine (around 5 millimetres). This elucidation can be justified clearly in Figures 4.14, 4,15 and 4.16, showing the concentration profiles of the ionic species of the inhibitors, which were obtained using their pK_a' values (pK_a for guanidine) and hydroxyl ion concentrations in pore solution. At the highest current density, $5A/m^2$, the predominant form of ethanolamine penetrating the specimens was molecular, except near the anode. Once

ethanolamine cations are converted into the molecules, they are no longer accelerated by the electrical field and their migration towards the cathode is not promoted. The results obtained after the passage of $5A/m^2$ for 7 days, therefore, indicate that further electrochemical treatment may not be effective for field-induced injection of ethanolamine for the specimens employed in this investigation. The main transport mode of ethanolamine near the cathode would be the diffusion of molecules. In contrast, guanidine mainly existed in the cationic form throughout the specimen, since the pK_a value of guanidine remained higher than the pH values of the re-alkalised pore solution. In addition, longer treatment would promote further injection of guanidine. In the case of arginine at the highest current density of $5A/m^2$, the dominant form of the inhibitor is molecular, at the cathode. When its pK_{a3} value (pK_{a3} 12.5) and the concentration of hydroxyl ions are taken into account, it can be seen that some of the inhibitor species take anionic form as shown in Figure 4.16, which are then driven back towards the anode by the action of the electric field. The anions migrating towards the anode are soon converted into molecules again as the anions leave the cathode and reach the area where the pH of the pore solutions is 10-11. Therefore, the accumulation of arginine molecules approximately 5-10mm from the steel cathode is attributable to two mechanisms: deprotonation of arginine cations migrating from the anolyte, and protonation of arginine anions from the cathode.

In the previous Chapter, the concentration threshold at which aqueous solutions of inhibitors can maintain passivation of steel was discussed, and the results showed that the threshold was between 10-100mmol/l for ethanolamine and arginine solutions, and below 10mmol/l for guanidine solutions. In the case of the highest current density ($5A/m^2$) applied for 7 days, the concentrations of all three inhibitors that accumulated in the vicinity of the cathode were obviously higher than 100mmol/l, thus it is expected that, in all three inhibitor cases, adequate concentrations of inhibitors were attained at the steel cathode for steel passivation. The passivity of the embedded steel in concrete specimens that were subjected to electrochemical injection treatments with the above three organic base corrosion inhibitors will be investigated in Chapter 6, wherein the long-term durability of the proposed remedial method is discussed.

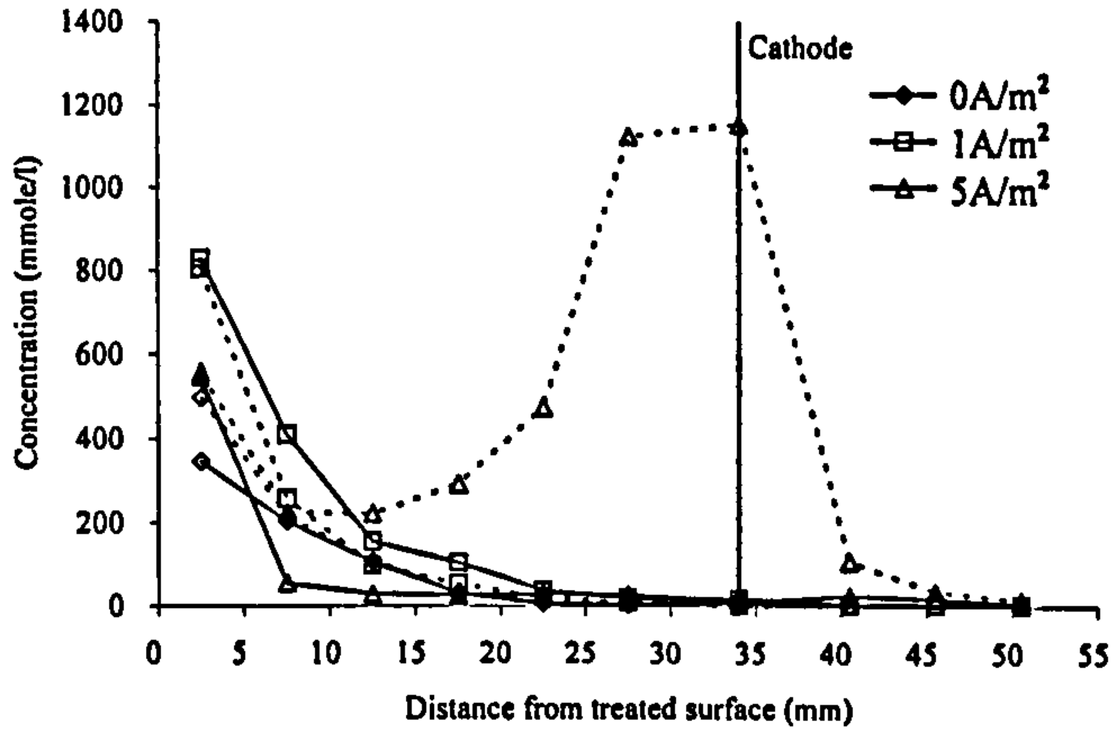

Figure 4.14 Concentration profile of ethanolamine in carbonated cement pastes of w/c 0.6 applied as 1M ethanolamine nitrate (Solid line: ethanolamine cations, Dotted line: total ethanolamine)

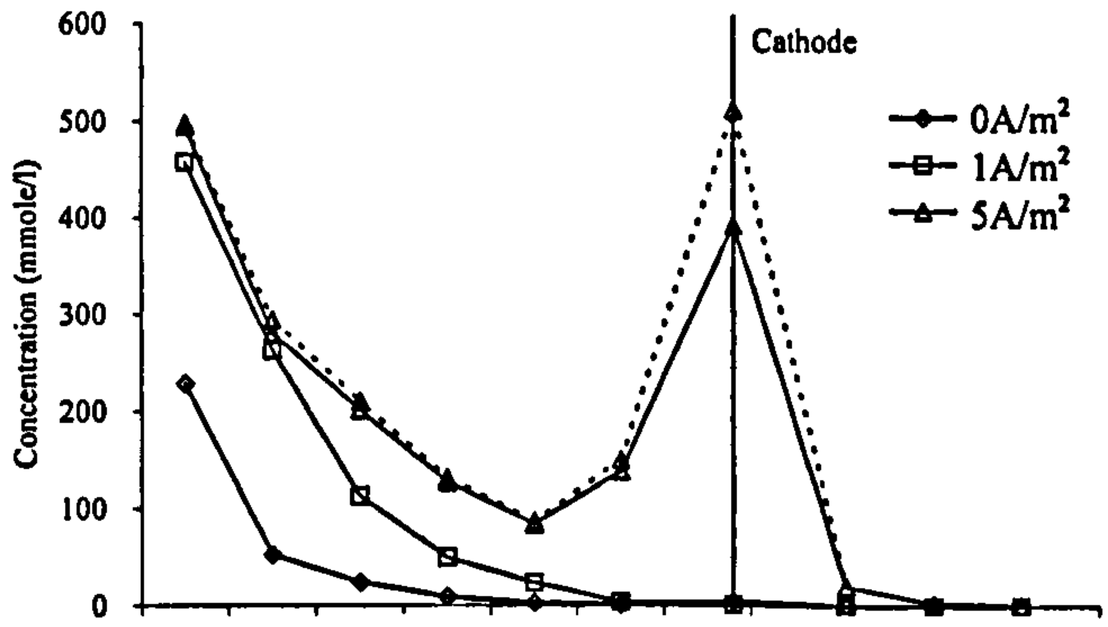

Figure 4.15 Concentration profile of guanidine in carbonated cement pastes of w/c 0.6 applied as 0.5M guanidine carbonate (Solid line: guanidine cations, Dotted line: total guanidine)

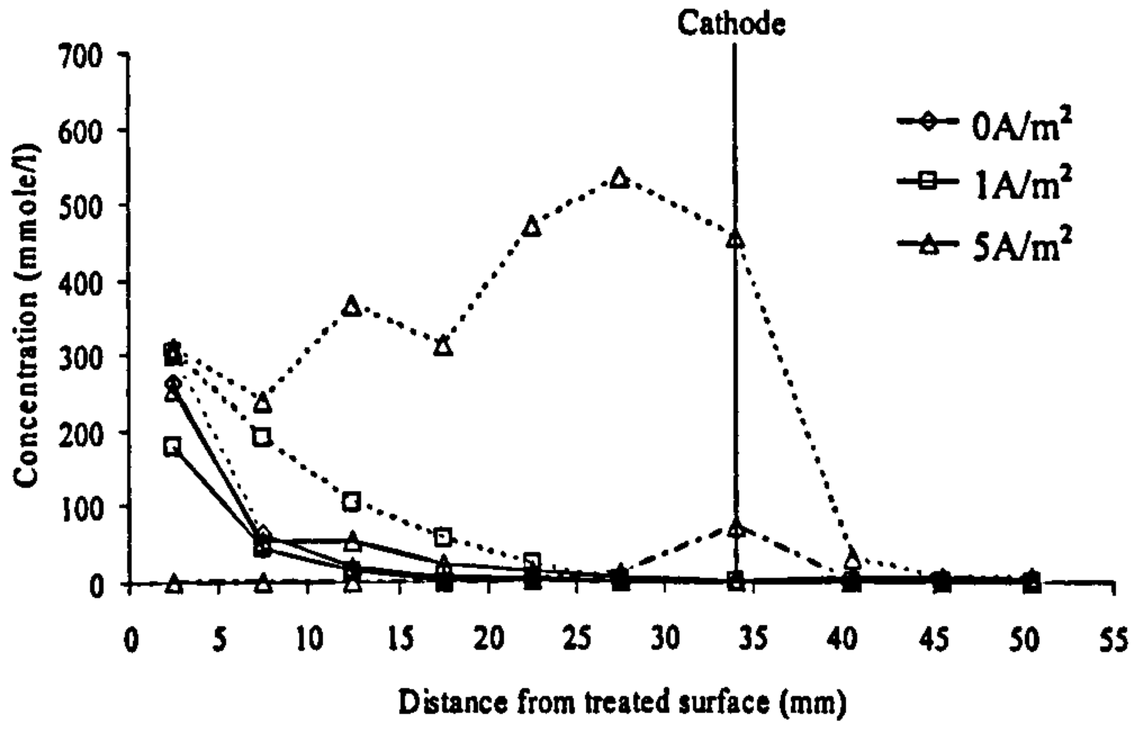

Figure 4.16 Concentration profile of arginine in carbonated cement pastes of w/c 0.6 applied as 0.5M arginine nitrate (Solid line: arginine cations, Dotted line: total arginine, Broken line: arginine anions)

The concentrations of the inhibitors remaining in the anolyte decreased with the progress of the electrochemical treatment, as shown in Table 4.3 and 4.4. In Figure 4.17, the quantities of inhibitors lost from the anolyte solution are plotted against the quantities of inhibitors injected into carbonated cement paste specimens, which were calculated from the data of inhibitor concentrations in the pore solution and the porosity of the specimens described in subsection 4.5.1. The amounts lost from the anolyte were larger than those penetrating into the cement matrix, especially in the case of guanidine carbonate. This difference can probably be attributed to the processes induced by the electrochemical treatment, such as anodic oxidation, evaporation or other side effects.

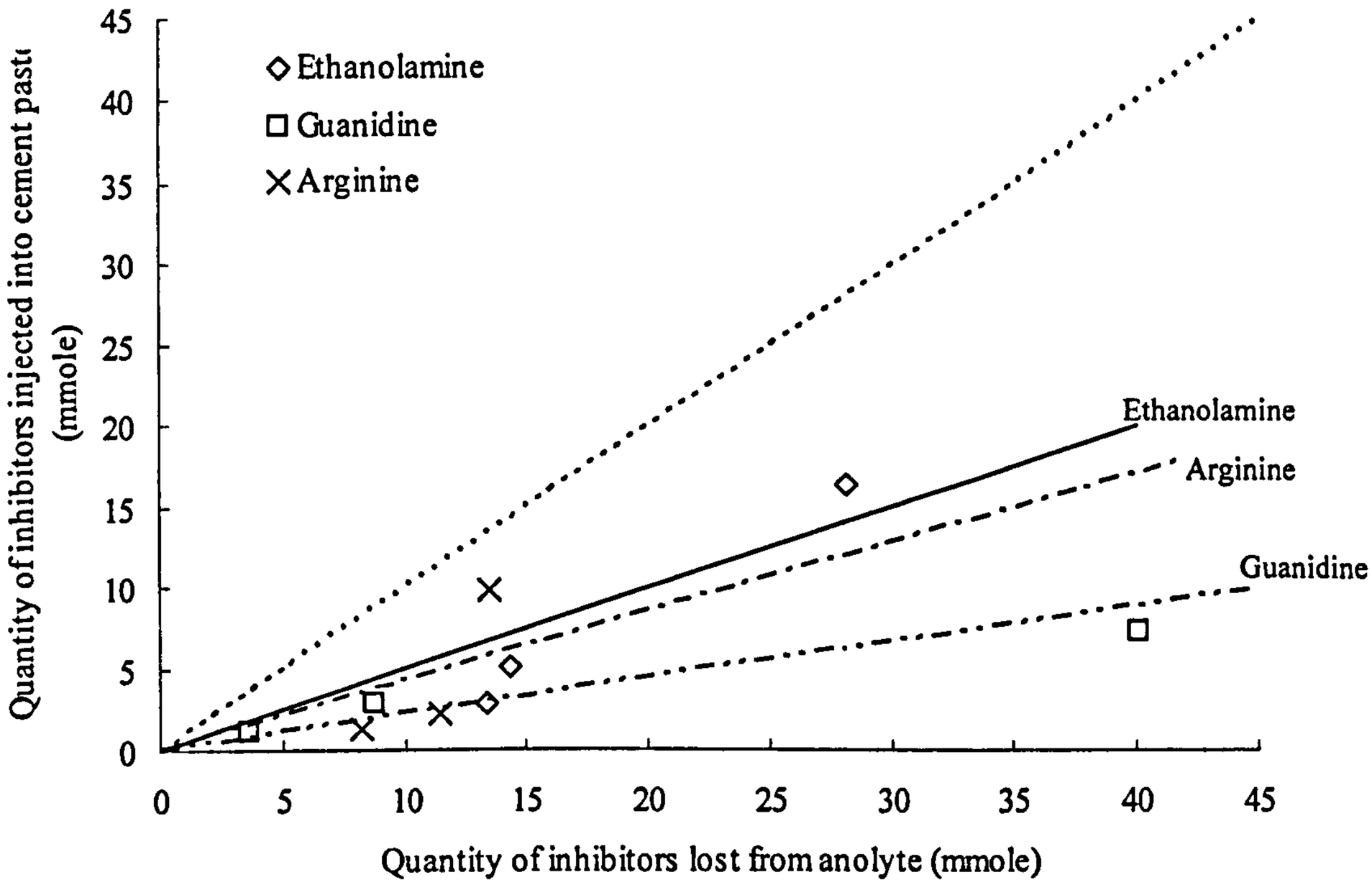

Figure 4.17 Comparison of quantity of corrosion inhibitors injected into carbonated cement paste with that lost in anolyte

4.6.2 Hydroxyl ions

The distributions of pH recorded for the various specimens are illustrated in Figure 4.18. In the case of ethanolamine and arginine, pH values progressively increased with the increase of circulated charge throughout the specimens, except near the anode. The low pH values near the anode resulted from the acidification of the anolyte owing to the generation of hydrogen ions by the anode reaction. In the case of guanidine, an increase in pH occurred only at the position of the cathode at the current density of $1A/m^2$, but the pore solutions

were re-alkalised to values of at least pH 12 over the length of specimens after the treatment of 5A/m^2 for 7 days. The cathodic region was effectively re-alkalised to the pH value of 13.08 in the case of guanidine, whereas re-alkalisation was moderate in the case of ethanolamine (pH value of 11.62) and arginine (pH value of 12.08)

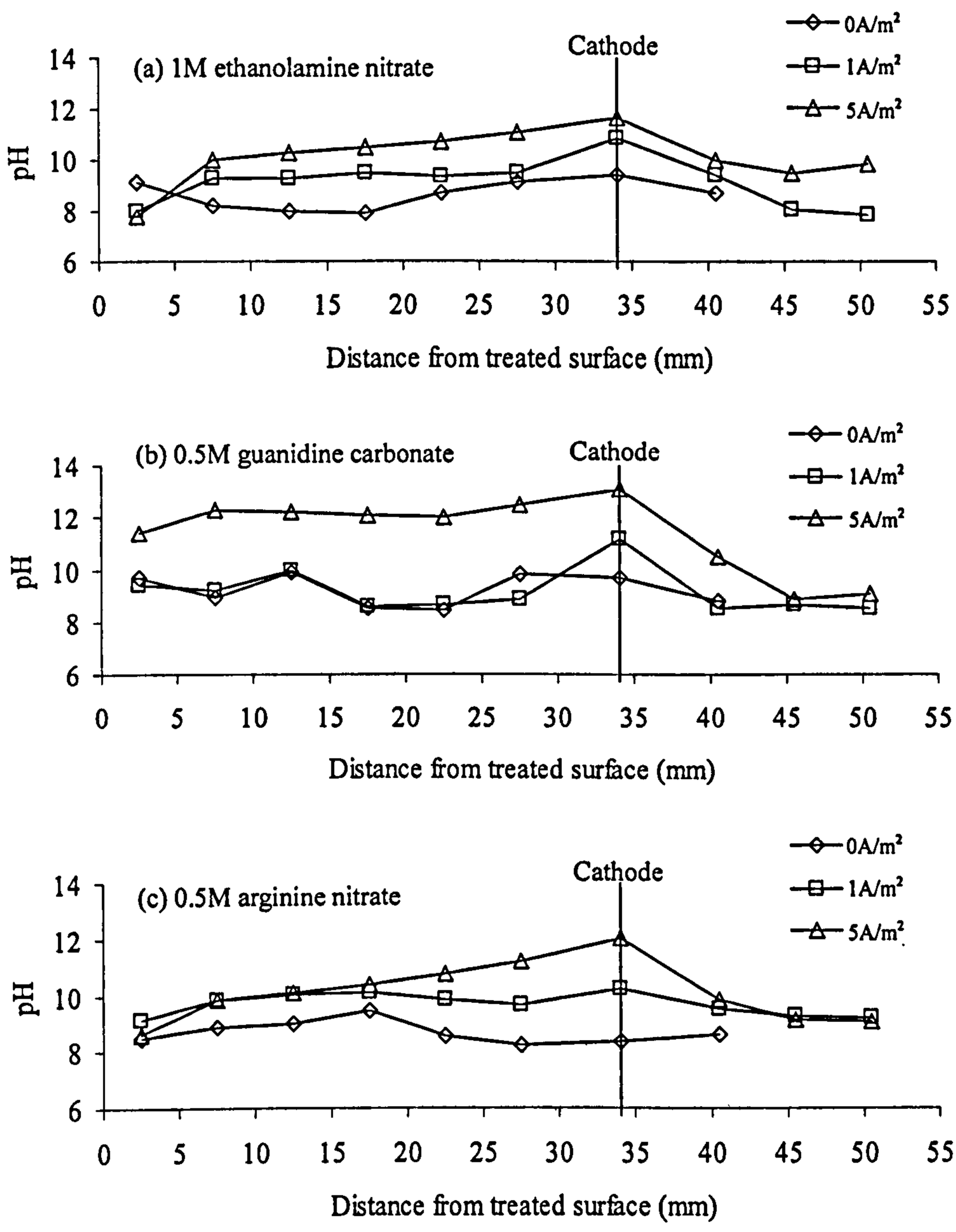

Figure 4.18 Distributions of pH values in carbonated cement pastes of w/c 0.6 treated with (a)1.0M ethanolamine nitrate, (b)0.5M guanidine carbonate and (c)0.5M arginine nitrate

Figure 4.19 shows the pH value in the cathodic region as a function of circulated charge. The pH values for the three inhibitors followed a similar trend rising until 6 $\times 10^5$ C/m^2 had been passed, but beyond that point the pH increase for ethanolamine was smaller than that for guanidine and arginine. At a current density of 1 A/m^2 (6 $\times 10^5$ C/m^2 charge passed in 7 days), none of the inhibitors was found to have reached the cathode region at significant concentrations (see Figures 4.5, 4.6, and 4.7) and thus the increase in pH therein was simply caused by water electrolysis. At a current density of 5 A/ m^2 (30 $\times 10^5$ C/m^2 charge passed in 7 days), however, significant concentrations of inhibitors penetrating to the cathode influenced the presence of cathodically generated hydroxyl ions to different extents. Ethanolamine with a pK_a value of 9.5 (pK_a' 9.75) consumed considerably more hydroxyl ions than guanidine with a pK_a value of 13.6. It is estimated that arginine with a pK_a value of 8.99 (pK_a' 9.30) consumed much more hydroxyl ions than ethanolamine, although the concentration of arginine accumulated near the cathode was much smaller than that of ethanolamine, resulting in a slightly more rapid increase in pH.

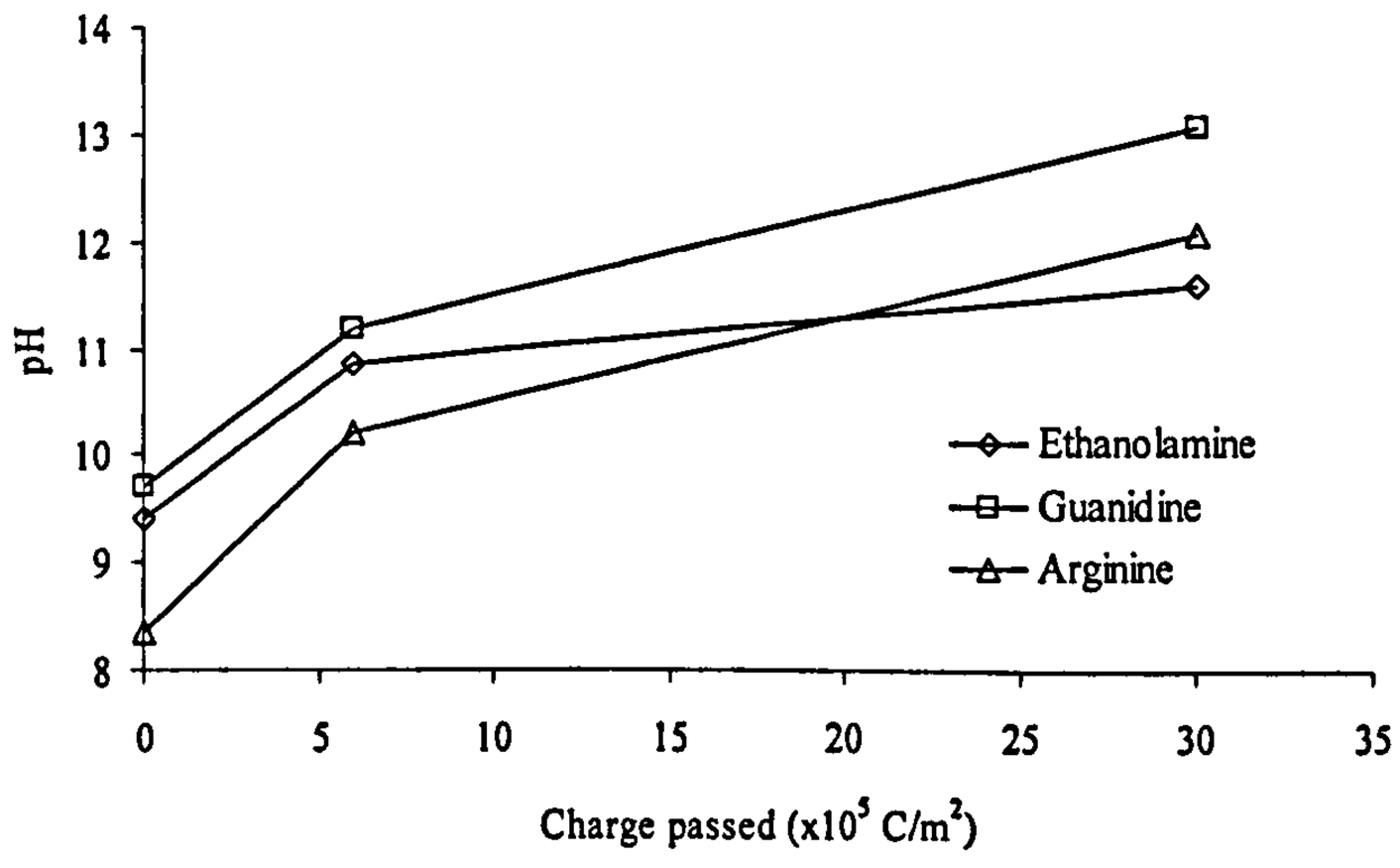

Figure 4.19 pH values at the cathode as a function of circulated charge

The moderate rise in pH at the cathode for the system using ethanolamine or arginine might be considered to be advantageous if the electrochemical injection of inhibitors were to be applied to concrete containing aggregates that are susceptible to the alkali-silica reaction. The phenomenon, which can cause local expansion and cracking of concrete, has been shown to be induced in the vicinity of embedded steel cathodes polarised at high current densities in non-carbonated concrete with certain types of potentially reactive siliceous aggregate (Sergi et al. 1991, Page et al. 1995).

4.6.3 Sulfate ions

As may be seen in Figures 4.11, 4.12, and 4.13, the concentrations of sulfate ions remarkably increased, particularly near the anodes, when an electrical field was applied. Moreover, in the case of guanidine without current, an increase in sulfate ion concentration near the external surface was also observed. These effects cannot be explained simply in terms of the redistribution of sulfate ions originally present in the initial pore solution toward the anode, since the magnitudes of the concentrations were far greater than expected. These results thus indicate that dissolution of sulfate ions from the solid cement carbonation products must have occurred during the electrical treatment. Since there was no significant variation in the concentration profile of sulfate ions in the case of ethanolamine treatment without current (see Figure 4.11) and there was no significant increase in sulfate ions near the cathode at the current density of $5A/m^2$ in the case of guanidine despite its high concentration (see Figure 4.12), it would seem that organic inhibitors have no direct role in promoting the dissolution of sulfate ions.

A tentative explanation of the evolution of sulfate ions in the cases without current for the three inhibitors can be given in terms of solubility equilibria involving calcium sulfate, which is expected to be present as gypsum produced in carbonated cement pastes, produced by the decomposition of ettringite resulting from carbonation of calcium sulfoaluminate hydrate phases in the cement (Grounds et al. 1988; Nishikawa et al. 1992). In the case of guanidine, calcium ions decreased in concentration near the anode due to precipitation of $CaCO_3$ (see Figure 4.9 (a)) and correspondingly the concentration of sulfate ions increased to preserve the solubility product of $CaSO_4$, as shown in Figure 4.12 (a). In contrast, in the case of ethanolamine and arginine, since there was a large amount of calcium ions due to the lower pH values of the pore solution resulting from the deprotonation of ethanolamine or arginine cations, corresponding sulfate concentrations were small, as can be seen in Figures 4.11 (a) and 4.13 (a). However, the significant changes in sulfate ion concentration associated with the application of the electrolytic treatments cannot be readily explained without resorting to mathematical modelling of the type proposed in the following Chapter.

4.6.4 Carbonate and bicarbonate ions

Substantial increases in the concentrations of carbonate ions at the cathode were observed when $5A/m^2$ had been applied for 7 days, especially in the case of specimens treated with

guanidine carbonate solution, as shown in Figures 4.6, 4.11 and 4.13. As there was no external source of carbonate ions in the case of ethanolamine and arginine, and it was difficult to imagine how carbonate ions could have moved from the anolyte to the cathode against the action of an electrical field in the case of guanidine, this local increase of carbonate ions is regarded as clear evidence of the dissolution of calcium carbonate in the vicinity of the stainless steel cathode. This might be simply explained in terms of the solubility equilibria of $Ca(OH)_2$ and $CaCO_3$, thus favouring the following reaction in the cathodic region:

$$CaCO_3 + 2OH^- \rightarrow Ca(OH)_2 + CO_3^{2-} \qquad (4\text{-B})$$

By the electrolysis of water the hydroxyl ion concentrations increased in the vicinity of the cathode, resulting in the decrease in calcium ion concentrations owing to the precipitation of $Ca(OH)_2$. This small concentration of calcium ions induced the release of carbonate ions from calcium carbonate in order to satisfy the solubility product of $CaCO_3$. As a result, the concentration of carbonate ions increased in the vicinity of the cathode. The support for this hypothesis is provided by Konno et al. (2002). In their study, the solubility of $Ca(OH)_2$ and $CaCO_3$ at high NaOH concentrations was determined and the results showed that the solubility of $CaCO_3$ was larger than that of $Ca(OH)_2$ at NaOH concentrations more than about 1 M at a temperature of 25 °C. The authors also found that the presence of $Ca(OH)_2$ was detected in solid samples obtained by adding NaOH solution at a concentration greater than 2M to saturated $CaCO_3$, and concluded that the solid phase of calcium carbonate was unstable and easily converted to calcium hydroxide in a high pH environment.

From the experimental results obtained in this chapter and the supporting evidence found in the literature, it may therefore be inferred that precipitation of $Ca(OH)_2$ can occur in the vicinity of the cathode under electrochemical treatment. This is expected to re-create a lime-rich layer of solid portlandite (and/or its reaction products with hydrous silica gel) in the interfacial zone between the steel and the carbonated cement matrix. The presence of a lime-rich interfacial transition zone at the steel/concrete interface is believed to have a significant role in stabilising the passive condition of the steel and thus in reducing the risk of corrosion under certain conditions (Page 1975). This could be practically relevant, particularly in cases where carbonated concrete is subject to chloride contamination. A related phenomenon, the induced precipitation of portlandite at cathodically polarised steel surfaces in non-carbonated mortars subjected to electrochemical chloride extraction treatments, has been observed

previously by Marcotte et al. (1999), and it has been suggested that this may significantly enhance the threshold level of chloride contamination for the corrosion of steel in concrete (Glass et al. 2000).

4.6.5 pH values of the anolyte after inhibitor injection treatment

After the electrical inhibitor injection treatment, the pH of external ethanolamine nitrate solutions was found to have most significantly decreased (pH 1.2), owing to the generation of hydrogen ions at the anode at the high current density ($5A/m^2$). This caused visible deterioration of the surface of the cement paste specimens immersed in these solutions, resulting in a markedly increased concentration of calcium ions due to the dissolution of carbonated cement matrix. In the case of arginine nitrate solutions, the final pH of the external solutions after the electrical treatment was slightly higher (pH 2.5). This would probably be attributable to the dissociation constant of arginine in an acid region (pK_{a1} 1.82), which therefore enabled the anolyte to act as a buffer solution by the following reaction:

$$RNH_3^+NH_2 + H^+ \Leftrightarrow R(NH_3^+)_2 \qquad (4\text{-}C)$$

In the case of guanidine carbonate, the external solutions, after the injection treatment, remained slightly alkaline (pH 8.8), even after the passage of $5A/m^2$ for 7 days, and no deterioration of the surface of the cement paste specimens was observed. This would be because of the equilibria involving carbonate/bicarbonate/carbonic acid concerned with the reactions with anodically generated hydrogen ions to lower the pH reduction rate as follows:

$$CO_3^{2-} + H^+ \Leftrightarrow HCO_3^- \ (pK_2\ 10.33) \qquad (4\text{-}D)$$

$$HCO_3^- + H^+ \Leftrightarrow H_2CO_3 \ (pK_1\ 6.35) \qquad (4\text{-}E)$$

It can be inferred from the final pH of the solutions (pH 8.8) that the reaction (4-D) was considered to have been dominant in the anolyte solutions. Thus in order to avoid surface dissolution due to rapid pH drop of the external solutions applied to the material surface, the use of such anolyte solutions as possess a buffer function with a pK value in a neutralised region would be beneficial.

4.7 CONCLUSIONS

(1) The three organic base corrosion inhibitors, namely ethanolamine, guanidine, and arginine, were effectively injected into carbonated cement paste (w/c 0.6) at depths corresponding to normal cover thickness to reinforcing steel when temporary electrochemical treatments of the types investigated were applied for up to a week at high current density ($5A/m^2$). The inhibitor penetration profiles observed were explicable in terms of the degrees of ionisation of ethanolamine (pK_a 9.5, pK_a' 9.75), guanidine (pK_a 13.6), and arginine (pK_a 8.99, pK_a' 9.30) in carbonated cement paste.

(2) The pH near the cathode was effectively raised to the value of 13.08 in the case of guanidine. The restoration of alkalinity was moderate in the case of ethanolamine (pH 11.62) and arginine (pH 12.08). This moderate rise of pH was attributable to the deprotonation of ethanolamine and arginine cations in high pH environments and may be a beneficial effect for reducing the risk of alkali-silica reaction.

(3) The concentrations of sulfate and carbonate/bicarbonate ions were significantly altered as a result of the electrochemical injection treatments applied. It appears that the effects observed involved dissociation of these anions from solid phases present in the carbonated cement pastes, satisfying the solubility equilibria of such species as calcium sulfate/carbonate/hydroxide in the pore solutions. The precipitation of $Ca(OH)_2$ in the vicinity of the steel cathode is expected to reduce the risk of corrosion.

(4) In the cases of the highest current density ($5A/m^2$) applied for 7 days, the concentration of all three inhibitors at the cathode exceeded a threshold value regarding whether an aqueous solution of inhibitors is inhibitive. Therefore it was demonstrated that the proposed electrochemical treatment allows inhibitors to penetrate into the vicinity of embedded steel cathodes in the adequate amounts required for the passivation of steel.

(5) Several important aspects could be clarified from the experimental investigation presented in Part 1 of this Chapter; however, it is still difficult to fully elucidate all the processes taking place in the cement matrix during the electrochemical treatment that are concerned with all relevant species. Thus, mathematical modelling is required for the theoretical and quantitative explanation of the phenomena, which is to be conducted in the following Chapter.

PART 2: MIGRATION OF CORROSION INHIBITORS INJECTED INTO PARTIALLY CARBONATED MEDIUM

4.8 INTRODUCTION

It is known that, in real concrete structures, the carbonation front is usually not uniform due to the inhomogeneity of the material or existing aggregates or cracks (see Figure 4.20). For example, the effect of existing cracks in concrete on carbonation depth is especially significant, and it is reported that the extreme rate of local carbonation has a quantitative relationship with crack width and length (De Schutter, 1999). Thus, it is likely that, in real concrete, the concrete cover may contain two regions with different material property: carbonated and non-carbonated sections. In Part 2 of this Chapter, the effect of partial carbonation of a cementitous material on the transport of species in the pore solutions, such as organic corrosion inhibitors, is investigated, employing the electrochemical inhibitor injection treatment studied in Part 1 of this Chapter. In this two-dimensional approach, it is expected that partial carbonation may induce the non-uniform current distribution in the material due to the special difference in material property, which may result in different efficiency in inhibitor migration. In addition, chemical phase interaction between two regions may influence the transport of species in the pore solution. The concentrations of inhibitors attained in the vicinity of the cathode by the electrochemical treatment are examined in terms of steel passivation, in a similar manner to those discussed in Part 1 of this Chapter.

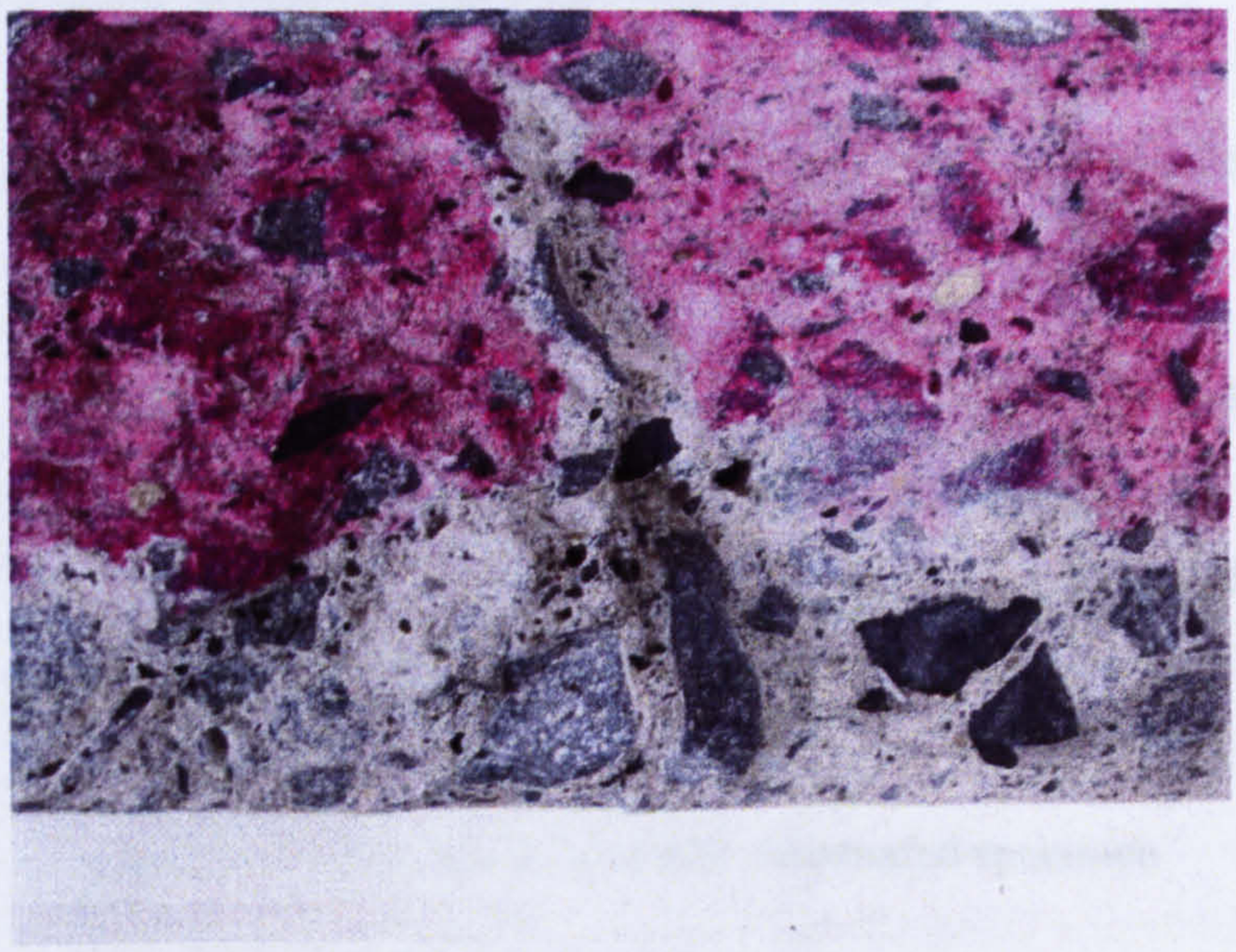

Figure 4.20 Partial carbonation of concrete
(After phenolphthalein test; pink region: non-carbonated, unchanged region: carbonated)

4.9 EXPERIMENTAL PROCEDURES

4.9.1 Overview of specimens

Figure 4.21 shows the overview of a set of cement paste specimens used in this experiment for the simulation of partially carbonated cementitious material. Five rectangular plate discs (area: 44mm×132mm), each of which has the thickness of 6mm, were stacked to form a single specimen. Steel reinforcement mesh acting as the cathode was embedded in the middle of layer 4 rectangular discs, and thus the cover depth was assumed to be 21mm (6+6+6+3). The bottom surface of the layer 1 rectangular plate disc was assumed to be the material surface contacting air, through which organic corrosion inhibitors were assumed to subsequently penetrate during the electrochemical treatment. Layer 1-2 plate discs were assumed to be fully carbonated, whilst for layers 3-5 plate discs, only the square sections (area: 44mm×44mm) in the middle were assumed to be carbonated and the other areas, on the both sides of the carbonated square sections, were non-carbonated. Therefore, the assumed profile of carbonation front in the specimen was as presented in a dotted curve in Figure 4.21 below.

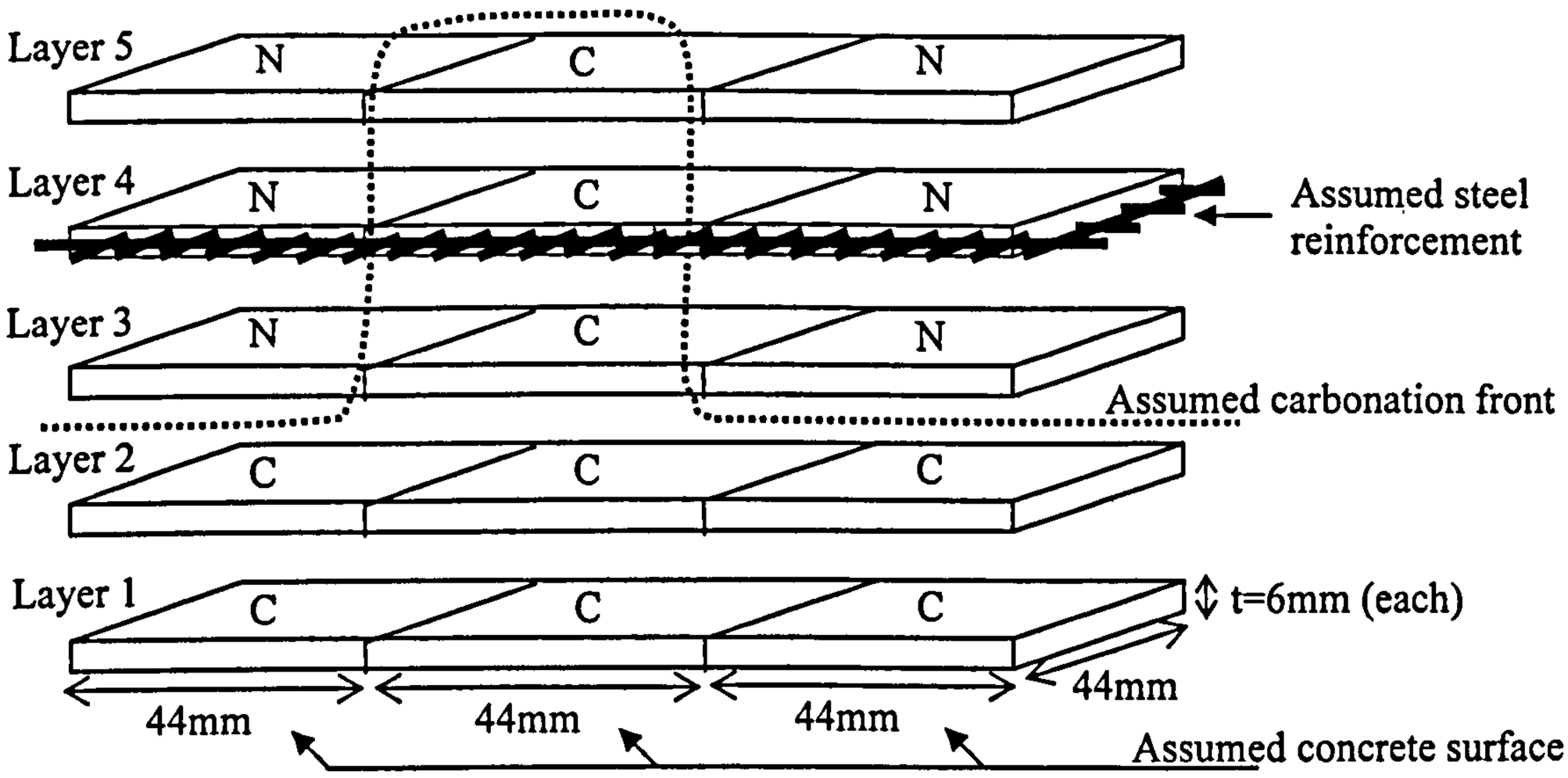

N: Non-carbonated, C: Carbonated

Figure 4.21 Overview of partially carbonated specimen

4.9.2. Specimen preparation

4.9.2.1 Layer 1-2 cement pastes

Ordinary Portland cement (OPC), whose chemical analysis is shown in Table 2.1 was used to produce cement paste specimens. After being sieved through a 150 μm mesh to remove coarse particles, the cement was then weighed and mixed with de-ionised water to produce paste of water/cement ratio 0.6. The mixture was poured into glass containers with dimensions of 44 × 132 × 6 mm. The containers were vibrated for approximately 2-4 minutes to get rid of any trapped air bubbles, and topped up with fresh paste. After the surface was flattened with a trowel, cling film was placed on the surface of the paste to prevent moisture loss. The specimens were cured in the same manner as described in subsection 4.4.1.1. When the samples were fully cured, the rectangular cement paste discs were ground with grade 600 emery paper and rinsed with distilled water before being exposed to rapid carbonation in the manner described in subsection 2.2.1. Three months later, completion of carbonation was confirmed by spraying phenolphthalein onto the surface of broken specimens. Then the fully carbonated discs were kept at 75% RH in air over saturated NaCl solutions until they were required for the electrochemical treatment detailed later in subsection 4.9.4.

4.9.2.2 Layer 3-5 cement pastes

For the preparation of layer 3-5 rectangular partially carbonated plate discs, carbonated specimens square sections in the middle were first produced. The cement pastes were made in the same manner as described in the previous subsection. For the production of layer-3 and layer-5 discs, the mixture was poured into square glass containers with 44 × 44 × 6 mm dimensions. For the production of layer-4 discs, the mixture was poured into specially prepared rectangular containers in which Type 316 stainless steel mesh (44 × 140 mm) was placed in the centre, as shown in Figure 4.22. The parts of the rectangular shaped stainless steel mesh were buried in Plasticine so that carbonated square cement pastes could be obtained at the right position in the middle of each glass container. After all the aforementioned square and rectangular containers had been vibrated for approximately 2-4 minutes to get rid of any trapped air bubbles and topped up with fresh paste, the surface was flattened with a trowel and then cling film was placed on the surface of the paste to prevent moisture loss. The specimens were cured in the same manner as described in the previous

subsection. When the samples were fully cured, the samples were ground with grade 600 emery paper and rinsed with distilled water before being exposed to rapid carbonation in the same manner as employed in the previous subsection. Three months later completion of carbonation was confirmed by spraying phenolphthalein onto the surface of broken specimens.

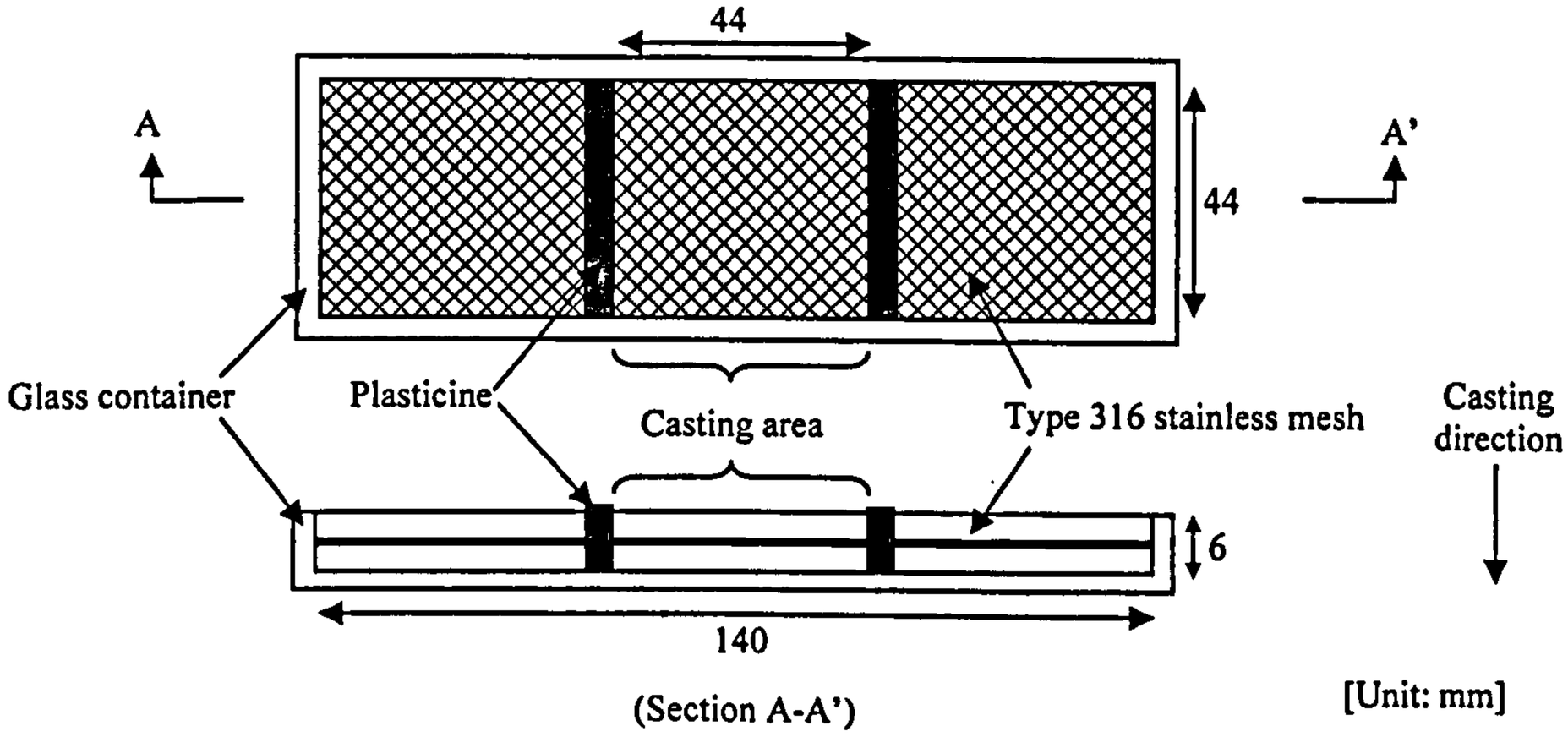

Figure 4.22 Container for producing carbonated partially carbonated discs for layer-4

After the carbonation of layer 3-5 specimens was completed, non-carbonated cement pastes were cast on both sides to form partially carbonated disc specimens. In order to avoid the re-alkalisation of obtained carbonated specimens due to the contact with newly cast non-carbonated cement pastes beside them, the carbonated specimens were converted to a saturated surface-dry condition in the manner described in subsection 4.4.3. For the production of layer-3 and layer-5 discs, the carbonated square discs were placed in the centre of glass containers with dimensions of 44 × 132 × 6 mm, and newly mixed cement pastes with the same mixture as described in the previous subsection were poured into two empty spaces with areas of 44 × 44 mm on both sides of the carbonated square discs as shown in Figure 4.23. For the production of layer-4 discs, the carbonated squares of cement paste with steel mesh were placed in the specially prepared containers again and newly mixed cement pastes were poured into the two empty spaces beside the carbonated paste as shown in Figure 4.23. The side edges of the rectangular shaped stainless steel mesh were buried in Plasticine so that wire could be attached to the electrode after the discs were demoulded. After all the containers had been vibrated for approximately 2-4 minutes to get rid of any trapped air bubbles and topped up with fresh paste, the surface was flattened with a trowel and then cling film was placed on the surface of the paste to prevent moisture loss and carbonation of

the newly cast pastes. The specimens were stored in a high humidity curing room at a temperature of 22±2°C for seven days. The samples were then demoulded and ground with grade 600 emery paper and rinsed with distilled water. The obtained samples were then immediately exposed to the full saturation procedure before they were used for electrochemical treatment.

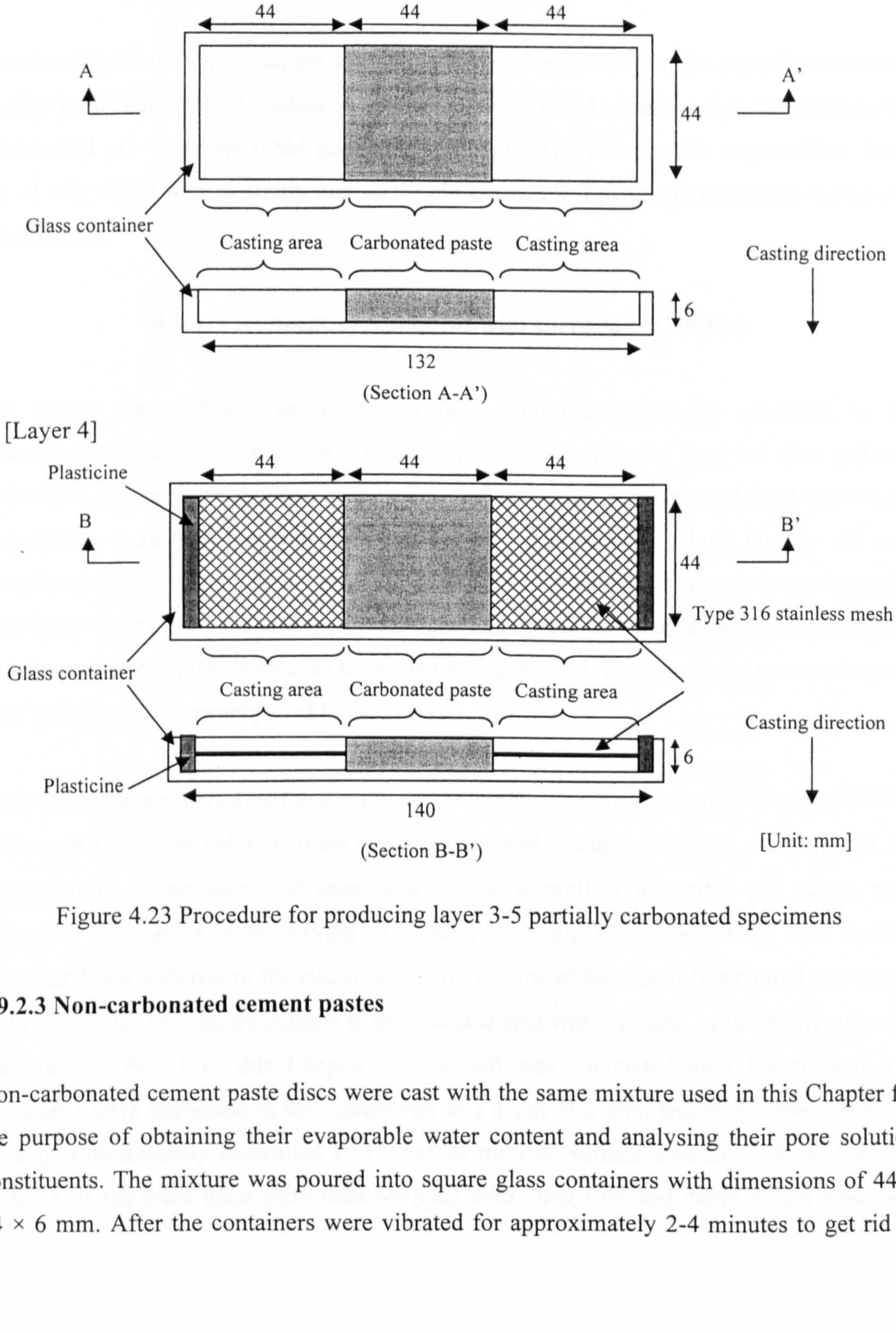

Figure 4.23 Procedure for producing layer 3-5 partially carbonated specimens

4.9.2.3 Non-carbonated cement pastes

Non-carbonated cement paste discs were cast with the same mixture used in this Chapter for the purpose of obtaining their evaporable water content and analysing their pore solution constituents. The mixture was poured into square glass containers with dimensions of 44 × 44 × 6 mm. After the containers were vibrated for approximately 2-4 minutes to get rid of

any trapped air bubbles and topped up with fresh paste, the surface was flattened with a trowel and then cling film was placed on the surface of the paste to prevent moisture loss and carbonation. Subsequently the specimens were cured and treated in the same manner as applied to non-carbonated sections within layer-4 partially carbonated discs described in subsection 4.9.2.2.

4.9.3. Organic corrosion inhibitors

The electrolyte solutions used for the electrochemical injection into the partially carbonated cement paste were 1M ethanolamine nitrate (mixture of 1M ethanolamine and 0.98M nitric acid: initial pH ~8.0) and 0.5M guanidine carbonate (1M with respect to guanidine: initial pH ~11.9), which were similarly used in the electrochemical treatment conducted in Part 1 of this Chapter.

4.9.4. Treatment of specimens with corrosion inhibitors

The cement paste discs were converted to a saturated surface-dry condition by the procedures detailed in subsection 4.4.3. Some spare fully carbonated layer 1-2 discs and non-carbonated square discs obtained in the manner described in subsections 4.9.2.1 and 4.9.2.3 respectively were then removed and used for the measurement of bulk density and total porosity according to the procedure detailed in section 2.7. Other discs were stacked together with damp filter papers (Whatman No.145) placed between two neighbouring layers of plate discs to ensure adequate contact as illustrated in Figure 4.24. Four specimens were set up for each test case and were subjected to electrolysis.

Each treatment was performed in a container whose atmosphere was kept at about 100% RH. After each electrolyte solution of the inhibitors outlined in subsection 4.9.3 was prepared, the concentration of inhibitors and associated anions, as well as the initial pH values, were measured. Six carbon rods, serving as anodes, were placed at the bottom of a shallow container filled with one of the electrolytes. The volume of the electrolyte poured was 360ml, so that the ratio of solution volume to disc surface area was the same as in the investigation presented in Part 1 of this Chapter. The circuit was completed after the stacked disc specimens were immersed in the electrolytes to a depth of 2 mm, and then current densities were galvanostatically controlled at 5 A/m^2 of the disc surface area for 7 days. The side surfaces of the piled discs were then wrapped with cling film and damp cotton wool was

placed on the top to restrict moisture loss caused by the temperature rise due to resistive heating during the electrochemical treatment.

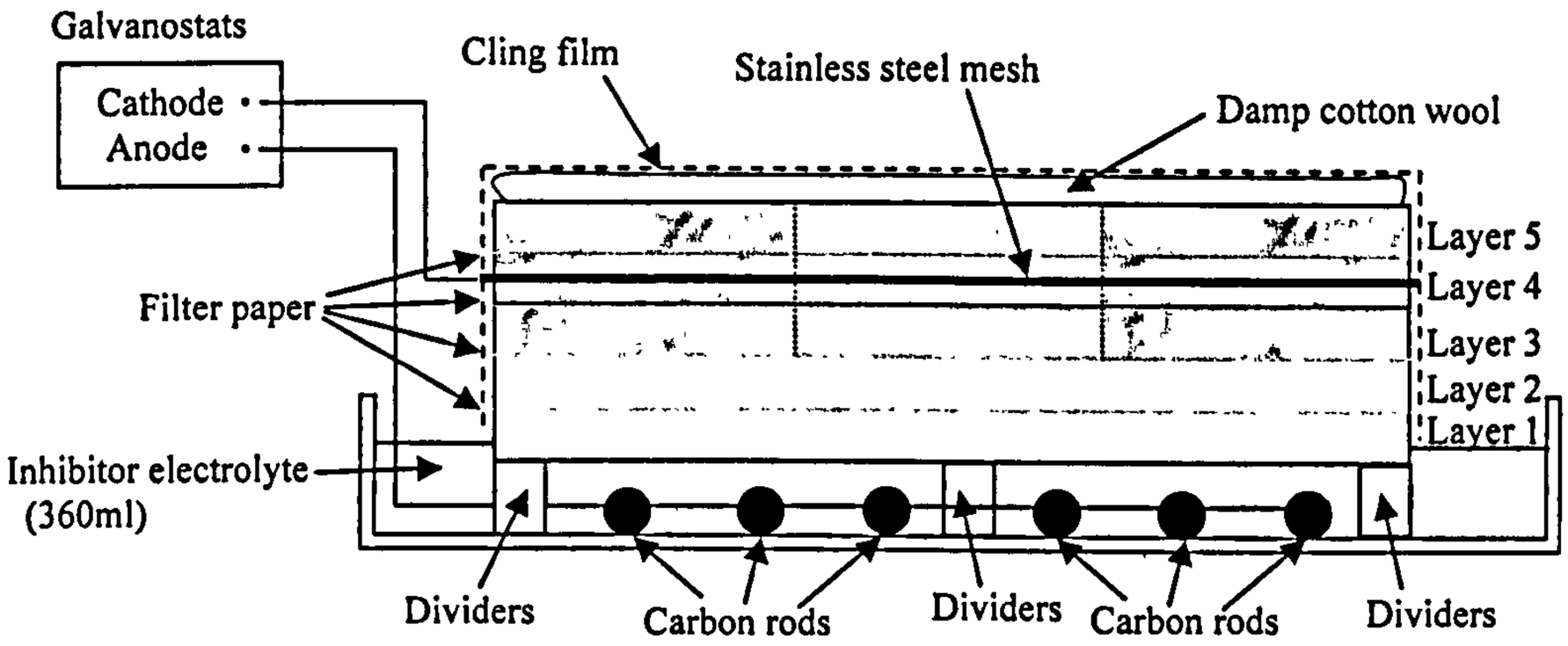

Figure 4.24 Experimental arrangement

4.9.5. Ionic distribution in pore solution

After the electrochemical treatment, the specimens were disassembled layer by layer and each rectangular disc was carefully broken into three square discs (area: 44 × 44 mm) with a screwdriver and a hammer. The three square discs that had formed one rectangular layer plate disc were respectively labelled as "left", "centre", or "right", according to the original horizontal position of each square disc during the electrochemical treatment. Then four discs located at the same position (labelled as layer number with horizontal position: e.g. 1-left, 1-centre, 1-right, ···, 5-right) were gathered from four sets of specimens and stored for one day in polythene bags inside a desiccator, in which distilled water was placed on the bottom. The four discs residing in the same position during the electrochemical treatment were used together as a sample for pore solution expression and pore solution constituents analysis as detailed in subsection 4.4.4. The spare carbonated and non-carbonated cement paste discs obtained in the manner described in subsections 4.9.2.1 and 4.9.2.3 were also used for the above analysis.

The anolytes were collected immediately after the treatments were completed. The concentrations of major ions and pH values of the anolytes were also determined as described in subsection 4.4.4.

4.10 RESULTS

4.10.1 Initial pore solution constituents of carbonated/non-carbonated cement paste

The ionic concentrations and pH values in the pore solution of carbonated and non-carbonated cement paste are shown in Tables 4.5 and 4.6. The values of bulk density were 2.21 and 1.89 g/cm^3 for the carbonated and non-carbonated cement pastes. Evaporable water contents, which were calculated from the loss of weight at 105 °C as described in section 2.7, were 0.18 and 0.29 g/g dry weight of sample respectively, from which the values of total porosity were determined to be 0.34 and 0.42. The concentrations of various ions in the carbonated pore solution are similar to those obtained in Part 1 of this Chapter as described in subsection 4.5.1. The concentrations of ions in the non-carbonated pore solutions showed similar magnitudes as those reported by Page et al. (1983). The carbonation process effectively reduced the pH value from above 13 to below 9, leading to increases in not only the binding of alkali metal cations into silica gel, but also the release of calcium, chloride, sulfate and carbonate species from solid carbonation products at the pore surfaces into pore solution as detailed in subsection 5.4.3.1 later.

Table 4.5 Concentration of cations (mmol/l) in the pore solution of cement paste

Type	Na^+	K^+	Mg^{2+}	Ca^{2+}	Sum of charge
Carbonated	11.7	6.6	15.9	24.9	99.9
Non-carbonated	99.3	140.6	0.4	4.7	250.0

Table 4.6 Concentration of anions (mmol/l) in the pore solution of cement paste

Type	pH	OH^-	Cl^-	SO_4^{2-}	CO_3^{2-}	HCO_3^-	Sum of charge
Carbonated	8.6	4.37E-03	38.6	22.4	0.1	5.8	89.3
Non-carbonated	13.3	213.8	2.5	1.9	2.6	0.0	225.3

4.10.2 Pore solution constituents after inhibitor injection treatment

Complete lists of data of pore solution constituents after inhibitor injection treatment are presented in Appendix C, for the samples at each horizontal position in each layer. The concentration of all relevant species in the discs of left and right columns in the same layer showed a reasonable agreement with each other, reflecting the symmetry of the assembled specimens to which current densities had been applied (see Figure 4.24). For the calculation of ethanolamine cation concentrations, 9.75 was used as the pK_a' value for the inhibitor in

order to take into account the interactions between inhibitor molecules and other species in the concentrated pore solutions, as in the cases described in subsections 4.5.2 and 5.4.4.

4.10.2.1 Organic corrosion inhibitors and associated anions

The concentration profiles of ethanolamine and nitrate ions in pore solutions are plotted in Figure 4.25. In the cases of the left and right columns that had had initial carbonation depths of only 12mm, leaving the embedded steel bars exposed to highly alkaline pore solutions before the treatment, the concentrations of ethanolamine at the cathode were approximately 400mmol/l. However, in the case of the centre column, which had been fully carbonated before the treatment, significant extra amounts of ethanolamine (over 1.0mol/l) were observed to migrate and accumulate around the stainless steel cathode, in accord with observations from Part 1 of this Chapter. The position of the concentration peak of ethanolamine was found to be just next to the initial carbonation depth in the former case (at around 10mm from the treated surface), and, on the other hand, a few millimetres from the steel cathode in the latter case. As for nitrate ions, the penetration of nitrate was similarly restricted to within the first 10 mm in the electric field.

The concentration profiles of guanidine and carbonate ions in the pore solutions after the treatment with 0.5M guanidine carbonate are plotted in Figure 4.26. Bicarbonate ions are not included in this figure since their concentrations were insignificant (see Appendix C). In the cases of the initially partially carbonated left and right columns, significant amounts of guanidine accumulated at the position of the stainless steel cathode, where the concentrations of guanidine were observed to be approximately 400-500mmol/l. On the contrary, in the case of the initially fully carbonated centre column, the concentrations of guanidine at the cathode were around 250mmol/l, which were not so significant compared with those observed in the side specimens or those obtained in Part 1 of this Chapter. The positions of the concentration peak of guanidine were different in different columns; the peak was found to be around 15mm from the treated surface in the side columns, though just at the steel cathode in the centre column. The penetration depths of carbonate ions were limited and smaller than those of guanidine except in the case of the centre column, where a notable increase in concentration of carbonate ions at the cathode was observed, in a similar manner as recorded in Part 1 of this Chapter.

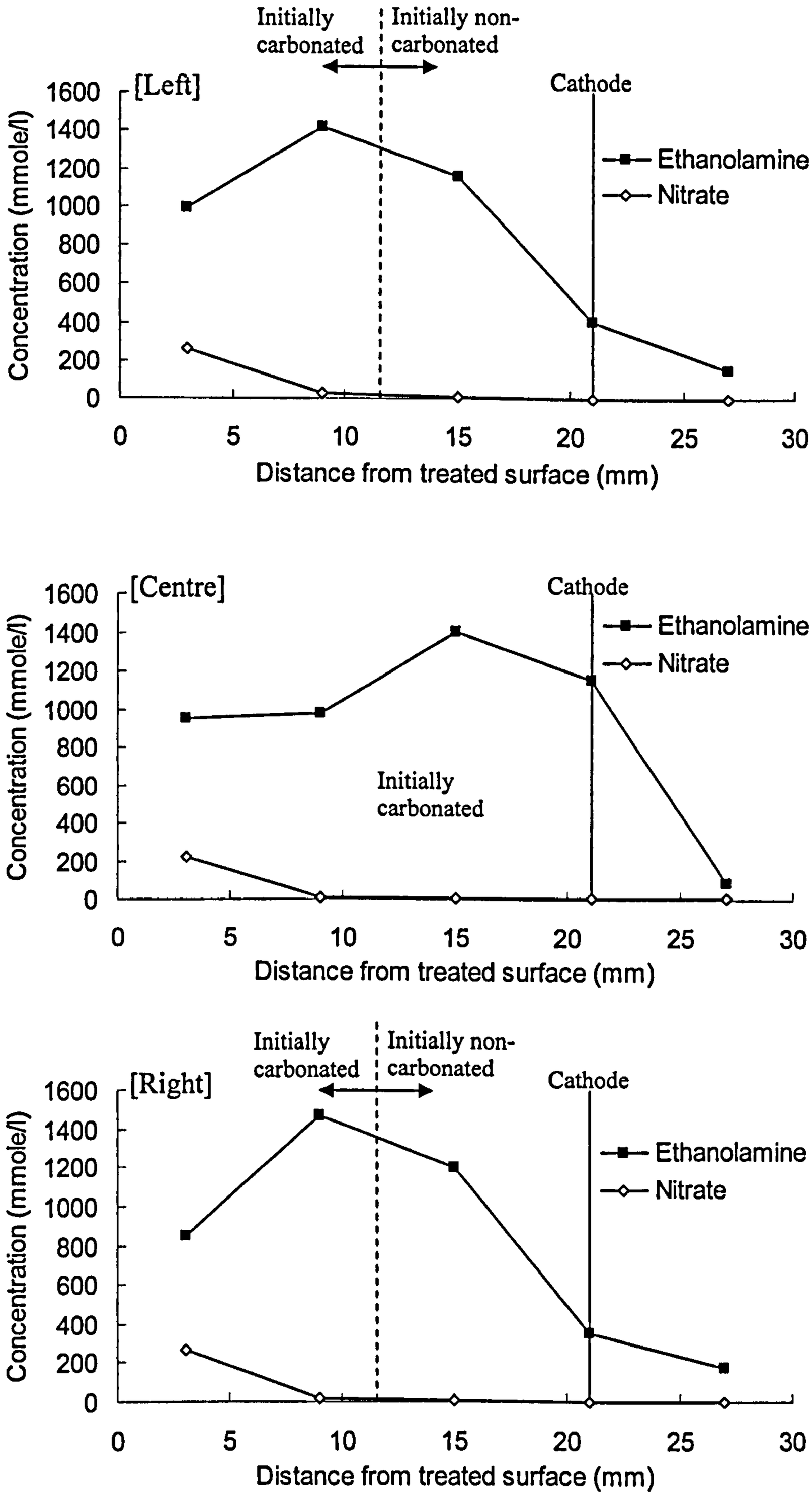

Figure 4.25 Concentration profiles of ethanolamine (applied as 1.0M ethanolamine nitrate) and nitrate ions in three different columns of partially carbonated cement paste after injection treatment at 5A/m^2 for 7 days (top: left, middle: centre, bottom: right)

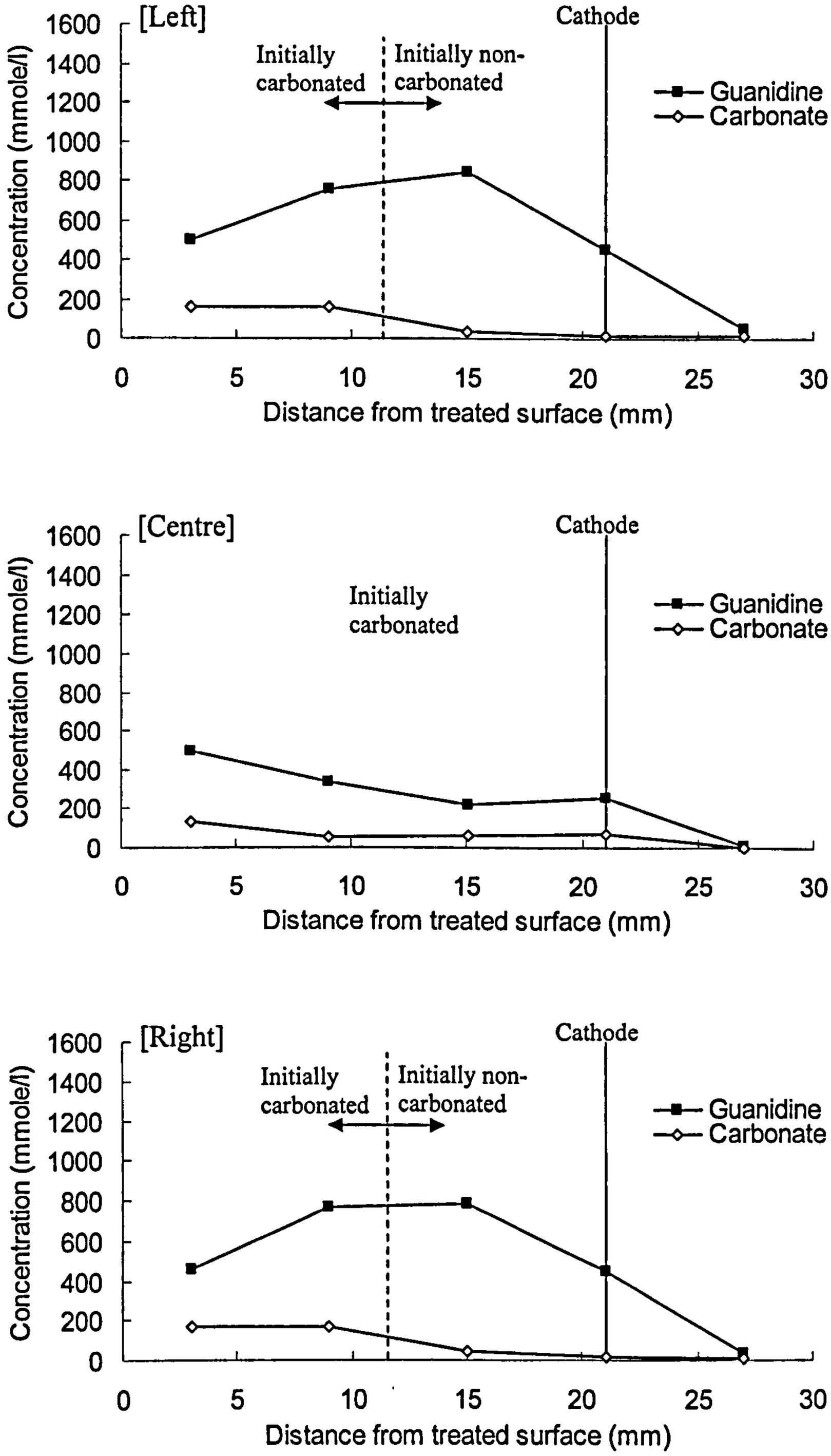

Figure 4.26 Concentration profiles of guanidine (applied as 0.5M guanidine carbonate) and carbonate ions in three different columns of partially carbonated cement paste after injection treatment at $5A/m^2$ for 7 days (top: left, middle: centre, bottom: right)

4.10.2.2 Evolutions in pH values

The distributions of pH recorded in the specimens after the electrochemical treatment are listed in Table 4.7 together with initial pH data. The pH values tended to rise throughout the cement paste specimens, except in the side columns of layer 3 treated with ethanolamine. In the case of guanidine, the environment in the vicinity of the steel cathode embedded in the initially carbonated centre column was highly re-alkalised to pH 12.91, and pH values over most of the entire area that had initially been carbonated were raised above 12. The centre square of layer 2 showed especially local enhancement of pH (to 12.85) in the centre column. On the other hand, in the case of ethanolamine, the pH value at the cathode in the centre column was restored to 11.85, and the pH rise of the initially carbonated areas of the specimens was moderate as a whole. These trends of rise in pH in the initially carbonated centre column specimens are similar to those observed in the investigation presented in Part 1 of this Chapter. The initially non-carbonated regions that contained the steel cathode (layer-4 discs in side columns) that were treated with guanidine showed higher increases in pH (to 13.60 and 13.62) than those treated with ethanolamine (to 13.48 and 13.51).

Table 4.7 pH evolutions in the cement paste specimens before and after treatment

Layer No.	[Initial] Left	Centre	Right	[Ethanolamine treated] Left	Centre	Right	[Guanidine treated] Left	Centre	Right
5	13.3	8.6	13.3	13.3	10.0	13.3	13.3	10.8	13.3
4	~~13.3~~	~~8.6~~	~~13.3~~	~~13.5~~	~~11.9~~	~~13.5~~	~~13.6~~	~~12.9~~	~~13.6~~
3	13.3	8.6	13.3	12.8	11.0	12.8	13.6	12.5	13.6
2	8.6	8.6	8.6	11.1	11.2	11.3	13.2	12.9	13.2
1	8.6	8.6	8.6	10.2	10.4	10.1	12.7	11.7	12.6

(The broken lines in the table indicate the position of steel cathode)

4.10.2.3 Major cations

The concentration profiles of other major cations, Na^+, K^+, and Ca^{2+}, in the pore solutions in the side and centre columns after treatment with 1M ethanolamine nitrate and 0.5M guanidine carbonate are plotted in Figure 4.27 and 4.28 respectively. For the profiles of the side specimens, the average concentrations at equal depths in left and right column specimens are used since their concentrations were similar (see Appendix C). The profiles of Mg^{2+} are not included in these profiles since the concentrations of the species were not significant compared to those of other cations (see Appendix C). The concentrations of both positively charged alkali metal ions were found to increase remarkably near the cathode in the side specimens. The increase in the concentrations of sodium and potassium near the

cathode was also observed in the cases of centre column, and the degree of the enhancement in the concentrations of the two ions near the cathode seemed to be higher than that recorded in the investigation presented in Part 1 of this Chapter. The peak concentrations of the alkali metal ions, namely sodium and potassium, near the cathode in the side specimens were higher in ethanolamine cases (around 140 and 210mmol/l respectively) than in guanidine cases (around 90 and 130mmol/l respectively). The concentrations of calcium ions were below 20mmol/l and the variations were small for both inhibitors' cases throughout the specimens, except near the anode in the case of ethanolamine.

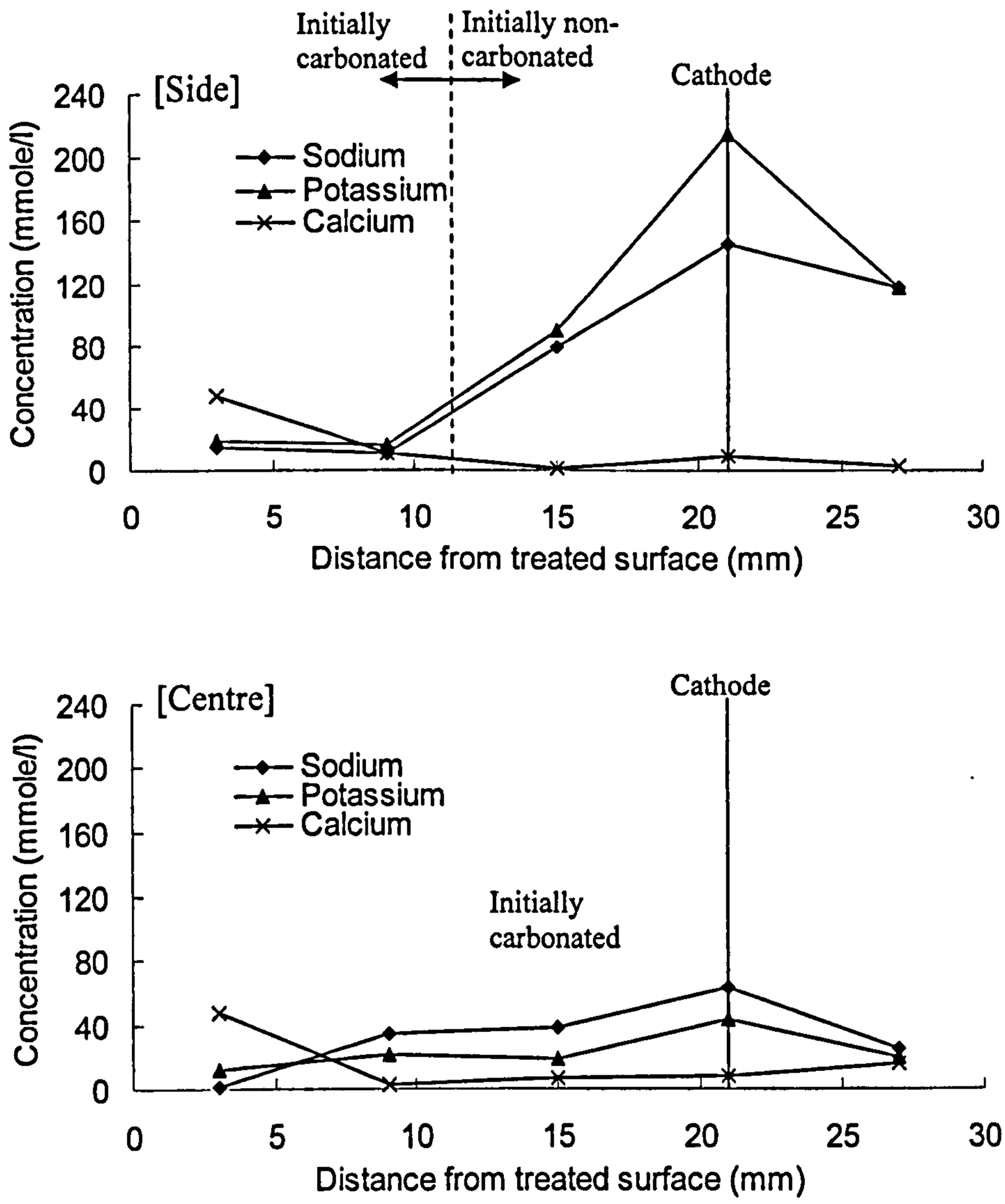

Figure 4.27 Concentration profiles of major cations (Na^+, K^+, and Ca^{2+}) in different columns of partially carbonated cement paste after specimen injection treatment with ethanolamine at $5A/m^2$ for 7 days (top: side columns (average), bottom: centre column)

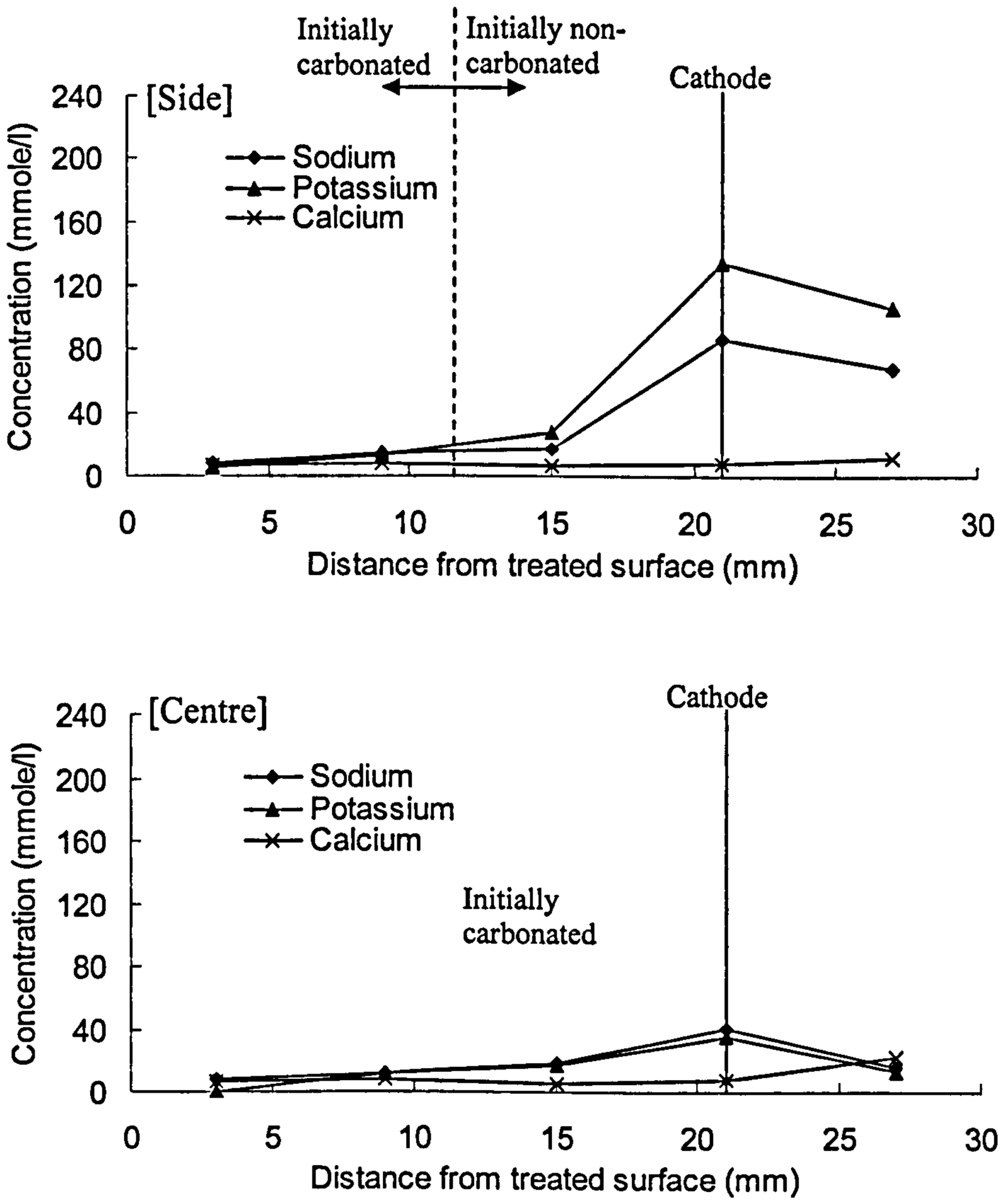

Figure 4.28 Concentration profiles of major cations (Na^+, K^+, and Ca^{2+}) in different columns of partially carbonated cement paste after specimen injection treatment with guanidine at $5A/m^2$ for 7 days (top: side columns (average), bottom: centre column)

4.10.2.4 Major anions

The concentration profiles of major anions, Cl^-, SO_4^{2-}, CO_3^{2-} and HCO_3^-, in the pore solutions after treatment with 1M ethanolamine nitrate are plotted in Figure 4.29. The concentration profiles of Cl^- and SO_4^{2-} in the pore solutions after treatment with 0.5M guanidine carbonate are plotted in Figure 4.30. The concentrations of OH^- are not included in these figures since they can be referred to in Table 4.7. The concentrations of chloride throughout the specimens were reduced progressively after the electrochemical treatment. In the case of ethanolamine, a significant increase in carbonate ions was observed especially around 5mm before the cathode for side column specimens, whilst observed throughout the cover depth for centre

column specimens. In the case of guanidine, a significant increase in sulfate ion concentration was observed, especially at around 10mm from the treated surface for side column specimens and near the surface for initially fully carbonated centre column specimens, as was the case in the investigation presented in Part 1 of this Chapter.

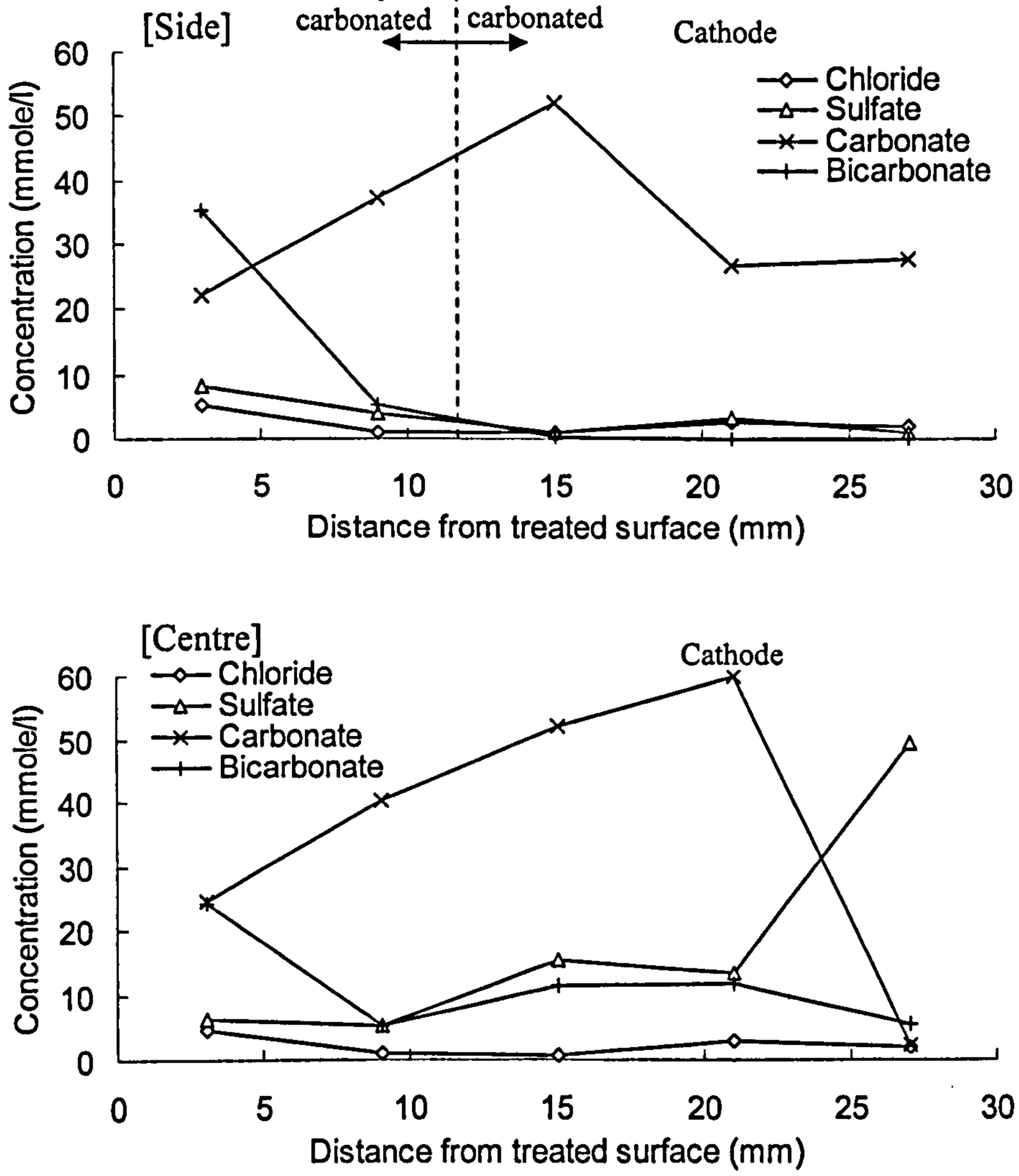

Figure 4.29 Concentration profiles of major anions (Cl^-, SO_4^{2-}, CO_3^{2-}, and HCO_3^-) in different columns of partially carbonated cement paste specimens after injection treatment with ethanolamine at $5A/m^2$ for 7 days (top: side columns (average), bottom: centre column)

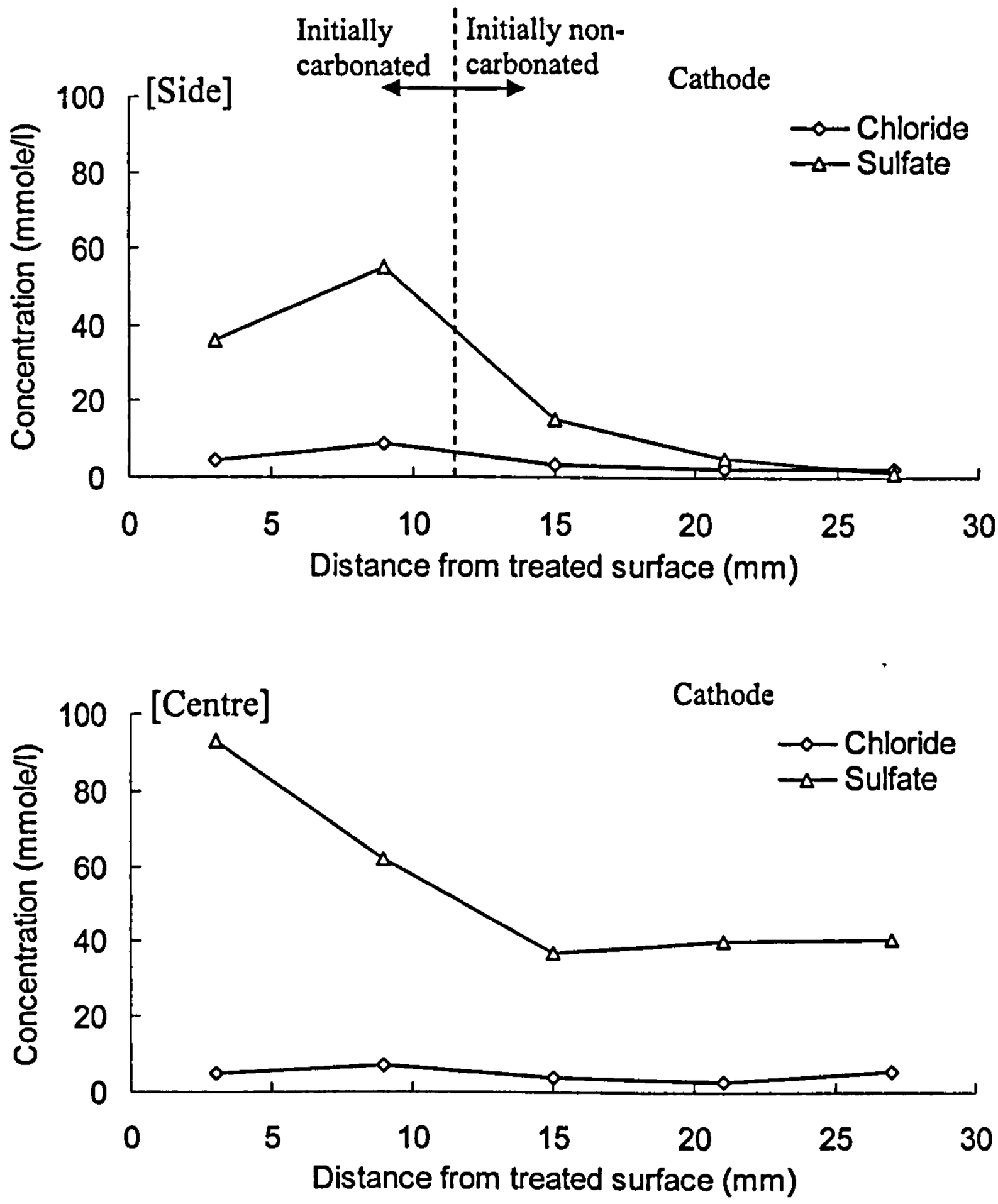

Figure 4.30 Concentration profiles of major anions (Cl^- and SO_4^{2-}) in different columns of partially carbonated cement paste specimens after injection treatment with guanidine at $5A/m^2$ for 7 days (top: side columns (average), bottom: centre column)

4.10.3 Chemical compositions of the anolyte after inhibitor injection treatment

The pH values and chemical compositions of the anolyte after treatment are presented in Tables 4.8 and 4.9, together with relevant initial values. The total charges for cations and anions detected in the anolyte showed reasonably similar values. The pH of ethanolamine nitrate solutions was found to have significantly decreased to the strong acid region (pH 1.55), resulting in visible deterioration of the surface of the cement paste specimens immersed in the solutions. The guanidine carbonate solution remained slightly alkaline (pH 9.21) after the treatment. The reductions in pH values were slightly more moderate than

those observed in the investigation in Part 1 of this Chapter (final pH 1.21 for ethanolamine nitrate and pH 8.80 for guanidine carbonate after the treatment).

Table 4.8 Concentrations of organic inhibitors and cations in the anolyte before and after treatment with inhibitors

Anolyte	State	Concentrations (mmol/l)							
		Organic inhibitors		Na^+	K^+	Mg^{2+}	Ca^{2+}	H^+	Sum of charge
		Total	Cationic						
1M ethanolamine nitrate	Treated	878.9	878.9	4.3	N/D	15.6	127.5	28.2	1197.4
	Initial	1081.6	1063.1	-	-	-	-	1.0E-05	1063.1
0.5M guanidine carbonate	Treated	835.3	835.3	8.9	N/D	0.0	4.1	6.2E-07	852.5
	Initial	990.2	974.0	-	-	-	-	1.5E-09	974.0

N/D: Not detectable

Table 4.9 Concentrations of anions in the anolyte before and after treatment with inhibitors

Anolyte	State	pH	Concentrations (mmol/l)						
			OH^-	Cl^-	SO_4^{2-}	NO_3^-	CO_3^{2-}	HCO_3^-	Sum of charge
1M ethanolamine nitrate	Treated	1.6	3.5E-10	4.0	10.1	1074.9	0.0	0.0	1099.0
	Initial	8.0	9.7E-04	-	-	981.7	-	-	981.7
0.5M guanidine carbonate	Treated	9.2	1.6E-02	1.6	56.4	-	50.2	677.7	892.6
	Initial	11.8	6.6E+00	-	-	-	481.2	15.6	984.6

4.11 DISCUSSION

In this section, the effect of partial carbonation of cement pastes, especially the interaction between initially non-carbonated and carbonated regions, on the behaviour of the major species (organic corrosion inhibitors, hydroxyl ions, alkali metal ions, and carbonate ions) which might be considered to have important roles by affecting other ions/species in the electrochemical injection approach, is discussed. Some of the phenomena discussed in the results section 4.10 can be justified by elucidation similar to that of Part 1 of this Chapter (see section 4.6), such as the concentration profiles of major anions (except hydroxyl and carbonate) and some other species. Thus, they are not discussed here.

4.11.1 Pore solution constituents

4.11.1.1. Organic corrosion inhibitors

Figures 4.31 and 4.32 show the concentration profiles of the ionic species of the inhibitors for ethanolamine and guanidine, which were obtained using their pK_a' values (pK_a value used for guanidine) and the pH values of the pore solution. The position of the concentration peak of the total inhibitors in each figure may be explicable in terms of the dissociation constants of ethanolamine (pK_a 9.5, pK_a' 9.75), and guanidine (pK_a 13.6), resulting in different degrees of ionisation of the inhibitors in the specimens, as discussed in Part 1 of this Chapter. This is why, for both inhibitors, the position of the concentration peak in the initially fully carbonated columns is closer to the steel cathode than it is in the partially carbonated side columns. It can also be seen that the predominant form of ethanolamine penetrating into the specimens was molecular, except near the anode, and that the main transport mode of ethanolamine near the cathode would be the diffusion of molecules. Thus the results obtained indicate that further electrochemical treatment may not be effective for field-induced injection of ethanolamine for the specimens employed in this investigation. In contrast, guanidine mainly existed in the cationic form throughout the specimen, even in the initially non-carbonated highly alkaline region, where the pH values were eventually raised to 13.6. These results demonstrate that longer treatment would promote further injection of guanidine.

It can be seen from the results that, when the concentrations of the two organic corrosion inhibitors that migrated to the steel cathode in the initially fully carbonated centre column are compared to those obtained in carbonated cement pastes in Part 1 of this Chapter, the

concentration of guanidine was disappointingly almost only half (513mmol/l for Part 1 and 256mmol/l for Part 2), whilst the concentrations remained at nearly full levels for ethanolamine (approximately 1,160mmol/l for both). It can also be observed that substantial concentrations of inhibitors reached the steel cathode through initially non-carbonated regions in the side columns, which seemed somewhat contradictory to the results demonstrated by Sawada et al. (2005), in which quite small migration of the inhibitors towards the cathode was observed when the same organic corrosion inhibitors were electrochemically injected into non-carbonated concrete at the same current density for the same period. These phenomena may be attributable to the interaction between the regions in the centre and side columns, which will be discussed later in subsection 4.11.2.

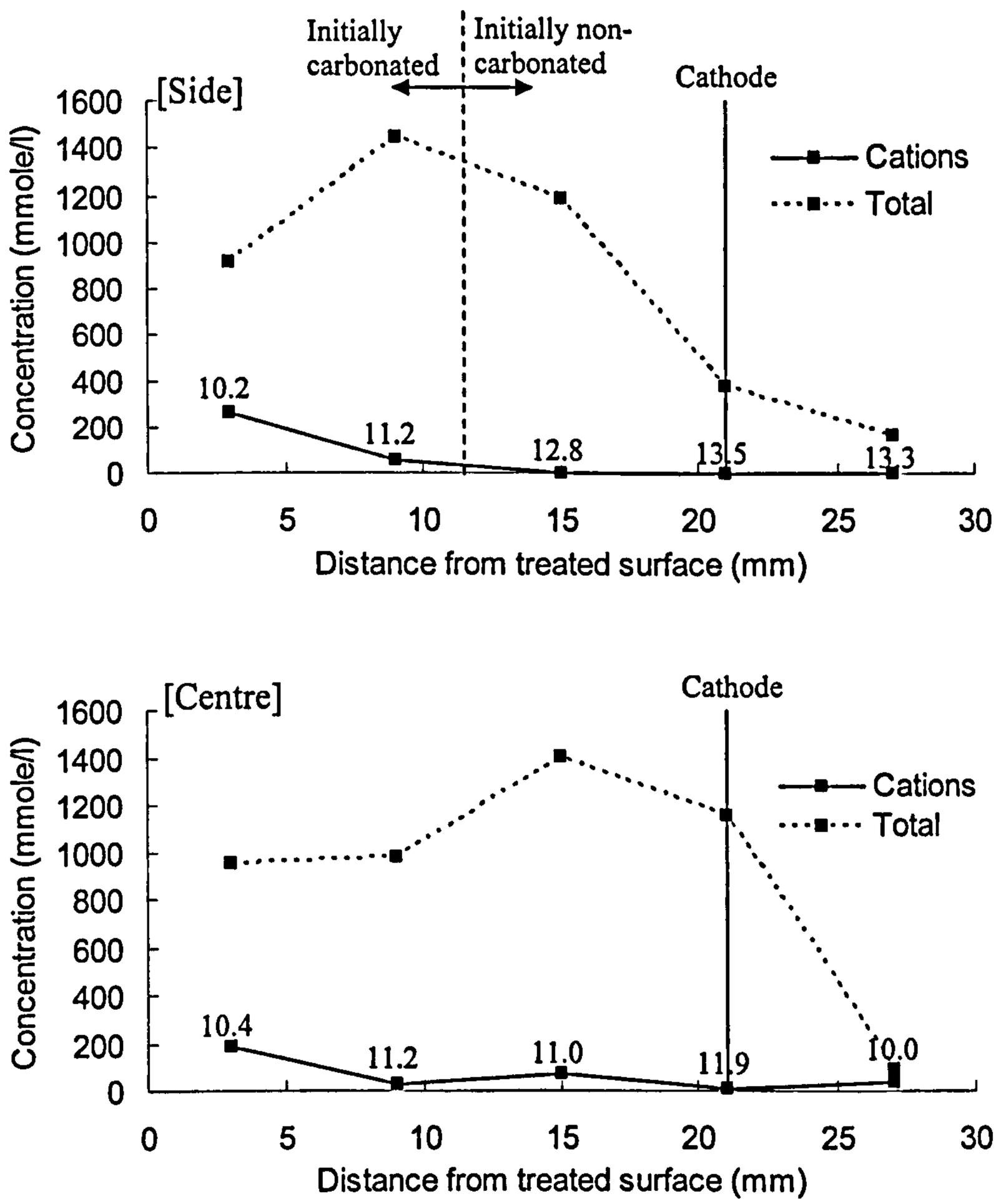

Figure 4.31 Concentration profiles of ethanolamine cations and total ethanolamine in different columns of partially carbonated cement paste specimens together with pH values of the pore solutions (top: side columns (average), bottom: centre specimen)

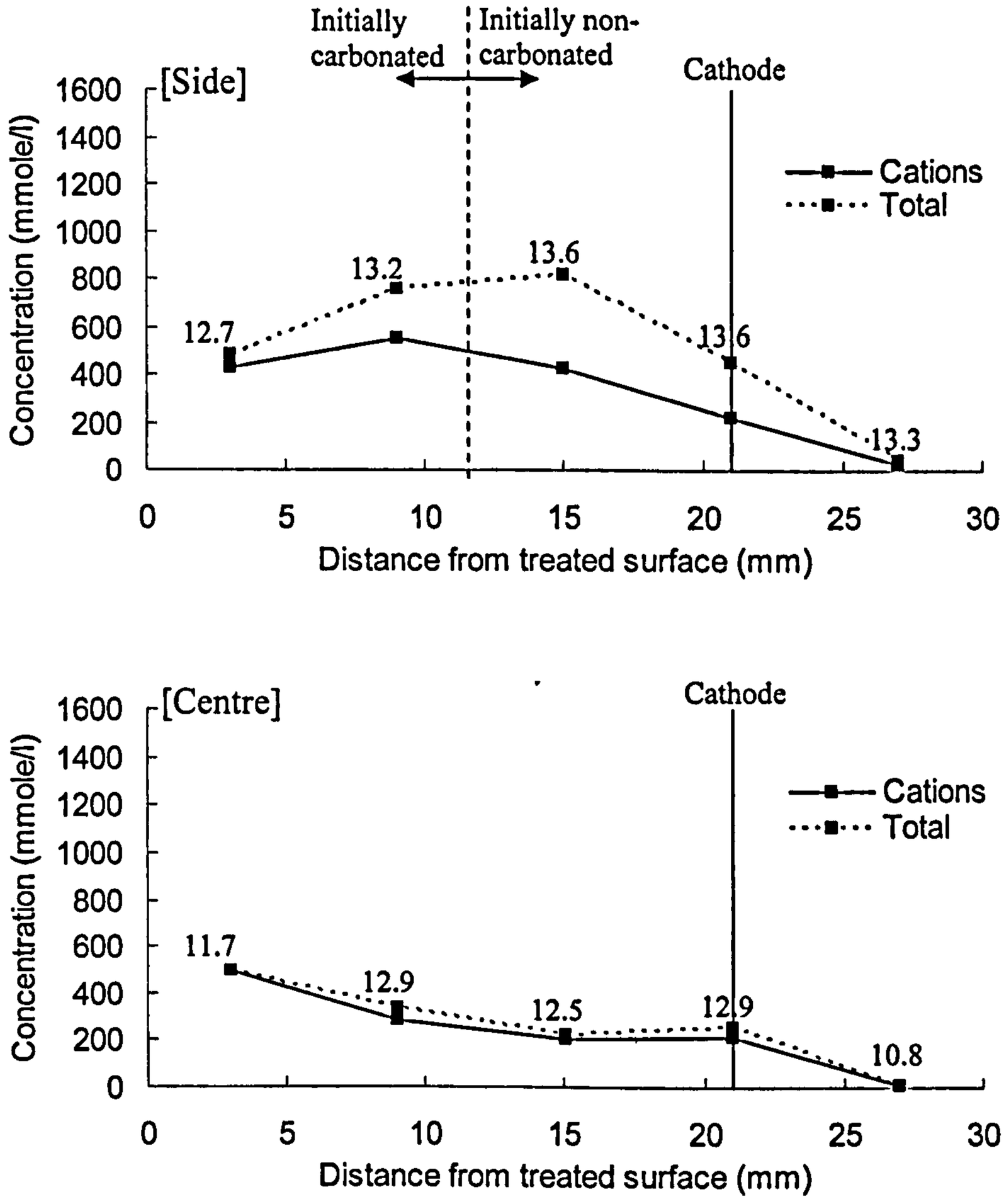

Figure 4.32 Concentration profiles of guanidine cations and total guanidine in different columns of partially carbonated cement paste specimens together with the pH values of the pore solutions (top: side columns (average), bottom: centre column)

As for the steel inhibition performance of the inhibitors injected, it was found in the previous Chapter that the threshold concentration at which aqueous solutions of inhibitors can maintain steel in a passivating condition was between 10-100mmol/l for ethanolamine, and below 10mmol/l for guanidine. From the experimental results obtained by applications of electrochemical inhibitor injections to partially carbonated cement paste specimens presented in this Chapter, it is obvious that the concentrations of both inhibitors attained in the vicinity of the steel cathode embedded in initially non-carbonated and carbonated cement pastes were higher than these threshold values, and thus it is expected that the injected corrosion inhibitors near the cathode will contribute to the passivation of steel even after the pore

solution is neutralised. The long-term effectiveness of this injection method on steel passivation will be discussed in Chapter 6.

The concentrations of both inhibitors remaining in the anolyte decreased with the progress of the electrochemical treatment, as shown in Table 4.8 and 4.9. The ratios of the quantities of inhibitors injected into partially carbonated cement paste specimens to the quantities of inhibitors lost from the anolyte solution were 68% for ethanolamine and 46% for guanidine, which are higher than those recorded in the investigation presented in Part 1 of this Chapter (58% for ethanolamine and 18% for guanidine). This can probably be attributed to the difference in area of the specimens covering the surface of anolyte, which might have prevented evaporation of the solutions.

4.11.1.2 Hydroxyl ions

The distributions of pH recorded for the centre and side columns are listed in Table 4.7. Similar to the observations gleaned from Part 1 of this Chapter, concentrations of inhibitors penetrating to the cathode significantly affected the presence of cathodically generated hydroxyl ions. Ethanolamine with a pK_a value of 9.5 (pK_a' 9.75) consumed considerably more hydroxyl ions than guanidine with a pK_a value of 13.6, and a significant concentration of ethanolamine penetrating layer-3 side column specimens even reduced the initial pH values from 13.3 to 12.8. The moderate rise in pH at the cathode for the system using ethanolamine might be considered to be advantageous in terms of the prevention of ASR (alkali-silica reaction), as discussed in Part 1 of this Chapter.

It was inferred that the concentration gradient of hydroxyl in the layer-4 discs containing the steel cathode caused diffusion of the ion from initially non-carbonated side column regions to initially carbonated centre column regions. The effect of interaction between two neighbouring columns will be discussed in subsections 4.11.1.4 and 4.11.2.

4.11.1.3 Alkali metal ions

Figures 4.27 and 4.28 show the concentration profiles of the ionic species of the alkali metal ions, namely sodium and potassium, in which, when compared to the initial concentrations of both ions in the carbonated pore solutions (see Table 4.5), significant concentrations can be found throughout the specimens in the centre column. The fact that the overall concentrations of the two alkali metal ions in the centre column are more significant than

those obtained in the fully carbonated cement pastes specimens obtained in Part 1 of this Chapter may be regarded as clear evidence of the flow of both ions from initially non-carbonated regions in side columns, in which sodium and potassium were abundant, to the centre column, which probably occurred due to the concentration gradient of these ions.

The results also show that higher concentrations of both ions can be observed in the case of ethanolamine than guanidine in the centre column specimens. In the case of ethanolamine, since the predominant form of the inhibitor penetrating into the specimens was molecular except near the anode, the two alkali metal ions were the main charge-carrying cations, resulting in more rapid migration of the two ions in the electric field than was the case for guanidine.

The concentrations of both alkali metal ions were remarkably high near the cathode in the side specimens as described in section 4.10.2.3. It is noted that the high concentrations of alkalis formed around the highly alkaline steel cathode area during the electrochemical treatment involve the possibility of generating damaging ASR (alkali-silica reaction) when susceptible aggregates are contained in concrete, since the applied current densities are of the similar magnitudes to those employed for ECR (electrochemical chloride removal), often in the range of A/m^2 (Page et al. 1994).

4.11.1.4 Carbonate ions

Substantial increases in the concentrations of carbonate ions observed in the case of centre column specimens treated with both inhibitors, except those after the steel cathode, can be attributed to the dissolution of calcium carbonate and the conversion of the species to calcium hydroxide, taking into account the solubility equilibria of $Ca(OH)_2$ and $CaCO_3$, as discussed in Part 1 of this Chapter. The reaction (4-B) in subsection 4.6.4 would be favoured in a high pH environment due to the flow of hydroxyl from the side columns in addition to the generation of hydroxyl at the steel cathode.

The re-establishment of the lime-rich region is expected to contribute to the stabilisation of the passive condition of steel, resulting in the reduction in corrosion risk, as discussed in Part 1 of this Chapter.

4.11.2 Interaction between centre and side column specimens

4.11.2.1. Current flow

In the investigation presented in Part 1 of this Chapter, the distribution of current density passing through the specimens was considered to be uniform since the material was fully carbonated, and thus homogeneous. However, in Part 2, the current density in partially carbonated specimens used in this investigation would vary at different positions within the material, due to partial difference in electrical resistivity resulting from such factors as porosity of the material and electrolyte conductance of the pore solutions. Carbonation causes a porosity reduction for normal Portland cement, since the calcium carbonate produced as a result of the carbonation reaction occupies a molar volume higher than that of hydrates (Ngala and Page 1997), and the carbonated cement pastes used in this experiment actually showed smaller values of porosity (see results in subsection 4.10.1). Carbonation also reduces the ionic concentration in the pore solution due to neutralisation of the electrolyte and the adsorption of alkali metal ions into silica gel as reported by Anstice et al. (2005). The same phenomena were observed in carbonated cement pastes in this experiment (see results in subsection 4.10.1). As for the effect of magnitude of concentration of pore solutions on their conductance, in general, conductivity (κ, reciprocal of resistivity, with the unit of S m^{-1} or Ω^{-1} m^{-1}) is approximately proportional to the concentration of the strong electrolyte (see subsection 5.8.5.2 for details) (Robinson and Stokes 1965, Bard and Faulkner 1980). Therefore, the carbonated cement pastes used in this experiment, with a smaller porosity value and with a smaller ionic concentration in the pore solutions, are estimated to have possessed higher electrical resistivity than the non-carbonated ones. The resistivity of carbonated concrete is actually significantly higher than that of non-carbonated concrete, as reported by Bertolini et al. (2004). The quantitative comparison of resistivity is to be detailed in the following mathematical modelling chapter. It can be inferred from the difference in resistivity of the two types of materials that the pattern of current flow within the partially carbonated specimens described in the form of arrows would be as illustrated in Figure 4.33, wherein the greater arrow thickness indicates higher current density. More current density is estimated to have been passed through the side columns than through the centre column, since the former material had higher conductivity than the latter material. The difference in resistivity between the centre and the side columns is considered to have caused lateral current flow between the two neighbouring columns and weakened the current flow in the upper layers (except layer-5) in the centre column as described in the aforementioned

Figure. The inferred current flow given here will be numerically confirmed in the following modelling chapter.

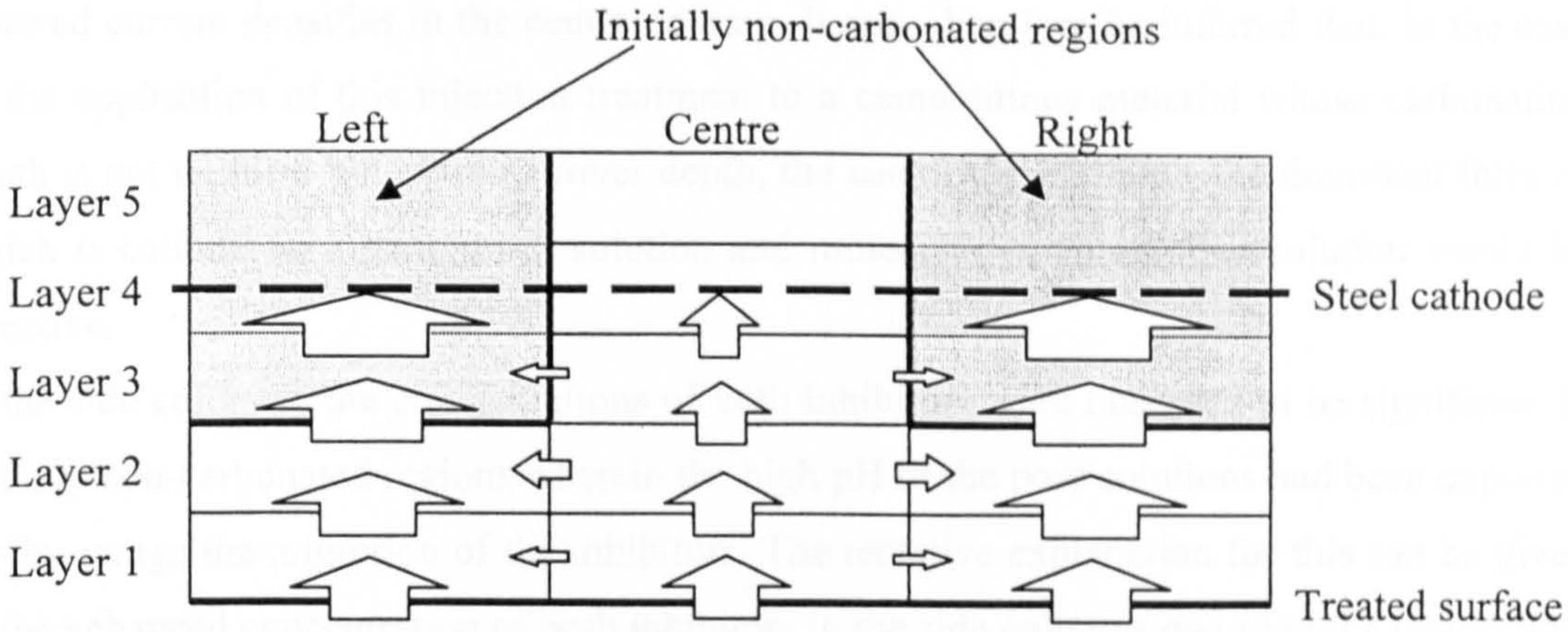

Figure 4.33 Inferred current flow in partially carbonated specimens during treatment

4.11.2.2. Transport of species between the centre and side columns

The lateral current flow from the centre column to side columns discussed in the previous subsection would cause migration of cations from the centre to the side columns and anions from the side columns to the centre column. The cation involved in this transport would be a cationic form of the inhibitor, since its concentration was significant compared to other cations in layers 1-2 of the centre column. The anion involved would be hydroxyl, which migrated downwards in the pore solutions after being generated at the cathode in the side columns by water electrolysis. Different lateral transport of species would also take place in layer 4. As discussed in subsection 4.11.1.3, the concentration gradient of sodium, potassium and cathodically generated hydroxyl ions at the interface between neighbouring columns would cause diffusive flow, conveying the three ions from the side columns to the centre column.

4.11.2.3. Organic corrosion inhibitors and other relevant ions

In the centre column, the concentration of guanidine that accumulated at the steel cathode was observed to be smaller than that recorded in the experiment presented in Part 1 of this Chapter, although the concentrations of ethanolamine at the cathode were, in both cases, similar. This can be explained by the smaller current densities substantially passed through layer 4 in the centre column, which slowed down the migration of guanidine cations, rather

than those applied to the whole specimen. On the other hand, in the ethanolamine case, the dominant form of the species penetrating towards the cathode is molecular, except near the treated surface, and thus the transport of the inhibitor was not significantly affected by the lowered current densities in the centre column. It may therefore be inferred that, in the case of the application of this injection treatment to a cementitious material whose carbonation depth is not uniform but close to cover depth, the use of the inhibitor, the dominant form of which is cationic in a neutralised solution and molecular in an alkaline solution would be effective.

In the side columns, the concentrations of both inhibitors were observed to be significant in initially non-carbonated regions wherein the high pH of the pore solutions had been expected to discourage the migration of the inhibitors. The tentative explanation for this can be given as the enhanced concentration of both inhibitors in the side columns owing to the lateral flow of both inhibitors in layers 1-3 from centre column, as discussed in the previous subsection. The inhibitors that were once highly accumulated in this region moved further towards the steel cathode by diffusion in the case of ethanolamine and by migration in the case of guanidine, by the action of higher current densities.

The lateral flow of hydroxyl in layers 1-2 from the side columns to the centre one may have affected the transport of both inhibitors in the vertical direction in the centre column. It is considered that there are two reactions that involve the hydroxyl ions flowing into this region, which are as follows:

$$RNH_3^+ + OH^- \rightarrow RNH_2 + H_2O \qquad (4\text{-F})$$

$$CaCO_3 + 2OH^- \rightarrow Ca(OH)_2 + CO_3^{2-} \qquad (4\text{-B})$$

In the case of ethanolamine, owing to its lower pK_a value (pK_a 9.5, pK_a' 9.75), the reaction (4-F) was dominant. This might account for the significant accumulation of ethanolamine in the region 5-10mm from the treated surface, which was not observed in the investigation presented in Part 1 of this Chapter. On the other hand, in the case of guanidine, since the higher pK_a value (pK_a 13.6) maintained most of the inhibitor in cationic form in the re-alkalised region, the influx of hydroxyl ions from side columns into this region led to a local increase of pH values, without reacting with inhibitor cations to deprotonate them. Instead, the enhancement of pH in this region caused precipitation of $Ca(OH)_2$ by the reaction (4-B) shown above, converting some of the hydroxyl ions to carbonate ions. This would elucidate the high pH values and significantly high carbonate concentrations in the bottom part of the centre column treated with guanidine.

The schematic views of the major transport of species within the partially carbonated specimens for ethanolamine and guanidine are shown in Figure 4.34.

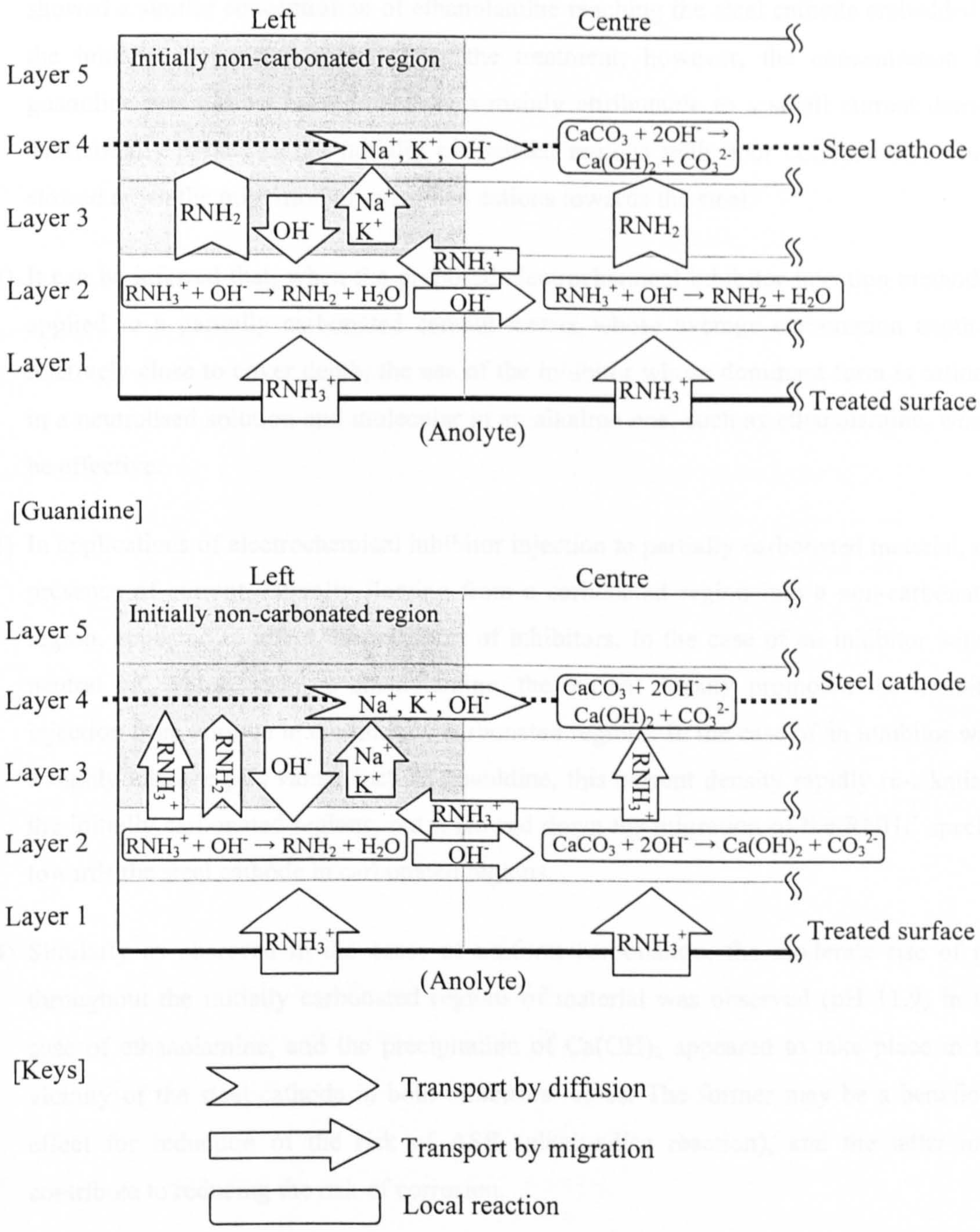

Figure 4.34 Schematic views of transport of species in partially carbonated specimens (Top: ethanolamine, bottom: guanidine)

4.12 CONCLUSIONS

(1) The two organic base corrosion inhibitors, namely ethanolamine and guanidine, were effectively injected into partially carbonated cement by similar electrochemical means to those discussed in Part 1. The comparison of the results to those obtained in Part 1 showed a similar concentration of ethanolamine reaching the steel cathode embedded in the initially carbonated region after the treatment; however, the concentration for guanidine was almost halved. This was mainly attributable to a small current density substantially passed to the initially carbonated regions with poor conductivity, which slowed down the migration of guanidine cations towards the steel.

(2) It can be inferred that, when the proposed electrochemical inhibitor injection method is applied to a partially carbonated cement matrix whose average carbonation depth is relatively close to cover depth, the use of the inhibitor whose dominant form is cationic in a neutralised solution and molecular in an alkaline one, such as ethanolamine, would be effective.

(3) In applications of electrochemical inhibitor injection to partially carbonated material, the presence of current, laterally flowing from a carbonated region into a non-carbonated region, appeared to affect the transport of inhibitors. In the case of an inhibitor with a neutral pK_a value, such as ethanolamine, the current density promoted the inhibitor injection from anolyte in the initially carbonated regions. In the case of an inhibitor with a highly alkaline pK_a value, such as guanidine, this current density rapidly re-alkalised the initially carbonated regions, but it slowed down the migration of the RNH_3^+ species towards the steel cathode in carbonated regions.

(4) Similarly as observed in the cases of uniform carbonation, the moderate rise of pH throughout the initially carbonated regions of material was observed (pH 11.9) in the case of ethanolamine, and the precipitation of $Ca(OH)_2$ appeared to take place in the vicinity of the steel cathode in both inhibitors' cases. The former may be a beneficial effect for reduction of the risk of ASR (alkali-silica reaction), and the latter may contribute to reducing the risk of corrosion.

(5) It is difficult to fully elucidate the current distribution in the material and all the processes taking place in the partially carbonated cement matrix under electrochemical treatment without resorting to mathematical modelling. In the following Chapter, further details are to be discussed with an established mathematical model.

CHAPTER 5

MATHEMATICAL MODELLING OF ELECTROCHEMICAL INJECTION OF ORGANIC CORROSION INHIBITORS

5.1 INTRODUCTION

In this chapter, a mathematical model is established for simulation of changes occurring in the pore solution phase chemistry of fully or partially carbonated hardened cement pastes when aqueous solutions of basic organic corrosion inhibitors, studied in the previous chapter, are electrochemically injected under externally applied constant current densities of varied magnitude (1-5A/m^2) and duration as described in the previous chapter. A multi-species migration model, based on the Nernst Planck equation, is used to predict the variation, as a function of depth from the concrete surface, of the quantities of the inhibitor that are electrochemically injected into the material and the nature and concentrations of the major ionic species present within the pore electrolyte. In order to elucidate the transport of basic corrosion inhibitors in carbonated cement pastes, not only the interactions of ions but also the self-interactions of inhibitor molecules need to be taken into consideration together with acid/base dissociation equilibria and the solubility products of relevant species in the pore solutions. For the three specific organic base inhibitors with widely different pK_a values, studied in the previous chapter, namely ethanolamine (pK_a 9.5), guanidine (pK_a 13.6), and arginine (pK_a 9.0), the model predictions are compared with the experimental data derived from electrochemical injection as described in the previous Chapter.

Following a literature review, this Chapter is divided into two Parts; each Part of this Chapter (Part 1 and Part 2, respectively) deals with mathematical modelling that simulates the migration of various species in the pore solutions of fully or partially carbonated material associated with electrochemical inhibitor injection, described in the corresponding Part of the previous experimental Chapter. Some of the work presented in Part 1 of this Chapter is included in the paper (Kubo et al. 2007, see Appendix G).

5.2 LITERATURE REVIEW

Several studies on the modelling of diffusion and migration of ions under an electric field have been reported, most of which are concerned with electrochemical chloride extraction. Andrade et al. (1995) calculated the duration of electrochemical chloride extraction based on the Nernst-Planck equation, for the case of constant chloride concentration in the concrete and for concentrations following the error function trend. In this study, the results obtained were compared with those of the practical treatment of a bridge deck by Elsener et al. (1993). The comparison showed the duration required to remove 99% of the chlorides was significantly shorter than that reported by Elsener. The authors thus concluded that the binding ratio of chloride ions should be considered. Later Hassanein et al (1998, 1999) modelled electrochemical chloride extraction and cathodic protection technology respectively, taking into consideration the concentration of free and bound chloride ions in the concrete. The aim of these studies was to predict the optimal time and current combination required to complete each process. In the former paper, three experimental cases carried out by other researchers (e.g. Bertolini et al. 1996) were simulated. The predicted removal of chloride ion showed good correlation with the experimental results. According to the model, electrochemical chloride removal may be approximated by a two-stage process; the initial stage involved rapid removal of free chloride ions and subsequently the process was dominated by the release rate of chlorides. In the latter research, the results derived from the model were compared to those of cathodic protection experiments using concrete specimens. It was demonstrated that the model, taking into consideration the binding ratio of chloride ions, was better than that without. In addition, this model predicted that the chloride distribution would reach a steady-state condition after four years, and the amount of chloride extracted would be limited. However these mathematical models considered the transport of only a single ionic species, namely chloride ion, in concrete.

An important issue in electrochemical migration is to understand how the various ions within the pore electrolyte phase move under the influence of an externally applied current density. Yu and Page (1996) simulated ionic migration associated with electrochemical chloride extraction from hydrated cement or concrete. Here electrostatic coupling of ions and electro-neutrality in the pore solution which contains four different ions, namely, sodium, potassium, chloride, and hydroxyl ion, were considered. The calculation results were compared with those observed experimentally (Bertolini et al. 1996) and it was found that this model overestimated the efficiency of chloride removal and the discrepancies could not be reduced

simply by changing the diffusion coefficient values. It was concluded in this study that the model may need to include the effect of ionic binding/desorption and ionic activities. As a further development of this simulation, Li and Page (1998) proposed a mathematical model for simulating electrochemical chloride extraction from concrete taking into consideration the effects of ionic concentration on diffusion and migration of charged ions. The results were then again compared with those measured in experiments (Bertolini et al. 1996) and it was found that the physical model might be much improved by considering the effects of activity coefficients and that further improvement could be achieved by taking into account other effects such as ion adsorption. Later Li and Page (2000) simulated chloride removal from concrete by the finite element method, where the adsorption and desorption of ions between the solid and liquid phases as well as electrostatic coupling of ions in a multi-component pore electrolyte were considered. This research also took into account the medium porosity and tortuosity of concrete. According to the authors, electrochemical removal could be reasonably well modelled by consideration of diffusion and migration of ions in a porous medium which allows ionic binding at the pore surface. Wang et al. (2001) conducted the same sort of mathematical modelling by means of a two-dimensional model. Truc et al. (2000) , by a numerical model based on the finite difference method, computed the concentration profiles of the chloride ion with several other relevant species in concrete under the influence of an electric field in order to demonstrate that the effective diffusion coefficient of chloride ion depends on the composition of pore solution. In their study the discrepancy was explained by the interactions with other ions and chloride binding. The method here determined the effective diffusion coefficient of chlorides with good accuracy.

No research has been found that deals with the mathematical modelling of migration of organic corrosion inhibitors under the influence of an electric field. In order to elucidate their migration in carbonated cementitious materials, it is necessary to examine the interactions of various ions in the pore solution phase, taking account of acid/base dissociation equilibria and the solubility products of relevant species, such as calcium carbonate, calcium sulphate and calcium hydroxide.

PART 1: MIGRATION OF CORROSION INHIBITORS INJECTED INTO FULLY CARBONATED MEDIUM

5.3 INTRODUCTION

In Part 1 of this Chapter, a mathematical model is established for simulation of changes in the pore solution phase chemistry of fully carbonated hardened cement paste under electrochemical injection of three organic base corrosion inhibitors with widely different pK_a values, studied in the previous chapter, namely ethanolamine (pK_a 9.5), guanidine (pK_a 13.6), and arginine (pK_a 9.0). Since it can be assumed that uniformly carbonated cement pastes have no significant spatial variation in the material properties, such as porosity or pore constituents, the mathematical modelling is based on a one-dimensional approach. For the elucidation of the migration of inhibitors in carbonated cementitious materials, it is necessary to examine the interactions of various ionic/molecular species in the pore solution phase, taking account of acid/base dissociation equilibria and the solubility products of relevant species, such as calcium carbonate, calcium sulphate and calcium hydroxide. The results derived from modelling are compared with the experimental data obtained in Part 1 of the previous Chapter.

5.4 MATHEMATICAL MODELLING

5.4.1 Transport of ions in porous media

It is well known that the transport of different ions in an ideal electrolyte can be described by the equations of mass balance, ionic flux (Nernst-Planck), current conservation and electroneutrality in one dimension as follows (Bard et al. 1980):

$$\frac{\partial C_i}{\partial t} = -\frac{\partial J_i}{\partial x} \tag{5-1}$$

$$J_i = -D_i \frac{\partial C_i}{\partial x} - z_i D_i \left(\frac{F}{RT}\frac{\partial \phi}{\partial x}\right) C_i \tag{5-2}$$

$$i = F\sum_{i=1}^{n} z_i J_i \tag{5-3}$$

$$\sum_{i=1}^{n} z_i C_i = 0 \tag{5-4}$$

where C_i is the concentration (mol/m^3), J_i is the flux (mol/m^2/s), D_i is the diffusion coefficient (m^2/s), z_i is the charge number of the ionic species i, F is the Faraday constant (9.64846×10^4 C/mol), R is the gas constant (8.3143 J/(mol K)), T is the temperature (K), ϕ is the potential (V), i is the current density applied to the pore solution (A/m^2), t is the time (s), and x is the position coordinate (m). Convection is assumed to be negligible in this model. Substituting Eq. (5-2) into (5-3), then into (5-1), we have:

$$\frac{\partial C_i}{\partial t} = \frac{\partial}{\partial x}[D_i \frac{\partial C_i}{\partial x} - z_i D_i (\frac{i/F + \sum z_i D_i \frac{\partial C_i}{\partial x}}{\sum z_i^2 D_i C_i}) C_i] \qquad (5\text{-}5)$$

Eq. (5-5) fully describes the transport behaviour of ions in an ideal electrolyte and gives the concentration profile of every ionic species for given initial and boundary conditions. The fact that electro-neutrality (Eq. (5-4)) is maintained in the case of constant externally applied current is shown by multiplying the valence numbers by Eq. (5-1) and summing both sides for all species:

$$\frac{\partial}{\partial t}\left(\sum_{i=1}^{n} z_i C_i\right) = -\frac{\partial}{\partial x}\left(\sum_{i=1}^{n} z_i J_i\right) = -\frac{1}{F}\frac{\partial i}{\partial x} = 0 \qquad (5\text{-}6)$$

For a porous medium, such as concrete or a hydrated cement paste, the porosity and tortuosity need to be taken into account, leading to the following:

$$\tau^2 \frac{\partial C_i}{\partial t} = \frac{\partial}{\partial x}[D_i \frac{\partial C_i}{\partial x} - z_i D_i (\frac{(\tau i)/(\varepsilon^{\frac{2}{3}} F) + \sum z_i D_i \frac{\partial C_i}{\partial x}}{\sum z_i^2 D_i C_i}) C_i] \qquad (5\text{-}7)$$

where τ is the tortuosity of pore structure and ε is the volume fraction of porosity.

5.4.2 Physical model

The physical system to which the above model is applied is shown in Figure. 5.1. It is assumed that an aqueous solution of the relevant corrosion inhibitor is applied to the surface of the carbonated cement paste and constant current density is passed between an anode placed in the inhibitor solution and a steel mesh cathode embedded within the cement paste. To simulate the dimensions of the specimens used in the experiments detailed in Part 1 of the previous chapter, the cover depth and the thickness of the medium behind the steel cathode

are set as x_1=34mm and x_2=16mm respectively. In this model, the species in the pore solution taken into consideration are the same (hydroxyl ion, hydrogen ion, sodium ion, potassium ion, calcium ion, inhibitor molecule/ion, carbonate ion, bicarbonate ion, carbonic acid, sulphate ion, chloride ion, and nitrate ion) as considered in the experiments described in the previous chapter except for magnesium since its concentration was insignificant. It is also assumed that, in carbonated cement pastes, the only solid phases with solubility products that have to be taken into account are calcite and gypsum; all other solid carbonation products at the surfaces of the pores (such as hydrated silica and alumina gels) are simply regarded as insoluble, non-reacting components, which have negligible influence on the pore solution composition. The tortuosity τ is assumed to be 2.0 (Li and Page 2000) and the porosity ε to be 0.34, the latter value being calculated from experimental data as described in subsection 4.5.1. The concentrations of all species in the anolyte are assumed to be uniform since the transport of ions in the external electrolyte is much faster than in the internal pore solution.

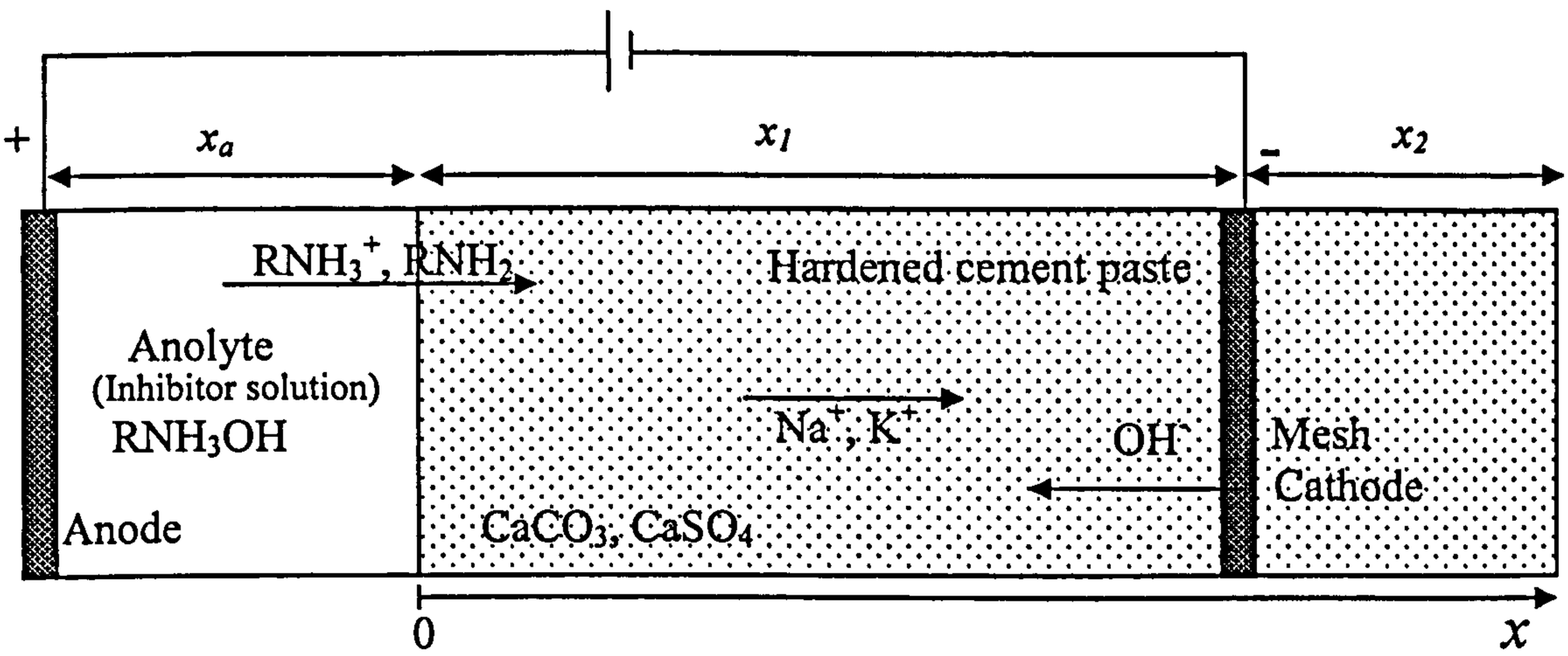

Figure 5.1 Physical model of transport in carbonated hardened cement

5.4.3 General and boundary conditions

5.4.3.1 General conditions in the pore solution

(1) General reactions

When an amine or alkanolamine-based corrosion inhibitor penetrates into an idealised carbonated cementitious material of the above type, the following chemical equilibria are assumed to be involved:

$$CaCO_3 \Leftrightarrow Ca^{2+} + CO_3^{2-} \quad (5\text{-A})$$

$$CaSO_4 \Leftrightarrow Ca^{2+} + SO_4^{2-} \quad (5\text{-B})$$

$$RNH_3^+ + OH^- \Leftrightarrow RNH_2 + H_2O \quad (5\text{-C})$$

$$HCO_3^- + OH^- \Leftrightarrow CO_3^{2-} + H_2O \quad (5\text{-D})$$

$$H_2O \Leftrightarrow H^+ + OH^- \quad (5\text{-E})$$

Since the pH of the pore solution within carbonated cementitious media is usually near 9.0 and the pK_a for the following reaction is 6.35 (Lide 2006), the concentration of carbonic acid is negligible.

$$CO_2(aq) + H_2O \Leftrightarrow HCO_3^- + H^+ \quad (5\text{-F})$$

(2) Carbamate product

In aqueous solutions, carbon dioxide reacts with alkanolamines, yielding carbamate products ($RNHCOO^-$) according to the following reaction (Blauwhoff et al. 1984). In this model, the formation of carbamate is assumed to be insignificant since the concentration of CO_2 (aq) is very low.

$$CO_2(aq) + 2RNH_2 \Leftrightarrow RNH_3^+ + RNHCOO^- \quad (5\text{-G})$$

(3) Binding of alkali ions in silica gel

It is known that sodium and potassium ions are released from cement minerals into the pore fluid during the early stage of cement hydration. In the pore solutions of non-carbonated concrete or cement, the alkali metal cations, namely sodium and potassium, are abundant and they keep a charge balance with hydroxyl ions. Longuet et al. (1973) found that not all the alkalis are in pore fluid and some sodium and potassium are bound into cement paste constituents. Taylor (1987) suggested a method for predicting alkali ion concentrations in cement pore solutions, in which all the positively charged ions are assumed to be sodium and potassium ions. He introduced a binding factor, which shows how much alkali ions are adsorbed in C-S-H and AFm phases.

Page and Vennesland (1983) found that there is no obvious increase of the two alkali ion concentrations in the pore solution of the OPC paste cured from 8-12 weeks, and for the OPC paste blended with microsilica there are continuous reductions of the concentrations in the pore solution from 1 up to 12 weeks. Glasser (1993) demonstrated that long-term carbonation of cement may reduce the Ca/Si ratio from typical non-carbonated cement, and Hong and Glasser (2000) showed decreasing Ca:Si ratio appeared to increase the overall

strength of alkali sorption into C-S-H. Brouwers and Eijk (2002) concluded that C-S-H is the only binder of alkali ions in hydrating OPC. Garrabrants et al (2004) confirmed that carbonation was observed to decrease sodium and potassium concentrations in the pore water, and the adsorption could be expressed as follows:

$$\text{C-S-H} + Na^+ + HCO_3^- \Leftrightarrow CaCO_3 + \text{Na-S(gel)} + H_2O \qquad (5\text{-H})$$

Quantitatively Anstice et al. (2005) showed a significant decrease of sodium and potassium ions in the pore solution of carbonated cement. In his research the concentration of both ions in carbonated cement was lowered to approximately between 1% and 5% of that in non-carbonated cement.

Figure.5.2 shows a concentration drop of free potassium ions associated with the reduced pH of the pore solution. The proportion of concentration of free ion in solution phase is provided by the researchers whose names appear in the Figure. This proportion was calculated with the potassium content of OPC given there as the content of K_2O and the concentration of potassium ion existing in the solution, taking into account the relationship between the porosity of the cement paste specimens and water/cement ratio given by Ngala and Page (1997). Garrabrants et al (2004) also showed that the concentration of alkali ions in the electrolyte drops sharply according to the pH reduction of the solution from 13.5 to 12.7, sodium ion being significantly reduced from 0.13mol/l to 0.009mol/l, and potassium ion from 0.18mol/l to 0.008mol/l respectively.

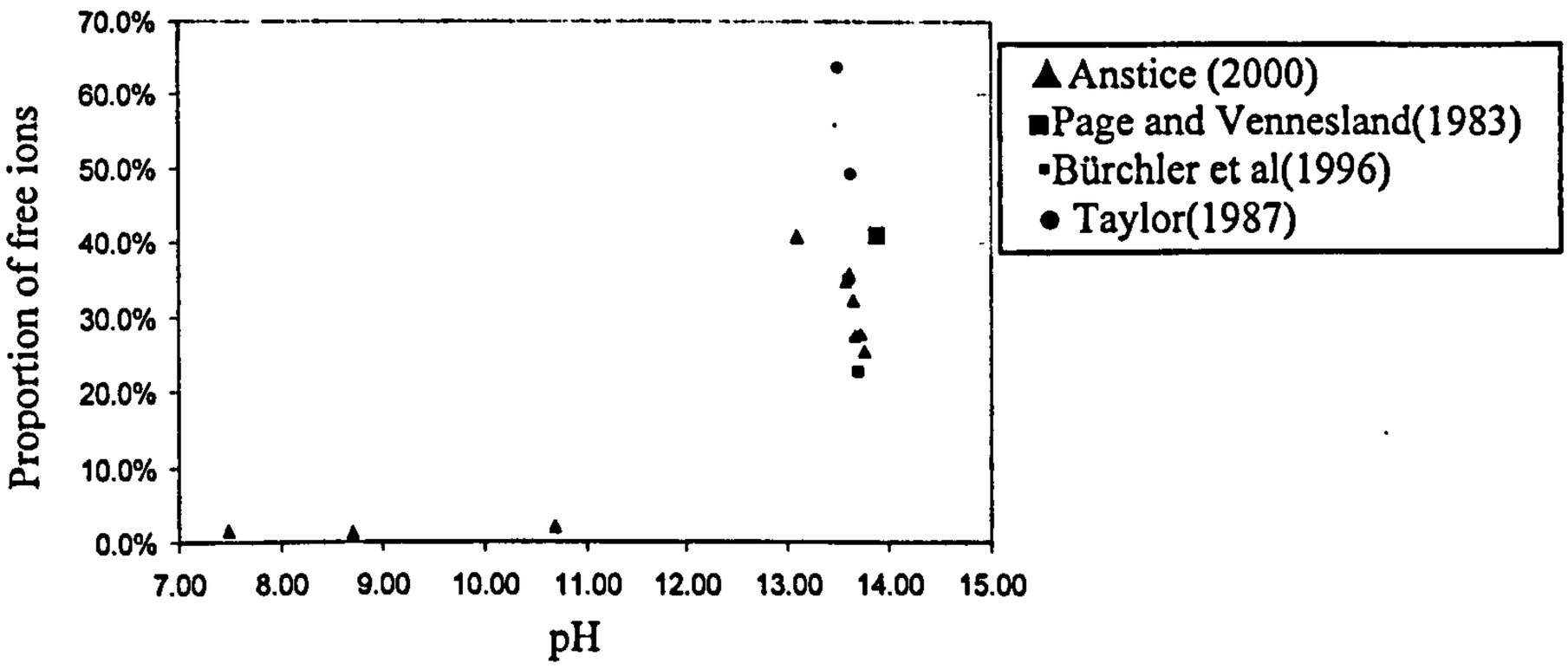

Figure 5.2 Proportion of free potassium ions in solution phase

As current is applied and the overall pH of the medium is increased, the release of these ions bound in silica gel might have to be taken into consideration. Sergi et al. (1996) applied

electrochemical re-alkalisation treatment to carbonated mortars using 2M lithium hydroxyl as an external electrolyte and monitored the concentration of sodium and potassium ions. After 5-10 days of the treatment, the mortar near steel was highly re-alkalised; however no significant increase of these two ions was seen in the vicinity of the steel. This might be interpreted as suggesting that these ions adsorbed in silica gels were not released to the re-alkalised pore solution. Thus the release of adsorbed alkali ions accompanied by the enhancement of the pH is neglected here.

(4) Binding of chloride ions in silica gel

It is believed that chloride ions are physically and chemically bound on pore surfaces within the cement matrix (Midgley and Illston 1984). The extent of chloride binding as a function of bulk concentration, usually described by a 'binding isotherm', is affected by a various parameters (Larsen 1989), such as chloride concentration or carbonation degree. Higher degree of carbonation decreases the chloride bindings and the carbonation-induced decomposition of bound chloride from solid phases, such as calcium chloro-aluminate hydrates is expressed as follows:

$$3CaO.Al_2O_3.CaCl_2.10H_2O + 3CO_2 + 3H_2O \Leftrightarrow 3CaCO_3 + 2Al(OH)_3 + CaCl_2 + 10H_2O \quad (5\text{-I})$$

As shown in section 5.2, Li and Page (2000) proposed a mathematical model simulating electrochemical chloride extraction applied to non-carbonated material taking into consideration the transient relationship between bound and free chloride concentrations. They found reasonable agreement when the modelling predictions were compared with the experimental results (Bertolini et al. 1996). This relationship is approximated by an equilibrium condition such as the Langmuir isotherm as follows:

$$S_{cl} = \frac{\alpha C_{cl}}{w(1+\beta C_{cl})} \quad (5\text{-}8)$$

where S_{cl} is the amount of bound chloride ions (mmol/g solid), C_{cl} is the concentration of chloride ions in solution (mol/l) and w is the content of water in which diffusion occurs (expressed per unit weight of cement), α and β are constants.

However, data for the binding ratio of bound chloride to free chloride with respect to pH value is unavailable. In addition, the magnitude of chloride concentration is not significant in this electrochemical treatment compared with that of injected inhibitors, thus the binding effect of chloride is neglected in this model to avoid increasing the complexity of the model unduly.

(5) General condition in the pore solution

If we consider an infinitesimal element of length, dx, as shown in Figure 5.3, the rates of change of concentration for each species i (caused by the inward and outward fluxes and the rates R_i of chemical reactions that produce species within the domain) can be expressed as follows:

$$\frac{\partial C_i}{\partial t} = \frac{J_i(x)}{dx} - \frac{J_i(x+dx)}{dx} + R_i \tag{5-9}$$

Note: R_i=0 for ions such as sodium, potassium, chloride, and nitrate that are assumed not to react chemically with other species in the domain. For these species, the time derivatives of concentration are obtained from this equation. For other species, after each R_i term is eliminated by the procedures shown in Appendix D-A, Eqs. (A1), (A2), (A5)-(A9) are obtained, which are the seven simultaneous equations to be solved to obtain time derivatives of concentration.

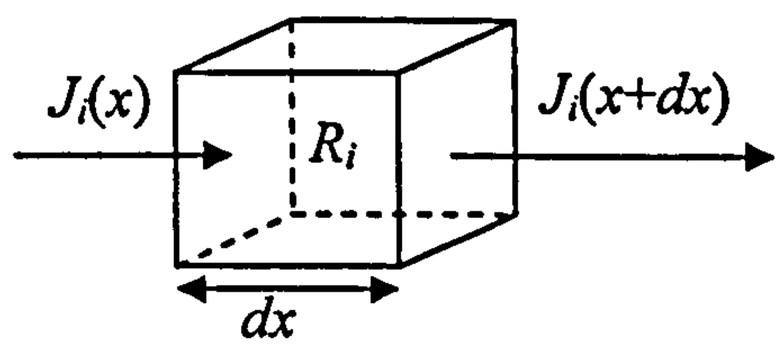

Figure 5.3 Introduced domain

5.4.3.2 Boundary conditions at the end of the specimen

Since the cement paste specimen was assumed to be wrapped with cling film to avoid moisture losses, at the end of the specimen ($x=x_1+x_2$), the flux of every species was assumed to be zero (i.e. J_i=0) in the model.

5.4.3.3 Boundary conditions at the cathode

At the steel cathode, there are two reactions generating hydroxyl ions due to water electrolysis:

$$2H_2O + 2e^- \rightarrow 2OH^- + H_2 \tag{5-J}$$

$$2H_2O + O_2 + 4e^- \rightarrow 4OH^- \tag{5-K}$$

Thus the boundary condition for hydroxyl ions at the cathode is simply expressed as follows:

$$J_{OH} = \frac{i}{z_{OH}F} = -\frac{i}{F} \tag{5-10}$$

Since (5-J) and (5-K) are the only reactions considered to take place at the cathode surface, it is assumed that the fluxes of other ion species are not affected by the existence of the steel.

5.4.3.4 Boundary conditions in the cathode region at a high pH

As shown in the previous chapter and in previous research (Anstice et al. 2005), the concentration of calcium ions present in the pore solution phase of carbonated cement pastes is typically > 20 mmol/l. Since the concentration of hydroxyl ions near the cathode is raised by reactions (5-J) and (5-K), it is to be expected that calcium hydroxide precipitation will occur locally when the concentrations of Ca^{2+} and OH^- ions exceed the solubility product for the reaction:

$$Ca^{2+} + 2OH^- \Rightarrow Ca(OH)_2 \tag{5-L}$$

After the system reaches this stage, the calcium ions consumed by reaction (5-L) are assumed to be replenished by reactions (5-A) and (5-B) so that the equilibrium saturation conditions for $CaSO_4$, $CaCO_3$ and $Ca(OH)_2$ are maintained. At the same time, in the case of arginine, the third dissociation equilibrium must be taken into account since the pK_a for the equilibrium lies in a highly alkaline region (pK_a 12.5):

$$R'NH_2COOH + OH^- \Leftrightarrow R'NH_2COO^- + H_2O \tag{5-M}$$

Thus at this stage the boundary condition must take into consideration the reactions (5-A)-(5-E), (5-L) and (5-M). In this case, for the species that are assumed to react chemically with other species in the domain, after each R_i term in Eq. (5-9) is eliminated by the procedures shown in Appendix D-B, Eqs. (A5)-(A8) and (B1)-(B4) are obtained as the eight simultaneous equations to be solved for the time derivatives of concentration.

5.4.3.5 Boundary conditions at the anolyte interface

The pH of the external anolyte is assumed to be lowered by the following two reactions taking place at the anode:

$$4OH^- \Rightarrow 2H_2O + O_2 + 4e^- \quad \text{(5-N)}$$

$$2H_2O \Rightarrow O_2 + 4H^+ + 4e^- \quad \text{(5-O)}$$

If the current density carried by each of the above reactions at the anode can be expressed as i^{OH} and i^{H} respectively, the boundary conditions for each ionic species are described as follows:

$$\left.\frac{\partial C_H}{\partial t}\right|_{x=0} = \frac{i^H/F}{x_a} - \frac{J_H^*}{x_a} + R_H^* \quad \text{(5-11)}$$

$$\left.\frac{\partial C_{OH}}{\partial t}\right|_{x=0} = -\frac{i^{OH}/F}{x_a} - \frac{J_{OH}^*}{x_a} + R_{OH}^* \quad \text{(5-12)}$$

$$\left.\frac{\partial C_i}{\partial t}\right|_{x=0} = -\frac{J_i^*}{x_a} + R_i^* \ (i \neq H \text{ and } i \neq OH) \quad \text{(5-13)}$$

where * denotes the values defined at the interface, x_a is the length of anolyte (x_a=63.6mm: derived by dividing the volume of the anolyte (120ml) by the cross section of the cement paste medium (a cylinder with a diameter of 49mm), and R_H^* and R_{OH}^* are the reaction rates of other chemical reactions at the interface involving H^+ and OH^- ions.

5.4.3.5.1 Anolyte with alkaline pH

Before the anolyte solution is neutralised by reactions (5-N) and (5-O), it is assumed that the three reactions (5-C), (5-D), (5-E) take place. For the species that are assumed to react chemically with other species in the anolyte, after each R_i term in Eqs. (5-11)-(5-13) is eliminated by the procedures shown in Appendix D-C, Eqs. (A7), (A8) and (C2)-(C4) are obtained as the five simultaneous equations to be solved for the time derivatives of concentration.

5.4.3.5.2 Anolyte with neutralised pH

As the pH value of the anolyte is lowered to the near-neutral region, but before it becomes low enough to start dissolving significant quantities of solid material from the surface of the carbonated cement paste, it is assumed that the following reactions occur as well as reaction (5-E):

$$RNH_2 + H^+ \Leftrightarrow RNH_3^+ \qquad (5\text{-C'})$$

$$CO_3^{2-} + H^+ \Leftrightarrow HCO_3^- \qquad (5\text{-D'})$$

For the species that are assumed to react chemically with other species in the anolyte, after each R_i term in Eqs. (5-11)-(5-13) is eliminated by the procedures shown in Appendix D-D, Eqs. (D1)-(D5) are obtained as the five simultaneous equations to be solved for the time derivatives of concentration.

5.4.3.5.3 Anolyte with acidic pH

The enhancement in concentration of hydrogen ion at the anode eventually causes dissolution of calcium carbonate that is assumed to be in the form of calcite from the surface of the carbonated cement paste. In this process, the following reaction is dominant under acidic conditions (pH<4) (Plummer et al. 1978):

$$CaCO_3 + H^+ \Rightarrow Ca^{2+} + HCO_3^- \qquad (5\text{-P})$$

the dissolution flux J_{Diss} being given by:

$$J_{Diss} = k_1[H^+] = k_1 C_H^* \qquad (5\text{-}14)$$

where k_1 is a dissolution rate constant. Note: J_{Diss} has a positive value if the flux goes in the negative x-direction. Therefore the boundary conditions for hydrogen, calcium, and bicarbonate are changed from Eqs.(5-11) and (5-13) as follows:

$$\left.\frac{\partial C_H}{\partial t}\right|_{x=0} = \frac{i^H/F}{x_a} - \frac{J_H^*}{x_a} - \frac{J_{Diss}}{x_a} + R_H^* = \frac{i^H/F}{x_a} - \frac{J_H^*}{x_a} - \frac{k_1 C_H^*}{x_a} + R_H^* \qquad (5\text{-}15)$$

$$\left.\frac{\partial C_{Ca}}{\partial t}\right|_{x=0} = -\frac{J_{Ca}^*}{x_a} + \frac{J_{Diss}}{x_a} = -\frac{J_{Ca}^*}{x_a} + \frac{k_1 C_H^*}{x_a} \qquad (5\text{-}16)$$

$$\left.\frac{\partial C_{HCO_3}}{\partial t}\right|_{x=0} = -\frac{J_{HCO_3}^*}{x_a} + \frac{J_{Diss}}{x_a} + R_{HCO_3}^* = -\frac{J_{HCO_3}^*}{x_a} + \frac{k_1 C_H^*}{x_a} + R_{HCO_3}^* \qquad (5\text{-}17)$$

Here the equilibrium between bicarbonate and hydrated carbon dioxide, for the equation shown below, needs to be introduced since pK_1 for the following reaction is 6.35 (Lide 2006):

$$HCO_3^- + H^+ \Leftrightarrow CO_2(aq) + H_2O \qquad (5\text{-}F')$$

At the same time, the first dissociation equilibrium must be taken into account in the case of arginine since the pK_a for the equilibrium lies in a strong acid region (pK_a 1.82) (Lide 2006):

$$R''NH_3^+NH_2 + H^+ \Leftrightarrow R''(NH_3^+)_2 \qquad (5\text{-}Q)$$

For the species that are assumed to react chemically with other species in the anolyte, after each R_i term in Eqs. (5-12), (5-13), (5-15)-(5-17) is eliminated by the procedures shown in Appendix D-E, Eqs. (D4), (D5), and (E2)-(E6) are obtained as the seven simultaneous equations whose solutions yield the time derivatives of concentration for each species. This condition is taken into account in the modelling to be described only when the pH of the anolyte is below 4.0. In this model, $k_l=1.65\times10^{-5}$ cm/s is derived from the average dissolution rate under non-stirring conditions, as reported by Brown and Glynn (2003). The generation of carbon dioxide gas accompanied by the dissolution of the surface material is mentioned later in section 5.4.5.

5.4.4 Activity coefficients

To account for the non-idealised behaviour of concentrated electrolytes, it is necessary to consider how to model the activity coefficients of the various ionic species (Davies 1962). These may be treated several ways in relation to modelling of electrochemical chloride extraction from concrete, as discussed by Li and Page (1998). A modified Davies equation (Eq. (5-18)) is used here, however, as this has been claimed to be usually fairly accurate over a range of ionic strengths up to 1,200mmol/l (Samson et al. 1999):

$$\ln\gamma_z = -\frac{Az^2\sqrt{I}}{1+Ba\sqrt{I}} + \frac{((-4.17\times10^{-5})I + C)Az^2I}{\sqrt{1000}} \qquad (5\text{-}18)$$

where γ_z is the activity coefficient for the ionic species with a charge number of z, I is the ionic strength of the solution defined by $I = 0.5\sum_{j=1}^{n} z_j^2 C_j$ (mmol/l), A and B are the Debye-Hückel constant and extended Debye-Hückel constant respectively, C is 0.2 and a is the mean radius of all ions, which is assumed to be 0.3nm in this model. The values of the equilibrium constants appearing in the previous sections are shown in Table 5.1 along with the corrections that need to be applied to them, taking into account the activity coefficients.

Whilst the activity coefficients of the ionic species referred to in Table 5.1 can be estimated by means of Eq. (5-18), those of the uncharged molecular species require further consideration. Thus the activity coefficient for hydrated carbon dioxide molecules, $CO_2(aq)$, is assumed to be 1.0 since their concentration in solution is quite low. Similarly, for guanidine solutions, the high pK_a value (13.6) implies that the proportion of guanidine existing in the molecular form is generally small enough for its activity coefficient to be assumed to be 1.0. In the case of ethanolamine or arginine solutions, however, the much lower pK_a value (9.5 for ethanolamine and 8.99 for arginine) means that the assumption would be invalid because a substantial proportion of the inhibitor exists as the molecular species in carbonated cement pore solutions. Thus for ethanolamine and arginine, a molecular activity coefficient, γ_m, must be introduced which can be incorporated into an apparent dissociation constant for the inhibitor, K_a', expressed as follows:

$$pK_a' = -\log\frac{[RNH_2]\cdot[H^+]}{[RNH_3^+]} = -\log\frac{\gamma_m\cdot[RNH_2]\cdot\gamma_1\cdot[H^+]}{\gamma_1\cdot[RNH_3^+]} + \log\gamma_m = pK_a + \log\gamma_m \quad (5\text{-}19)$$

The activity coefficient of a neutral solute in an electrolyte solution may be estimated by means of the Pitzer model (Pitzer 1987, 1991), from which the molecular activity coefficient, γ_m, of a species such as RNH_2 can be represented as follows:

$$\log\gamma_m \approx 2(\lambda_{RNH_2\cdot RNH_2}C_{RNH_2} + \sum_{i\neq RNH_2}\lambda_{RNH_2\cdot i}C_i) \quad (5\text{-}20)$$

where λ_{ij} are binary interaction parameters representing the short range interactions between the species i and j in the solution. This equation indicates that the activity coefficient is affected by the self-interaction between the inhibitor molecules and by the inhibitor molecule-ion interactions. Unfortunately, however, published λ_{ij} values relating to ethanolamine or arginine are not available. Thus, to provide some indication of the likely contributions to γ_m of the two different interactions, ethanolamine solutions at concentrations of 0.01, 0.1, 0.5 and 1.0M and arginine solutions at concentrations of 0.01, 0.1 and 0.5M were titrated against 1.0M nitric acid. The solutions also contained Na_2SO_4 at concentrations of 0.0, 0.01, and 0.05M because the two ions (Na^+ and SO_4^{2-}) are important constituents of the pore solution phase of carbonated cement pastes and they have been found to exhibit relatively large λ_{ij} values in aqueous ammonia solutions as discussed by Clegg and Brimblecombe (1989). The titration curves are shown in Figure 5.4 for the cases of 0.01M, 0.1M, 1.0M ethanolamine and 0.01M, 0.1M, 0.5M arginine without Na_2SO_4. The total number of moles was kept as 0.005 by adjusting the volume of the ethanolamine or arginine

solutions. Since the point of inflexion of a titration curve indicates the pK_a' value of the initial solution, as shown in Appendix D-H, the pK_a' values were estimated from the zero points of the second derivatives of the titration curves, the latter being interpolated with a third order polynomial function. The results obtained for pK_a' and γ_m are shown in Table 5.2, from which the molecular self-interaction appeared to be dominant and the pK_a' value was approximately constant for ethanolamine or arginine solutions at concentrations > 0.1M. For the sake of simplicity, constant pK_a' values of 9.75 and 9.30 for ethanolamine and arginine respectively were therefore assumed in the modelling. This also tends to reduce the discrepancies in charge balance that were found in the experimental data for specimens treated at a current density of $5A/m^2$ to more reasonable values.

Table 5.1 Equilibrium constants used in the model and their corrections

Species	Equilibrium constant	-log K	Corrections (K')
$R''(NH_3^+)NH_2$	$K_{a1}=\gamma_1 [R''NH_3^+ NH_2]$ $\gamma_1[H^+]/\gamma_2[R''(NH_3^+)_2]$	1.82 (Arginine)	$K_{a1}\gamma_2/\gamma_1^2$
RNH_2	$K_{a2}=\gamma_m[RNH_2]\ \gamma_1[H^+]/\ \gamma_1\ [RNH_3^+]$	9.5 (Ethanolamine) 13.6 (Guanidine) 8.99 (Arginine)	K_a/γ_m
$R'NH_2COO^-$	$K_{a3}=\gamma_1[R'NH_2COO^-]\ \gamma_1[H^+]/$ $\gamma_m\ [R'NH_2COOH]$	12.5 (Arginine)	$K_{a3}\gamma_m/\gamma_1^2$
HCO_3^-	$K_1=\gamma_1\ [HCO_3^-]\ \gamma_1\ [H^+]/[CO_2(aq)]$	6.35	K_1/γ_1^2
CO_3^{2-}	$K_2=\gamma_2\ [CO_3^{2-}]\ \gamma_1\ [H^+]/\ \gamma_1\ [HCO_3^-]$	10.33	K_2/γ_2
$CaCO_3$	$K_{s1}=\gamma_2\ [Ca^{2+}]\ \gamma_2\ [CO_3^{2-}]$	8.47	K_{s1}/γ_2^2
$CaSO_4$	$K_{s2}=\gamma_2\ [Ca^{2+}]\ \gamma_2\ [SO_4^{2-}]$	4.31	K_{s2}/γ_2^2
$Ca(OH)_2$	$K_{s3}=\gamma_2\ [Ca^{2+}]\ \gamma_1^2[OH^-]^2$	5.30	$K_{s3}/\gamma_1^2\gamma_2$
H_2O	$K_w=\gamma_1\ [H^+]\ \gamma_1\ [OH^-]$	14.0	K_w/γ_1^2

Table 5.2 pK_a' values of ethanolamine and arginine obtained from titrations

(a) Ethanolamine

Concentration of inhibitor (mole/l)	Without Na_2SO_4		0.01M Na_2SO_4		0.05M Na_2SO_4	
	pK_a'	γ_m	pK_a'	γ_m	pK_a'	γ_m
Dilute solution	9.5	1.000	-	-	-	-
0.01	9.65	1.412	9.65	1.412	9.67	1.480
0.10	9.76	1.819	9.75	1.778	9.79	1.950
0.50	9.75	1.778	9.75	1.778	9.78	1.905
1.00	9.75	1.778	9.75	1.778	9.78	1.905

(b) Arginine

Concentration of inhibitor (mole/l)	Without Na_2SO_4		0.01M Na_2SO_4		0.05M Na_2SO_4	
	pK_a'	γ_m	pK_a'	γ_m	pK_a'	γ_m
Dilute solution	8.99	1.000	-	-	-	-
0.01	9.17	1.514	9.18	1.549	9.18	1.549
0.10	9.29	1.995	9.27	1.905	9.30	2.041
0.50	9.30	2.041	9.29	1.995	9.32	2.138

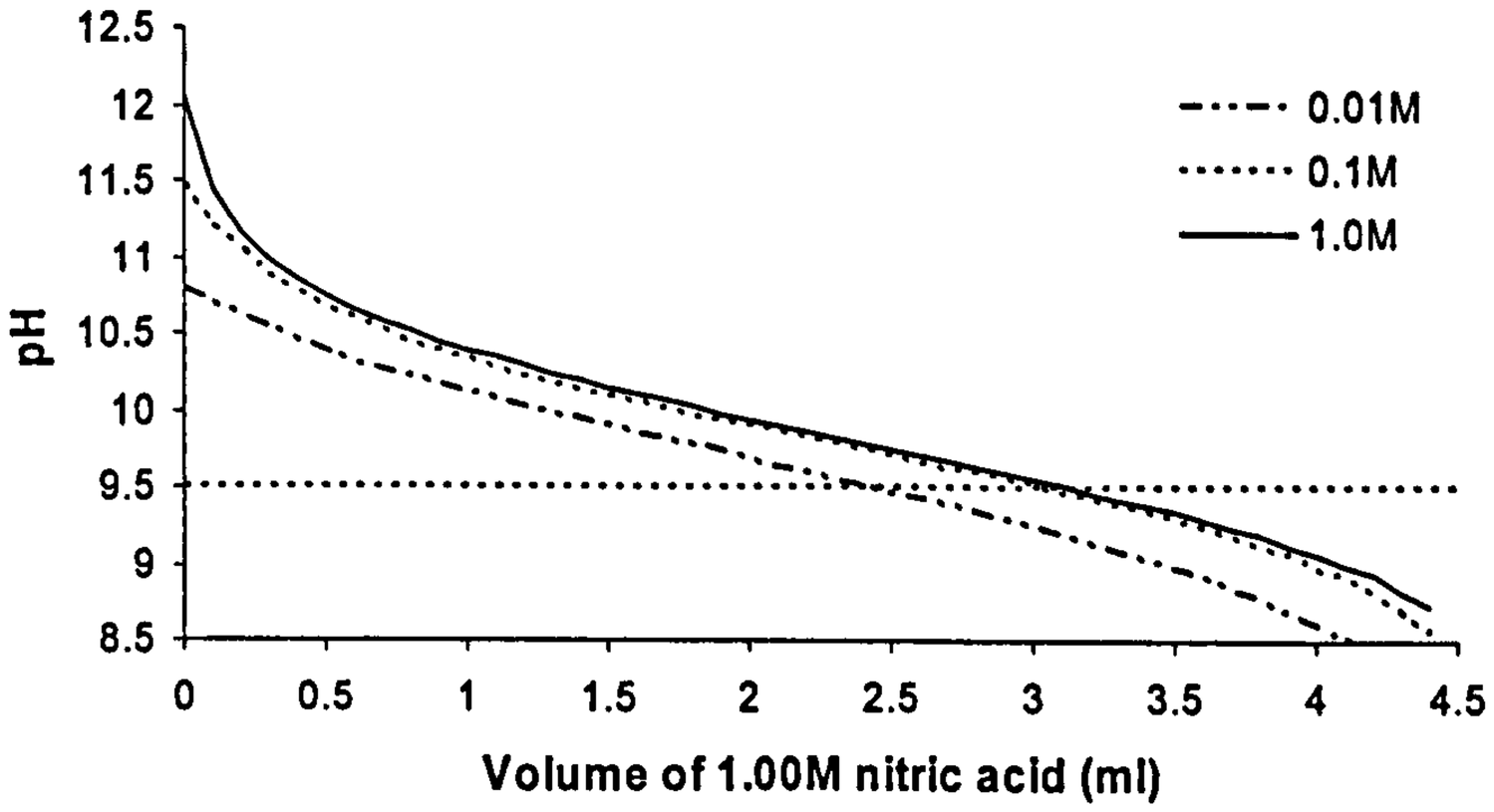

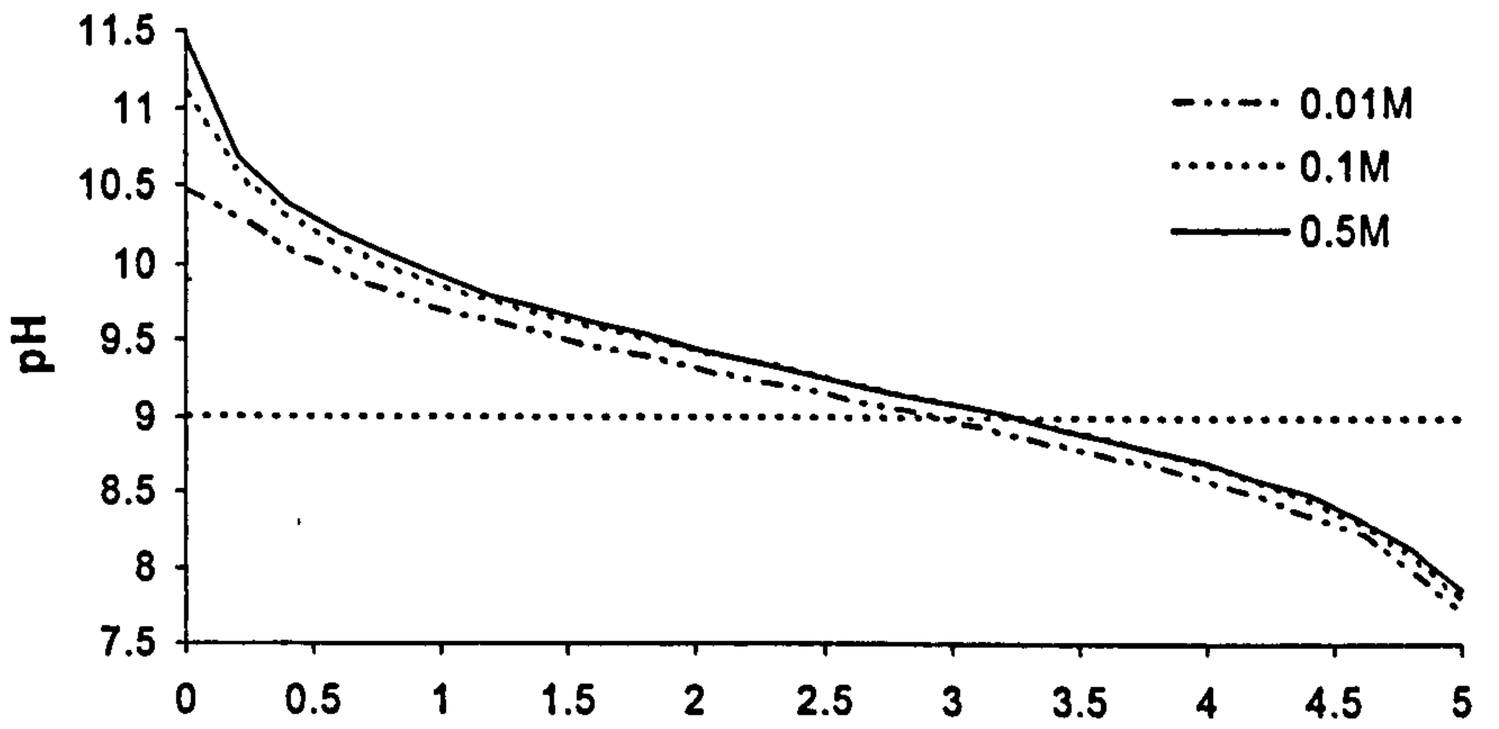

Figure 5.4 Titration curves for 0.01M, 0.1M and 1.0M ethanolamine solutions (top) and 0.01M, 0.1M and 0.5M arginine solutions (bottom) against 1.0M nitric acid

5.4.5 Application of the model

A finite difference method (Noye 1982) was used to compute the concentration profiles through the domain that is assumed to consist of infinitesimal elements with a length of dx as shown in Figure 5.3. It was also assumed that each element has a representative value at its central node, $x=x_j$, where j is the number of the discrete area, thus the concentration of the species i in a certain element j can be represented as follows:

$$C_i(x_j) \approx \int_{x_j-\frac{1}{2}dx}^{x_j+\frac{1}{2}dx} C_i(x)dx \Big/ dx \qquad (5\text{-}21)$$

For example, the first and second order derivative of the concentration with respect of x is given at the element as follows:

$$\left.\frac{\partial C_i(x)}{\partial x}\right|_{x=x_j} \approx \frac{C_i(x_{j+1}) - C_i(x_{j-1})}{2dx} \tag{5-22}$$

$$\left.\frac{\partial^2 C_i(x)}{\partial x^2}\right|_{x=x_j} \approx \frac{C_i(x_{j+1}) - 2C_i(x_j) + C_i(x_{j-1})}{dx^2} \tag{5-23}$$

The fourth order Runge Kutta method (Hundsdorfer 2003) was applied for the integration of Eq. (5-7). The system of equations was solved with a FORTRAN 95 programme (Lee 2003), the algorithm of which is described as follows:

1. The initial concentrations of each species ($C_i(x)$ at t=0) are given at each element as described in the following section.
2. Activity coefficients γ_i are calculated for each species and the values of the equilibrium constants are corrected as shown in Table 5.1.
3. The time derivatives of concentration for each species are calculated by the procedures already mentioned in the general or boundary conditions section above based on Eq. (5-9).
4. The concentrations of each species at the next time step are obtained by the integration of Eq. (5-7) at all nodes.
5. The routines of 2-4 above are repeated for the time steps required after which the final concentrations of each species are obtained.

The numbers of elements and the time steps required to obtain results with good accuracy and to ensure convergence of the numerical solutions were investigated until a stable solution was obtained (see Appendix F), from which the computations were performed with 500 elements and with a constant time step of 0.1 second for the first 10,000 loops and then a time step of 10 seconds.

When the pH of the anolyte is reduced below pH4, the generation of carbon dioxide gas may need to be taken into account. According to Henry's law, the partial pressure of carbon dioxide (P_{CO2}) is related to the concentration of (CO_2 (aq)) as follows:

$$CO_2(g) + H_2O \Leftrightarrow CO_2(aq) \tag{5-R}$$

$$K_H = [CO_2(aq)]/P_{CO_2} \tag{5-24}$$

where K_H is Henry's constant. The naturally occurring partial pressure of CO_2 (g) is $10^{-3.5}$ atm at 1atm total pressure. With $K_H=10^{-1.42}$ M/atm at 25°C (Pagenkopf 1978), the saturation concentration of CO_2 (aq) is assumed to be $10^{-4.92}$M. In the computation, after CO_2 (aq) reaches this value, the excess of this species is assumed to be converted to carbon dioxide gas due to the reaction (5-R) from the right to the left hand side. Since CO_2 (aq) is not electrically charged, this conversion does not affect the overall charge balance among the species at the interface.

5.4.6 Initial conditions

Anolyte solutions of volume 120ml containing 1.0M ethanolamine nitrate at pH 8.0 (produced by mixing equal volumes of 2M ethanolamine and 1.97M nitric acid), 0.5M guanidine carbonate (1M with respect to guanidine), and 0.5M arginine nitrate at pH 8.0 (produced by dissolving 0.5 mole arginine in 1,000ml of 0.98M nitric acid) were used, as detailed in Part 1 of Chapter 4. The assumed initial concentrations of the internal and external solutions as well as the diffusion coefficients and the charge numbers of the various ions are given in Table 5.3. The pH values and the concentrations of sodium and potassium ions in the pore solution and initial anolyte solution were based on experimental measurements recorded in Part 1 of the previous Chapter. Experimentally determined calcium and sulphate ion concentrations, which exceeded the solubility product of calcium sulphate recorded in Table 5.1, were adjusted by dilution to yield the assumed equilibrium values. The concentrations of carbonate species were then calculated from the solubility product of calcium carbonate and the other relevant equilibrium constants shown in Table 5.1. The diffusion coefficients of the each inhibitor were calculated from applying this model to diffusion specimens (0 A, 7 days) appearing in the previous Chapter, where the ionic or molecular inhibitors were assumed to have the same diffusion coefficient values.

Table 5.3 Initial conditions of species in pore and external solutions

	Charge number (z_i)	In pore solution (mole/l) [pH=9.0]	Diffusion coefficient (D_i) (m^2/s)	In external solution (mol/l)	
				Ethanolamine/ arginine nitrate [pH=8.0]	Guanidine carbonate [pH=11.74]
OH^-	-1	A) 1.00×10^{-5}	G) 5.3×10^{-10}	A) 1.00×10^{-6}	A) 5.50×10^{-3}
Na^+	+1	B) 9.00×10^{-3}	G) 2.8×10^{-11}	-	-
K^+	+1	B) 6.00×10^{-3}	G) 4.0×10^{-11}	-	-
Ca^{2+}	+2	C) 7.43×10^{-3}	G) 1.6×10^{-11}	-	-
RNH_3^+	+1	-	H) 6.0×10^{-11} (for ethanolamine) 3.0×10^{-11} (for guanidine) 5.2×10^{-11} (for arginine)	E) 9.83×10^{-1} (for ethanolamine) 4.70×10^{-1} (for arginine)	E) 9.86×10^{-1}
RNH_2	0	-	H) 6.0×10^{-11} (for ethanolamine) 3.0×10^{-11} (for guanidine) 5.2×10^{-11} (for arginine)	E) 1.75×10^{-2} (for ethanolamine) 2.97×10^{-2} (for arginine)	E) 1.36×10^{-2}
$R'NH_2COO^-$	-1	-	H) 5.2×10^{-11} (for arginine only)	-	-
CO_3^{2-}	-2	D) 6.68×10^{-7}	I) 9.2×10^{-11}	-	E) 4.81×10^{-1}
HCO_3^-	-1	E) 1.43×10^{-5}	I) 1.2×10^{-10}	-	E) 1.87×10^{-2}
$CO_2(aq)$	0	E) 3.42×10^{-8}	-	-	E) 7.61×10^{-8}
SO_4^{2-}	-2	C) 9.56×10^{-3}	I) 1.1×10^{-10}	-	-
Cl^-	-1	F) 1.07×10^{-2}	G) 1.0×10^{-10}	-	-
NO_3^-	-1	-	I) 1.9×10^{-10}	9.83×10^{-1} (for ethanolamine) 4.70×10^{-1} (for arginine)	-
H^+	+1	A) 1.00×10^{-9}	I) 9.3×10^{-10}	A) 1.00×10^{-8}	A) 1.82×10^{-12}

A): determined from pH of electrolyte

B): experimental data recorded in the previous chapter

C): calculated by adjusting experimental data taking solubility product of $CaSO_4$ into account

D): calculated from solubility product of $CaCO_3$

E): calculated from dissociation constants of relevant species at each pH

F): set to maintain charge balance

G): Li and Page (2000)

H): calculated from model applied to diffusion specimens

I): estimated by dividing diffusion coefficient of species in dilute solution (Lide 2006) by ratio of diffusion coefficient of hydroxyl ion in dilute solution (Lide 2006) to that in porous medium (Li and Page 2000).

5.5 RESULTS AND DISCUSSION

5.5.1 Organic corrosion inhibitors in the pore solution

The computed concentration profiles of the three inhibitors after treatments at $1A/m^2$ and $5A/m^2$ for 7 days are plotted in Figure 5.5 and Figure 5.6 respectively along with the corresponding experimental data. It may be seen that the results from modelling are in general agreement with those obtained from experiment, showing that all three inhibitors penetrate into the carbonated medium progressively with increase in current density and that they attain a significant concentration at the cathode (x=34mm) when a current density of $5A/m^2$ is applied for seven days. This supports the observations in the previous Chapter and confirms that the intensity and duration of the required treatment are similar to those used for electrochemical re-alkalisation of carbonated concrete claimed by Mietz (1998).

In the case of arginine, at a current density of $5A/m^2$ applied for seven days, the only major difference between the results from the modelling and the experimental data can be seen in the concentration of the inhibitor at the cathode. Unlike the case of ethanolamine and guanidine, owing to the third dissociation equilibrium (5-M) (pK_a 12.5), it was expected that when arginine cations or molecules approach the cathode with high alkalinity, some of them would be turned into anions, which would be then pushed back from the cathode region towards the material surface in the electric field. The diffusion coefficient of an inhibitor anion ($R'NH_2COO^-$) was assumed to be the same (5.2×10^{-11} m^2/s) as that of an inhibitor cation (RNH_3^+) as shown in Table 5.2; however, it might be overestimated.

The computed pH profiles and the concentration profiles of ionic and molecular species of the inhibitors are shown in Figure 5.7 and Figure 5.8 along with the values of pH obtained from experiment. In the case of ethanolamine at a current density of $5A/m^2$, it is clear that the predominant form of the inhibitor at the cathode is molecular and that the highest concentration is observed just a few millimetres from the cathode where the concentration of the inhibitor ions approaches zero. In contrast for the case of guanidine at a current density of $5A/m^2$, the peak concentration occurs at the cathode where almost half of the inhibitor exists in the cationic form. The difference in pH profiles recorded for the two inhibitors is simply due to the lower pK_a value of ethanolamine, which results in its consuming more of the migrating hydroxyl ions generated at the cathode by the following reaction:

$$RNH_3^+ + OH^- \Leftrightarrow RNH_2 + H_2O \qquad (5\text{-}C)$$

In the case of arginine at a current density of $5A/m^2$, the region near the cathode is moderately re-alkalised as is similarly observed in the ethanolamine case due to the its lower pK_a value than that of guanidine; however the mechanism of the accumulation of arginine near the cathode is more complicated. The computed concentration profiles for inhibitor ions and molecules show that at the cathode, with a pH of approximately 12.5, half of arginine is in molecular form ($R'NH_2COOH$) and the rest in anionic form ($R'NH_2COO^-$) as illustrated in Figure 5.8. Unlike the pH profile in the case of ethanolamine or guanidine, a plateau region can be seen in the pH profile of arginine between 25mm and just before the cathode. This can be explained as follows. The inhibitor anions ($R'NH_2COO^-$) near the cathode migrate towards the negative direction in the electric field, however, once they reach the region with less alkalinity, they are turned back into the molecules again by the following reaction (5-M') as shown below, leaving hydroxyl ions in this region, which in turn are consumed by the inhibitor cations to settle in this region as molecules by the equilibrium (5-C).

$$R'NH_2COO^- + H_2O \Rightarrow R'NH_2COOH + OH^- \qquad (5\text{-}M')$$

The pH values are in agreement with those obtained in the experiments in the case of the applied current density of $5A/m^2$ for all three inhibitors. However, there are some unexplained discrepancies near the cathode at the current density of $1A/m^2$.

Figure 5.9 shows the concentration evolution of the three inhibitors electrochemically injected into the cement medium during 7 days of the treatment at the current density of $5A/m^2$ calculated by means of this model. It can be seen that in all inhibitor cases, the concentration increases with the increasing duration of the treatment. In the case of guanidine, the concentration of the inhibitor at the cathode continues to increase with the peak of the concentration profiles just at the cathode. On the other hand, in the case of ethanolamine and guanidine, the peak of the concentration gradually approaches the cathode with the increasing duration of the current application. This might be because the pH value near the cathode region is slightly decreased by the accumulation of the inhibitors owing to the reaction (5-C), allowing the inhibitor in an ionic form to penetrate further towards the cathode.

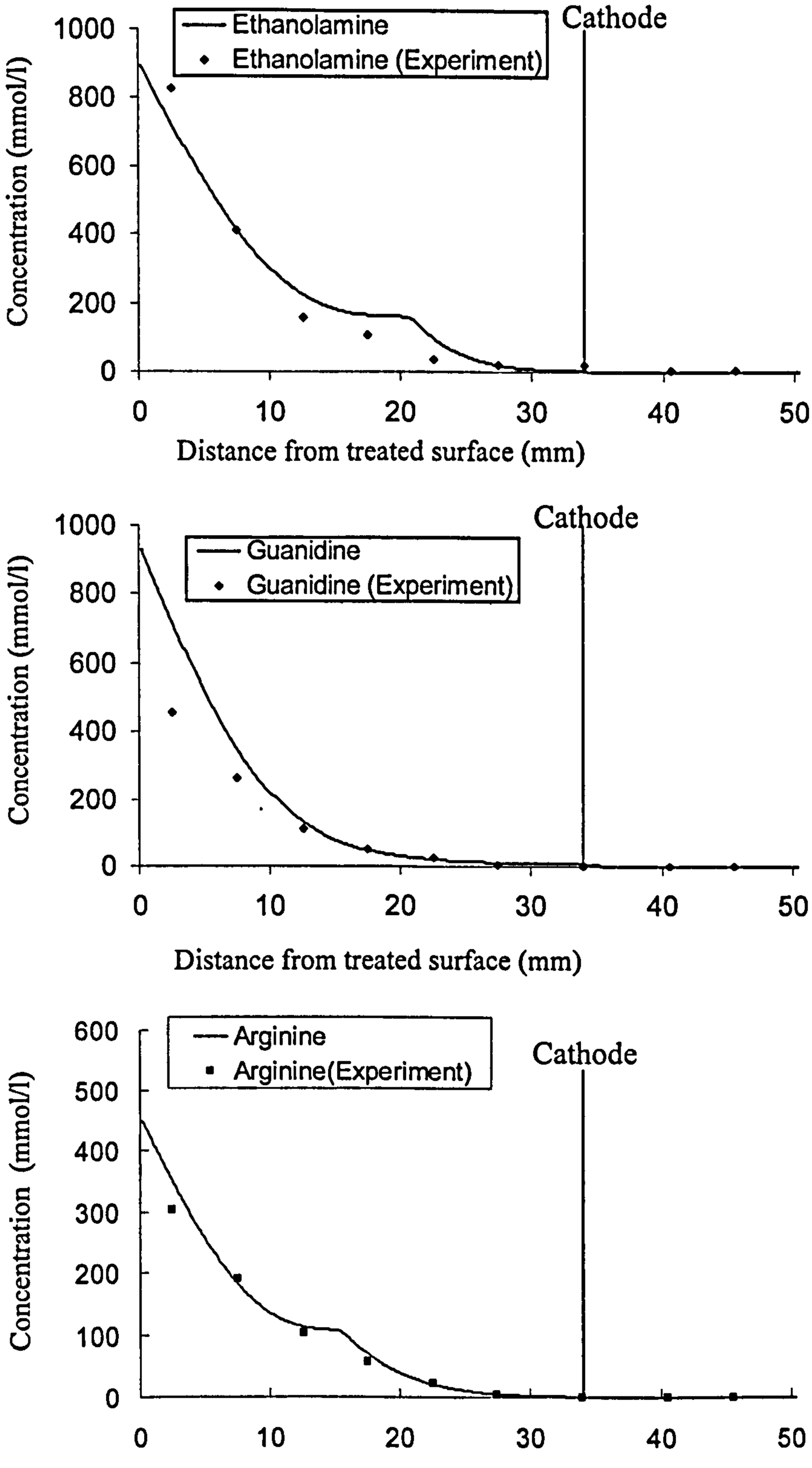

Figure 5.5. Computed and experimental concentration profiles for ethanolamine (top), guanidine (middle), and arginine (bottom) after galvanostatic treatments at 1A/m^2 applied for 7 days

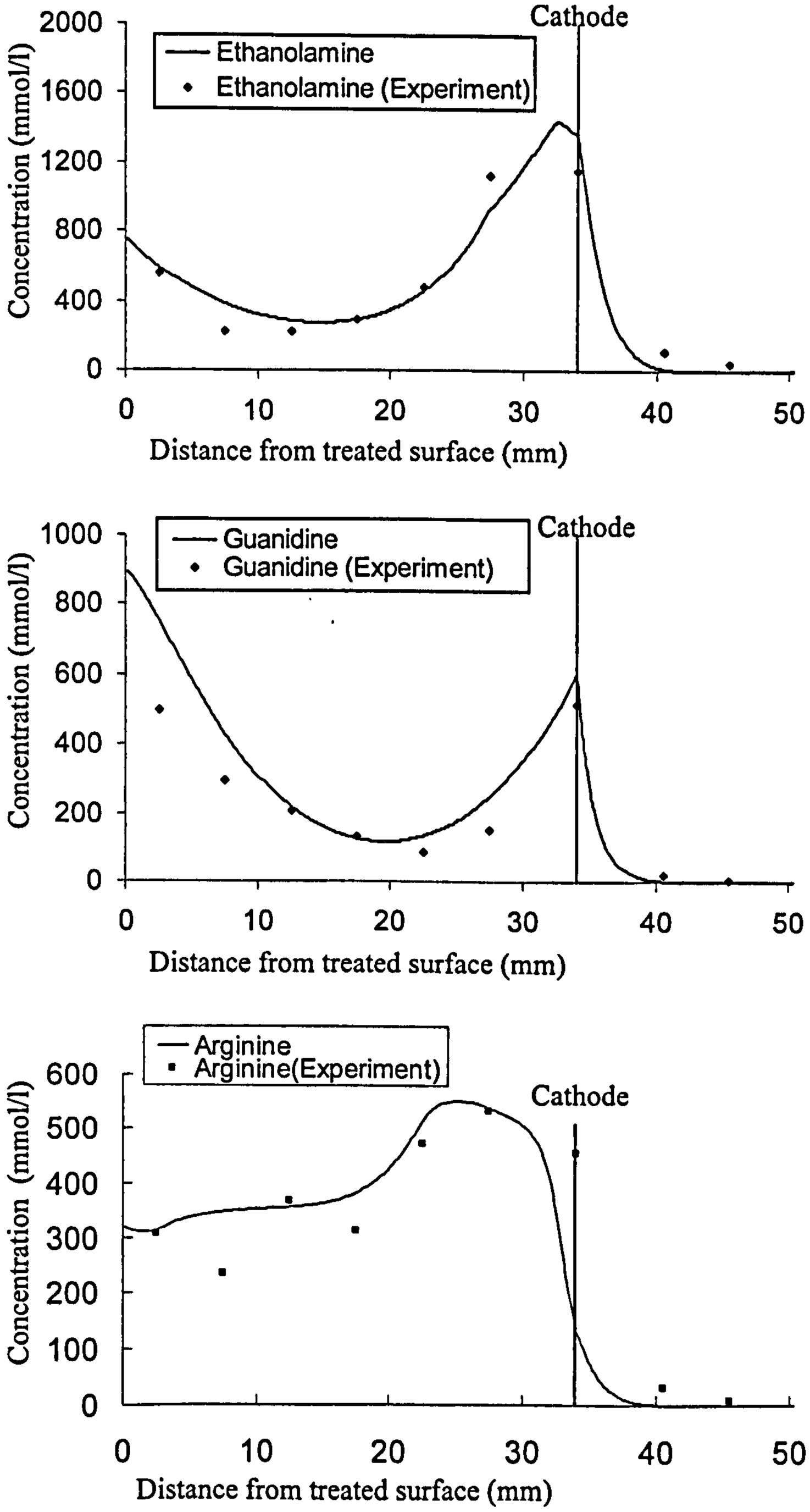

Figure 5.6. Computed and experimental concentration profiles for ethanolamine (top), guanidine (middle), and arginine (bottom) after galvanostatic treatments at 5A/m^2 applied for 7 days

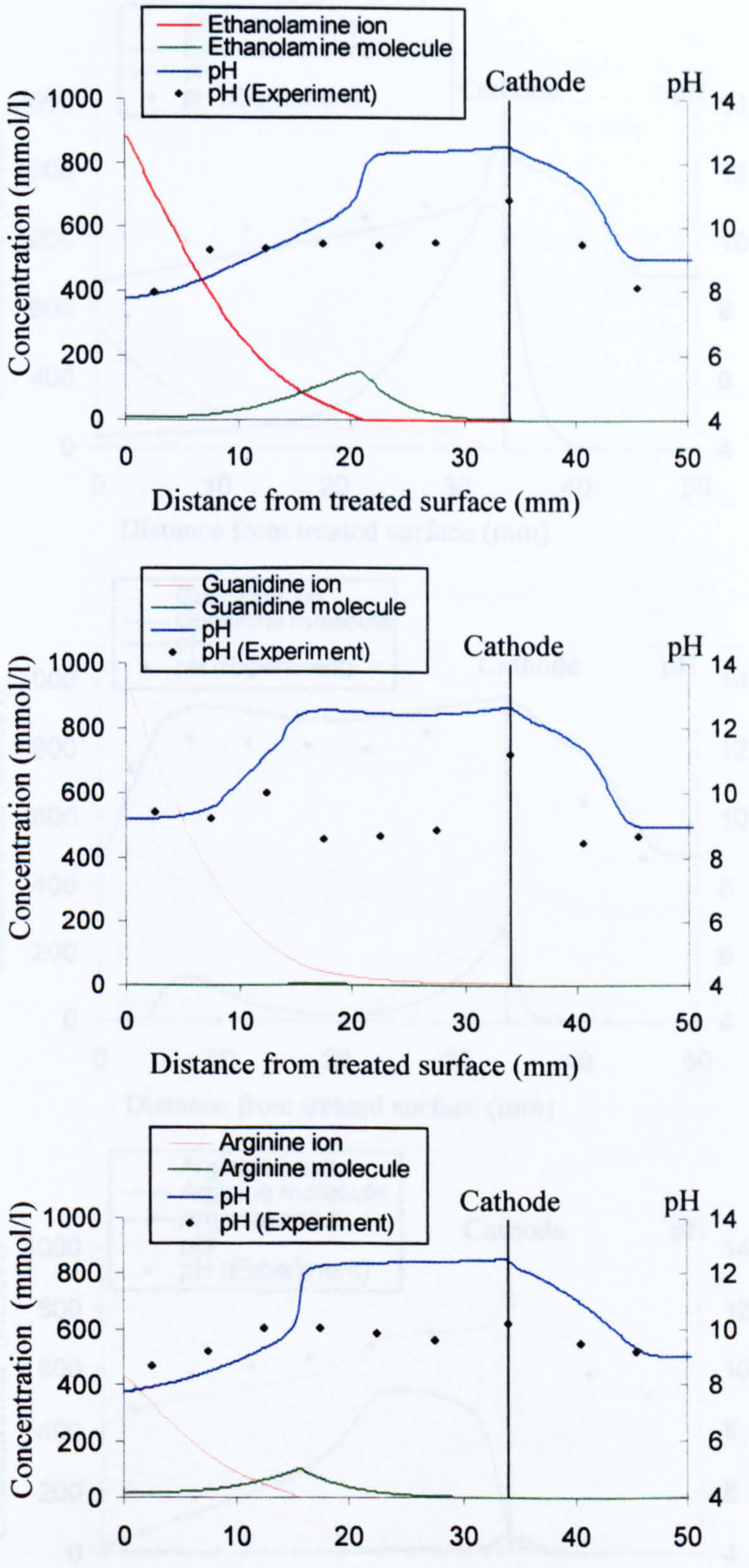

Figure 5.7. Computed and experimental pH profiles and concentration profiles for inhibitor ions and molecules after galvanostatic treatments applied for 7 days at $1A/m^2$

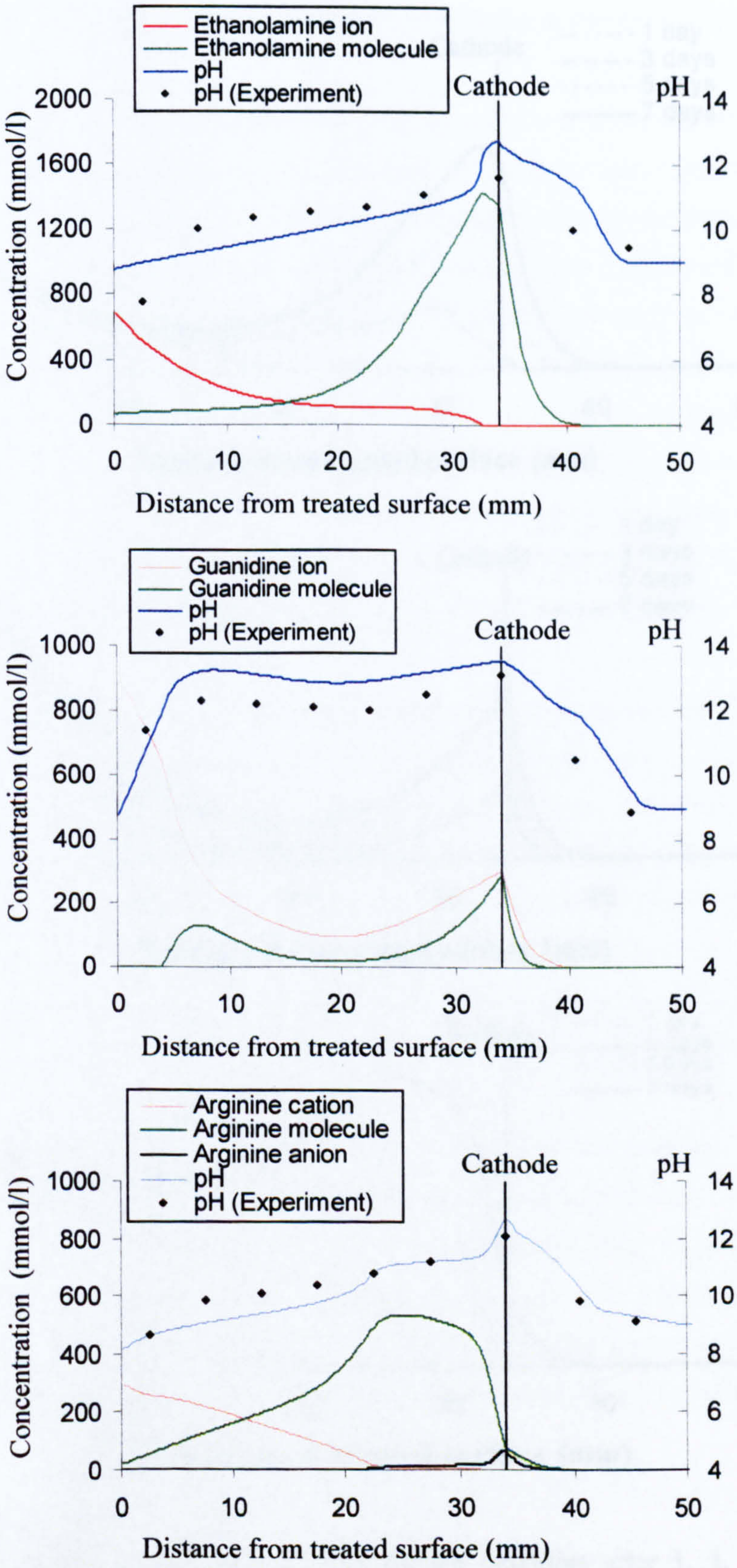

Figure 5.8. Computed and experimental pH profiles and concentration profiles for inhibitor ions and molecules after galvanostatic treatments applied for 7 days at $5A/m^2$

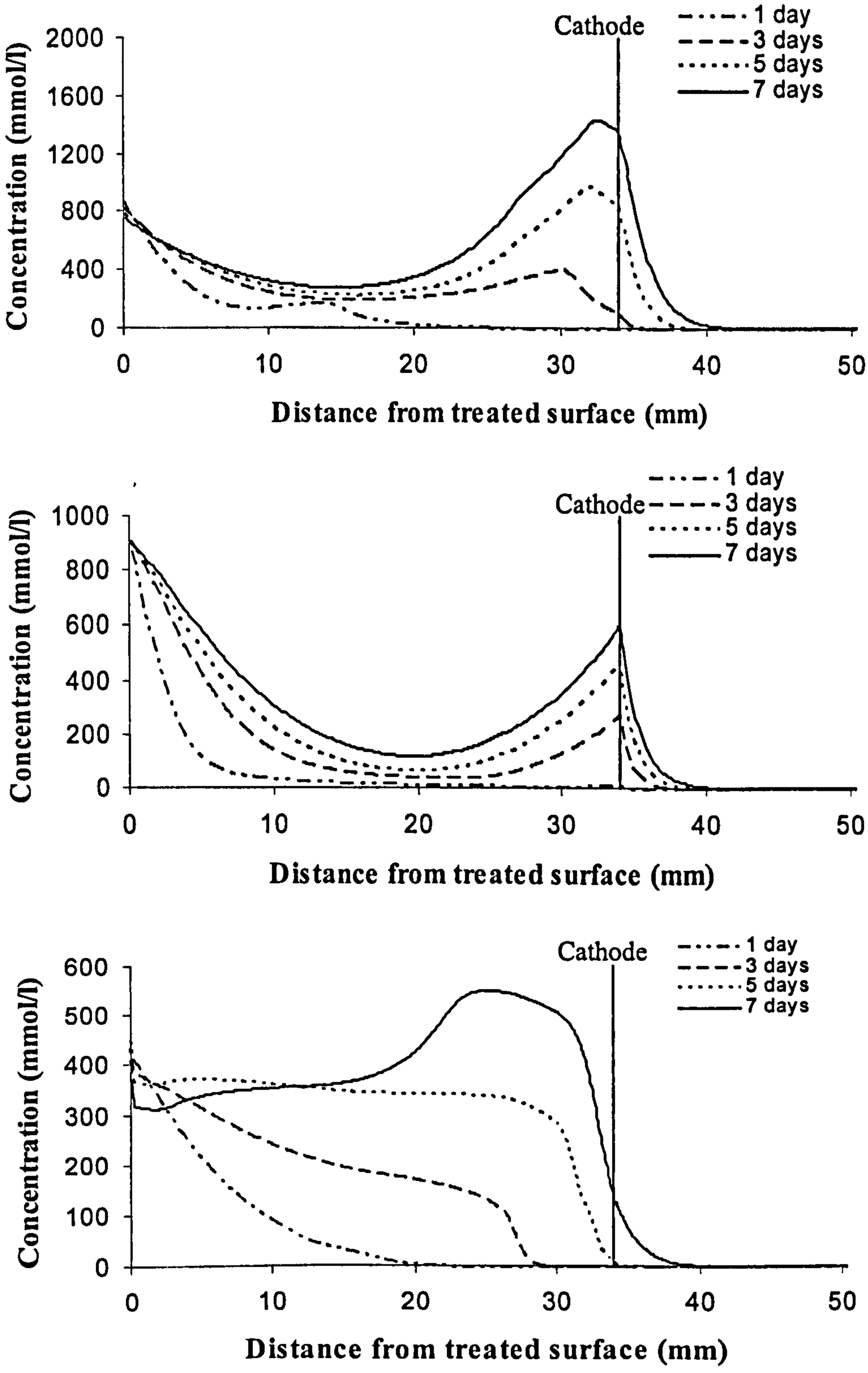

Figure 5.9. Computed concentration profiles for the inhibitors after 1, 3, 5, 7 days of galvanostatic treatments at 5A/m^2 (top: ethanolamine, middle: guanidine, bottom: arginine)

5.5.2 Organic corrosion inhibitors remaining in the anolyte

The concentrations of the inhibitors remaining in the anolyte at each current density are shown in Table 5.4 along with the concentrations of other cationic species while the concentrations of the anions are shown in Table 5.5. The reason for the substantial difference in the concentration of guanidine measured experimentally after treatment for 7 days at $5A/m^2$, compared with that predicted by the model, is unclear but might be attributable to anodic oxidation and/or evaporation losses.

The results show that the extent to which the pH reduction of the anolyte electrolytes agrees with the experimentally obtained data in the case of all three inhibitors and that the rate is more moderate in the case of guanidine compared with that in the case of other two inhibitors. This can be attributable to the buffer function of carbonate ions in the original anolyte solution (guanidine carbonate) that can be expressed by the equilibrium (5-D') (pK_a 10.33).

Although the initial pH values of ethanolamine and arginine solutions were the same (pH 8.0), the pH reduction of the anolyte solutions is slightly more moderate in the case of arginine than in the case of ethanolamine. This can be attributable to the buffer function of arginine cations concerned with the first dissociation equilibrium (5-Q) (pK_a 1.82), when the arginine single positively charged cations react with hydrogen ions to become in the form of $R"(NH_3^+)_2$. However it can be said that it does not affect the migration of the inhibitor ions towards the cathode significantly, since almost all of the inhibitor is in a cationic form, not a molecular form, thus the inhibitor can migrate in the externally applied electric field toward the cathode.

The difference in the magnitude of calcium and sulphate ion concentration in the anolyte solutions after 7 days of treatment can be seen between experimentally and numerically obtained results. This may be because that the solubility product of calcium sulphate calculated using experimentally obtained calcium and sulphate ion concentrations is much higher than the value used in this model as shown in Table 5.1. But it can be inferred that the occurrence of dissolution of the surface material can be successfully simulated by means of this model.

Table 5.4 Concentration of inhibitors and cations in anolytes after 7 days of treatment

Anolyte	Current density (A/m^2)	Method	Concentrations (mmol/l)							
			Inhibitors		Na^+	K^+	Mg^{2+}	Ca^{2+}	H^+	Sum of charge
			Total	Cationic						
1M ethanolamine nitrate	1	Modelling	912.9	912.9	0.6	0.4	-	3.6	9.7	930.8
	1	Experiment	970.8	970.8	2.1	N/D	5.7	38.5	9.5	1071.0
	5	Modelling	808.6	808.6	0.3	0.2	-	31.3	110.4	982.2
	5	Experiment	856.2	856.2	10.5	12.4	16.6	168.4	61.7	1310.7
0.5M guanidine carbonate	1	Modelling	957.6	955.1	0.3	0.2	-	0.0	0.0	955.6
	1	Experiment	912.1	912.0	3.8	N/D	3.0	2.5	0.0	926.8
	5	Modelling	922.5	922.4	0.1	0.1	-	0.0	0.0	922.7
	5	Experiment	651.1	651.1	5.0	N/D	0.0	1.5	0.0	659.0
0.5M arginine nitrate	1	Modelling	432.7	421.8 (10.1)	0.3	0.2	-	2.4	0.4	448.5
	1	Experiment	405.0	397.4 (7.6)	4.8	2.4	3.1	33.5	0.3	493.2
	5	Modelling	370.2	332.1 (46.8)	0.2	0.1	-	40.2	2.2	499.9
	5	Experiment	388.7	326.5 (62.2)	13.8	1.0	10.0	165.6	2.9	819.8

Note: the values inside ( ) denote the concentrations of $R(NH_3^+)_2$ type cations

Table 5.5 Concentration of anions in anolytes after 7 days of treatment

Anolyte	Current density (A/m^2)	Method	pH	Concentrations (mmol/l)						
				OH^-	Cl^-	SO_4^{2-}	NO_3^-	CO_3^{2-}	HCO_3^-	Sum of charge
1M ethanolamine nitrate	1	Modelling	2.01	0.0	1.8	0.7	927.4	0.0	0.0	930.8
	1	Experiment	2.01	0.0	6.5	6.9	971.9	0.0	0.0	992.3
	5	Modelling	0.96	0.0	3.2	0.1	978.8	0.0	0.0	982.2
	5	Experiment	1.21	0.0	9.8	26.8	1092.7	0.0	0.0	1156.1
0.5M guanidine carbonate	1	Modelling	10.92	0.8	1.0	52.0	-	385.1	79.7	955.6
	1	Experiment	9.7	0.1	5.6	11.1	-	284.9	299.6	897.3
	5	Modelling	9.25	0.0	2.8	181.3	-	38.8	480.0	922.7
	5	Experiment	8.8	0.0	6.6	57.0	-	23.6	516.8	684.5
0.5M arginine nitrate	1	Modelling	3.44	0.0	1.5	1.1	444.9	0.0	0.0	448.5
	1	Experiment	3.5	0.0	4.5	5.8	453.7	0.0	0.0	469.7
	5	Modelling	2.66	0.0	10.0	0.1	489.8	0.0	0.0	499.9
	5	Experiment	2.54	0.0	26.5	27.6	598.6	0.0	0.0	680.3

5.5.3 Sodium, potassium, chloride and nitrate

In this model, sodium, potassium, chloride and nitrate were not assumed to react chemically with other species in the pore electrolytes. The computed concentration profiles of sodium, potassium, and chloride are shown in Figure 5.10 together with the experimental data when the three organic corrosion inhibitors are electrochemically injected at $5A/m^2$ for seven days. The computed concentration profiles of nitrate are shown in Figure 5.11 for ethanolamine and arginine together with the experimental data.

(1) Sodium and potassium

Similarly, as was observed in the experimental results detailed in the previous chapter, the concentration profiles of sodium and potassium have a peak at the cathode (x=34mm). It is easy to elucidate this phenomenon since the two ions are positively charged and the ions in the pore solution migrate in the electric field towards the cathode where they accumulate. The initial concentrations of these two ions in the domain before the electrical treatment were assumed to be 9mmol/l and 6mmol/l respectively; however after galvanostatic treatments at $5A/m^2$ for seven days, the computed concentrations at the cathode are over 40mmol/l and 30mmol/l. Judging from the concentration profiles of the ions after the cathode, it can be seen that the electric field has no effect the movement of the ions after 40mm.

From the concentration profiles, it can be seen that the computed concentrations of the two ions are almost zero and seem to be lower than those observed in the experimental results in the region within approximately 30mm from the treated surface. This discrepancy might be attributable to the assumption of this model that the release of adsorbed alkali ions owing to the enhancement of the pH within the domain caused by the generation of hydroxyl ions at the cathode is neglected as detailed in section 5.4.3.1. However, this assumption would not affect the migration of the inhibitors significantly since the concentrations of these two alkali ions (in the magnitude of 1-10mmol/l) are small compared to those of inhibitors injected (in the magnitude of several hundred to one thousand mmol/l).

It may be interesting to discuss the difference in shape of concentration peak at the cathode for the three inhibitors studied. The profiles of both alkali ions in the case of ethanolamine and guanidine look similar, but the profiles in the case of arginine have a higher and more pointed peak than those in the case of other two inhibitors. This can be explained as follows. Since the pK_a value of arginine is lower (8.99) than that of the other two inhibitors (9.5 for ethanolamine and 13.6 for guanidine), most of the arginine species are in the form of the

molecule as shown in Figure 5.8. Therefore in the case of arginine, there are fewer positively charged ions in the domain, resulting in the necessity of more rapid migration of the two alkali ions towards the cathode to meet not only the generation of hydroxyl ions but also the accumulation of arginine anions in the highly re-alkalised region. The slight difference in shape of concentration peaks of the two alkali ions (20-34mm) between ethanolamine and arginine cases can also be explained by the difference in the concentration of total cations in this region that affects the migration rate of the above two ions.

(2) Chloride

Similarly as observed in the experimental results detailed in the previous chapter, in the case of all three inhibitors, it can be seen that chloride is extracted to the anolyte solutions by the help of the applied electric field. The initial concentrations of chloride in the domain before the electrical treatment were assumed to be approximately 11mmol/l in this model. Judging from the concentration profiles of the ions after the cathode, it can be seen that the electric field has no effect the movement of the ions after 40mm.

From the concentration profiles, it can be seen that the computed results show that almost all chloride has been extracted in the region of 10-34mm after 7 days for all three inhibitors and that the concentrations seem to be lower than those observed in the experimental results in this region. This discrepancy might be attributable to the assumption of this model that the binding of chloride ions is neglected as detailed in section 5.4.3.1, and the efficiency of chloride extraction is overestimated by this model similarly as seen in the numerical results of Yu and Page (1996) (see section 5.2). However, this assumption would not affect the migration of the inhibitors significantly since the concentration of chloride (in the range of 1-10mmol/l) is small compared to those of inhibitors injected (in the range of several hundred to one thousand mmol/l).

(3) Nitrate

As seen in Figure 5.11, the computed concentration profiles of nitrate show that the penetration of nitrate into the material becomes more restricted with increasing current density ($1A/m^2$ to $5A/m^2$), similarly as observed in the experimental results. The concentrations of the ion predicted by this model are slightly higher than those by experiments near the treated surface; however, the reason for this is unclear.

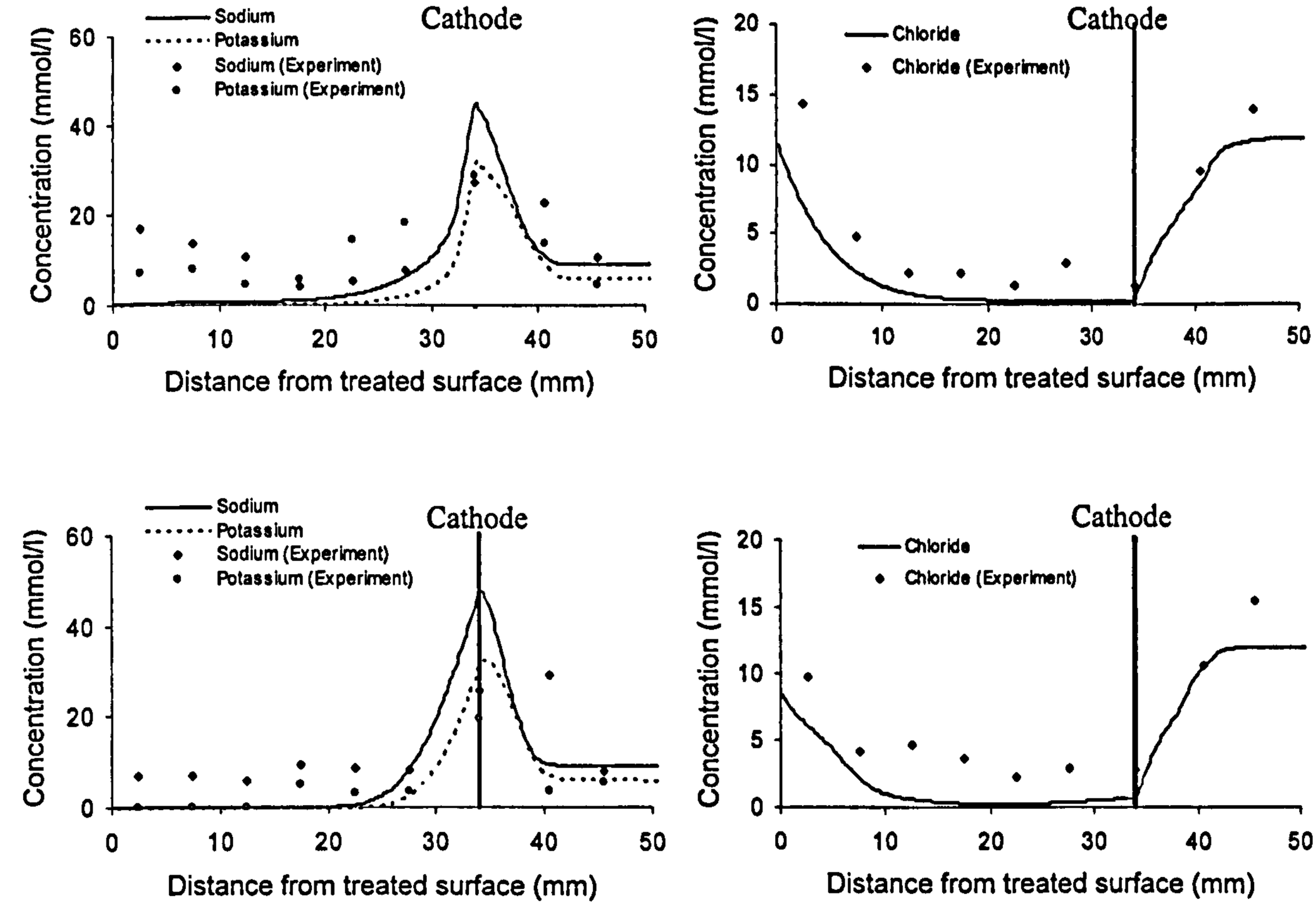

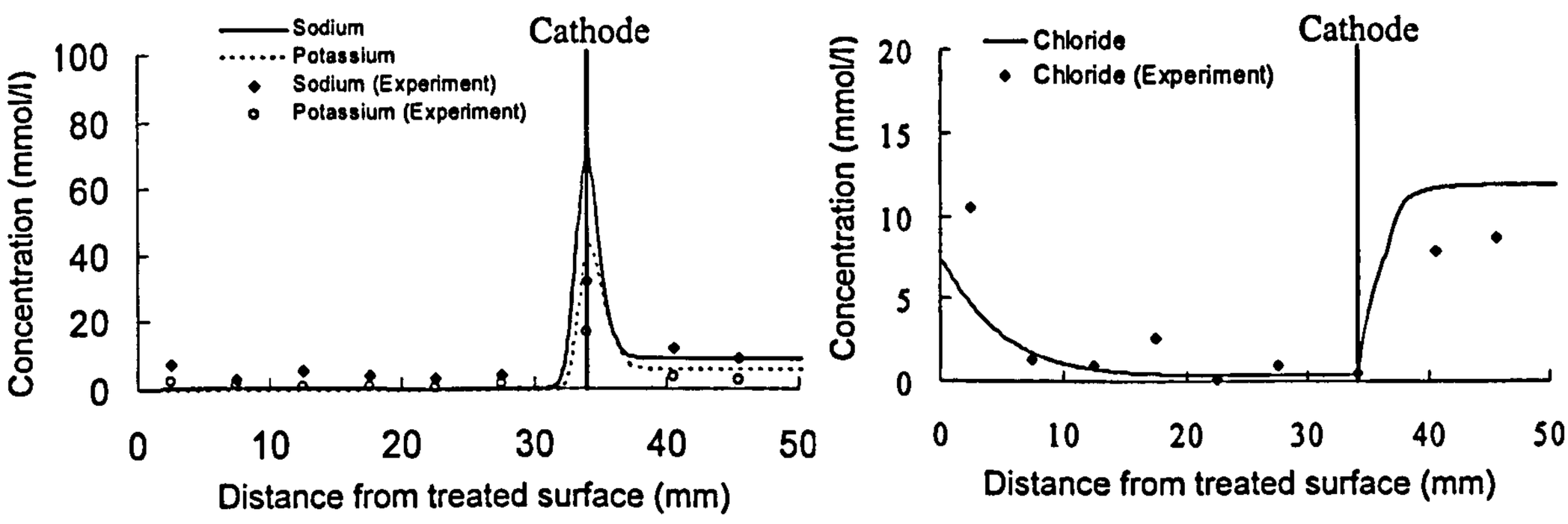

Figure 5.10. Computed concentration profiles for sodium, potassium, and chloride ions after galvanostatic treatments applied for 7 days (top:ethanolamine, middle: guanidine, bottom: arginine; left: 1A/m^2, right: 5A/m^2)

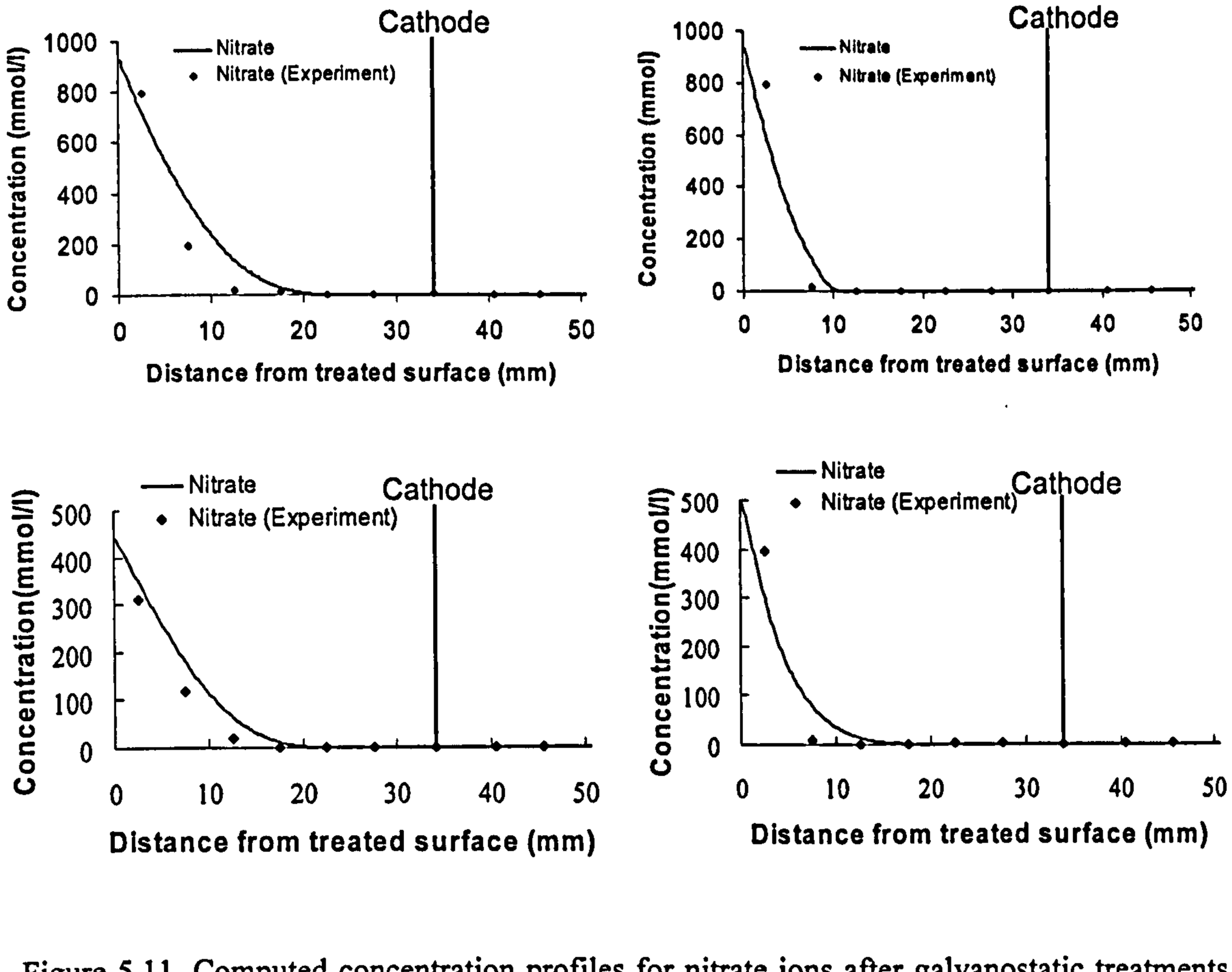

Figure 5.11. Computed concentration profiles for nitrate ions after galvanostatic treatments applied for 7 days (top: ethanolamine, bottom: arginine; left: 1A/m^2, right: 5A/m^2)

5.5.4 Effect of the solubility product of calcium carbonate

The concentration profiles of carbonate and bicarbonate ions, as well as those of sulphate, are represented in Figure 5.12 for the case of guanidine at $5A/m^2$ for 7 days. From these results, it is apparent that whilst the concentration of sulphate predicted by this model agrees with that obtained experimentally, the computed concentrations of carbonate and bicarbonate are generally about two orders of magnitude smaller than the corresponding experimental values. These discrepancies may be attributable to supersaturation of the pore solutions with calcium carbonate. If it is arbitrarily assumed that the solubility of calcium carbonate is governed by an apparent solubility product ($K'_{sl} = 3.36\times10^{-5}\ mol^2/l^2$) which is 10^4 times greater than the normal value reported in the literature ($K_{sl} = 3.36\times10^{-9}\ mol^2/l^2$) (Lide 2006), the computed concentration profiles of CO_3^{2-}, HCO_3^- and SO_4^{2-} at a current density of $5A/m^2$ in the case of guanidine are as shown in Figure 5.13. It can be seen from these results that a much better fit to the experimental data is thus obtained. In addition, a peak of carbonate concentration at the cathode that was observed in the experiments in the previous Chapter is simulated. This peak is caused by the displacement of calcium ions from $CaCO_3$ to $Ca(OH)_2$ which precipitates at the cathode owing to the high pH by the following reaction:

$$CaCO_3 + 2OH^- \Rightarrow Ca(OH)_2 + CO_3^{2-} \qquad (5\text{-}S)$$

A further significant finding here is that the large change in the assumed value for the apparent solubility product of calcium carbonate has relatively little effect on the computed concentration profiles of the inhibitors, as shown in Figure 5.14, in the case of ethanolamine and guanidine. This is because the calculated contributions to the ionic strength of CO_3^{2-}, HCO_3^- and SO_4^{2-} are almost unchanged and hence have little effect on the potential gradient in the pore solution, as defined by the following equation:

$$\frac{\partial \phi}{\partial x} = -\frac{RT}{F} \cdot \frac{i/F + \sum z_i D_i \partial C_i / \partial x}{\sum z_i^2 D_i C_i} \qquad (5\text{-}25)$$

Thus changes in the assumed value of the solubility product of calcium carbonate have little influence on the concentration of other ions involved.

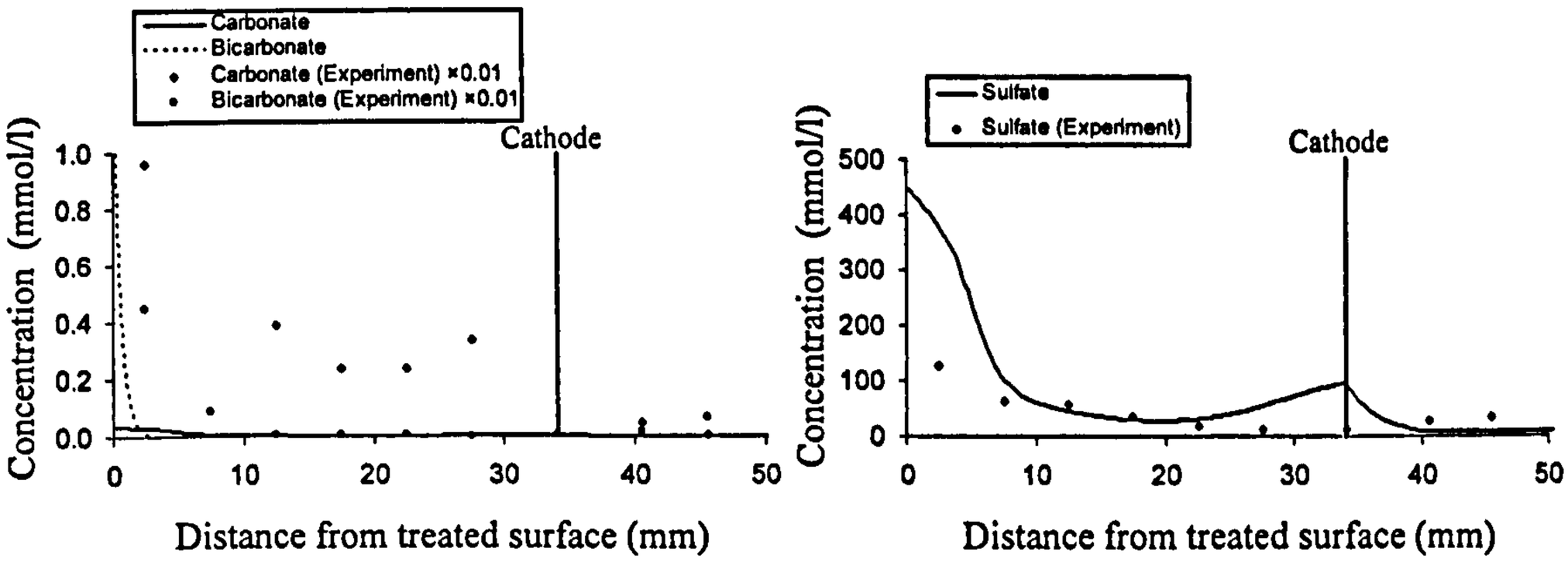

Figure 5.12. Computed concentration profiles of carbonate, bicarbonate and sulphate ions after guanidine treatment at 5A/m^2 for 7 days (left: carbonate and bicarbonate, right: sulphate)

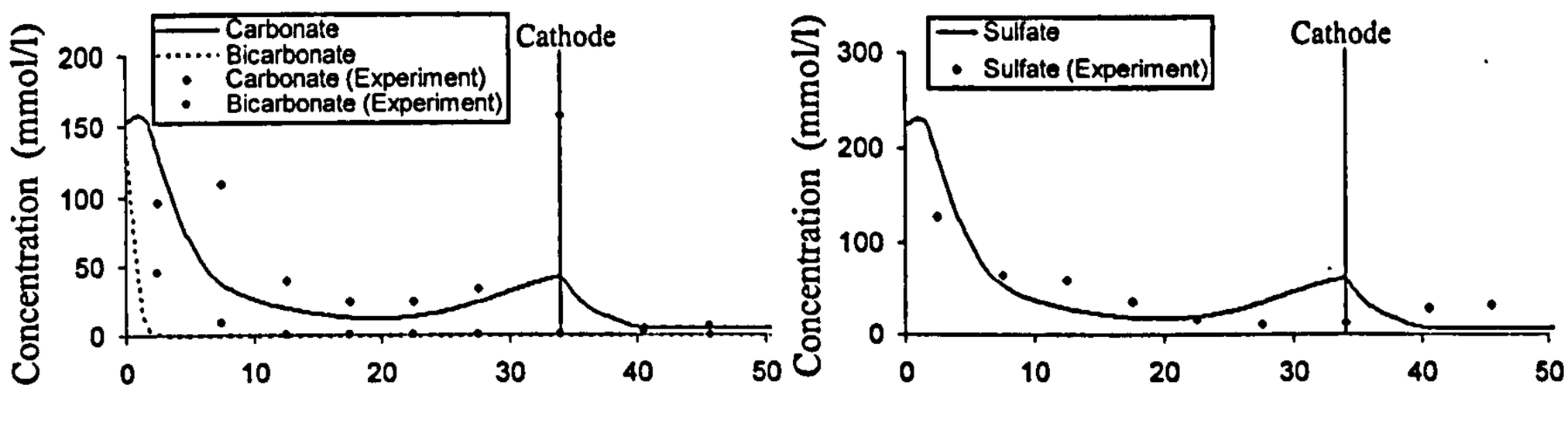

Figure 5.13. Computed concentration profiles of carbonate, bicarbonate and sulphate ions, assuming 3.36×10^{-5} mol^2/l^2 as solubility product of calcium carbonate, after guanidine treatment at 5A/m^2 for 7 days (left: carbonate and bicarbonate, right: sulphate)

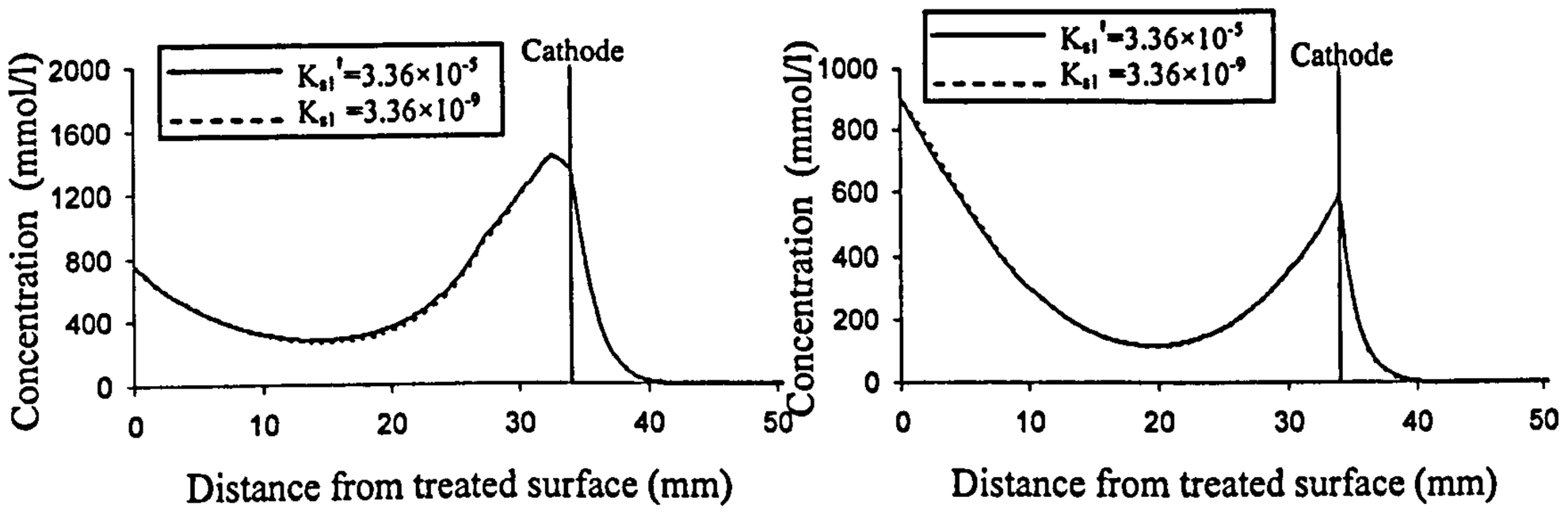

Figure 5.14. Computed concentration profiles of inhibitors, assuming 3.36×10^{-5} mol^2/l^2 as solubility product of calcium carbonate after guanidine treatment at 5A/m^2 for 7 days (left: carbonate and bicarbonate, right: sulphate)

5.5.5 Environment near the cathode

Figure 5.15 shows the computed changes in pH at the cathode at a current density of 5A/m^2 for the three inhibitors, together with the result of similar computations made, for the case of guanidine, without taking into consideration the precipitation of calcium hydroxide at the cathode. It is clear that the pH of the initially near-neutral pore solution (pH 9.0) is raised at almost the same rate to just over 12.5 at the cathode during the first day of treatment in all four cases. Thereafter, for ethanolamine and arginine, the pH value tends to decrease slowly owing to the consumption of hydroxyl ions that occurs when the inhibitor arrives in the vicinity of the steel. In contrast, for guanidine, the pH progressively rises towards about 13.5 if calcium hydroxide precipitation is considered and to somewhat higher values if this process is not taken into account. This implies that, in the cases of the three inhibitors, calcium hydroxide precipitated at the cathode functions as a buffer of moderate alkalinity. This may be considered a beneficial phenomenon, providing enhanced corrosion protection to the steel, as discussed in the previous Chapter.

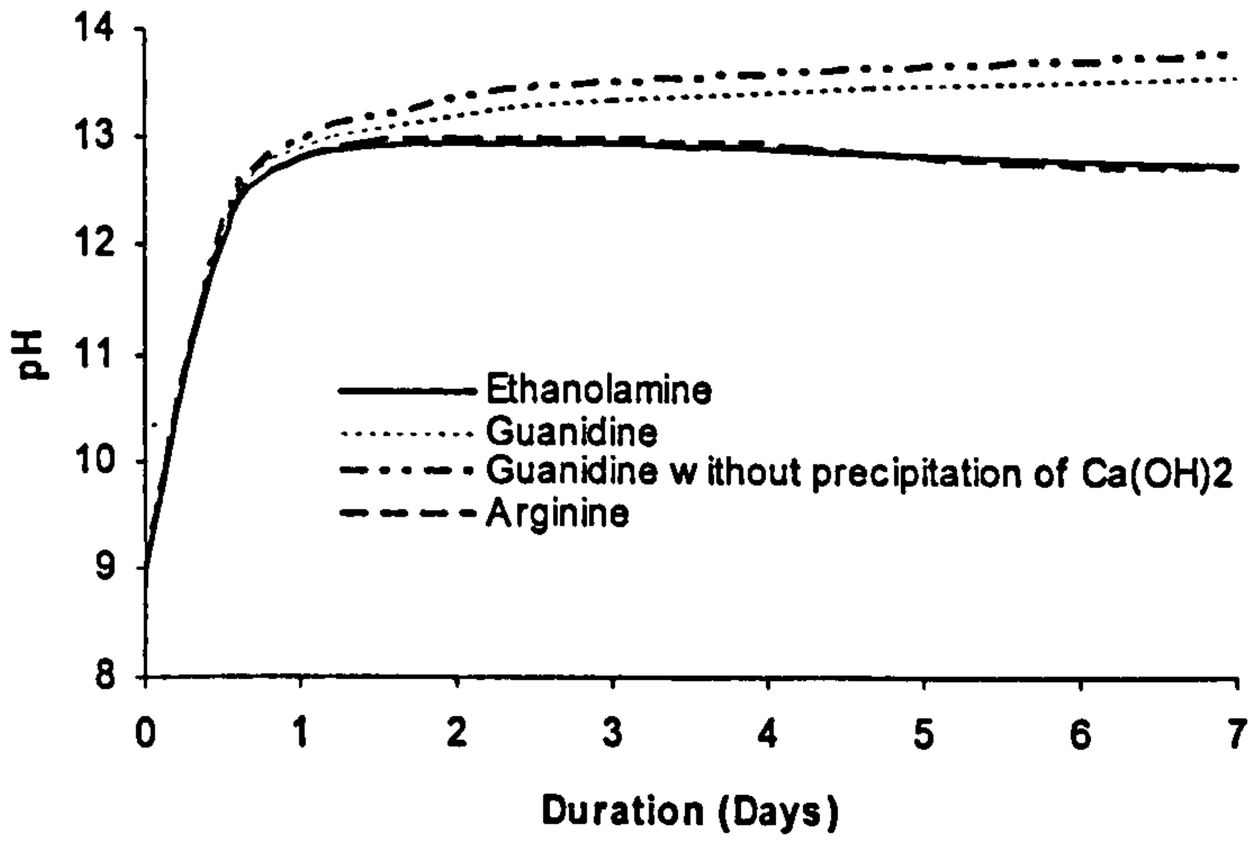

Figure 5.15 Evolution of pH at cathode at current density of 5A/m^2 for three inhibitors and, for guanidine, without considering precipitation of calcium hydroxide

5.5.6 Effect of molecular interactions

As noted in section 5.4.4, in the case of ethanolamine and arginine, the effects of molecular interactions cannot be ignored but may be simply offset by replacing the thermodynamic pK_a value (9.5 for ethanolamine, and 8.99 for arginine) with a higher apparent pK_a' value (9.75 for ethanolamine, and 9.30 for arginine). The concentration profiles of ethanolamine and arginine calculated with and without consideration of molecular interactions are shown in Figure 5.16 from which it appears that the use of the pK_a' value results in a somewhat better fit to the experimental data.

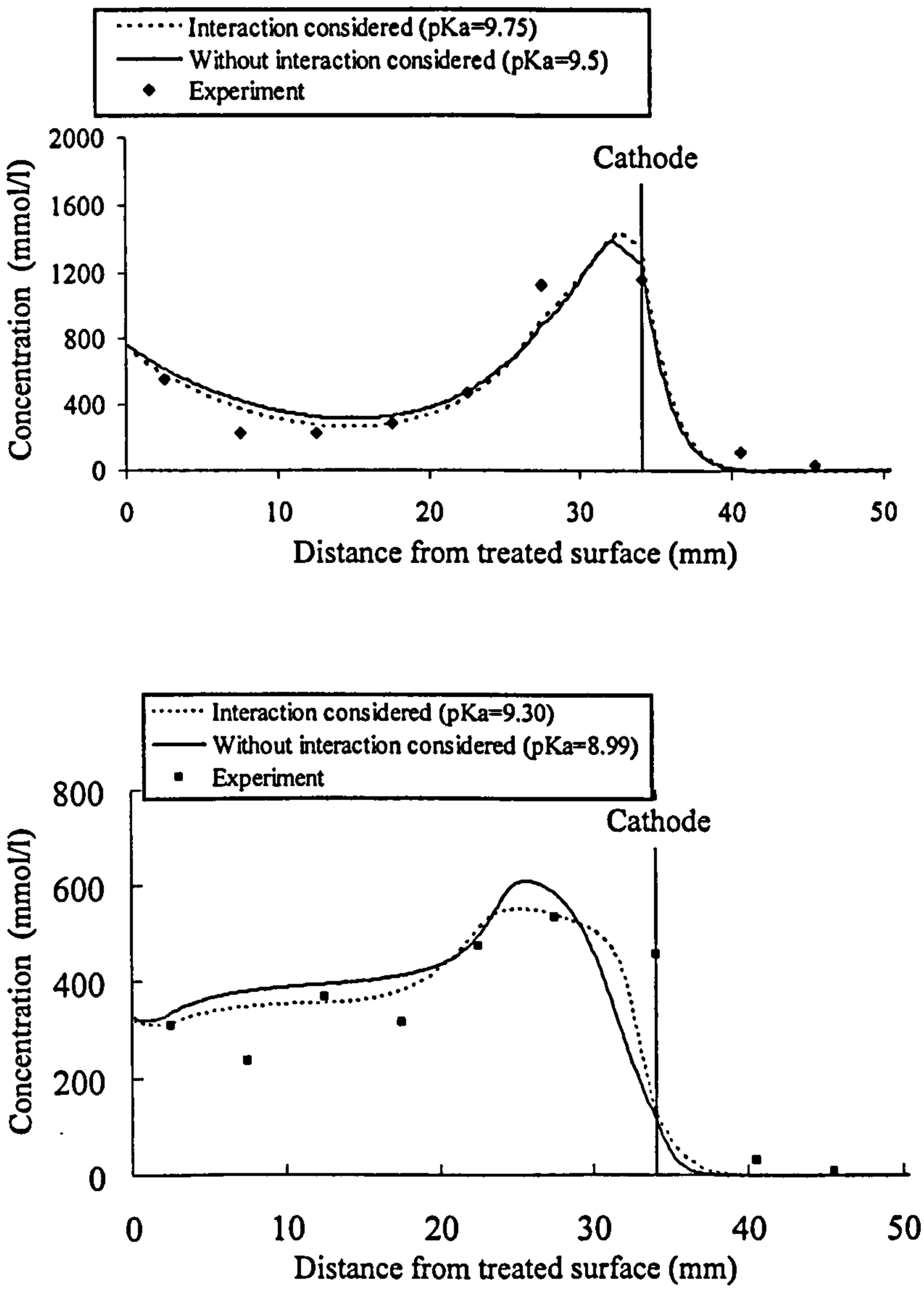

Figure 5.16 Computed concentration profile of ethanolamine (top) and arginine (bottom) with and without consideration of molecular activity coefficient.

5.6 CONCLUSIONS

The main conclusions of this part of the investigations may be summarised as follows.

(1) The proposed model yields reasonable general agreement with experimentally determined concentration profiles for three organic base inhibitors of widely varying pK_a values that were subjected to electrochemical injection into carbonated cement paste.

(2) In the cases of ethanolamine (pK_a 9.5) and arginine (pK_a 8.99), improved agreement between modelling and experiment was obtained when molecular interactions were represented by the introduction of an activity coefficient, γ_m, which raised the apparent pK_a' value of the inhibitor to 9.75 (ethanolamine) and 9.30 (arginine) respectively; for guanidine (pK_a 13.6), no such modification was required.

(3) In the cases of all three inhibitor injection treatments, calcium hydroxide precipitation at the cathode was shown to affect the evolution of pH in the vicinity of the embedded steel as a function of current density and time, the precipitated calcium hydroxide functioning as a buffer of moderate alkalinity.

(4) To obtain reasonable correspondence between modelling predictions and experimental concentration profiles determined for carbonate, bicarbonate and sulphate ions, it was necessary to assume a much larger apparent solubility product for calcium carbonate than that reported in the literature; this had only minor influence on the computed concentration profiles of the two corrosion inhibitors. In addition a peak of carbonate concentration at the cathode that was observed in the experiments is simulated by this modification of solubility product value.

(5) In the case of arginine at a current density of $5A/m^2$ applied for 7 days, difference in the concentration of the inhibitor at the cathode can be seen between in the model prediction results and the experimental data. This can be attributable to the third dissociation equilibrium (pK_a 12.5) of arginine and the diffusion coefficient of the inhibitor anion ($R'NH_2COO^-$) needs to be carefully determined.

(6) The concentrations of inhibitor cations that migrate towards the cathode in the pore solutions significantly affect the migration rates of other cations, viz. sodium and

potassium. The consideration of decomposition of adsorbed alkali ions, namely sodium and potassium in C-S-H gel and binding of chloride ions in C-S-H gel might improve the computed results, however the discrepancies are negligible compared to the concentrations of inhibitor species injected in the material.

(7) Further development of the model described may lead to improved understanding of the rates of dispersion of electrochemically injected corrosion inhibitors on cessation of treatments of the sort employed in this research; this should allow the long-term effectiveness of the corrosion inhibition conferred on embedded steel to be predicted quantitatively. The work on this is presented in the following Chapter (Chapter 6).

PART 2: MIGRATION OF CORROSION INHIBITORS INJECTED INTO PARTIALLY CARBONATED MEDIUM

5.7 INTRODUCTION

In Part 1 of this Chapter, it was confirmed that the proposed one-dimensional multi-species migration model could reasonably simulate the electrochemical injection of the three organic base corrosion inhibitors, studied in this thesis, into fully carbonated material. In Part 2 of this Chapter, for simulation of electrochemical injection of inhibitors into partially carbonated material, the mathematical model established in Part 1 of this Chapter is developed into a two-dimensional model, in which the spatial difference in material properties, such as porosity, is taken into consideration. The effect of partial carbonation of the material on the migration of inhibitors or other relevant species existing in the pore solution phase is investigated, taking account of the non-uniform distribution of the applied current densities within the material that may arise from the spatial difference in material properties as discussed in the previous Chapter. The results derived from modelling are compared with the experimental data obtained in Part 2 of the previous Chapter for the two inhibitors, namely ethanolamine and guanidine.

5.8 MATHEMATICAL MODELLING

5.8.1 Transport of ions in porous media

In a two-dimensional model, the equations of mass balance, ionic flux, current conservation and electroneutrality discussed in subsection 5.3.1 can be described for the transport of different ions in an ideal electrolyte as follows (Bard et al. 1980):

$$\frac{\partial C_i}{\partial t} = -\nabla \cdot J_i \tag{5-26}$$

$$J_i = -D_i \nabla C_i - z_i D_i (\frac{F}{RT} \nabla \phi) C_i \tag{5-27}$$

$$i = F \sum_{i=1}^{n} z_i J_i \tag{5-28}$$

$$\sum_{i=1}^{n} z_i C_i = 0 \tag{5-29}$$

where ∇ is a differential operator defined as $\nabla = \left[\frac{\partial}{\partial x}, \frac{\partial}{\partial z}\right]$, acting on scalar fields and vector fields to express the gradient and divergence of the fields, respectively. From the above three equations, similarly as derived in Part 1, the full transport behaviour of ions in an ideal electrolyte can be expressed as follows:

$$\frac{\partial C_i}{\partial t} = \nabla \cdot [D_i \nabla C_i - z_i D_i (\frac{i/F + \sum z_i D_i \nabla C_i}{\sum z_i^2 D_i C_i}) C_i] \tag{5-30}$$

Since there is no divergence of the current in the material, the current density satisfies the following equation:

$$\nabla \cdot i = 0 \tag{5-31}$$

Thus, the fact that electro-neutrality (Eq. (5-29)) is maintained is shown by multiplying the valence numbers by Eq. (5-26) and summing both sides for all species:

$$\frac{\partial}{\partial t}\left(\sum_{i=1}^{n} z_i C_i\right) = -\nabla \cdot \left(\sum_{i=1}^{n} z_i J_i\right) = -\frac{1}{F} \nabla \cdot i = 0 \tag{5-32}$$

When porosity and tortuosity are taken into consideration for a porous medium, the above equation (Eq. (5-30)) leads to the following:

$$\tau^2 \frac{\partial C_i}{\partial t} = \nabla \cdot [D_i \nabla C_i - z_i D_i (\frac{(\pi i)/(\varepsilon^{\frac{2}{3}} F) + \sum z_i D_i \nabla C_i}{\sum z_i^2 D_i C_i}) C_i] \tag{5-33}$$

where τ is the tortuosity of pore structure and ε is the volume fraction of porosity.

5.8.2 Physical model

The physical system to which the above model is applied is illustrated in Figure. 5.17. Since the specimens used in the experiments detailed in Part 2 of the previous Chapter were symmetric (see Figure 4.24), only the left half side of the specimens was modelled in order to save time required for calculation. As shown in the Figure, it is defined in this model that the x-axis is the horizontal axis and the z-axis is the vertical axis. To simulate the dimensions of the specimens used in the experiments detailed in Part 2 of the previous chapter, the

carbonation depth in initially non-carbonated regions, the cover depth, and the thickness of the medium behind the steel cathode are set as z_c=12mm, z_1=21mm, and z_2=9mm respectively. In addition, the half length of the initially carbonated region and the length of initially non-carbonated regions are set as x_1=22mm and x_2=44mm respectively. z_a is the length of the anolyte, which is detailed later in the boundary condition subsection 5.8.3.3. It is assumed that an aqueous solution of the relevant corrosion inhibitor is applied to the surface of the carbonated cement paste and constant current density (5A/m^2) is passed between an anode placed in the inhibitor solution and a steel mesh cathode embedded within the cement paste. The species in the pore solution taken into consideration are the same as were considered in Part 1 of this Chapter. It is also assumed that the only solid phases with solubility products that have to be taken into account are calcite and gypsum for carbonated cement pastes similarly as assumed in Part 1 of this Chapter, and hydrated lime for non-carbonated cement pastes. The tortuosity τ is assumed to be 2.0 (Li and Page 2000) and the porosity ε to be 0.34 for carbonated cement pastes and 0.42 for non-carbonated cement pastes (see subsection 4.10.1). The concentrations of all species in the anolyte are assumed to be uniform since the transport of ions in the external electrolyte is much faster than in the internal pore solution.

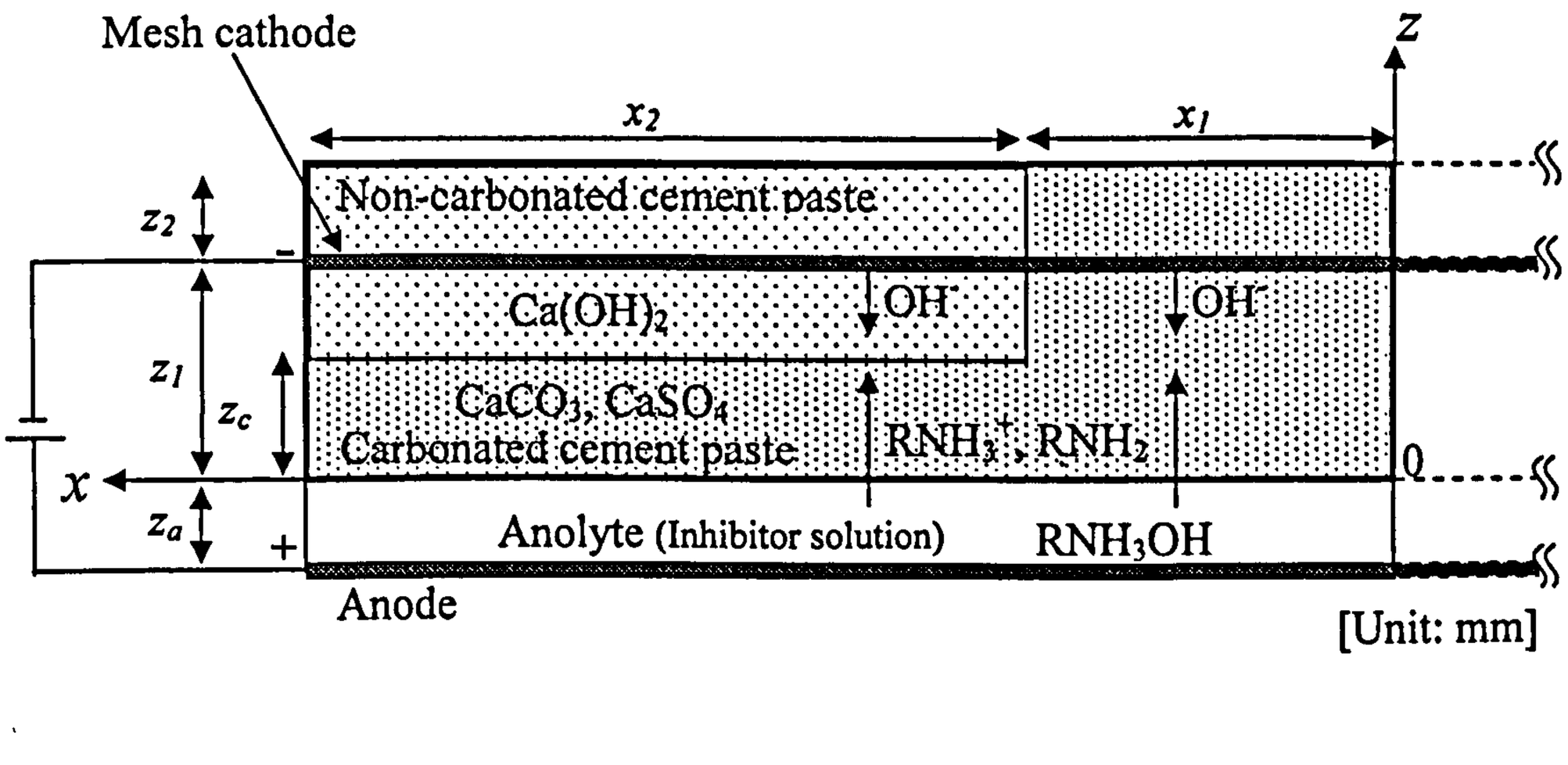

Figure 5.17 Physical model of transport in partially carbonated material

5.8.3 General and boundary conditions

5.8.3.1 General conditions in the pore solution

As assumed in the one-dimensional model presented in subsection 5.4.3.1, binding of alkali metal ions and chloride ions in silica gel is neglected in the initially carbonated region in this model. In the initially non-carbonated region, binding of alkali metal ions is also neglected since the pH of the pore solution in this region is expected to be maintained at high values owing to the migration of hydroxyl ions generated at the cathode during the electrochemical treatment (see Figure 5.2 for proportion of free alkali ions with respect to pH of the pore solution). Binding of chloride ions is also neglected in initially non-carbonated region in this model, since the concentration of the ion is initially insignificant (see Table 4.6) in this region and the migration of this ion from initially chloride-rich carbonated regions into this region against the action of an electrical field is assumed to be negligible. The formation of carbamate products ($RNHCOO^-$) is also assumed to be negligible in this model, similarly as discussed in subsection 5.4.3.1.

(1) General reactions

In initially carbonated regions, the chemical equilibria (5-A)-(5-E) in subsection 5.4.3.1 are assumed to be involved as follows:

$$CaCO_3 \Leftrightarrow Ca^{2+} + CO_3^{2-} \quad (5\text{-A})$$

$$CaSO_4 \Leftrightarrow Ca^{2+} + SO_4^{2-} \quad (5\text{-B})$$

$$RNH_3^+ + OH^- \Leftrightarrow RNH_2 + H_2O \quad (5\text{-C})$$

$$HCO_3^- + OH^- \Leftrightarrow CO_3^{2-} + H_2O \quad (5\text{-D})$$

$$H_2O \Leftrightarrow H^+ + OH^- \quad (5\text{-E})$$

On the other hand, in initially non-carbonated regions with high pH values, the chemical equilibria that are assumed to be involved are as follows:

$$Ca(OH)_2 \Leftrightarrow Ca^{2+} + 2OH^- \quad (5\text{-T})$$

$$RNH_3^+ + OH^- \Leftrightarrow RNH_2 + H_2O \quad (5\text{-C})$$

where the solubility products of calcium carbonate and calcium sulphate are neglected. Since the pK_a values for the equilibria (5-D) and (5-F) in subsection 5.4.3.1 are 10.33 and 6.35 respectively (Lide 2006), the concentrations of bicarbonate and CO_2(aq) are assumed to be

negligible. The concentration of hydrogen ions ($[H^+]$) is also assumed to be negligible in this highly alkaline environment.

(2) General condition in the pore solution

If we consider an infinitesimal element of length, dx, and of height, dz, as shown in Figure 5.18, the rates of change of concentration for each species i (caused by the inward and outward fluxes and the rates R_i of chemical reactions that produce species within the domain) can be expressed as follows:

$$\frac{\partial C_i}{\partial t} = \left(\frac{J_i(x)}{dx} - \frac{J_i(x+dx)}{dx}\right) + \left(\frac{J_i(z)}{dz} - \frac{J_i(z+dz)}{dz}\right) + R_i \qquad (5\text{-}34)$$

Note: R_i=0 for ions such as sodium, potassium, chloride, and nitrate that are assumed not to react chemically with other species in the domain. For these species, the time derivatives of concentration are obtained from this equation. For other species, in initially carbonated regions, after each R_i term is eliminated by the procedures shown in Appendix D-A, Eqs. (A1), (A2), (A5)-(A9) are obtained, which are the seven simultaneous equations to be solved to obtain time derivatives of concentration. In initially non-carbonated regions, after each R_i term is eliminated by the procedures shown in Appendix D-F, Eqs. (F1)-(F4) are obtained, which are the four simultaneous equations to be solved.

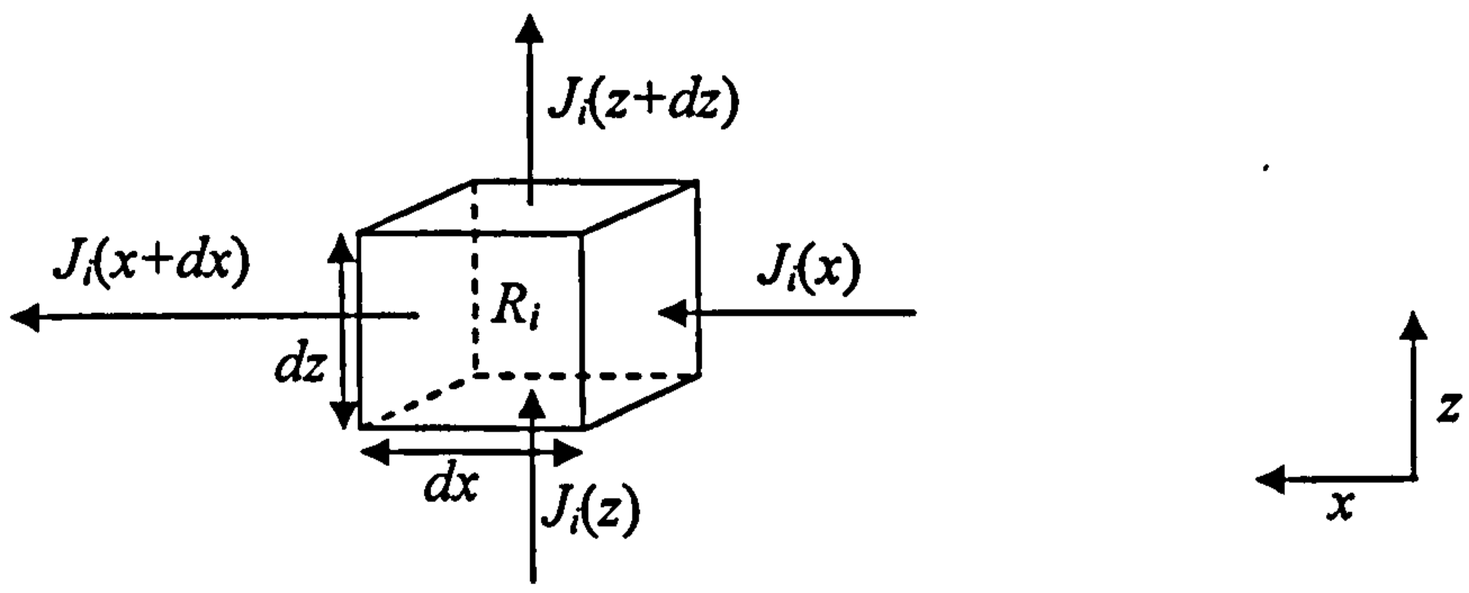

Figure 5.18 Introduced domain

5.8.3.2 Boundary conditions at the cathode

Similarly as discussed in subsection 5.4.3.3, the boundary condition at the cathode embedded in both initially carbonated and non-carbonated regions is simply expressed as follows:

$$J_{OH(z)} = \frac{i_{(z)}}{z_{OH}F} = -\frac{i_{(z)}}{F} \tag{5-35}$$

where $J_{OH(z)}$ is a vertical component of flux of hydroxyl ion and $i_{(z)}$ is a vertical component of the current density.

In the case of the boundary condition at the cathode in initially carbonated cement pastes, as discussed in subsection 5.4.3.4, the precipitation of calcium hydroxide needs to be taken into account when the concentration of calcium and hydroxyl ions exceed the solubility product associated with the pH rise in the vicinity of the cathode. In this case, for the species that are assumed to react chemically with other species in the domain, after each R_i term in Eq. (5-34) is eliminated by the procedures shown in Appendix D-B, Eqs. (A5)-(A8) and (B1)-(B3) are obtained as the seven simultaneous equations to be solved for the time derivatives of concentration. Note that the terms in Appendix D-B that are concerned with $RCOO^-$ are 0, simply because arginine is not used in Part 2.

5.8.3.3 Boundary conditions at the anolyte interface

Similarly as discussed in subsection 5.4.3.5, the pH of the external anolyte is assumed to be lowered by the following two reactions taking place at the anode:

$$4OH^- \Rightarrow 2H_2O + O_2 + 4e^- \tag{5-N}$$

$$2H_2O \Rightarrow O_2 + 4H^+ + 4e^- \tag{5-O}$$

If the current density consumed by each of the above reactions at the anode can be expressed as i^{OH} and i^{H} respectively, the boundary conditions for each ionic species are described as follows:

$$\left.\frac{\partial C_H}{\partial t}\right|_{z=0} = \frac{i^H_{(z)}/F}{z_a} - \frac{J^*_{H(z)}}{z_a} + R^*_H \tag{5-36}$$

$$\left.\frac{\partial C_{OH}}{\partial t}\right|_{z=0} = -\frac{i^{OH}_{(z)}/F}{z_a} - \frac{J^*_{OH(z)}}{z_a} + R^*_{OH} \tag{5-37}$$

$$\left.\frac{\partial C_i}{\partial t}\right|_{z=0} = -\frac{J^*_{i(z)}}{z_a} + R^*_i \quad (i \neq H \text{ and } i \neq OH) \tag{5-38}$$

where * denotes the values defined at the entire interface, z_a is the length of anolyte (z_a=62.0mm: derived by dividing the volume of the anolyte (180ml: half of 360ml used in experiments in previous chapter) by the cross section of the cement paste medium (a rectangle with a dimensions of 44mm×66mm: half of 44mm×132mm used in experiments), and R_H^* and R_{OH}^* are the reaction rates of other chemical reactions at the interface involving H^+ and OH^- ions. $i_{(x)}^H$, $i_{(x)}^{OH}$, and, $J_{i(x)}^*$ are neglected since they are insignificant. $J_{i(z)}^*$ and R_i^* are represented as follows:

$$J_{i(z)}^* = \frac{1}{L}\int_0^L J_{i(z)}(x,0)dx \tag{5-39}$$

$$R_i^* = \frac{1}{L}\int_0^L R_i(x,0)dx \tag{5-40}$$

where L is the half length of the specimen used in the experiments ($L=x_1+x_2$, see Figure 5.17).

As for anolyte with the pH being lowered during the electrochemical treatment, the assumed boundary conditions are the same for each categorised pH region, as detailed in subsections 5.4.3.5.1, 5.4.3.5.2, and 5.4.3.5.3.

5.8.3.3.1 Anolyte with alkaline pH

In the case of anolyte with alkaline pH, for the species that are assumed to react chemically with other species in the anolyte, after each R_i term in Eqs. (5-36)-(5-38) is eliminated by the same procedures as shown in Appendix D-C, Eqs. (A7), (A8) and (C2)-(C4) are obtained as the five simultaneous equations to be solved for the time derivatives of concentration. Note that, for this two dimensional model, (C1) can be derived by subtraction of Eq. (5-37) from (5-36) at z=0. All time derivatives in the Appendix D-C are discussed at z=0, and J_i^*, i, and x_a need to be replaced with $J_{i(z)}^*$, $i_{(z)}$, and z_a.

5.8.3.3.2 Anolyte with neutralised pH

For the species that are assumed to react chemically with other species in the anolyte, after each R_i term in Eqs. (5-36)-(5-38) is eliminated by the same procedures as shown in Appendix D-D, Eqs. (D1)-(D5) are obtained as the five simultaneous equations to be solved for the time derivatives of concentration. Note that, for this two dimensional model, all time

derivatives in the Appendix D-D are discussed at z=0, and J_i^*, i, and x_a need to be replaced with $J_{i(z)}^*$, $i_{(z)}$, and z_a.

5.8.3.3.3 Anolyte with acidic pH

The boundary conditions for hydrogen, calcium and bicarbonate associated with the dissolution of the material surface are changed from Eqs. (5-15)-(5-17) as follows:

$$\left.\frac{\partial C_H}{\partial t}\right|_{z=0} = \frac{i_{(z)}^H/F}{z_a} - \frac{J_{H(z)}^*}{z_a} - \frac{J_{Diss}}{z_a} + R_H^* = \frac{i_{(z)}^H/F}{z_a} - \frac{J_{H(z)}^*}{z_a} - \frac{k_1 C_H^*}{z_a} + R_H^* \tag{5-41}$$

$$\left.\frac{\partial C_{Ca}}{\partial t}\right|_{z=0} = -\frac{J_{Ca(z)}^*}{z_a} + \frac{J_{Diss}}{z_a} = -\frac{J_{Ca(z)}^*}{z_a} + \frac{k_1 C_H^*}{z_a} \tag{5-42}$$

$$\left.\frac{\partial C_{HCO_3}}{\partial t}\right|_{z=0} = -\frac{J_{HCO_3(z)}^*}{z_a} + \frac{J_{Diss}}{z_a} + R_{HCO_3}^* = -\frac{J_{HCO_3(z)}^*}{z_a} + \frac{k_1 C_H^*}{z_a} + R_{HCO_3}^* \tag{5-43}$$

For the species that are assumed to react chemically with other species in the anolyte, after each R_i term in Eqs. (5-37)-(5-38) and Eqs. (5-41)-(5-43) is eliminated by the same procedures as shown in Appendix D-E, Eqs. (D4), (D5) and (E2)-(E5) are obtained as the six simultaneous equations to be solved for the time derivatives of concentration. Note that for this two dimensional model, all time derivatives in the Appendix D-E are discussed at z=0, and J_i^*, i, and x_a need to be replaced with $J_{i(z)}^*$, $i_{(z)}$, and z_a. Also note that the terms in Appendix D-E that are concerned with $RCOO^-$ are 0, simply because arginine is not used in Part 2.

5.8.4 Activity coefficients

In this model, in order to elucidate the non-idealised behaviour of concentrated electrolytes, a modified Davies equation (see Eq. (5-18)) is also used for the estimation of the activity coefficients of the ionic species referred to in Table 5.1, as discussed in subsection 5.4.4. A molar activity coefficient is also introduced by means of Pitzer model (see Eq. (5-20)) for ethanolamine, by which constant pK_a' value of 9.75 is assumed in the modelling (pK_a value 9.5).

5.8.5 Application of the model

5.8.5.1 Discrete system

A finite difference method (Noye 1982) was used to compute the concentration profiles through the domain that is assumed to consist of infinitesimal elements with a length of dx and dz as shown in Figure 5.18. It was also assumed that each element has a representative value at its central node, $x=x_m$ and $z=z_n$, where m and n are the number of the discrete area, thus the concentration of the species i in a certain element j can be represented as follows:

$$C_i(x_m,z_n) \approx \frac{1}{dxdz}\int_{z_n-\frac{1}{2}dz}^{z_n+\frac{1}{2}dz}\int_{x_m-\frac{1}{2}dx}^{x_m+\frac{1}{2}dx} C_i(x,z)dxdz \tag{5-44}$$

For example, the first order derivative of the concentration (scalar) and the current density (vector), and the second order derivative of the concentration, with respect of x and z is given at the element P (with a centre node of $x=x_m$, $z=z_n$) as follows:

$$\nabla C_i\big|_{atP} = \left[\frac{\partial C_i}{\partial x},\frac{\partial C_i}{\partial z}\right]_{atP} \approx \left[\left.\frac{C_i(x_{m+1})-C_i(x_{m-1})}{2dx}\right|_{z=z_n},\left.\frac{C_i(z_{n+1})-C_i(z_{n-1})}{2dz}\right|_{x=x_m}\right] \tag{5-45}$$

$$\nabla\cdot i\big|_{atP} = \left(\frac{\partial i_{(x)}}{\partial x}+\frac{\partial i_{(z)}}{\partial z}\right)_{atP} \approx \left.\frac{i_{(x)}(x_{m+1})-i_{(x)}(x_{m-1})}{2dx}\right|_{z=z_n} + \left.\frac{i_{(z)}(z_{n+1})-i_{(z)}(z_{n-1})}{2dz}\right|_{x=x_m} \tag{5-46}$$

$$\nabla\cdot(\nabla C_i)\big|_{atP} = \nabla^2 C_i\big|_{atP} = \left(\frac{\partial^2}{\partial x^2}+\frac{\partial^2}{\partial z^2}\right)C_i\Big|_{atP} = \left(\frac{\partial^2 C_i}{\partial x^2}+\frac{\partial^2 C_i}{\partial z^2}\right)_{atP}$$

$$\approx \left.\frac{C_i(x_{m+1})-2C_i(x_m)+C_i(x_{m-1})}{dx^2}\right|_{z=z_n} + \left.\frac{C_i(z_{n+1})-2C_i(z_n)+C_i(z_{n-1})}{dz^2}\right|_{x=x_m} \tag{5-47}$$

5.8.5.2 Current density distribution

In this two-dimensional model, owing to the spatial difference in material properties in the medium, it is expected that the distribution of the current density is not uniform. In order for Eq. (5-33) to be solved, the current density distribution inside the medium needs to be given. Since there is no divergence of the current densities in the material, the current density satisfies $\nabla\cdot i=0$ (Eq. (5-31)). Thus, the approximate current density distributions can be numerically obtained by applying Kirchhoff's circuit laws to the domain, where the whole

circuit covering the domain is assumed to consist of square grid-patterned infinitesimal resistors in x and z directions (number of arrays: Nx for z direction and Nz for x direction) as shown in Figure 5.19.

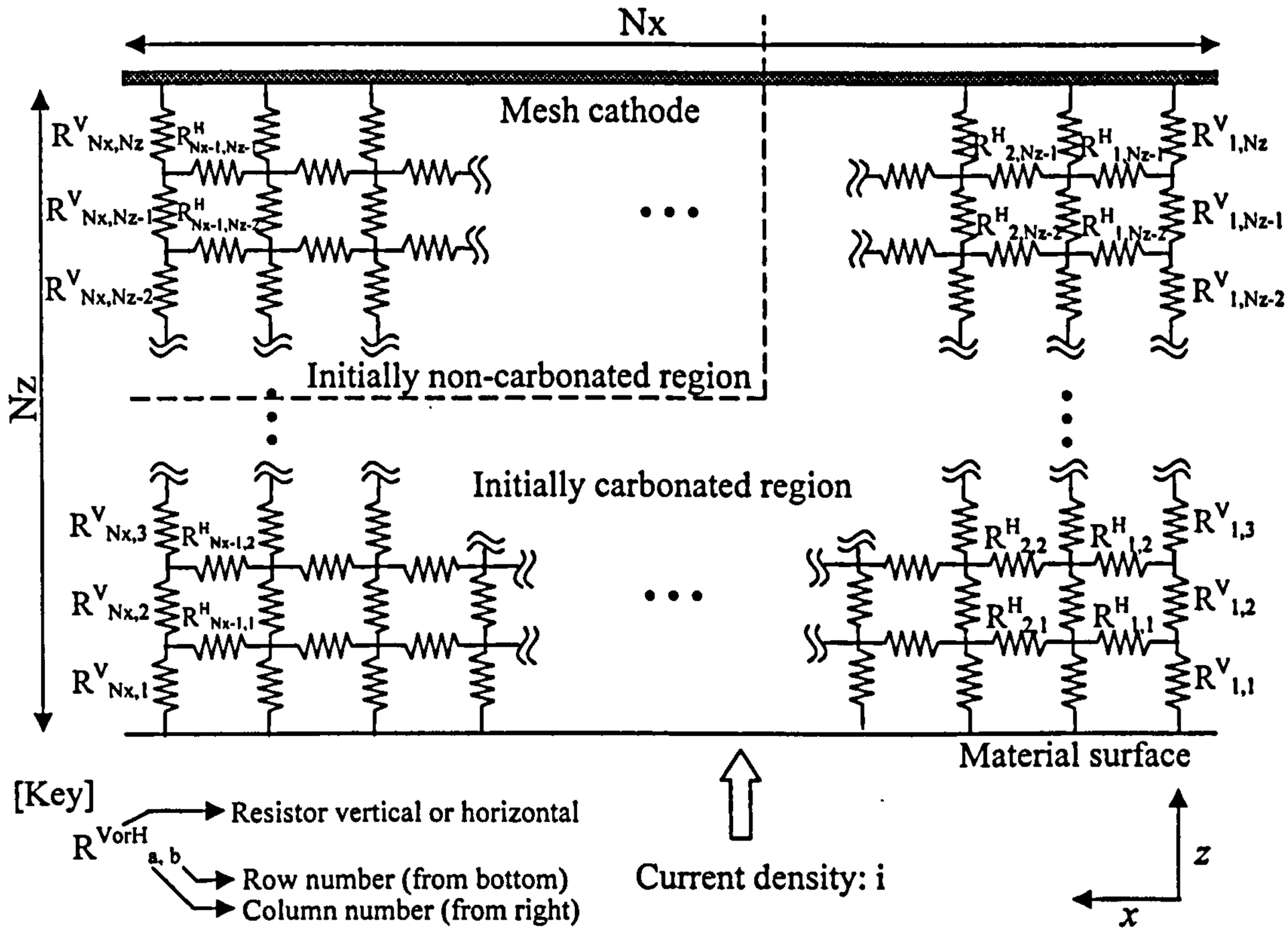

Figure 5.19 Circuit model for material

Each resistance of a square element can be expressed as follows:

$$R = \frac{1}{\kappa}\frac{L}{A} \propto \frac{1}{\kappa \varepsilon^{2/3}} \tag{5-48}$$

where R is element resistance (Ω), κ is the electrical conductivity of pore electrolytes (S/m or $\Omega^{-1}m^{-1}$), L is the length (m), A is the conductive cross section (m^2), and ε is the porosity of the material in the element. Electrical conductivity, in general, may be written in terms of the mobilities of all the ions present in an electrolyte as follows (Robinson and Stokes 1965, Bard and Faulkner 1980):

$$\kappa = F\sum_i |z_i|\, u_i C_i = \Lambda C \tag{5-49}$$

where F is the Faraday constant (9.64846×10^4 C/mol), z_i is the charge number, u_i is the mobility ($S/C/cm^2$), C_i is the concentration of ion i (mol/cm^3) respectively, Λ is molar conductivity (or sometimes "equivalent conductivity") ($S\cdot cm^2/mol$), and C is the total ionic concentration (mol/cm^3). Data for the relationships between conductivity and concentration are available for some electrolytes as shown in Figure 5.20 (Lide 2006), which are concerned with the constituents of the pore solution of non-carbonated or carbonated cement pastes (see Table 4.5 and 4.6 in subsection 4.10.1).

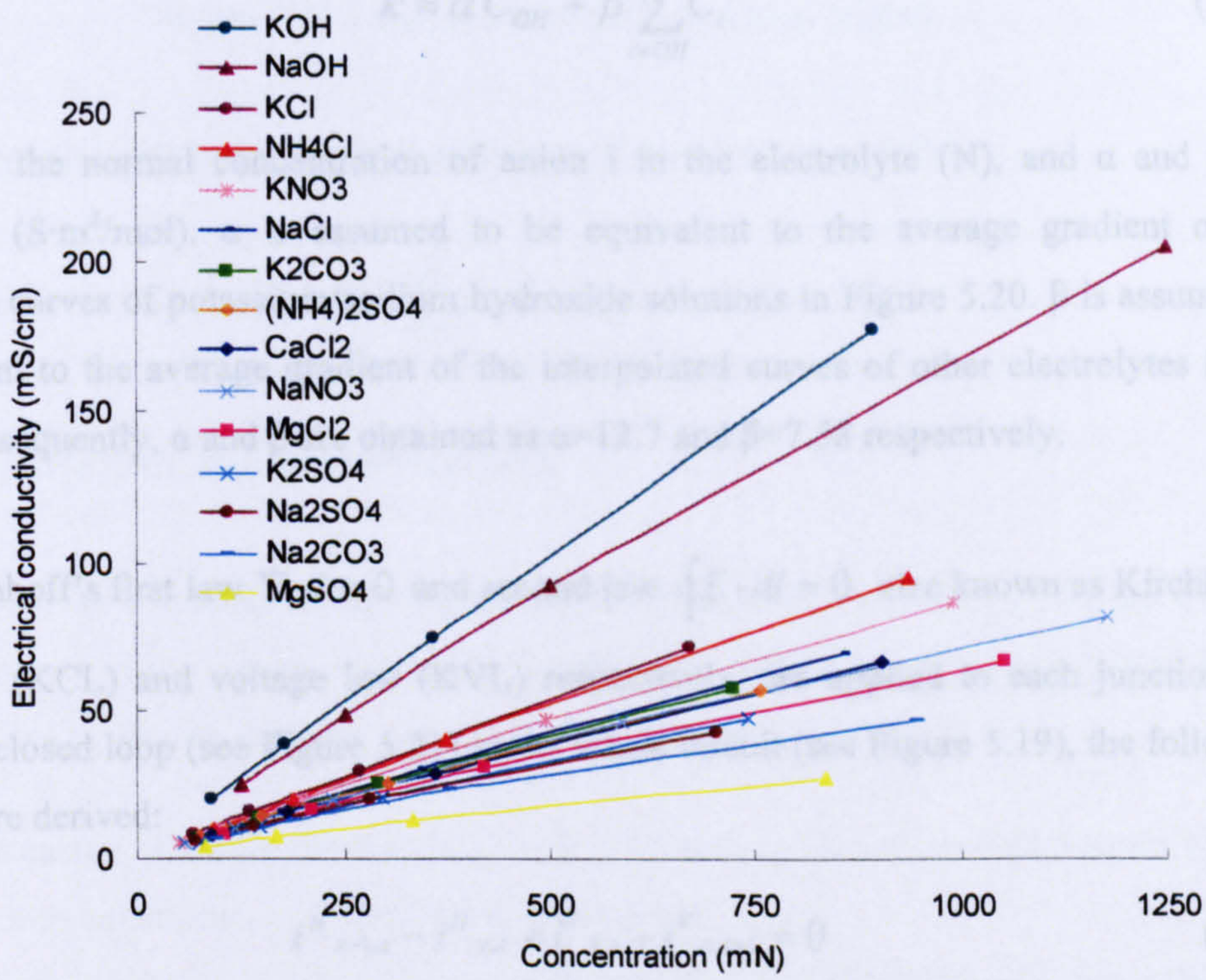

Figure 5.20 Electrical conductivity of electrolytes (Lide 2006)

It may be seen from this Figure that the electrolytes of potassium hydroxide and sodium hydroxide, both of which are strong bases, especially have large electrical conductivity compared with other electrolytes. It can thus be inferred that, from the concentration data of the pore constituents presented in Table 4.5 and 4.6, the pore solution of non-carbonated cement pastes is more conductive than that of carbonated cement pastes.

The molar conductivity Λ is, in fact, concentration dependent, which can be expressed by an equation known as Kohlrausch's Law as follows (Bard and Faulkner, 1980):

$$\Lambda = \Lambda^0 - k\sqrt{C} \tag{5-50}$$

where Λ^0 is the molar conductivity at infinite dilution ($S \cdot cm^2/mol$), k is Kohlrausch's constant and C is the total ionic concentration (mol/cm^3). However, it is known that the molar conductivity does not change significantly with concentration for solutions of strong electrolytes such as those presented in Figure 5.20 (Bard and Faulkner, 1980). Therefore, for the sake of simplicity, the electrical conductivity of a given multi-component pore solution is assumed to have a linear relationship with its ionic concentration and to be approximated as follows:

$$\kappa \approx \alpha C_{OH} + \beta \sum_{i \neq OH} C_i \tag{5-51}$$

where C_i is the normal concentration of anion i in the electrolyte (N), and α and β are coefficients ($S \cdot m^2/mol$). α is assumed to be equivalent to the average gradient of the interpolated curves of potassium/sodium hydroxide solutions in Figure 5.20. β is assumed to be equivalent to the average gradient of the interpolated curves of other electrolytes in the Figure. Consequently, α and β are obtained as α=12.7 and β=7.58 respectively.

When Kirchhoff's first law $\nabla \cdot i = 0$ and second law $\oint_c E \cdot dl = 0$, also known as Kirchhoff's current law (KCL) and voltage law (KVL) respecitvely, are applied to each junction and each small closed loop (see Figure 5.21) in the whole circuit (see Figure 5.19), the following equations are derived:

$$i^H{}_{x-1,z} - i^H{}_{x,z} + i^V{}_{x,z} - i^V{}_{x,z+1} = 0 \tag{5-52}$$

$$i^H{}_{x,z+1} R^H{}_{x,z+1} - i^H{}_{x,z} R^H{}_{x,z} + i^V{}_{x,z+1} R^V{}_{x,z+1} - i^V{}_{x+1,z+1} R^V{}_{x+1,z+1} = 0 \tag{5-53}$$

where, $i^{VorH}{}_{x,z}$ is the current density passing through the resistor $R^{VorH}{}_{x,z}$. Since R satisfies Eq. (5-48), Eq. (5-53) can be altered as follows:

$$\frac{i^H{}_{x,z+1}}{\kappa^H{}_{x,z+1} \cdot \varepsilon^H{}_{x,z+1}{}^{2/3}} - \frac{i^H{}_{x,z}}{\kappa^H{}_{x,z} \cdot \varepsilon^H{}_{x,z}{}^{2/3}} + \frac{i^V{}_{x,z+1}}{\kappa^V{}_{x,z+1} \cdot \varepsilon^V{}_{x,z+1}{}^{2/3}} - \frac{i^V{}_{x+1,z+1}}{\kappa^V{}_{x+1,z+1} \cdot \varepsilon^V{}_{x+1,z+1}{}^{2/3}} = 0 \tag{5-54}$$

where, $\kappa^{VorH}{}_{x,z}$ and $\varepsilon^{VorH}{}_{x,z}$ are the local electrical conductivity and porosity. Note that each resistor is assumed to have the same length.

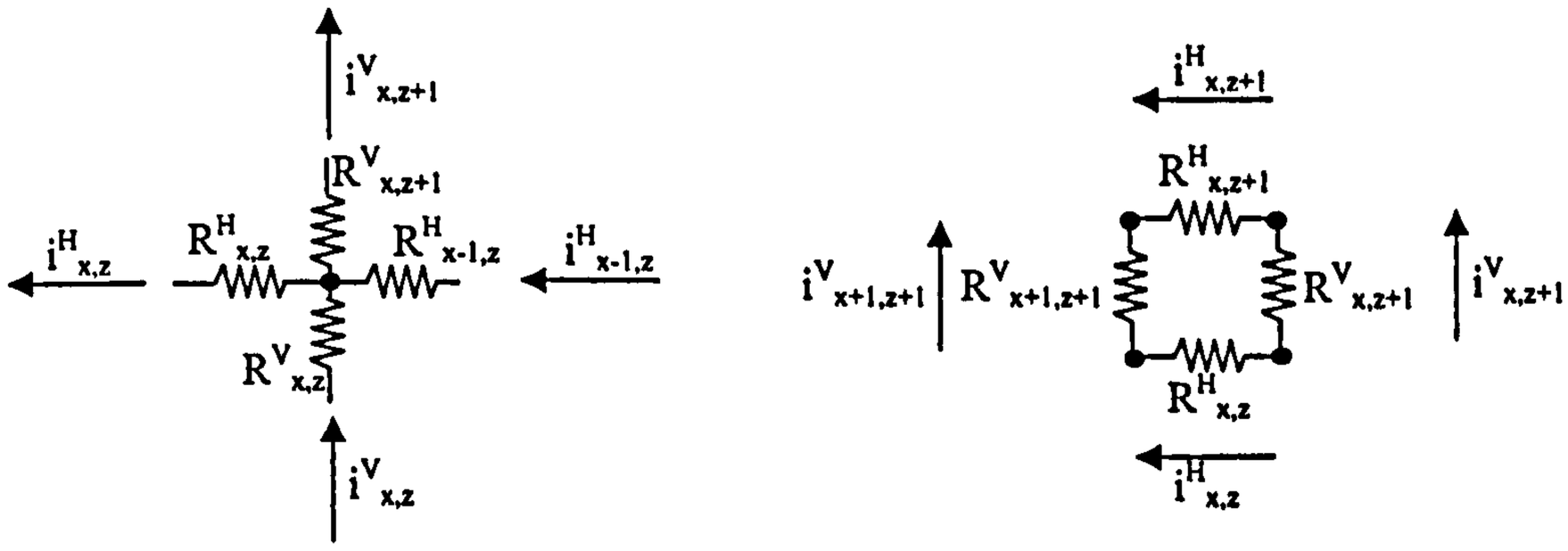

Figure 5.21 Local junction (left) and loop (right)

The boundary condition at the material surface can be expressed as follows:

$$\sum_{j=1}^{Nx} i^V_{j,1} = N_X \cdot i \tag{5-55}$$

where i is the externally applied current density.

Each $i^{VorH}_{x,z}$ can be obtained by solving simultaneous equations (5-52), (5-54), and (5-55), since the numbers of the unknowns and the simultaneous equations are the same (both being 2NxNz-Nx-Nz+1), shown as below:

·Unknown current densities: (Nx-1)·(Nz-1)+Nx·Nz (horizontal and vertical, respectively)

·Simultaneous equations: (Nz-1) ·Nx+(Nx-1)·Nz+1

(Eqs. (5-52), (5-54), and (5-55), respectively)

In the 2-D mathematical model for the simulation of electrochemical chloride removal presented by Wang et al. (2001), the initial current distribution, obtained by solving the Laplace equation, was assumed to remain unchanged during the treatment, probably due to the homogeneity of the material and the high pH values of the pore solutions. However, in the present model, for example, the initially diluted carbonated pore solutions were expected to become concentrated by electrolysis, possibly raising the conductivity of the region and altering the current distribution within the material during the treatment. Therefore it was assumed that the current distribution would be determined by the concentration distribution of various ions within the material during the treatment.

5.8.5.3 Numerical solution

The fourth order Runge Kutta method (Hundsdorfer 2003) was applied for the integration of Eq. (5-33). The system of equations was solved with a FORTRAN 95 programme (Lee 2003), the algorithm of which is described as follows:

1. The initial concentrations of each species ($C_i(x, z)$ at $t=0$) are given at each element as described in the following section.
2. Electrical conductivity κ is calculated for each node by Eq. (5-51), and the current density distribution in the domain is obtained by the procedure described in the previous subsection.
3. Activity coefficients γ_i are calculated for each species and the values of the equilibrium constants are corrected as shown in Table 5.1 in subsection 5.4.4.
4. Applying the current density field in the domain obtained in the procedure 2 above to Eq. (5-33), the time derivatives of concentration for each species are calculated by the procedures already mentioned in the general or boundary conditions section above based on Eq. (5-34).
5. The concentrations of each species at the next time step are obtained by the integration of Eq. (5-33) at all nodes.
6. The routines of 2-5 above are repeated for the time steps required after which the final concentrations of each species are obtained.

The numbers of elements and the time steps required to obtain results with good accuracy and to ensure convergence of the numerical solutions were investigated until a stable solution was obtained, from which the computations were performed with 7,920 square elements (vertically sectioned 60 elements × horizontally sectioned 132 elements) and with a constant time step of 0.1 second for the first 10,000 loops and then a time step of 10 seconds.

5.8.5.4 Generation of carbon dioxide gas

The generation of carbon dioxide gas is taken into account in the same manner as detailed in subsection 5.4.5, when the pH of the anolyte is reduced below pH 4.

5.8.6 Initial conditions

Anolyte solutions of volume 360ml containing 1.0M ethanolamine nitrate at pH 8.0 (produced by mixing equal volumes of 2M ethanolamine and 1.97M nitric acid) and 0.5M guanidine carbonate (1M with respect to guanidine) were used, as detailed in Part 2 of Chapter 4. The assumed initial concentrations of the various species in the carbonated pore solutions and external solutions as well as the diffusion coefficients are the same as used in Part 1 of this Chapter (see Table 5.3 in subsection 5.4.6).

The pH value and the initial concentrations of the species in the pore solutions of non-carbonated cement pastes are assumed to be as shown in Table 5.6, based on experimental measurements recorded in Part 2 of the previous Chapter. Experimentally determined calcium and hydroxyl ion concentrations, which exceeded the solubility product of calcium hydroxide recorded in Table 5.1 in subsection 5.4.4, were adjusted by dilution to yield the assumed equilibrium values. The concentration of potassium was determined so that the charge balance could be maintained in the solution. The initial concentrations of carbonate species are assumed to be negligible.

Table 5.6 Initial conditions of species in non-carbonated pore solutions

	Charge number (z_i)	In pore solution (mole/l) [pH=13.3]
Na^+	+1	9.90×10^{-2}
K^+	+1	1.16×10^{-1}
Ca^{2+}	+2	1.15×10^{-4}

	Charge number (z_i)	In pore solution (mole/l) [pH=13.3]
OH^-	-1	2.09×10^{-1}
SO_4^{2-}	-2	1.90×10^{-3}
Cl^-	-1	2.50×10^{-3}

5.9 RESULTS AND DISCUSSION

In this section, the factors that arise from partial carbonation of the material and affect the transport of electrochemically injected organic corrosion inhibitors in the partially carbonated material are discussed.

5.9.1 Current density distribution

The calculation of conductivity κ, by means of Eq. (5-51), of the pore solutions in carbonated and non-carbonated cement pastes used in the experiment in the previous Chapter showed that the conductivity of the pore solutions in non-carbonated specimens was around 6.56 times as high as that in carbonated specimens. The ratio of conductivity/resistivity of carbonated and non-carbonated pore solutions is in the same range as was determined for mature real concrete reported by Bertolini et al. (2004).

An initial current density distribution (just after the current was assumed to be switched on) in carbonated and non-carbonated regions in the left half of the cover specimen, obtained by solving simultaneous equations (5-52), (5-54), and (5-55), is described in Figure 5.22, where vertical and horizontal components of the current density are given in an arrow form; a thicker arrow indicates a higher current density. The values presented in the Figure mean the average current densities passed in each rectangular (3mm×1mm or 3mm×2mm) or square element (3mm×3mm) by using the calculated current densities at the nodes (note that the distance between the two neighbouring nodes employed in the numerical analysis was 0.5mm, see subsection 5.8.5.3). The results show that when current density of 5A/m^2 was applied at the material surface, the magnitude of the current densities inside the material was varied for different positions. The vertical components were higher than 5A/m^2 (around 5.0-5.6A/m^2) in the initially carbonated region below the initially non-carbonated region; however, the components were smaller in the other initially carbonated regions. Significantly small current densities were found in the vicinity of the steel along the boundary of initially carbonated and non-carbonated regions (smaller than 3.0A/m^2). It may be inferred that this effectively smaller current density discouraged the migration of guanidine towards the steel cathode embedded in initially carbonated regions, as observed in Chapter 4. On the other hand, the calculation revealed quite high current densities in the initially non-carbonated region near the boundary (around 6.0-8.4A/m^2). The horizontal components with a significant current density were observed within 6-9mm areas from the position ((x, z) =

(22mm, 12mm)) at the boundary, with the highest current density around 3.1A/m^2, which demonstrated the presence of lateral current flow from initially carbonated regions to non-carbonated regions near the boundary as discussed in Chapter 4.

The current density distribution in the material after the inhibitor injection treatment applied for 7 days is shown in Figure 5.23. In the case of ethanolamine, the vertical current density distribution after the treatment has the similar trend to that just after the treatment, and the degree of the difference in current density at the boundary of the two columns (x=22mm) became moderate after the 7-day treatment. This may be attributable to the phenomenon that most of the migrating ethanolamine was deprotonated by reacting with hydroxyl ions (see reaction (5-C) in subsection 5.5.1), by which the initially carbonated pore solutions remained diluted in the layers 1 and 2. In addition, the pores in layer 3 and 4 in the centre column gradually became concentrated by the migration of alkali metal ions and hydroxyl ions thus increasing conductivity, resulting in smaller lateral current density flowing between the two columns (see Figure 5.23 (B)). In contrast, in the case of guanidine, the difference in the average current density in the two columns was increased after the treatment. This may be explained as follows. Since the initial current density in the layer 1 and 2 of the side column was higher than that of the centre column (see Figure 5.22), the migration of guanidine was estimated to be more significant in the side column than in the centre column in these layers. The generated ionic concentration discrepancy in these two different regions might have gradually increased the difference in conductivity of the two regions, which, in turn, again affected the migration of the inhibitor, resulting in greater difference in conductivity. Therefore it may be said that the initial current density distribution in the material significantly influences the subsequent penetration of the inhibitor whose transport depends on migration, towards the steel cathode in carbonated material. However, similarly as in the case of ethanolamine, the lateral current density became smaller as pores in the layers 3 and 4 in the centre column became concentrated during the electrochemical treatment (see Figure 5.23 (D)). This may indicate that, when an inhibitor with a high pK_a value is used, since the carbonation front is usually not uniform in real concrete structures (for example, see Figure 4.20), care needs to be taken for the practical application of this method in order to avoid causing an inadequate level of inhibitor injection to the steel bars embedded in carbonated regions. It may be thus useful to investigate the distribution of carbonation depth within the concrete by taking out a core or drilling a hole at as many points as possible prior to the application of the electrochemical method.

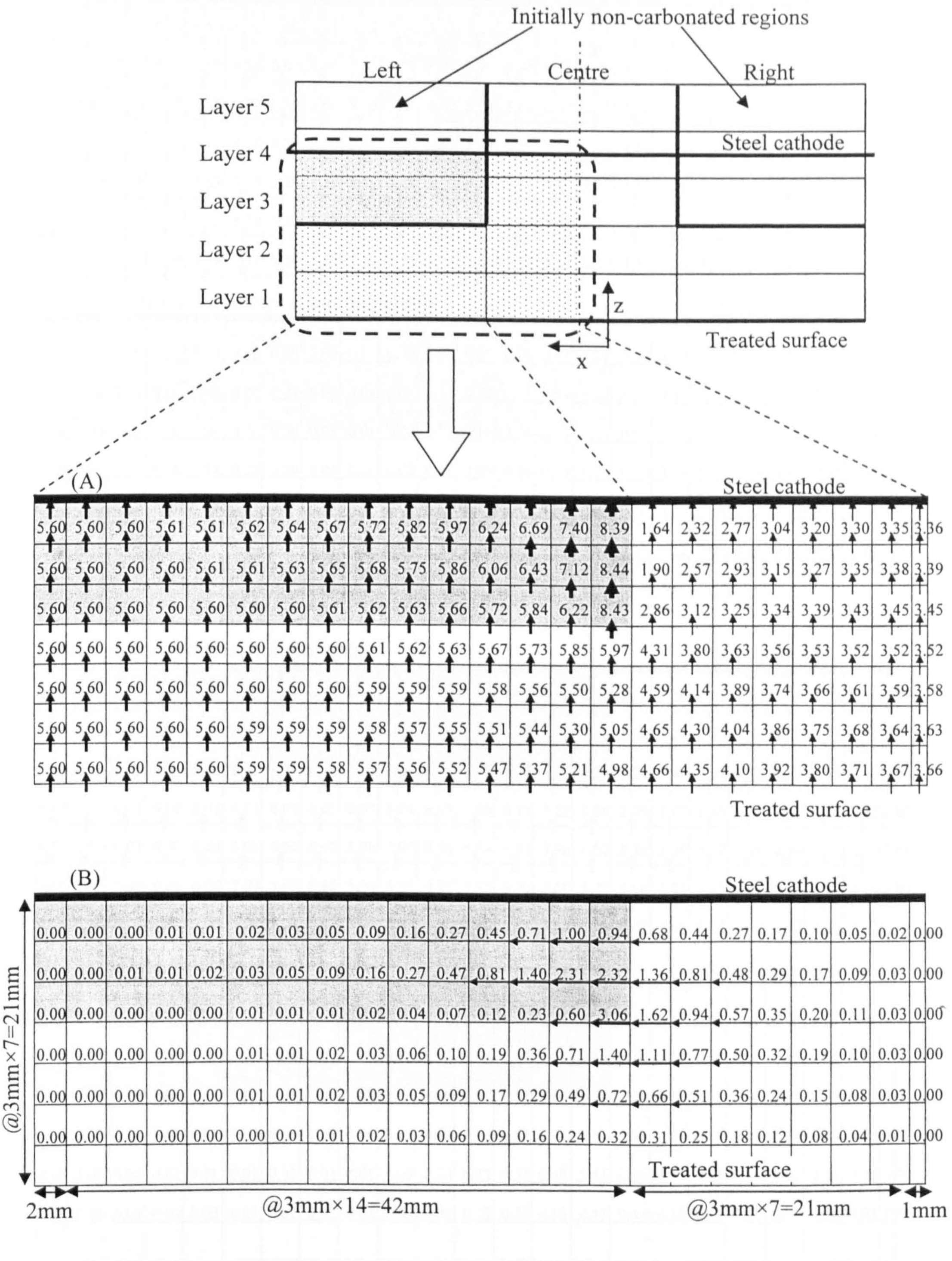

Figure 5.22 Calculated current density distribution in partially cabonated specimens at the commencement of galvanostatic treatment at 5A/m^2: (A) vertical components, (B) horizontal components (Unit: A/m^2)

(A) Ethanolamine (vertical components)

Steel cathode

5.59	5.59	5.59	5.59	5.59	5.60	5.60	5.61	5.62	5.64	5.69	5.79	5.98	6.41	7.49	2.40	3.04	3.35	3.52	3.61	3.66	3.68	3.69
5.59	5.59	5.59	5.59	5.59	5.59	5.60	5.60	5.61	5.63	5.67	5.75	5.90	6.19	6.65	3.07	3.31	3.48	3.59	3.65	3.68	3.70	3.70
5.59	5.59	5.59	5.59	5.59	5.59	5.59	5.60	5.60	5.61	5.62	5.64	5.69	5.80	6.21	3.56	3.65	3.68	3.70	3.71	3.72	3.72	3.72
5.59	5.59	5.59	5.59	5.59	5.59	5.59	5.59	5.59	5.60	5.60	5.59	5.59	5.55	5.40	4.19	3.93	3.83	3.78	3.76	3.75	3.74	3.74
5.59	5.59	5.59	5.59	5.59	5.59	5.59	5.59	5.59	5.58	5.57	5.55	5.51	5.41	5.20	4.32	4.06	3.92	3.84	3.79	3.77	3.76	3.76
5.59	5.59	5.59	5.59	5.59	5.59	5.59	5.58	5.58	5.56	5.54	5.51	5.44	5.35	5.21	4.28	4.12	3.99	3.90	3.84	3.81	3.79	3.78
5.59	5.59	5.59	5.59	5.59	5.59	5.58	5.58	5.57	5.55	5.53	5.48	5.42	5.32	5.20	4.27	4.13	4.02	3.93	3.86	3.82	3.80	3.80

(B) Ethanolamine (horizontal components)

Steel cathode

0.00	0.00	0.00	0.00	0.00	0.00	0.00	0.00	0.01	0.02	0.03	0.07	0.15	0.37	1.21	0.54	0.27	0.24	0.08	0.04	0.02	0.01	0.00
0.00	0.00	0.01	0.00	0.00	0.00	0.01	0.01	0.03	0.06	0.11	0.22	0.44	0.83	1.27	0.78	0.44	0.25	0.14	0.07	0.04	0.01	0.00
0.00	0.00	0.00	0.00	0.00	0.00	0.00	0.01	0.01	0.02	0.05	0.10	0.20	0.45	1.25	0.62	0.34	0.19	0.11	0.06	0.03	0.01	0.00
0.00	0.00	0.00	0.00	0.00	0.00	0.00	0.01	0.01	0.03	0.05	0.09	0.16	0.30	0.50	0.37	0.24	0.14	0.09	0.05	0.03	0.01	0.00
0.00	0.00	0.00	0.00	0.00	0.01	0.01	0.02	0.03	0.05	0.08	0.13	0.19	0.26	0.26	0.30	0.25	0.18	0.12	0.07	0.04	0.01	0.00
0.00	0.00	0.00	0.00	0.00	0.00	0.01	0.01	0.02	0.03	0.04	0.07	0.10	0.12	0.13	0.14	0.12	0.09	0.06	0.04	0.02	0.01	0.00

(C) Guanidine (vertical components)

Steel cathode

6.01	6.01	6.01	6.01	6.02	6.03	6.04	6.06	6.10	6.15	6.23	6.35	6.52	6.74	6.95	2.21	2.36	2.51	2.62	2.69	2.73	2.76	2.76
6.01	6.01	6.01	6.01	6.02	6.02	6.02	6.05	6.08	6.13	6.20	6.31	6.48	6.75	7.18	2.06	2.36	2.53	2.64	2.71	2.75	2.77	2.77
6.01	6.01	6.01	6.01	6.01	6.01	6.01	6.03	6.05	6.08	6.12	6.20	6.34	6.61	7.24	2.22	2.49	2.63	2.71	2.75	2.78	2.79	2.80
6.00	6.00	6.00	6.00	6.01	6.01	6.01	6.01	6.02	6.03	6.05	6.08	6.15	6.25	6.36	2.96	2.87	2.86	2.85	2.85	2.85	2.85	2.85
6.00	6.00	6.00	6.00	6.00	6.00	6.00	5.99	5.98	5.97	5.96	5.94	5.91	5.90	6.02	3.35	3.20	3.07	2.99	2.94	2.91	2.90	2.89
6.00	6.00	6.00	6.00	6.00	5.99	5.99	5.98	5.96	5.94	5.91	5.85	5.76	5.60	5.28	3.94	3.51	3.27	3.12	3.03	2.97	2.94	2.93
6.00	6.00	6.00	6.00	6.00	5.99	5.98	5.97	5.95	5.92	5.88	5.80	5.67	5.45	5.09	4.07	3.65	3.37	3.19	3.07	3.00	2.97	2.96

(D) Guanidine (horizontal components)

Steel cathode

0.00	0.00	0.00	0.01	0.01	0.01	0.02	0.03	0.05	0.07	0.21	0.15	0.20	0.19	0.15	0.10	0.10	0.07	0.05	0.03	0.02	0.00	0.00
0.00	0.00	0.01	0.01	0.01	0.02	0.04	0.06	0.09	0.14	0.22	0.33	0.47	0.62	0.56	0.40	0.27	0.18	0.11	0.07	0.04	0.01	0.00
0.00	0.00	0.01	0.01	0.01	0.02	0.03	0.05	0.08	0.13	0.20	0.32	0.51	0.86	1.74	1.00	0.62	0.39	0.24	0.14	0.08	0.02	0.00
0.00	0.00	0.01	0.01	0.01	0.02	0.04	0.06	0.09	0.15	0.24	0.38	0.62	0.97	1.31	0.92	0.60	0.38	0.24	0.14	0.08	0.02	0.00
0.00	0.00	0.00	0.01	0.01	0.01	0.02	0.03	0.05	0.08	0.14	0.22	0.38	0.68	1.43	0.84	0.53	0.33	0.21	0.12	0.07	0.02	0.00
0.00	0.00	0.00	0.00	0.00	0.01	0.01	0.02	0.03	0.05	0.08	0.13	0.22	0.36	0.55	0.42	0.28	0.18	0.11	0.07	0.04	0.01	0.00

Figure 5.23 Current density distribution in partially cabonated specimens after 7 days' inhibitor injection treatment (Unit: A/m^2, scale: same as Figure 5.22)

5.9.2 Organic corrosion inhibitors

5.9.2.1 Organic corrosion inhibitors in the pore solutions

The computed concentration profiles of ethanolamine and guanidine after the treatments had been applied at 5A/m^2 for 7 days to partially carbonated material are shown in Figure 5.24 and 5.26 respectively. The computed average concentration profiles of the two inhibitors in side and centre columns are shown in Figure 5.25 and 5.27 along with the corresponding experimental data. It may be seen that the results from modelling are in good accord with those obtained from the experiment, showing that the two inhibitors penetrate into the partially carbonated medium with a significant concentration attained at the cathode (z=21mm). In both inhibitors cases, the calculated concentration profiles have a respective peak at a different position in each column. As discussed in the previous Chapter and Part 1 of this Chapter, this can be interpreted in terms of the difference in the degrees of protonation of the two inhibitors in the pore solutions whose pH values were raised by the electrolysis to very high level (pH >13, in the initially non-carbonated region of the side column) and moderately high (pH 11-13, in the centre column). The concentration peak of ethanolamine in the side column was found in the initially carbonated region (around at 10mm from the treated surface), whilst the concentration peak of guanidine in the side column was found in the initially non-carbonated region (at around 14mm). In addition, in the centre column, the highest concentration was observed just a few millimetres from the cathode in the case of ethanolamine, whilst it was observed at the cathode in the case of guanidine. These are simply attributable to the difference in pK_a value of the two inhibitors, similarly as discussed in Part 1 of this Chapter. Ethanolamine has high peaks (both around 1,500mmol/l) in the side and centre column respectively, whilst guanidine has two peaks with significantly different heights (one around 860mmol/l in the side column and the other around 310mmol/l in the centre column). This provides clear evidence that in the case of guanidine with a high pK_a value (pK_a 13.6), the transport of the species depends on the ionic migration, since the effective current densities passed in each column were significantly different as described in the previous subsection. As may be inferred from Figure 5.24 and Figure 5.26, the effect of interaction of the species associated with the difference in material property in the two regions is restricted, just within a few millimetres from the boundary (x=22mm).

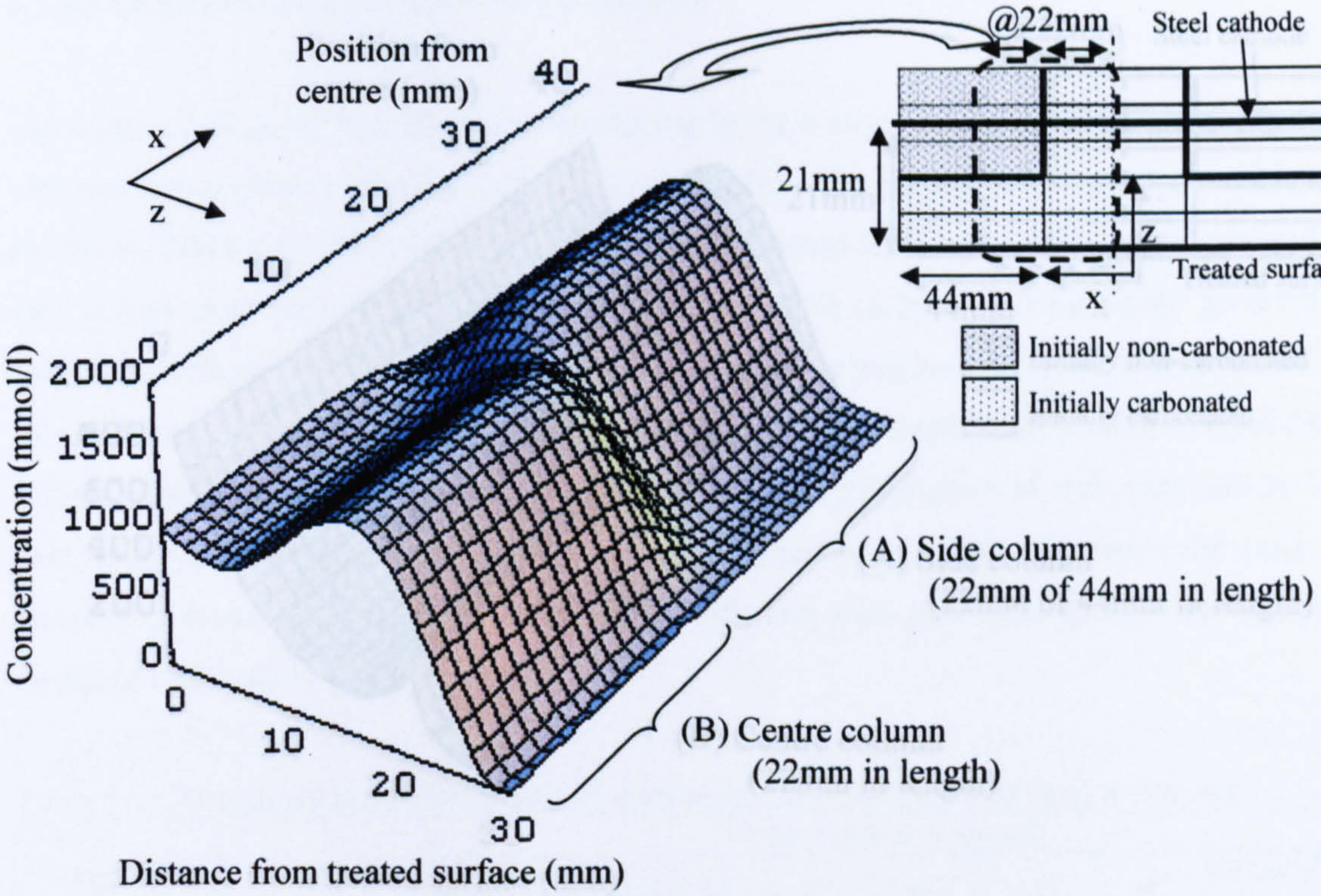

Figure 5.24 Computed concentration profile for ethanolamine after galvanostatic treatments at 5A/m^2 applied for 7 days

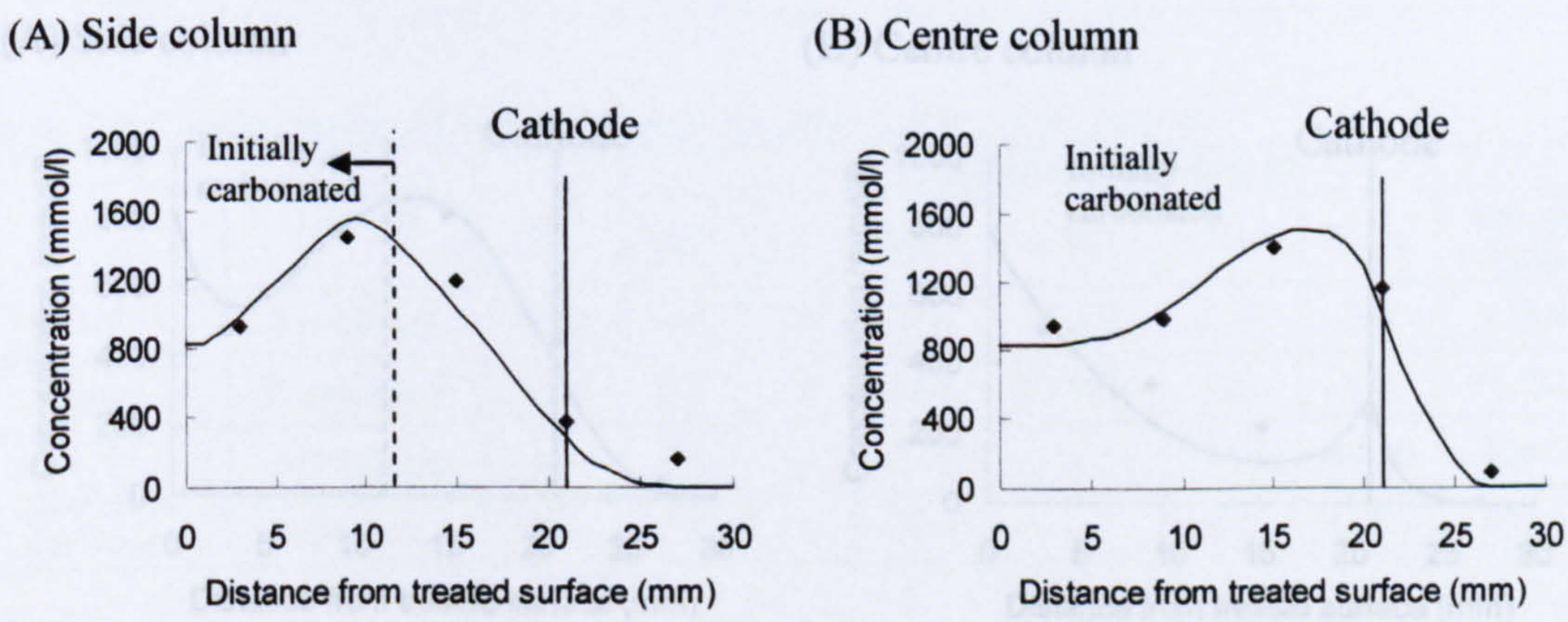

Figure 5.25 Computed average concentration profiles of ethanolamine in (A) side column and (B) centre column (line: model prediction, dots: experimental data)

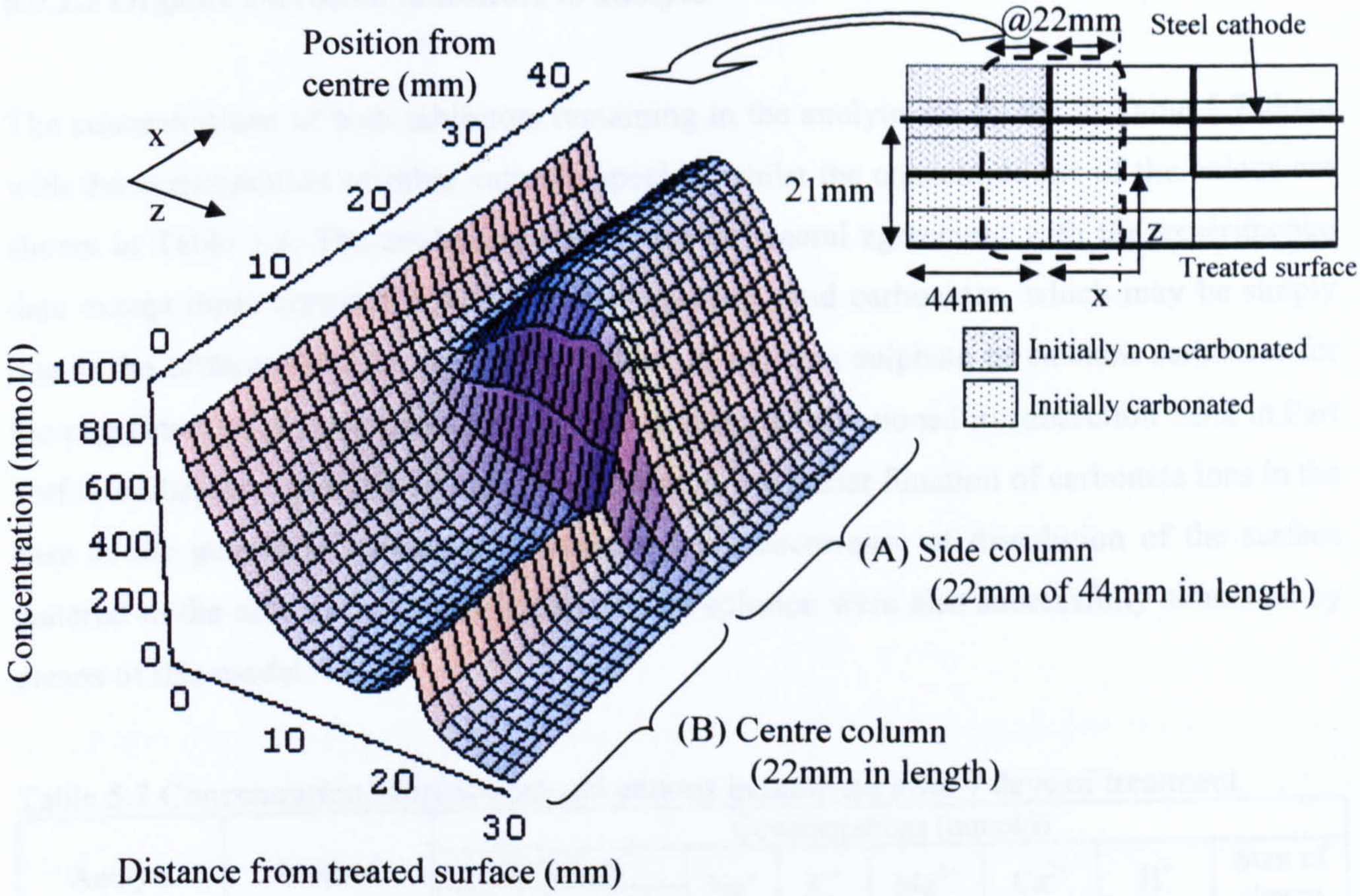

Figure 5.26 Computed concentration profile for guanidine after galvanostatic treatments at 5A/m^2 applied for 7 days

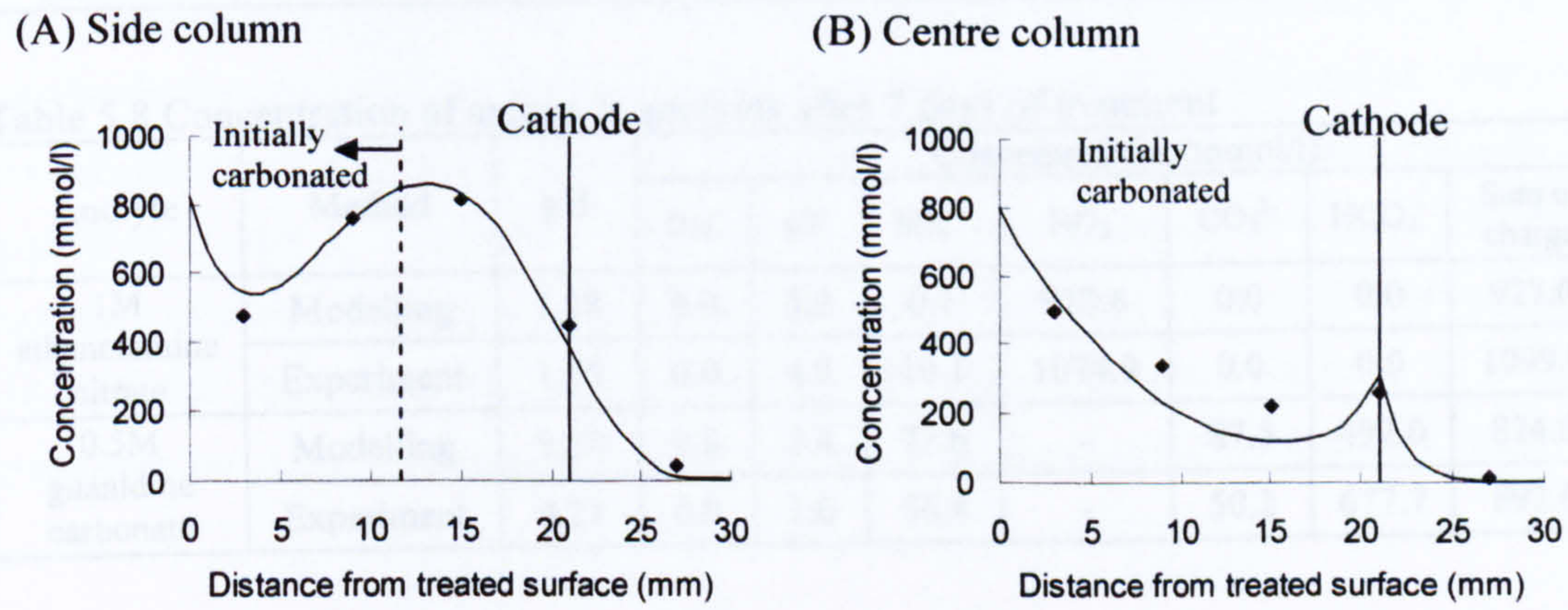

Figure 5.27 Computed average concentration profiles of guanidine in (A) side column and (B) centre column (line: model prediction, dots: experimental data)

5.9.2.2 Organic corrosion inhibitors in anolyte

The concentrations of both inhibitors remaining in the anolyte are shown in Table 5.7 along with the concentration of other cationic species, whilst the concentrations of the anions are shown in Table 5.8. The modelling results are in general agreement with the experimental data except those concerned with calcium, sulphate, and carbonates, which may be simply due to the difference in the solubility product of calcium sulphate or calcium carbonate for the experimental and mathematical modelling cases, as mentioned in subsection 5.5.2 in Part 1 of this Chapter. Similarly as discussed in Part 1, the buffer function of carbonate ions in the case of the guanidine carbonate solution and the occurrence of dissolution of the surface material in the case of the ethanolamine nitrate solution were also successfully simulated by means of this model.

Table 5.7 Concentration of inhibitors and cations in anolytes after 7 days of treatment

Anolyte	Method	Concentrations (mmol/l)							
		Inhibitors		Na^+	K^+	Mg^{2+}	Ca^{2+}	H^+	Sum of charge
		Total	Cationic						
1M ethanolamine nitrate	Modelling	828.6	828.6	0.2	0.2	-	22.7	52.5	927.0
	Experiment	878.9	878.9	4.3	N/D	15.6	127.5	28.2	1197.4
0.5M guanidine carbonate	Modelling	824.3	824.3	0.2	0.1	-	0.0	0.0	824.6
	Experiment	835.3	835.3	8.9	N/D	0.0	4.1	0.0	852.5

Table 5.8 Concentration of anions in anolytes after 7 days of treatment

Anolyte	Method	pH	Concentrations (mmol/l)						
			OH^-	Cl^-	SO_4^{2-}	NO_3^-	CO_3^{2-}	HCO_3^-	Sum of charge
1M ethanolamine nitrate	Modelling	1.28	0.0	3.2	0.1	923.6	0.0	0.0	927.0
	Experiment	1.55	0.0	4.0	10.1	1074.9	0.0	0.0	1099.0
0.5M guanidine carbonate	Modelling	9.58	0.0	2.4	77.6	-	87.5	492.0	824.6
	Experiment	9.21	0.0	1.6	56.4	-	50.2	677.7	892.6

5.9.3 Hydroxyl ions

The computed concentrations profiles of hydroxyl ions are shown in Figure 5.28 and the computed pH profiles are shown in Figure 5.29 along with the values of pH obtained from experiment (see Table 4.8). The predicted pH profiles are in reasonable agreement with the experimental data. Again it is clear that the difference in the profiles recorded for the two inhibitors is simply attributable to the lower pK_a value of ethanolamine (apparent pK_a' value of 9.75), resulting in its consuming more of the hydroxyl ions generated at the cathode. These results also indicate that the transport of the inhibitor species towards the cathode mainly depends on molecular diffusion in the case of ethanolamine and ionic migration in the case of guanidine.

In the case of ethanolamine, the pH value at the cathode showed a moderate rise (around pH 12.5) as was observed in the investigation presented in Part 1 of this Chapter. On the other hand, in both inhibitors' cases, the calculated pH values at the cathode in the side column specimen were higher than 13.6, indicating a potential risk of deleterious ASR (alkali-silica reaction) when susceptible aggregates are contained in concrete, as discussed in the subsection 4.11.1.3.

An interesting phenomenon may be that a bulge can be seen at around 10mm in the pH profiles in the centre column for both inhibitors, which was not observed in the simulation of the electrochemical inhibitor injection treatment applied to fully carbonated material, as described in Part 1. This may be attributable to the lateral current flow from the centre column to the side column in the layers 1-2 (see subsection 5.9.1), promoting the migration of hydroxyl ions from the side column to the centre column, resulting in a local concentration increase of hydroxyl ions in this region, as discussed in subsection 4.11.2.2.

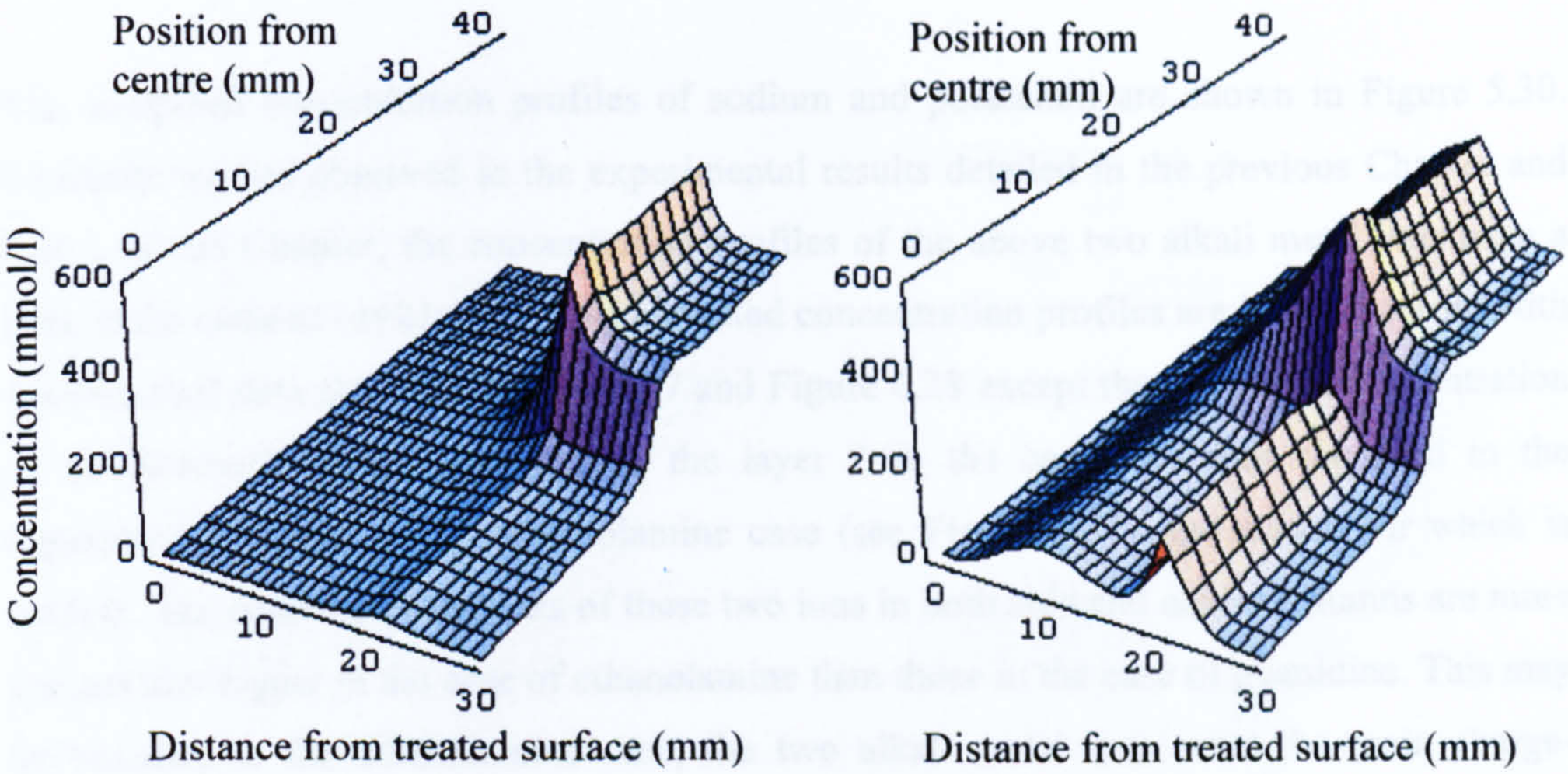

Figure 5.28 Computed concentration profile for hydroxyl ions after galvanostatic treatments at 5A/m^2 applied for 7 days (Left: ethanolamine, right: guanidine)

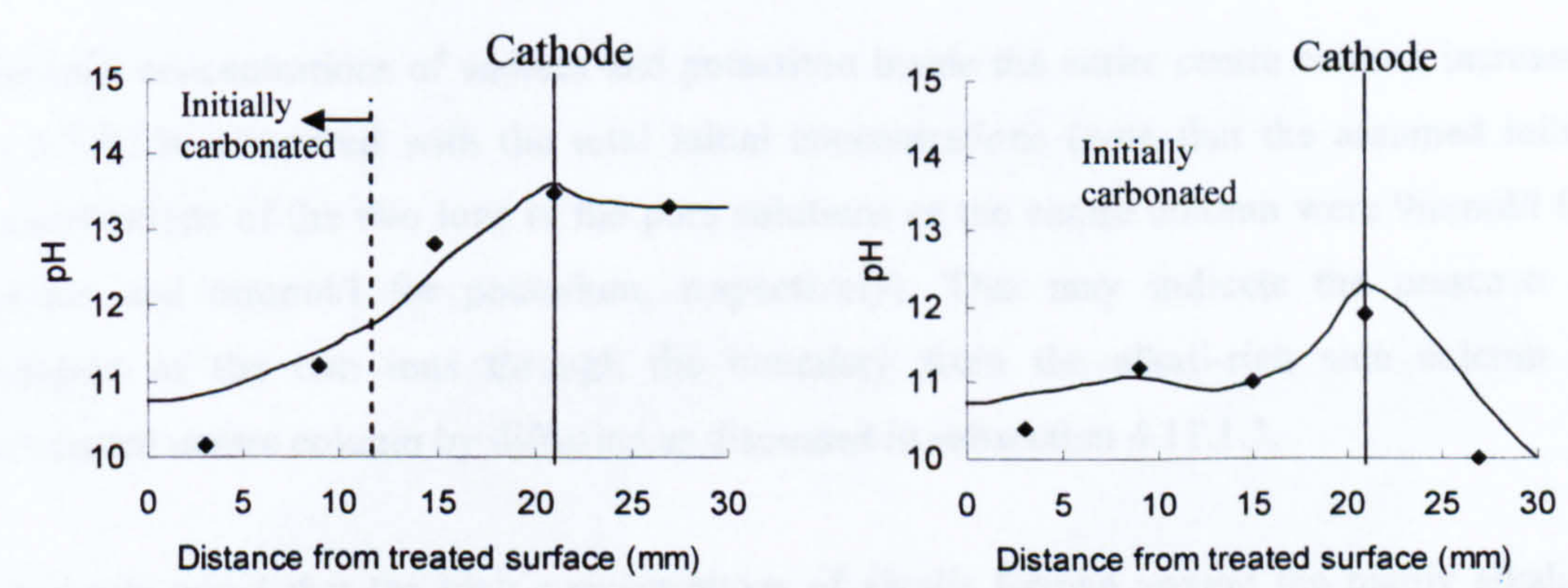

Figure 5.29 Computed pH profiles in the material electrochemically treated with (A) ethanolamine and (B) guanidine (left: side solumn, right: centre column, line: model prediction, dots: experimental data)

5.9.4 Alkali metal ions

The computed concentration profiles of sodium and potassium are shown in Figure 5.30. Similarly, as was observed in the experimental results detailed in the previous Chapter and Part 1 of this Chapter, the concentration profiles of the above two alkali metal ions have a peak at the cathode (z=21mm). The calculated concentration profiles are in good accord with experimental data shown in Figure 4.27 and Figure 4.28 except the plateau of concentration of 20-40mmol/l of the two ions in the layer 2 in the centre column observed in the experimental results for the ethanolamine case (see Figure 4.27), the reason for which is unclear. The concentration peaks of these two ions in both side and centre columns are more pointed and higher in the case of ethanolamine than those in the case of guanidine. This may be because, in the ethanolamine case, the two alkali metal ions were the main charge-carrying cations, since the predominant form of ethanolamine penetrating into the specimens was molecular, resulting in more rapid migration of the two ions in the electric field than was the case for guanidine.

The total concentrations of sodium and potassium inside the entire centre column increased by 5.7-9.3% compared with the total initial concentrations (note that the assumed initial concentrations of the two ions in the pore solutions of the centre column were 9mmol/l for sodium and 6mmol/l for potassium, respectively). This may indicate the presence of transport of the two ions through the boundary from the alkali-rich side column to carbonated centre column by diffusion as discussed in subsection 4.11.1.3.

It is again noted that the high concentrations of alkalis formed around the highly alkaline steel cathode area during the electrochemical treatment may involve the possibility of generating damaging ASR when susceptible aggregates are contained in concrete.

(A) Ethanolamine

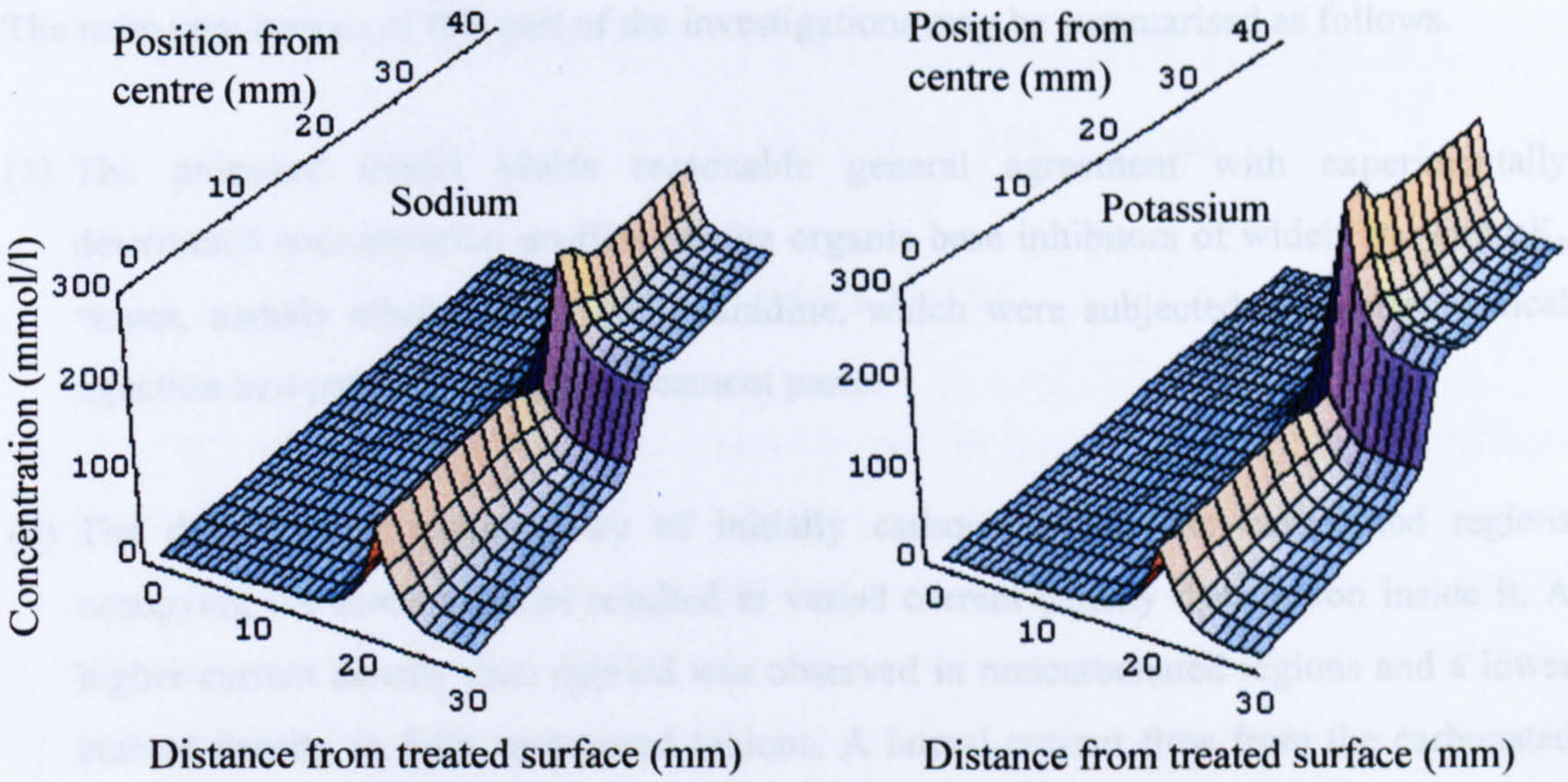

(B) Guanidine

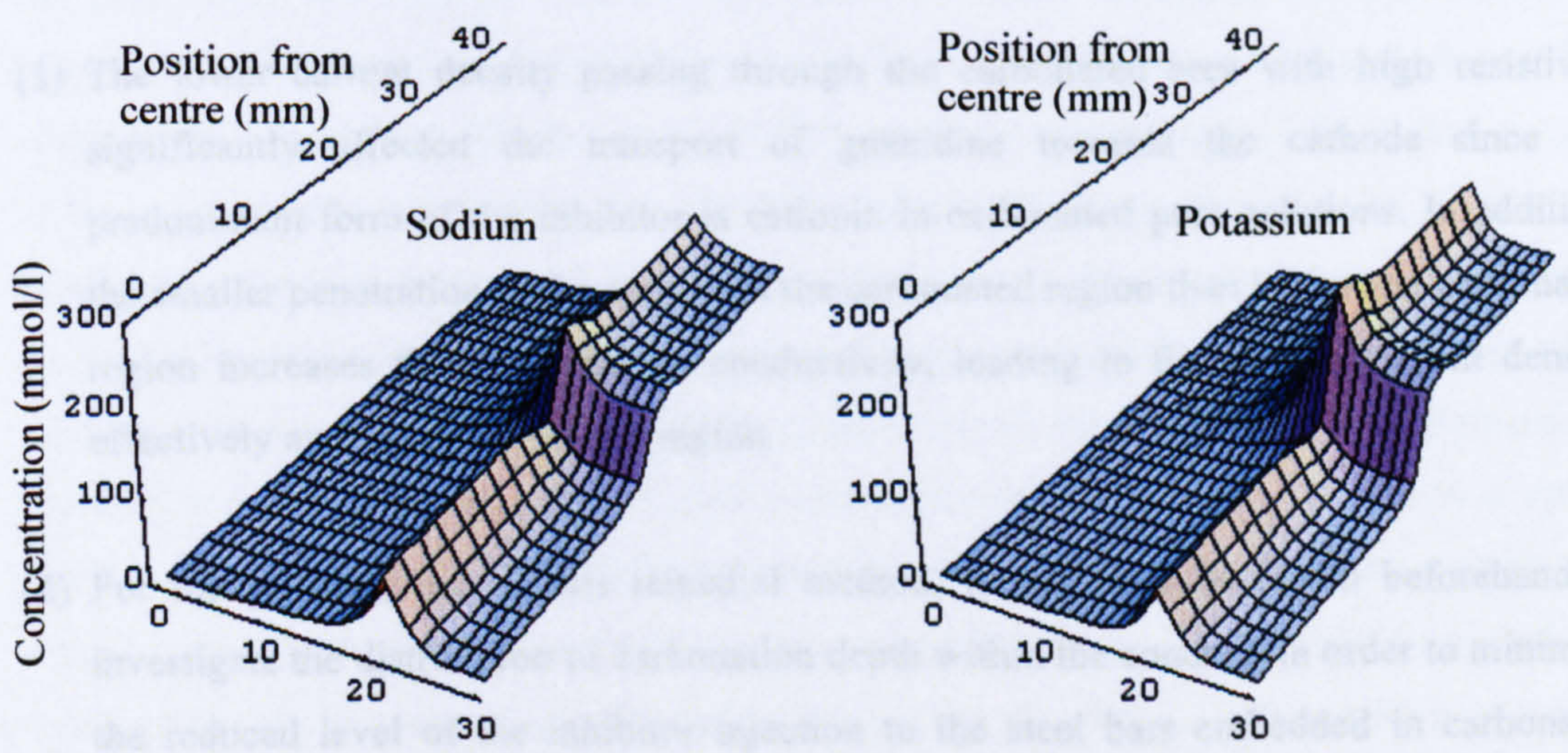

Figure 5.30 Computed concentration profiles of sodium and potassium in the material electrochemically treated with (A) ethanolamine and (B) guanidine (left: sodium, right: potassium)

5.10 CONCLUSIONS

The main conclusions of this part of the investigations may be summarised as follows.

(1) The proposed model yields reasonable general agreement with experimentally determined concentration profiles for the organic base inhibitors of widely varying pK_a values, namely ethanolamine and guanidine, which were subjected to electrochemical injection into partially carbonated cement paste.

(2) The difference in conductivity of initially carbonated and non-carbonated regions occupying the same material resulted in varied current density distribution inside it. A higher current density than applied was observed in noncarbonated regions and a lower current density in fully carbonated regions. A lateral current flow from the carbonated region to the non-carbonated region near the boundary, which was expected to cause migration of hydroxyl ions from the latter region to the former region, was also simulated.

(3) The lower current density passing through the carbonated area with high resistivity significantly affected the transport of guanidine towards the cathode since the predominant form of the inhibitor is cationic in carbonated pore solutions. In addition, the smaller penetration of the cations in the carbonated region than in the non-carbonated region increases the difference in conductivity, leading to far smaller current density effectively applied in the former region.

(4) For the practical use of this remedial method, it may thus be useful beforehand to investigate the distribution of carbonation depth within the concrete in order to minimise the reduced level of the inhibitor injection to the steel bars embedded in carbonated regions, when an inhibitor with a high pK_a value is employed.

(5) Sodium and potassium are the major charge-carrying cations in the side column with high pH. The two alkali metal ions were observed to move towards the initially carbonated centre column by diffusion; however the accumulation of the ions in the vicinity of the cathode in the side column was significant, thus care must be taken when the method is applied to concrete that contains aggregate susceptible to ASR.

CHAPTER 6

LONG-TERM DURABILITY OF ELECTROCHEMICAL INHIBITOR INJECTION METHOD

6.1 INTRODUCTION

It was confirmed in the previous two Chapters that the organic base corrosion inhibitors studied in this thesis were, by means of the proposed electrochemical injection treatments, successfully injected into fully/partially carbonated cement paste at depths corresponding to normal cover thickness to reinforcing steel with substantial concentrations that had been found to be adequate for steel passivation in Chapter 3. When it comes to the issues of long-term passivation of embedded steel, it should be noted that, after the completion of electrochemical treatment, the injected inhibitors that once accumulated in the vicinity of steel cathode by the help of the electric field may gradually migrate inside the material or dissipate from the material surface over time by such mechanisms as diffusion or evaporation. This may lead to a reduction in inhibitor concentration near the steel, possibly affecting its passivation. Elsener et al. (1999) pointed out that, especially in the case of inhibitor of volatile compounds, the durability of the inhibitor action may be affected by evaporation through the porous material. In this Chapter, the longevity of the proposed method is investigated, where the condition of the steel embedded in concrete samples after inhibitor injection treatment was electrochemically monitored through the measurements of potential and corrosion rates of the steel under reasonably long-term exposure to a cyclic wet/dry regime. Then the re-distribution profiles of the inhibitor concentration inside the material were probed by means of ion chromatography after a fairly long period of the exposure for the investigations of whether or not the injected corrosion inhibitors would remain at the steel in an adequate concentration required for steel passivation.

The main two factors which were found, in the previous two Chapters, to possibly affect the passivation of the embedded steel were the concentrations of inhibitors and hydroxyl ions that were accumulated and generated at the steel cathode at the completion of the galvanostatic treatment. In this study, in order to elucidate which of the above two factors more significantly influences the long-term passivation of the embedded steel exposed to the electrochemical inhibitor injection treatment, the samples treated with electrochemical re-

alkalisation (using a 1M sodium carbonate solution as external anolyte) were introduced as "blank samples", in which the passivation of the steel embedded in carbonated concrete was considered to be mainly controlled by restored alkalinity associated with the generation of hydroxyl ions at the cathode during the treatment. Besides such corrosion monitoring methods as potential monitoring and corrosion rates measurements by means of linear polarisation conducted, the effect of the injected inhibitors and the electrochemical re-alkalisation on the inhibition of embedded steel was also investigated by the interrogation of the steel bars by means of EIS (electrochemical impedance spectroscopy) technique, highlighting the change in such interface properties on the steel surface as double layer capacitance.

A technique is desirable for confirmation of long-term passivation of steel bars in concrete by which the steel is easily or quickly driven to passivation and the passivation is maintained for a long period. It is known (Hancock and Mayne 1957) that anodic polarisation rapidly enhances the potential of steel in electrolytes if it is passivated. In this Chapter, the effectiveness was also investigated of anodic polarisation applied to steel embedded in concrete for the purpose of securing long-term passivation as well as for the purpose of instant determination of its passivation. The steel potential, which was expected to be significantly lowered due to the electrolysis during the proposed electrochemical treatment, was intentionally raised by anodic polarisation after the completion of the treatment, and then the potential profiles were monitored for an investigation of whether anodic polarisation would indicate the steel condition in a reasonably short period and would maintain the steel potential in a noble region for a fairly long period.

6.2 LITERATURE REVIEW

6.2.1 Long-term effectiveness of corrosion inhibitor in concrete

There are some researches concerned with remedial treatment for reinforcing steel in concrete with corrosion inhibitors aiming at the evaluation of long-term durability after treatment.

Qian and Cusson (2004) investigated the effectiveness of several commercial organic/inorganic corrosion inhibitors from a 5-year field survey of highway bridges where the inhibitors were used as admixtures at the construction stage. The authors monitored the condition of the embedded steel by measuring its half-cell potential and corrosion rate every year (1997-2001). Since the obtained corrosion rate was lower than 0.5μA/cm^2 but was increasing, the conclusion derived by the authors was that more time would be required to see the significant corrosion activity and to evaluate the effectiveness of the systems. However the information on concentration of the inhibitor remaining in the vicinity of the steel or inside the concrete during the testing period is not available.

Elsener et al. (1999 and 2000) investigated the efficiency of MCI (migratory corrosion inhibitor) in reducing corrosion of steel in saturated calcium hydroxide solution with chloride additions and chloride-contaminated or carbonated/non-carbonated mortar. The threshold concentration of inhibitor required for steel passivation was first determined (to be 10%) by the recovery of the corrosion potential and polarisation resistance observed when pre-corroding steel bars were immersed in saturated $Ca(OH)_2$ + 1M NaCl containing inhibitor. In Part 1 of their research (1999), an addition of the inhibitor satisfying the concentration threshold for steel passivation predetermined in aqueous solutions, to mortar as admixture was found to yield no significant reduction in corrosion rate for chloride-contaminated specimens and for specimens exposed to CO_2 for around 380 days. In Part 2 of their report (2000), mortar specimens containing pre-corroding steel bars were immersed into the inhibitor solution for around 130 days until the samples took up more than the dosage recommended by the manufacturer. The results showed that no increase in polarisation resistance was obtained and the corrosion potential did not indicate repassivation despite low cover to the embedded steel and high porosity of the mortar used. The authors attributed this to the assumption that the non-volatile fraction of the inhibitor, which had major inhibiting properties, did not diffuse through the mortar because of precipitation of

calcium ions in the pore solution. In addition, the authors mentioned that significant rates of evaporation from treated mortar samples might be observed in atmospheres of RH 80%; however, the actual concentrations of the constituents of the surface applied corrosion inhibitor that migrated and remained in the vicinity of the steel bars are not clear.

Ngala et al. (2002) found that when calcium nitrite was introduced into moderately pre-corroded reinforced concrete specimens by means of repeated ponding with an aqueous solution of recommended dosage of the inhibitor, significant reductions in the overall rates of corrosion of bars embedded were achieved at depths of 12mm after a cyclic wet/dry regime for over 700 days, provided that the initial chloride content was relatively low for non-carbonated concrete or very low for carbonated concrete. At the end of exposure period, the concentrations of the penetrating inhibitors and chloride ions in chloride-contaminated specimens (w/c: 0.65) were obtained by means of an ion-chromatography, and the obtained concentration ratio of the former to the latter anion was found to be close to the threshold value for borderline passivation reported by Jazairi et al. (1990). It was also found that the penetration of nitrite was much lower in the case of carbonated specimens (w/c 0.8). In the second Part of the series of the investigations (Ngala et al. 2003), the authors used sodium monofluorophosphate and obtained similar results. Later, the authors (Ngala et al. 2004) investigated the effectiveness of surface applied ethanolamine-based corrosion inhibitors for carbonated concrete with a cover depth of 5mm and 12mm and demonstrated that there was no evidence of passivation of steel bars embedded in carbonated concrete after exposure to a wet/dry regime for a fairly long period (around 18 months), although ethanolamine had been shown to penetrate to depths > 25mm (approximately 2mg/g concrete was detected) by means of ion chromatographic analysis. The results derived in this research demonstrated that surface application of ethanolamine-based corrosion inhibitor was not effective for long-term steel passivation, as indicated by Page et al. (2000); however, the information on the evolution of inhibitor concentration inside the samples associated with re-dosage or wash-out of the inhibitor with respect to time in the cyclic wetting and drying conditions may be desired.

For the minimisation of dissipation of the inhibitors from the material, Fedrizzi et al. (2005) claimed that simultaneous use of surface applied inhibitor with a good barrier coating offered substantial protection against rebar corrosion by preventing the volatile substances of the inhibitors from coming out from the system, although no quantitative information on the long-term performance of this treatment was provided. Batis et al. (2003) also demonstrated

that, for carbonated concrete specimens, the simultaneous use of the alkanolamine corrosion inhibitor (as admixture) with inorganic coatings improved the corrosion resistance of embedded bars more than the use of either of the remedial systems individually after 10 months of immersion in the corrosive environment of a 3.5% NaCl solution; in spite that the steel bars used for all cases in the experiment were not observed to be passivated.

In the cases of corrosion inhibitors injected into concrete by the help of applied electric field, Phanasgaonkar et al. (2000) and Holloway et al. (2004) investigated the efficiency of electrochemically injected corrosion inhibitors on the long-term passivation of the embedded steel, as described in Chapter 4 (subsection 4.2). In the former study, the authors claimed that the combined system of both applied field and inhibitors showed the higher level of inhibition than that observed in the case of control specimens that were exposed to applied electric field only. However, as mentioned in Chapter 4, such high accumulation of the inhibitors with low pK_a values at the steel cathode appears somewhat unlikely, and the passivation of the embedded steel might be mainly attributable to the generation of hydroxyl ions due to the electrolysis. In the latter study, the samples that had been electrochemically treated with MCI were exposed to external chlorides for 300 days and then exposed to a laboratory environment for additional 4 years without further interference. After 1 year's exposure to external chlorides, the treated specimens showed passivation, however, after additional 4 years' exposure, the polarisation resistance was observed to decrease with lowered steel potential (around -430mV vs SCE), although the injected inhibitor was confirmed to still remain inside the samples. The evolution of inhibitor concentration inside the specimens over time is not presented in the report, but this reduction in passivation might be attributable to the dissipation of some proportion of the injected inhibitor from concrete by diffusion or evaporation.

6.2.2 Anodic polarisation technique

It is desired that a quick and simple method to evaluate the long-term durability of a remedial treatment system for embedded steel be established, which can be applied soon after treatment. Galvanostatic anodic polarisation is reported as a possible rapid method of determining whether the environment surrounding the steel is corrosive or not (Hancock and Mayne, 1957). According to these authors, anodic current density of $10\mu A/cm^2$ raises the potential of steel dramatically if it is readily passivated.

Assuming the system response approximates to that of a Randles equivalent circuit (Randles 1947), Elsener et al (1994) gave the theoretical basis, the experimental details and field experience with this rapid galvanostatic pulse technique. When an instantaneous current step I_{app} is applied to a corrosion system, the potential, V_t, at a given time t can be expressed as follows:

$$V_t = I_{app}[R_p[1-\exp(-\frac{t}{R_p C_{dl}})]+R_\Omega] \qquad (6\text{-}1)$$

where R_p is polarisation resistance, C_{dl} is double layer capacitance, and R_Ω is ohmic resistance. As is shown in Figure 6.1, extrapolation of the fitted potential jump at t=0 allows us to calculate the ohmic resistance $R_\Omega(E_{ohm}/I_{app})$, while from extrapolation to infinity at t=∞ the steady state polarisation resistance R_p is determined.

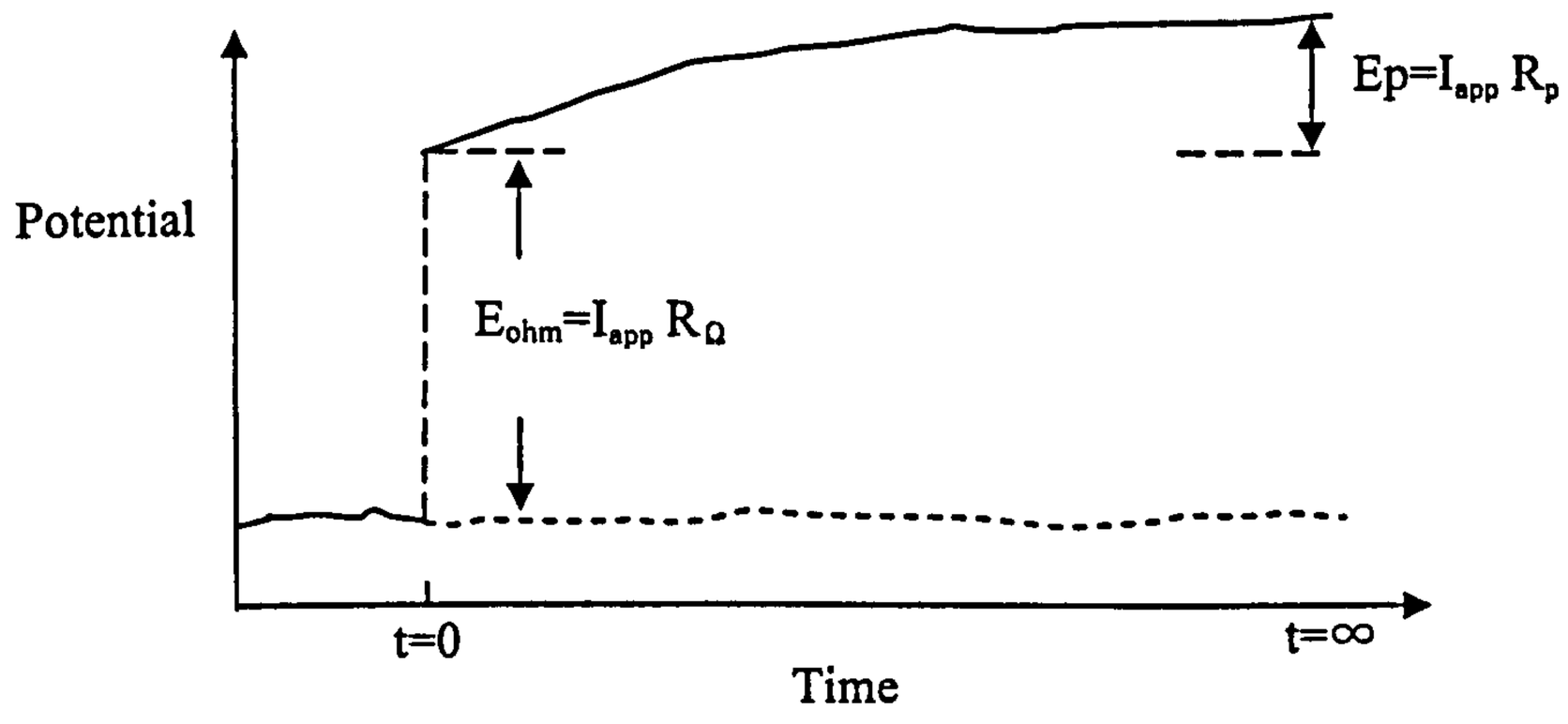

Figure 6.1 Calculation of resistivity by extrapolation of the potential

Here it is planned to apply this method to the steel bars shortly after the electrical remedial treatment described in Chapter 4 and 5 in order to evaluate the ease of passivation of the reinforcement and the durability of passivation.

The long-term performance of electrochemical re-alkalisation will be investigated in this study. In spite of the fact that this technology has widely been used, there still remain several unanswered questions to be resolved. One of them is that the durability of this method has yet to be demonstrated and the acceptance criteria to decide the completion of a successful treatment have not been agreed (Page, 2002).

Phenolphthalein indicator is commonly used in practical applications to assess the depth of re-alkalisation; however, the test only gives information on whether the pH value of the concrete pore solution is above or below 10, and is therefore not sufficient proof of repassivation of the steel. Mietz (1995) investigated the repassivasion of steel after re-alkalisation treatment by anodic polarisation, and concluded that the phenolphthalein test is not a sufficient tool to prove the repassivation of the steel. Half-cell potential is often measured to evaluate the passivation of embedded steel after several months of completion of the electrical treatment. However, Sergi et al (1996) applied the anodic polarisation technique at a constant current density of $20\mu A/cm^2$ for 20 hours and demonstrated that potential survey after electrochemical re-alkalisation could sometimes be misleading because it is likely that the depolarisation of steel takes considerable periods of time. Here the current density and the duration of anodic polarisation, which are required for an accurate judgement of the passivasion of the steel and an adequate durability, have been unclear. Thus, the anodic polarisation technique with several combinations of current density and duration will be applied to evaluate the long-term performance of electrochemical re-alkalisation technology in this study.

6.2.3 EIS technique

It is widely claimed that EIS (Electrochemical Impedance Spectroscopy) is not only a powerful non-destructive method of characterising many of the electrical properties of materials and their interfaces, but also a convenient method to analyse the corrosion phenomena of steel in concrete. The response to an AC input is a complex impedance that has both real and imaginary components Z' and -jZ", where j is the imaginary unit ($j=\sqrt{-1}$). The data analysis method is used on the basis of an equivalent circuit correlated to the properties of concrete and electrochemical mechanisms. For example, the most common equivalent circuit used to model corrosion of bare metal in aqueous electrolyte is the Randles circuit (Randles 1947), as shown in Figure 6.2, where corroding interface is described by an interfacial polarisation ohmic resistance R_p and a double layer capacitance C_{dl} in parallel. The impedance is given by the following:

$$Z=\left(1/R_p+j\omega C_{dl}\right)^{-1} \tag{6-2}$$

where ω is angular frequency of AC input (ω=2πf). The double layer capacitance value is obtained by the frequency f at the highest point on the semicircle as follows:

$$C_{dl} = \left(2\pi R_p f\right)^{-1} \tag{6-3}$$

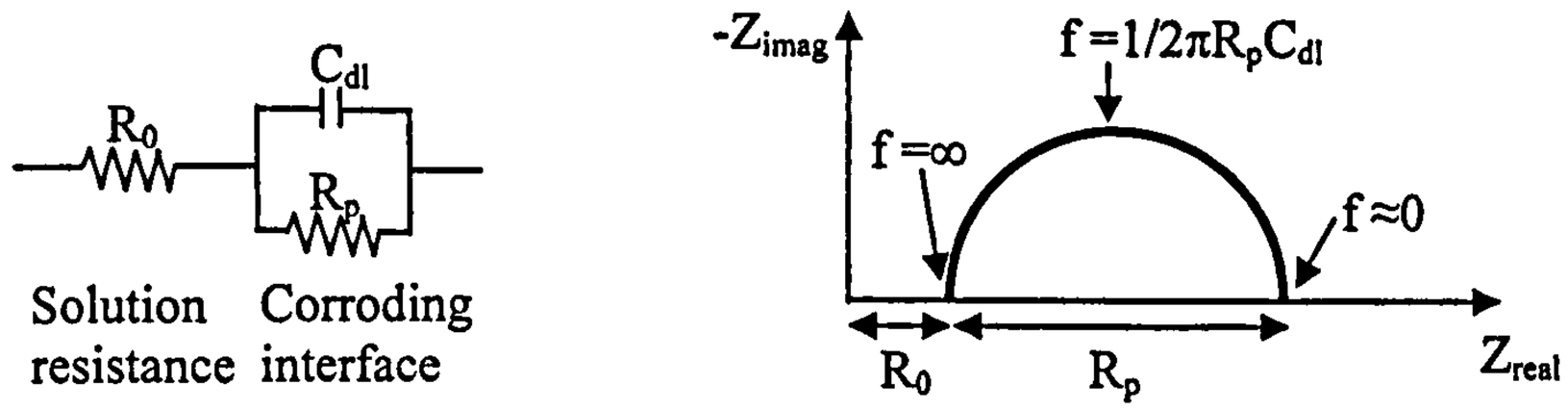

Figure 6.2 Randles equivalent circuit

EIS measurements in reinforced concrete were carried out from the first studies of Dawson et al. (1978). Dawson and his co-workers (John et al. 1981) modelled steel in concrete as an equivalent circuit form shown in Figure 6.3 for semi-quantitative interpretations of impedance plots, where two time constants were reported; The left hand components are the solution resistance (R_s), and the concrete film/dielectric relaxation (R_f, C_f), observed in high frequency. The electrochemical response, which is typically observed below 10Hz, results from the double layer capacitance (C_{dl}), the charge transfer resistance (R_{ct}) and the diffusion impedance (W).

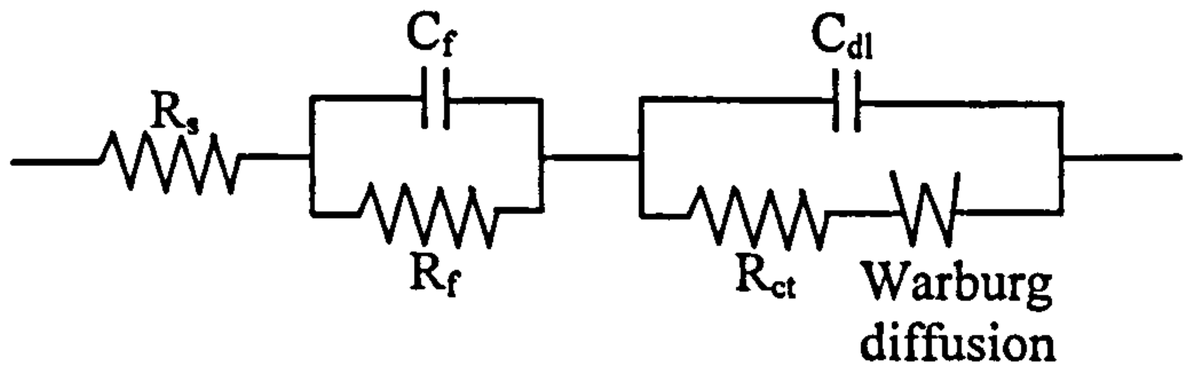

Figure 6.3 Equivalent circuit for steel in concrete proposed by John et al. (1981).

The elucidation of physical meaning of the EIS results obtained has been attempted by many researchers. The high frequency loop (over 10^5 Hz) was ascribed to the concrete properties (Keddam et al. 1997, Andrade et al. 1995, Ford et al. 1998) or to the ionic motion of free ions in the electrolyte filling the pores (Alonso et al. 1998). In the middle frequency region (10^4-10 Hz), the loop has been claimed to be concerned with the dielectric properties of a layer often formed on the steel surface and reputed to be constituted by the effect of an interfacial layer of $Ca(OH)_2$ crystals (Lemoine et al. 1990, Sagoe-Crentsil et al. 1992, Hachani et al. 1992, Gu et al. 1997) or by the rust oxides (John et al. 1981). In the low frequency region (from a few to a few tenths of Hz), EIS spectra are affected by the Faradaic corrosion process occurring on the embedded steel electrodes (Andrade et al. 1995). At even

lower frequencies, the EIS spectra, for which insufficient experimental evidence has been obtained to justify the assumption of diffusion control processes (oxygen diffusion), may be affected by redox processes ($Fe^{2+} \Leftrightarrow Fe^{3+}$) (Andrade et al. 1995).

It is reported that the changes in double layer capacitance (C_{dl}) obtained from EIS measurements gives some information about the inhibitor film formation. The inhibition mechanism is based on adsorption of the inhibitor to metal surfaces (see Chapter 3). In general, the raise in C_{dl} values may suggest an increase of the active area (Montemor et al. 1995), and the decrease in the values, which can result from a decrease in local dielectric constant and/or an increase in the thickness of the electrical double layer, can be attributable to the adsorption of the inhibitors on the metal surface (McCafferty and Hackerman 1972, Ravichandran and Rajendran 2004, Jamil et al. 2005) or a denser inhibitor molecular structure in the layers (Tan et al. 1996). Therefore it might be useful to investigate double layer capacitance (C_{dl}) by EIS for evaluations of steel inhibition induced by corrosion inhibitors.

Andrade et al. (1995) claimed three main frequency regions of different processes in an EIS response, where the magnitude of capacitances is characterised as follows:

(1) High (in the range of KHz) – where the electrolyte (concrete) itself presents a response. The capacitances are in the order of pF/cm^2. More than one time constant may appear due to the moisture content of the concrete or the different constituents of the solid phases.
(2) Medium (few to tenths of Hz) – where faradic processes present a response and typical capacitances are in the order of $\mu F/cm^2$. More than one time constant may be found when localised attack is developing, as reported by Mansfeld (1990) and Carnot et al. (2003) (see Figure 6.4).
(3) Low (below 1Hz) – where the redox process, indicating the presence of the reaction $Fe_3O_4 \Leftrightarrow \gamma\text{-}Fe_2O_3$ equilibrium in the passive layer, may occur depending on the potential, which is supported by Joiret et al. (2002). The capacitances recorded are in the magnitude of mF/cm^2.

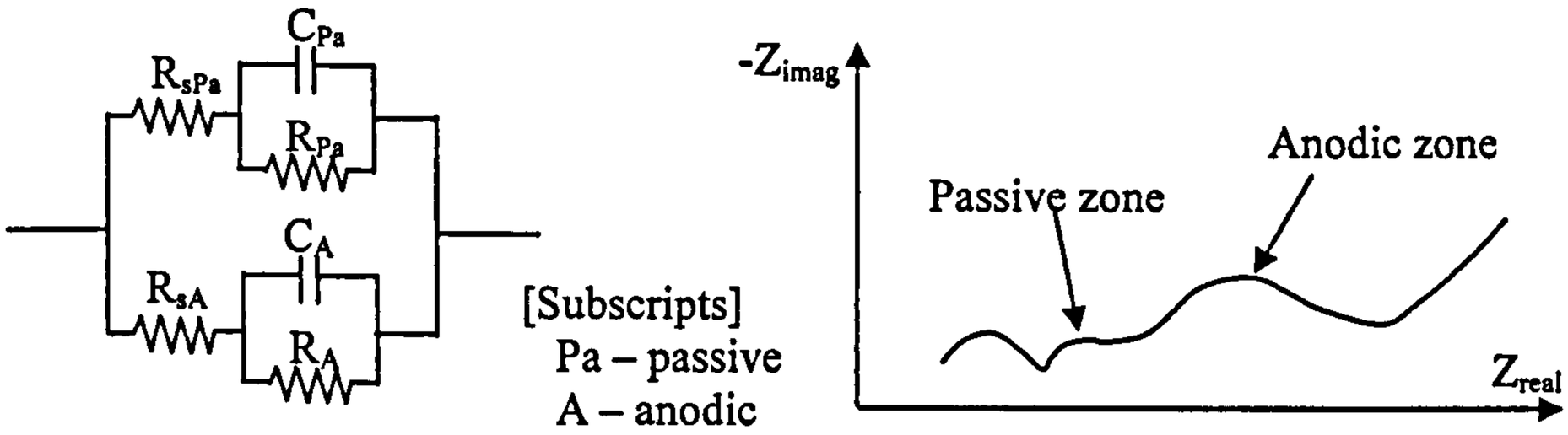

Figure 6.4 Equivalent circuit for pitting corrosion model and corresponding impedance plot in the complex plane (Nyquist plot) (Andrade et al. 1995).

For an investigation of corrosion inhibitor performance (using sodium nitrite and dinitrobenzonic acid as admixture) in chloride-contaminated concrete, Gu et al. (1997) adopted a modified electrical equivalent circuit as shown in Figure 6.5, similar to that reported by Sagoe-Crentsil et al. (1992), each parallel combination of a pure resistor and a frequency dependent capacitor (also called a constant phase element, CPE (Pajkossy 1994), see subsection 6.4.3.2.2), simulating concrete matrix, interfacial film, and double layer respectively. As a result, the concrete matrix C_C was obtained in high frequency (10kHz and higher) with the magnitude of pF-nF/cm^2, the film capacity C_f to be in medium frequency (10kHz to 1Hz) with the magnitude of few μF/cm^2, and the double layer capacitance C_{dl} to be in low frequency with the magnitude of a few hundred of μF/cm^2. It appeared that the both corrosion inhibitive substances did not make a significant difference to the values of C_c and C_f, whilst they increased the values of R_p (polarisation resistance) and lowered the values of C_{dl} remarkably.

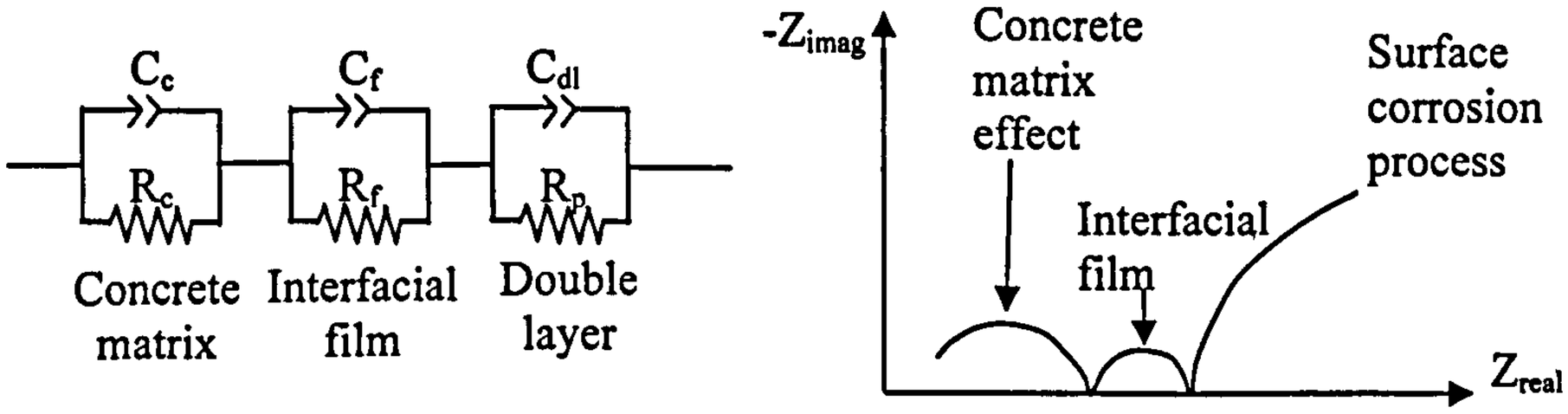

Figure 6.5 Equivalent circuit and corresponding impedance plot in the complex plane (Nyquist plot) used by Gu et al. (1992) for inhibitor performance analysis.

Trabanelli et al. (2005) evaluated the inhibitive action of some organic corrosion inhibitors such as the sodium salts of benzoic acid and dicarboxylic acids in carbonated concrete by means of EIS. An equivalent circuit as shown in Figure 6.6 was employed for the extrapolation of data, where R_0 and R_C correspond to the resistance of electrolyte inside the

concrete pores and to the resistance of the concrete itself, respectively; R_f and CPE_f are related to the resistive and capacitive properties of the surface film at the steel/concrete interface, and R, r, W, and CPE are connected to the process occurring at steel/concrete interface. The results also showed the decrease in CPE in the case of inhibitor applications.

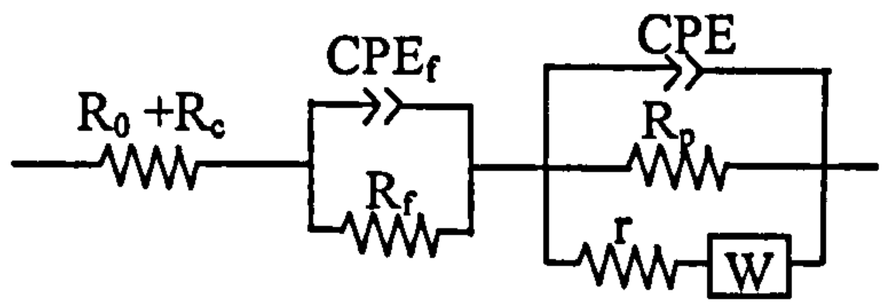

Figure 6.6 Equivalent circuit used by Trabanelli et al. (2005)

Ford et al. (1998) proposed a useful table for making impedance spectroscopy feature assignments based on capacitances as shown in Table 6.1. The derived capacitance values may sometimes be used to determine which parts of the response are due to the corrosion process, although it is often difficult to separate the response into different parts, making a clear interpretation quite difficult (Gowers et al. 1999).

Table 6.1 Capacitance values and their possible interpretations (Ford et al. 1998)

Capacitance (F)	Phenomena responsible	Origin	Frequency region
10^{-11}	Bulk	Bulk	MHz
10^{-10}-10^{-8}	Internal space charge layers	Bulk	kHz-MHz
10^{-7}-10^{-4}	Product layers	Electrode	mHz-Hz
10^{-4}	Electrochemical reactions	Electrode	mHz

Although EIS is a useful tool that provides some information about materials and interfaces, indicating corrosion properties as mentioned above, the fitting is still mere a mathematical operation without physical basis (Andrade et al. 1995). It may be said that the properties gained from complicated EC are questionable unless a convincing physical meaning to the components presented in the EC is fully given.

6.3 EXPERIMENTAL PROCEDURES

6.3.1 Objectives and overview of experiment

The experimental work presented in this Chapter was carried out at two places at two different periods of this research. Preliminary experiments were carried out in Leeds University, UK (hereafter termed as "Leeds experiments"), and, due to the author's personal circumstances, further experiments were subsequently conducted at the Research Institute of Japan Central Railway Company in Nagoya, Japan (hereafter termed as "Nagoya experiments"). All of the concrete specimens studied in this Chapter were produced at Leeds University, UK by the procedure detailed in subsection 6.3.2. Some of the specimens were transferred by air from Leeds to Japan after they were fully carbonated, and these were to be subsequently used for Nagoya experiments. The parametric plan of the experiments carried out at the different two sites for this Chapter is described in Table 6.2. For specimen preparation, injection treatment, and inhibitor concentration analysis in this Chapter, the experimental technique presented by Sawada et al. (2005) was used.

6.3.1.1 Leeds experiments

There were three objectives for the experiments. The first was to investigate the effect of anodic polarisation on the electrochemical conditions of embedded steel. As shown in Figure 6.7, it was not clear how the potential of passivated steel once raised by anodic polarisation would behave after application of anodic current was terminated, although it was desired that the enhanced steel potential would reduce slowly, but remain in the noble region until it stabilised (shown as the dotted line (a) in the Figure) or would reduce soon, but finally approach higher potential value than initial (dotted line (b) in the Figure). Anodic current was applied to steel embedded in non-carbonated concrete specimens with or without chloride at varied current densities for varied periods (see (A) in Table 6.2) and the evolution of steel potential was monitored after application of anodic current was terminated, by which the magnitude of current density that was to be applied to electrochemically treated specimens in (B) was optimised.

The second objective was to investigate preliminarily the long-term durability of inhibition of steel bars embedded in the carbonated concrete that had been electrochemically treated with organic corrosion inhibitors and had been exposed to anodic polarisation at the current

densities determined in experiments (A) at different timings after treatment (see (B) in Table 6.2). The inhibition performance was evaluated by monitoring the potential and corrosion current density of the steel embedded in the concrete specimens whilst the specimens were exposed to cyclic wet and dry conditions. Among the three organic corrosion inhibitors studied in this thesis, guanidine was used in this experiment. The timing of anodic current application that contributed to the long-term passivation of steel most significantly was determined from the results, and this was employed in anodic polarisation applied to the electrochemically treated specimens in Nagoya experiments (D) detailed in the following subsection.

The third objective was to obtain a concentration profile of electrochemically injected inhibitor into a concrete specimen soon after the treatment was finished. The procedure is described in subsection 6.3.5. Among the three inhibitors studied in this thesis, the concentration profile of arginine was obtained in the experiment (see (C) in Table 6.2), since the injected concentration profiles of the other two inhibitors, namely ethanolamine and guanidine, soon after the treatment were available in the literature (Sawada et al. 2005). For the investigation of the dissipation effect of the injected inhibitors from the embedded steel bars, the concentration profile of arginine in specimen LPA (see Table 6.2) obtained in this experiment was compared with that in the specimen subsequently obtained 160 days after the injection treatment in Nagoya experiments (see NPA in Table 6.2 (E)).

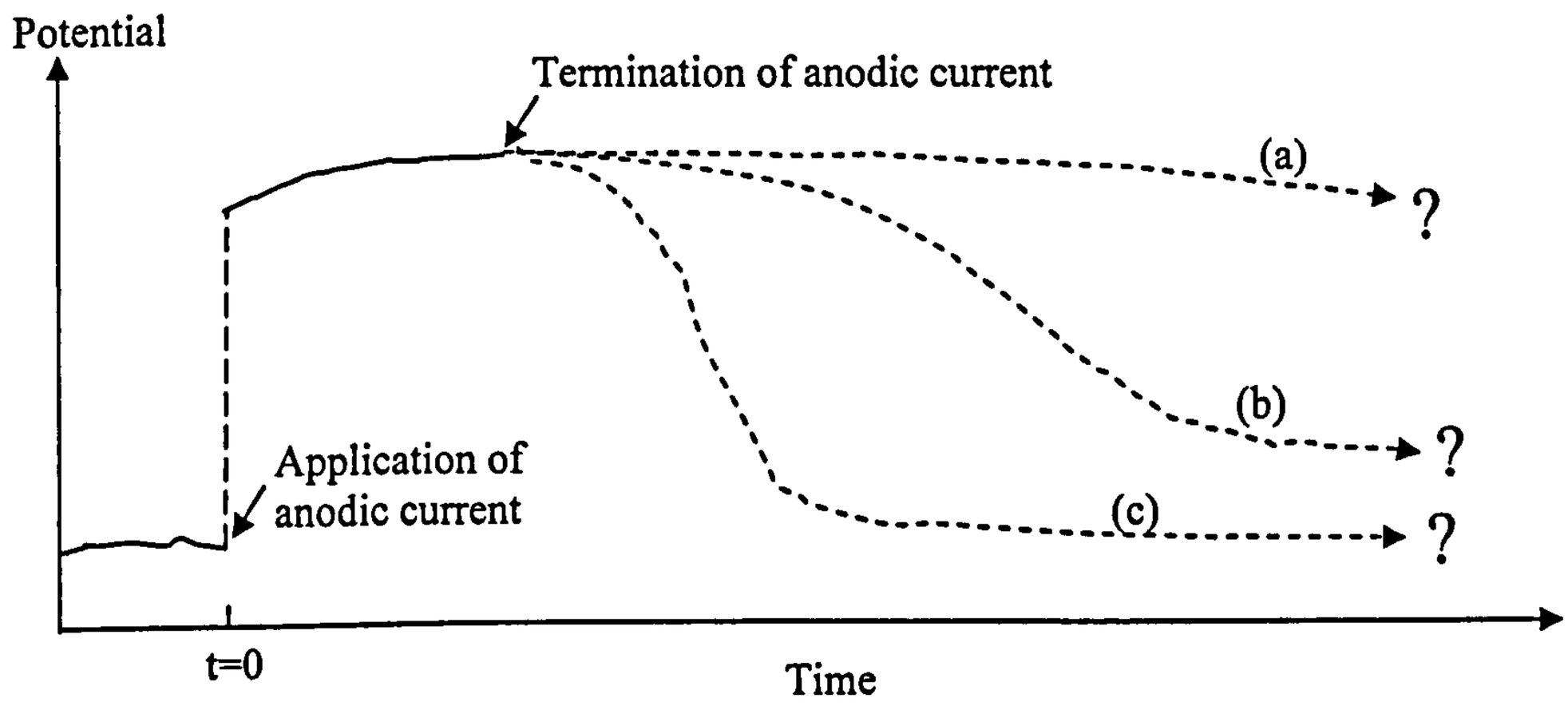

Figure 6.7 Evolution of potential predicted prior to experiments

6.3.1.2 Nagoya experiments

The long-term durability of electrochemical inhibitor injection into the carbonated concrete specimens transferred from Leeds was investigated with three inhibitors studied in this thesis. After applications of the injection treatment and anodic polarisation, the corrosion-related electrochemical features, such as steel potential, corrosion current density and electrochemical impedance, were monitored over 240 days for the embedded steel in the concrete specimens that were exposed to cyclic wet/dry or dry conditions (see (D) in Table 6.2). In order for the effect of the inhibitor injected in the vicinity of the steel on its corrosion reduction to be investigated, the inhibitive performance of the inhibitor-treated specimens was compared with that of other specimens treated without inhibitors. Thus, specimens treated with 1M sodium carbonate intended for simulation of electrochemical re-alkalisation were employed in this experiment (specimens NR and NRD in Table 6.2 (D)). Carbonated ethanolamine solutions were also prepared as anolyte in the experiment (NEc and NEcD in Table 6.2, (D)), which were expected to minimise the surface dissolution of concrete during the injection treatment owing to the buffer function of carbonate ions in the electrolytes as described in subsection 4.6.5. It was necessary to confirm whether the effect of transfer of the specimens from Leeds to Nagoya on the features of the specimens was considered to be negligible, thus the corrosion monitoring results after the injection of guanidine (specimens NG) were compared with those obtained in Leeds experiments (specimens LG7). The measured corrosion rates of the steel embedded in the specimens under wet/dry condition for 240 days (NEn, NEc, NG, NA, NR, and NC) were justified by the gravimetric analysis of the steel bars.

For the investigation of the dissipation of injected inhibitors that might affect longevity of the injection method, approximately 160 days after the injection treatment was finished, the concentration profiles of the three inhibitors remaining in the concrete specimens were obtained (NPE, NPG and NPA). These profiles were compared with those obtained just after the treatment (data presented by Sawada et al. 2005 for ethanolamine and guanidine, and LPA for arginine).

Table 6.2 Experimental plan (Keys in next page)

[Leeds experiments]

(A) Preliminary investigation on anodic polarisation parameters

Label	Tri.	Chemical injected	Anodic polarisation		Note
			Current density.	Period applied	
LA	-	None	10 -200μA/cm^2	10secs-100mins	Non-carbonated
LAC	-	None (5%Cl inc.)	10 -200μA/cm^2	10secs-100mins	Non-carbonated

(B) Inhibitor injection, anodic polarisation and corrosion monitoring

Label	Tri.	Chemical injected	Expo.	Anodic polarisation		Corrosion monitoring			Grav. analysis
				1 day	7 days	Pot.	Rate	EIS	
LG	Yes	Guanidine C.	W/D	-	-	Yes	Yes		-
LG1	Yes	Guanidine C.	W/D	Yes	-	Yes	Yes	-	-
LG7	Yes	Guanidine C.	W/D	-	Yes	Yes	Yes	-	-
LC	Yes	None (Control)	W/D	-	-	Yes	Yes	-	-

(C) Inhibitor injection and concentration profile analysis

Label	Tri.	Chemical injected	Expo.	Anodic polarisation		Concentration profile analysis	
				1 day	7 days	0 days	160 days
LPA	-	Arginine N.	-	-	-	Yes	-

[Nagoya experiments]

(D) Inhibitor injection, anodic polarisation, corrosion monitoring and gravimetric analysis

Label	Tri.	Chemical injected	Expo.	Anodic polarisation		Corrosion monitoring			Grav. analysis
				1 day	7 days	Pot.	Rate	EIS	
NEn	Yes	Ethanolamine N.	W/D	-	Yes	Yes	Yes	Yes	Yes
NEnD	Yes	Ethanolamine N.	D	-	Yes	Yes	Yes	-	-
NEc	Yes	Ethanolamine C.	W/D	-	Yes	Yes	Yes	Yes	Yes
NEcD	Yes	Ethanolamine C.	D	-	Yes	Yes	Yes	-	-
NG	Yes	Guanidine C.	W/D	-	Yes	Yes	Yes	Yes	Yes
NGD	Yes	Guanidine C.	D	-	Yes	Yes	Yes	-	-
NA	Yes	Arginine N.	W/D	-	Yes	Yes	Yes	Yes	Yes
NAD	Yes	Arginine N.	D	-	Yes	Yes	Yes	-	-
NR	Yes	Na_2CO_3	W/D	-	Yes	Yes	Yes	Yes	Yes
NRD	Yes	Na_2CO_3	D	-	Yes	Yes	Yes	-	-
NC	Yes	None (Control)	W/D	-	-	Yes	Yes	Yes	Yes

(E) Inhibitor injection, anodic polarisation and concentration profile analysis

Label	Tri.	Chemical injected	Expo.	Anodic polarisation		Concentration profile analysis	
				1 day	7 days	0 days	160 days
NPE	-	Ethanolamine N.	W/D	-	Yes	-	Yes
NPG	-	Guanidine C.	W/D	-	Yes	-	Yes
NPA	-	Arginine N.	W/D	-	Yes	-	Yes

[Keys]

Tri.: triplicate specimens (otherwise, single specimen), Expo.: exposure (W/D: under cyclic wet and dry condition, D: under dry condition), Pot: steel potential (Ecorr), Rate: corrosion rate (Icorr), EIS: electrochemical impedance spectroscopy, Grav. analysis: Gravimetric analysis, C.(in Chemical): carbonate, N.(in Chemical): nitrate, Na_2CO_3: used for simulation of electrochemical re-alkalisation

- Anodic polarisation
  1 day: anodic polarisation was applied 1 day after electrochemical injection treatment
  7 days: anodic polarisation was applied 7 days after electrochemical injection treatment
- Concentration profile analysis
  0 days: profile was obtained immediately after electrochemical injection treatment
  160 days: profile was obtained 160 days after electrochemical injection treatment

6.3.2 Specimen preparation

6.3.2.1 Carbonated concrete specimens

OPC was used to manufacture the concrete specimens, the chemical analysis of the cement being shown in 2.1.1. All of the concrete specimens used in the investigation presented in this Chapter were produced in Leeds University, UK. The specimens were made with a w/c of 0.86 in order to obtain permeable concrete in which carbonation would be considered to be rapid. The mix proportions of the concrete are shown in Table 6.3. Cement was first mixed with distilled water for about 2 minutes in a mechanical mixer. Fine aggregate and coarse aggregate were added to the cement pastes in sequence and the mixture was agitated for about 3 minutes. The slump of the fresh concrete ranged from 35 to 165 mm. The mixed concrete was then poured into metal containers of dimensions 100 × 100 × 80 mm with four mild steel bars, which were 8 mm in diameter at intervals of 20 mm and cover depths of 35 mm from one face as shown in Figure 6.8 (a). The end surfaces of the steel bars were masked with epoxy resin and the electrical wire was attached to one end of the steel. The specimens were then compacted on a vibration table for about 1 minute. A piece of cling film was placed on the surface of the concrete in each of the containers to prevent moisture loss. After demoulding and storage in a high humidity room for 7 days, the specimens were sliced into slabs of about 15mm thickness by cutting between each of the steel bars, as shown in Figure 6.8 (b). This ensured that full carbonation across the thickness was achieved rapidly. Other sliced slabs were placed upright in a sealed tank and subjected to the accelerated carbonation treatment as described in subsection 2.2.1. After about two months of this treatment it was found that the specimens were fully carbonated throughout their thickness as shown by the phenolphthalein test. They were then kept at 75% RH in air, which was conditioned by saturated sodium chloride solution, for a further period of 4-5

months. Some of the specimens were used for Leeds experiments (specimens LG, LG1, LG7, LC and LPA), and others were transferred by air to Research Institute of Central Japan Railway Company in Nagoya, Japan, where they were again kept at 75% RH in air over saturated sodium chloride solution for 2-3 months until Nagoya experiments ((D) and (E) in Table 6.2) were started.

6.3.2.2 Non-carbonated specimens

Non-carbonated specimens LA and LAC were produced in same manner as described in the previous subsection until being sliced into slabs of about 15mm thickness, except that sodium chloride (with Cl 5% by cement mass) was added during mixing for the specimens LAC. The slices were kept non-carbonated by wrapping them with cling film to avoid contact to the air at room temperature for 2 weeks, until they were used to investigate the effect of anodic polarisation applied for specimens whose embedded steel bars were passivated or depassivated (Leeds experiments (A)).

Table 6.3 Mix proportions of concrete

W/C	Max. size of aggregate (mm)	Water (kg/m^3)	Cement (kg/m^3)	Fine aggregate (kg/m^3)	Coarse aggregate (kg/m^3)
0.86	10	173	201	803	803

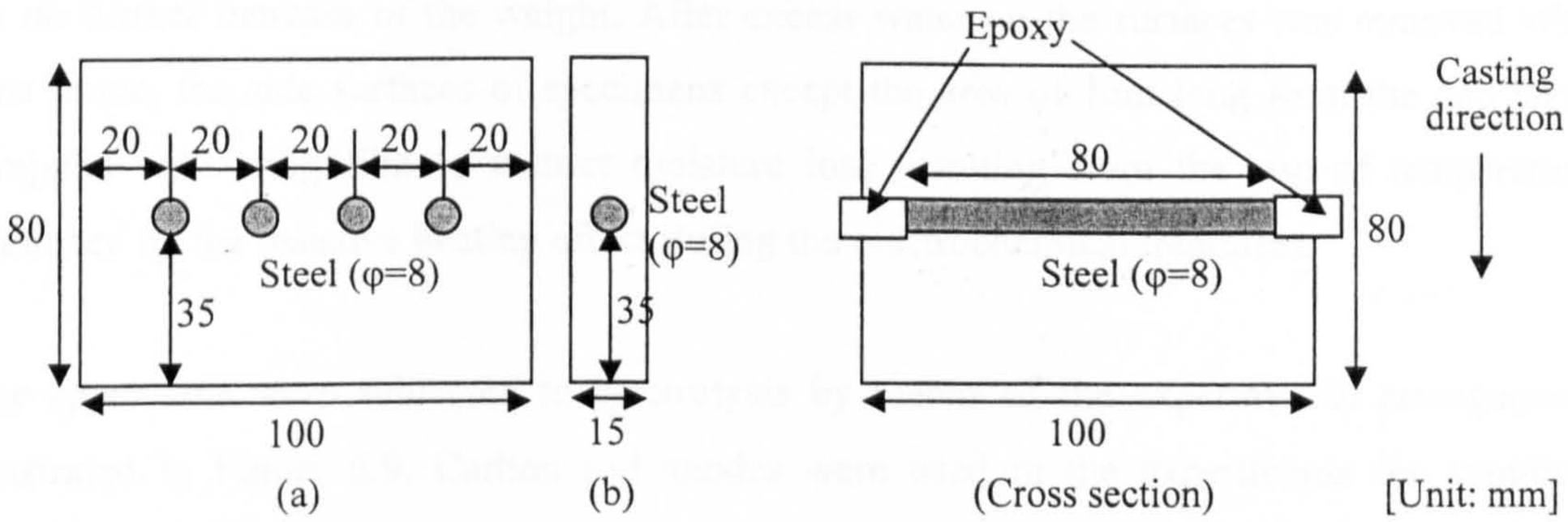

Figure 6.8 Dimension of specimen

6.3.3 Chemicals

The three organic corrosion inhibitors studied in this thesis, namely, ethanolamine, guanidine, and arginine, were investigated in the experimental work presented in this Chapter. The same electrolyte solutions as were used as anolytes in the experimental work presented in Chapter 4 were prepared: 1M ethanolamine nitrate (mixture of 1M ethanolamine and 0.98M nitric

acid, initial pH ~8.0), 0.5M guanidine carbonate (1M with respect to guanidine, initial pH ~11.9) and 0.5M arginine nitrate (mixture of 0.5M L-arginine and 0.48M nitric acid, initial pH ~8.0). In addition, the electrolyte solution of carbonated 1M ethanolamine was produced by injecting carbon dioxide from a carbon dioxide cylinder through plastic tubes into a 1M ethanolamine solution (initial pH ~12.1) until the pH value was lowered to 9.2, at which the solutions could contain substantial concentrations of not only ethanolamine cations but also carbonate ions. The reason for this was that this solution was expected, by the help of the buffer function of carbonate ions, to avoid the dissolution of concrete surface by inducing moderate drop of pH of the anolyte solution during the injection treatment (see subsection 4.6.5). 1M sodium carbonate solution (initial pH ~11.8) was also prepared for a simulation of electrochemical re-alkalisation (NR and NRD).

The above electrolytes were prepared with chemicals listed in Table 2.5 for Leeds and Nagoya experiments respectively, just before they were used as anolyte for electrochemical treatments detailed in the following subsection.

6.3.4 Treatment of specimens with corrosion inhibitors and sodium carbonate

Before the treatment of inhibitor injection or electrochemical re-alkalisation was carried out, the thin slab carbonated specimens (as shown in Figure 6.8 (b)) had been immersed in distilled water for 5 hours to attain a saturated condition. Complete saturation was confirmed by no further increase of the weight. After excess water on the surfaces was removed with lens tissue, the side surfaces of specimens except the area of 1cm long from the end were wrapped with cling film to restrict moisture loss resulting from the rise of temperature produced by the resistive heating effect during the electrochemical treatment.

The specimens were subjected to electrolysis by means of the experimental arrangement illustrated in Figure 6.9. Carbon rod anodes were used in the experiments for avoiding corrosion of the electrodes. The anodes were placed in the bottom of a shallow dish filled with 120 ml of one of the electrolytes described in the previous subsection. For Leeds experiments (B), solutions of only guanidine carbonate were used, whilst for Nagoya experiments (D), solutions of ethanolamine nitrate, ethanolamine carbonate, guanidine carbonate, arginine nitrate, and sodium carbonate were used. Before the specimens were immersed to a depth of 2 mm in the electrolytes, the initial pH values of the anolytes were measured. The anodes were connected to the positive terminal of a galvanostat and the electric wires which were attached to the steel bars were connected to the negative terminal.

The current densities were galvanostatically controlled for 7 days at 5 A/m^2 of steel area for inhibitor solutions whilst at 1 A/m^2 for sodium carbonate solutions, thus equivalent to a total charge of $168Ah/m^2$, which is sufficient in corrosion protection when the recommendation by Hondel and Polder (1998) for Portland cement concrete is referred to ($100Ah/m^2$), but insufficient when the CEN draft (2000) is referred to ($200Ah/m^2$) – see also Bertolini et al (2004). Each setup of specimens was placed in a container in which the atmosphere was kept at about 100% RH during the experiments. The anolyte was collected after the experiments and pH values of the solution were measured. The treated surfaces of the specimens were visually examined and photographed. The specimens were prepared in triplicate for each condition except for the specimens for concentration profile analysis (LPA, NPE, NPG, and NPA).

After the electrochemical treatment, the specimens were removed and kept at 35% RH in air, which was conditioned over saturated magnesium chloride solution. This is because the exposure of the specimens to a dry atmosphere, which provides easier oxygen access than a wet atmosphere, was expected to accelerate the recovery of potential of the steel that had been depressed to the hydrogen discharge region during the galvanostatic treatment.

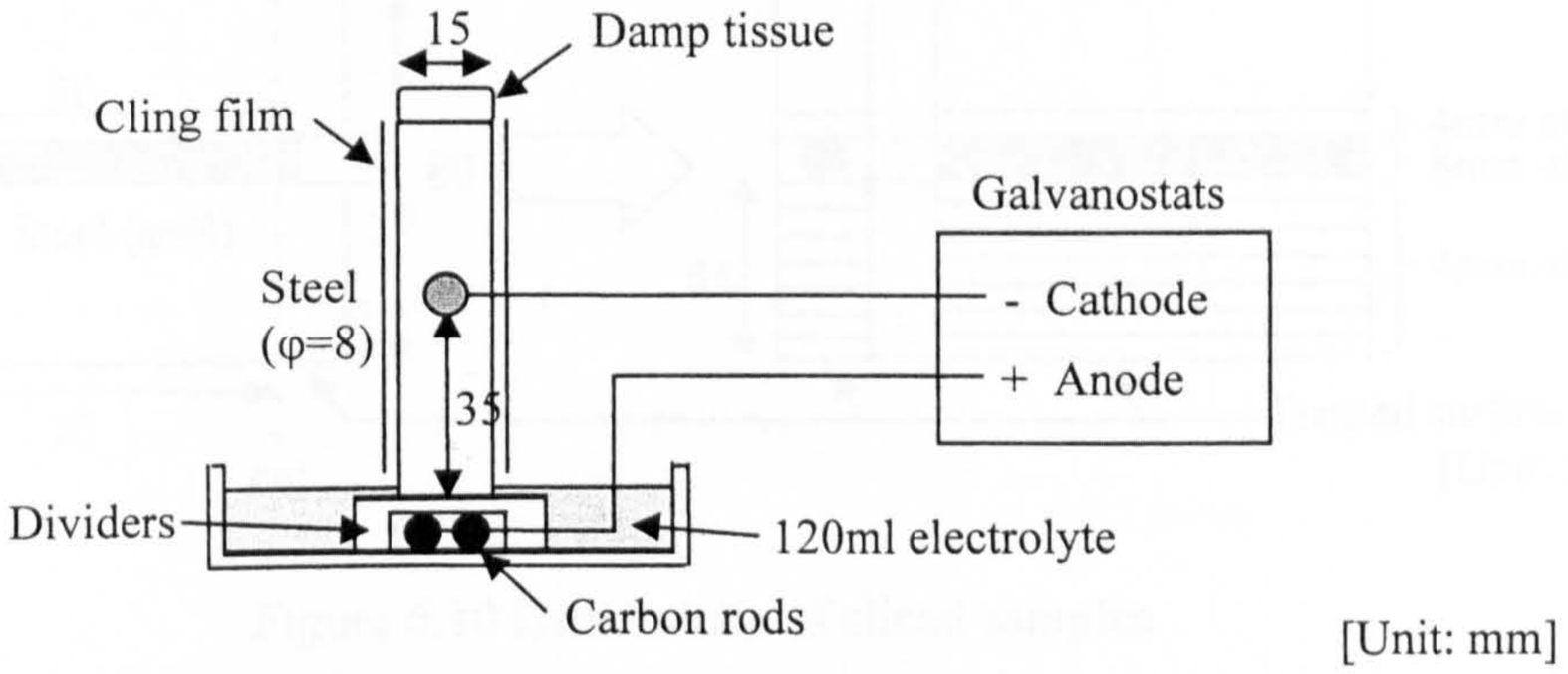

Figure 6.9 Experimental arrangement

6.3.5 Penetration profiles of corrosion inhibitors

The concentration profiles were obtained by the following procedure, in the case of arginine just after the inhibitor injection was completed (Leeds experiment (C)), and in the case of all three inhibitors studied (ethanolamine, guanidine, and arginine) after the specimens exposed to injection treatment were subsequently subjected to a wetting and drying regime for 160 days (Nagoya experiment (E)).

Both sides of the specimen through which the steel bars emerged were cut off leaving a prism of about 70 × 80 × 15 mm as shown in Figure 6.10. The prisms were cut parallel to their treated surface into 4mm slices, except at the position of the steel where the slice was 8mm, by means of a diamond saw lubricated with a small amount of distilled water. Each slice was crushed in a mortar with a pestle until most parts of the slices except the coarse aggregate were reduced to fine particles which were less than 425 μm. Each crushed concrete sample including coarse aggregate was divided into two portions and weighed separately. One of the portions was dried at 105 °C for 24 hours to obtain the dry weight of the sample. The other portion was used for extracting organic corrosion inhibitor which had penetrated into the concrete slice during the electrochemical treatment. This second portion was mixed thoroughly with 100 ml of distilled water and agitated by means of a mechanical shaker (Stuart Flask Shaker) for 100 minutes. The solutions were filtered through Whatman No.3 filter paper and collected in plastic tubes. Concentrations of corrosion inhibitor in the solutions were determined by a Dionex DX500 ion chromatography system, operated as described in section 2.4.

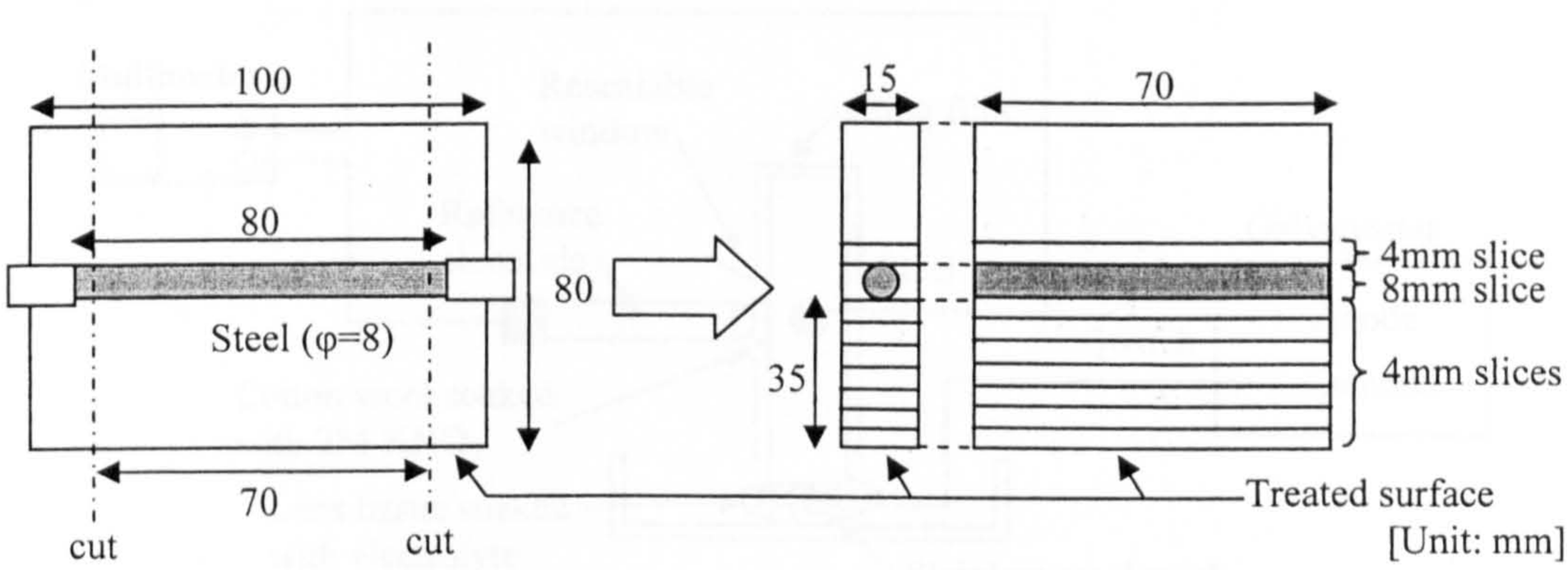

Figure 6.10 Dimensions of sliced samples

6.3.6 Anodic polarisation treatment

6.3.6.1 Leeds experiments (A)

Non-carbonated slice specimens with or without chloride (LA and LAC), which had been produced in the manner described in section 6.3.2.2, were used in the experiments. Prior to application of anodic current, the specimens were immersed in distilled water for 5 hours to attain a saturated condition. A re-sealable window was installed on the side of the specimens to confirm the contact of the SCE reference electrode to the specimen via cotton wool soaked with 2M potassium nitrate. The corrosion rates of the embedded steel in the specimens were

measured by linear polarisation as detailed in subsection 6.3.7. The embedded steel was then connected to the positive terminal of a galvanostat with copper wire. A Type 316 stainless steel mesh was embedded in lens tissue soaked with distilled water, which was placed beneath the treated surface of the specimen as the cathode to be connected to the negative terminal of a galvanostat. The reference electrode and the embedded steel were connected to multi-meter for measurement of the steel potential. The final setup for anodic current treatment is illustrated in Figure 6.11. Anodic current densities of 10, 100 and 200μA/cm^2 were applied to the embedded steel by means of the galvanostat for the period of 10 seconds, 1 minute, 10 minutes, and 100 minutes. The evolution of the steel potential was monitored by means of a multi-meter until it became constant with respect to time during and after the application of the current densities. The current density of anodic polarisation that kept the steel potential in noble area for a significant period after termination of the current was determined from the results, and this value was to be employed in the subsequent experiments (Leeds experiments (B) and Nagoya experiments (D)).

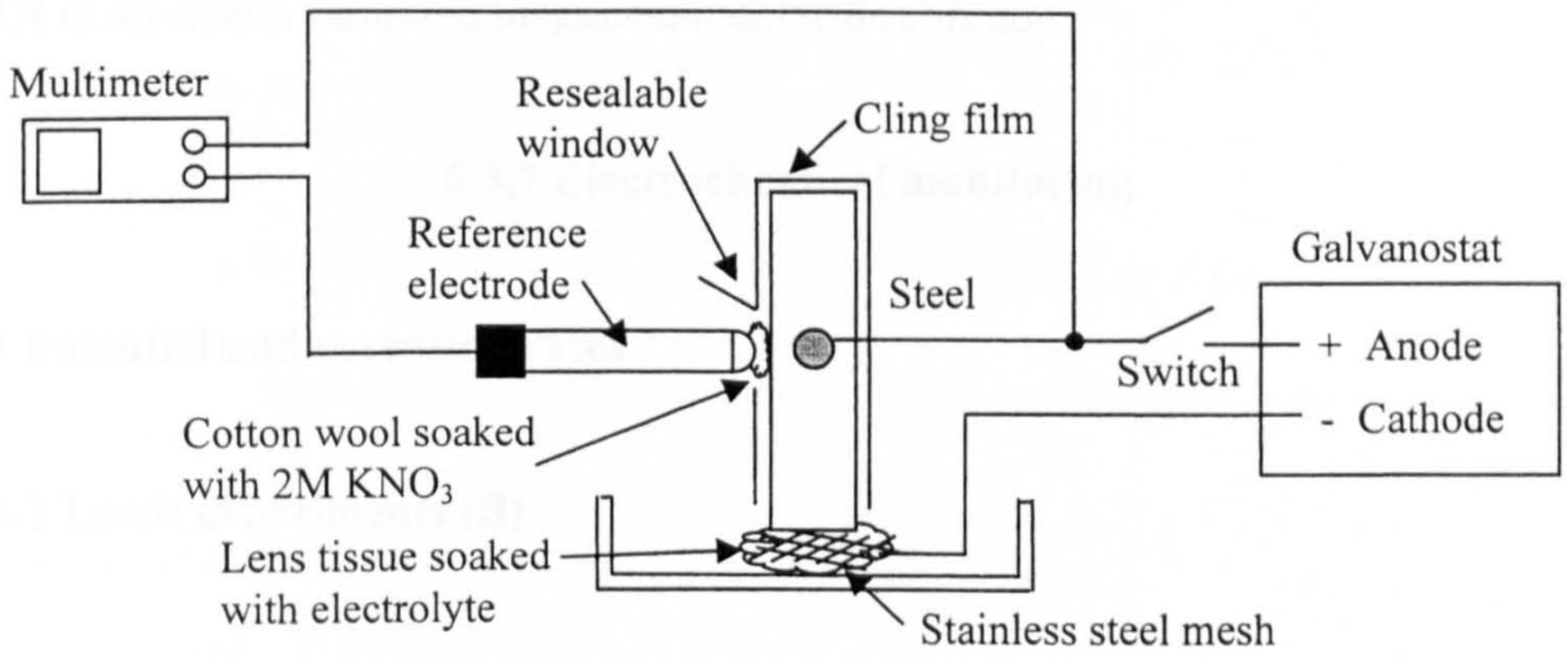

Figure 6.11 Anodic polarisation treatment

6.3.6.2 Leeds experiments (B)

Anodic polarisation treatment with the current density determined by Leeds experiments (A) was carried out 1 day and 7 days after carbonated concrete specimens were treated with guanidine carbonate by the experimental procedure presented in subsection 6.3.4 (LG1 and LG7). Anodic current was applied to the two specimens in the same manner as described in the previous subsection until the potential of the steel was raised to around +500mV, when the current was switched off. The evolution of the steel potential was recorded during and after the anodic polarisation until the steel potential was observed to become constant. When

the measurement was finished, the specimens were again kept at 35% RH in air over a saturated magnesium chloride solution. The corrosion rates of the embedded specimens were subsequently monitored under cyclic wet/dry conditions as detailed in 6.3.7, together with the specimens without application of anodic polarisation and control specimens. The timing of anodic polarisation application that subsequently gave the best influence on passivation of embedded steel was determined, which was then employed for electrochemically treated specimens in Nagoya experiments (D).

6.3.6.3 Nagoya experiments (D), (E)

Anodic polarisation treatment with the current density determined by Leeds experiments (A) was applied to carbonated concrete specimens that had been electrochemically treated with 5 different electrolytes detailed in subsection 6.3.4. The anodic current was applied to the specimens in the same manner as described in the previous subsections at the timing determined in Leeds experiments (B). After the treatment, the specimens were again kept at 35% RH in air over a saturated magnesium chloride solution.

6.3.7 Electrochemical monitoring

6.3.7.1 Potential and corrosion rates

6.3.7.1.1 Leeds experiments (B)

After the guanidine injection treatment was completed, the potential of steel was measured every 12 hours. Prior to the potential measurement, so that the specimen could easily have a contact with a reference electrode (SCE) via cotton wool soaked with 2M potassium nitrate, a $1cm^2$ square section of the cling film just close to the steel on the either side of the specimen was removed and a small re-sealable window was installed instead with the same cling film. Two weeks after the injection treatment, the specimens (LG, LG1, and LG7) were subjected to a wetting and drying regime for 4 weeks, which consisted of a period of immersing the treated surface of the specimens in distilled water to a depth of 3mm in shallow dishes for 24 hours and a period of storing the specimens in air over a saturated magnesium chloride solution (35% RH) for 6 days. During the wetting, the dishes were stored in a clear box whose atmosphere was kept at about 100% RH. At the end of each wetting and drying cycle, the potential and instantaneous corrosion rates (I_{corr}) of the

embedded steel bars were determined by the method of linear polarisation detailed in subsection 3.3.6. A Type 316 stainless steel mesh, embedded in lens tissue soaked with 1M guanidine carbonate solution (the same electrolyte as used in injection treatment), was placed beneath the treated surface of the specimens as the counter electrode. In the experiment, the same potentiostat/galvanostat with positive feedback IR compensation as had been used in the measurement of potential and corrosion rates of steel presented in Chapter 3 was employed. The final cell arrangement is shown in Figure 6.12. Carbonated specimens without inhibitor treatment were also used as control specimens (LC) that were simultaneously exposed to 4-week wetting and drying cycles with the guanidine-treated specimens.

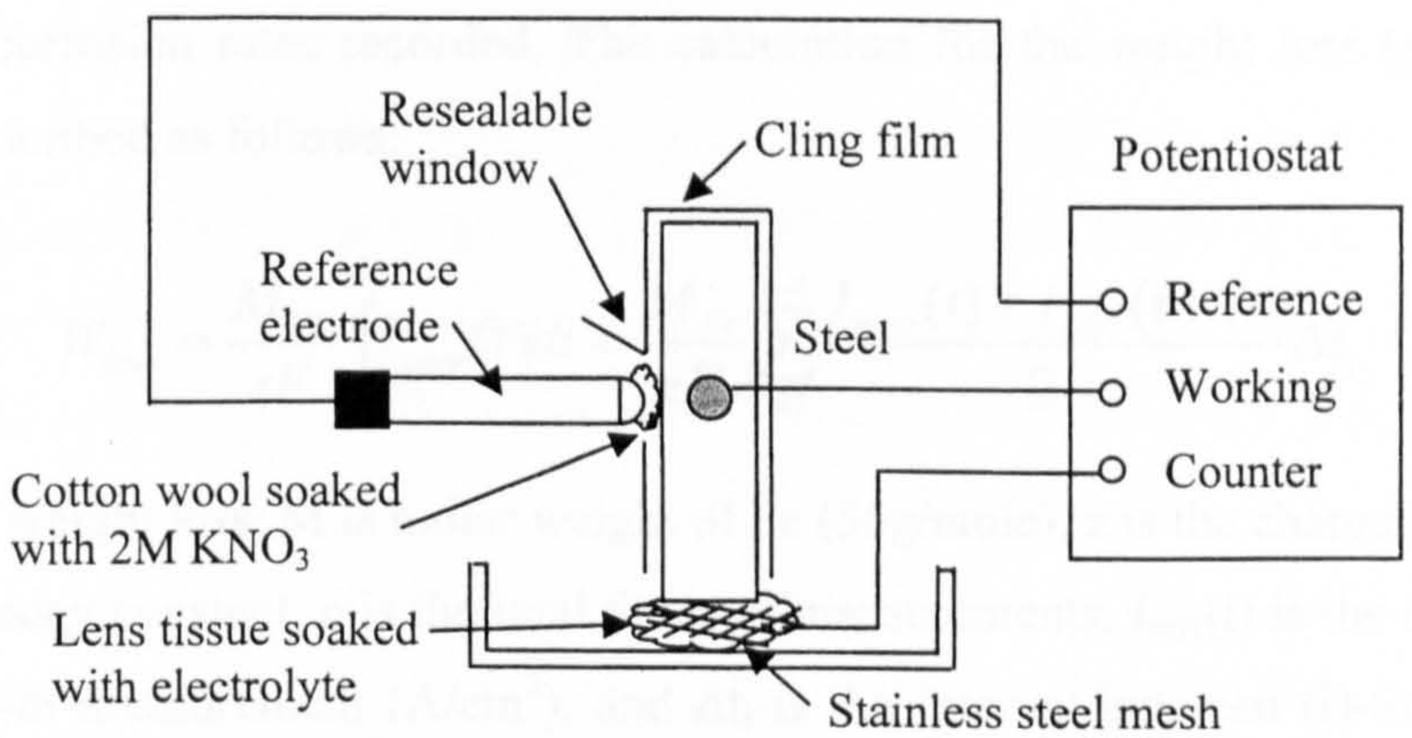

Figure 6.12 Cell arrangement for corrosion measurements

6.3.7.1.2 Nagoya experiments (D)

The potential of steel was measured after 2, 4, 7, 10, 20, 28, 35 days of the cessation of the electrical treatment with the solutions of corrosion inhibitors or sodium carbonate. Prior to the measurement of the potential, a small part of the cling film was replaced by the re-sealable window near the steel in the same manner as detailed in the previous subsection. Five weeks after the electrochemical treatment was finished, the specimens were divided into two groups; the first group was exposed to a cyclic wetting and drying regime (NEn, NEc, NG, NA, and NR), and the second group was exposed to a dry condition (NEnD, NEcD, NGD, NAD, and NRD).

The wetting and drying regime employed in this experiment was the same as described in the Leeds experiments (B) for the first 4 weeks; however it was slightly different in interval for the next 6 months, which consisted of 1 day wetting and 13 day drying. Carbonated specimens without electrochemical treatment were used as control specimens (NC) that were

simultaneously exposed to the above wetting and drying cycles, together with the specimens treated with corrosion inhibitors or sodium carbonate. At the end of each wetting and drying cycle, the potential and instantaneous corrosion rates (I_{corr}) of the embedded steel bars were determined by linear polarisation. For the measurement of linear polarisation, a potentiostat/galvanostat 1280Z, manufactured by Solartron was used. Type 316 stainless steel mesh, embedded in lens tissue soaked with the same electrolyte as had been used as anolyte during the electrochemical treatment, was placed beneath the treated surface of the specimens as the counter electrode. The setup of the specimens was the same as described in the previous subsection (see Figure 6.12). The corrosion weight loss was estimated by integrating the measured corrosion rates throughout the experimental period for each steel bar, where the evolutions of the rates were assumed to have been linear between two neighbouring corrosion rates recorded. The calculation for the weight loss (g/cm^2) of the steel can be described as follows:

$$W_{loss} = \frac{M_{Fe}}{zF}\int I_{corr}(t)dt \approx \frac{M_{Fe}}{zF}\sum_{i=1}^{n-1}\frac{I_{corr}(i)+I_{corr}(i+1)}{2}\cdot\Delta t_i \qquad (6\text{-}4)$$

where, W_{loss} is weight loss, M is molar weight of Fe (56g/mole), z is the charge number of Fe (z=2), F is Faraday constant, n is the total times of measurements, $I_{corr}(i)$ is the corrosion rate obtained at (i)-th measurement (A/cm^2), and Δt_i is the interval between (i)-th and (i+1)-th measurement (seconds).

The specimens exposed to drying conditions were kept at 35% RH over saturated magnesium chloride solutions throughout the experiment. The potential and the corrosion rates of the embedded steel were measured at the same occasion when the measurement for the specimens under wet/dry conditions was carried out.

6.3.7.2 Measurement of AC impedance

The electrochemical impedance spectroscopy was measured for the steel embedded in specimens NEn, NEc, NG, NA, NR, and NC, around every two months after the cessation of the electrical treatment, when the specimens were finished with exposure to one-day wet conditions. The first measurement was performed at the end of the first wet/dry regime (1 day wetting and 6 day drying), and the other three measurements were conducted during or at the end of the second wet/dry regime (1 day wetting and 13 day drying). The impedance measurements were carried out by means of a Solartron apparatus (1280Z: EI (electrochemical interface) and FRA (frequency response analyser) combined, with a

frequency domain ranging from 20 kHz to 1 mHz) with a three-electrode cell as shown in Figure 6.12. An excitation signal of maximum amplitude of 35mV was applied for the interrogation of the system over a frequency swept from 20 kHz to 5 mHz through a Spectrum, taken at five points per decade. This is because much lower frequencies may take away the potential from its rest value due to long imposed polarisation (Andrade et al. 1989). The results were represented as Nyquist plot format (-imaginary vs. real impedance). The double layer capacitance and polarisation resistance were estimated by fitting, which was performed using associated software "Zplot" presented by Solartron.

6.3.8 Gravimetric analysis of corrosion

After the whole cyclic wetting and drying regime was completed in Nagoya experiments (D), weight loss measurements were performed for the steel bars embedded in the concrete slice specimens that had been treated with corrosion inhibitors or sodium carbonate. The concrete specimens were carefully broken using a vice and the embedded bars were removed. After removing epoxy coating and smoothing the ends with emery paper, taking care not to damage the steel surface, the bars were visually examined and photographed. Then, in order to obtain a clear view of the final corrosion state at different positions of the steel bars, the middle part of the bars (with a length of 80mm; see Figure 6.10) that had not been coated with epoxy were cut into eight of equal sections with a length of just 10mm using the precision wire erosion method (see section 2.6) with the wire diameter of 200μm, making sure that each cut was exactly perpendicular to the axis of the bar. After the small pieces of steel bars were labelled, they were put into test tubes containing 10% diammonium hydrogen citrate solution with 150ppm 2-Mercaptobenzothiazole as corrosion inhibitor, as indicated by Japan Concrete Institute (1987). The test tubes were placed in an ultrasound bath and shaken for two minutes. The bars were then removed and washed in hot water before returning to the test tubes containing 10% diammonium hydrogen citrate solution with inhibitor. The process was repeated five times to ensure all corrosion products were removed. The bars were then placed in test tubes filled with hot water to ensure removal of acid before being washed with distilled water, wiped dry with tissue and degreased by washing in acetone and ethanol. Each cleaned bar was wrapped in a tissue, placed in a polythene bag and stored in a desiccator. In addition, 10 control bars were prepared and treated in the same manner as described above. The weight loss (mg/cm^2) of the test bars could then be obtained by evaluating the difference between the weight of the control bars (initial weight) and the test bars (final weight).

6.4 RESULTS

6.4.1 Change in anolyte after electrochemical treatment

During the electrochemical inhibitor injection or electrochemical re-alkalisation treatment, the pH of the anolyte was lowered due to the generation of hydrogen ions near the anode by water electrolysis. The pH reductions observed in the five electrolytes that were used as anolyte during the electrochemical treatment in Leeds experiments and Nagoya experiments are shown in Table 6.4, together with the visually examined surface condition concerned with surface deterioration. The results indicate that the pH values of the anolyte dropped to the acid region in the case of nitrate solutions (ethanolamine nitrate and arginine nitrate), whilst the pH values of the carbonated solutions were lowered moderately. The surfaces of the specimens after electrochemical treatment for seven days were photographed as shown in Figure 6.13. It can be seen that surfaces of the specimens treated with ethanolamine nitrate and arginine nitrate dissolved in anolyte with acidity, resulting in a rough surface condition with discolouration from initially grey (see control specimens in Figure 6.13) to finally white.

Table 6.4 pH reduction of anolyte after 7 days of treatment at $5A/m^2$

Anolyte	Initial pH	Final pH	Surface deterioration
Ethanolamine nitrate(**)	8.09	1.60	Yes
Ethanolamine carbonate(**)	9.20	8.72	No
Guanidine carbonate	11.64(*)/11.77(**)	8.76(*)/8.88(**)	No(*)/No(**)
Arginine nitrate	7.69(*)/8.04(**)	3.08(*)/3.11(**)	Yes(*)/Yes(**)
Sodium carbonate ($1A/m^2$)(**)	11.83	10.55	No

(*): Leeds experiments, (**): Nagoya experiments

Figure 6.13 Surfaces of the specimens after electrical treatment for 7 days (From left: control, sodium carbonate (electrochemical re-alkalisation), arginine nitrate, ethanolamine carbonate, ethanolamine nitrate, guanidine carbonate, control)

6.4.2 Anodic current treatment

6.4.2.1 Leeds experiments (A)

The initial potential of the steel prior to the application of the anodic current to the non-carbonated slice concrete specimens with or without chloride (LA and LAC) ranged between -140mV and -280mV vs SCE for specimens LA and -530mV and -620mV for specimens LAC respectively. The corrosion rates obtained by linear polarisation before the anodic polarisation treatments were <0.08μA/cm^2 for specimens LA and >1.2μA/cm^2 for specimens LAC, thus it was confirmed that the steel bars embedded in the non-carbonated concrete slices LA were passivated and those in chloride-contaminated slices LAC were depassivated. The evolutions of the potential of embedded steel with respect to time when anodic current (10μA/cm^2 to 200μA/cm^2) was applied to specimens LA and LAC for 10 seconds to 100 minutes are shown in Figure 6.14. It can be seen from the results that the anodic current applied to specimens LA quickly raised the steel potential significantly to between +350mV and +1,000mV (inclusive of IR drop), depending on the anodic current density and the applied period. It was observed that, after a sharp rise, the enhanced potential soon became constant with respect to time until the current was switched off. The current applied to chloride-contaminated specimens LAC, however, did not show a sharp rise of the potential, just gradually raising the potential by 100mV or 200 mV towards the noble direction.

In the case of chloride-free specimens LA, the significantly enhanced steel potential was observed to drop and approach the initial potential value with time, immediately after the current was switched off. It can also be seen that in the case of short-term applications of the polarisation (10 seconds and 1 minute), rapid potential drop was observed right after the cessation of the treatments. In the case of the longer applications of the polarisation (100 minutes), the potential gradually dropped, and it took more than 100 minutes for the value to approach the initial value after the termination of the applied current. On the other hand, the slightly raised potential of steel embedded in chloride-contaminated specimens LAC soon returned to the initial potential value after the cessation of the treatment, regardless of the applied current density or the treatment period.

The difference in current density seems to affect the degree in potential enhancement for both specimens; however, does not seem to affect the period required for the potential to return to the initial potential value significantly, if compared under the same duration of the polarisation treatment. The period rather seems to be influenced by the duration of the treatment. It was determined that the current density of 100μA/cm^2 would be employed for

the anodic polarisation applied to concrete specimens after being exposed to electrochemical inhibitor injection in the subsequent experiments (Leeds experiments (B)).

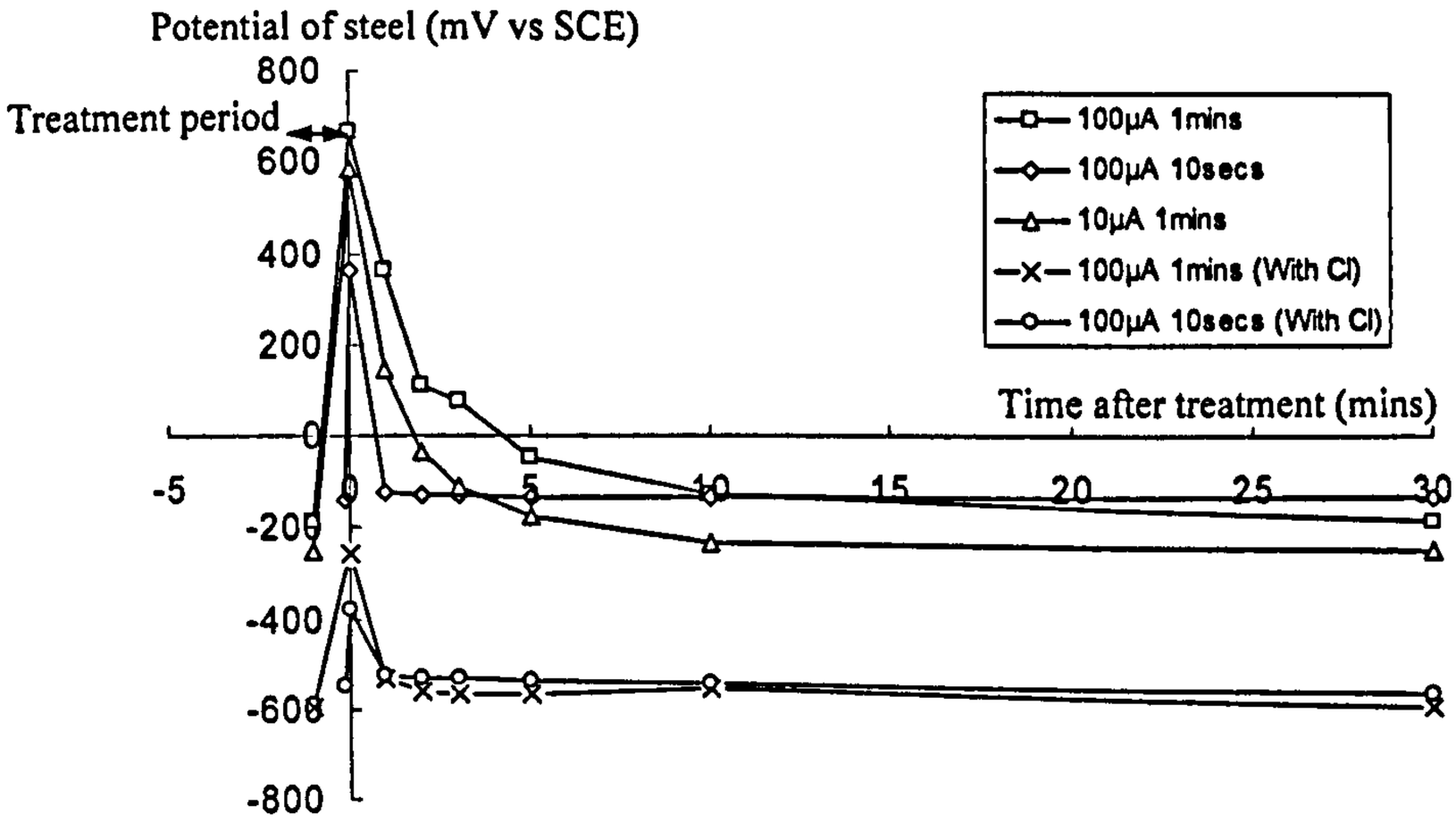

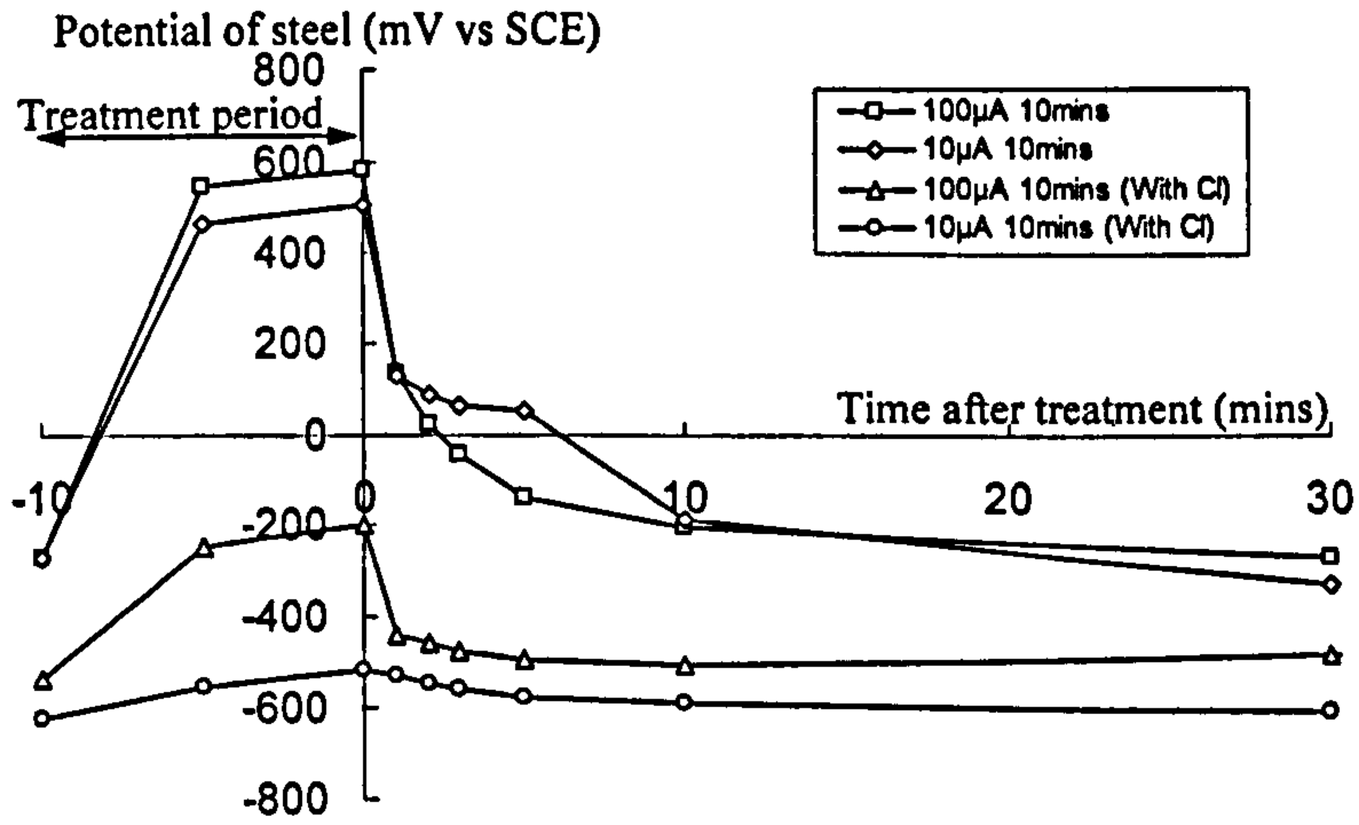

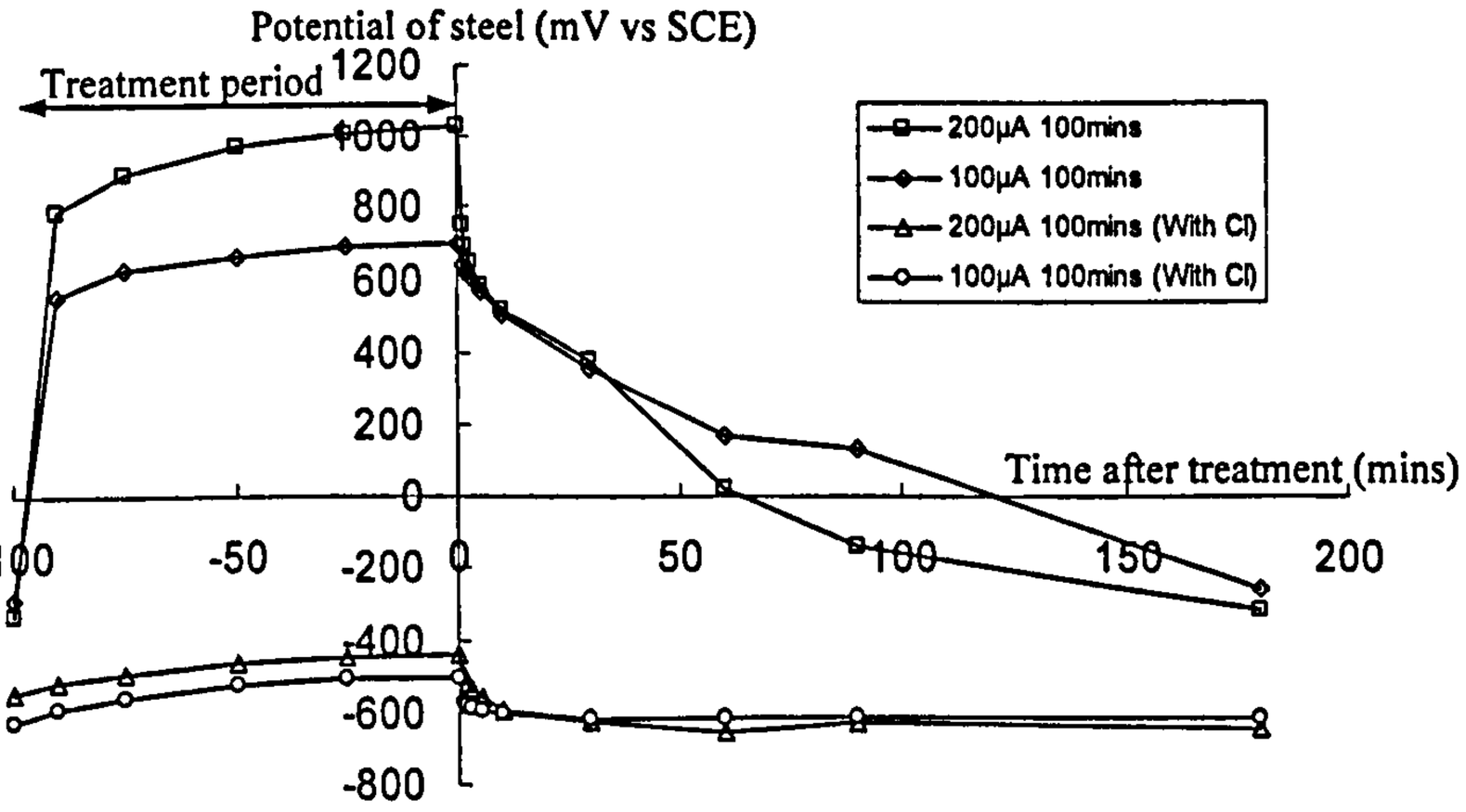

Figure 6.14 Evolutions of steel potential by applications of anodic polarisation (With no inhibitors; Top: treatment period of 10secs-1min, middle: 10mins, bottom: 100mins)

6.4.2.2 Leeds experiments (B)

Figure 6.15 shows the evolution of potential of steel bars embedded in concrete slices when the anodic polarisation at the current densities determined in the previous subsection was applied to the specimens 1 day and 7 days after the electrochemical guanidine injection had been finished (LG1 and LG7, respectively). Right after the completion of the electrochemical injection, the potential of the steel, which had been used as the cathode during the treatment, showed quite negative values, ranging between -1,070 and -1,010mV (vs SCE), resulting from the electrolysis

1 day after the treatment was finished, the potential was observed to slightly recover to between -750 and -800mV (vs SCE), when anodic polarisation was applied at the current density of 100μA/cm^2 for LG1 specimens. As seen in the Figure, the enhancement rate of the steel potential was moderate compared to that in the previous investigation (Leeds experiments (A)), and it took almost 3 hours for the potential to reach approximately +500mV (vs SCE). When the current was switched off, the potential immediately dropped and reached the initial potential value in around half an hour.

7 days after the electrochemical inhibitor injection treatment was finished, the potential of the embedded steel bars in specimens LG7 had recovered to between -380 and -210 mV (vs SCE), when anodic polarisation was applied at the current density of 100μA/cm^2 for these specimens. It can be seen from the results that, similarly as observed in the previous investigation (Leeds experiments (A)), the application of the anodic polarisation raised the potential of the steel significantly to approximately +500mV (vs SCE) in just around a few minutes, which indicates that the steel bars were successfully passivated. After the anodic current was switched off, also similarly as observed in the previous investigation, the enhanced potential slowly returned to the initial potential value recorded at the commencement of the application of anodic polarisation.

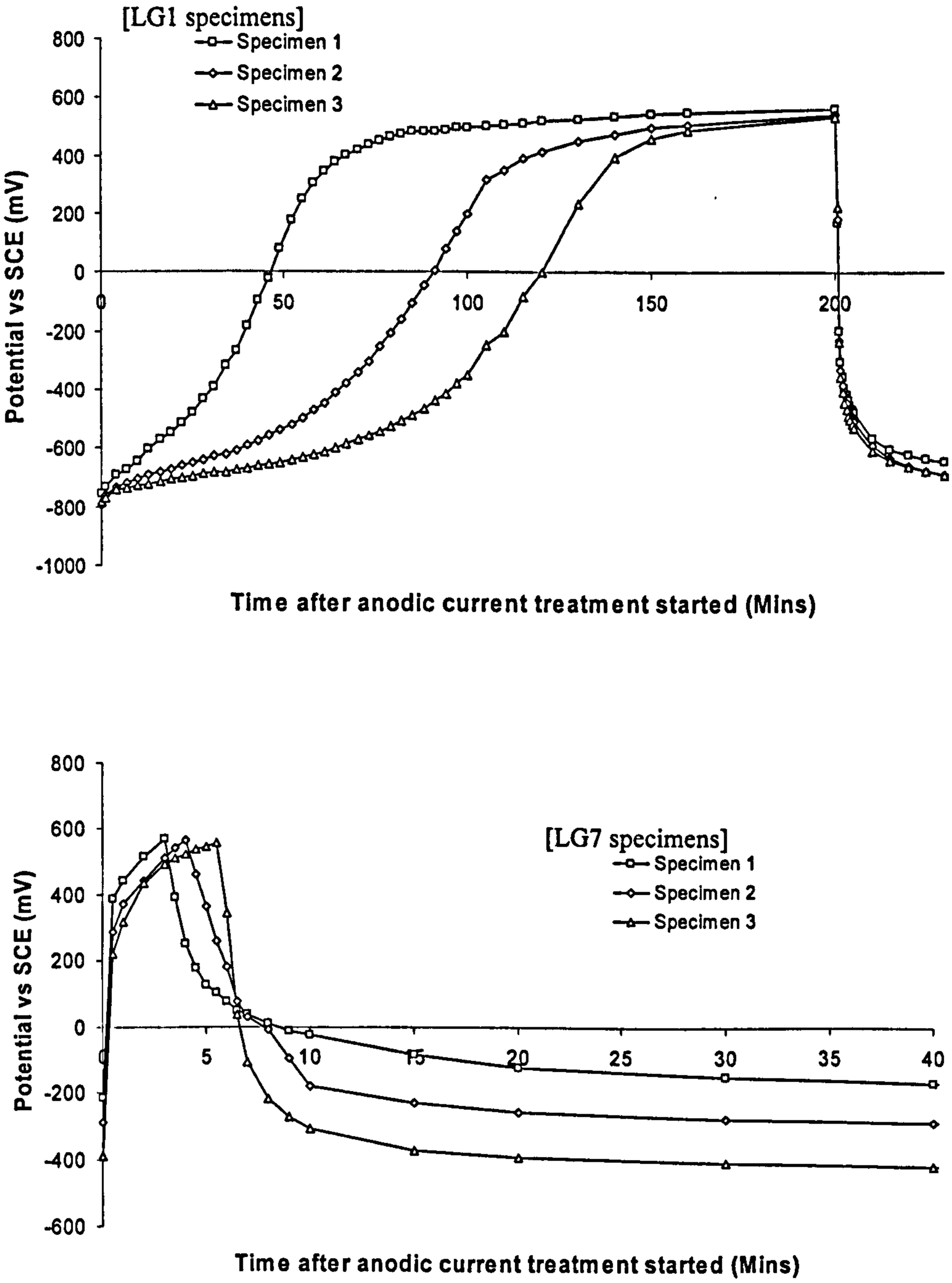

Figure 6.15 Evolutions of steel potential by applications of anodic polarisation at 100μA/cm^2 after electrochemical guanidine injection (Top: 1 day after injection, bottom: 7 days after injection)

6.4.2.3 Nagoya experiments (D)

The potential values of the embedded steel recorded soon after the inhibitor injection or electrochemical re-alkalisation treatment are shown in Table 6.5, together with the restored potential values obtained 7 days after the electrochemical treatment was finished.

Figure 6.16 and Figure 6.17 show the evolution of potential of steel bars embedded in concrete slices when the anodic polarisation at 100μA/cm^2 was applied to the specimens 7 days after the electrochemical inhibitor injection or electrochemical re-alkalisation had been finished with different electrolytes (NEn, NEc, NG, NA, and NR).

Table 6.5 Potential of steel after the electrochemical treatment (mV vs SCE)

Anolyte	Just after treatment	7 days after treatment
Ethanolamine nitrate	-999 ~ -984	-238 ~ -222
Guanidine carbonate	-1,070 ~ -1,009	-342 ~ -322
Arginine nitrate	-1,060 ~ -1,005	-348 ~ -332
Ethanolamine carbonate	-1,055 ~ -1,029	-237 ~ -227
Sodium carbonate (1A/m^2)	-1,076 ~ -1,042	-461 ~ -433

In all cases, the potential of the steel was once significantly raised to approximately between +450mV and +500mV (vs SCE) within around 7 minutes, which indicates that the steel bars were successfully passivated. Rapid enhancement of the steel potential was observed in ethanolamine cases and most of the guanidine cases, where the potential reached around +450mV in a few minutes. On the other hand, the potential enhancement was observed to be the slowest for sodium carbonate that had also shown the slowest recovery of potential after the electrochemical re-alkalisation treatment was finished (see Table 6.5).

After the anodic current was switched off, the enhanced potential quickly returned to the initial potential values within a few minutes in the case of ethanolamine nitrate/carbonate, and sodium carbonate, whilst the raised potential relatively slowly returned to the initial potential values in the case of guanidine and arginine. The similar trend was observed between in the profiles of the steel potential in the cases of guanidine in Leeds experiments (B) presented in the previous subsection and Nagoya experiments (D) presented in this subsection.

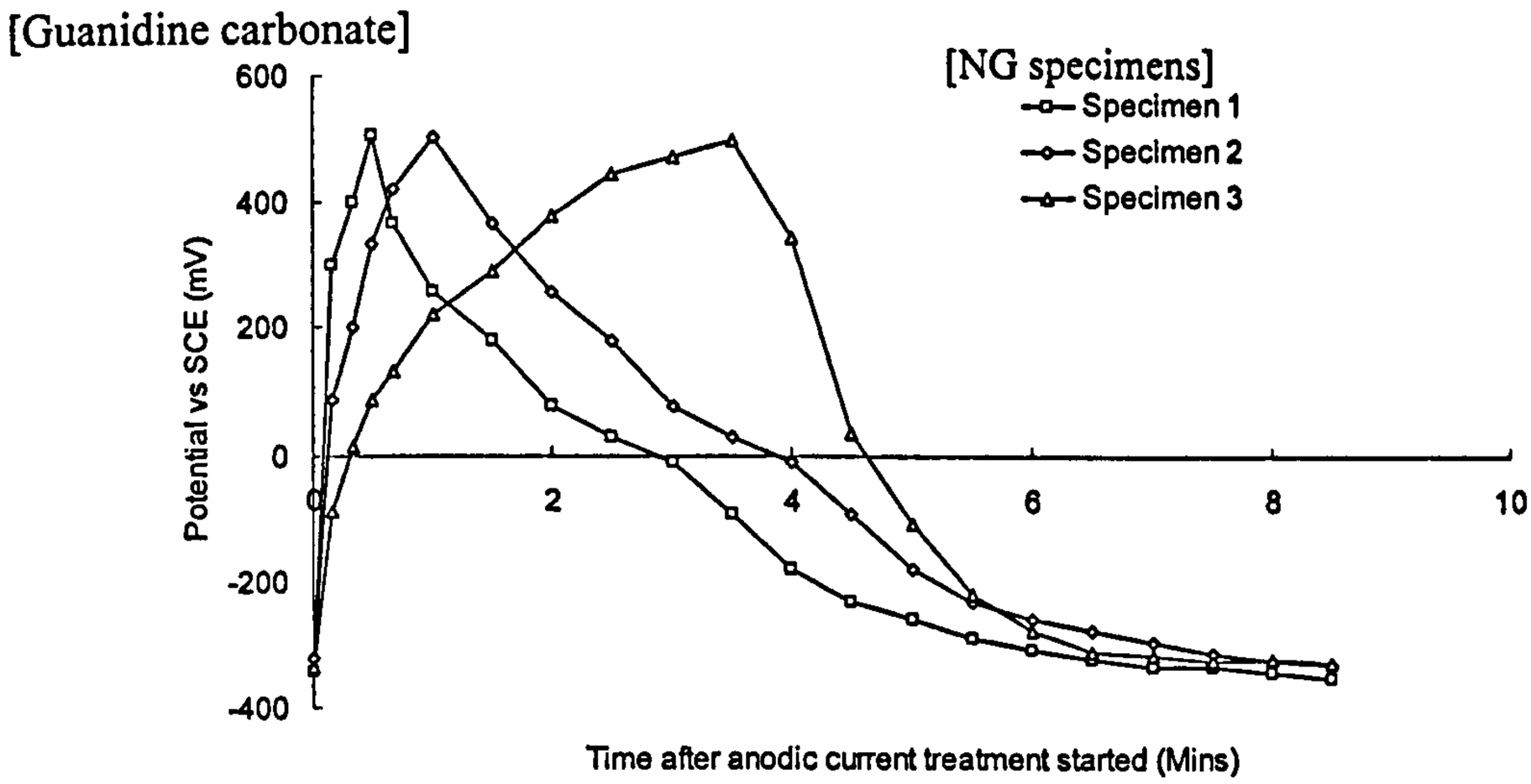

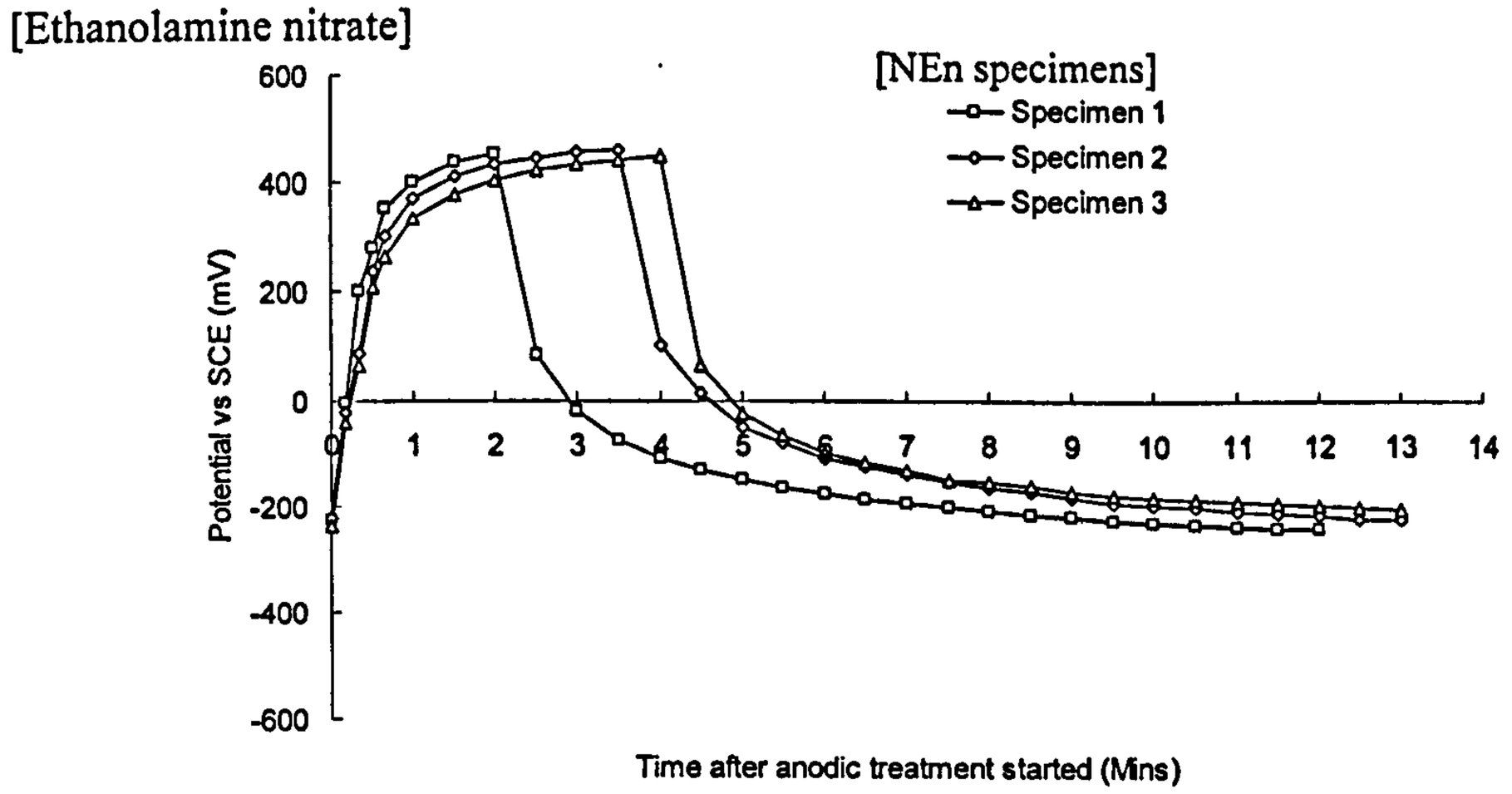

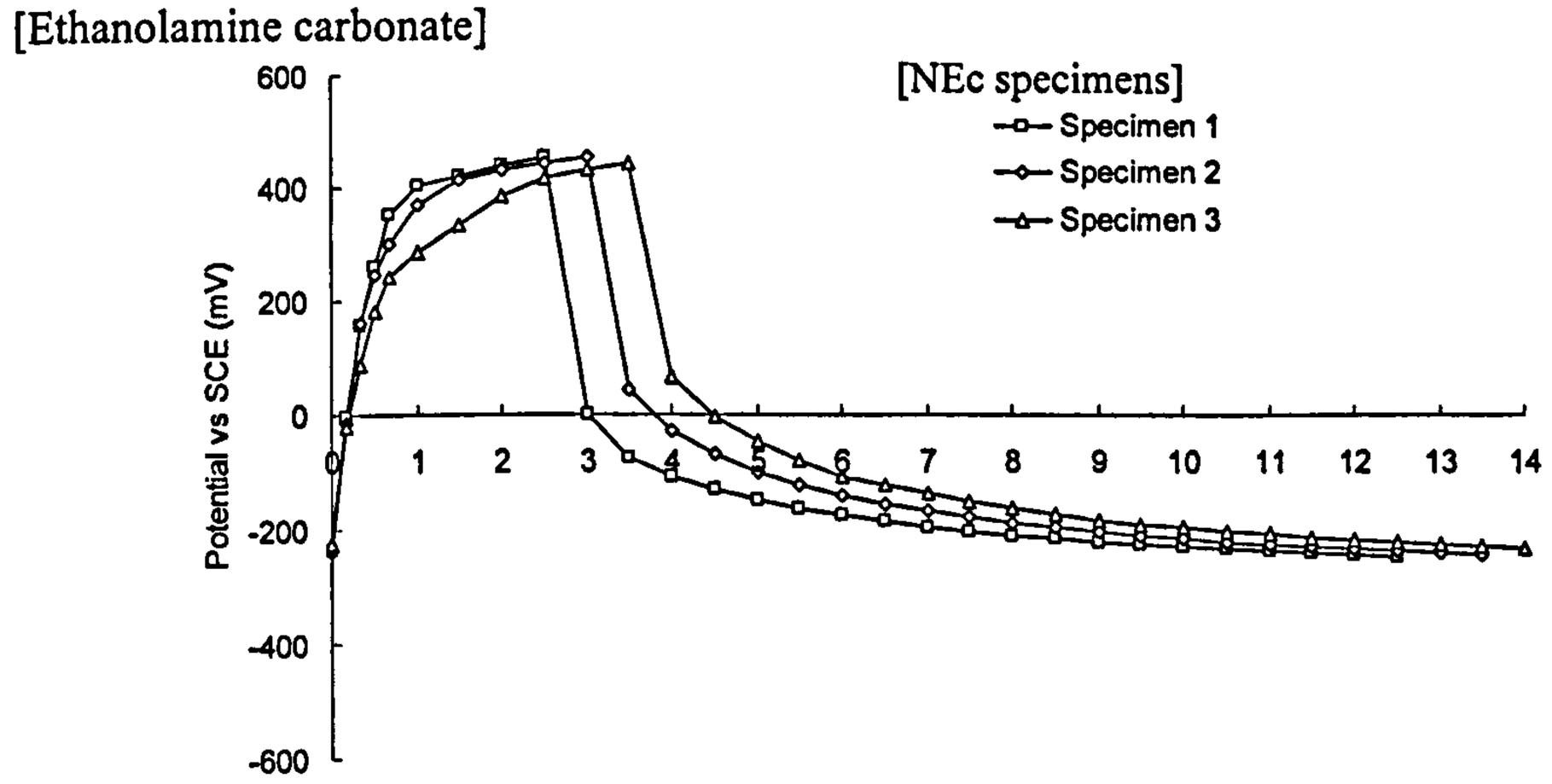

Figure 6.16 Evolutions of steel potential by applications of anodic polarisation at 100μA/cm^2 7 days after electrochemical injection (Top: guanidine carbonate, middle: ethanolamine nitrate, bottom: ethanolamine carbonate)

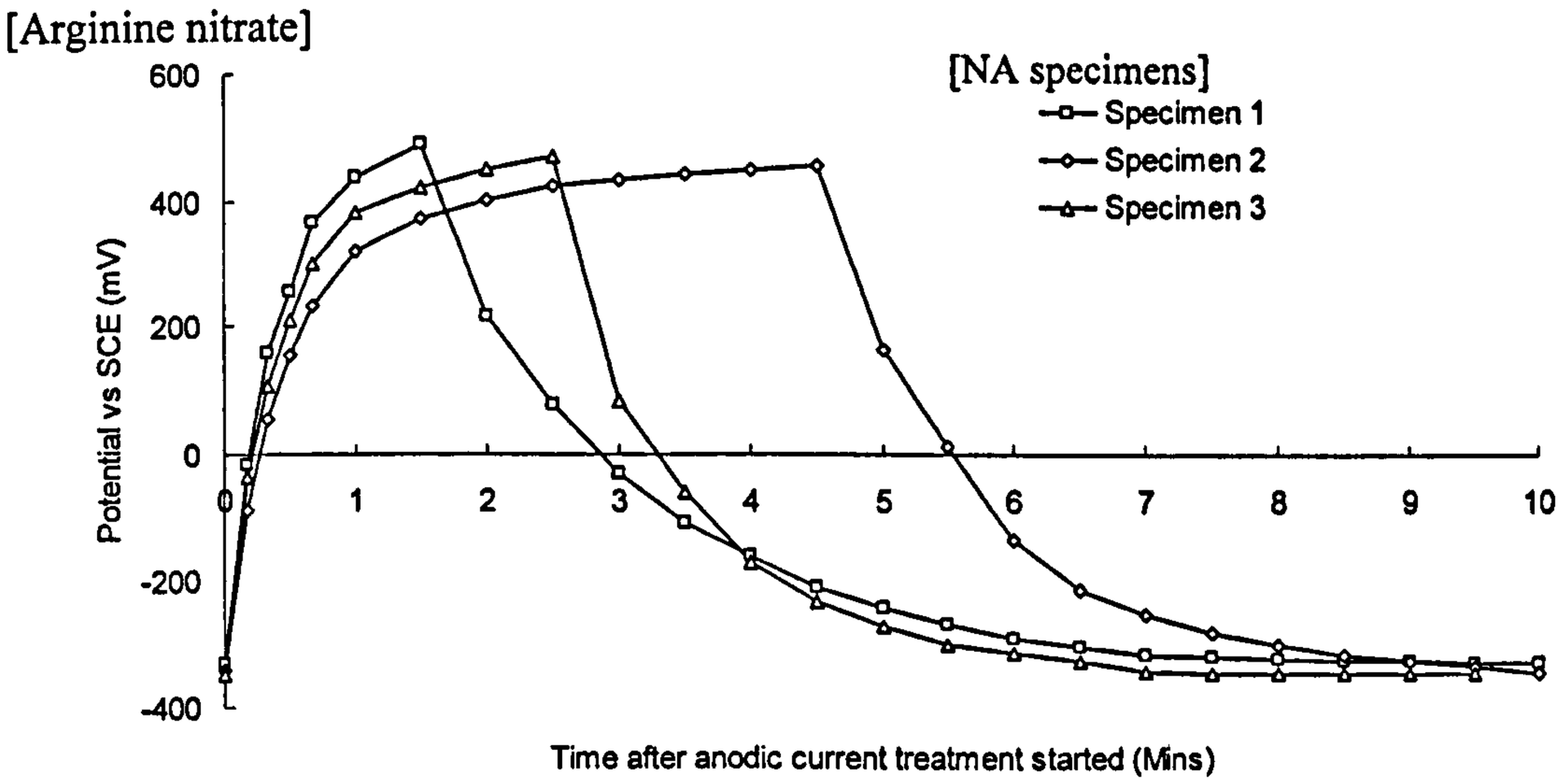

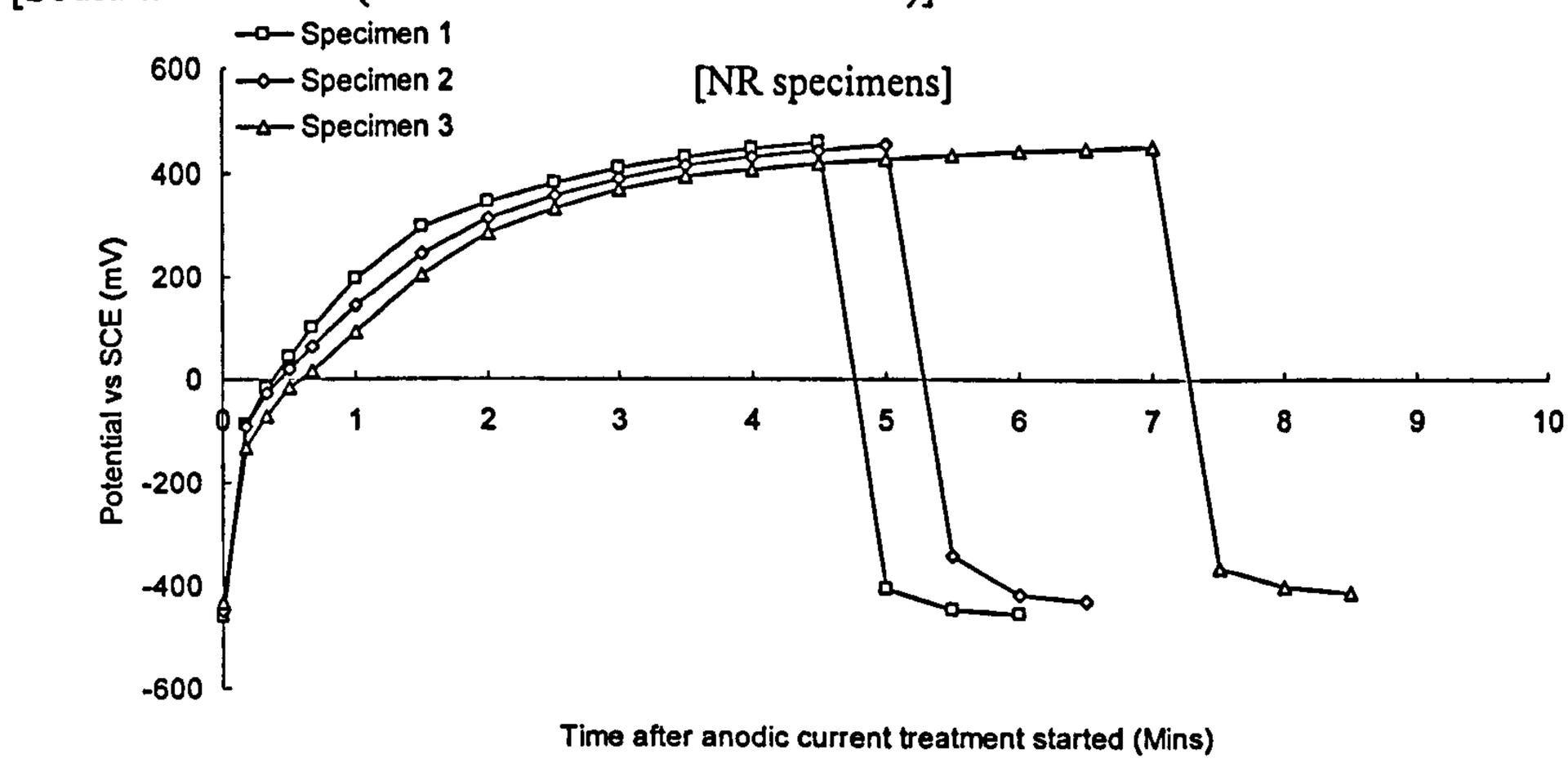

Figure 6.17 Evolutions of steel potential by applications of anodic polarisation at 100μA/cm^2 7 days after electrochemical injection (Top: arginine nitrate, bottom: sodium carbonate (electrochemical re-alkalisation))

6.4.3 Electrochemical monitoring

6.4.3.1 Leeds experiments (B)

Figure 6.18 shows the evolution of potential of steel bars embedded in the guanidine treated concrete slice specimens that were treated with or without anodic polarisation at 100μA/cm^2 1 day or 7 days after the treatment and exposed to wetting and drying regime for 4 weeks (LG, LG1 and LG7). It can be seen from the results that the steel potential that once dropped to below -1000mV (vs SCE) by the electrolysis recovered to between -400 and -200 mV in almost 5 days and became stable in around 10 days after the guanidine injection treatment was finished. However, relatively large potential variance was observed between the triplicate samples of LG7 and LG specimens. Six weeks after the injection treatment, when the specimens were broken with a hammer and the corrosion state of the removed embedded steel bars was visually examined, corrosion probably due to incomplete coverage of the steel edges with epoxy was unfortunately found on the edge surfaces of the steel bars embedded in the specimen 3 of LG7 and the specimen 2 and 3 of LG. This can be attributable to the relatively low steel potential of above three samples, resulting in variance in steel potential for LG7 and LG specimens. In order to avoid this unfavourable corrosion due to poor coverage, the steel edges were carefully recoated with epoxy before and after the electrochemical treatment in the subsequent Nagoya experiments (D).

The potential of the steel bars in the three series of the specimen (LG1, LG7 and LG) showed similar evolution throughout the experiment period except the bars with unexpected corrosion, finally approaching to around -200mV (vs SCE) indicating that the steel was successfully passivated. The steel bars embedded in control carbonated specimens (LC) were observed to be depassivated, the potential fluctuating in the range of between around -500 and -400 mV (vs SCE) during the wet/dry cycles as shown in Figure 6.19.

The evolutions of average corrosion rates for each series of the specimens during the wet/dry cycles are shown in Figure 6.20, in which the samples that encountered with unfavourable corrosion on the edge surfaces are excluded. The Icorr values were observed to be the smallest (just close to 0.1μA/cm^2) in the case of LG7 specimens, and LG specimens showed Icorr values of below 0.2μA/cm^2. The bars in LG1 specimens showed slightly higher corrosion current densities; however the rates were still around 0.2μA/cm^2. On the other hand, the steel bars in control carbonated specimens (LC) were observed to be higher than 1.0μA/cm^2 whilst the specimens were exposed to the cyclic wetting/drying conditions.

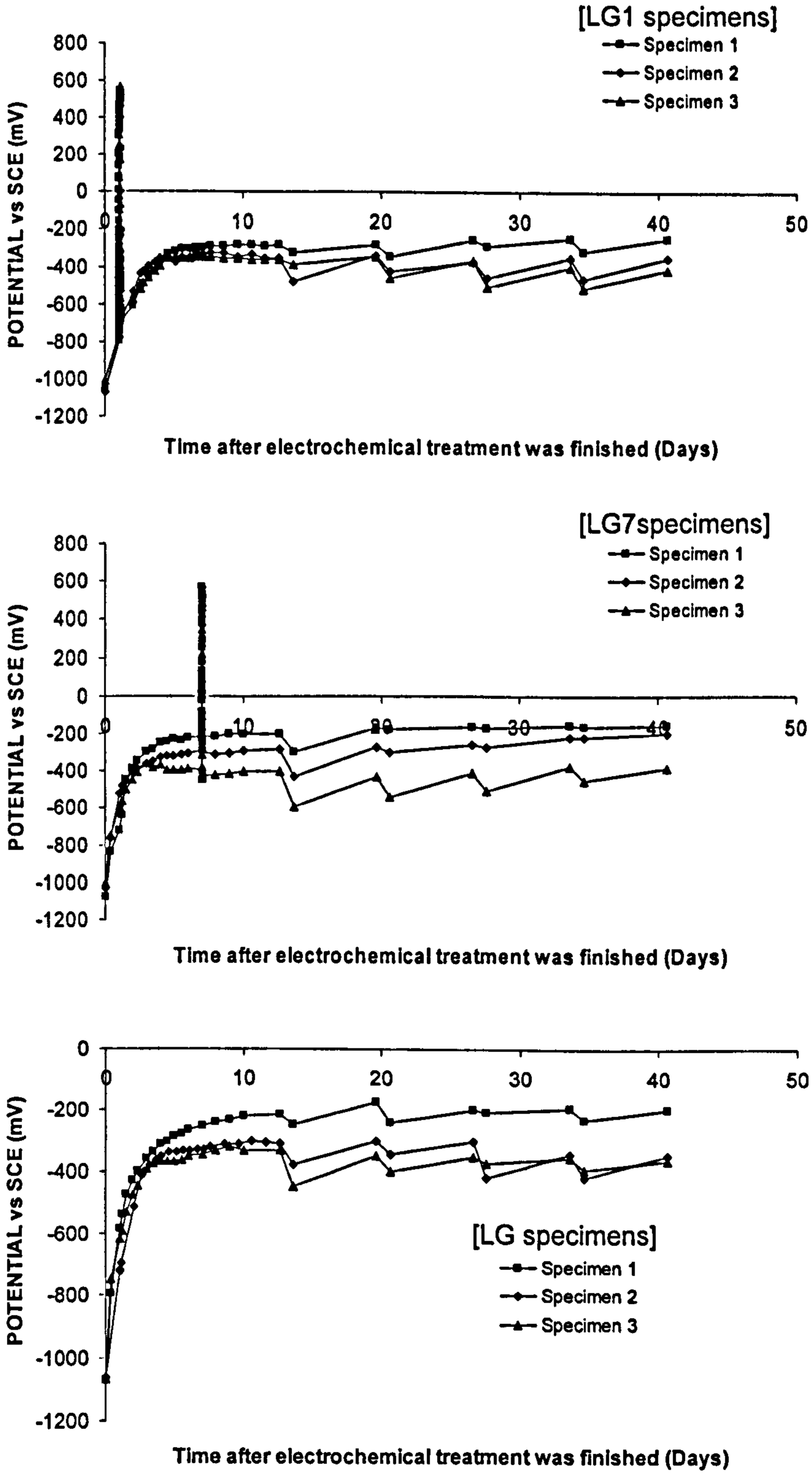

Figure 6.18 Evolutions of steel potential for six weeks after electrochemical injection (Top: anodic polarisation applied 1 day after electrochemical inhibitor injection treatment, middle: anodic polarisation applied 7 days after treatment, bottom: without anodic polarisation)

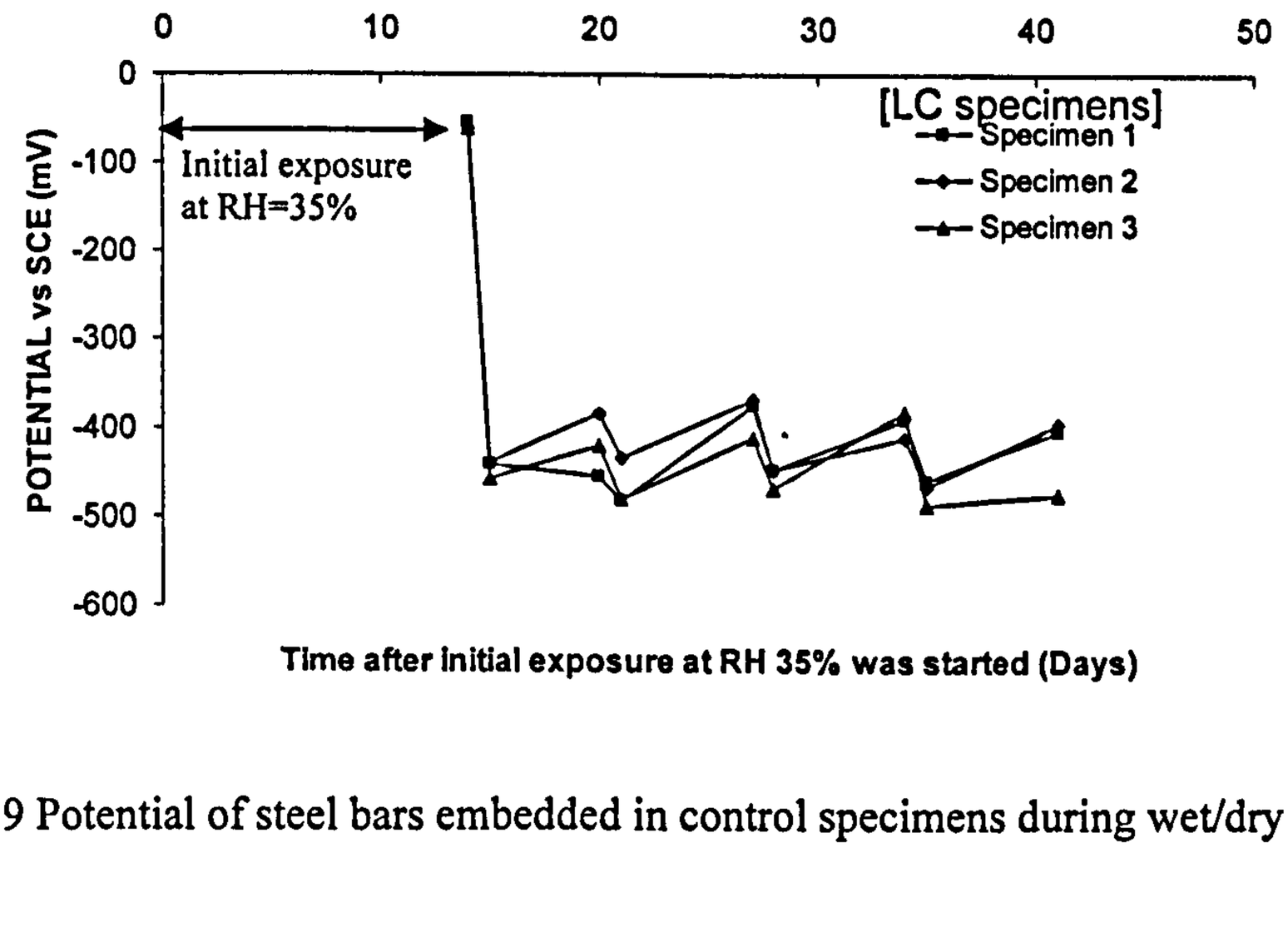

Figure 6.19 Potential of steel bars embedded in control specimens during wet/dry cycles

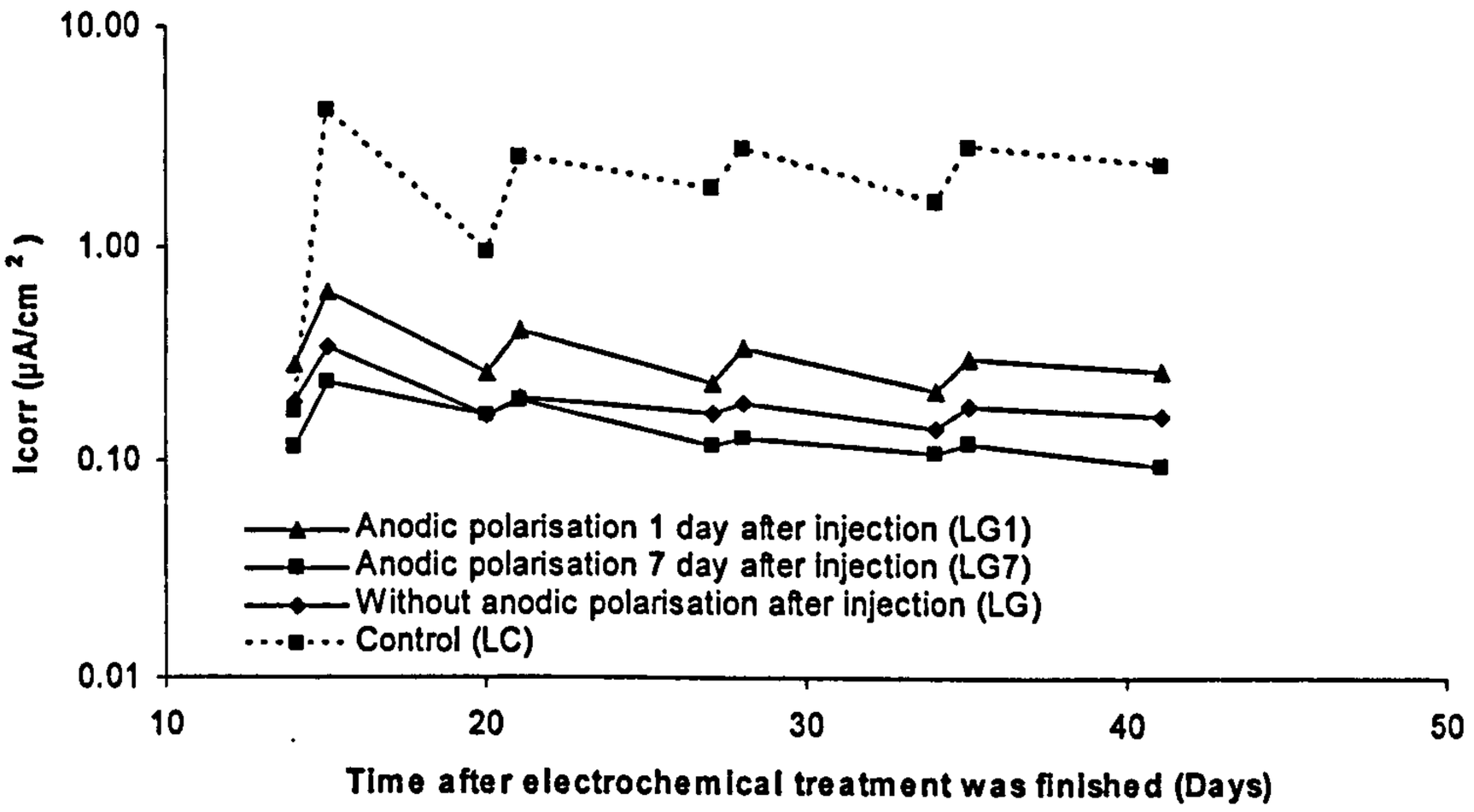

Figure 6.20 Corrosion rates of steel bars during wet/dry cycles

6.4.3.2 Nagoya experiments (D)

6.4.3.2.1 Steel potential and corrosion rates

Figure 6.21 and Figure 6.22 present the evolutions of the potential of steel bars embedded in electrochemically treated and control concrete slice specimens that were exposed to wetting and drying regime for totally 7 months. The anodic polarisation treatment at 100μA/cm^2 was performed 7 days after the completion of electrochemical treatment, based on the electrochemical monitoring results obtained in Leeds experiments (B) presented in the previous subsection. The potential evolutions accompanied by anodic polarisation are not included in these Figures.

In all specimens except control, the steel potential just after the electrochemical treatment was observed to be below -1,000mV (vs SCE) owing to electrolysis, and gradually recover with time, reaching the potential value of -250mV to -50mV (vs SCE) in 35 days. In dry specimens for all five cases (NGD, NEnD, NEcD, NAD and NRD), the potential still continued to rise until it became constant at around 0 to +100 mV (vs SCE). In the cases of the specimens that were exposed to wetting and drying regime, the trend in potential profiles seems to depend on the different electrochemical treatment. The ethanolamine specimens (NEn and NEc, both treated with ethanolamine nitrate and ethanolamine carbonate) showed typically passive behaviour with a steady potential range of between -200 mV and -50 mV (vs SCE) during the wet/dry cycles until 240 days. This also applies to the guanidine specimens (NG), the potential ranging between -250 mV and 0mV vs (SCE). The arginine specimens, however, showed uncertainty of passivation of the steel with the potential range in slightly more negative region (between -400mV and -150mV) than above two inhibitor cases.

In the case of sodium carbonate (NR, used for simulation of electrochemical re-alkalisation), the potential seems to be more significantly affected by the wet/dry cycles. The steel potential dropped to around -450mV soon after the wet/dry cycles started, and continued to show large amplitude during the exposure to the cycles. After the interval of the wet/dry regime was changed at 60 days, the amplitude of the potential evolution became still larger with the maximum potential of near 0 mV and the minimum potential of -350mV (vs SCE), and it can be said that the trend of the potential evolution for this case is similar to that observed in the control specimens (NC).

The average corrosion rate profiles of the embedded steel bars during wet/dry cycles are shown in Figure 6.23 for different types of treatment together with control, where the

average values of NEn and NEc specimens were used for the ethanolamine case, since they were similar. It can be seen from these results that the corrosion rates of the steel embedded in ethanolamine treated concrete specimens were the smallest throughout the experiment period of 8 months, showing the significantly low corrosion rates of 0.1-0.2μA/cm^2. Guanidine showed a similar profile of corrosion rates to that of ethanolamine with the small corrosion rates of 0.1-0.2μA/cm^2 until 150 days; however, the rate started to increase after 150 days to 0.3-0.4μA/cm^2. The corrosion rates in the specimens treated with arginine was higher than those of above two inhibitors during the wet/dry cycles (over 0.5μA/cm^2), but gradually decreased with time, reaching 0.2-0.3μA/cm^2 after 100 days. In the case of electrochemical re-alkalisation, the corrosion current once decreased to below 0.2μA/cm^2 until 35 days; however, at the commencement of wet/dry cycles, the rate suddenly increased to above 1.0μA/cm^2 and fluctuated with larger amplitude, compared with those in inhibitor treated cases, near 1.0μA/cm^2 until the completion of the experiment. The corrosion current densities observed in the case of electrochemical re-alkalisation were similar to those of control specimens, indicating that the embedded steel may not be passivated in the both series of specimens.

Before above-mentioned experiments (Nagoya experiments (D)) were started, when the concrete specimens had arrived at the Research Institute in Nagoya from the University of Leeds by air, the specimens had been immediately visually examined. As a result, it had been confirmed that no cracks or damage associated with transportation were seen in the specimens. The similarity in the results of anodic polarisation and corrosion monitoring obtained in both Leeds experiments (B) and Nagoya experiments (D) with guanidine also indicates that the effect of the transportation was not significant.

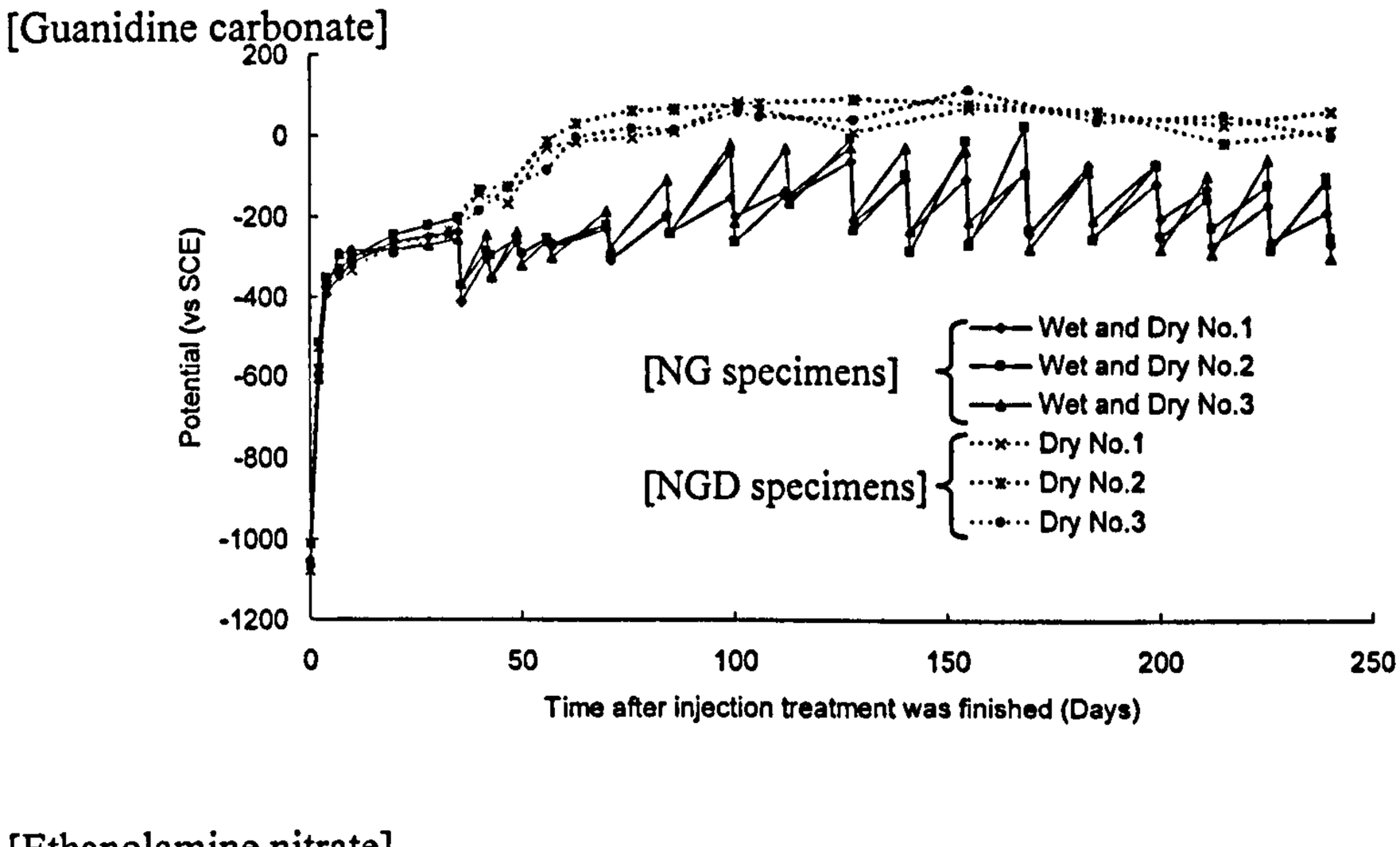

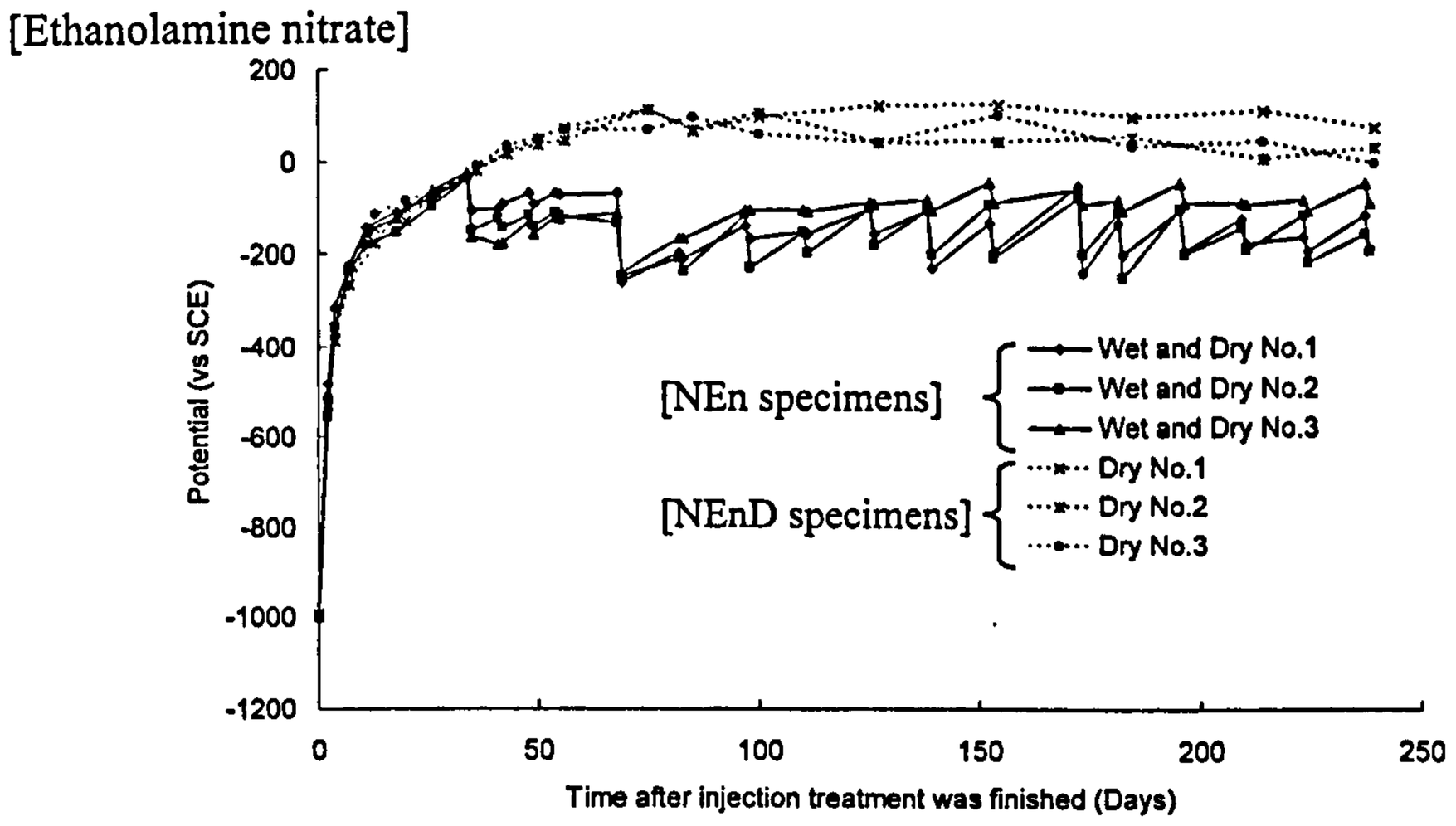

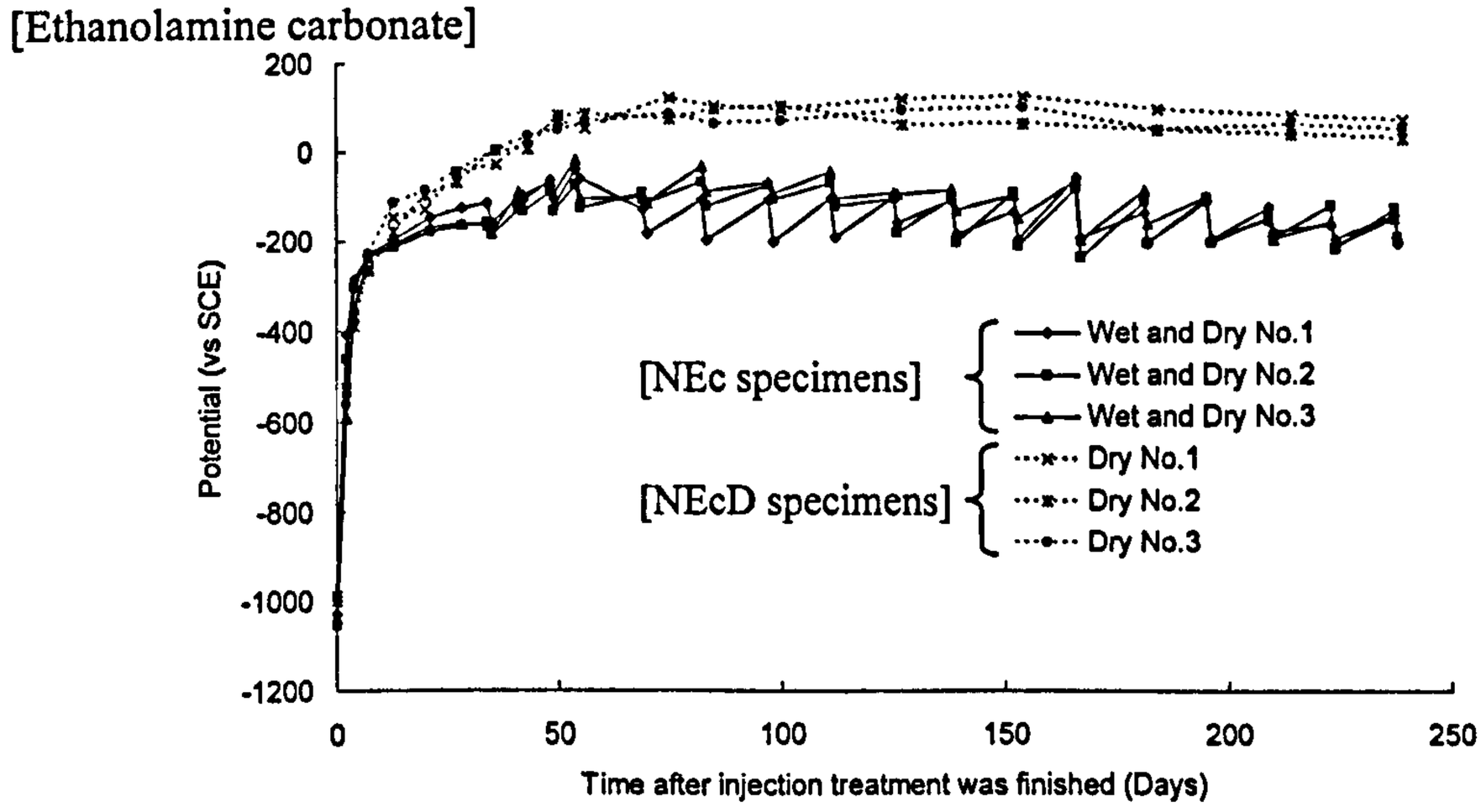

Figure 6.21 Evolutions of steel potential after electrochemical injection (Top: guanidine carbonate, middle: ethanolamine nitrate, bottom: ethanolamine carbonate)

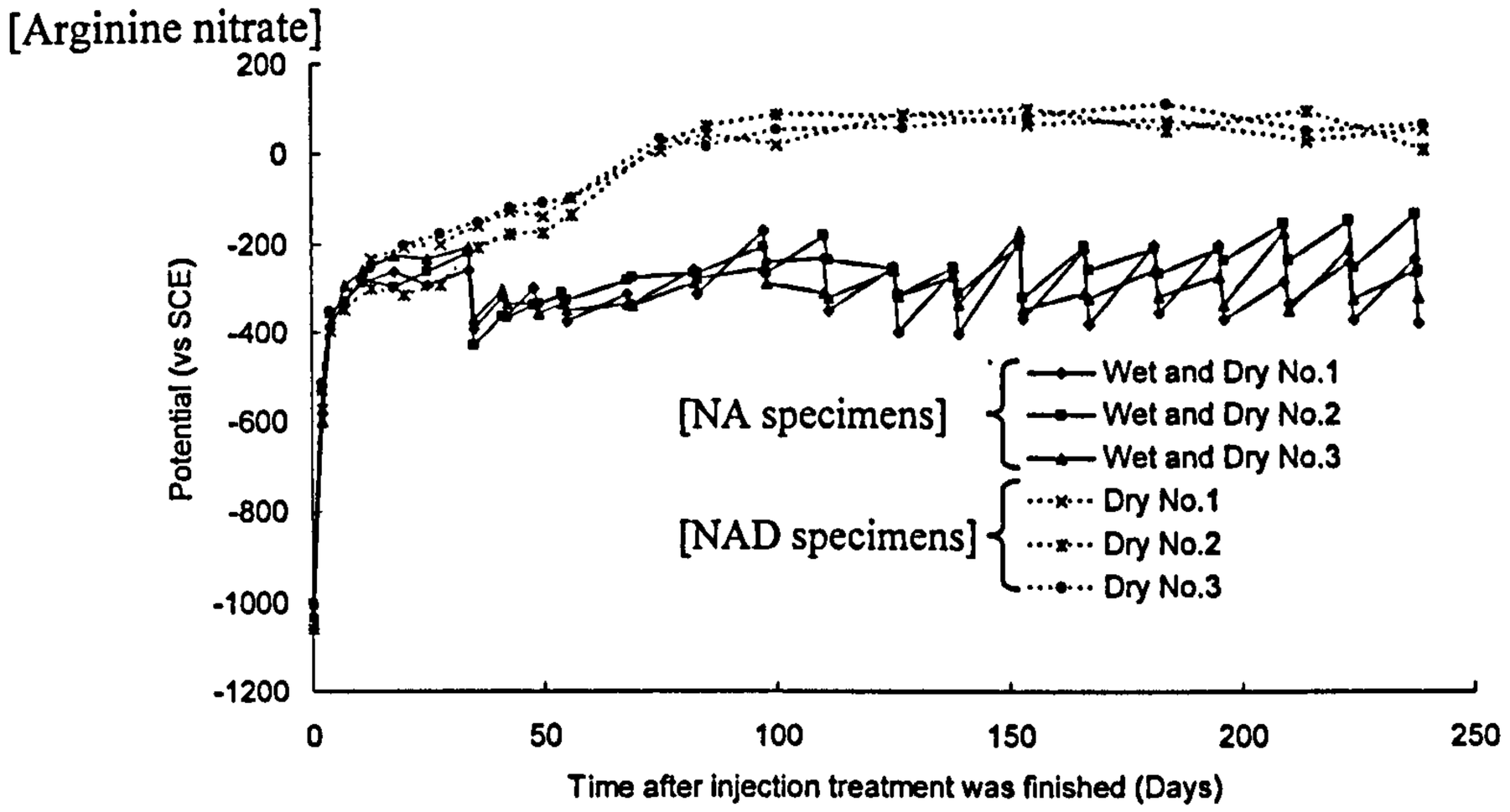

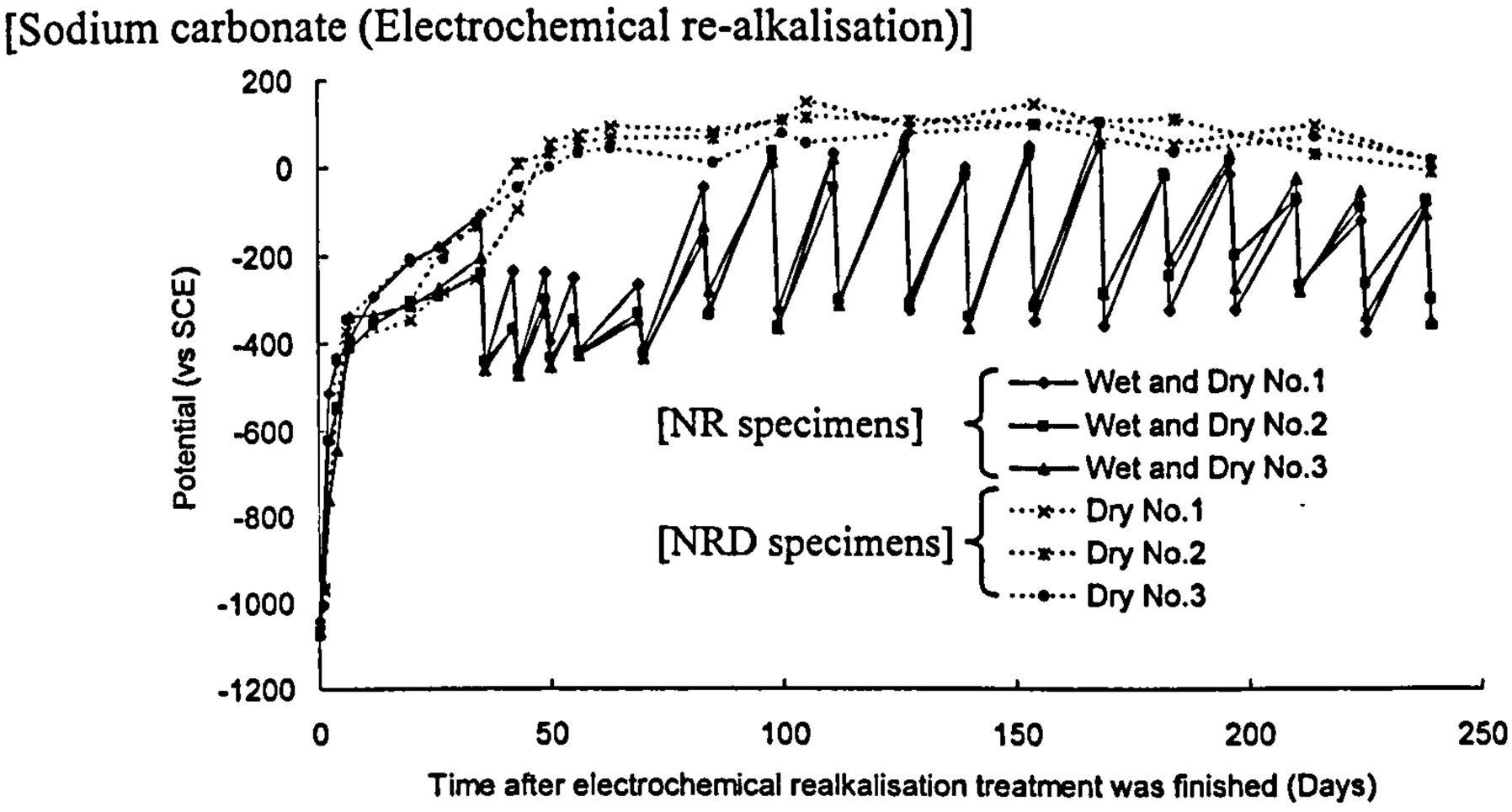

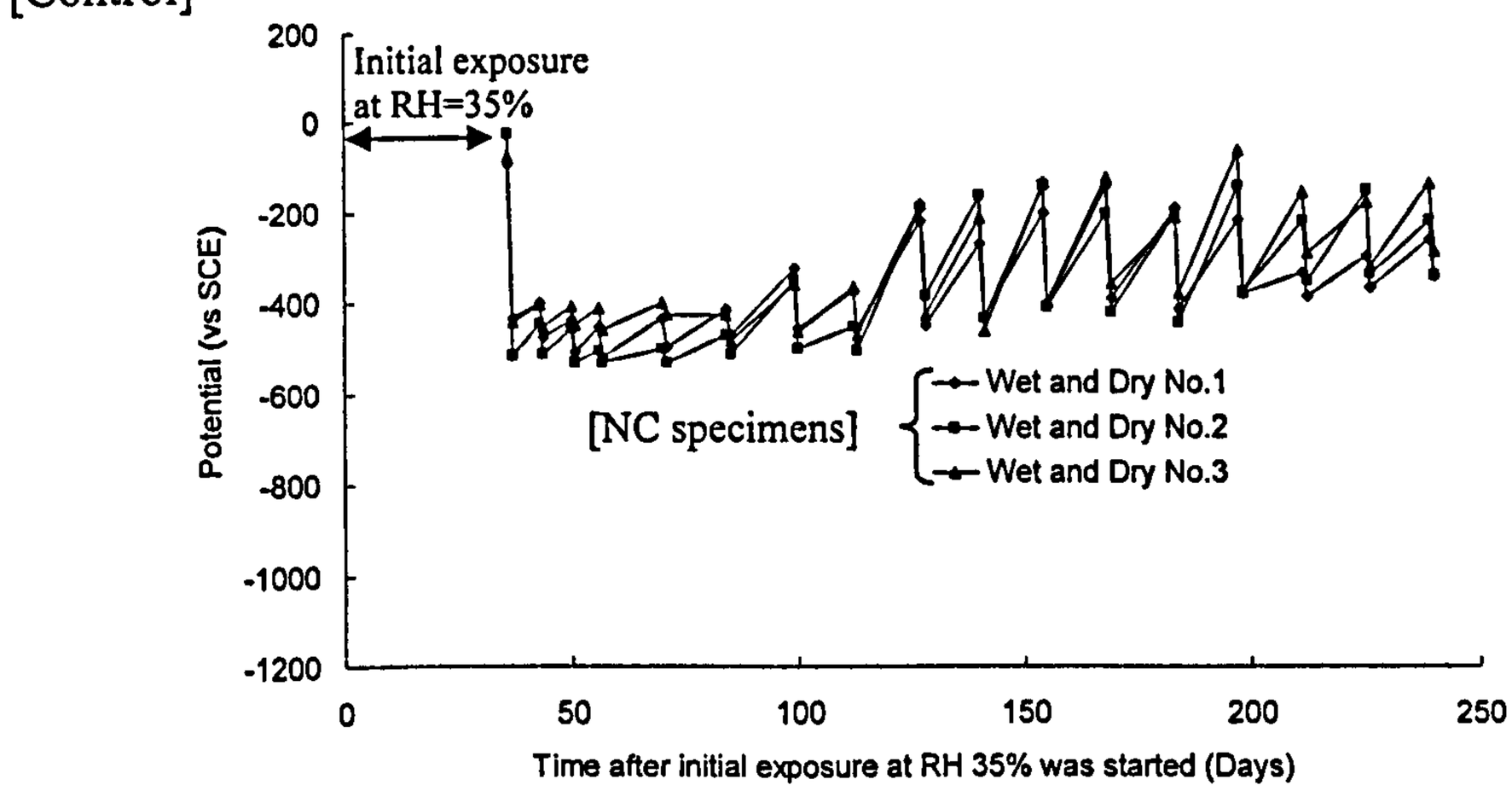

Figure 6.22 Evolutions of steel potential after electrochemical injection (Top: arginine nitrate, middle: sodium carbonate (electrochemical re-alkalisation), bottom: control)

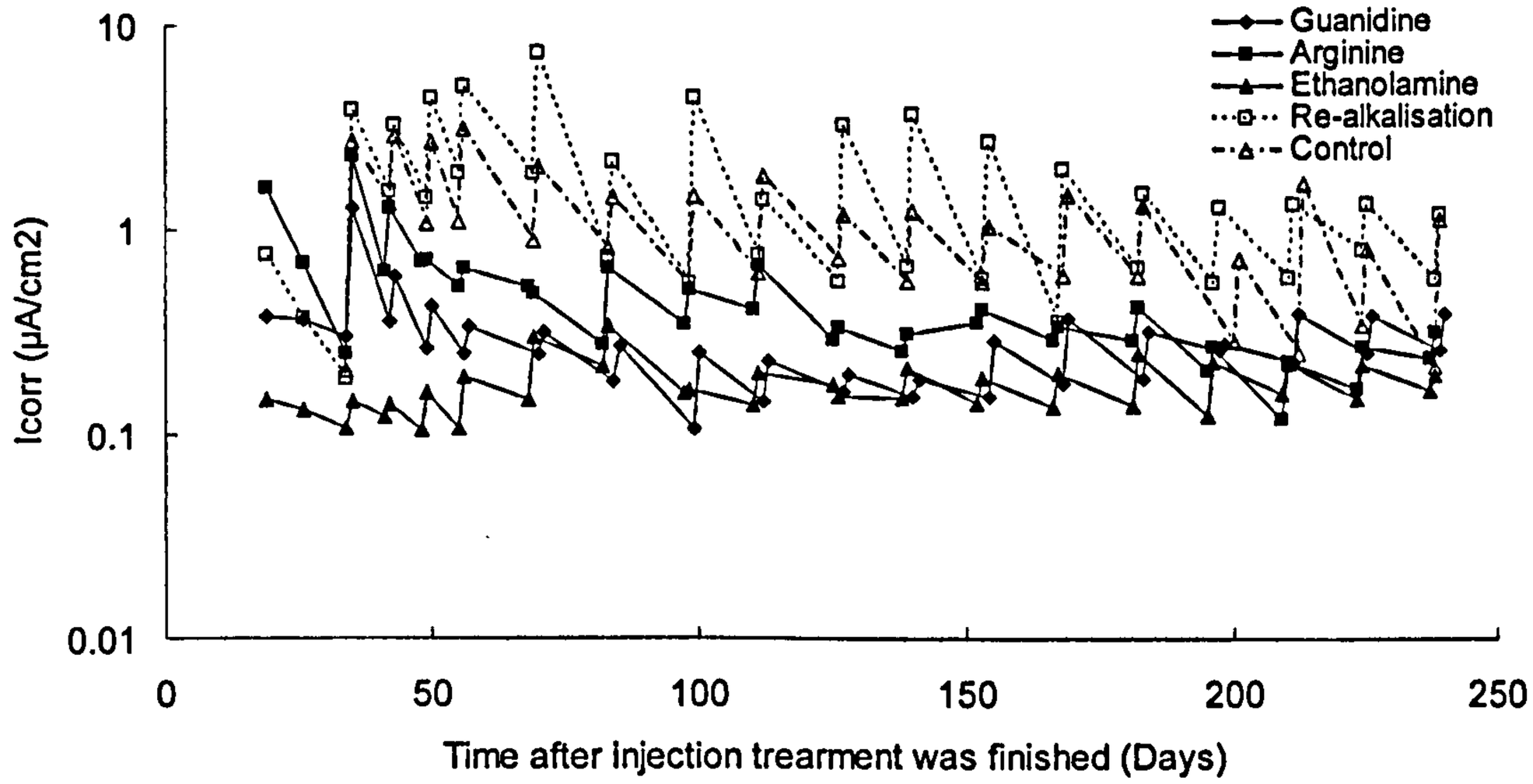

Figure 6.23 Corrosion rates of steel after electrochemical injection/re-alkalisation treatment

6.4.3.2.2 EIS measurement

The impedance responses of electrochemically treated specimens, measured approximately 60, 120, 180, and 240 days after the treatment are shown in Figure 6.24 and 6.25, together with those of control. The obtained Nyquist plots with the input frequency range of 20kHz-5mHz looked different for the different treatment methods. In the cases of guanidine of an early stage and ethanolamine, the response profiles showed high angles at low frequencies. The responses in the intermediate frequency (20kHz-10Hz) were too small to be recognised in the impedance plots for guanidine and ethanolamine-treated specimens. This indicates that the embedded steel was in an electrochemically passive state, according to Andrade et al. (1989) and Dawson et al. (1990). On the other hand, in the cases of arginine of an early stage (60 and 120 days) and electrochemical re-alkalisation, the obtained arcs looked similar (note that the scales in the figures for the two treatment methods are different) and both seemed to be a part of a flattened and deformed semi-circle. The loops were even flattened and deformed for control specimens, which is representative of multiple pits or generalised corrosion, as produced in carbonated concrete (Andrade et al. 1989). A linear tail can be seen in the low frequency (below few Hz) in the cases of guanidine and arginine of a late stage (180 and 240 days) and in the cases of electrochemical re-alkalisation and control, indicating the existence of Warburg impedance where active corrosion might be combined with diffusion (Andrade et al. 1989). A significant change was observed in the impedance response plots for arginine-treated specimens after 180 days.

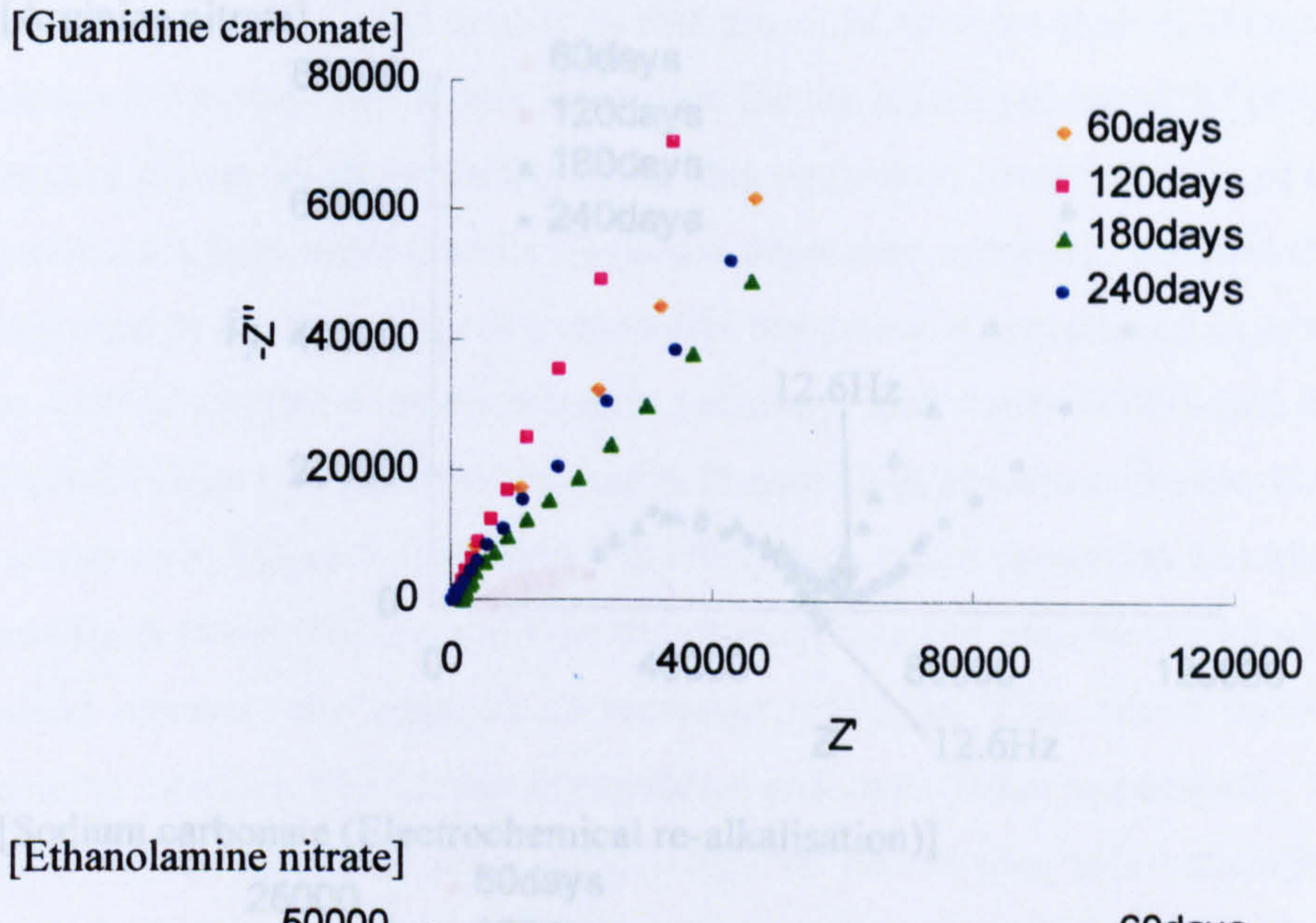

Figure 6.24 Nyquist plot (20kHz-5mHz) for steel bars embedded in carbonated concrete specimens after electrochemical treatment ($\Omega \cdot cm^2$) (Top: guanidine carbonate, middle: ethanolamine nitrate, bottom: ethanolamine carbonate)

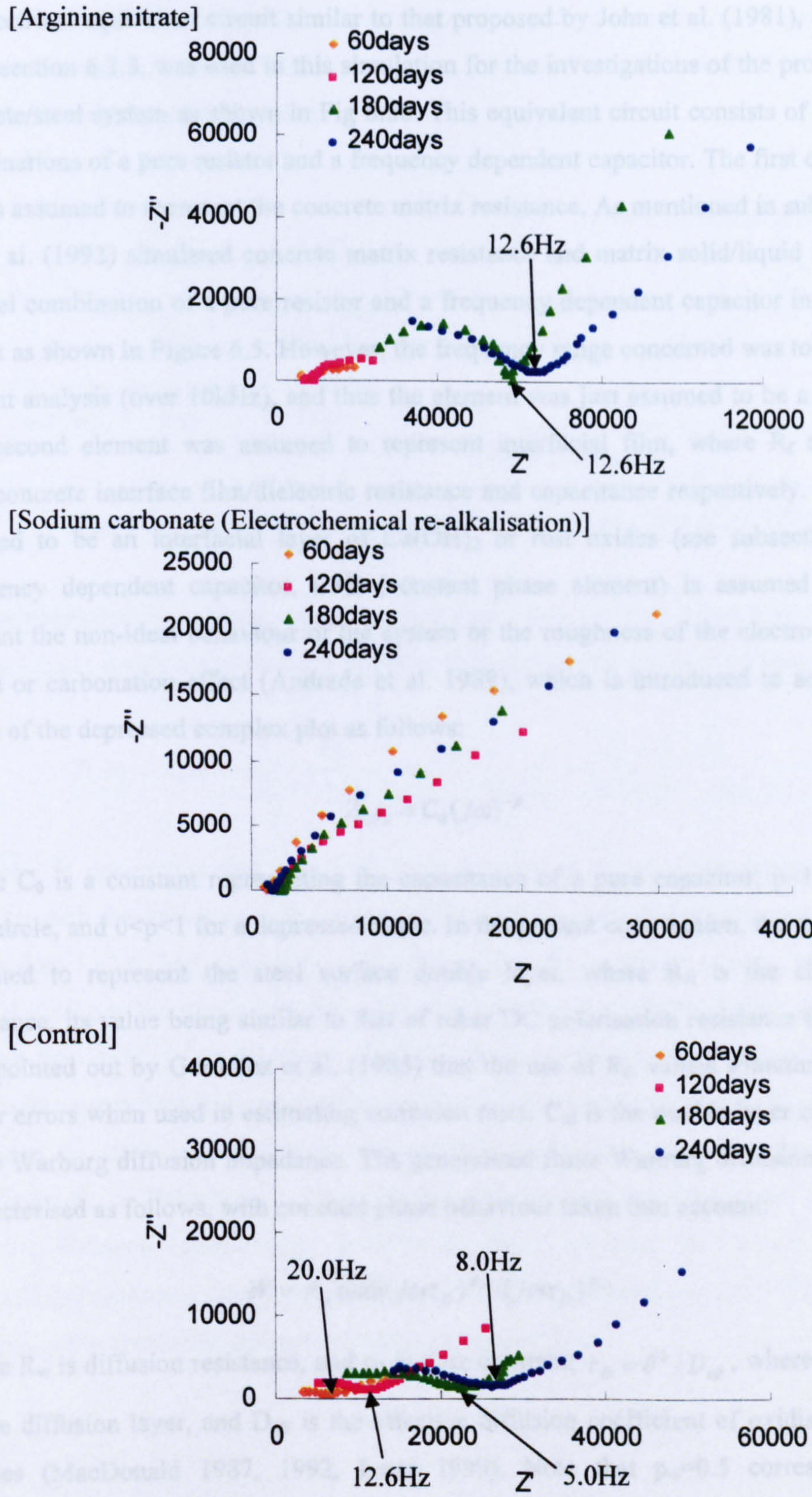

Figure 6.25 Nyquist plot (20kHz-5mHz) for steel bars embedded in carbonated concrete specimens after electrochemical treatment ($\Omega \cdot cm^2$) (Top: arginine nitrate, middle: sodium carbonate (electrochemical re-alkalisation), bottom: control)

An electrical equivalent circuit similar to that proposed by John et al. (1981), as introduced in subsection 6.2.3, was used in this simulation for the investigations of the properties of the concrete/steel system as shown in Fig 6.26. This equivalent circuit consists of three parallel combinations of a pure resistor and a frequency dependent capacitor. The first element (from left) is assumed to represent the concrete matrix resistance. As mentioned in subsection 6.2.3, Gu et al. (1992) simulated concrete matrix resistance and matrix solid/liquid interface as a parallel combination of a pure resistor and a frequency dependent capacitor in his proposed circuit as shown in Figure 6.5. However, the frequency range concerned was too high for the present analysis (over 10kHz), and thus the element was just assumed to be a pure resistor. The second element was assumed to represent interfacial film, where R_f and CPE_f are steel/concrete interface film/dielectric resistance and capacitance respectively. The film was claimed to be an interfacial layer of $Ca(OH)_2$ or rust oxides (see subsection 6.2.3). A frequency dependent capacitor, CPE (constant phase element) is assumed to take into account the non-ideal behaviour of the system or the roughness of the electrodes (Pajkossy 1994) or carbonation effect (Andrade et al. 1989), which is introduced to account for the shape of the depressed complex plot as follows:

$$Z_{CPE} = C_0 (j\omega)^{-P} \tag{6-5}$$

where C_0 is a constant representing the capacitance of a pure capacitor, p=1 for a perfect semicircle, and 0<p<1 for a depressed circle. In the present contribution, the third element is assumed to represent the steel surface double layer, where R_{ct} is the charge transfer resistance, its value being similar to that of rebar DC polarisation resistance R_p, although it was pointed out by González et al. (1985) that the use of R_{ct} values sometimes introduces larger errors when used in estimating corrosion rates. C_{dl} is the double layer capacitance. W is the Warburg diffusion impedance. The generalised finite Warburg diffusion impedance is characterised as follows, with constant phase behaviour taken into account:

$$W = R_w \tanh(j\omega\tau_D)^{P_w} / (j\omega\tau_D)^{P_w} \tag{6-6}$$

where R_w is diffusion resistance, and τ_D is time constant; $\tau_D = \delta^2 / D_{eff}$, where δ is thickness of the diffusion layer, and D_{eff} is the effective diffusion coefficient of oxidised or reduced species (MacDonald 1987, 1992, Lasia 1999). Note that p_w=0.5 corresponds to the theoretical value for pure Warburg impedance in an infinite diffusion layer, when the impedance angle becomes 45° in the complex plot.

The concrete samples used for the electrochemical treatment in this study were chloride-free and carbonated; therefore, only generalised corrosion was assumed as a corrosion process

(Glass et al. 1991). Thus, the element that represents pitting corrosion in equivalent circuits, proposed by Andrade et al. (1995) (see Figure 6.4) and Trabanelli et al. (2005) (see Figure 6.6), was not employed in this simulation.

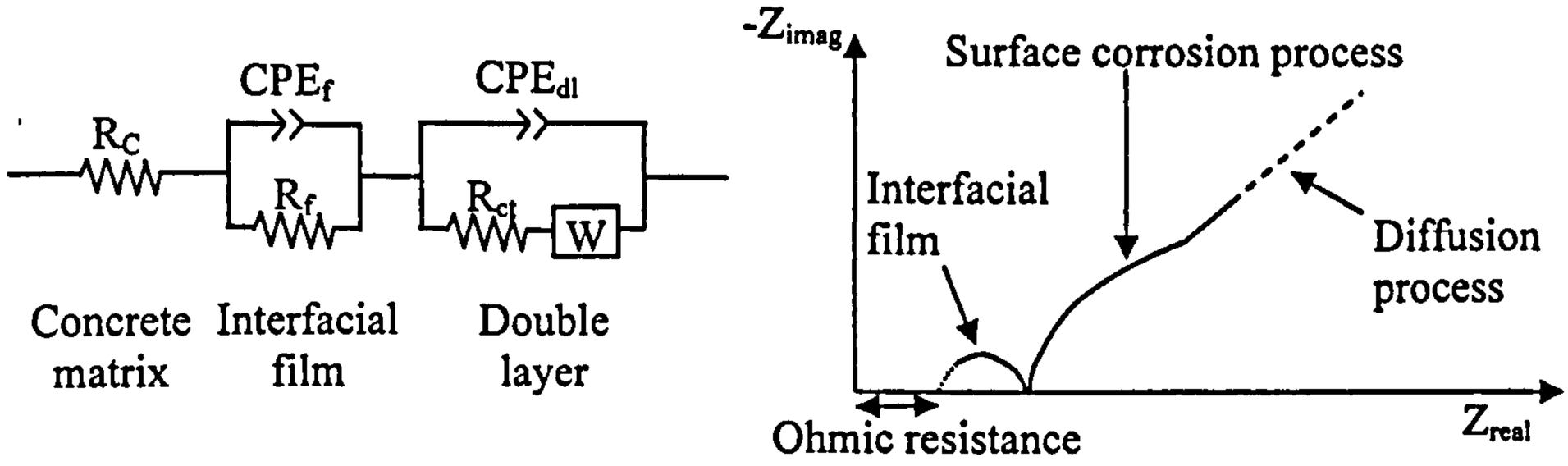

Figure 6.26 Equivalent circuit used for simulation (John et al. 1981)

The experimental impedance data were modelled using the equivalent circuit as shown in Figure 6.26 to which the impedance function of the following equation corresponds:

$$Z(\omega) = R_c + \frac{R_f}{1 + R_f C_f(\omega)(j\omega)^{p_f}} + \frac{R_{ct} + W(\omega)}{1 + (R_{ct} + W(\omega))C_{dl}(\omega)(j\omega)^{p_{dl}}} \qquad (6\text{-}7)$$

The best-fit parameters that give the fitting data using Eq. (6-7) are listed in Table 6.6, together with the values of polarisation resistance (R_p) obtained by linear polarisation (see subsections 3.3.6 and 6.4.3.2.1). The values for the concrete matrix resistance (R_c), corresponding to the ohmic resistance (IR drop), are not listed in the Table, since they were smaller than 1kΩ·cm^2 in all cases. The calculated charge transfer resistance (R_{ct}) was in reasonable agreement with polarisation resistance (R_p), except for a few results, which may probably be attributable to poor extrapolation of the data with the significantly high resistance (R_{ct} > 200 kΩ·cm^2). The p_w values, which were assumed to be associated with Warburg diffusion impedance as shown in Eq. (6-6), are listed for the cases in which the effect of diffusion was observed. The evaluation of the values presented in this table will be detailed in the discussion subsection (see subsection 6.5.3).

Table 6.6 Parameters obtained from fitting data and measured polarisation resistance values

Treatment/ Time	R_f ($\Omega \cdot cm^2$)	CPE_f ($\mu F/cm^2$)	p_f	R_{ct} ($k\Omega \cdot cm^2$)	CPE_{dl} ($\mu F/cm^2$)	p_{dl}	p_w	R_p ($k\Omega \cdot cm^2$)
[Guanidine carbonate]								
60 days	9	0.0	0.578	179	103	0.741	-	216
120 days	95	0.1	0.587	216	181	0.749	-	104
180 days	105	0.1	0.545	29	155	0.763	0.534	44
240 days	302	0.1	0.574	36	199	0.706	*0.708	30
[Ethanolamine nitrate]								
60 days	954	0.1	0.638	96	265	0.768	-	123
120 days	1742	0.0	0.699	133	150	0.786	-	136
180 days	1666	0.0	0.834	201	158	0.855	-	232
240 days	2093	0.0	0.870	180	187	0.828	-	136
[Ethanolamine carbonate]								
60 days	747	0.1	0.521	298	285	0.821	-	152
120 days	1330	0.0	0.765	325	174	0.875	-	325
180 days	1805	0.0	0.800	205	189	0.826	-	162
240 days	2255	0.0	0.887	324	195	0.869	-	288
[Arginine nitrate]								
60 days	8722	2.3	0.277	34	263	0.501	0.384	32
120 days	7161	1.2	0.254	25	221	0.502	0.462	50
180 days	41156	0.1	0.690	239	88	0.753	0.631	162
240 days	61996	0.1	0.480	82	66	0.557	0.537	105
[Sodium carbonate (Electrochemical re-alkalisation)]								
60 days	1462	0.1	0.316	38	283	0.761	*0.849	36
120 days	2273	0.1	0.516	10	267	0.784	0.507	10
180 days	3006	0.1	0.509	12	270	0.804	0.491	11
240 days	2073	0.0	0.526	41	278	0.756	0.454	41
[Control]								
60 days	5949	2.0	0.412	16	320	0.349	0.255	16
120 days	12403	1.9	0.375	22	250	0.513	0.348	18
180 days	24555	1.4	0.333	10	329	0.500	0.431	13
240 days	28098	1.0	0.325	43	284	0.438	0.421	50

*) may include an extrapolation error since the diffusion tail was not long enough for fitting.

6.4.4 Gravimetric analysis of corrosion

The complete list of corrosion weight losses is shown in Appendix E on sections of steel bars obtained by means of gravimetric analysis. In Figure 6.27 the distribution of average corrosion weight losses is presented by means of gravimetric analysis (presented in bar charts) together with average weight loss obtained through integration of the corrosion rate measured by means of linear polarisation (presented in dotted lines). This shows that a fairly good correlation has been achieved between the weight loss measurement and the electrochemical monitoring.

It may be noted that a corrosion current density of 1.0μA/cm^2 passing for around 240 days would correspond to average loss of 6.0mg/cm^2 recorded. The average weight loss calculated by integration of the corrosion rates was the smallest in the case of ethanolamine (ethanolamine nitrate: 0.96mg/cm^2, ethanolamine carbonate: 0.85mg/cm^2), followed by guanidine (1.43mg/cm^2) and arginine (2.71 mg/cm^2), whilst the weight loss values were 3.78mg/cm^2 and 5.55mg/cm^2 respectively for control and electrochemically re-alkalised specimens.

Compared with the weight loss observed in control specimens, it was found that injected guanidine and ethanolamine (nitrate and carbonate) were significantly effective in reducing the weight loss of the embedded steel bars by approximately 60% and 75% respectively.

Ngala et al (2004) demonstrated that relatively uniform attack can be seen in the weight loss distribution profiles of steel bars embedded in carbonated concrete with very low levels of chloride, with no sections of steel bars showing an outstanding weight loss, and this was the case with the bars in all of the specimens in this experiment.

Figure 6.28(a) and (b) shows corrosion states of the embedded steel bars photographed just after they were extracted from concrete slices by means of a hammer and a chisel and also shows the surface conditions of the sectioned bars photographed immediately after the corrosion products were removed by immersion of the samples in 10% diammonium hydrogen citrate solution with 150ppm 2-mercaptobenzothiazole as corrosion inhibitor. As can be seen in the photos, in the cases of electrochemical re-alkalisation and the control, the colour of the rust covering the steel bars was brown or even orange, indicating that the corrosion levels of the steel bars in the specimens for the above two cases were more severe than those embedded in inhibitor treated specimens, whose rust colour ranged between dark brown or dark grey. The occurrence of pitting was not seen in any sectioned samples in the photo, although it might be noted that some unexpected damage by means of a chisel can be seen on some of the sample surfaces.

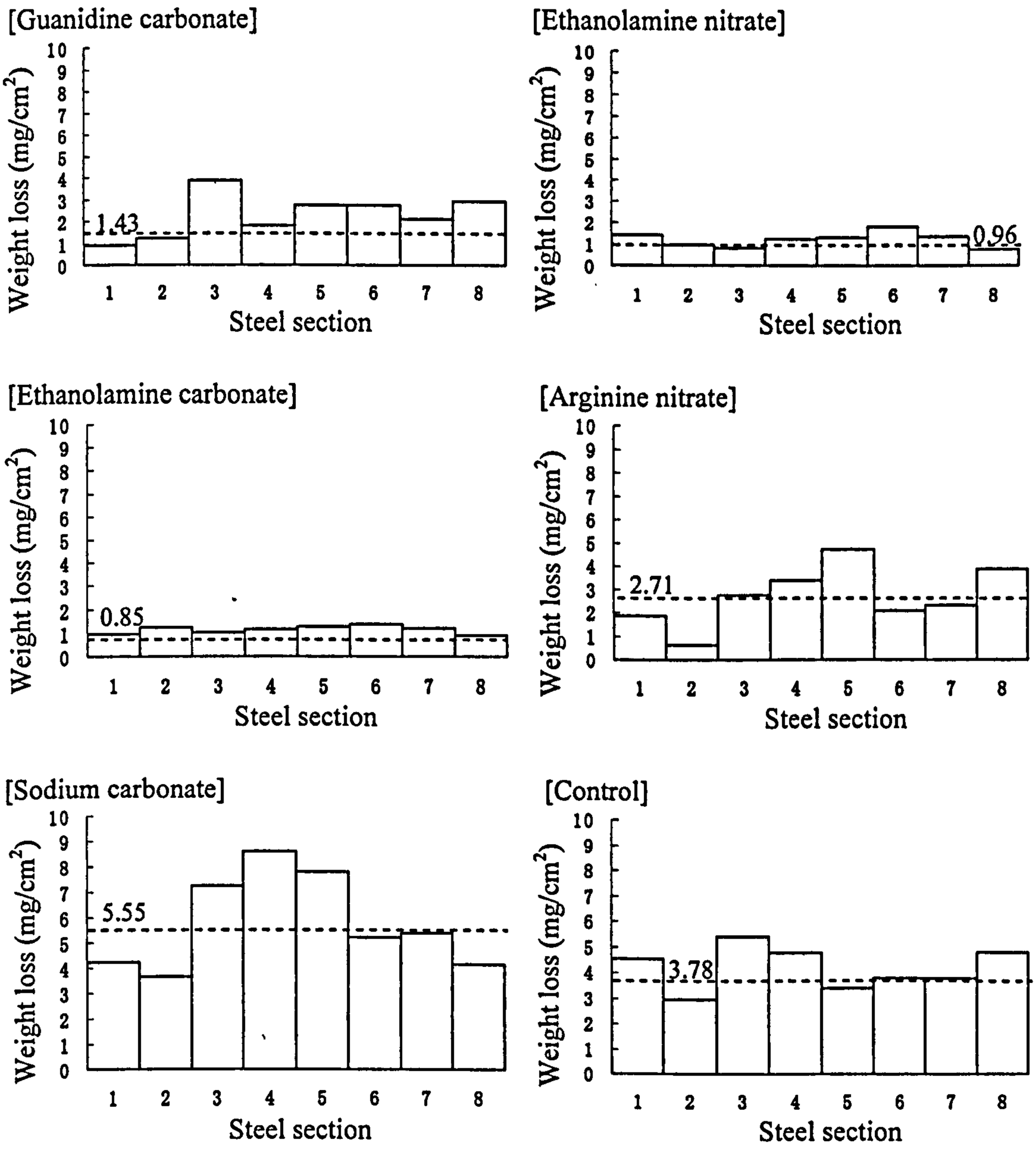

Figure 6.27 Distribution of corrosion weight losses on sections of steel bars obtained by means of gravimetric analysis together with average weight loss obtained by means of linear polarisation

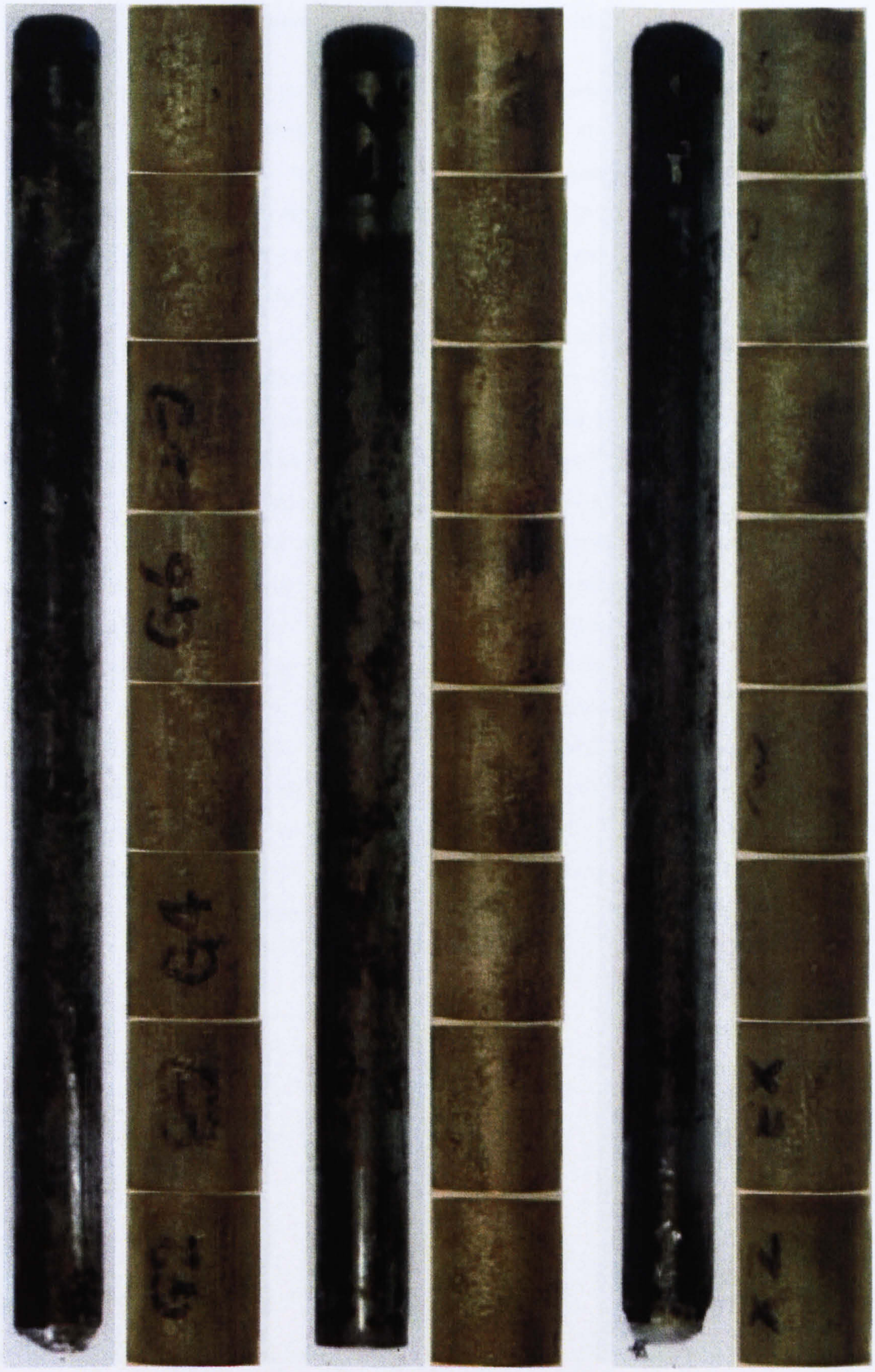

Figure 6.28(a) Extracted embedded steel bars and cleaned sectioned pieces (left: treated with guanidine carbonate, centre: ethanolamine nitrate, right: ethanolamine carbonate)

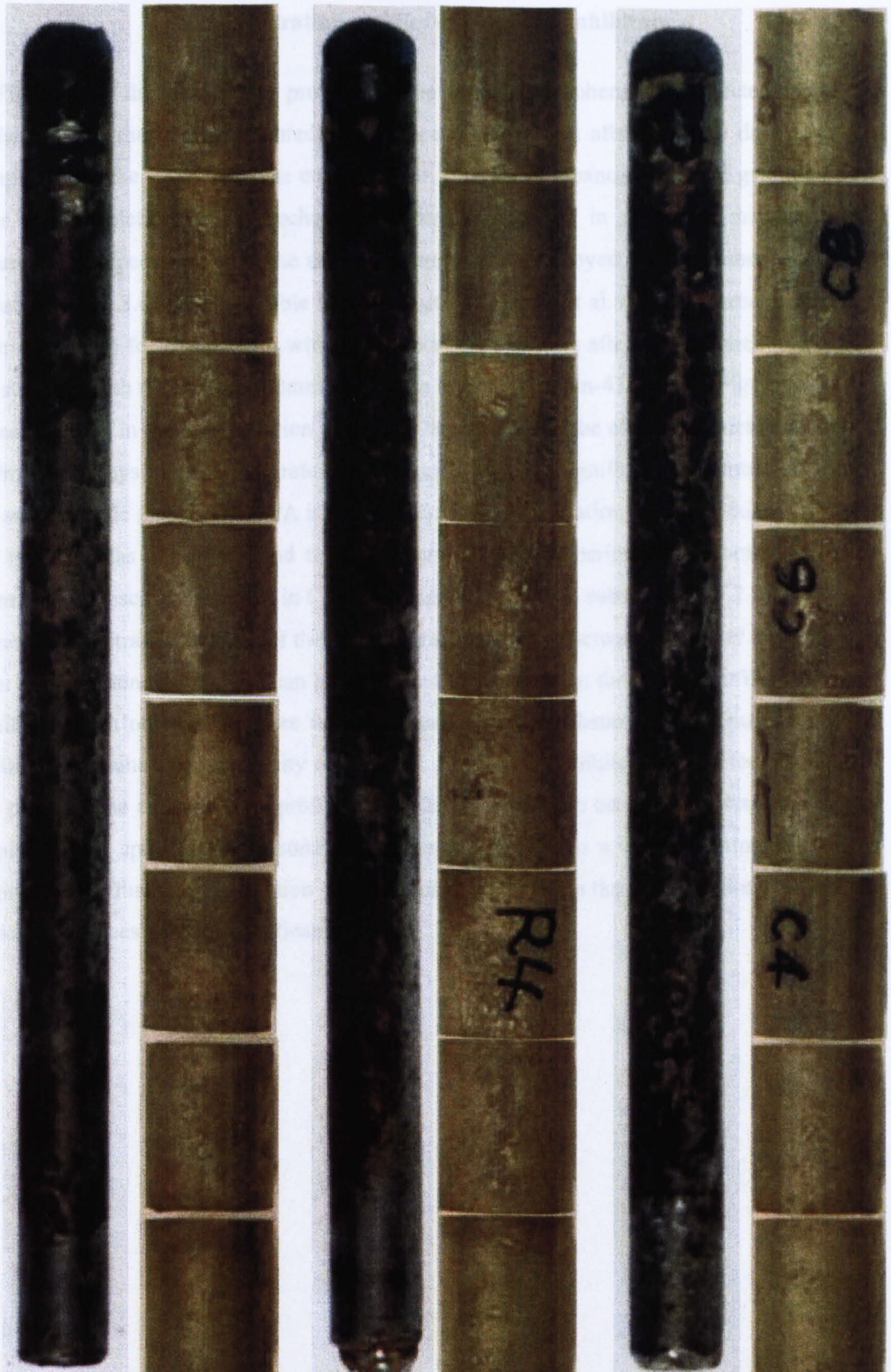

Figure 6.28(b) Extracted embedded steel bars and cleaned sectioned pieces (left: treated with arginine nitrate, centre: sodium carbonate (electrochemical re-alkalisation), right: control)

6.4.5 Penetration profiles of corrosion inhibitors

In Figure 6.29 the penetration profiles of the three electrochemically injected inhibitors studied in this thesis are presented; these were obtained just after and 160 days after the completion of the treatment. The concentration profiles of ethanolamine and guanidine just after the completion of electrochemical treatment (applied in the same manner to the concrete slice specimens with the same mixture as was employed the experiment described in subsection 6.3.4) were available in the report by Sawada et al. (2005). These profiles are referred to here for comparison with those obtained 160 days after the treatment. Note that the steel bar with a diameter of 8mm covers the region of 35mm-43mm (see Figure 6.8).

As can be seen in the concentration profiles of arginine, after the electrochemical injection at $5A/m^2$ for 7 days, arginine migrated and accumulated at a significant concentration around the steel cathode (specimens LPA in Table 6.2). The concentration profile obtained just after the injection has a similar trend to that observed in the experiments performed by using cement paste discs as described in Chapter 4 (see Figure 4.7 in subsection 4.5.2.1).

When the penetration profiles of the inhibitors are compared between just after and 160 days after the injection treatment, it can be seen from the results that the paired profiles look quite similar to each other in all three inhibitor cases and that substantial concentrations of the inhibitors remained in the vicinity of the steel. In all three inhibitors' cases, the positions of the peaks of the concentration profiles were the same on both occasions. These results may imply that, in spite of the reasonably long-term exposure to a cyclic wetting and drying regime, the diffusion or dissipation of the injected inhibitors in the pore solutions or from the concrete surfaces was not significant.

[Guanidine]

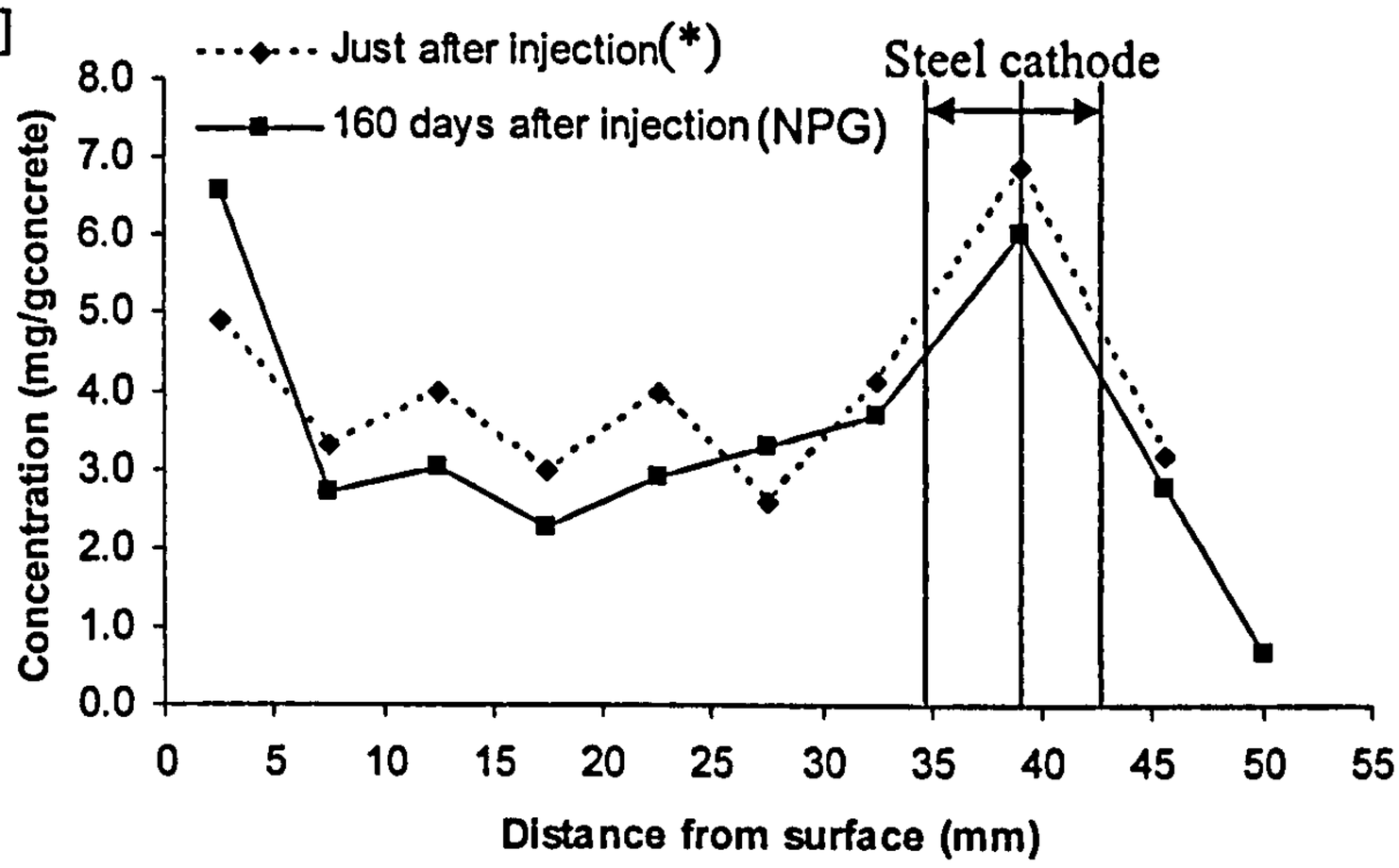

[Ethanolamine]

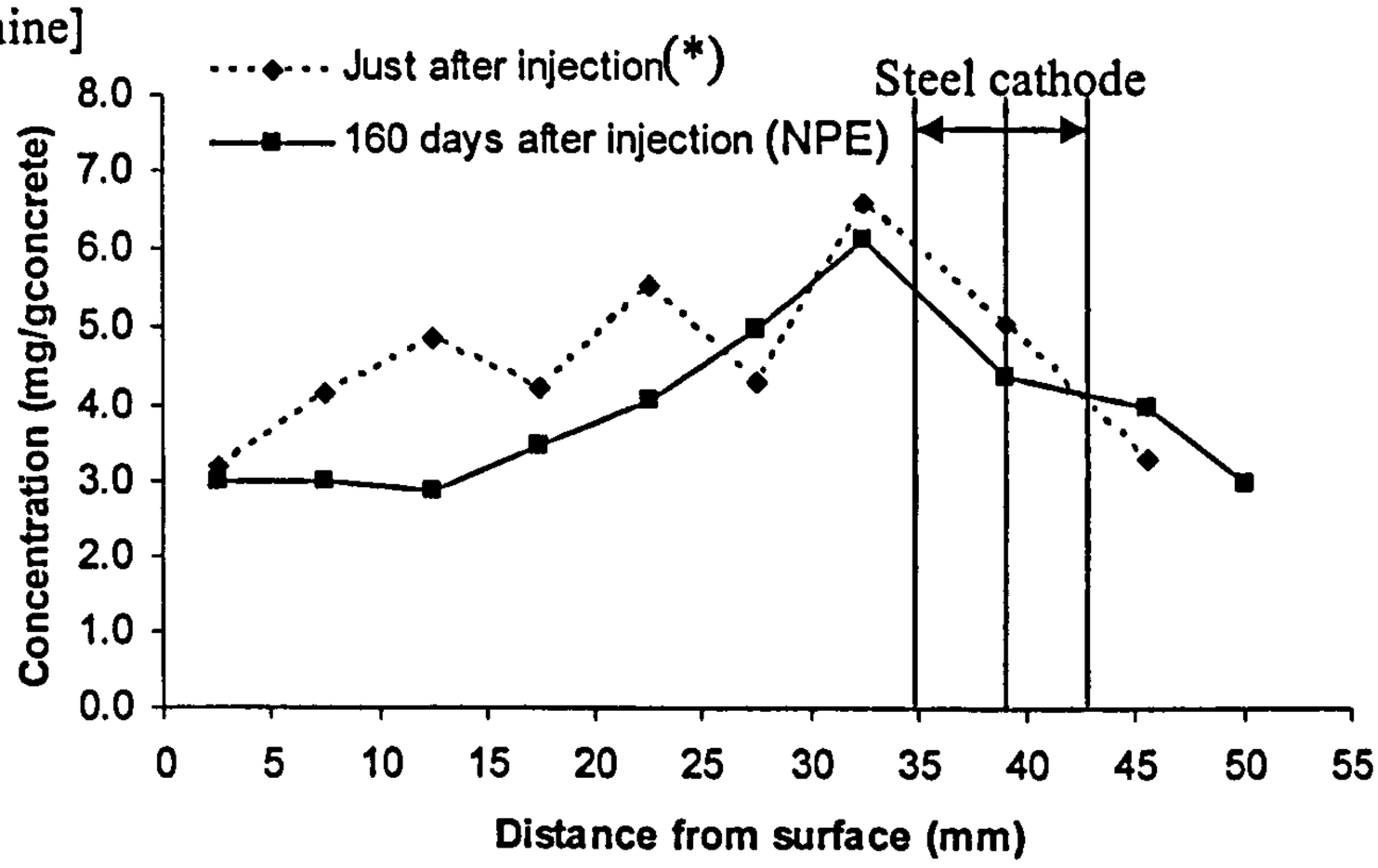

[Arginine]

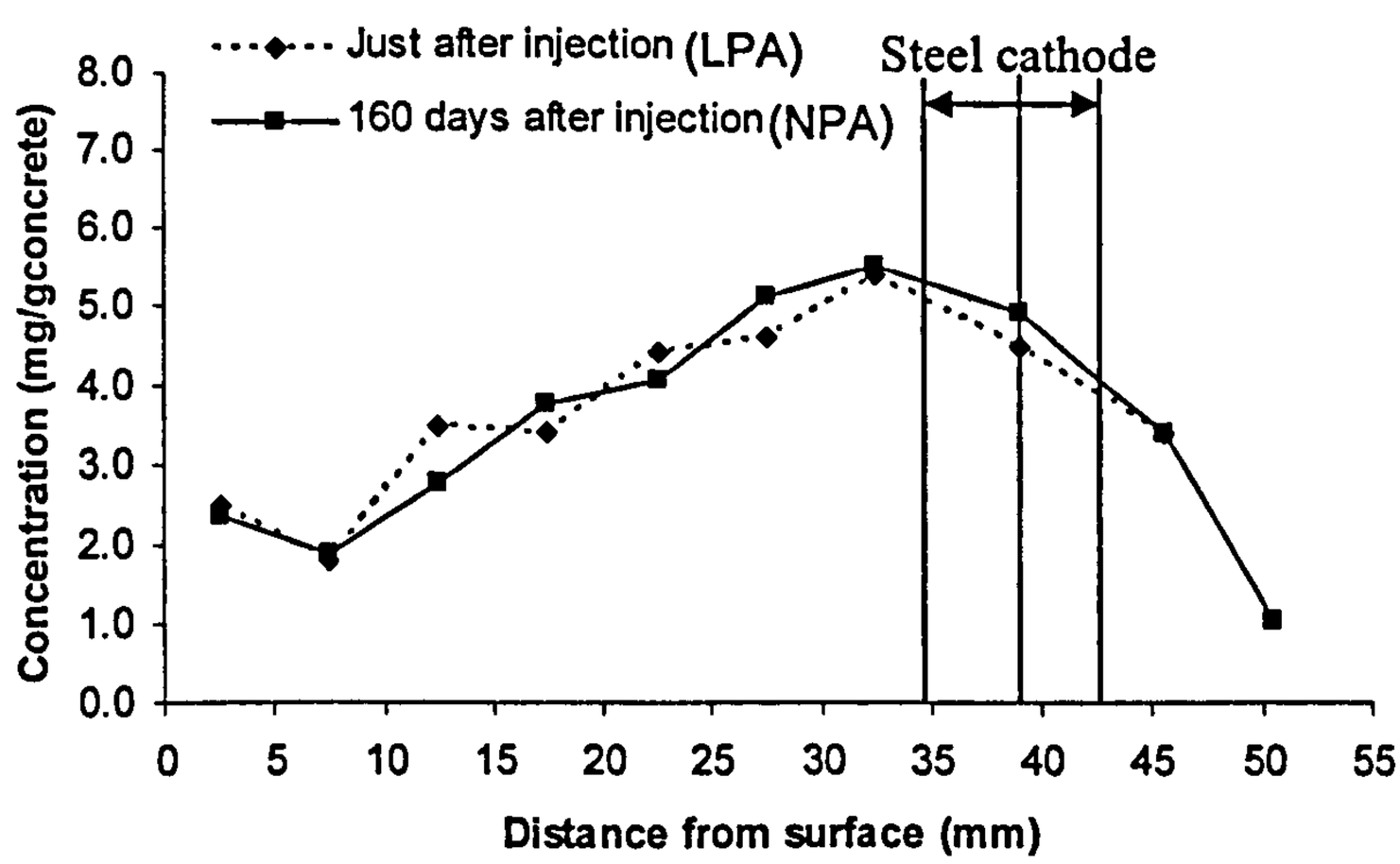

Figure 6.29 Concentrations of inhibitor in concrete specimens ((*): Sawada et al. (2005))

6.5 DISCUSSION

In this section, the effect of anodic polarisation on electrochemical behaviour of embedded steel in concrete specimens is first discussed. Then the effect of the different electrochemically injected inhibitors or electrochemical re-alkalisation on the long-term passivation of steel embedded in concrete is discussed with the results of monitored potential, corrosion rates and electrochemical impedance of the steel under cyclic wet/dry conditions for each treatment case. The changes in concentration profiles of the electrochemically injected inhibitors with respect to time, which might have affected the long-term durability of the steel inhibition, are also discussed in this section.

6.5.1 Anodic polarisation

By comparing the potential enhancement when anodic polarisation was applied to the non-carbonated specimens with or without chloride in subsection 6.4.2.1 (specimens LA and LAC in Leeds experiments (A)), it was found that the polarisation technique provides a means of determination of the ease of passivation of steel embedded in concrete, in a similar way to that devised for steel in aqueous solutions (Hancock and Mayne, 1957). Figure 6.14 indicates that, for passivated specimens, longer anodic polarisation application resulted in a more moderate drop of the enhanced potential after the termination of the anodic current application. However, it was not observed that the highly raised potential by means of the polarisation method continued to be sustained at the enhanced level (between +400 and +1,000mV vs SCE, inclusive of IR drop) in any cases with different anodic current densities and different treatment periods. It was thus found that the evolution of the steel potential associated with the application of anodic polarisation was disappointingly similar to the curve (c) in Figure 6.7. From these results, it can be concluded that the anodic polarisation method is effective for determination of the ease of passivation of steel embedded in concrete, whilst the application of the method does not contribute to the long-term passivation of the steel significantly.

In Leeds experiments (B), when anodic polarisation was applied to the embedded steel one day after completion of the electrochemical injection treatment with guanidine, the potential evolution showed that the steel was not passivated at that stage. Seven days after the treatment, the potential of the embedded steel in concrete recovered to around –300mV (vs SCE) and the passivation of the steel was confirmed by the application of anodic polarisation.

However, it was again observed that the potential raised by the polarisation soon dropped to the value recorded before the application of the anodic current densities. This drop was also observed when anodic polarisation was applied in Nagoya experiments (D) (see subsection 6.4.2.3), in which, 7 days after the completion of various electrochemical treatments including electrochemical re-alkalisation treatment, the passivation of the embedded steel was confirmed by the anodic polarisation method, but the raised potential dropped back to the original values in only a few minutes. It can be concluded that the anodic polarisation has little effect on the long-term passivation of steel bars embedded in concrete after being exposed to various electrochemical treatments. This suggestion is supported by the fact that there was no significant difference in corrosion rates of the steel bars in the guanidine-treated specimens to which anodic polarisation was applied at different times (see Figure 6.18 in subsection 6.4.3.1).

6.5.2 Electrochemical monitoring and gravimetric analysis

As shown in the results of Nagoya experiments (D) (see subsection 6.4.3.2), for all electrochemical treatment cases with five different electrolytes, the potential of the steel embedded in concrete specimens was depressed to below -1,000mV by electrolysis soon after the completion of the treatment. During the 7 days after the treatment, the potential was observed to recover and, 7 days after the treatment, the passivation of the steel was confirmed for all cases by applications of the anodic polarisation technique. The rate of the potential recovery was different, depending on the treatment method. The recovery rate was the smallest in the case of electrochemical re-alkalisation, which was probably attributable to the smaller current density ($1A/m^2$) applied to the specimens during the treatment than that ($5A/m^2$) applied to inhibitor specimens.

As shown in Figures 6.21 and 6.22, for all the treatment cases including electrochemical re-alkalisation, when the specimens continued to be kept in dry conditions after the electrochemical treatment, the embedded steel bars were observed to be maintained passivated with the potential values more noble than 0mv (vs SCE) for almost 8 months.

However, when the specimens were exposed to cyclic wet/dry conditions, the behaviour of the steel potential and corrosion rates was observed to be significantly different for different treatment methods. The results of potential and corrosion current density evolutions in Figures 6.21, 6.22, and 6.23, showed that electrochemical injection treatments with three

inhibitors, namely ethanolamine, guanidine, and arginine, were effective in promoting long-term steel passivation. It can thus be inferred that, as predicted in Chapters 4 and 5, the accumulation of the inhibitors at the steel cathode was higher than the threshold concentration required for steel inhibition obtained in Chapter 3. It was found that among the treatments with five different electrolytes, ethanolamine nitrate/carbonate demonstrated the best performance in terms of the steel inhibition, showing relatively high potential and low corrosion current density of steel bars. It may be seen from the results that the second best was guanidine carbonate and the third arginine nitrate. The reason for high corrosion inhibition in the case of ethanolamine may be attributable to the significant concentration of the inhibitor accumulated at the steel cathode during the electrochemical treatment, as observed in Chapter 4. In addition, the use of carbonated ethanolamine would be useful since it avoided surface dissolution of concrete during the electrochemical treatment by the help of buffer function of carbonate ions, which prevented the pH of anolyte from dropping severely.

On the contrary, the obtained results showed relatively a poor long-term passivation effect in the case of electrochemical re-alkalisation, where the potential and corrosion rates of the steel were somewhat similar to those of control specimens. The reasons for this might be as follows. The hydroxyl ions, generated at the steel cathode during the electrochemical treatment, continued to passivate the embedded steel; however, as soon as the cyclic wet/dry conditions were started, the ions might have dissipated through the quite porous material (w/c 0.86), in the view of the high diffusion coefficient of the hydroxyl ion (see Table 5.3). The other reason would be that, since the total charge delivered to the reinforcement was 168A/m^2 (see subsection 6.3.4), the treatment was considered to be insufficient for corrosion protection, according to the statement in the CEN draft (2000), which requires a total charge of 200 A/m^2 for the treatment. The poor long-term passivation effect of electrochemical re-alkalisation observed in this experiment, attributable to the dissipation of hydroxyl ions from the steel as mentioned above, may indicate that the long-term passivation of the steel in the cases of inhibitor applications is secured by not cathodically generated hydroxyl ions but the injected inhibitors.

The gravimetric analysis revealed similar trends as shown in Figure 6.27. The weight losses of the steel bars embedded in concrete treated with two inhibitors, namely ethanolamine and guanidine, were especially smaller than those observed in control specimens. The comparisons of the weight losses of the embedded steel reveal that the carbonated concrete treated with ethanolamine or guanidine has approximately 4 times or 3 times as long

durability as the specimens without treatment. However, the weight losses in the case of arginine and re-alkalisation seemed to be higher than those of specimens treated with the above two inhibitors and to be somewhat similar to that observed in control specimens. For the evaluation of the difference between the weight losses of bars embedded in electrochemically treated specimens (NG, NEn, NEc, NA and NR) and those in control specimens (NC), the distributions of the weight loss values are statistically analysed with the weight loss data presented in Appendix E. Student's t-test is employed as a test of the null hypothesis that the means (μ) of two normally distributed populations of independent observations are equal. Given two data sets, each of characterised mean, standard deviation and number of data points, it can be determined by using this test whether the means are distinct, provided that the underlying distributions can be assumed to be normal. The t-statistic for the null hypothesis H_0: $\mu_1=\mu_2$ can be calculated as follows (Snedecor and Cochran, 1967):

$$t = \frac{\overline{X_1} - \overline{X_2}}{\sqrt{\frac{(N_1-1)\sigma_1^2 + (N_2-1)\sigma_2^2}{N_1+N_2-2}\left(\frac{1}{N_1}+\frac{1}{N_2}\right)}} \qquad (6\text{-}8)$$

where, $\overline{X}$ and σ^2 are the unbiased estimators of the mean and the variance respectively, N is the number of data, 1 and 2 are group numbers, N-1 is the number of degrees of freedom for each group, and the total sample size minus 2 is the total number of degrees of freedom.

The t-statistic t_{XC} for each null hypothesis H_0: $\mu_{NX}=\mu_{NC}$, calculated by using a statistical table for the total number of degrees of freedom = 46 (24+24-2) (Snedecor and Cochran, 1967), is shown in Table 6.7 with the significance level. It can be seen from these results that, at the 99% confidence level, the null hypothesis H_0: $\mu_{NA}=\mu_{NC}$ is rejected, whilst, at the 95% confidence level, the null hypothesis H_0: $\mu_{NR}=\mu_{NC}$ is accepted. It can be thus concluded that at the latter confidence level, there was no significant difference between the corrosion weight losses recorded for the controls and the electrochemically re-alkalised specimens, whilst there was a difference between the corrosion weight losses recorded for the controls and the arginine-treated specimens. As for the corrosion weight loss levels for guanidine or ethanolamine-treated specimens, at the 99.9% confidence level, the three null hypotheses H_0: $\mu_{NG}=\mu_{NC}$, H_0: $\mu_{NEn}=\mu_{NC}$, H_0: $\mu_{NEc}=\mu_{NC}$ are rejected, indicating that there was a difference between the corrosion weight losses recorded for the controls and guanidine or ethanolamine-treated specimens.

Table 6.7 t-statistics for mean value of corrosion rates compared with those of control

	Mean	Variance	t_{xC}	Significance level α
Arginine	2.72	2.16	-2.848	< 1%
Re-alkalisation	5.79	12.15	+1.982	Not significant
Guanidine	2.29	2.26	-3.673	< 0.1%
Ethanolamine nitrate	1.20	0.58	-6.780	< 0.1%
Ethanolamine carbonate	1.15	0.35	-7.062	< 0.1%
Control	4.17	4.02	-	-

6.5.3 Properties obtained from EIS measurement

As may be seen in Figure 6.24, in the cases of guanidine and ethanolamine, the arcs in the intermediate frequency region (20kHz-10Hz), corresponding to the properties of the second element described in Figure 6.26, were too small to be distinguished, compared with those observed in the low frequency (a few Hz-5mHz). This is reflected by the relatively smaller R_f values shown in Table 6.6, compared to R_{ct} values. It has been reported by Sagoe-Crentsil et al. (1992) that this phenomenon is representative for the fresh or non-corroded reinforced concrete or for the steel in calcium hydroxide solution systems. Also as claimed by Gu et al. (1997), although the use of this arc to quantify the corrosion rate would not be accurate, this arc, which might indicate the corrosion products or the rust, might be used as a qualitative indication for rebar corrosion. Indeed, the passivation of the specimens treated with the two inhibitors was confirmed by the linear polarisation measurements. The increase in R_f values with respect to time, which was also observed in the experiment carried out by John et al. (1981), Andrade et al. (1989) and Sagoe-Crentsil et al. (1992), might suggest the increasing corrosion products formed on the steel surface for all cases. On the other hand, arginine, re-alkalisation and control specimens showed higher ratio of R_f values to R_{ct} values, probably indicating depassivation of steel, which was also supported by the smaller R_p values of the relevant specimens. An interesting interpretation can be that the significantly small R_f value in the case of guanidine ($9\Omega \cdot cm^2$) at the first EIS measurement might indicate the protection of the steel bars by $Ca(OH)_2$ that had possibly precipitated during the electrochemical treatment as suggested in Chapter 4. In the guanidine case, the precipitation of $Ca(OH)_2$ during the treatment is estimated to have been the most significant, since the pH in the vicinity of the steel cathode was the highest. Note that in the case of electrochemical re-alkalisation, the current density applied was smaller ($1A/m^2$), which might have resulted in lower pH at the cathode than in guanidine case.

The capacitances of the arc observed in this intermediate region (CPE_f) were in the range of 10^{-8}-$10^{-6}\mu F/cm^2$, suggesting surface layer formation, as demonstrated by Sagoe-Crentsil et al.

(1992) and Ford et al. (1998) (see Table 6.1). Relatively higher values of this capacitance can be found in the case of arginine of an early stage and control (1.0-2.3μF/cm^2). The reason for this is not clear; however, it might seem to be relevant to corrosion products formed on the steel surface, with the polarisation resistance for the two cases taken into consideration.

The double layer capacitance values of the low frequency impedance arcs (CPE_{dl}) were in the magnitude of several hundred of μF/cm^2, which can be regarded as typical indicators for electrochemical reactions on the steel surface when other relevant reports are referred to (Hachani et al. 1991, Sagoe-Crentsil et al. 1992, Andrade et al. 1995, Gu et al. 1997, Ford et al. 1998). As presented in Table 6.6, the measured double layer capacitances in the corroded specimens (electrochemical re-alkalisation, control and arginine in an early stage) were observed to be higher (around 250-320μF/cm^2) than in passivated specimens (around 150-200μF/cm^2, except for the first measurement of ethanolamine specimens at 60 days), and remained high throughout the measurements for 240 days. A similar trend has been reported by many researchers, based on the claims that the increase or the decrease in the capacitance value may respectively suggest an increase of the active area or the adsorption of the inhibitors on the metal surface (see subsection 6.2.3). It can therefore be said that the electrochemically injected ethanolamine and guanidine might have successfully adsorbed on the metal surface, maintaining the steel in a passive condition. No significant change in the capacitance values with respect to time was observed for all specimens except arginine-treated ones. Arginine specimens showed a significant change in impedance response after 180 days, with a significant reduction in the capacitance to the smallest values after 180 days (less than 100μF/cm^2). The reason for this phenomenon is unclear; however, it might be attributable to corrosion protection mechanism of arginine via its carboxyl group ($RCOO^-$), forming a strong chemical bond with iron, which lowers the reactivity of iron atoms on the surface and facilitates passivation (Rozenfeld 1981).

The smaller p_{dl} values of control specimens compared with electrochemically treated specimens show that the impedance plots for control specimens were significantly deformed throughout the exposure period of 240 days, as is typically observed in carbonated concrete (Andrade et al. 1989). It may be seen that the values were raised by means of the various electrochemical treatments applied; however, it is still unclear that the values in the case of arginine-treated specimens were similar to those of the control for the first 120 days. The calculated p_w values were close to the theoretical value of 0.5 for pure Warburg impedance

in the cases of guanidine and electrochemical re-alkalisation; however the values were again smaller for the control specimens with smaller gradient of the diffusional tails. According to Sagoe-Crentsil et al. (1992), the lower value of p_w indicates that diffusional rather than activation process dominated kinetics at the interface; however, the corrosion rates were observed to be especially high in control specimens, thus the low p_w values would be merely attributable to the constant phase behaviour effects of the diffusion impedance associated with carbonation.

As discussed in this subsection, electrochemical impedance measurement in the intermediate frequency and low frequency regions may provide substantial information related to the surface state of steel bars embedded in carbonated concrete that has been exposed to various electrochemical treatments. The application of the equivalent circuit shown in Figure 6.26 does not seem to be far from realistic for the estimation of concrete/steel interface properties, but thorough elucidation of the physical meaning of the circuit still needs to be undertaken.

6.5.4 Penetration profiles of corrosion inhibitors

The penetration profiles in Figure 6.29 showed small diffusion or dissipation of the injected inhibitors for the period of 160 days after the completion of the electrochemical treatment. The concentrations of the inhibitors that had accumulated in the vicinity of the embedded steel during the treatment remained high during the cyclic wet and dry regime for 160 days, probably contributing to the steel passivation. The reason for this may be that, since the concrete specimens were kept at RH 35% most of the time after the treatment, the migration of the inhibitor inside the concrete was expected to be negligible in the relatively dry condition if the effect of volatility of the inhibitor, i.e. ethanolamine, was neglected.

For the investigation of the diffusive effect of the corrosion inhibitors in the specimens after the injection treatment, the mathematical model presented in Part 1 of Chapter 5 was employed for the simulation. It was desirable that the evaporation of the injected inhibitor from the material surface and the volatility of the inhibitor in the dry pores were taken into account for the prediction; however, it was expected that the model might become quite complicated. Then, in view of the limited period of this research, a particular case was investigated, which could be simply modelled with the following assumptions: After the application of the electrochemical inhibitor injection treatment to cement paste specimens studied in Chapter 4, the material surface was assumed to be coated by an impermeable

coating, by which the dissipation of the inhibitors from the surface was prevented and the pores in the material were assumed to remain fully saturated with the aqueous solution phase, leading to the following boundary condition at the surface (see Figure 5.1):

$$J_i = 0 \text{ (at x=0)} \tag{6-9}$$

Eq. (5-7) in subsection 5.4.1 is numerically solved with no externally applied current density (thus, simply applying i=0). The concentration data that were obtained from the simulation of the electrochemical treatment at $5A/m^2$ for 7 days described in Part 1 of the previous Chapter are used as initial concentration data for the calculation. The computation was performed with 500 elements and with a constant time step of 60 seconds, after the numbers of elements and the time steps required to obtain results with good accuracy and to ensure convergence had been investigated (see Appendix F).

The predicted concentration profile evolutions for 160 days after the completion of the electrochemical treatment are shown in Figure 6.30 for the three corrosion inhibitors studied. The concentrations of inhibitors at the embedded steel are found to gradually decrease by diffusion in the cases of guanidine and ethanolamine, and after 160 days, the concentrations at the cathode are around 200mmol/l and 400mmol/l respectively, which are still regarded as sufficient concentrations for steel passivation according to the threshold obtained in Chapter 3. After 160 days, the concentration profile of ethanolamine is fairly flattened mainly because of its large diffusion coefficient (see Table 5.3). On the other hand, the concentration of arginine at the steel cathode was found to increase by degrees from around 150mmol/l to 250mmol/l during the 160 days. It should be noted that, without the assumed impermeable coating applied on the material surface, the total concentrations of the inhibitors remaining within the material would be different due to evaporation of the pore solutions containing inhibitors or volatility of the inhibitors at the material surface.

Therefore, the results presented in Figure 6.29 may indicate that the storage of the concrete specimens in the dry condition resulted in small diffusion or evaporation of the inhibitors inside or from the material, if the effect of the volatility of the inhibitors is neglected. In the cases of guanidine or arginine with smaller volatility compared with ethanolamine, this might be a beneficial aspect in applying the proposed injection treatment to carbonated concrete structures, since it is generally accepted that rapid penetration of carbonation may be found in atmospheres of moderate humidity (Tuutti, 1982). However, the effect of volatility needs to be considered in dry pores, which will be undertaken in the future work.

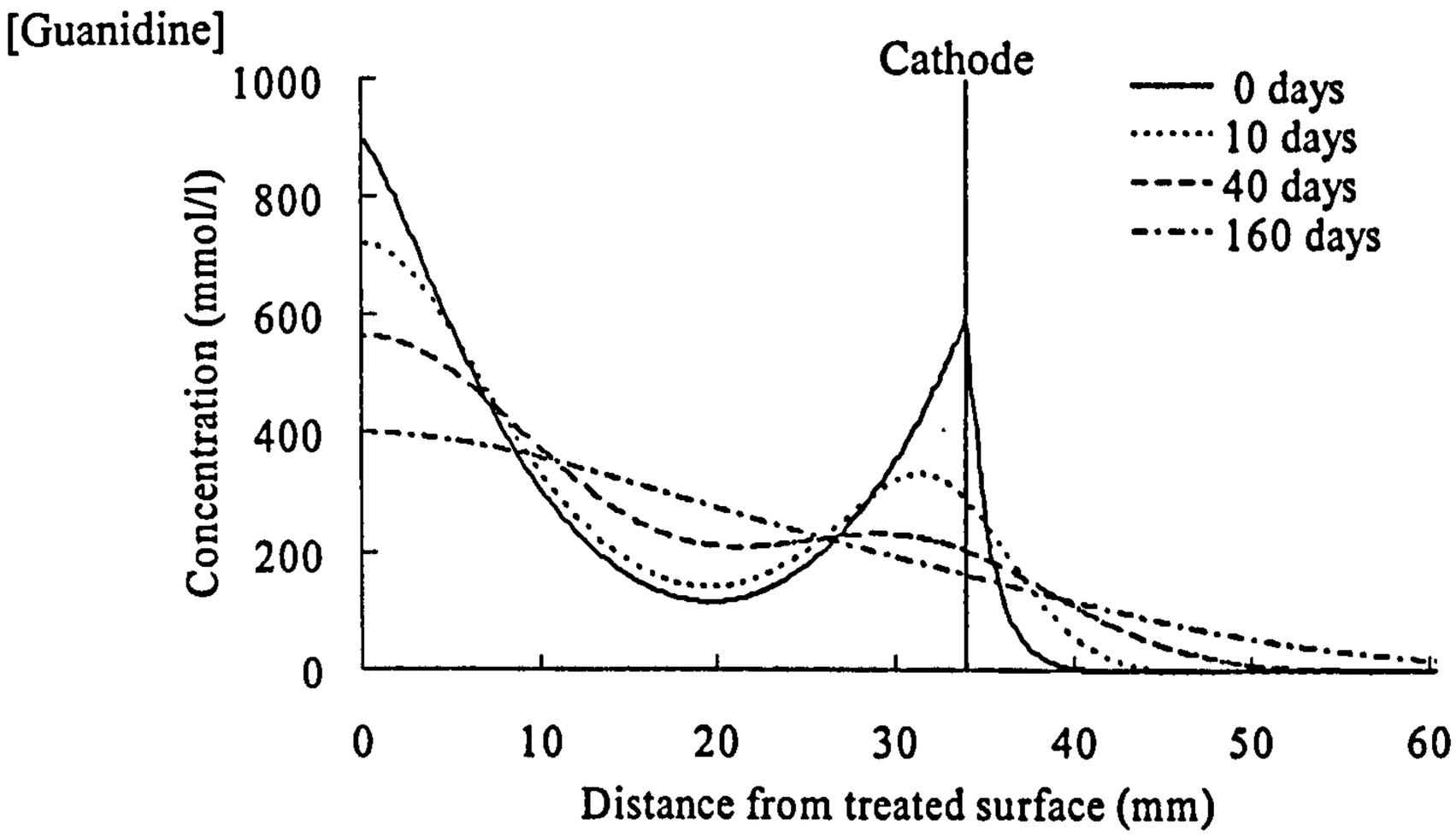

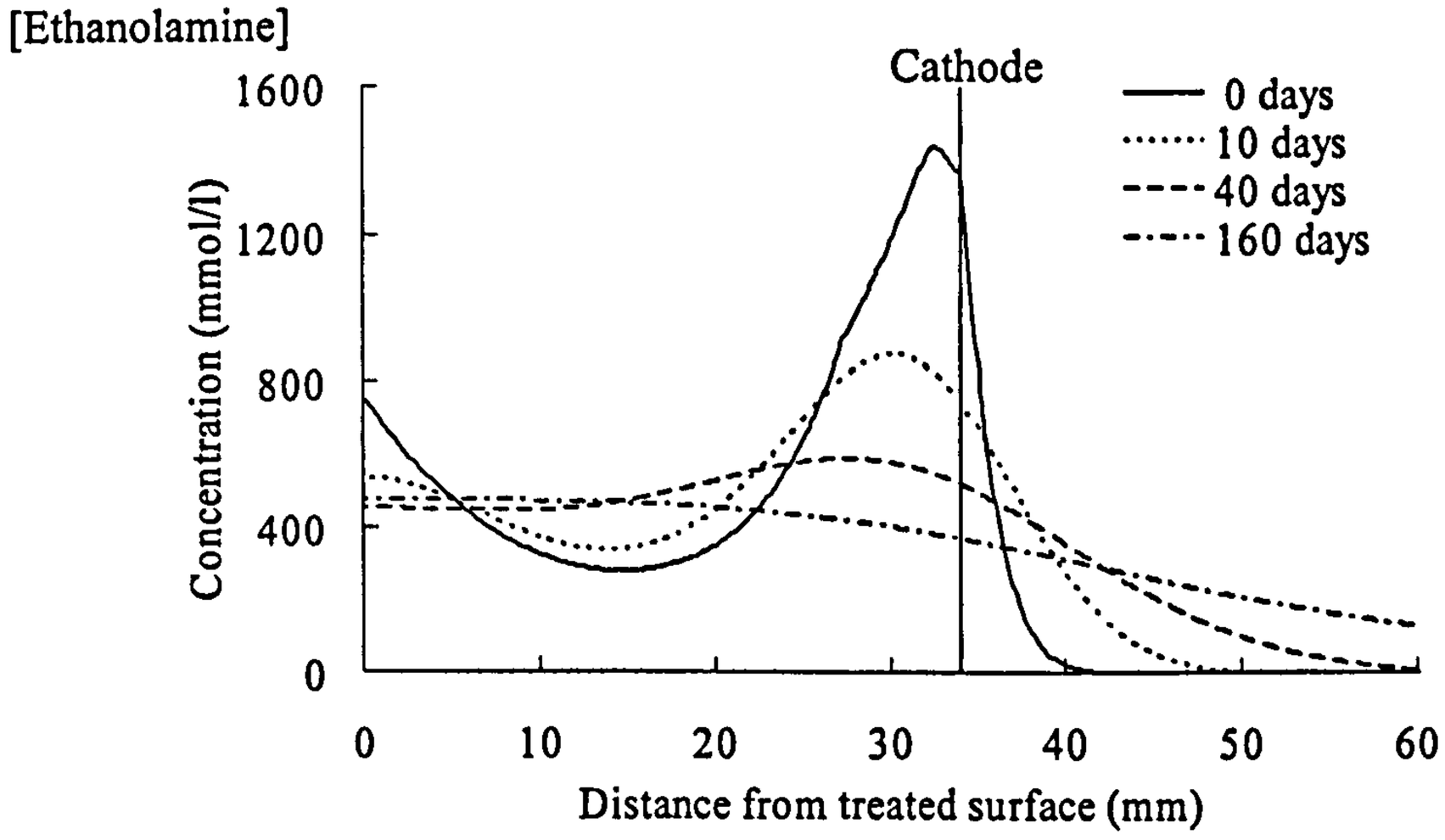

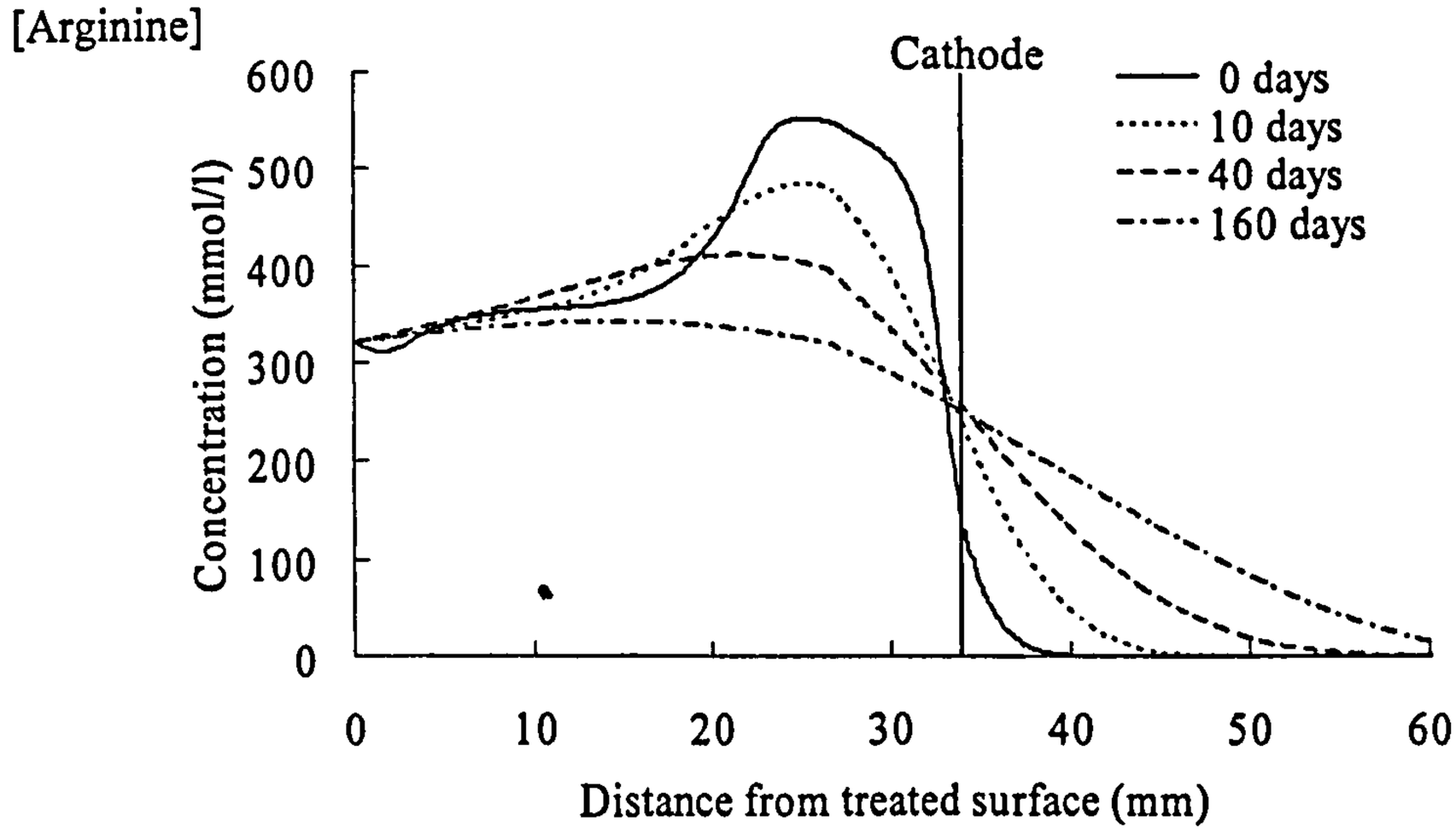

Figure 6.30 Concentration profiles of inhibitors in cement pastes after completion of electrochemical injection treatment (predicted by mathematical modelling)

6.6 CONCLUSIONS

The main conclusions of this part of the investigations may be summarised as follows.

(1) The proposed anodic polarisation method is effective for determination of the ease of passivation of steel embedded in concrete; however, the application of the method does not significantly contribute to the long-term passivation of the embedded steel. In addition, the application of the current densities used in this study has little effect on the long-term passivation of steel bars embedded in concrete treated with electrochemical inhibitor injection or electrochemical re-alkalisation.

(2) When long-term durability of electrochemical treatment is compared among the three organic inhibitor injection methods and electrochemical re-alkalisation, the use of ethanolamine demonstrated the best performance in terms of steel inhibition. This may be attributable to the high concentration of the inhibitor accumulated in the vicinity of steel cathode during the treatment. For practical applications, the use of a carbonated solution of the inhibitor would be beneficial, since it would minimise the deterioration of the concrete surface. Guanidine also demonstrated substantial long-term durability.

(3) Electrochemical re-alkalisation applied to steel bars embedded in carbonated concrete in this study showed relatively poor long-term passivation under the conditions investigated. This is probably because of the dissipation of hydroxyl ions from the steel in the highly porous concrete studied, and because of the insufficient total charge delivered to the reinforcement, compared with the required charge values stated in CEN draft (2000).

(4) The corrosion rates obtained by means of linear polarisation during electrochemical monitoring were in good accord with the corrosion weight losses determined by gravimetric analysis for all specimens studied.

(5) EIS measurement was found to provide some useful information related to the condition of the steel interface. The calculated film resistance in the intermediate frequency ranges appeared to indicate steel passivation in ethanolamine and guanidine-treated specimens. The measurements in the low frequency range showed reduced values of capacitance for the specimens treated with the passivating inhibitors, possibly indicating the adsorption of the inhibitor on the metal surface.

(6) The penetration profiles of the inhibitors inside the concrete specimens were almost unchanged for 160 days after the electrochemical treatment. This may result from the rather dry conditions applied in the experiment, where diffusion or dissipation of the injected species was expected to be limited. This might be the reason for the long-term passivation of the embedded steel.

(7) The application of the mathematical model proposed in the previous Chapter for the simulation of the concentration profile evolutions of injected inhibitors after the treatment showed a rapid reduction in concentration of ethanolamine and guanidine at the steel bars, when the pores were assumed to remain saturated and the effect of evaporation and volatility of the inhibitors was neglected. The humidity inside carbonated concrete is usually low, which might thus be a beneficial aspect in applying the proposed electrochemical inhibitor injection treatments. However, the effect of evaporation and volatility needs to be carefully taken into account in the future research.

CHAPTER 7

FATIGUE RESISTANCE OF COATINGS

7.1 INTRODUCTION

A significant consideration in reaching any repair strategy is whether to coat the concrete surface to inhibit the ingress of penetrating substances such as carbon dioxide, water, and chloride salts. The question that arises is how we can protect and preserve our existing stock of structures so that they remain safe, serviceable and usable for many years to come. The obvious solution is to cut off the transportation path of these aggressive agents, and appropriate surface or barrier coatings on the concrete can be expected to do this efficiently, effectively, and economically due to an ease of application and low cost. The application requires thorough surface preparation, because a durable bond to the substrate is essential for coating effectiveness.

There are now a wide range of proprietary products that are claimed to delay or retard corrosion by reducing chloride or carbonation ingress or by allowing concrete to dry out. However, they may not necessarily work as they are expected to. The stress applied on coatings due to temperature changes or wet and drying may degrade their barrier properties. The appearance of cracks can make carbon dioxide or chloride penetrate increasingly fast. For instance, as reported by Seneviratne et al. (2000), high bond strength can lead to localised failure of coatings, resulting in corrosion of embedded steel by allowing moisture ingress.

According to the European Standard EN 1504-2 (2004), "Products and systems for the protection and repair of concrete structures – Definitions, requirements, quality control and evaluation of conformity – Part 2: Surface protection systems for concrete", which has the status of a British Standard (BS EN 1504-2:2004), coating is defined as treatment to produce a continuous protective layer on the surface of concrete with a typical thickness of 0.1mm to 5.0mm. In this standard, performance requirements for coatings are described, which are concerned with, for example, linear shrinkage, permeability to CO_2 or water vapour, adhesion, chemical resistance, crack-bridging ability, pull-off test, and diffusion of chloride ions.

DD ENV 1504-9 (1997) describes general principles for the use of products and systems for the protection and repair of concrete structures, in which a surface coating can be a method based on the several principles related to defects in concrete: protection against ingress and moisture control. This European Prestandard also states that a coating can be a method in terms of reinforcement corrosion based on the principle of increasing electrical resistivity of the concrete by limiting moisture content. According to the CRA (Concrete Repair Association 2005), this is currently being revised for publication as a full BS EN.

(1) Coatings as carbon dioxide barriers

Klopfer (1978) investigated protective coatings on concrete as carbon dioxide barriers, and discussed the effectiveness of protective coatings in terms of an equivalent air layer thickness, R, which is defined as

$$R=\mu \cdot S \tag{7-1}$$

Where S is the thickness of the coating and μ is the diffusion resistance coefficient to carbon dioxide. Klopfer (1978) suggested that an anti-carbonation coating must maintain an R value in excess of R=50m for it to be deemed effective. EN 1504-02 (2004) requires the resistance to CO_2 to be greater than 50m for coatings obtained by the test method EN 1062-6 (2002). According to Bassi and Davies (1996), a wide range of organic coatings had an acceptable carbon dioxide resistance immediately after the application; however, R values dropped significantly during artificial or natural weathering. Sanjuan and Olmo (2001) used a mortar coating for the same objectives. They found that the use of the mortar coating with a thickness of 2mm as a CO_2 barrier led to diffusion coefficients 3 orders of magnitude lower than that of uncoated concrete. David and Harrison (1990) carried out an experiment to evaluate how the effectiveness of acrylic-based coatings as carbon dioxide barriers varied with their thickness by means of accelerated carbonation (4% carbon dioxide). They indicated that the coats were more effective in terms of carbonation prevention as the number of coats or total coverage (g/m^2) increased.

(2) Control of reinforcement corrosion

It is desirable that a coating can reduce the ingress of water from the environment, whole allowing the evaporation of moisture from the inside, so that the concrete consequently will reach lower values of humidity in particular in wetting/drying situations. According to Seneviratne et al. (2000), in the case of carbonated concrete without any chlorides, when the RH was maintained at or below 80%, the concrete had a high enough resistivity to restrict

the corrosion rate of the reinforcement to levels below 0.1μA/cm^2, which are within the range typically recorded for corrosion rates of passive steel in non-carbonated concrete and are therefore not considered to be significantly detrimental (Andrade et al. 1990).

Sergi et al. (1990) investigated the corrosion rates of the steel bars embedded in the non-carbonated, partially carbonated, and fully carbonated parts of sectioned concrete blocks obtained from 30 years old RC beams removed from a demolished building. Three water repellent surface treatments, silane, and siloxane, and silicone were applied to the concrete and their abilities to control corrosion were assessed under a regime of cyclic wetting and drying. As a result, the surface treatments proved to be effective in resisting water penetration by lining the pores of concrete with hydrophobic layers and thus limited the corrosion rate of steel in carbonated regions of the specimens during exposure to cycles of wetting and drying.

Swamy and Tanikawa (1993) investigated the protective effect of coatings to prevent penetration of chloride ions by evaluation of the extent of corroded areas on rebars embedded in the concrete prisms subjected to a salt exposure regime, where the specimens were sprayed continuously with 3% NaCl in water for 5000 h at 35°C. The four coating systems used were acrylic rubber, polyurethane rubber, poly-butadiene rubber and epoxy resin, all having a thickness of approximately 1100μm. The results indicated that the epoxy resin coating showed the best performance in protection of the reinforcement corrosion with no corroded area, followed by the acrylic rubber coating with a corroded area of 7% of the entire rebar surface, while the corroded area was almost 60% in the case of an uncoated control specimen.

Seneviratne et al. (1996) used three elastomeric coating systems of a similar thickness (>400 μm) with good crack-bridging abilities and showed that they were successful over a period of 2 years in controlling reinforcement corrosion in carbonated concrete free from chloride. However, later in their research (1999), over the longer term, two of them were found to be only partially effective in retaining their waterproofing character after weathering, resulting in significant corrosion.

Ibrahim et al. (1999) applied six types of coatings, namely sodium silicate, silicone resin, silane/siloxane, silane/siloxane with acrylic topcoat, silane, and acrylic coating respectively, to the surface of concrete cylinders that were subsequently immersed into 5% NaCl solution and compared the performance against the corrosion of the pre-corroded embedded

reinforcement bars by monitoring the corrosion current densities. The results showed that after four months of application, all six coatings maintained the corrosion current density at approximately 0.1μA/cm^2, and performed better than uncoated control specimens. They concluded that the reduction in the corrosion current density may be attributed to the reduced diffusion of oxygen and moisture. However, if oxygen diffusion was a rate-limiting factor, the potential of steel would be expected to be depressed to more negative values. Since this potential drop was not observed in their experiment, the reduction of corrosion current density should be probably attributed just to moisture reduction in concrete.

Batis et al. (2003) compared the protective action against carbonation penetration and chloride-induced corrosion of an acrylic dispersion and an inorganic coating applied on concrete specimens in which steel bars were embedded. It was found that both coatings reduced the carbonation depth compared to control specimens, and that the reduction offered by the former was higher than the latter. This was also the case with corrosion rate. They concluded that the difference could be attributed to the fact that the acrylic dispersion forms a continuous film over the substrate surface, whereas the inorganic coating reacts chemically with the surface and just reduces the diameter of the surface pores. They also mentioned that the simultaneous use of alkanolamine-based corrosion inhibitor as an admixture (1.0% of cement by weight) together with the coating still reduced the corrosion rate by approximately 40%.

A protective surface coating demands reasonably good adhesion to the concrete, high durability, UV and weather resistance, prevention of water ingress, high resistance against carbon dioxide diffusion, but adequate water vapour permeability. Seneviratne et al. (2000) demonstrated that the use of an elastomeric coating system with particular properties can protect carbonated concrete from water ingress, and that it is desirable for coatings to develop only a modest adhesional bond to the substrate so that they can tolerate the stress associated with movements of the concrete without cohesional failures, which thus extends the service life of a structure.

Certain basic engineering requirements, such as crack-bridging ability, elasticity, strain capacity, adhesion and fatigue resistance are also essential for the successful protection of concrete. Crack-bridging ability is also one of the most important factors which surface coatings should have. Concrete has a relatively low tensile strength and may crack easily. The cracking of concrete may arise from the inherent volume and thermal changes that occur

during hydration of the cement, such as heat of hydration, plastic shrinkage, thermal/moisture movements or drying shrinkage, or they may be due entirely to applied stresses. Cracking may also originate from basic deteriorating processes such as freezing and thawing or alkali-aggregate reactions. Cracking is a common cause of the degradation of concrete, since cracks may affect its durability, by providing easier access to aggressive agents. If a coating has been applied over a concrete structure where shrinkage cracks or working cracks develop, the coating will tend to crack with the structure. Thus a coating without adequate crack-bridging ability will eventually break, losing its barrier properties, leading to reinforcement corrosion. Thus crack-bridging ability is a fundamental property when protective coatings are considered for concrete.

7.2 LITERATURE REVIEW

There have been some researches concerned with crack-bridging ability. Delucchi et al. (2002) investigated crack-bridging ability of several sorts of coatings for the purpose of correlating the results of crack-bridging ability with the intrinsic properties of the coatings. The six coating systems they used were: acrylic (thickness: 1200μm), acrylic with polyurethane top coating (1500μm), epoxy-polyurethane with polyurethane top coating (220μm), epoxy with fluorinated polyurethane top coating (300μm), epoxy with acrylic top coating (300μm), epoxy with fluorinated rubber top coating (1050μm). They applied each coating to specimens as shown in Figure 7.1, and the samples were slightly bent to break the substrate without damaging the coating, and then subjected to continuous opening of the crack with a cross-head speed of 0.5mm/min. Then the crack-bridging ability was evaluated by the displacement measured at the break in the coating. An analysis of the behaviour of the coatings in the area surrounding the concrete crack was also performed for the better interpretation of the recorded stress/displacement diagrams. From the results they concluded that the coatings that have a better chance of bridging cracks have an appreciable thickness as well as some extensibility and rather low stiffness. Later they (2004) evaluated the relationship between thickness and crack-bridging ability for an acrylic coating and an epoxy-polyurethane coating applied on a similar type of concrete specimen as that used in their previous work. They found that thicker coatings reached higher value of crack-bridging ability, and that as thickness increased the crack-bridging ability of acrylic coatings increased more rapidly than that of epoxy-polyurethane coatings. This difference was attributed to the difference in intrinsic mechanical properties of the two coatings, specifically

the capability of the coating molecules to reorient themselves by moving into free volumes spaces in the film under applied stress.

Another research was carried out by Almusallam et al. (2002), trying to establish a performance criterion related to crack-bridging ability for selection of coatings. They used five generic types of coating; acrylic, polymer emulsion, epoxy resin, polyurethane, and rubber coatings to compare the crack-bridging ability applied on a cement mortar specimen with two glued steel plates on its wings as shown in Figure 7.2. A tensile load was applied through the steel plates until the time of coating failure. They concluded that the epoxy resin coatings exhibited the highest adhesion to concrete, followed by rubber and polyurethane coatings and that since the acrylic and polymer emulsion were poor in adhesion they should be used only in situations where adhesion is not the basic requirement. They also claimed that the crack-bridging ability of the epoxy was the best and that the acrylic and polymer emulsion coatings were not effective in bridging the cracks. Based on their experimental results they finally demonstrated that the crack-bridging ability of over 0.5mm is recommended as a performance criterion for the selection of coatings, but, the reason for this was not clear.

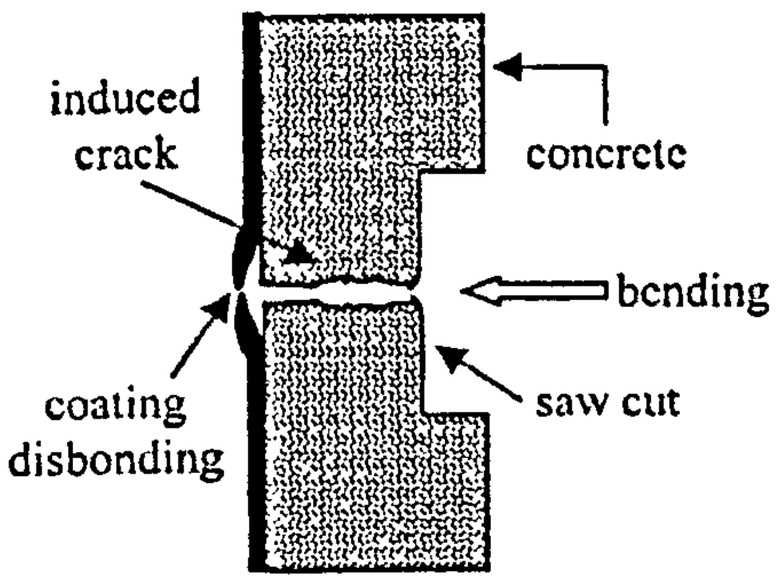

Figure 7.1 Specimen (Delucchi et al.)

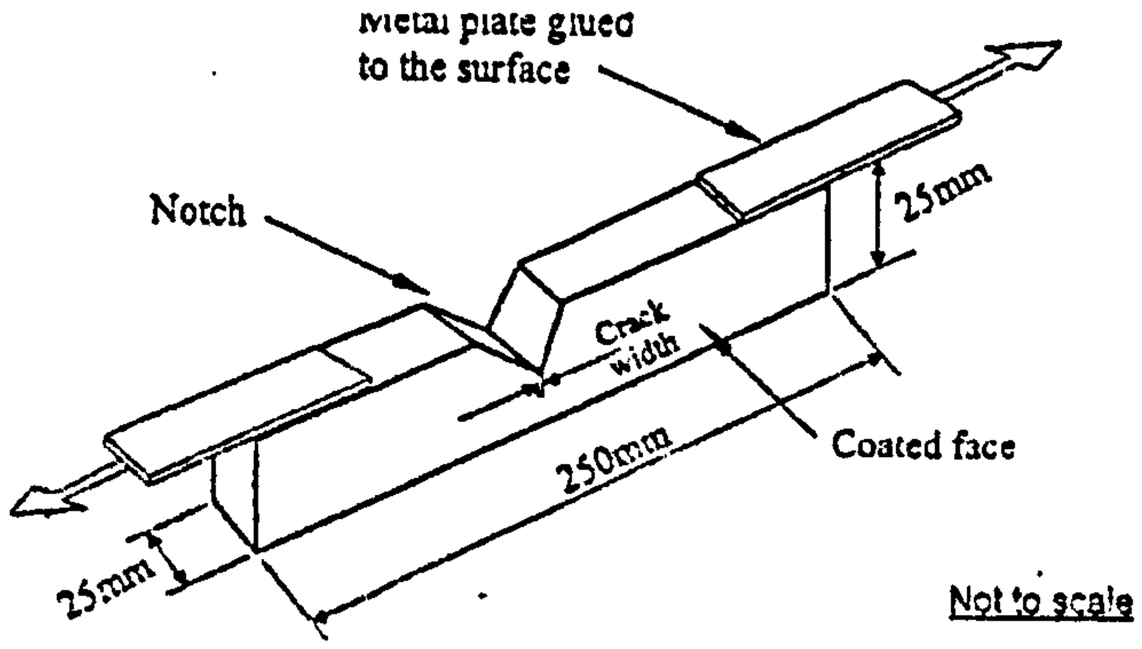

Figure 7.2 Specimen (Almusallam et al.)

In the experiment to test the crack-bridging ability of a coating described in the above researches, the coatings to be examined were rapidly pulled just one time until they were broken. When durability of crack-bridging property is concerned, Swamy and Tanikawa (1993) examined the long-term stability of surface coatings in "extended states", in which acrylic rubber coatings bridging cracks on concrete prisms (200mm × 200mm × 300mm) were exposed for five years to a hot and humid coastal environment or soaked in seawater in hot and humid conditions. This was to investigate whether the coating had the ability to accommodate movements in the underlying substrate and allow opening and closing of

cracks without fracturing. The results showed that the widths of the cracks on uncoated control specimens ranged from 0.3 to 1.5mm after 5 years' exposure to sea water and from 0.4 to 0.8mm after 5 years' exposure outdoors; however, the acrylic rubber coating showed no blisters, peeling or cracking after 5 years of the exposure conditions.

There have been few researches concerned with the performance of surface coatings applied on cracks that are forced to respond to cyclic loading where performance may depend on the fatigue resistance of the coatings. The coating materials which have been applied underneath the motorway bridges or railways viaducts have high crack-bridging ability in order to withstand the stress due to the active loads which are generated by running automobiles and trains. However after several months or years of application, in spite of its adequate crack-bridging ability, cracks are likely to appear on the coating just along the line of the original concrete cracks, which indicates lack in fatigue resistance. Swamy and Tanikawa (1989) mentioned that fatigue resistance is essential for successful protection of concrete as well as crack-bridging ability, elasticity, strain capacity, and adhesion of coatings. In this chapter fatigue resistance of coatings is focused on to have better understanding of the durability of surface coatings.

As for crack-bridging ability, BS EN 1504-2 (2004) specifies the required test conditions in two ways based on BS EN 1062-7 (2004) which are continuous and cyclic opening of cracks. The former is similar to the manner in which Delucchi et al. (2002) or Almusallam et al. (2002) investigated crack-bridging ability of coatings. The latter is concerned with the investigation of fatigue resistance, when a specimen, as shown in Figure 7.3 can be used for the test. After making an immediate crack into the coated substrate of the test piece, the ends of the reinforcing steel are fixed in the clamps of the testing apparatus. Then the dynamic test is carried out under displacement control at a recommended temperature (-10°C), using a crack width function as shown in Figure 7.4 during which the surface of the test piece is monitored in order to see if cracks occur or grow. In this test displacement is applied as a basic trapezoidal waveform (maximum crack width: Wo, minimum crack width: Wu) with superimposed sinusoidal waveform of higher frequency and smaller amplitude as shown in Figure 7.4. The classification and test conditions are shown in Table 7.1. According to the standard, the requirement of coatings is that after testing no failures may occur. The standard also states that the required crack-bridging ability shall be selected by the designer with respect to local conditions such as climate, crack width and crack movement.

Dimensions in millimetres

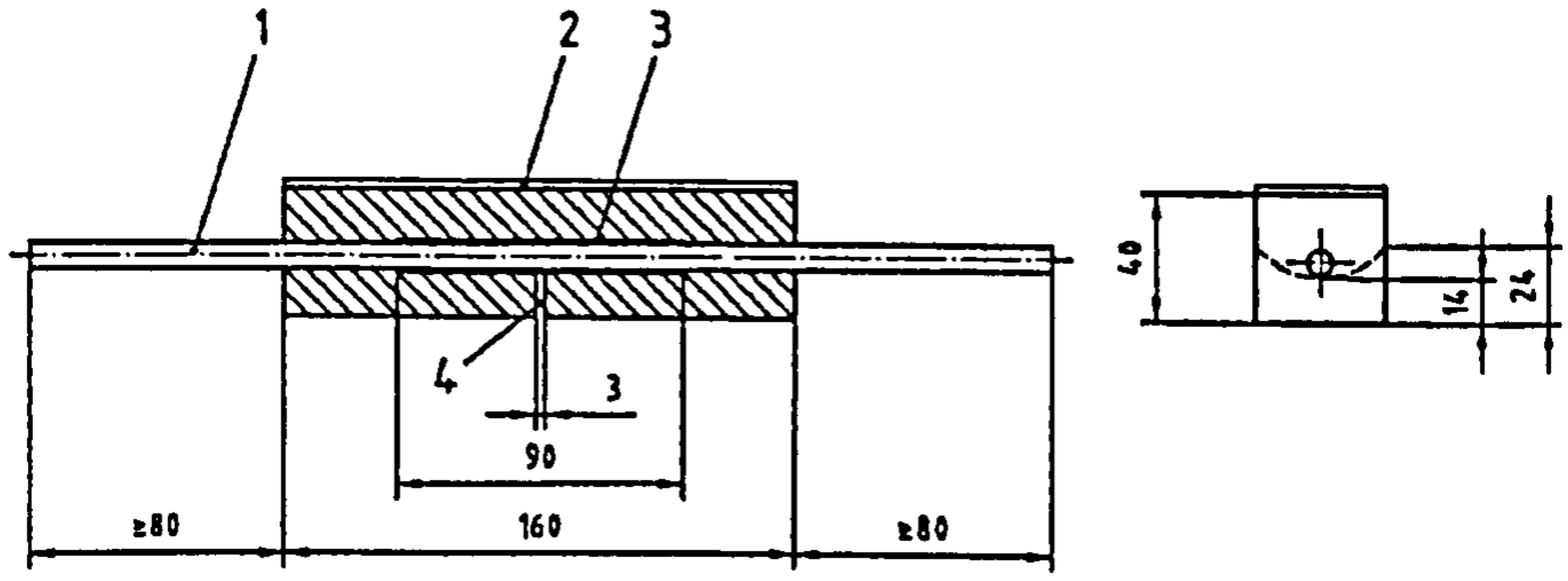

Key

1 Steel with a diameter of 8 mm
2 Coating
3 Plastic tube with an internal diameter of 8 mm, wall thickness $d = 2$ mm
4 Predetermined breaking point

Figure 7.3 Dimension of coated prisms for dynamic crack-bridging test described in BS EN 1504-2 (2004)

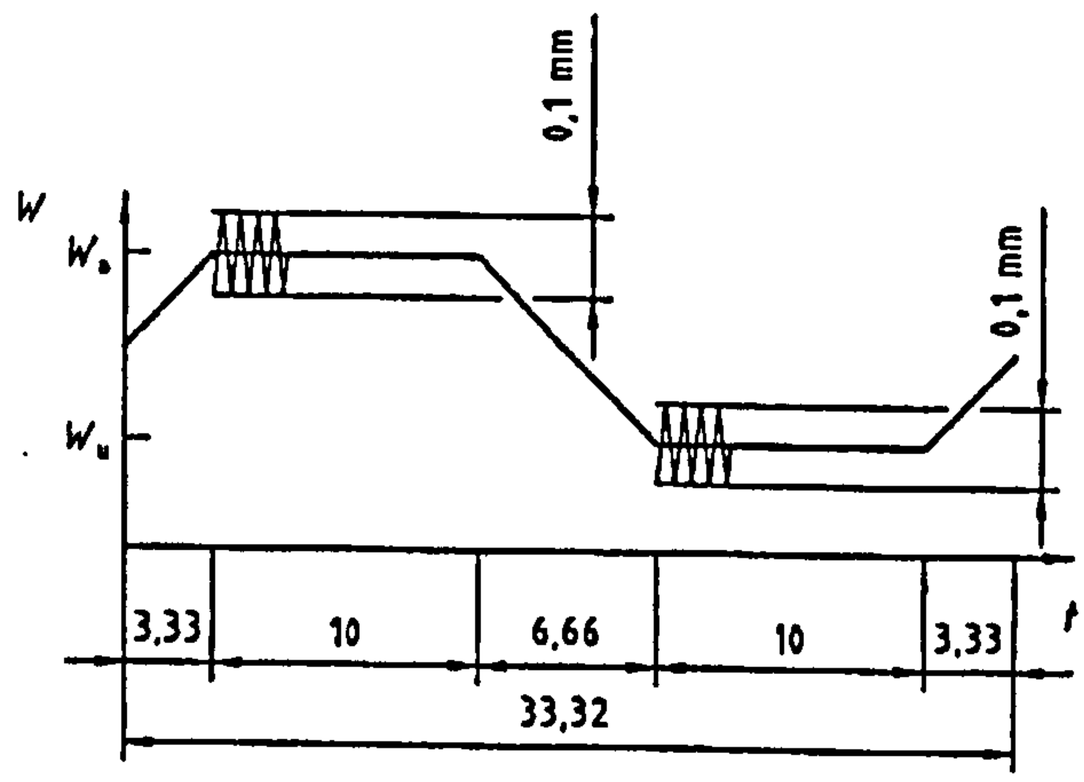

Key

t Time in seconds
w Crack width in millimetres

Figure 7.4 Change of crack width as a function of time (crack cycles as a trapezoidal function using 0.03Hz, superimposed crack cycles as a sinusoidal function using 1Hz, Wo: maximum crack width, Wu: minimum crack width)

Table 7.1 Classification and test conditions

Class	trapezoidal				sinusoidal	
	Wo (mm)	Wu (mm)	n (times)	f (Hz)	n (times)	f (Hz)
B1	0.15	0.10	100	0.03	-	-
B2	0.15	0.10	1000	0.03	-	-
B3.1	0.30	0.10	1000	0.03	-	-
B3.2	0.30	0.10	1000	0.03	20000	1.00
B4.1	0.50	0.20	1000	0.03	-	-
B4.2	0.50	0.20	1000	0.03	20000	1.00

7.3 PREVIOUS EXPERIMENTAL WORK ON FATIGUE RESISTANCE

In previous research carried out in 1999 at the author's company (Central Japan Railway Company), the author and co-workers (Seki et al. 1999, internal report) focused on the fatigue resistance of coatings which were applied beneath RC railway viaducts for the purpose of preventing further carbonation of concrete. Unlike such concrete structures as static buildings or dams, RC motorway bridges and railway viaducts are exposed to numerous repetitions of dynamic loadings caused by the vehicles passing on them when the impacts often force the initially existing cracks on the concrete to move.

Crack movements were measured by means of a π-shaped strain gauge fixed to bridge a 0.1mm wide crack in a concrete longitudinal beam when a train passed at approximately 120km/h on a 20.5m long viaduct in Tokyo that consists of three continuous spans of 6m as shown in Figure 7.5. One example of the crack movement is shown in Figure 7.6. As seen from the wave pattern in this figure and the fact that a train consists of 16 coaches, each of which has 2 bogies, it can be derived that the number of repetitions of main crack opening is 32 for every single passage of a train. The number of the train services is approximately 140 every day, thus in the case of the concrete structures owned by the author's company, the total number of repetitions of crack opening every year due to the passages of the trains may be calculated as follows:

$$32 \times 140 \times 365 \approx 1{,}600{,}000 \text{ times/year.} \qquad (7\text{-}2)$$

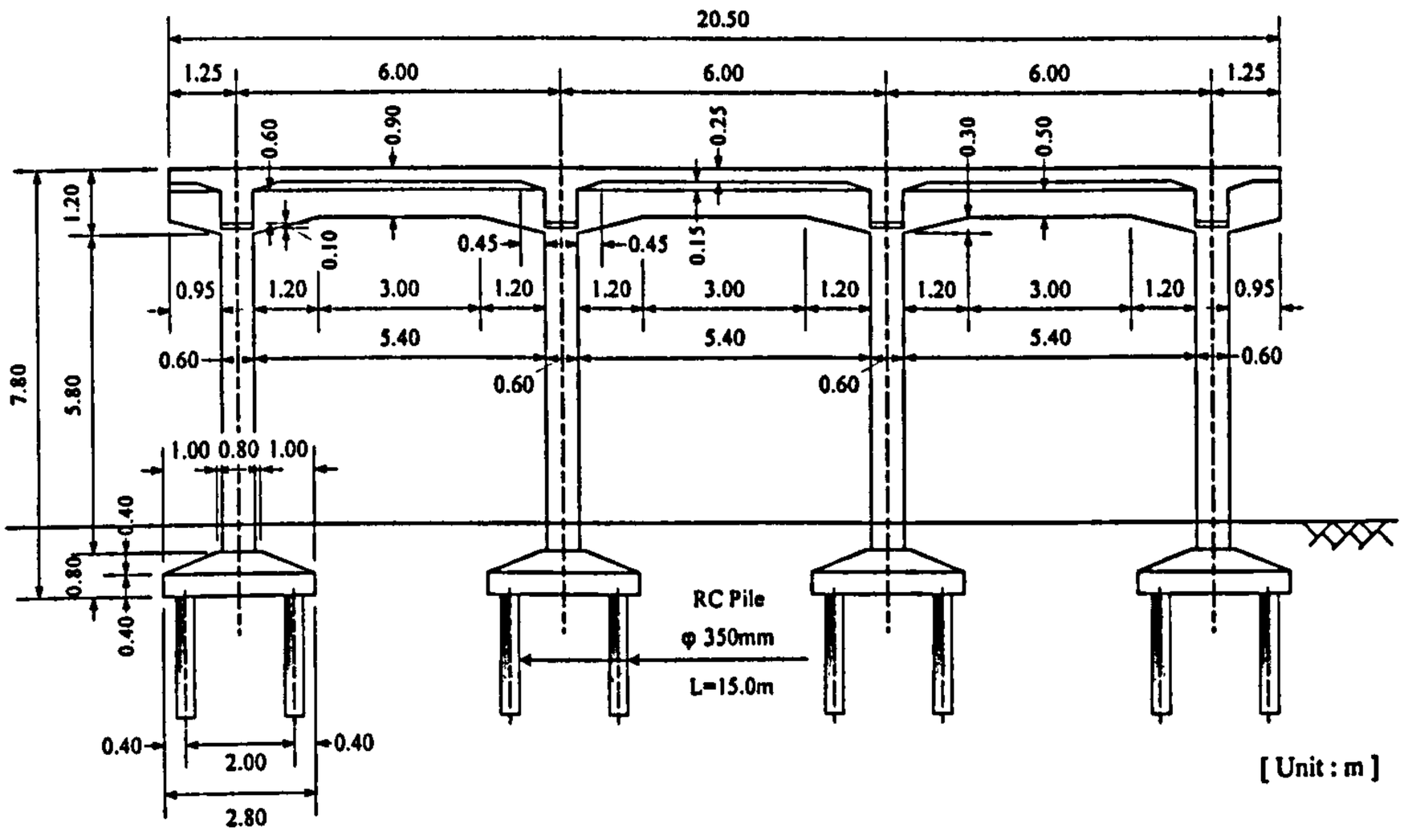

Figure 7.5 Schematic view of measured RC viaduct

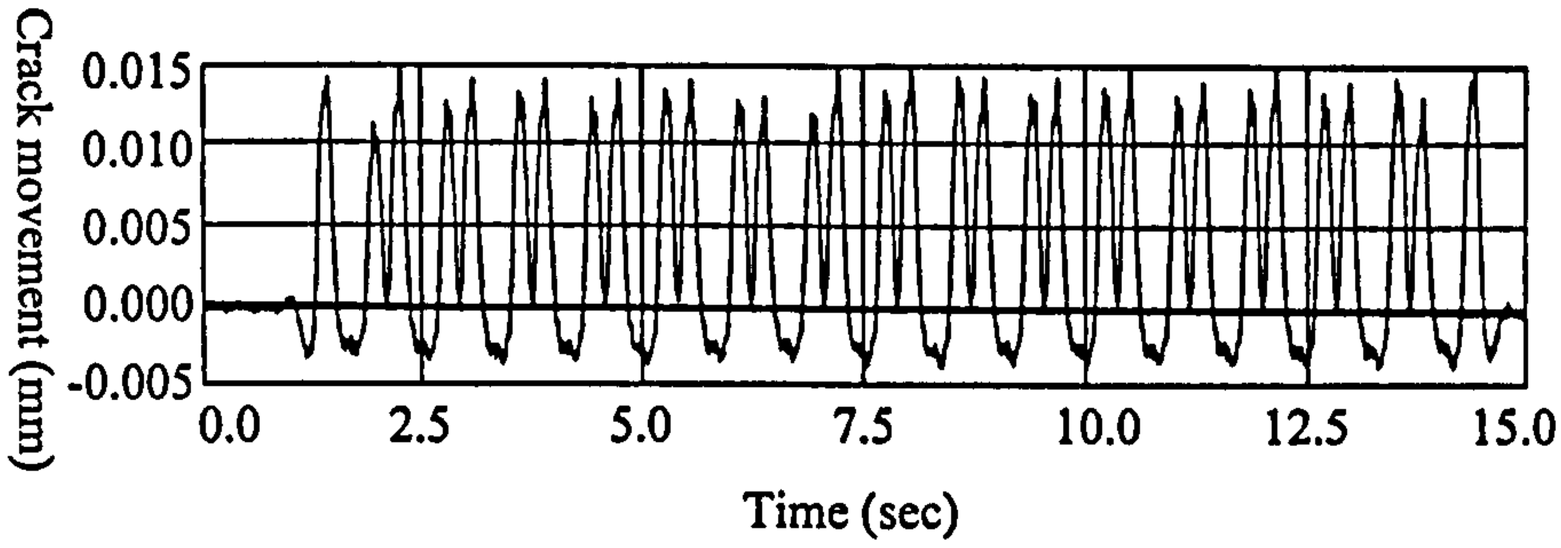

Figure 7.6 Example of crack movement due to train passage

The concrete beams of the structures have a wide variety of cracks, and for the investigations of the cracks, the crack width and the amplitude of the crack movement under active train loadings were measured. Crack gauge sheets were used for the measurement of crack width and π-shaped strain gauges were used for measuring the crack movement amplitude whilst the trains were passing on the structures. Crack movement was investigated at randomly selected 46 viaducts from total approximately 4200 viaducts with various length of span as shown in Table 7.2. As the minimum number of cracks visibly observed on the investigated viaducts was 18, 18 cracks were randomly selected on each viaduct for the measurement (20 cracks were selected on some viaducts). The on-site measurement results are shown in Figure 7.7, where it can be seen that the crack width ranges from 0.01mm to 0.3mm with the cracks movement amplitude within approximately 0.03mm.

The coatings that had been applied on the concrete surface have a crack-bridging ability strong enough (>0.6mm) to tolerate the movement of cracks; however, within several years after the application, visible cracks began to appear on the coatings resulting from failure to accommodate the crack movements. This may imply that fatigue resistance needs to be taken into account for the selection of coatings applied to the concrete surface that has cracks with dynamic movement.

Table 7.2 Crack measurement plan

Span (m)	Number of viaducts	Number of cracks	Span (m)	Number of viaducts	Number of cracks
6	16	314	15	9	162
8	2	36	17.5	4	72
10	7	130	20	3	54
12	2	36	25	3	54

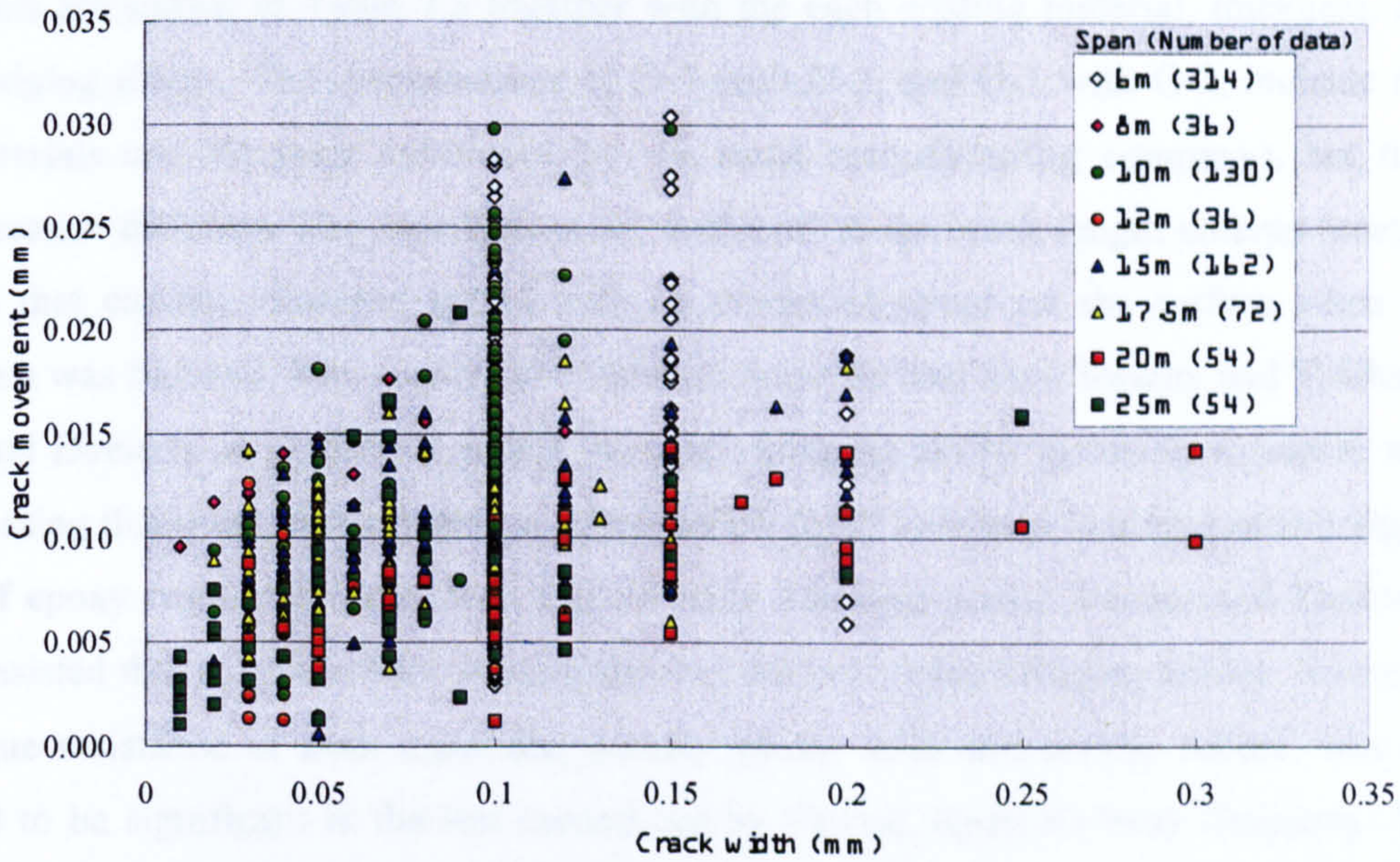

Figure 7.7 Crack movement amplitude versus crack width under active loadings

It was expected that the coatings would endure the dynamic movement of the cracks with their crack-bridging ability for a while once they are applied over the cracks on the concrete. Thus the authors assumed that fatigue resistance has some correlation with crack-bridging ability and that if a coating has a better crack-bridging ability, it has a higher fatigue resistance. Later in the subsequent research (Seki et al. 2001), the author and co-workers carried out an experiment to obtain the correlation between crack-bridging ability and fatigue resistance. 15 coatings of six material types, namely epoxy, acrylic rubber, poly-butadiene, PCM, polyurethane and chloroprene synthetic rubber, presented by 13 coating manufacturers were selected. Prism cement specimens (70mm × 70mm × 400mm, W/C 0.65) with a reinforcing steel bar (φ=8mm) penetrating along the axis were prepared in triplicate with a 0.2mm wide slit in the centre and the coatings were applied on the two sides of the prisms as shown in Figure 7.8. Prior to the fatigue tests, the crack-bridging ability of every coating was measured at room temperature according to JSCE-K 532-1999 (1999). After the both ends of the reinforcing steel were fixed in the clamps of the fatigue testing machine, the coatings were deliberately pre-stressed until the width of the crack became 0.4mm so that they could be damaged more easily by the fatigue cycles. Then a fatigue test of one million cycles was applied to the specimens at 10Hz with amplitude of 0.04mm. The temperature was maintained at 20±2°C. The fatigue resistance of each coating examined was evaluated by measuring the average of the crack length appearing on the coatings of triplicate specimens after the whole number of cycles.

The results are shown in Table 7.3 together with the each coating material, thickness, and crack-bridging ability. The combinations of D-1 with D-2, and G-1 with G-2, indicate that their materials are the same (produced by the same manufacturing company), but their thicknesses are different. The descriptions of "0.00mm" in the crack length column (coating E) mean that coating remained sound with no cracks observed on the surface when the fatigue test was finished. The results coincide with those derived from Swamy and Tanikawa (1993) and Delucchi et al. (2004) in that the crack-bridging ability generally increases with the increasing thickness of the coatings. Almussalam (2002) claimed that the crack-bridging ability of epoxy resin was better than that of other coatings, whilst Swamy and Tanikawa (1993) insisted that acrylic rubber coating showed the best crack-bridging ability. However, the fatigue resistance of both materials, namely epoxy resin and acrylic rubber, was not observed to be significant in the test carried out by Central Japan Railway Company. The results show a coating of chloroprene synthetic rubber (coating E) has quite strong fatigue resistance with no cracks appearing on the surfaces and shows the best performance.

The results show that the cracks appearing on the PCM coating were relatively small (coating L) throughout the fatigue test in spite of its small thickness. It is known that PCM has relatively weak bond strength (Almusallam et al. 2002), thus it might be that the coating applied just close to the cracks lost adhesion during the cyclic loading, which eventually made it easier for the coating to accommodate the crack movement with a longer span thus with smaller strain. In order for a coating to have a long durability in accommodating the movement of concrete cracks, it might be desirable that the coating does not have too much bond strength with the substrate. As mentioned before, Seneviratne et al. (2000) also claimed that it is desirable for coatings to develop only a modest adhesional bond to the substrate so that they can tolerate the stress associated with movements of the concrete without cohesional failures, which thus extends the service life of a structure.

Figure 7.9 shows the correlation between the crack-bridging ability and the fatigue resistance evaluated by the length of the crack that appeared on the surface of the specimens. It can be concluded that a coating with a higher fatigue resistance has a higher crack-bridging ability.

When a coating applied on such structures as motorway bridges or railway viaducts is intended to maintain a sound condition against fatigue cyclic stress for over ten years, it has to tolerate more than ten million cycles of crack openings. In the work to be described in the following section of this chapter in order to investigate the fatigue resistance of coatings

under such large numbers of cycles, fatigue tests are carried out with realistic crack width and crack movement referring to the on-site measurement results shown in Figure 7.7. Taking into consideration the fluctuating temperature throughout a year in the author's country, the tests need to be carried out at high and low temperature as well as room temperature at which the previous research was performed.

Table 7.3 Length of crack on the coating after one million cycles of fatigue test.

Coating No.	Material	Thickness (μm)	Crack-bridging ability (mm)	Length of crack after fatigue test (mm)
A	Acryl rubber	1,135	2.47	13.02
B	Poly butadiene	1,345	2.64	0.76
C	Acryl rubber	985	3.03	3.23
D-1	Epoxy resin	350	1.81	32.51
D-2	Epoxy resin	950	2.83	4.71
E	Chloroprene synthetic rubber	150	2.60	0.00
F	Epoxy resin	595	2.33	16.40
G-1	Epoxy resin	185	1.88	52.48
G-2	Epoxy resin	505	2.01	30.07
H	Polyurethane	350	1.80	46.96
I	Epoxy resin	330	2.56	4.91
J	Polyurethane	1,171	2.59	17.67
K	Epoxy resin	270	2.36	8.62
L	PCM	120	2.56	0.35
M	Epoxy resin	690	2.73	0.50

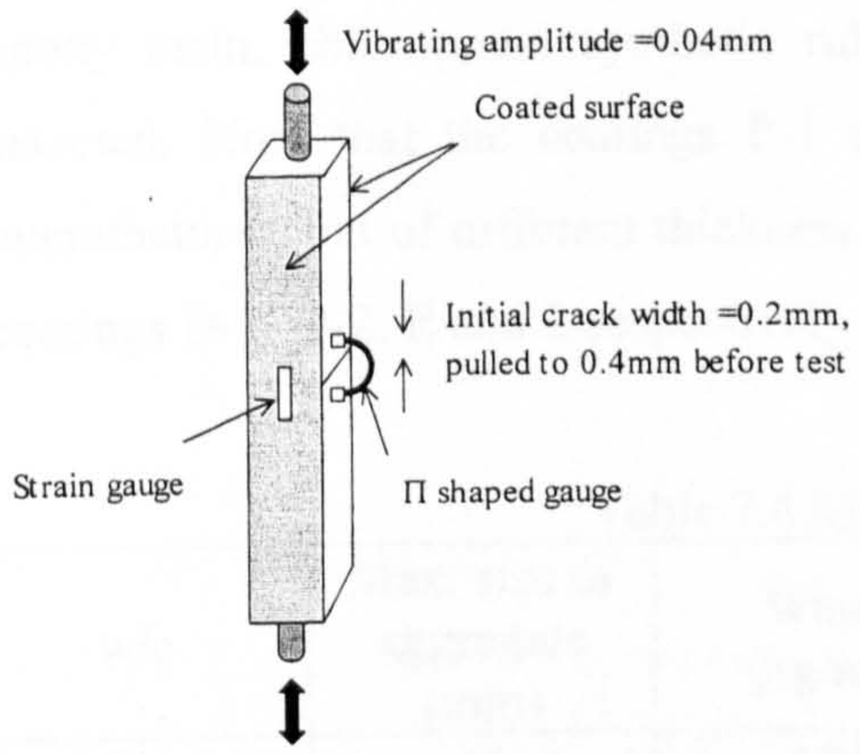

Figure 7.8 Specimen used in fatigue test

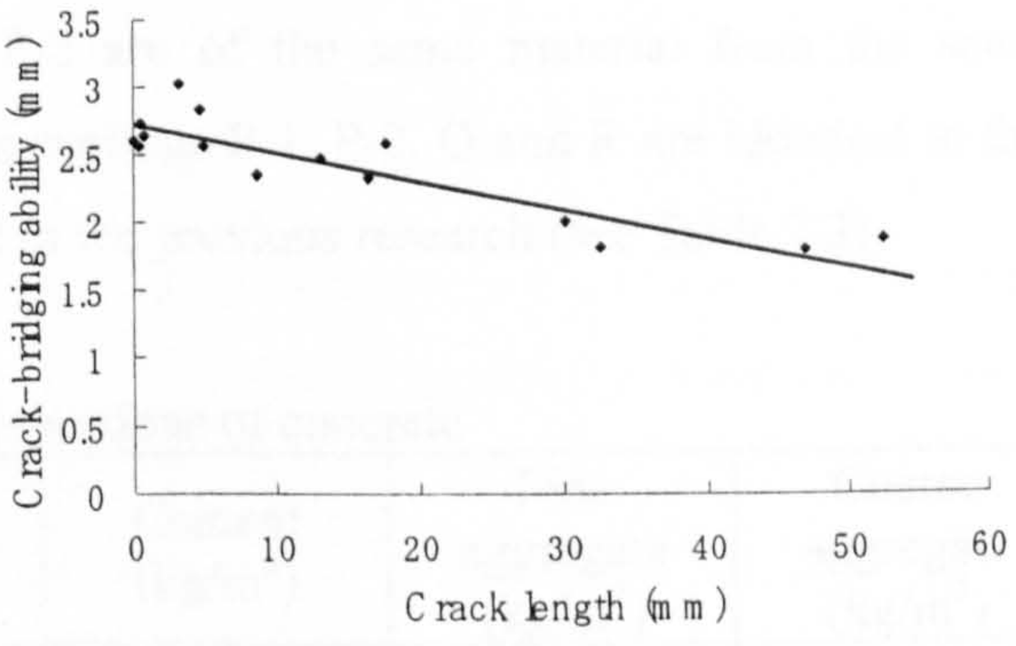

Figure 7.9 Effect of crack-bridging ability on fatigue resistance

7.4 EXPERIMENTAL PROCEDURES

7.4.1. Specimen preparation

OPC was used to produce concrete prisms (width 90mm, length 230mm, and height 50mm) with water/cement ratio of 0.6 and maximum size of aggregate of 15mm. The mix proportions of the concrete are shown in Table 7.4. After having been cured in water for 28 days, each prism was carefully cut by means of a concrete cutter into two pieces with same length, which were subsequently exposed to accelerated carbonation until the carbonation depth reached 10mm, at 20°C and 60% RH in a chamber where the concentration of carbon dioxide was maintained at 5%. After 2 months of carbonation, two of the specimens were broken and the carbonation depth was confirmed by a phenolphthalein test. Then all the surfaces of the concrete blocks were cleaned with a concrete grinder and each block was, by means of epoxy resin adhesives, fixed to a cement mortar board strengthened with fibre. The cement mortar board had been drilled to have six holes so that it could be fixed to a fatigue apparatus with bolts. Each pair of concrete blocks was arrayed with a 0.2mm thick plastic plate touching the sides of the both blocks in the middle to simulate a concrete specimen with a 0.2mm wide crack, after which a selected coating was applied on the surface of the concrete according to the manufacturer's instructions at a room temperature in the rectangular area of 50mm×150mm over the crack to form a single fatigue specimen. The schematic view of the specimen is as shown in Figure 7.10. The list of the coatings used in this test is as shown in Table 7.5 together with their thickness and crack-bridging ability at a room temperature, where seven types of coatings of five different generic materials, namely epoxy resin, chloroprene synthetic rubber, PCM, poly butadiene, and polyurethane are selected. Note that the coatings P-1 and P-2 are of the same material from the same manufacturer, but of different thickness. The coatings P-1, P-2, Q and R are identical to the coatings D-1, D-2, E and L respectively used in the previous research (see Table 7.3).

Table 7.4 Mix proportions of concrete

w/c	Max. size of aggregate (mm)	Water (kg/m^3)	Cement (kg/m^3)	Fine aggregate (kg/m^3)	Coarse aggregate (kg/m^3)
0.6	15	174	290	917	898

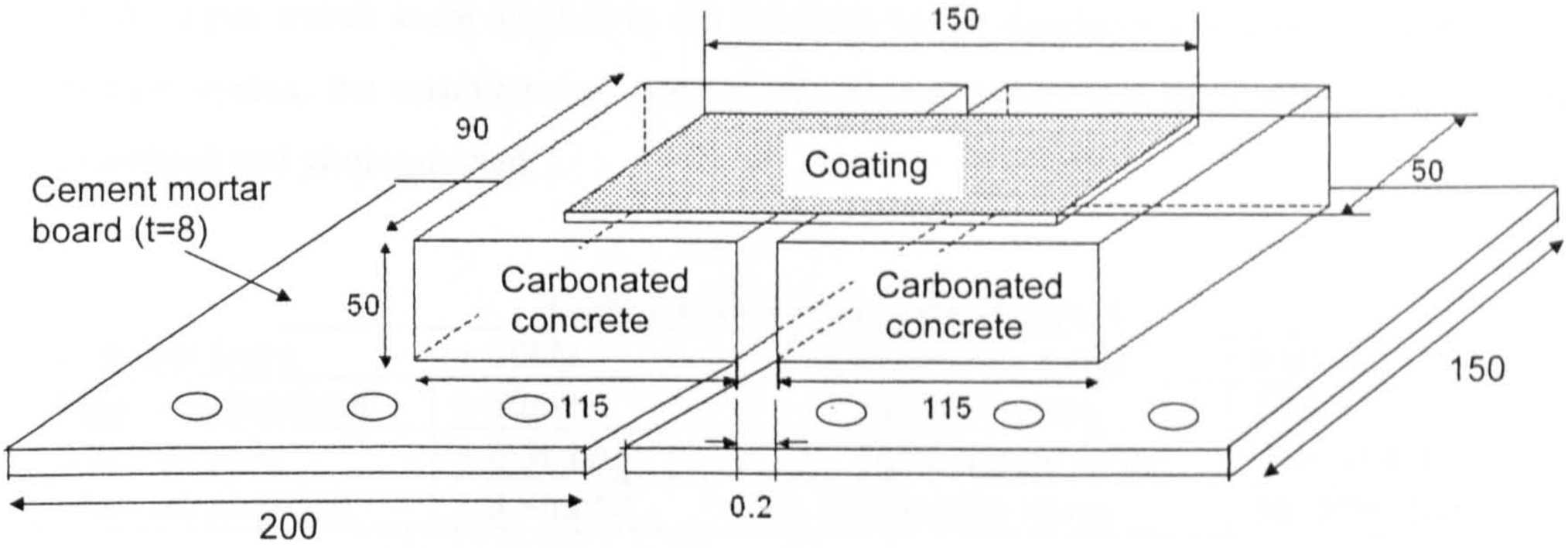

Figure 7.10 Specimen used in the fatigue test

Table 7.5 coatings used in the fatigue test

Coating No.	Material	Thickness (μm)	Crack-bridging ability (mm)
P-1 (D-1)	Epoxy resin	350	1.81
P-2 (D-2)	Epoxy resin	950	2.83
Q (E)	Chloroprene synthetic rubber	150	2.60
R (L)	PCM	120	2.56
S	Poly butadiene	1,060	3.50
T	Polyurethane	730	1.85
U	Polyurethane	2,060	88.31

7.4.2. Fatigue test

The fatigue test apparatus used in this investigation was a "Dynamic Servo V-2728" manufactured by Saginomiya Co. Ltd. in Japan. The whole test system includes a large testing chamber (1000mm×1670mm×689mm) where the temperature and humidity can be controlled as desired. The performance of this system is described in Table 7.6. The chamber can contain 9 specimens (3 types of coating in triplicate) at one time as shown in Figure 7.11. One of the cement mortar boards is placed on a fixed plate of the machine and the other on a flexible plate that moves according to the cyclic vibrations given. Since the number of the cycles of crack openings to which a coating on a real viaduct is exposed during 10 years is calculated to be approximately 16 million times from Eq. 7-2, therefore, JIS A 1436 "Test methods for movement capability of coatings and sheets fully adhered on substrate" is adopted in this experiment, under which fatigue cycles of 6 million times are applied at 10 Hz to the specimens at 20°C, then at 60°C, and finally at -10°C respectively. The humidity was maintained at 60% RH except at -10°C. Referring to the on-site measurement of the maximum crack movement (approximately 0.03mm as seen in Figure 7.7), and allowing a margin of 0.01mm, fatigue testing amplitude was determined as 0.04mm, and sinusoidal

cyclic input waves were applied to the coatings under displacement control. After every 1 million cycles, the machine was stopped for several hours and the coatings were visually examined and photographed.

Table 7.6 Test system performance

Nominal force	± 30kN	Frequency range	0.01~10 Hz
Max. displacement	± 30mm	Rated Pressure	20.5 MPa
Max. velocity	± 6.3cm/s	Temperature range	-20~70°C (±2°C)
Max. acceleration	± 3.96m/s^2	Humidity range	30~90%RH

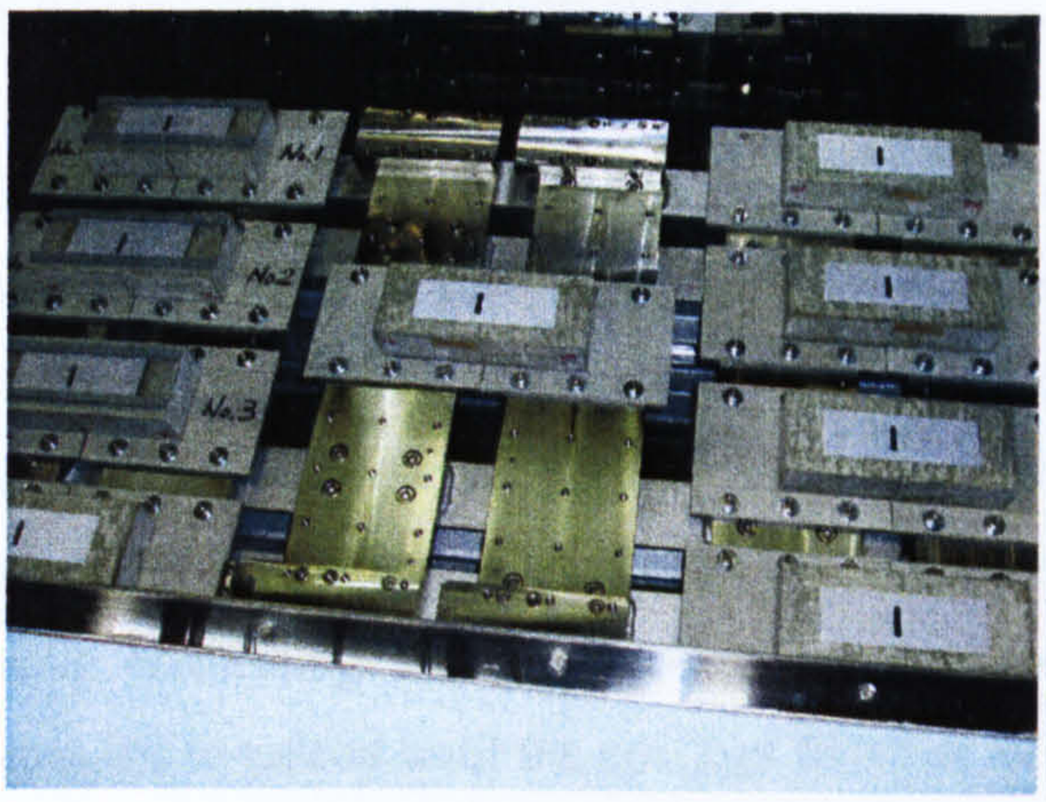

Figure 7.11 Inside the chamber (left) and an installed specimen (right)

7.5 RESULTS

The fatigue test results are shown in Table 7.7, where the experiment was carried out in triplicate. The solid lines correspond to the period during which the coating was observed to be sound. The point at which the solid line ends and the broken line starts indicates the moment when a crack or defect started to appear on the coating. The end of the broken lines corresponds to the failure, when the coating was broken over its whole length on the cracks.

The surface conditions of all the seven coatings during the fatigue tests were photographed as shown in Figures 7.12-18 respectively. These photos were taken from just above the initial concrete crack after 1, 2, 6, 9, 12, 15, and 18 million cycles of stress repetitions had been given to the specimens. The specimen numbers from left to right appearing in these figures correspond to those in Table 7.7 from top to bottom for each coating. The black rectangle in each picture is for concealing the information regarding to the coating brand or the manufacturer and thus has no connection with the experimental results.

As shown in Table 7.7 and Figure 7.12, the epoxy resin coating with a smaller thickness (Coating P1, t=350 μm) showed poor fatigue resistance performance. Cracks started to appear on the coatings soon after 1 or 2 million of cycles at 20°C and gradually extended while the temperature inside the chamber was maintained at 60°C. After the temperature was decreased to -10°C at 12 million cycles, the rate of the crack extension was suddenly observed to accelerate and the coating finally failed at between 13 and 17 million cycles. However as shown in Figure 7.13, the coating with the same material with a larger thickness (Coating P2, t=950 μm) showed good performance and remained undamaged until the end of the fatigue cycles (18 million cycles).

The chloroprene synthetic rubber specimens (Coating Q, t=150 μm) showed a different cracking pattern as shown in Figure 7.14. Within the first several millions cycles after the experiment was started, the coatings began to have a couple of spots with a diameter of a few millimetres on the initial substrate cracks, and the spots gradually became larger with the increasing fatigue cycles. After the temperature was changed to 60°C at 6 million cycles, cracks connecting the neighbouring spots appeared on the coatings. Then the cracks continued to extend until the coatings failed at around 15-17 millions of cycles. This coating had remained undamaged and performed best according to the results of one million cycle fatigue test carried out in the previous research; however, in this experiment with more cycles at various temperatures, this coating was observed to show poor fatigue resistance.

Figure 7.15 shows the crack view of the PCM coating (Coating R, t=120 μm). The PCM coating had shown relatively good fatigue resistance performance in the previous fatigue test detailed in the previous section. In the present experiment, the coating remained sound while the specimens were exposed to the first 6 million cycles at 20°C, and then almost invisible cracks with a small width appeared on the two of the three specimens during the next 6 million cycles at 60°C. However, after the temperature was changed to -10°C, the coatings were significantly damaged with vivid cracks appearing on them. One of the three specimens failed at 13 million cycles. As seen in the other two specimens, the crack extended in almost whole length on the coatings on the initial substrate crack at 15 million cycles.

On the other hand, poly-butadiene (Coating S, t=1,060 μm) and polyurethane (Coating T, t=730 μm; Coating U, t=2,060μm) coatings remained sound until the end of the fatigue test as shown in Figures 7.16-18 except one of the specimens T (T-2 in Figure 7.17), which was found to be fixed to the fatigue machine unfortunately in a wrong manner with unintended

torsional stress given to the specimen at the commencement of the fatigue experiment. No adhesion loss between the coatings and the substrate that could have tolerated the stress of the coatings and made it easier to accommodate the underlying substrate crack movements was observed in all specimens.

Table 7.7 Results of fatigue tests

No.	Material (thickness (μm))	20°C						60°C						-10°C					
		1	2	3	4	5	6	7	8	9	10	11	12	13	14	15	16	17	18
														(million times)					
P-1	Epoxy resin (350)	P-1-1																	
		P-1-2																	
		P-1-3																	
P-2	Epoxy resin (950)	P-2-1																	
		P-2-2																	
		P-2-3																	
Q	Chloroprene synthetic rubber (150)	Q-1																	
		Q-2																	
		Q-3																	
R	PCM (120)	R-1																	
		R-2																	
		R-3																	
S	Poly Butadiene (1,060)	S-1																	
		S-2																	
		S-3																	
T	Polyurethane (730)	T-1																	
		T-2																	
		T-3																	
U	Polyurethane (2,060)	U-1																	
		U-2																	
		U-3																	

	P-1-1	P-1-2	P-1-3
1 mil.	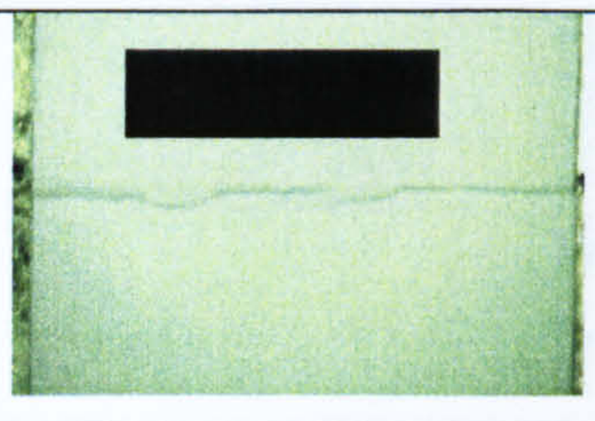	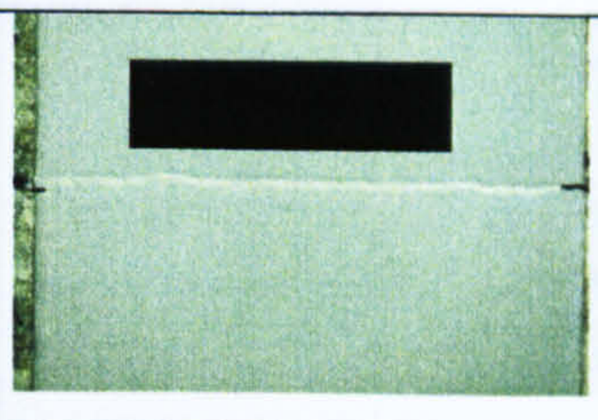	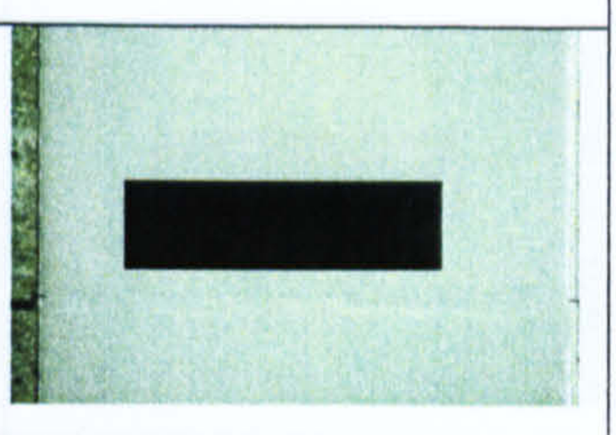
2 mil.	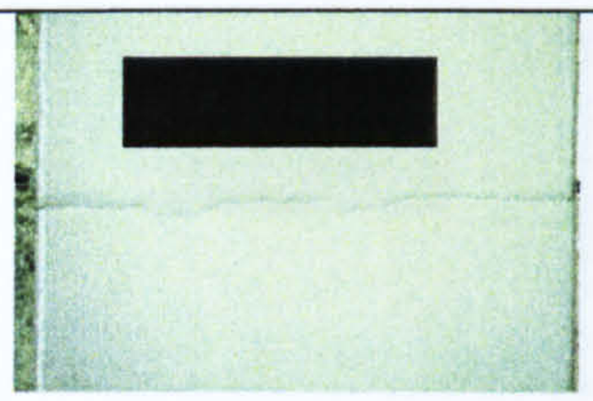	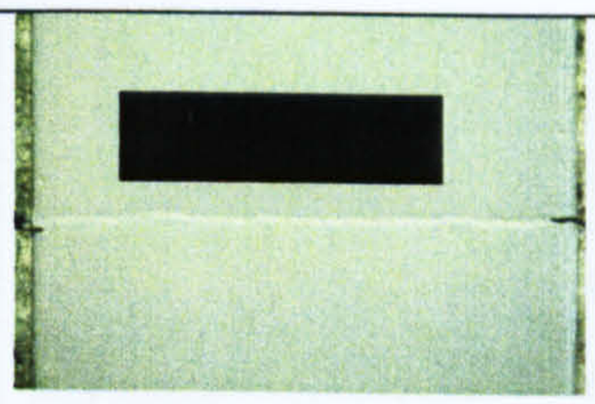	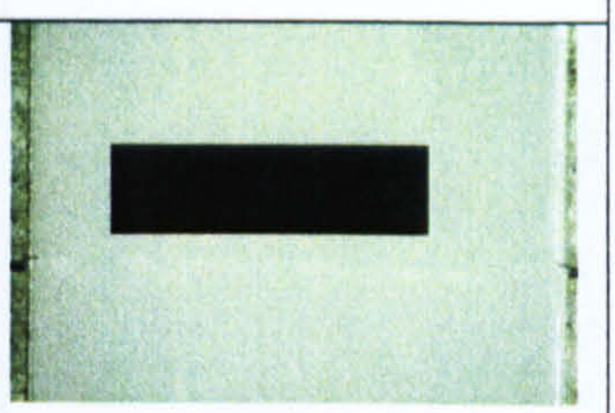
6 mil.	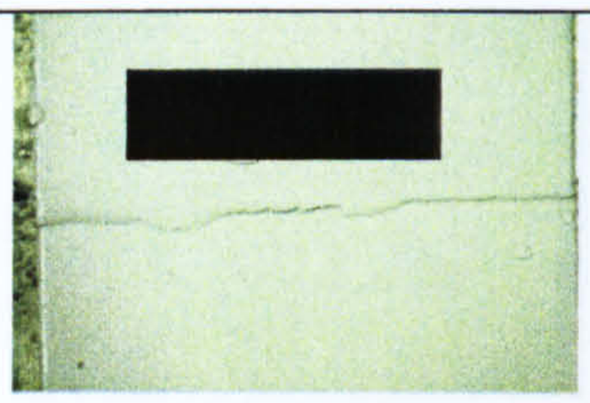	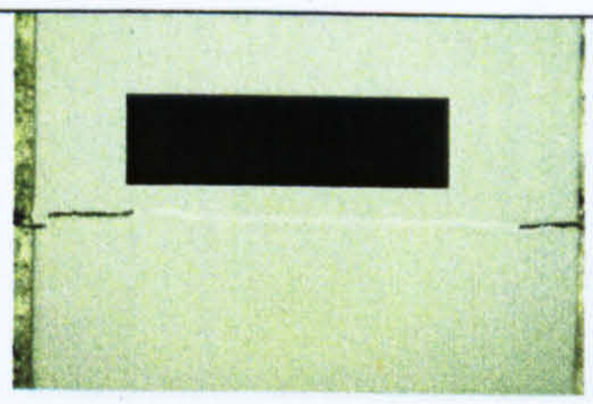	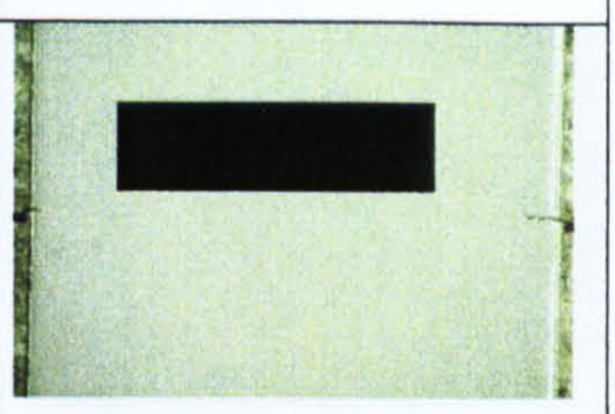
9 mil.	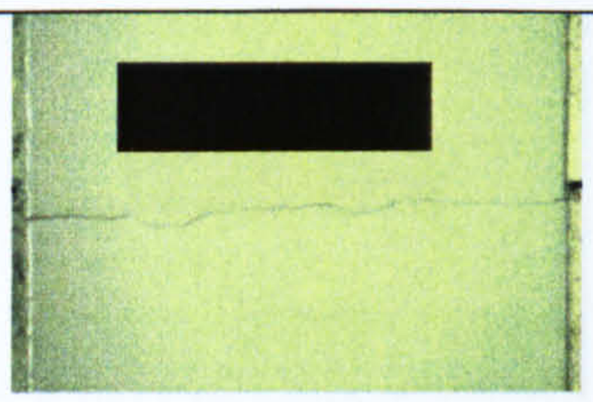	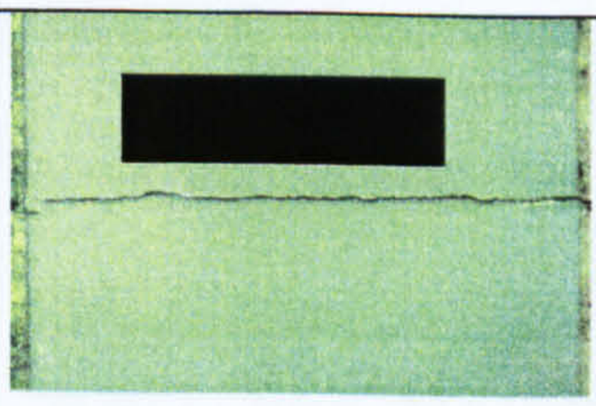	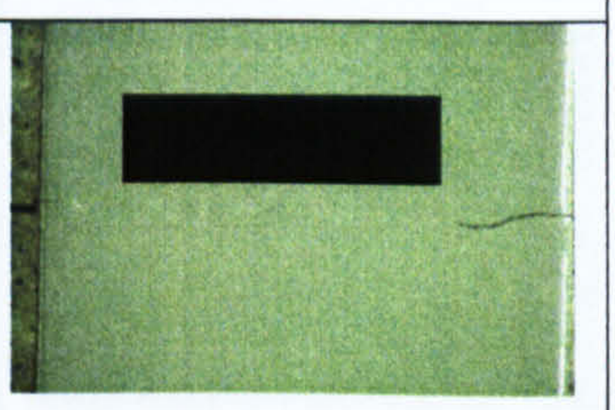
12 mil.	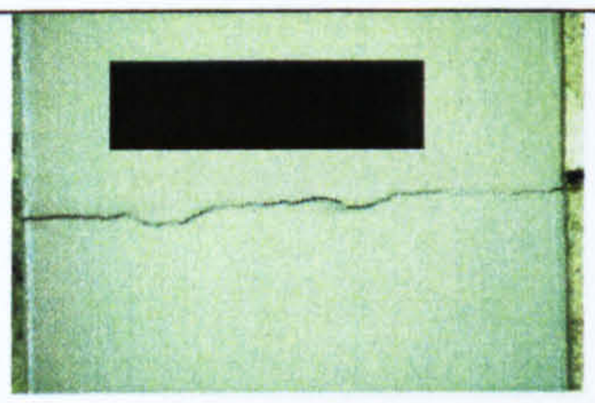	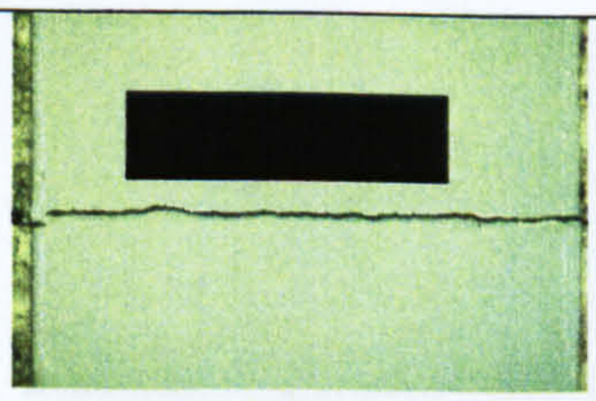	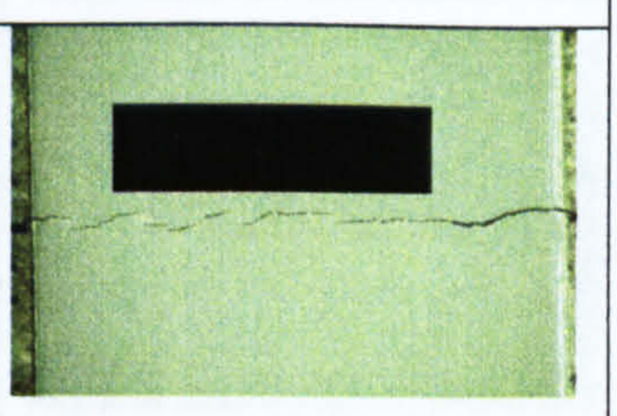
15 mil.	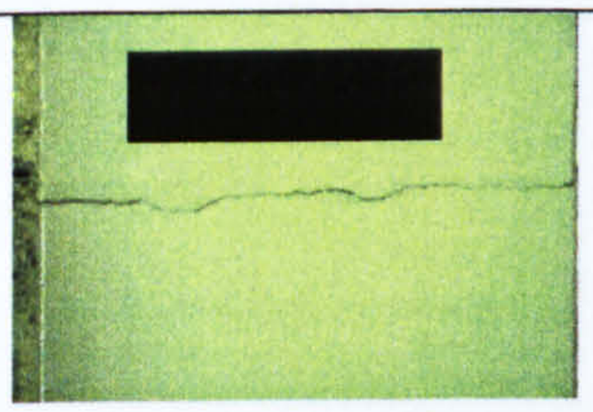	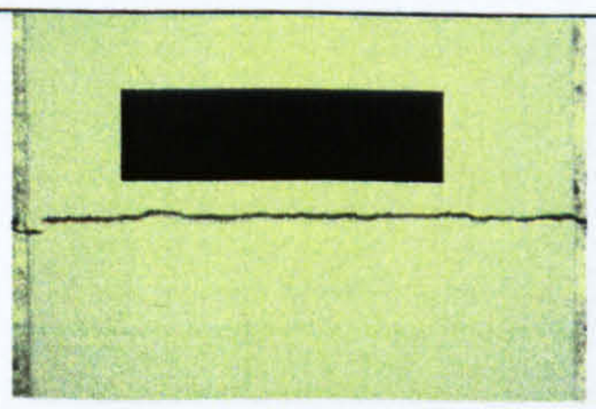	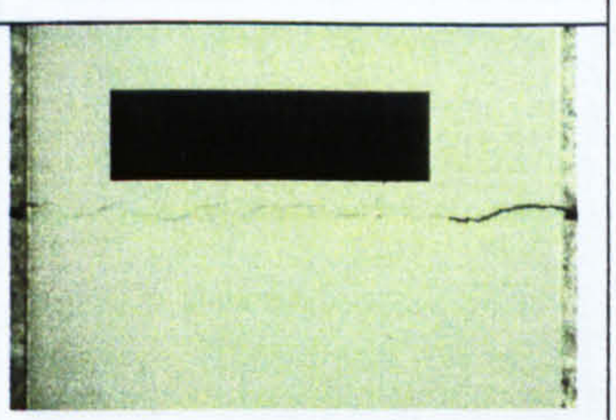
18 mil.	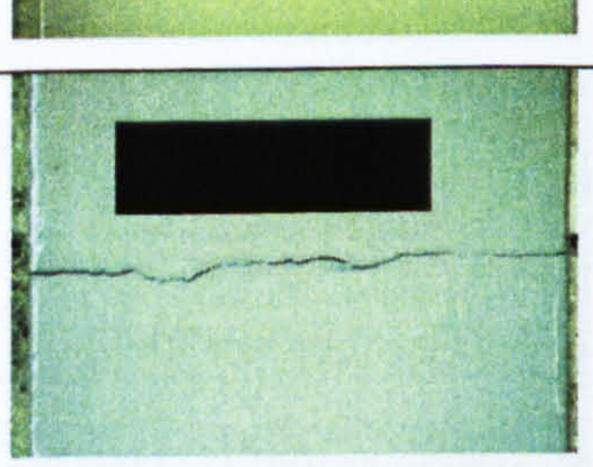	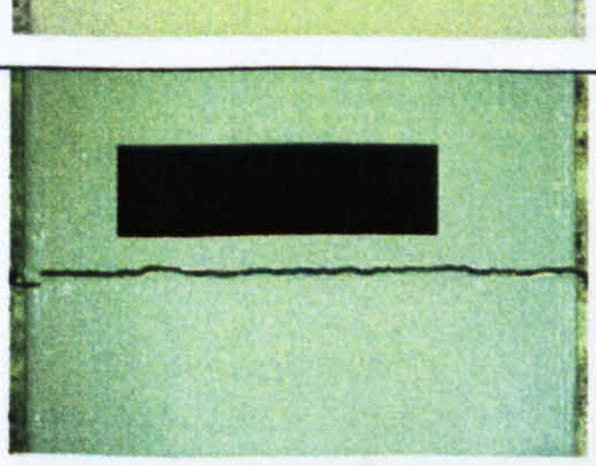	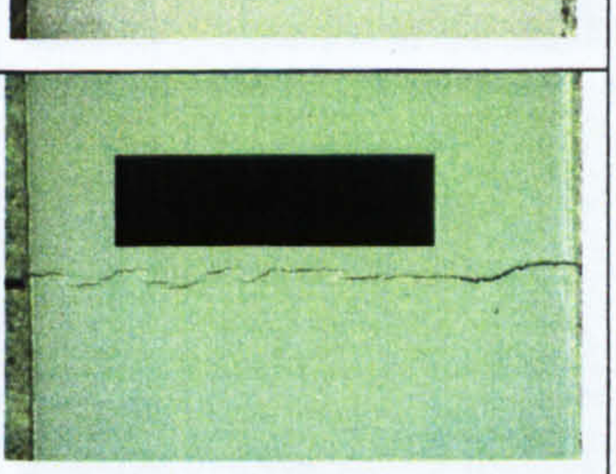

Figure 7.12 Crack view on coating P-1

	P-2-1	P-2-2	P-2-3
1 mil.	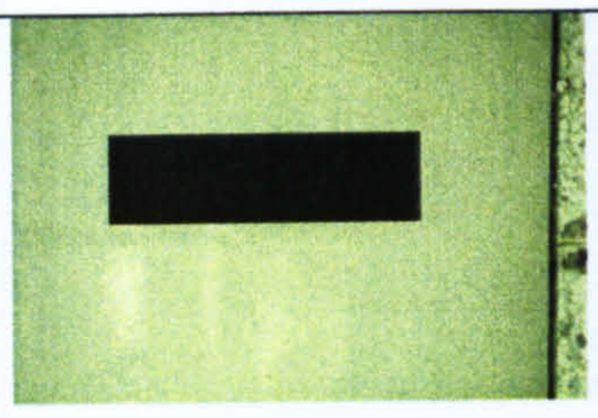	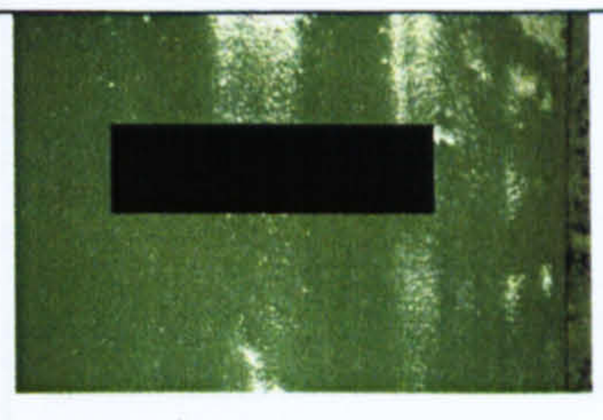	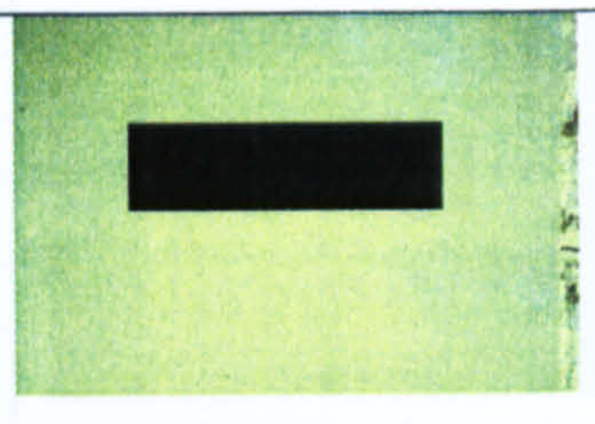
2 mil.	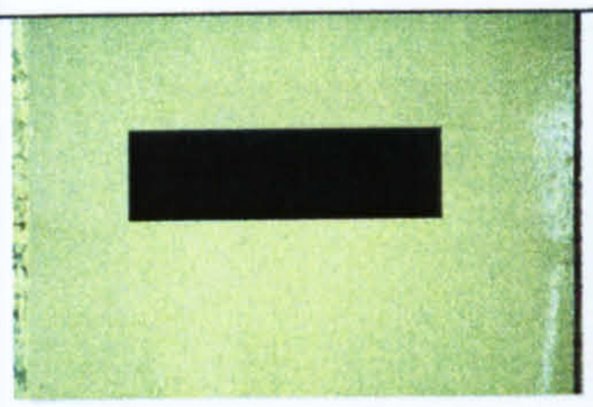	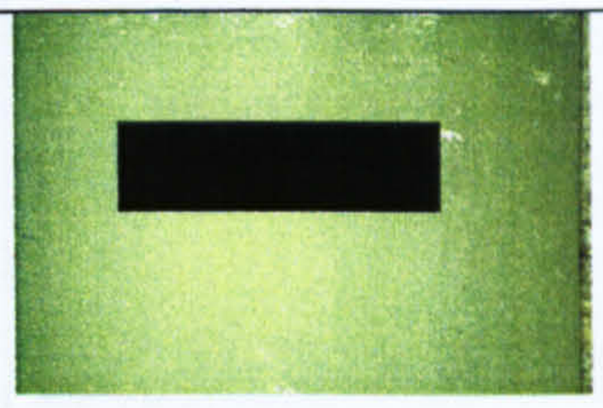	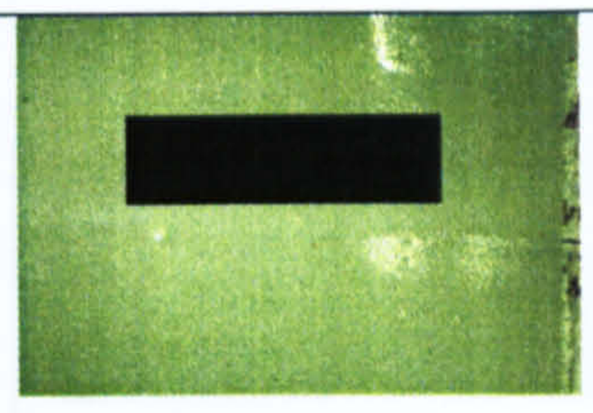
6 mil.	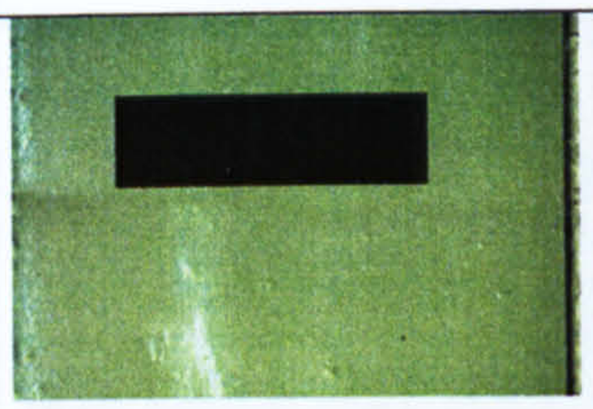	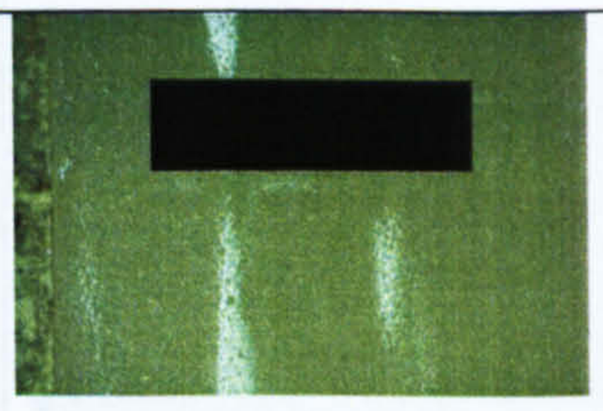	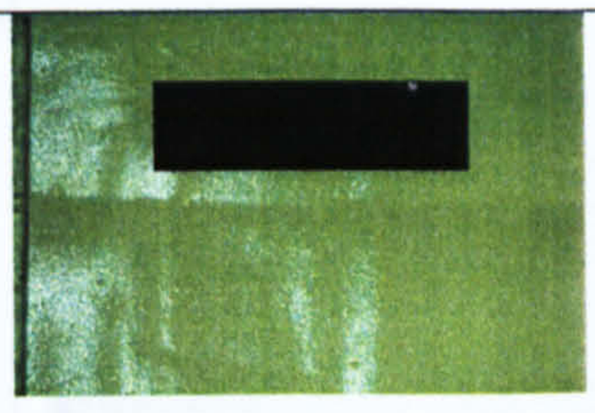
9 mil.	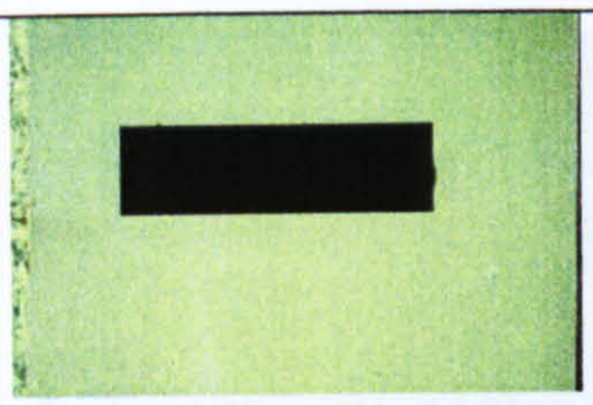	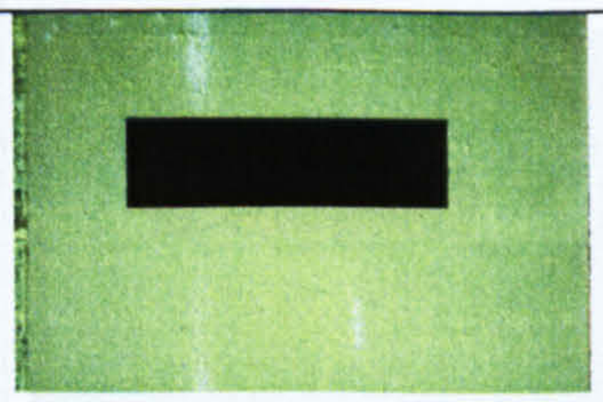	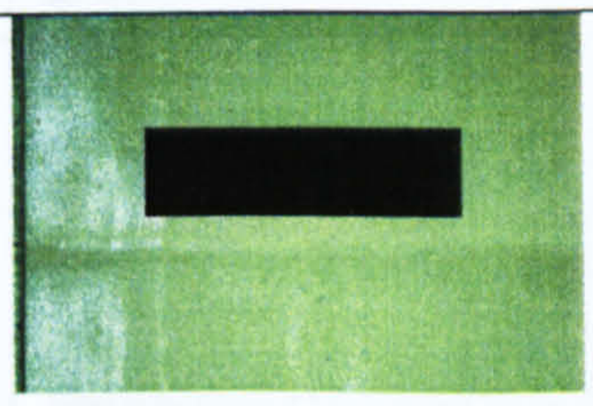
12 mil.	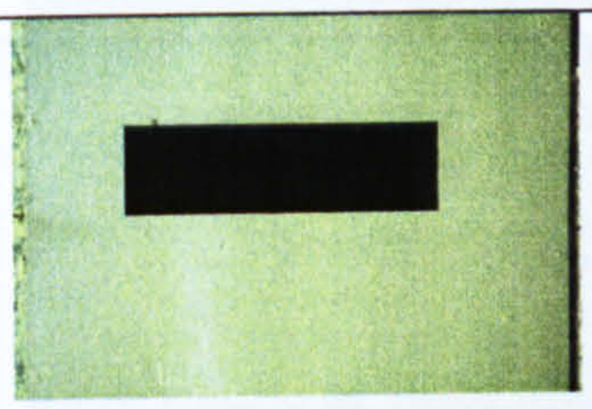	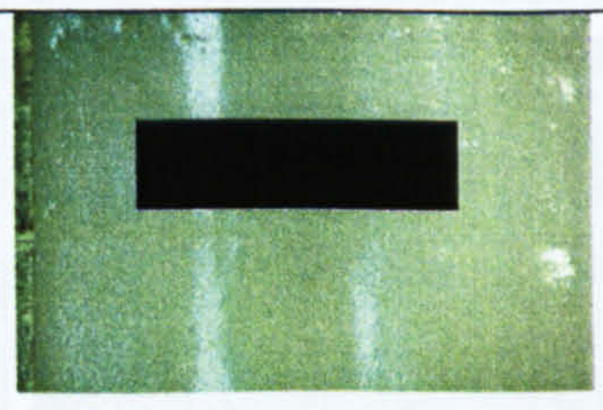	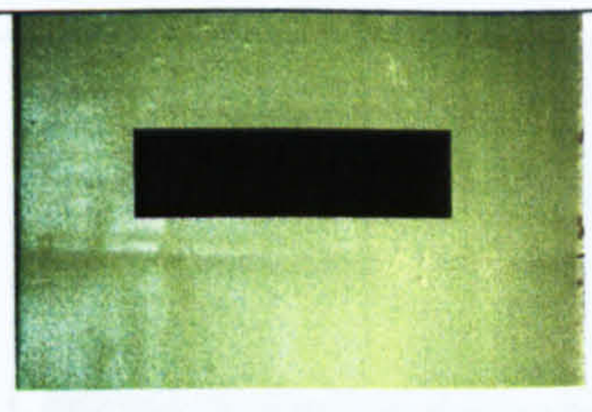
15 mil.	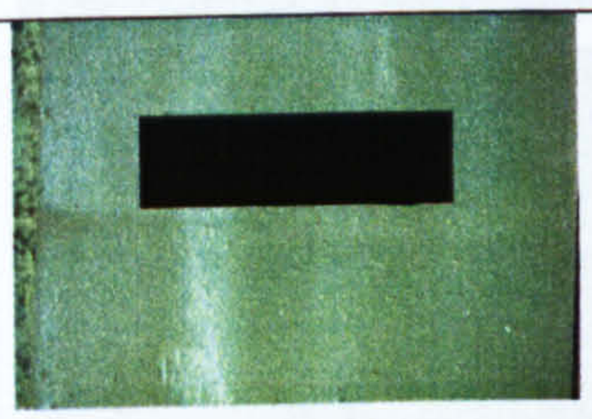	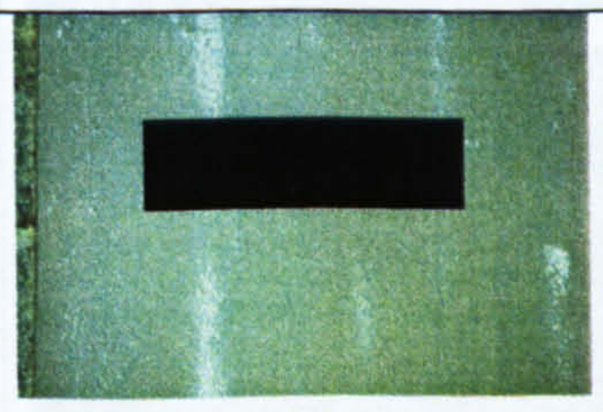	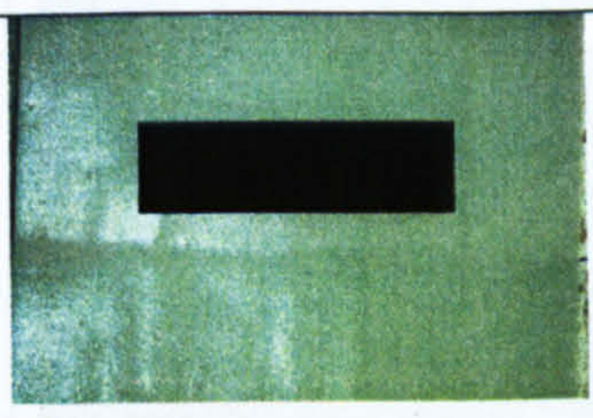
18 mil.	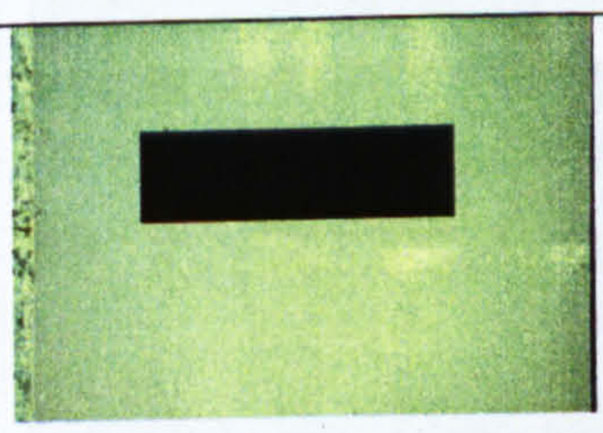	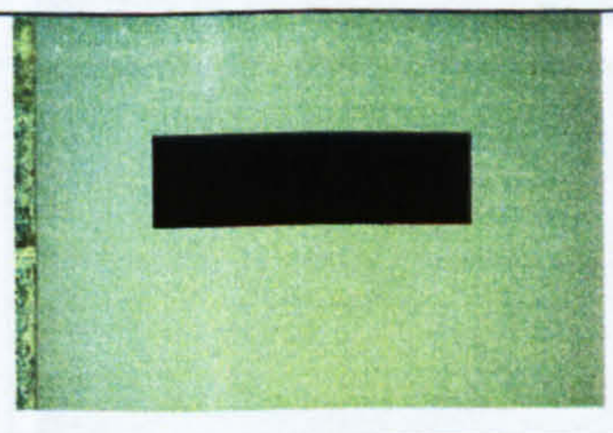	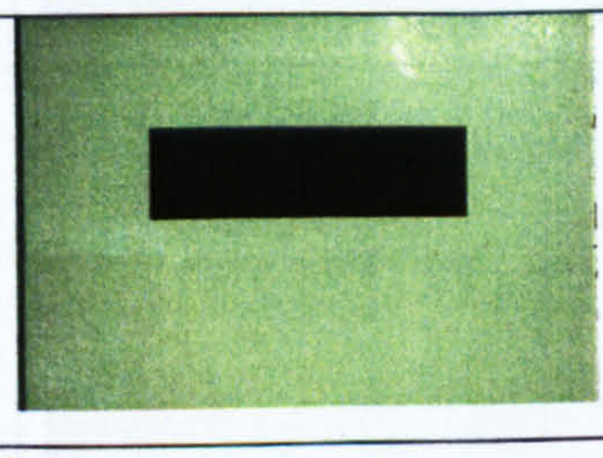

Figure 7.13 Crack view on coating P-2

	Q-1	Q-2	Q-3
1 mil.	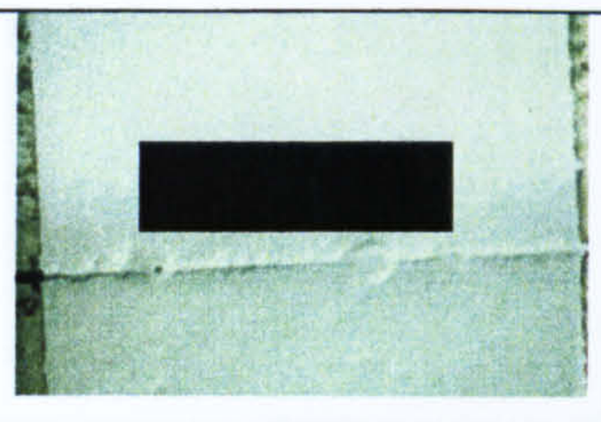	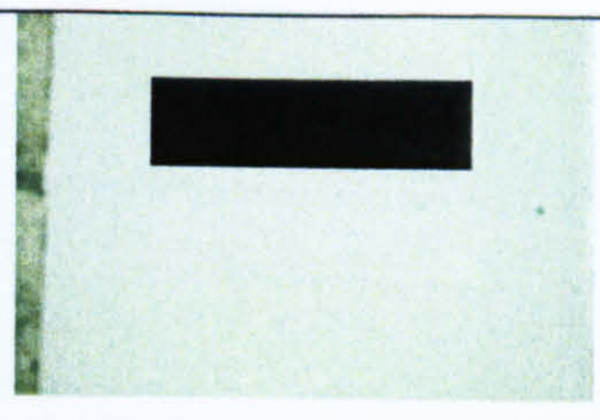	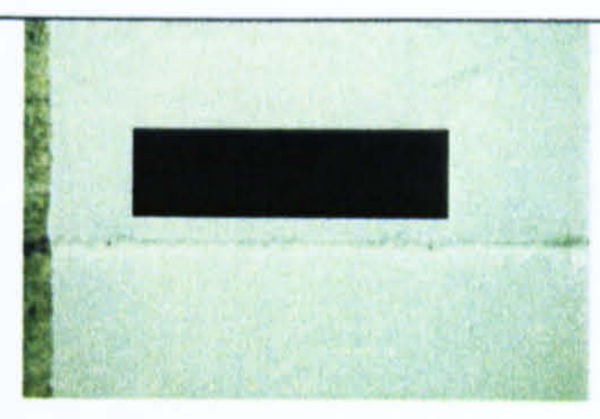
2 mil.	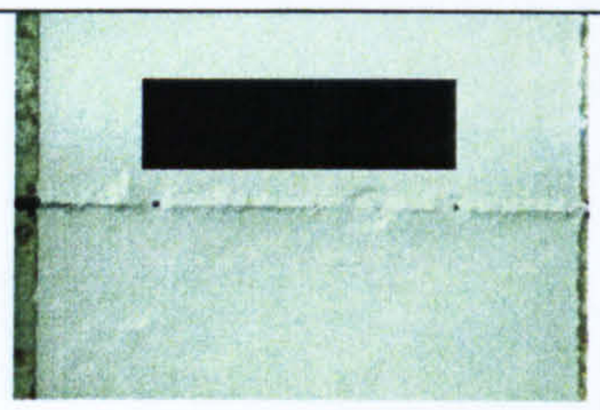	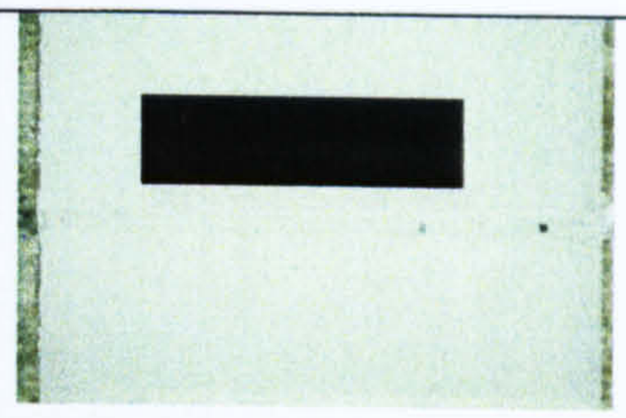	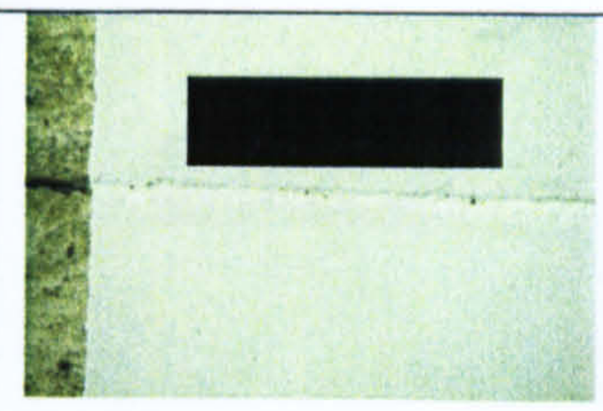
6 mil.	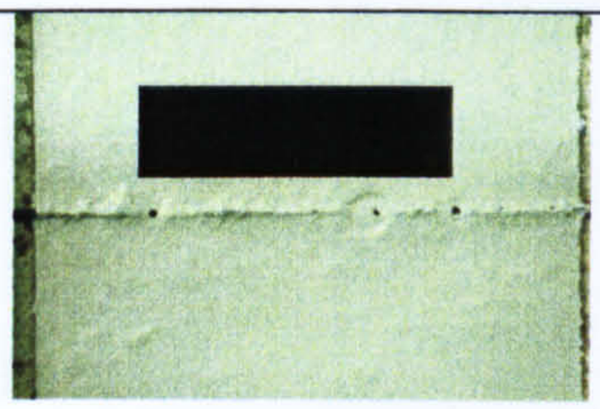	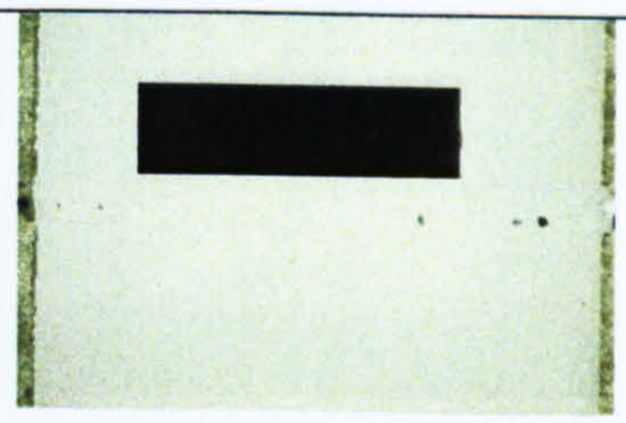	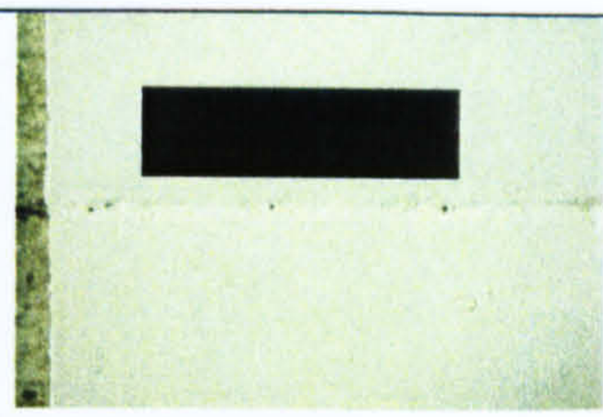
9 mil.	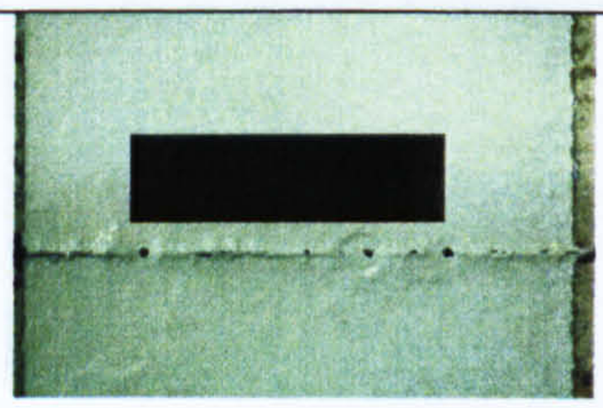	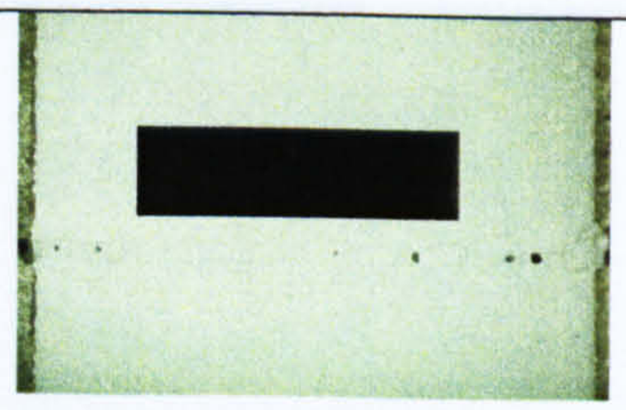	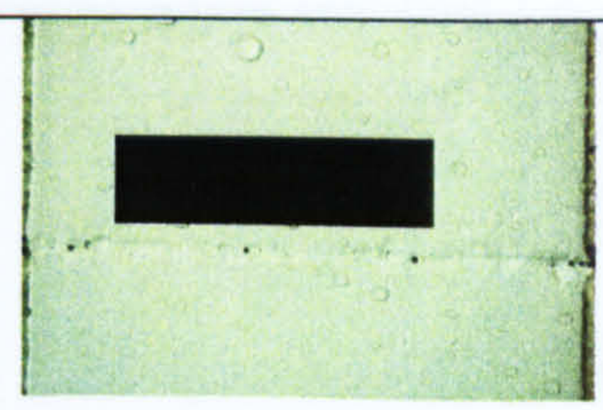
12 mil.	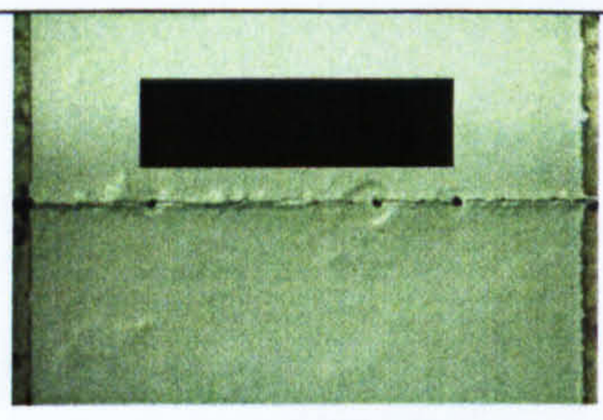	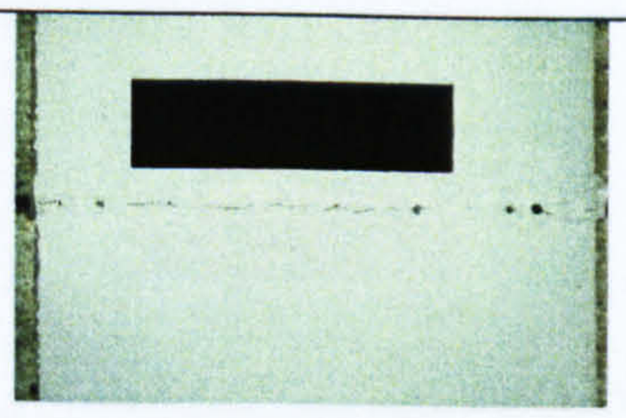	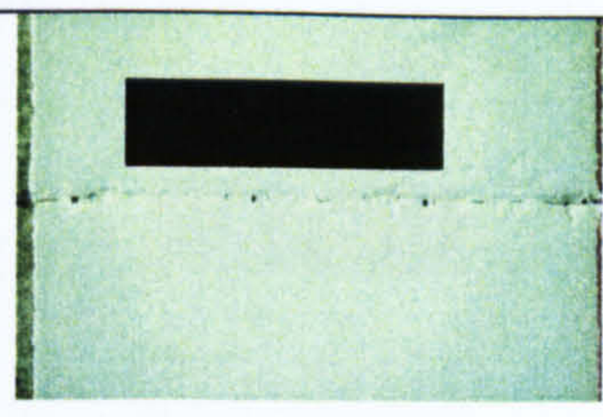
15 mil.	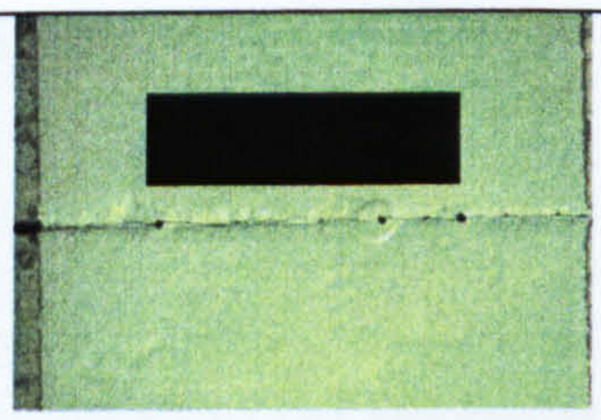	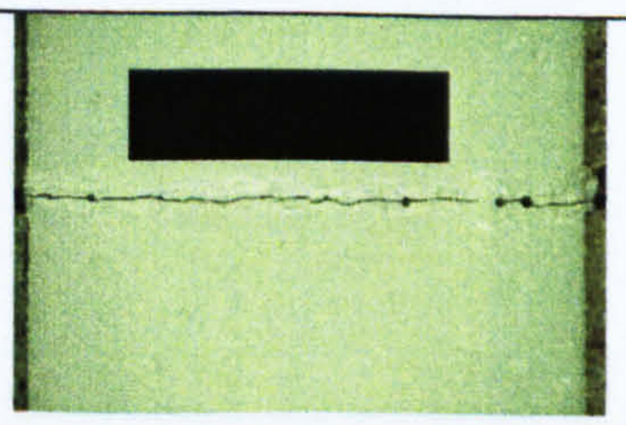	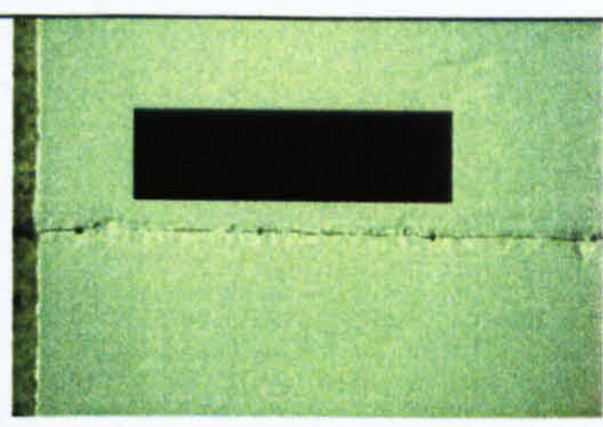
18 mil.	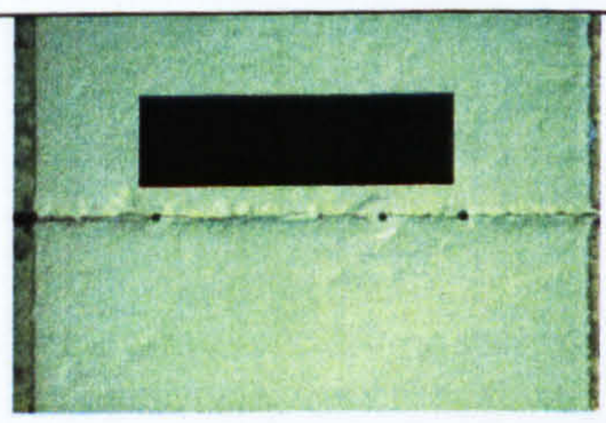	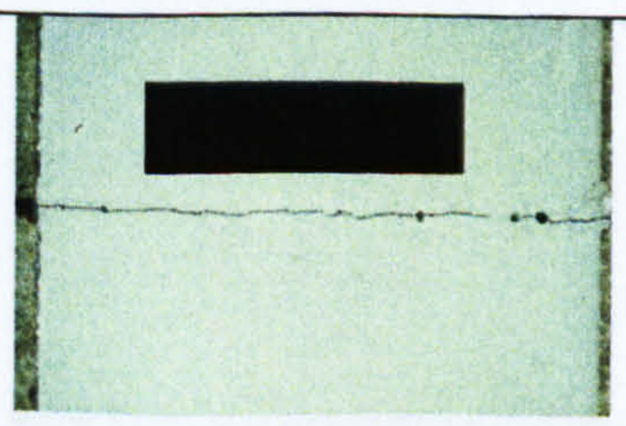	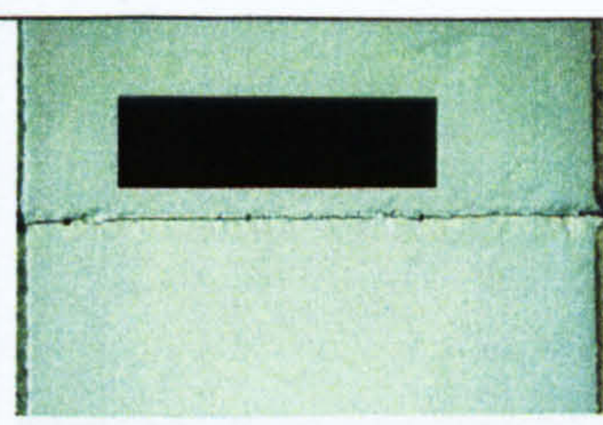

Figure 7.14 Crack view on coating Q

	R-1	R-2	R-3
1 mil.	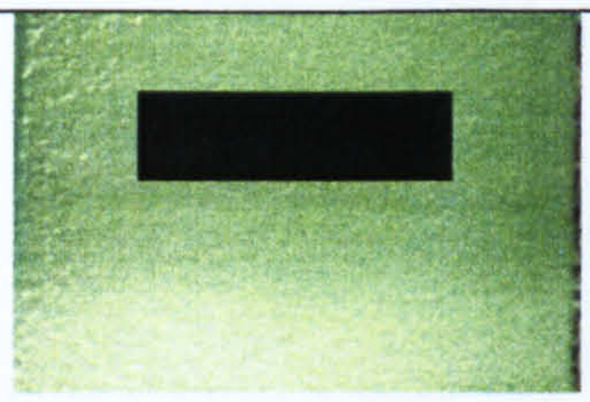	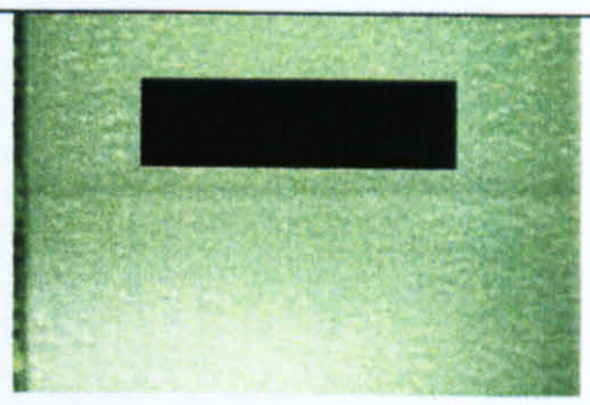	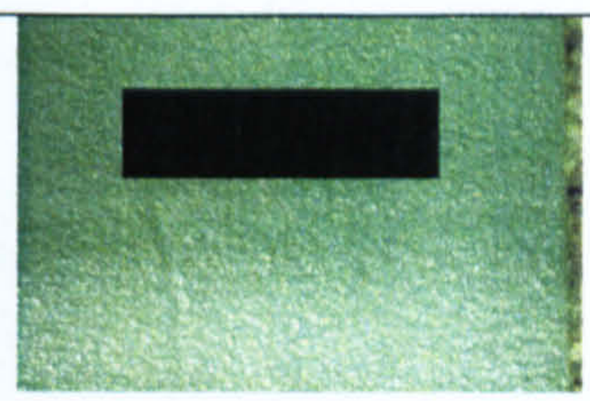
2 mil.	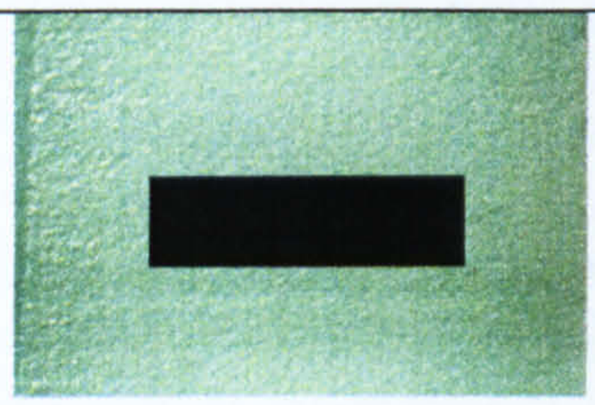	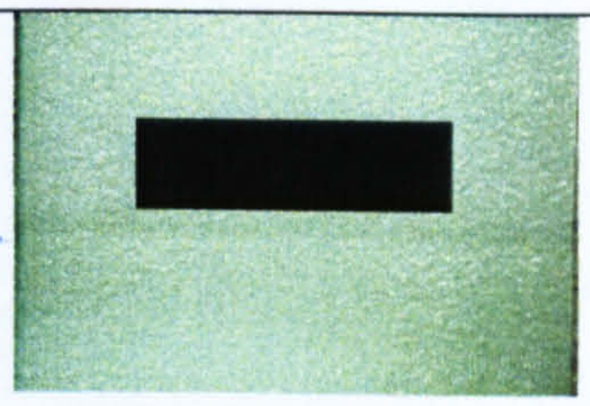	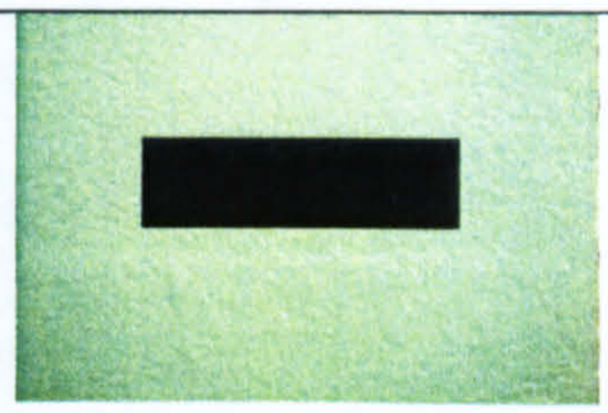
6 mil.	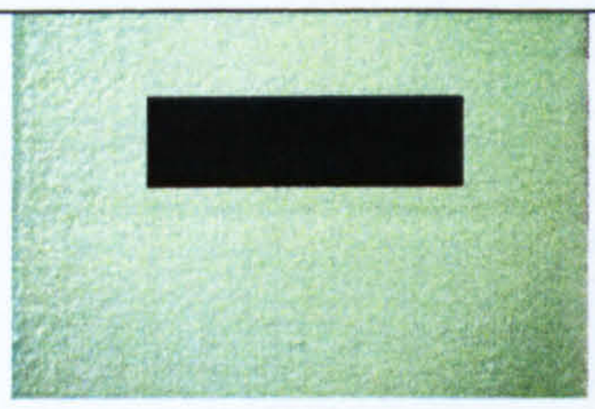	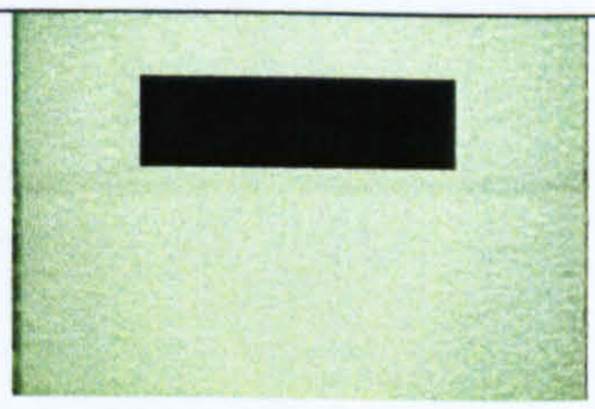	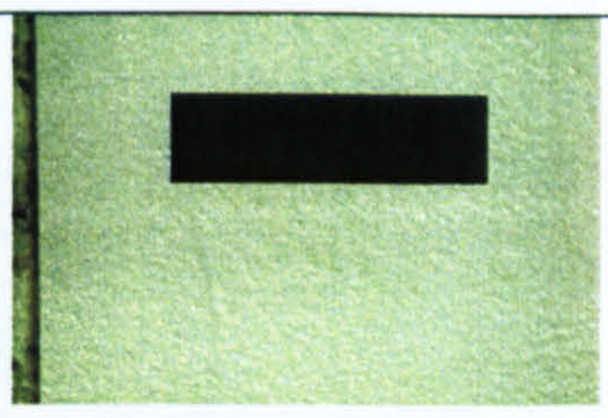
9 mil.	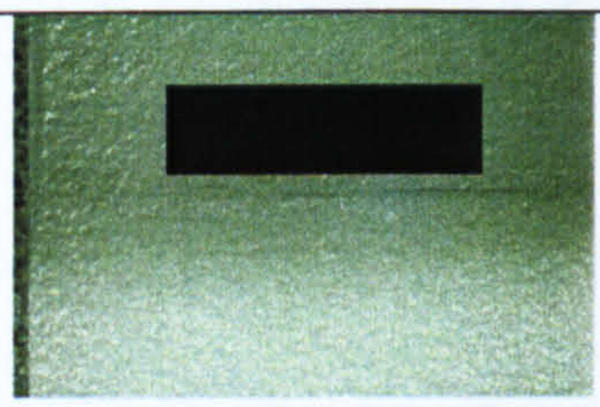	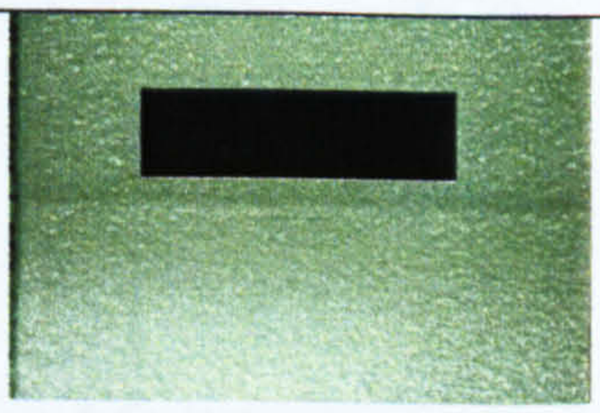	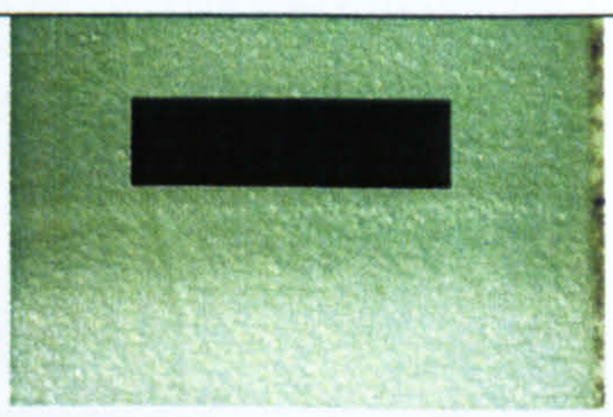
12 mil.	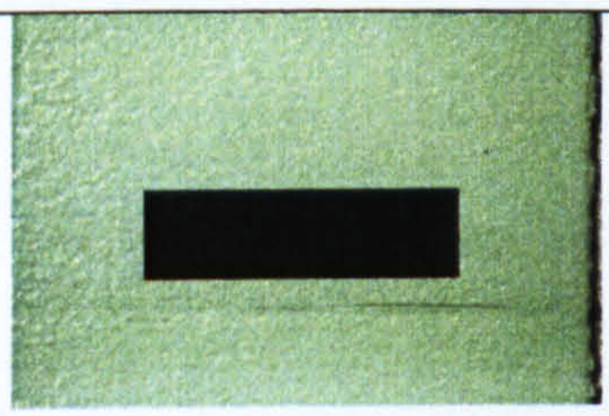	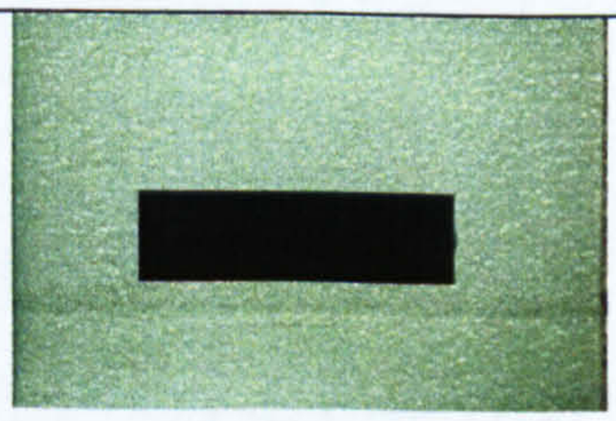	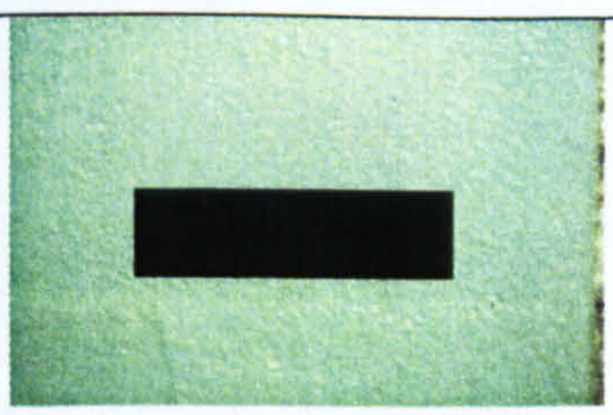
15 mil.	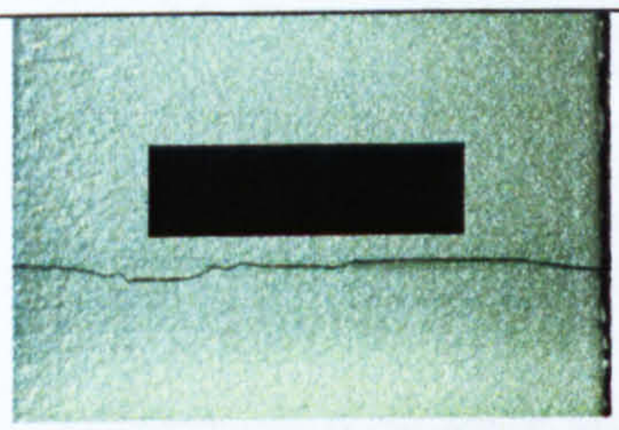	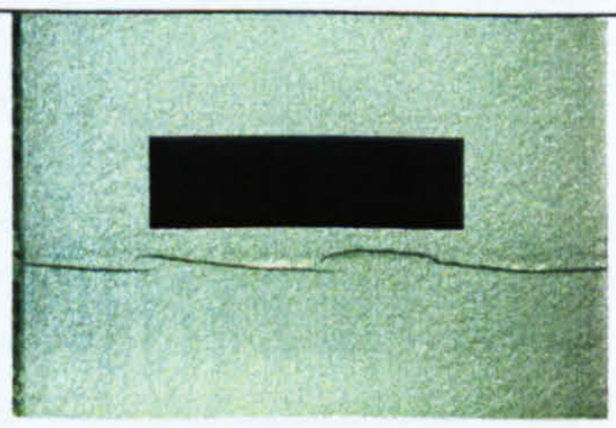	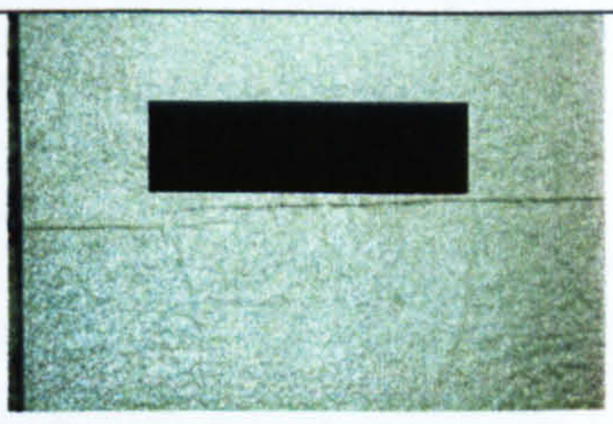
18 mil.	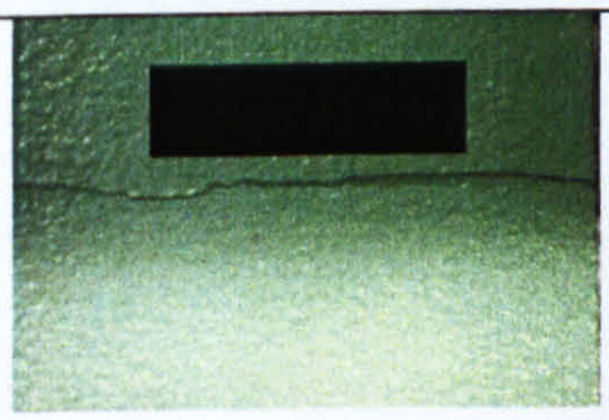	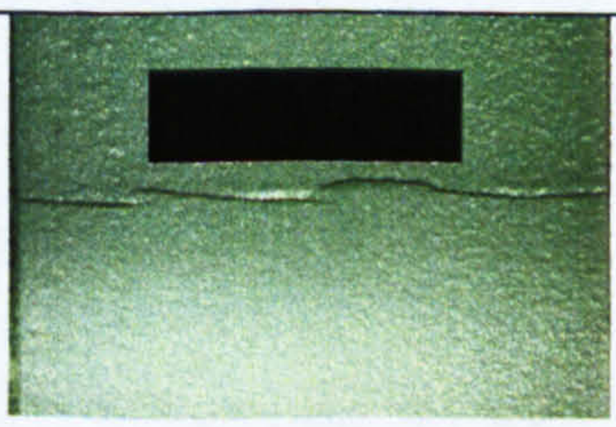	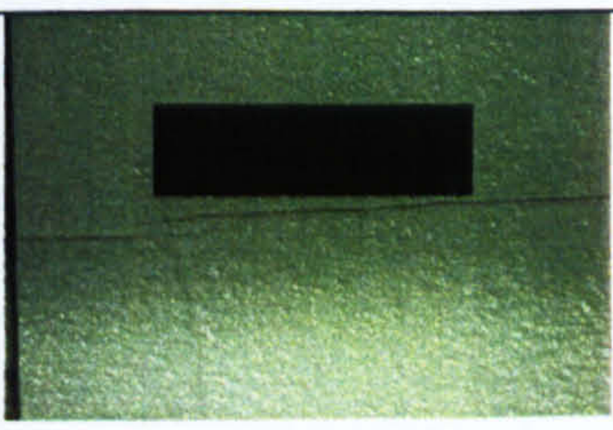

Figure 7.15 Crack view on coating R

	S-1	S-2	S-3
1 mil.	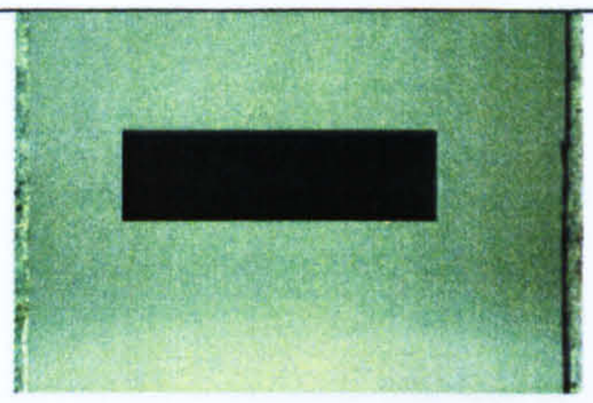	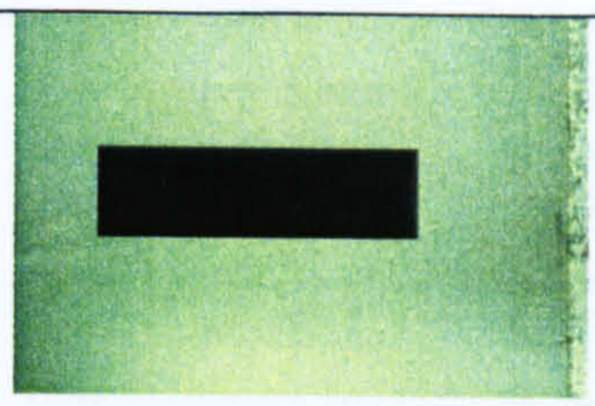	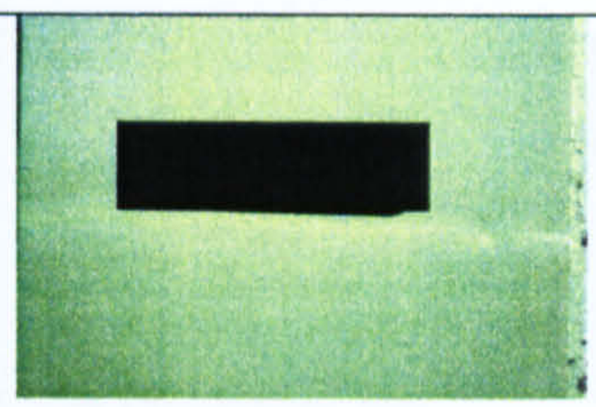
2 mil.	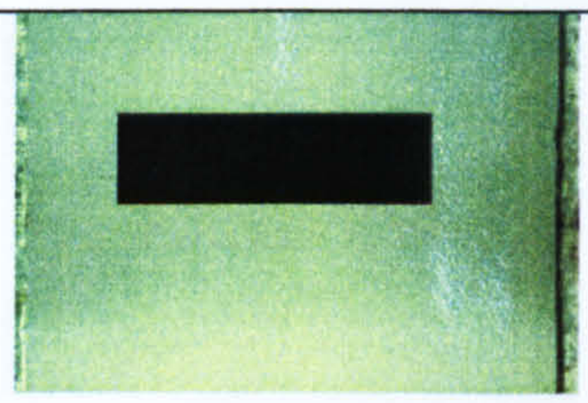	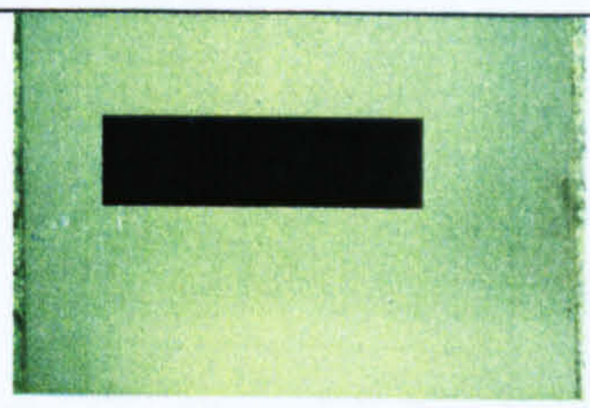	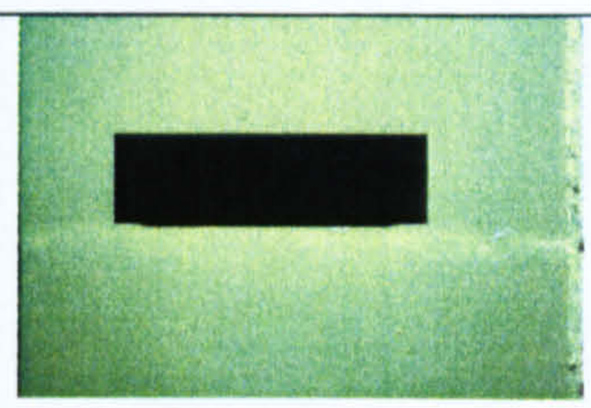
6 mil.	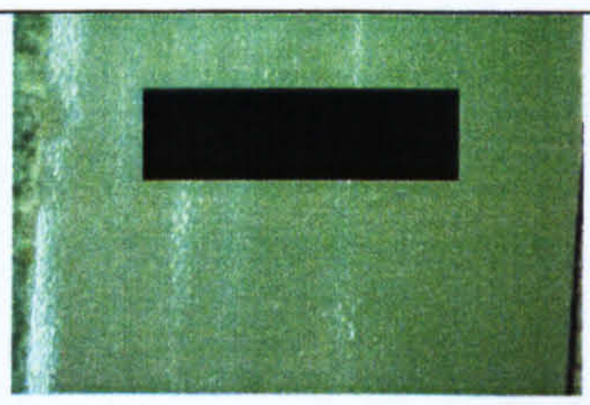	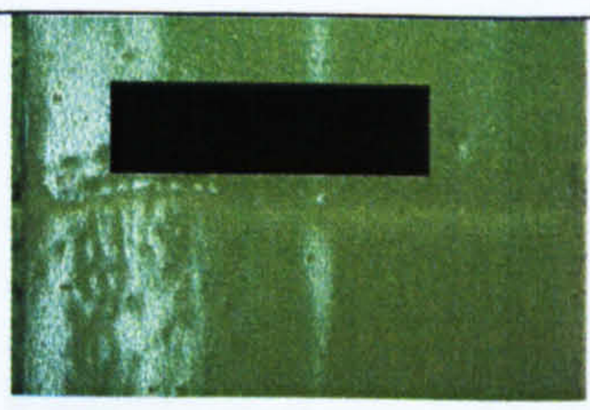	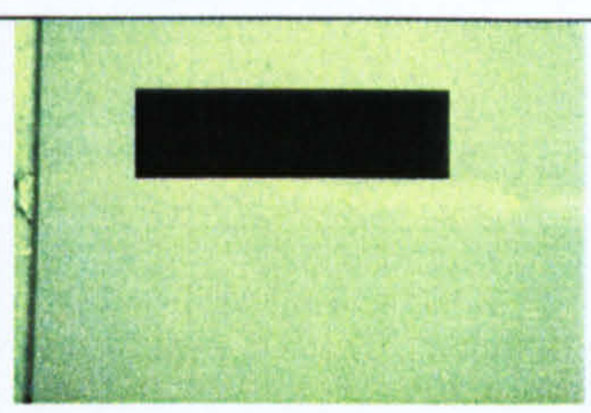
9 mil.	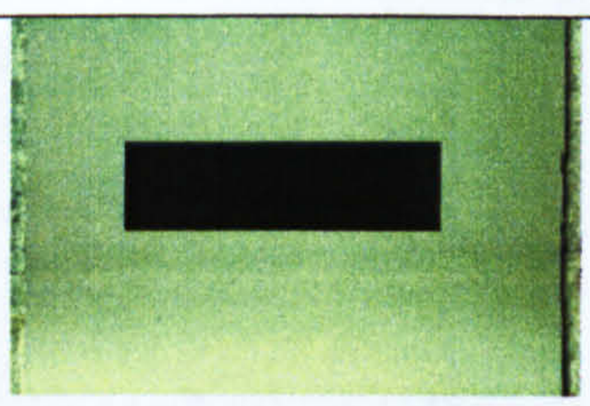	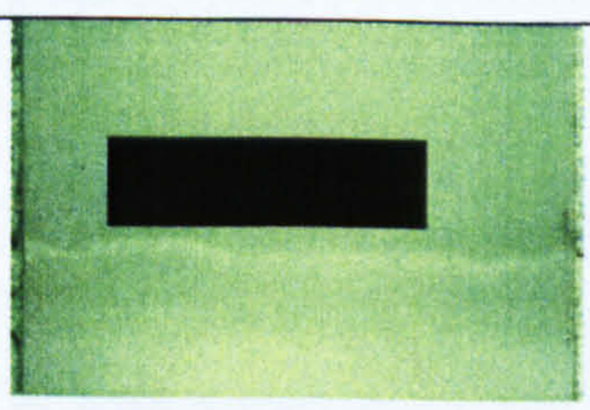	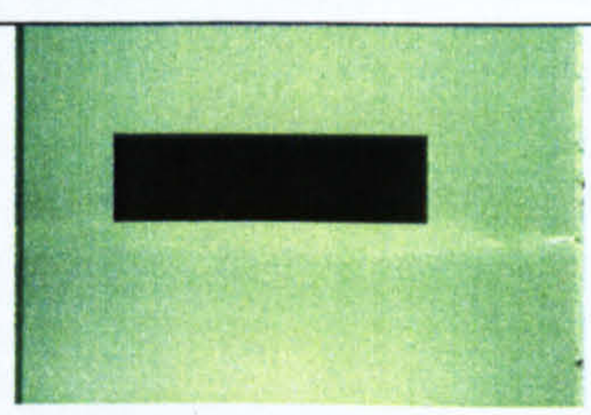
12 mil.	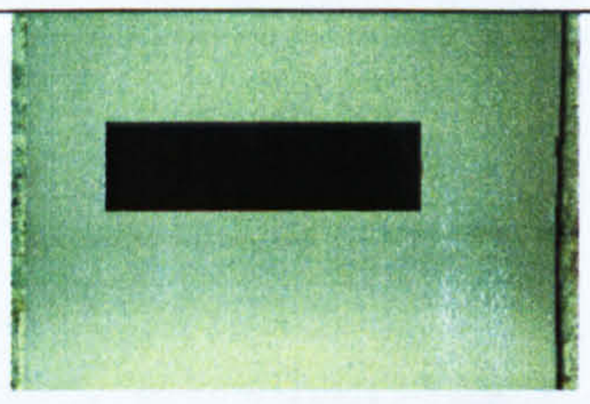	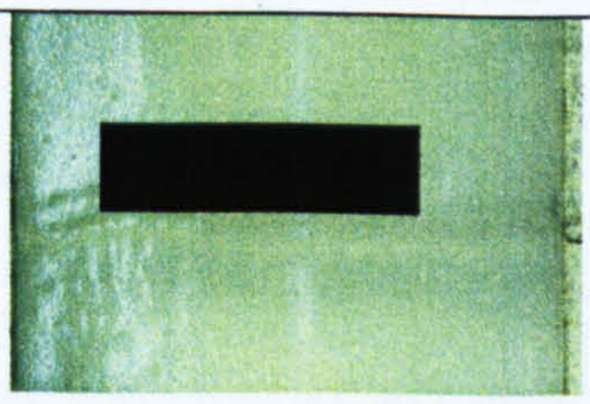	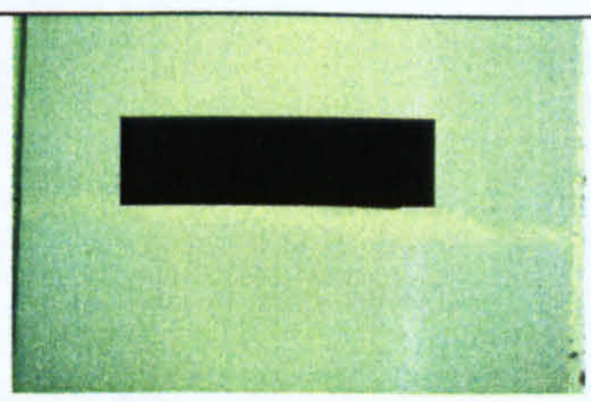
15 mil.	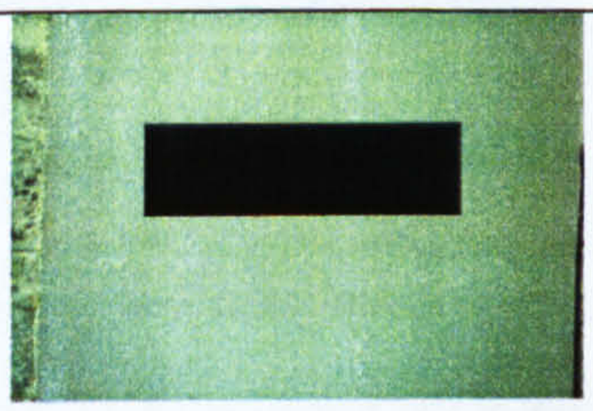	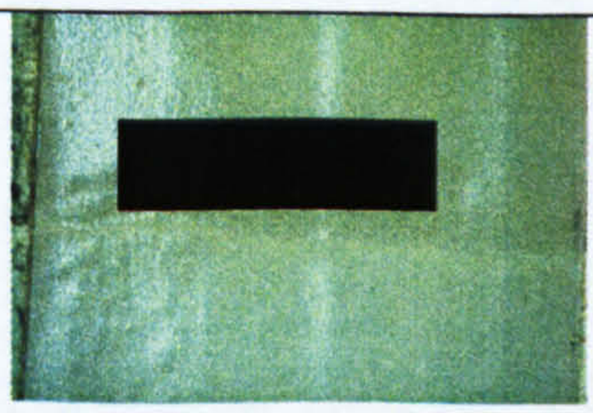	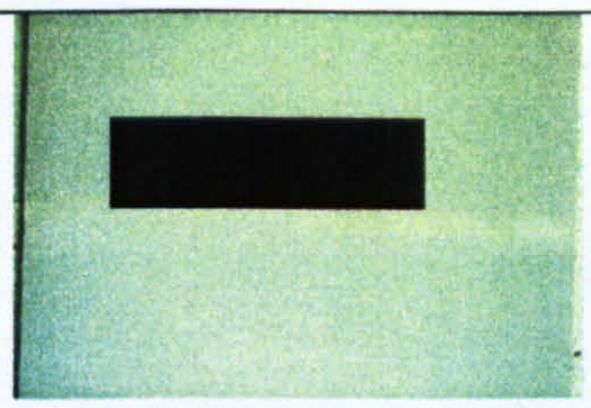
18 mil.	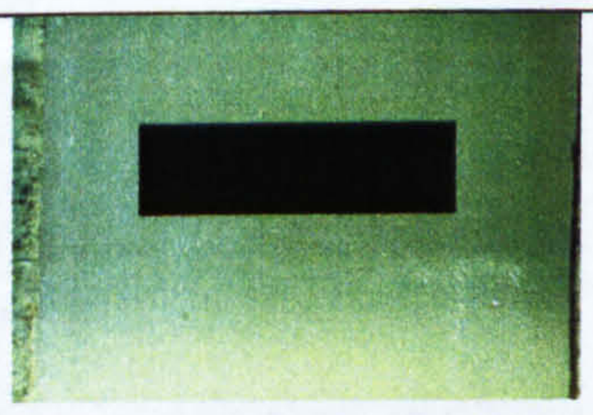	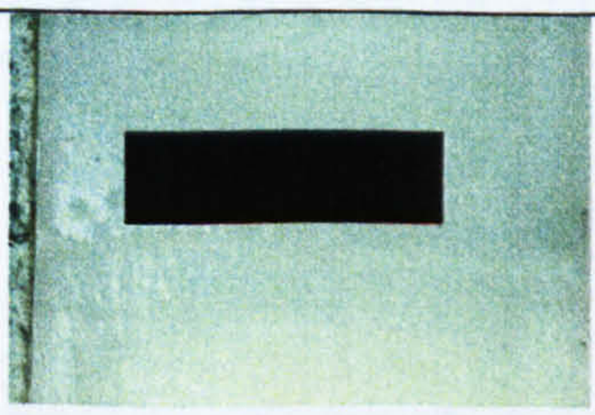	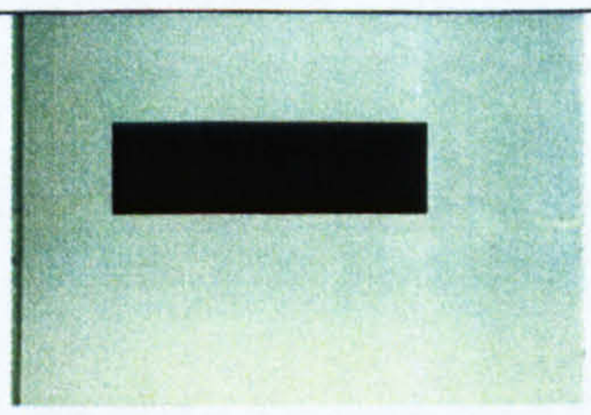

Figure 7.16 Crack view on coating S

	T-1	T-2	T-3
1 mil.	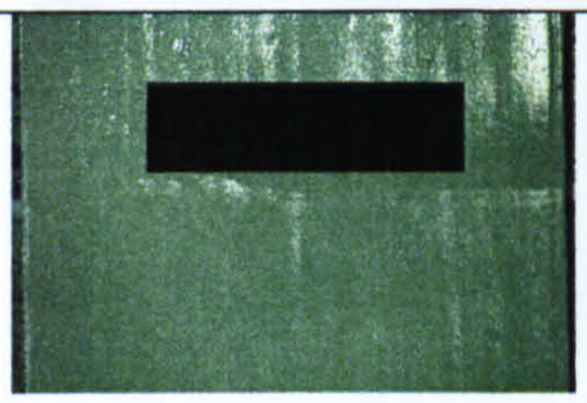	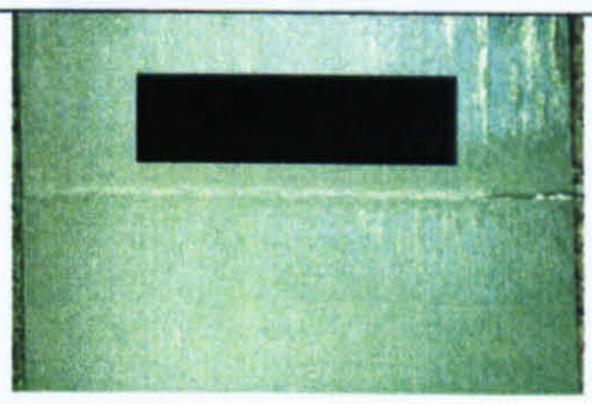	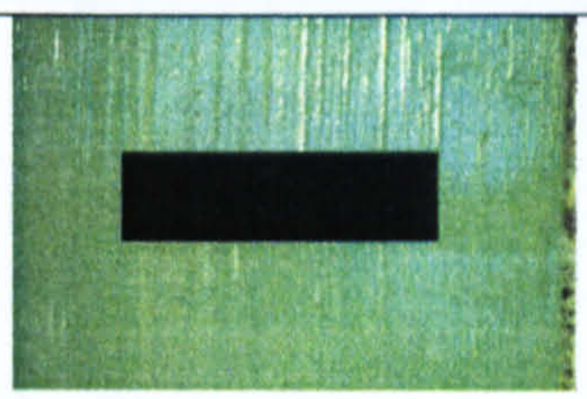
2 mil.	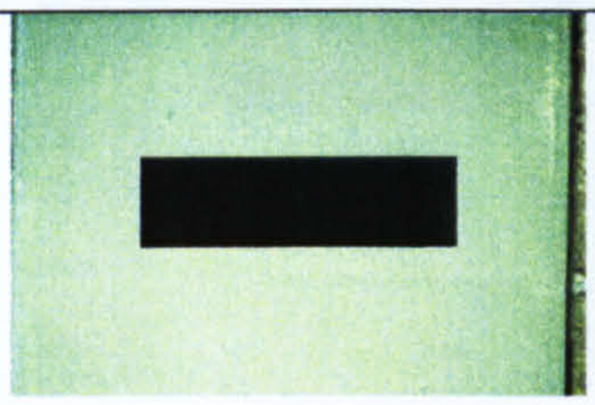	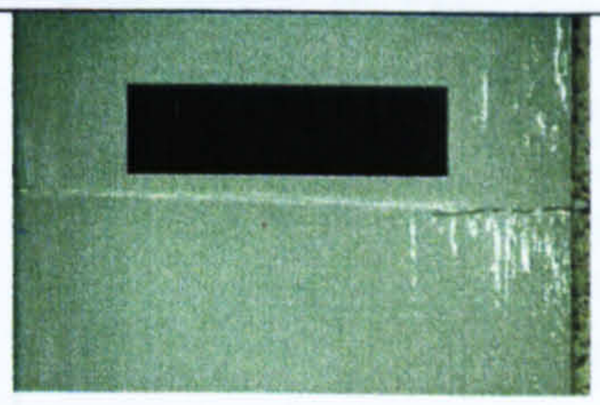	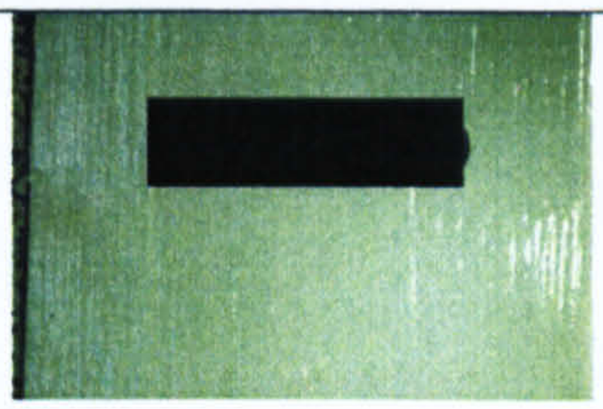
6 mil.	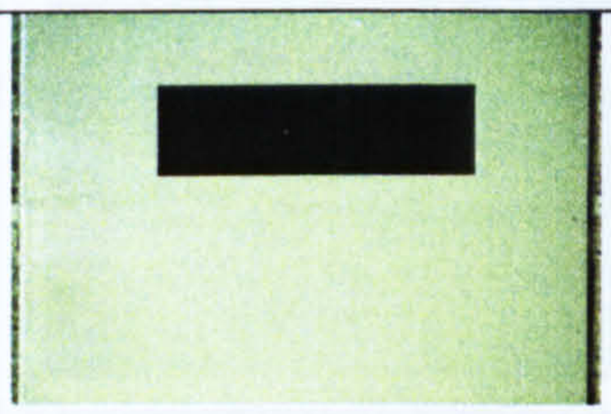	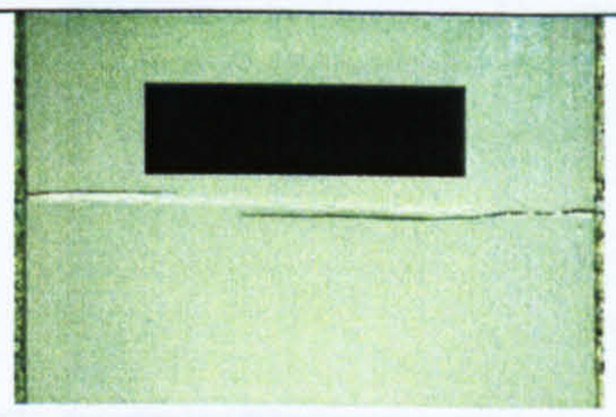	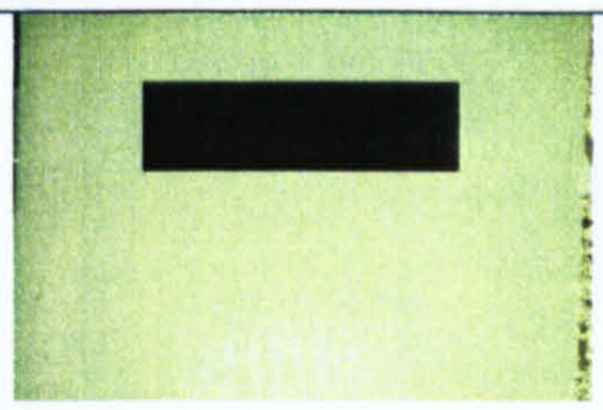
9 mil.	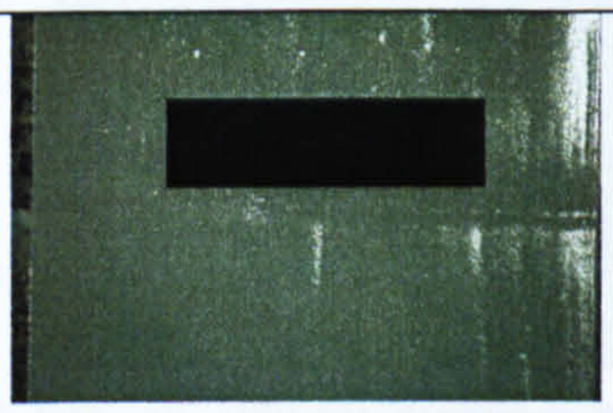	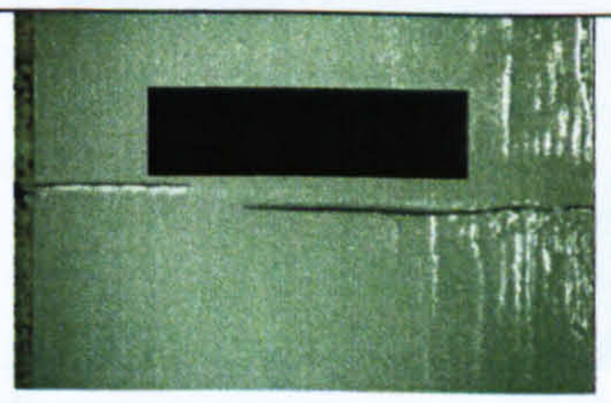	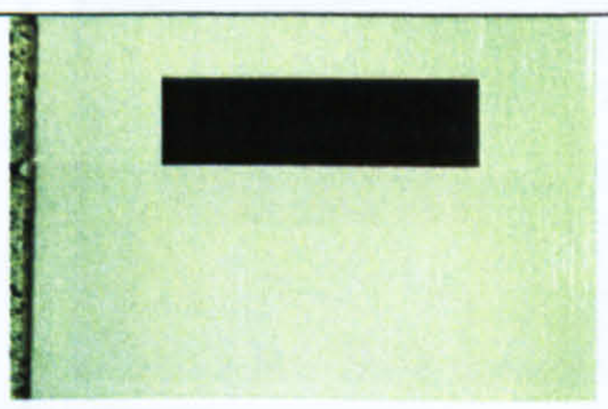
12 mil.	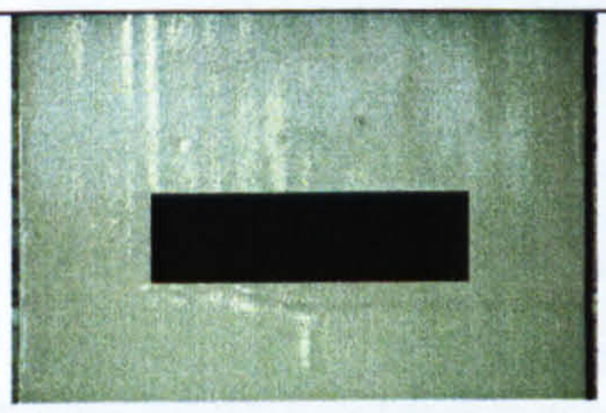	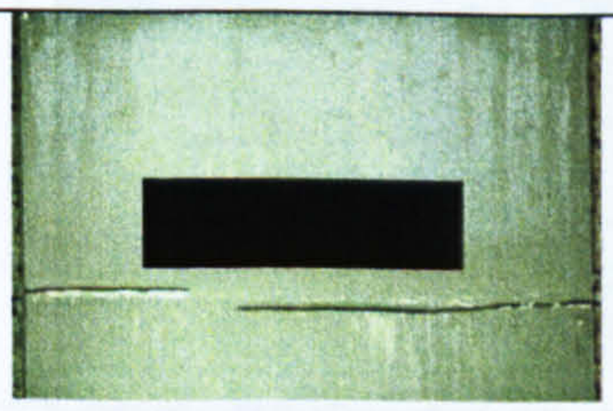	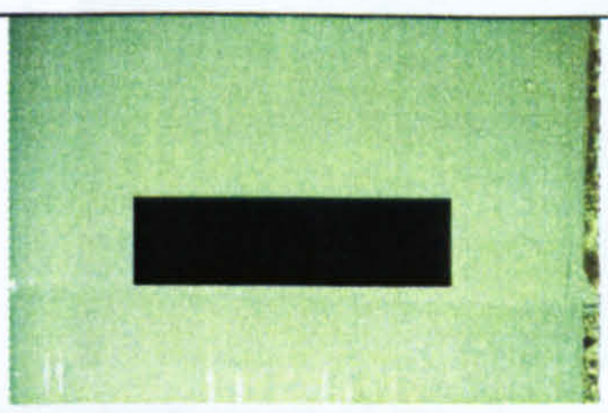
15 mil.	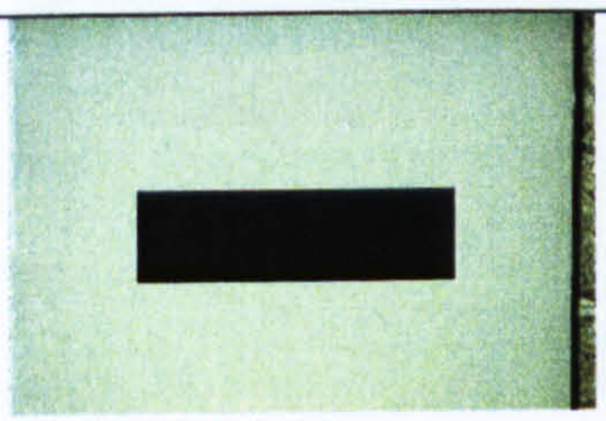	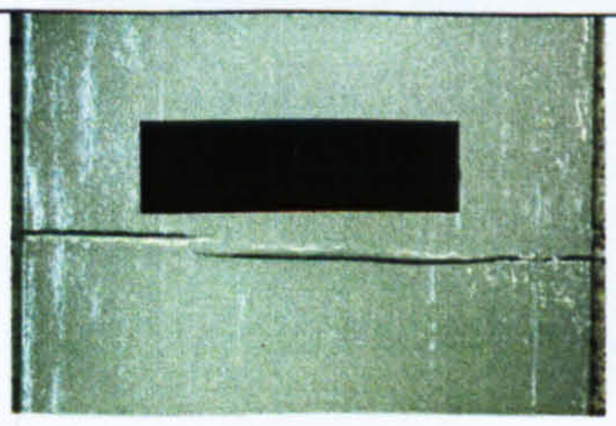	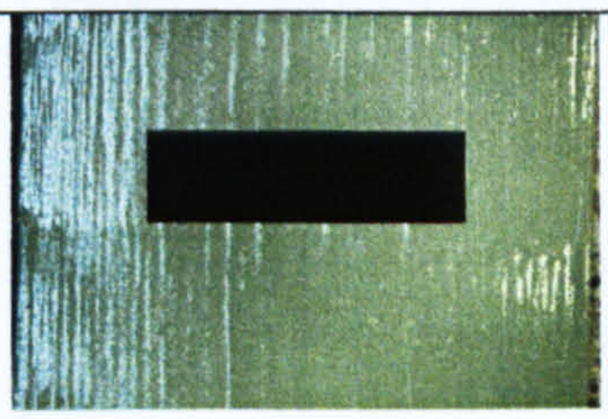
18 mil.		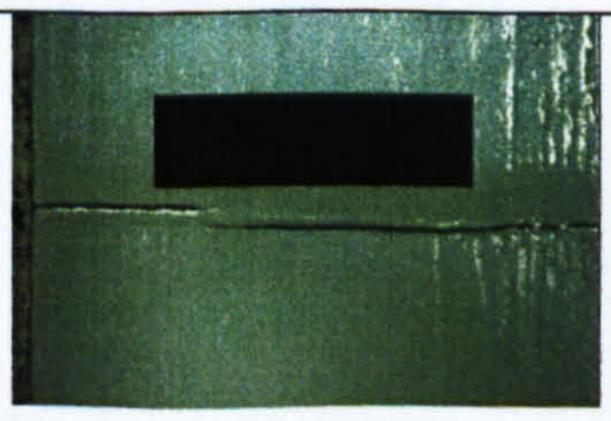	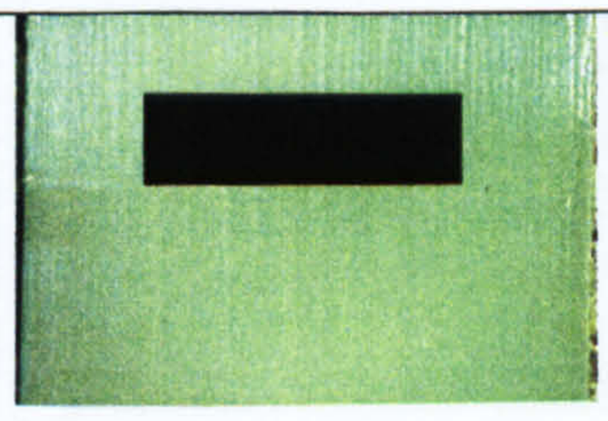

Figure 7.17 Crack view on coating T

	U-1	U-2	U-3
1 mil.	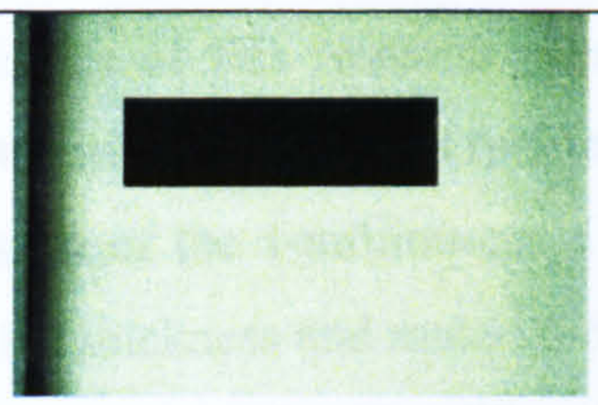	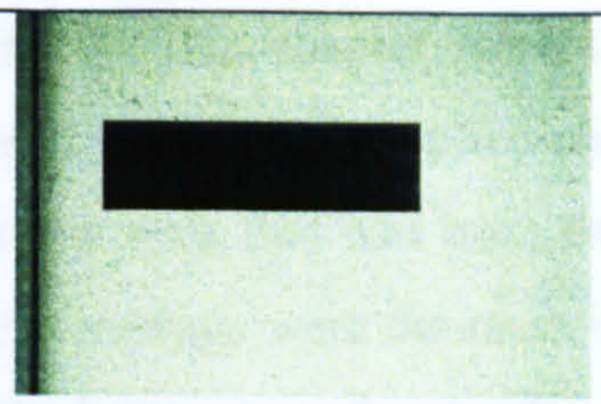	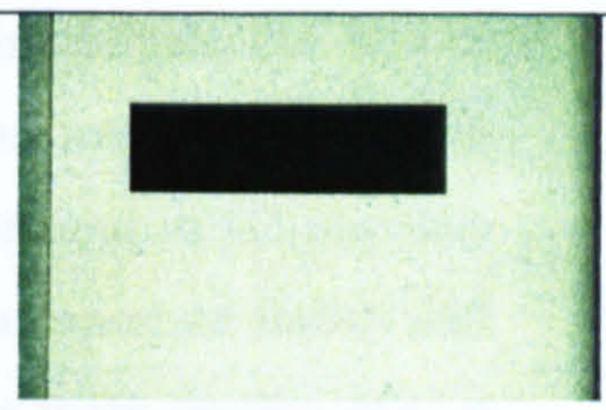
2 mil.	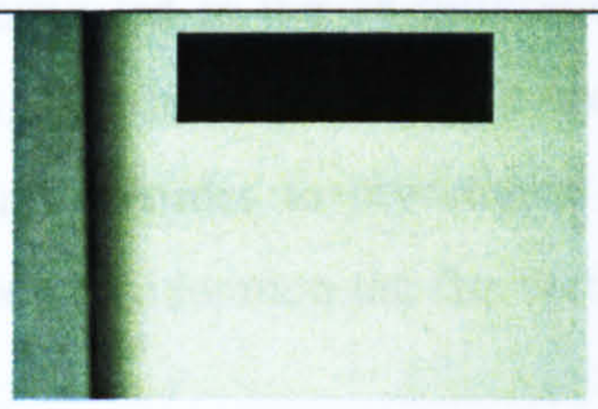	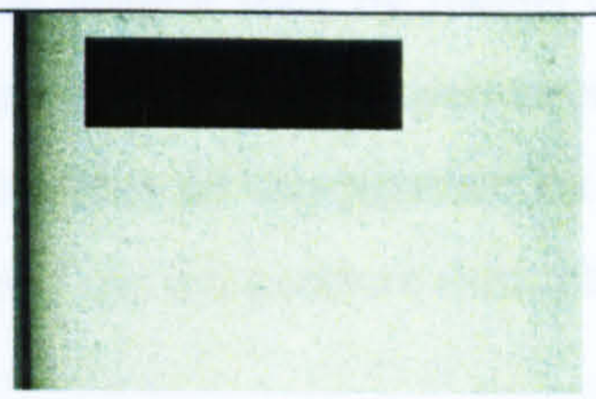	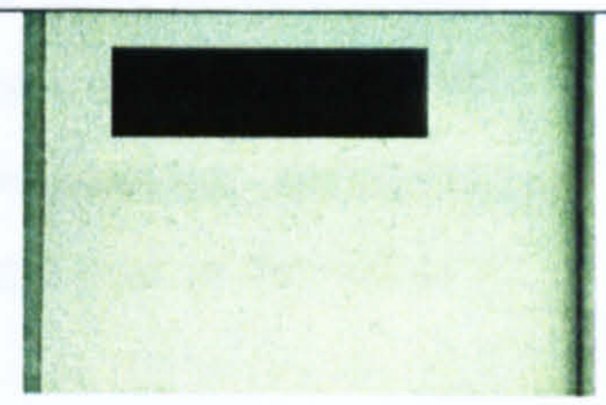
6 mil.	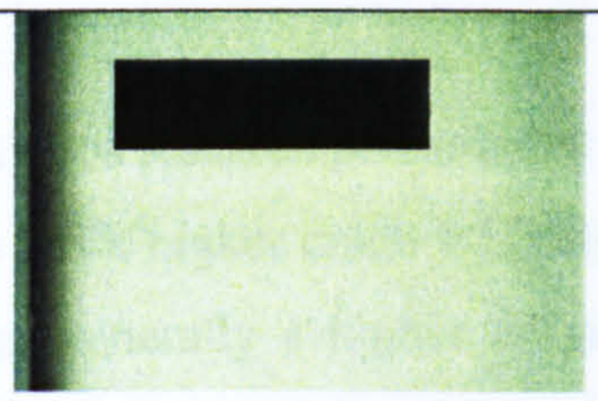	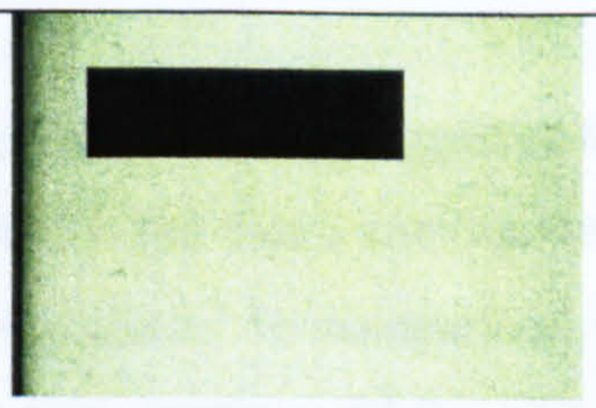	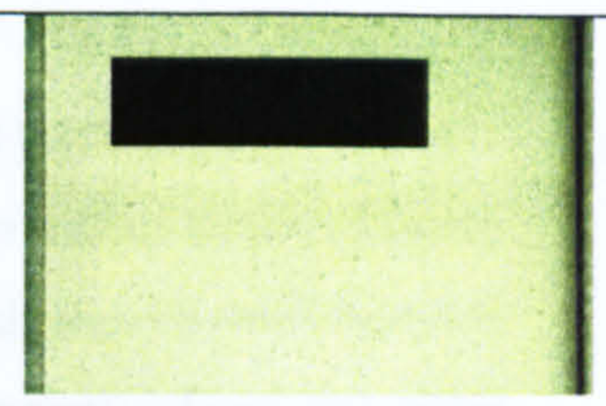
9 mil.	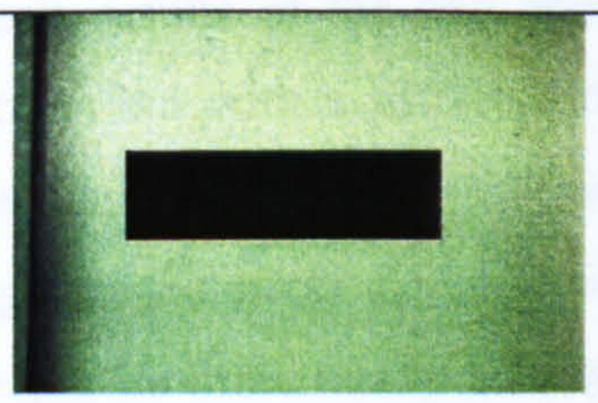	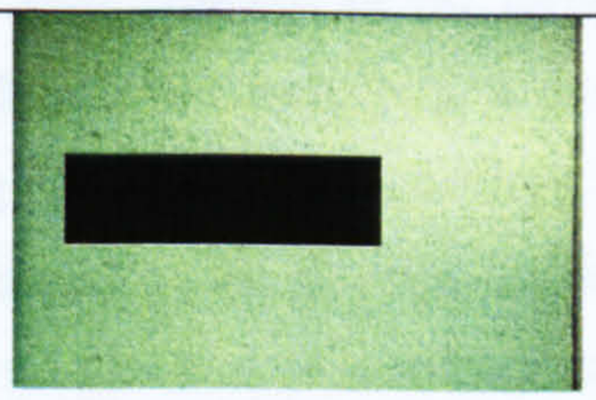	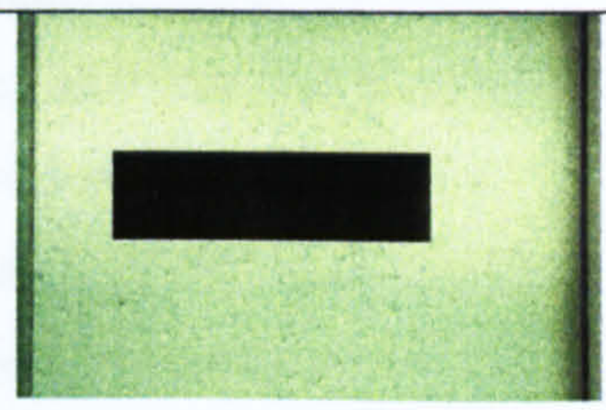
12 mil.	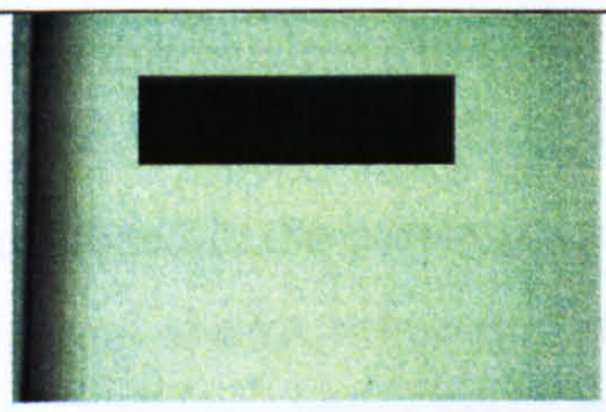	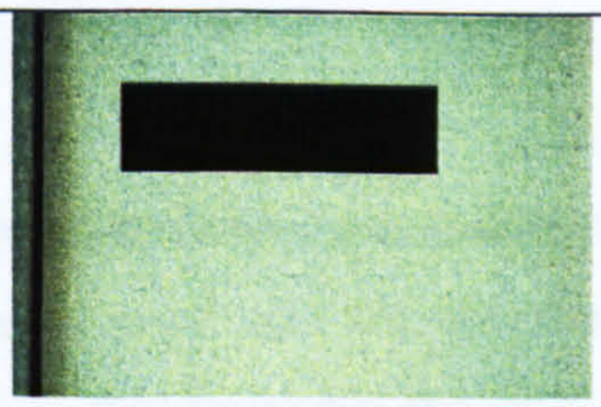	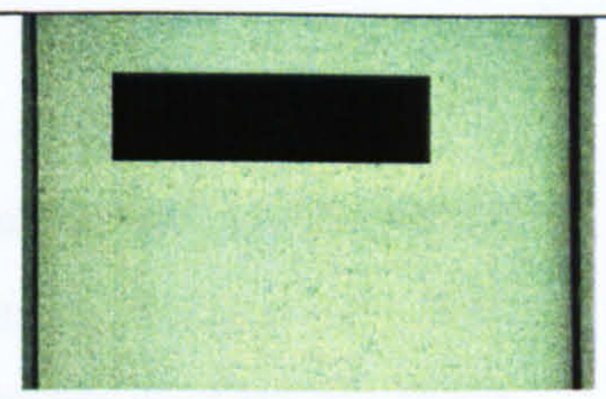
15 mil.	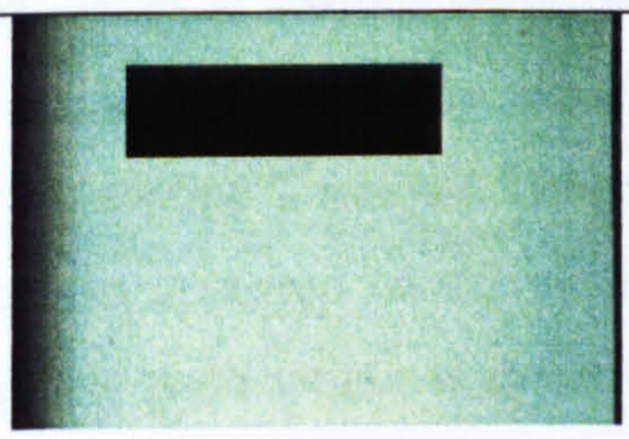	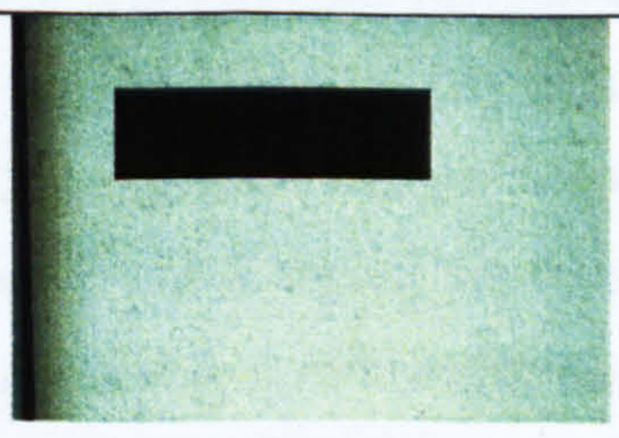	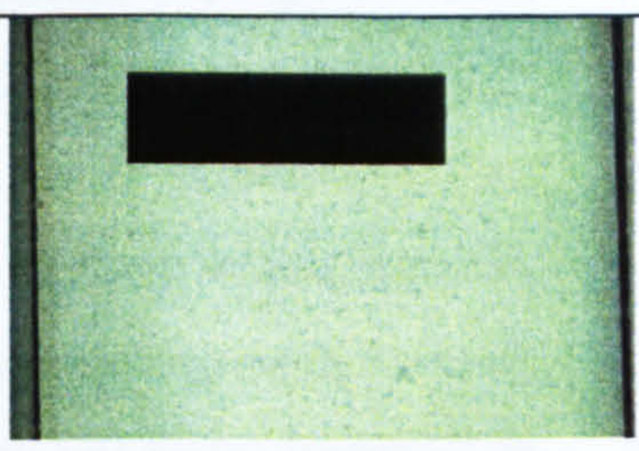
18 mil.	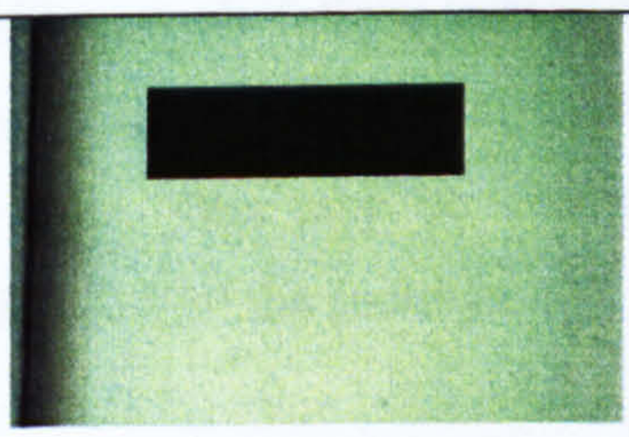	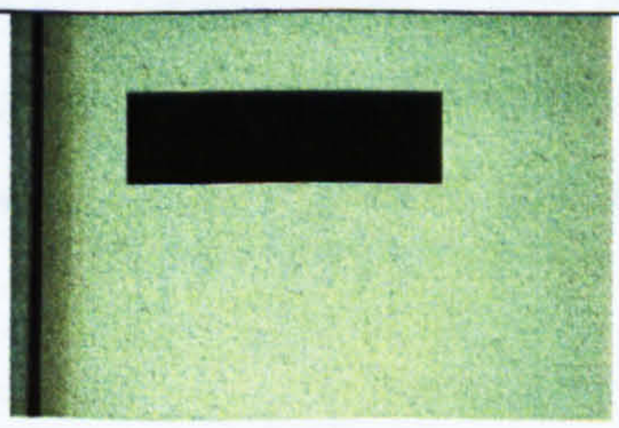	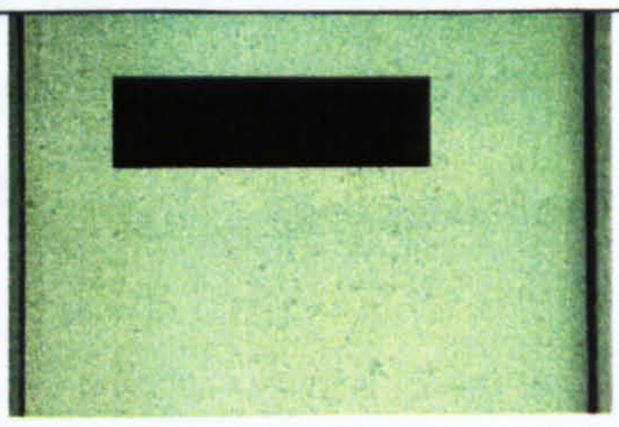

Figure 7.18 Crack view on coating U

7.6 DISCUSSION

The objectives of this research presented in this chapter were to investigate the factors affecting the long-term fatigue resistance of the coatings applied on concrete surfaces. Based on the results of the 1-million-cycle fatigue tests that had been carried out in the previous research, the thickness and material of the coatings were the main two important factors that were investigated in the 18-million-cycle fatigue tests by means of a more precise fatigue apparatus. The tests were conducted at high or low temperatures as well as at a normal temperature in order to investigate the effect of temperature on the coatings' durability, taking into consideration the fluctuation of the temperature throughout a year in the author's country.

In the previous research presented in section 7.3, it was suggested that a coating with a larger thickness has a higher crack-bridging ability and that a coating with a higher crack-bridging ability has generally a higher fatigue resistance. In comparison with the 18-million-cycle fatigue tests results of the two epoxy resin coatings of the same material from the same manufacturer but with a different thickness (P-1 and P-2), it can be said that the fatigue resistance increases with the increasing thickness of the coatings. This can be interpreted as indicating that the stress distribution caused by the movements of cracks in the underlying substrate can be more easily tolerated in the case of a thicker coating, resulting in longer durability of this repair method.

It was concluded in the previous research that fatigue resistance increases with an increasing crack-bridging ability, however, the same trend was not observed in the fatigue tests with extended cycles at various temperatures. For example, the polyurethane coating, T, has a smaller crack-bridging ability of 1.85 than coatings Q (2.65) or R (2.56) as shown in Table 7.5, but the coating T was not damaged throughout the entire fatigue test of 18 million cycles, whilst cracks appeared on the coatings Q and R during the tests. These two coatings had shown pretty good fatigue resistance performance without having almost any cracks during the 1-million-cycle fatigue tests in the previous research, where they had been examined as coatings E and L respectively; however, they were damaged during the present longer fatigue tests. This may be attributable to the different characteristics of the different materials used for the coatings.

For instance, it is known that epoxy resin and PCM are generally susceptible to cold temperature and they become hard in such conditions, resulting in reduced ability to accommodate the substrate crack movements (Swamy and Tanikawa, 1993). The results of the long-term fatigue tests in the present research show that the coatings of both materials, namely epoxy resin and PCM, revealed sudden acceleration of cracking soon after 12 million cycles, when the temperature was changed to -10°C.

Another example might be that it is also known that rubber is more susceptible to heat than other generic materials and that even among the various rubber materials, chloroprene synthetic rubber possesses more susceptibility to heat than other rubbers such as silicone rubber, fluorine rubber, or acrylic rubber. The material is also susceptible to cold. Although the chloroprene synthetic rubber coatings had shown no cracks during the fatigue tests presented in the previous research, the coatings showed accelerating rate of cracking at high and low temperatures in the second and final 6-million-cycle periods (60°C and -10°C) after generating several small spots in the first stage in the present long-term experiment.

In terms of the ability of the coatings to prevent the further penetration of carbonation, the applications of the epoxy resin coating with a smaller thickness (P-1) or the chloroprene synthetic rubber coating (Q) might not be effective since they would lose the barrier property by generating cracks or small spots approximately in only one year according to the fatigue experiment results and Eq (7-2). It can be also inferred that the use of the PCM coating (R) might not be recommended where the temperature is extremely high or cold. It can be suggested that the use of the poly-butadiene (S) or the polyurethane coatings (T or U) would be effective by protecting the concrete from carbon dioxide ingress for over 10 years. However the applications of a thicker chloroprene synthetic rubber or PCM coating might be effective, just as the epoxy resin coating with a larger thickness (P-2) showed a good fatigue resistance.

7.7 CONCLUSIONS

(1) Crack-bridging ability and fatigue resistance of a coating generally increase with the increasing thickness if compared among the coatings of the same material.

(2) The difference in materials of the coatings affects the manner in which the coatings are broken by the repetitive cyclic fatigue stress applied.

(3) The temperature regime to which a coating is exposed may significantly influence the long-term durability under a fatigue condition.

(4) In the case of applications of surface coatings to concrete structures where crack movements can be a significant problem, it is important to determine the appropriate thickness and material of the coating so that it can tolerate the movements of the substrate cracks for the required period.

CHAPTER 8

GENERAL CONCLUSIONS AND RECOMMENDATIONS FOR FUTURE WORK

The aim of the present study, as mentioned in the introductory chapter, was to contribute to the better understanding of the issues underlying the remedial treatment of carbonation-induced corrosion of steel in concrete and to improve the applications of such treatments intended for alleviation of carbonation-induced corrosion as surface-applied corrosion inhibitors and surface coatings. As regards corrosion inhibitors, attempts were made to study the detailed inhibition/migration mechanisms and long-term durability of proposed electrochemical inhibitor injection treatments for carbonated concrete. Work was also carried out to establish a mathematical model, intended to provide a general basis for the prediction of migration of relevant species in the pore solutions of concrete during or after the inhibitor injection treatment. Fatigue tests were also carried out for investigations of the properties of surface coatings crucial for long-term fatigue resistance.

8.1 GENERAL CONCLUSIONS

8.1.1 Electrochemical injection of corrosion inhibitors

From the research described in Chapters 3-6, the electrochemical injection of organic corrosion inhibitors, namely ethanolamine, guanidine, and arginine, into carbonated cementitious material was proved to be capable of allowing inhibitors to penetrate carbonated concrete into the vicinity of embedded steel in adequate concentrations for keeping the steel passivated. The method was also demonstrated to be effective in controlling carbonation-induced corrosion of the steel embedded in concrete when the latter was exposed to cyclic wetting and drying for several months after inhibitor injection treatment. The conclusive statements are presented in the form of giving answers to the issues raised in the introductory chapter (Chapter 1) as follows:

(1) Evidence that inhibitors can stop or at least reduce corrosion rates of steel in concrete that suffers from carbonation

The immersion tests carried out in Chapter 3 showed that the inhibitors, if present at a sufficient concentration in the carbonated electrolytes simulating the pore solutions of

carbonated concrete, could reduce the corrosion rates of the immersed steel. In Chapter 6, the inhibitive ability of the corrosion inhibitors in carbonated concrete was demonstrated by the small corrosion rates of steel observed after the proposed electrochemical treatment.

(2) Inhibitor concentrations required at the steel for its passivation

As described in Chapter 3, the threshold concentration at which each of the three inhibitors studied is inhibitive or corrosive was confirmed by immersing mild steel bars in the solutions at various pH that simulated the pore solutions of carbonated concrete. The concentration value was found to lie between 0.01M and 0.1M for ethanolamine and arginine, and below 0.01M for guanidine, except at a considerably reduced pH value of 7.0.

(3) Method of introducing the required concentrations of corrosion inhibitors at the reinforcing steel

As described in Chapter 4, the amine/alkanolamine-based organic corrosion inhibitors with widely varying dissociation constants studied were effectively injected into fully/partially carbonated cement pastes at depths corresponding to normal cover thickness to reinforcing steel when temporary electrochemical treatments were applied for up to a week at similar current density as applied in the case of electrochemical chloride extraction. The concentration of the inhibitors penetrating to the steel cathode was found to exceed a threshold value required for the steel passivation that had been obtained from the immersion tests. The different inhibitor penetration profiles observed were found to be explicable in terms of the degrees of ionisation of the different inhibitors in carbonated cementitious materials. The injected arginine converted to an anionic form in the highly alkaline cathodic region moved back towards the anode in the electrical field, resulting in a concentration profile having a plateau before the steel cathode.

In the case of applying electrochemical injection of inhibitors to partially carbonated materials, it should be noted that, owing to the poor conductivity of the carbonated region, the effective current density passed through this region is smaller than that applied to the whole surface, which discourages the migration of ionic inhibitors towards the steel. In addition, the current density flowing from carbonated region into non-carbonated region at the boundary between the two regions tended to remove cationic inhibitors from the carbonated region. It can therefore be suggested that the use of the inhibitor whose dominant form is cationic in a neutralised solution and molecular in an alkaline solution, such as

ethanolamine, would be effective when the injection treatment is applied to partially carbonated materials.

The experimentally determined concentration profiles were reasonably simulated by the mathematical model developed in this thesis, which was based on the Nernst-Planck equation, taking account of acid/base dissociation equilibria and solubility products of relevant species, as shown in Chapter 5. The proposed model yielded reasonable agreement with experimentally determined concentration profiles of the organic base corrosion inhibitors of widely different pK_a values. In the cases of ethanolamine and arginine, the model yielded better agreement with the experimental data when molecular interactions were represented by the introduction of an activity coefficient, which raised the apparent pKa' value of the inhibitors. This enhancement in pKa' value also helped to minimise the apparent charge imbalances observed in the experimental data in the cases of ethanolamine and arginine. In the cases of application of this model to partially carbonated material (Chapter 5 Part 2), with the assumption that the material consisted of a network of resistors whose resistance depended on the local porosity and ionic constituents, the current distribution within the material (that is, the lowered current density effectively applied to the carbonated region) was successfully simulated, yielding reasonable prediction of concentrations of species in the material that had been determined by the experiment (Chapter 4 Part 2). The presence of lateral current flow was also simulated by application of the proposed model, and the current flow was found to affect the transport of species in the material. It may thus be inferred that for the practical use of this remedial method, it may be useful beforehand to investigate the distribution of carbonation depth within the concrete in order to minimise the reduced level of the inhibitor injection to the steel bars.

An additional benefit, inferred from the increase in concentration of carbonate ion near the steel cathode after the electrochemical treatment as presented in Chapter 4, was that calcium hydroxide may precipitate in the vicinity of the cathode, contributing to reducing the risk of corrosion by producing a buffer to maintain alkaline conditions around the embedded steel. This precipitation of calcium hydroxide also might be indicated by the increase in film resistance observed in the intermediate frequency range of EIS measurements (Chapter 6). This phenomenon may be encouraged by the increase in pH during the injection treatment with guanidine as derived from mathematical modelling (Chapter 5). As observed in Chapter 4, in addition to the effect of the corrosion inhibitors injected to carbonated concrete, the alkalinity of the pore solution was restored by the migration of hydroxyl ions generated by

reduction of water at the steel cathode. Furthermore, chloride ions present in the pore solution were driven away from the steel by ionic migration. These two phenomena are beneficial in terms of passivation of the steel.

(4) Deleterious side effects that might arise by application of the treatment

As shown in Chapter 4, high alkalinity was generated around the steel cathode by water electrolysis in the electrochemical treatment and this might cause a problem, i.e. ASR (alkali-silica reaction), if the concrete has susceptible aggregates. In the case of application of this treatment to fully carbonated concrete, however, the risk is expected to be reduced when corrosion inhibitors with near neutral pKa values, such as ethanolamine or arginine, are used as the anolyte, since the rise of the pore solution pH at the cathode is restricted due to the deprotonation of such inhibitors migrating towards the cathode. This moderate pH rise was successfully simulated by mathematical modelling detailed in Chapter 5. On the other hand, in the case of application of this treatment to partially carbonated concrete, in spite of the moderate pH rise owing to the deprotonation of inhibitors, the remarkably high concentrations of alkali metal ions induced near the cathode in non-carbonated regions involve the possibility of ASR, similarly as may be observed in ECR (electrochemical chloride removal) treatment, with similar magnitudes of current densities employed.

During the treatment, the dissolution of surface concrete was observed when a nitrate solution was used as anolyte. This was because of the rapid reduction in pH value of the solution due to water electrolysis occurring at the anode. The use of a carbonated solution as anolyte, instead, was found to minimise this surface deterioration owing to its buffering capacity which served to accommodate the generated hydrogen ions.

(5) Durability of the method

The electrochemical monitoring of the embedded steel in carbonated concrete conducted for a reasonably long period after exposure to the electrochemical inhibitor injection showed that the use of ethanolamine and guanidine significantly reduced the corrosion rates and maintained passivation of embedded steel, compared with control specimens. Ethanolamine demonstrated the best performance, which might be attributable to the high concentration of the inhibitor accumulated near the steel. Treatment with arginine caused semi-passivating conditions. EIS measurements in the low frequency range showed reduced values of capacitance in the cases of passivating inhibitors, possibly indicating the adsorption of the inhibitors on the steel surface.

The penetration profiles of the three inhibitors inside the concrete specimens were found to be almost unchanged by 160 days of exposure to a cyclic wet/dry regime after the injection treatment. This may be a reason for the long-term passivation of embedded steel in the case of inhibitor applications. The application of the proposed mathematical model to the simulation of the concentration evolutions of injected inhibitors, however, showed rapid concentration changes due to diffusion, when the pores of carbonated concrete were assumed to be fully saturated. Therefore it was suggested that the partially dry conditions minimised the diffusion or dissipation of the injected inhibitors. This might be a beneficial aspect in applying the proposed injection treatment to carbonated concrete, which has low humidity inside the material. However, longer exposures to more aggressive environmental conditions would be necessary to provide further confirmation of the durability of the inhibitor injection method.

Electrochemical re-alkalisation applied to carbonated concrete in the present research showed a poor long-term passivation effect, and the degree of the effect was similar to that of control specimens. This may be attributable to the dissipation of cathodically generated hydroxyl ions through the highly porous material and to the insufficient total charge applied during the electrochemical treatment.

Anodic polarisation had been expected to be effective for instant determination of steel passivation and for encouraging long-term passivation by the enhanced potential of the steel. It was found that the polarisation was effective for the former purpose, but it showed insignificant effect for the latter purpose.

8.1.2 Fatigue resistance of coatings

In the case of application of surface coatings intended to alleviate the carbonation penetration and carbonation-induced corrosion on such concrete structures as railway viaducts that are exposed to millions of dynamic active loading cycles generated by the passage of trains, fatigue resistance of a coating has an important influence on long-term durability. The objective of the study presented in Chapter 7 was to investigate the factors affecting the long-term fatigue resistance of the coatings applied on concrete surfaces. Fatigue tests with a total of 18 million cycles were conducted at varied temperatures using several coatings of different materials with varied thickness, bridging a moving crack in carbonated concrete specimens.

As a result, it was found that the two properties that significantly affected the fatigue resistance of coatings were their thickness and composition. As regards the former property, the reason may be that the stress distribution caused by the movements of cracks in the underlying substrate was more easily tolerated in the case of a thicker coating. As for the latter property, some materials were observed to be susceptible to the effect of heat (rubber) or cold (epoxy resin, PCM and rubber).

When a surface coating, as a repair method to retard carbonation-induced deterioration processes, is applied to concrete structures where crack movements with significantly large numbers of cycles can be a problem, it is important to determine the appropriate thickness and composition of the coating, taking into consideration the temperature of the environment to which the coating is exposed, so that it can tolerate the movements of the substrate cracks for the required period.

8.2 RECOMMENDATIONS FOR FURTHER WORK

8.2.1 Electrochemical injection of corrosion inhibitors

The study on the electrochemical inhibitor injection method described in Chapter 3-6 revealed features of the mechanism of migration of inhibitors during the injection treatment and the long-term durability of the treatment in terms of the inhibition of the embedded steel in carbonated concrete. However the following points are still unclear and further investigations would be necessary to clarify them:

(1) The interface between the steel cathode and cement matrix needs to be investigated after the electrochemical treatment by means of microscopy in order to obtain direct evidence of the proposed phenomenon whereby calcium carbonate is converted to calcium hydroxide in the vicinity of the steel cathode. It may also be important to investigate the possibility of re-carbonation of this precipitated calcium hydroxide, since the precipitated lime near the steel is expected to reduce the corrosion risk.

(2) There are still some mysteries concerning arginine injection. The inconsistency in concentrations of arginine at the cathode after the injection treatment at $5A/m^2$ that were derived by experiment and mathematical modelling needs to be elucidated by further investigating the appropriate modification of pKa_3' value of the inhibitor. The moment at

which arginine initiated inhibition after the injection treatment was quite late compared with other two inhibitors' cases. The inhibition mechanism of arginine may also need to be clarified.

(3) The long-term durability of electrochemical re-alkalisation needs to be further investigated. The application of the treatment under a combination of a current density and duration which satisfies the required total charge (200Ah/m^2, see subsection 6.3.4) to carbonated concrete with quite high porosity would be interesting.

In addition, the following issues are raised if the electrochemical inhibitor injection treatment is to be practically applied to real structures in the future:

(4) The following properties involved in the electrochemical injection of inhibitors may need to be optimised: concentration of inhibitors to be applied as anolyte, magnitude and duration of current density to be applied. The simulations by means of the proposed mathematical model with the above three properties as the parameters are expected for the optimisation. The clarification of this issue is expected to contribute to the better practical applications of this remedial treatment to real structures that suffer from carbonation-induced reinforcing corrosion.

(5) The proposed mathematical model may need to be developed so that not only the evaporation of the injected inhibitors from the material surface but also the transport of the inhibitors in the dry pores after the injection treatment can be simulated, taking into account the volatility of the inhibitors. This development will help to estimate the long-term durability of the injection method applied under various environmental conditions.

The electrochemical inhibitor injection is planned to be applied to sections of concrete slabs with dimensions of 70cm×150cm×25cm (see Figure 8.1, left) which were taken from a real RC viaduct in Shinagawa, Tokyo, when it was demolished in 2000. The cover depth is 25mm and the bar arrangement is as shown on the right side of Figure 8.1. The chloride-free concrete has been carbonated for more than 40 years since the viaduct was constructed in the early 1960s. Before the treatment, several core samples will be extracted to examine the constituents of the pore solution as well as the carbonation depth and the porosity of the concrete. After the treatment, some sections of the treated concrete will be used for the analyses of the concentrations of relevant species by the same procedure as employed in the

present research (see Chapter 4), and other sections will be used for the investigation of long-term durability by means of electrochemical monitoring and inhibitor re-distribution measurements over a long time scale, similarly as conducted in Chapter 6,.

Figure 8.1 Real concrete slab specimens (left: overview, right: bar arrangement)

8.2.2 Fatigue resistance of coatings

The temperature regime employed in the fatigue tests carried out in Chapter 7 (20°C for the first 6 million cycles, 60°C for the next 6 million cycles, and -10°C for the final 6 million cycles) might be at least reasonable for investigating the factors affecting the long-term fatigue resistance of a coating, but might not be reasonable for the simulation of the environment to which the real concrete structures with coating applications are usually exposed. In addition, other environmental factors than temperature which may lead to the deterioration of coatings under cyclic stress need to be taken into account for the better prediction of the service life of surface coatings. Recommendations for further work on this issue are given as follows:

(1) Fatigue tests need to be carried out under fluctuating temperature characterised by seasonal/daily variations of the local climate.

(2) Simultaneous exposure of the coatings to accelerated illumination by UV rays during the fatigue tests would be interesting.

REFERENCES

Almusallam A., Khan F. M., and Maslehuddin M., 2002, Performance of concrete coatings under varying exposure conditions, Materials and Structures, 35, pp. 487-494.

Alonso C., Andrade C., Argiz C. and Malric B., 1996, Na_2PO_3F as inhibitor of corroding reinforcement in carbonated concrete, Cement and Concrete Research, Vol.26, pp. 405-415.

Alonso C., Andrade C., Izquierdo M., Nóvoa X. R., and Pérez M. C., 1998, Effect of protective oxide scales in the macrogalvanic behaviour of concrete reinforcements, Corrosion Science, 40, pp. 1379-1389.

Andrade C. and González J. A., 1978, Quantitative measurements of corrosion rate of reinforcing steels embedded in concrete using polarization resistance measurements, Materials and Corrosion, 29, pp. 515-519.

Andrade C., Alonso C., and González J. A., 1989, Results of polarization resistance and impedance of steel bars embedded in carbonated concrete contaminated with chlorides, Materials Science Forum, Trans Tech Publications, Switzerland, 44-45, pp. 329-336.

Andrade C., Alonso M. C., and Gonález J. A., 1990, An initial effort to use corrosion rate measurements for estimating rebar durability, "Corrosion Rates of Steel in Concrete", ASTM STP 1065, Berke N. S. et al. Eds. ASTM, Philadelphia, pp. 29-37.

Andrade C., Diez J. M., Alamaan A., and Alonso C., 1995, Mathematical modelling of electrochemical chloride extraction from concrete, Cement and. Concrete Research, 25, pp.727-740.

Andrade C., Soler L., and Nóvoa X. R., 1995, Advance in electrochemical impedance measurements in reinforced concrete, Materials Science Forum, Trans Tech Publications, Switzerland, 192-194, pp. 843-856.

Andrade C., Merino P., Nóvoa X. R., Pérez M. C., and Soler L., 1995, Passivation of reinforcing steel in concrete, Materials Science Forum, Trans Tech Publications, Switzerland, 192-194, pp. 891-898.

Andrade C., Keddam M., Nóvoa X. R., Pérez M. C., Rangel C. M., and Takenouti H., 2001, Electrochemical behaviour of steel bars in concrete: influence of environmental factors and cement chemistry, Electrochemica Acta, 46, pp. 3905-3912.

Andrade C. and Alonso C. with contributions from Gulikers J., Polder R., Cigna R., Vennesland Φ., Salta M., Raharinaivo A., and Elsener B., 2004, Test methods for on-site corrosion rate measurement of steel reinforcement in concrete by means of the polarization resistance method, Materials and Structures, 37, pp. 623-643.

Anstice D. J., 2000, Corrosion inhibitor systems for the rehabilitation of reinforced concrete, Ph.D. thesis, Aston University.

Anstice D. J., Page C. L., and Page M. M., 2005, The pore solution phase of carbonated cement pastes, Cement and Concrete Research, 35, pp.377-383.

Aramaki K., Mizoguchi M., and Nishihara H., 1991, Relationship between the HSAB principle and effects of various anions and a tetra-n-butylammonium ion as a passive film of iron in a borate buffer solution, Journal of the Electrochemical Society, 138, pp. 394-398.

Aramaki K., Tomihari M., Furuya S., Yamaguchi M., and Nishihara H., 1994, The inhibitive effect of organic cations on passive film breakdown of iron in a chloride-containing borate buffer solution, Corrosion Science, 36, pp. 1133-1141.

Asaro M. F., Gaynor A. T., and Hettiarachchi S., 1990, Electrochemical chloride removal and protection of concrete bridge components, National Research Council, Washington DC., Strategic Highway Research Program Report SHRP-S-310, pp. 1-53.

Bard A. J. and Faulkner L. R., 1980, Electrochemical Methods: Fundamentals and Applications, Wiley, New York, pp. 64-67.

Barneyback Jr. R. S. and Diamond S., 1981, Expression and analysis of pore fluids from hardened cement pastes and mortars, Cement and Concrete Research, 11, pp.279-285.

Batis G., Pantazopoulou P., and Routoulas A., 2003, Corrosion protection investigation of reinforcement by inorganic coating in the presence of alkanolamine-based inhibitor, Cement and Concrete Composites, 25, pp. 371-377.

Bentur A., Diamond S., and Berke N. S. (Eds.), 1997, Steel corrosion in concrete: fundamentals and civil engineering practice, Modern Concrete Technology; 6, E & FN Spon, pp. 118-123.

Bertolini L., Yu S.W., and Page C.L., 1996, Effects of electrochemical chloride extraction on chemical and mechanical properties of hydrated cement paste, Advances in Cement Research, 8, No.31, July, pp. 93-100.

Bertolini L., Elsener B., Pedeferri P., and Polder R., 2004, Corrosion of Steel in Concrete: Prevention, Diagnosis, Repair, Wiley, New York, pp. 38-39, 71-77, 369-373.

Bjegović D., Sipos L., Ukrainczyk V., and Mikšić B., 1994, Diffusion of MCI 2020 and 2000 corrosion inhibitors into concrete, in: Proceedings of International Conference on Corrosion and Corrosion Protection of Steel in Concrete, Sheffield Academic Press, Sheffield, Swamy R. N. (Ed.), pp. 865-877.

Blauwhoff P. M. M., Versteeg G. F., and van Swaaij W. P. M, 1984, A study on the reaction between CO_2 and alkanolamines in aqueous solutions, Chemical Engineering Science, 39, pp. 207-225.

Brasher D. M., 1969, Stability of oxide film on metals in relation to inhibition of corrosion, British Corrosion Journal, 4, pp. 122-128.

British Standard Institute: BS 812-103.1, 1985, Testing aggregates, Part 103: Methods for determination of particle size distribution, Section 103.1 Sieve tests.

British Standard Institute: BS 882, 1992, Specification for aggregates from natural sources for concrete.

British Standards EN 1062-6:2002, 2002, Paints and varnishes - Coating materials and coating systems for exterior masonry and concrete – Part 6: Determination of carbon dioxide permeability.

British Standards EN 1062-7:2004, 2004, Paints and varnishes - Coating materials and coating systems for exterior masonry and concrete – Part 7: Determination of crack bridging properties, British Standards, London.

Brouwers H.J.H. and van Eijk R.J., 2003, Alkali concentration of pore solution in hydrating OPC, Cement and Concrete Research No. 33, pp. 191-196.

Brown J. G. and Glynn P. D., 2003, Kinetic dissolution of carbonates and Mn oxides in acidic water: measurement of in situ field rates and reactive transport modeling, Applied Geochemistry, 18, pp. 1225-1239.

Bürchler D., Elsener B., and Böhni H., 1996, Electrical resistivity and dielectric properties of hardened cement paste and mortar, Materials Research Society Symposium – Proceedings, Vol. 411, Electrically Based Microstructural Characterization, pp. 407-412.

Buenfeld N. R., Glass G. K., Hassanein A. M., and Zhang J-Z., 1998, Chloride transport in concrete subjected to an electric field, Journal of Materials in Civil Engineering, 10, pp. 220-228.

Canham I., Page C. L., and Nixon P. J., 1987, Aspects of the pore solution chemistry of blended cements related to the control of alkali silica reaction, Cement and Concrete Research, 17, pp. 839-844.

Cansell F., Chevalie B., Demourgues A., Etourneau J., Even C., Garrabos Y., Pessey V., Petit S., Tressaud A., and Weill F., 1999, Supercritical fluid processing: a new route for materials synthesis, Journal of Materials Chemistry, 9, pp. 67-75.

Carnot A., Frateur I., Zanna S., Tribollet B., Dubois-Brugger I., and Marcus P., 2003, Corrosion mechanisms of steel concrete moulds in contact with a demoulding agent studied by EIS and XPS, Corrosion Science, 45, pp. 2513-2524.

CEN, 2000, Electrochemical re-alkalisation, chloride extraction treatments for reinforced concrete – Part 1 Re-alkalisation, prEN 14038-1: 2000.

Clegg S. L. and Brimblecombe P., 1989, Solubility of ammonia in pure aqueous and multicomponent solutions, Journal of Physical Chemistry, 93, pp. 7237-7248.

Concrete Repair Standards News – Latest news on new British Standards for concrete repair, 2005, Concrete repair association, http://www.concreterepair.org.uk.

COST (European cooperation in the field of scientific and technical research), 2003, Corrosion of steel in reinforced concrete structures, Final report, COST Action 521, EC publication, pp. 141-148.

David W. S. and Harrison R. S., 1990, Influence of surface coatings on carbonation of concrete, Journal of Materials in Civil Engineering, 2, pp. 35-44.

Davies C. W., 1962, Ion Association, Butterworths, London, pp. 34-54.

Dawson J. L., Callow L. M., Hladky K., and Richardson, J. A., 1978, Use of electrochemical impedance measurements applied to the corrosion of reinforcing steel in concrete, Corrosion '78, Paper No. 125, NACE, Houston, 1978.

Dawson J. L., John D. G, Jafar M. I., Hladky K., and Sherwood L., 1990, Electrochemical methods for the inspection and monitoring of corrosion of reinforcing steel in concrete, Corrosion of Reinforcement in Concrete, Page C. L., Treadaway K., and Bamforth P. (Eds.), Elsevier, London: Published for the Society of Chemical Industry by Elsevier Applied Science, pp. 358-371.

Delucchi M., Barbucci A., Temtchenko T., Poggio T., and Cerisola G., 2002, Study of the crack-bridging ability of organic coatings for concrete: analysis of the mechanical behaviour of unsupported and supported films, Progress in Organic Coatings, 44, pp. 261-269.

Delucchi M., Barbucci A. and Cerisola G., 2004, Crack-bridging ability of organic coatings for concrete: influence of the method of concrete cracking, thickness and nature of the coating, Progress in Organic Coating, 49, pp. 336-341.

De Shutter G., 1999, Quantification of the influence of cracks in concrete structures on carbonation and chloride penetration, Magazine of Concrete Research, 51, pp. 427-435.

Draft for Development ENV 1504-9:1997, 1997, Products and systems for the protection and repair of concrete structures – Definitions, requirements, quality control and evaluation of conformity, Part 9: General principles for the use of products and systems, European Prestandard, Brussels.

Elsener B., Molina M., Böhni H., 1993, The electrochemical removal of chlorides from reinforced concrete, Corrosion science, 35, pp. 1563-1570.

Elsener B., Wojtas H., and Böhni H., 1994, Galvanostatic pulse measurements – rapid on site corrosion monitoring, Corrosion and Corrosion Protection of Steel in Concrete, Sheffield Academic Press, Vol. 1, pp. 236-246.

Elsener B., Büchler M., Stalder F., and Böhni H., 1999, Migrating corrosion inhibitor blend for reinforced concrete: Part 1 – Prevention of corrosion, Corrosion, 55, pp. 1155-1163.

Elsener B., Buchler M., Stalder F., and Böhni H., 2000, Migrating corrosion inhibitor blend for reinforced concrete: Part 2 – Inhibitor as repair strategy, Corrosion, 56, pp. 727-732.

Elsener B. (Ed.), 2001, Corrosion inhibitors for steel in concrete – State of the art report, European Federation of Corrosion Publications, No. 35, Maney Publishing on behalf of The Institute of Materials, London, p38.

European Standard EN 1504-2, 2004, British Standards Institution, London.

Fedrizzi L., Azzolini F., and Bonora P. L., 2005, The use of migrating corrosion inhibitors to repair motorway's concrete structures contaminated by chlorides, Cement and Concrete Research, 35, pp. 551-561.

Feliu V, González J. A., Andrade C., and Feliu S., 1998, Equivalent circuit for modelling the steel-concrete interface. I. Experimental evidence and theoretical predictions, Corrosion Science, 40, pp. 975-993.

Feliu V, González J. A., Andrade C., and Feliu S., 1998, Equivalent circuit for modelling the steel-concrete interface. II. Complications in applying the Stern-Geary equation to corrosion rate determinations, Corrosion Science, 40, pp. 995-1006.

Fold S. J., Shane J. D., and Mason T. O., 1998, Assignment of features in impedance spectra of the cement-paste/steel system, Cement and Concrete Research, 28, pp. 1737-1751.

Gaidis J. M. and Rosenberg A. M., 1979, The mechanism of nitrite inhibition of chloride attack on reinforcing steel in alkaline aqueous environments, Materials Performance, 18 (11), pp. 45-48.

Garrabrants A.C., Sanchez F., and Kosson D.S., 2004, Changes in constituent equilibrium leaching and pore water characteristics of a Portland cement mortar as a result of carbonation, Waste Management, 24, pp. 19-36.

Gilroy D. and Mayne J. E. O., 1965, The oxidation of iron at room temperature, Corrosion Science, 5, pp. 55-58.

Glass G. K., Page C. L., and Short N. R., 1991, Factors affecting the corrosion rate of steel in carbonated mortars, Corrosion Science, 32, pp. 1283-1294.

Glass G. K., and Buenfeld N. R., 2000, The inhibitive effects of electrochemical treatment applied to steel in concrete, Corrosion Science, 42, pp. 923-927.

Glasser F. P., 1993, Chemistry of cement-solidified waste forms. In RD. Spence Chemistry, Microstructure of Solidified Waste Forms. Lewis Publishers, Baton Rouge, LA, pp. 1-40.

González J. A., Algaba S., and Andrade C., 1980, Corrosion of reinforcing bars in carbonated concrete, British Corrosion Journal, 15, pp. 135-139.

González J. A., Molina A., Escudero M. L., and Andrade C., 1985, Errors in the electrochemical evaluation of very small corrosion rates – I. Polarization resistance method applied to corrosion of steel in concrete, Corrosion Science, 25, pp. 917-930.

González J. A., Molina A., Escudero M. L., and Andrade C., 1985, Errors in the electrochemical evaluation of very small corrosion rates – II. Other electrochemical techniques applied to corrosion of steel in concrete, Corrosion Science, 25, pp. 519-530.

González J. A., Miranda J. M., Birbilis N., and Feliu S., 2005, Electrochemical techniques for studying corrosion of reinforcing steel: Limitations and advantages, Corrosion, 61, pp. 37-50.

Gowers K. R. and Millard S. G., 1999, Electrochemical techniques for corrosion assessment of reinforced concrete structures, Proceedings of the Institution of Civil Engineers, Structures and Buildings, 134, pp. 129-137.

Granata R. D., Santiesteban P. C., and Leidheiser H. Jr., 1986, Mechanism for corrosion inhibition by carboxylates, Proceedings of an International Symposium Honoring Doctor Norman Hackerman on his Seventy-Fifth Birthday: Surfaces, Inhibition, and Passivation, Held at the 170th Meeting of the Electrochemical Society, San Diego, 86-87, pp. 69-81.

Grounds T., Midgley H. G., and Nowell D. V., 1988, Carbonation of ettringite by atmospheric carbon dioxide, Thermochemica Acta, 135, pp. 347-352.

Hachani L., Carpio J., Fiaud C., Raharinaivo A., and Triki E., 1992, Steel Corrosion in concretes deteriorated by chlorides and sulfates: Electrochemical study using impedance spectrometry and "Stepping down the current" method, Cement and Concrete Research, 22, pp. 56-66.

Hancock P. and Mayne J. E. O., 1957, Anodic polarisation as a possible rapid method of deciding whether a given solution is corrosive or inhibitive, Journal of Applied Chemistry, No. 7, pp. 700-708.

Hassanein A. M., Glass G. K., and Buenfeld N. R., 1998, A mathematical model for electrochemical removal of chloride from concrete structures, Corrosion, 54, pp. 323-332.

Hassanein A. M., Glass G. K., and Buenfeld N. R., 1999, Chloride removal by intermittent cathodic protection applied to reinforced concrete in the tidal zone, 1999, Corrosion, 55, pp. 840-850.

Haynes M. and Malric B., 1997, Use of migratory corrosion inhibitors, Construction Repair, (July/August), 10.

Hettiarachchi S. and Gaynor A. T., 1992, Corrosion inhibitors for rebar corrosion control, Materials Performance, 31, 3, pp. 62-66.

Hladky K., Callow L. M., and Dawson J. L., 1980, Corrosion rates from impedance measurements: An introduction, British Corrosion Journal, 15, pp. 20-25.

Hoar T. P., 1937, The corrosion of tin in nearly neutral solutions, Transactions of the Faraday Society, 33, pp. 1152-1167.

Holloway L., Narin K., and Forsyth, M., 2004, Concentration monitoring and performance of a migratory corrosion inhibitor in steel-reinforced concrete, Cement and Concrete Research, 34, pp. 1435-1440.

Hondel, A. W. M. Van den, and Polder R. B., 1998, Laboratory investigation of electrochemical re-alkalisation of reinforced concrete, Eurocorr' 98, European Federation of Corrosion, Utrecht, 28 September- 1 October 1998 (CD-ROM).

Hong. Sung-Yoon and Glasser F.P., 1999, Alkali binding in cement pastes, Part I. The C-S-H phase, Cement and Concrete Research 29, pp. 1893-1903.

Hundsdorfer W. H., 2003, Numerical solution of time-dependent advection-diffusion-reaction equations, Hundsdorfer W. H. and Verwer J., (Eds.), Springer, London, Chapter 3.

Ibrahim M., Al-Gahtani A. S., Maslehuddin M., and Dakhil F. H., 1999, Journal of Materials in Civil Engineering, 11, pp. 36-40.

Jamil H. E., Montemor M. F., Boulif R., Shriri A., and Ferreira M. G. S., 2003, An electrochemical and analytical approach to the inhibition mechanism of an amino-alcohol-based corrosion inhibitor for reinforced concrete, Electrochemica Acta, 48, pp. 3509-3518.

Jamil H. E., Shriri A., Boulif R., Montemor M. F., and Ferreira M. G. S., 2005, Corrosion behaviour of reinforcing steel exposed to an amino-alcohol-based corrosion inhibitor, Cement and Concrete Composites, 27, pp. 671-678.

Japan Concrete Institute: JCI-SC1, 1987, Method and standard for evaluation of steel corrosion in concrete (Japanese only), pp. 1-4.

Japanese Industrial Standard: JIS A 5005, 1993, Crushed stone and manufactured sand for concrete.

Japanese Industrial Standard: JIS A 5308, 1998, Ready-mixed concrete.

Jazairi B. E. and Berke N. S., 1990, The use of calcium nitrite as a corrosion inhibiting admixture to steel reinforcement in concrete, Page C. L., Treadaway K. W. J., and Bamforth P. B. (Eds.), Corrosion of Reinforcement in Concrete, Elsevier, London, pp. 571-585.

JIS A 1436, 1991, Test methods for movement capability of coatings and sheets fully adhered on substrate, Japan Industrial Standards Committee, Tokyo (Japanese only).

John D. G., Searson P. C., and Dawson J. L., 1981, Use of AC impedance technique in studies on steel in concrete in immersed conditions, British Corrosion Journal, 16, pp. 102-106.

Joiret S., Keddam M., Nóvoa X. R., Pérez M. C., Rangel C., and Takenouti H., 2002, Use of EIS, ring-disk electrode, EQCM and Raman spectroscopy to study the film of oxides formed on iron in 1M NaOH, Cement and Concrete Composites, 24, pp. 7-15.

Jones R., 1998, New process converts ordinary cements into low cost advanced composites, Materials Technology, 13 (3), pp. 104-106.

Jones R. and Tingley L., 1999, Environmentally beneficial alternatives to thermoplastics and composites, in: Proceedings of the 6th Meeting on Supercritical Fluids, Chemistry and Materials, Nottingham, edited by Poliakoff M., George M. W., and Howdle S. M., pp. 65-70.

JSCE-K 532-1999, 1999, Test methods for crack-bridging-ability of surface coatings, Japan Society of Civil Engineers, Tokyo (Japanese only).

Kaesche H. and Hackerman N., 1958, Corrosion inhibition by organic amines, Journal of the Electrochemical Society, 105, pp. 191-198.

Keddam M., Takanouti H., Nóvoa X. R., Andrade C., and Alonso C., 1997, Impedance measurement on cement paste, Cement and Concrete Research, 27, pp. 1191-1201.

Klopfer H., 1978, The carbonation of external concrete and the control of it, Bautenshutz und Bausanierung.

Konno H., Nanri Y., and Kitamura M., 2002, Crystallisation of aragonite in the causticizing reaction, Powder Technology, 123, pp. 33-39.

Kubo J., Sawada S., Page C. L., and Page M. M., 2007, Electrochemical injection of organic corrosion inhibitors into carbonated cementitious materials: Part II – Mathematical modelling, Corrosion Science, 49, pp. 1205-1227.

Larsen, C.K., 1998, Chloride binding in concrete: Effect of surrounding environment and concrete composition, Doctoral Thesis, The Norwegian University of Science and Technology, Trondheim, p. 61

Lasia A., 1999, Modern aspects of electrochemistry, In: Conway B. E., Bockris J. O'. M., and White R. E. (Eds.), Kluwer Academic, New York.

Lee H. J., 2003, Ordinary and partial difference equation routines in C, C++, Fortran, Java, Maple, and MATLAB, Lee H. J. and Schiesser W. E., (Eds.), CRC Press, Boca Raton, Florida, Chapter 4.

Lemoine L., Wenger F., and Galland J., 1990, Study of the corrosion of concrete reinforcement by electrochemical impedance measurement, ASTM Technical Publication, 1065, pp. 118-133.

Li L. Y. and Page C. L., 1998, Modelling of chloride extraction from concrete: influence of ionic activity coefficients, Computational Materials Science, 9, pp. 303-308.

Li L. Y. and Page C. L., 1998, Mathematical modelling of electrochemical chloride removal from concrete, in: de Borst R. et al. (Eds.), Computational Modelling of Concrete Structures, Balkema, Rotterdam/Brookfield, pp. 497-503.

Li L. Y. and Page C. L., 2000, Finite element modelling of chloride removal from concrete by an electrochemical method, Corrosion Science, 42, pp. 2145-2165.

Lide D. R. (Ed.), 2006, Handbook of Chemistry and Physics, 87th edition, CRC Press, Boca Raton, Florida, 5.72, 5.76-5.78, 8.41-8.52, 8.119-8.121.

Longuet P., Burglen P., and Zellwer A., 1973, Phase liquid du ciment hydrate (The liquid phase of hydrated cement), Materiaux de Construction et Travaux Publics, 676, pp. 35-41.

MacDonald J. R. (Ed.), 1987, Impedance spectroscopy: Emphasizing solid materials and systems, Wiley, New York, pp. 20-26, 56-61.

MacDonald J. R., 1992, Impedance spectroscopy, Annals of Biomedical Engineering, 20, pp. 289-305.

Maedar U., 1994, A new class of corrosion inhibitors, Corrosion and Corrosion Protection of Steel in Concrete, Swamy R. N., Ed., Proceedings of International Conference held at the University of Sheffield, Sheffield Academic Press, pp. 851-864.

Maitra A., Singh G., and Chakraborty B. B., 1983, Study of corrosion inhibitor/stimulator characteristics of guanidine derivatives, British Corrosion Journal, 18, pp. 152-155.

Maitra A., Singh G., and Chakraborty B. B., 1984, Adsorption kinetics and inhibition by some guanidine derivatives during corrosion of pure iron in neutral aqueous solutions, 1984, Proceedings – International Congress on Metallic Corrosion, Natl Research Council of Canada, Toronto, pp. 120-124.

Mansfeld F., Kendig M. W., and Lorenz W. J., 1985, Corrosion inhibition in neutral, aerated media, Journal of the Electrochemical Society, 132, pp. 290-296.

Mansfeld F., 1990, Electrochemical impedance spectroscopy (EIS) as a new tool for investigating methods of corrosion protection, Electrochemica Acta, 35, pp. 1533-1544.

Marcotte T. D., Hansson C. M., and Hope B. B., 1999, The effect of electrochemical chloride extraction treatment on steel-reinforced mortar: Part 2 – Microstructural characterisation, Cement and Concrete Research, 29, pp. 1561-1568.

Mayne J. E. O. and Page C. L., 1974, Inhibition of the corrosion of iron by benzoate and acetate ions, British Corrosion Journal, 9, pp. 223-226.

McCafferty E. and Hackerman N., 1972, Double layer capacitance of iron and corrosion inhibition with polymethylene diamines, Journal of the Electrochemical Society, 119, pp. 146-154.

Midgley, H.G. and Illston, J.M., 1984, The penetration of chlorides into hardened cement pastes, Cement and Concrete Research, Vol. 14, No.4, pp. 546-558

Mietz J., 1995, Electrochemical re-alkalisation for rehabilitation of reinforced concrete structures, Materials and Corrosion, No. 46, pp. 527-533.

Mietz J. (Ed.), 1998, Electrochemical rehabilitation methods for reinforced concrete structures – A state of the art report, European Federation of Corrosion Publications, No. 24, Maney Publishing on behalf of The Institute of Materials, London, pp. 9-34.

Montemor M. F., Simóes A. M. P., Salta M. M., and Ferreira M. G. S., 1995, Carbonation of fly-ash-containing concrete: Electrochemical studies, Material Science Forum, Trans Tech Publications, Switzerland, 192-194, pp. 867-876.

Montemor M. F, Simóes A. M. P., and Salta M. M., 2000, Effect of fly ash in concrete reinforcement corrosion studied by EIS, Cement and Concrete Composites, 22, pp. 175-185.

Newman J. S., 1973, Electrochemical Systems, Prentice-Hall, Englewood Cliffs, NJ.

Ngala V. T. and Page C. L., 1997, Effects of carbonation on pore structure and diffusional properties of hydrated cement pastes, Cement and Concrete Research, 27, pp. 995-1007.

Ngala V. T., Page C. L., and Page M. M., 2002, Corrosion inhibitor systems for remedial treatment of reinforced concrete. Part 1: calcium nitrite, Corrosion Science, 44, pp. 2073-2087.

Ngala V. T., Page C. L., and Page M. M., 2003, Corrosion inhibitor systems for remedial treatment of reinforced concrete. Part 2: sodium monofluorophosphate, Corrosion Science, 45, pp. 1523-1537.

Ngala V. T., Page C. L., and Page M. M., 2004, Investigations of an ethanolamine-based corrosion inhibitor system for surface treatment of reinforced concrete, Materials and Corrosion, 55, No.7, pp. 511-519.

Nishikawa T., Suzuki K., Ito S., Sato K., and Takebe T., 1992, Decomposition of synthesized ettringite by carbonation, Cement and Concrete Research, 22, pp. 6-14.

Noye J. (Ed.), 1982, Numerical solutions of partial differential equations, Elsevier North-Holland, pp. 9-34.

Page C. L., 1970, The mechanism of inhibition of the corrosion of iron in aqueous solutions, Ph.D. thesis, Cambridge University.

Page C. L. and Mayne J. E. O., 1972, The anomalous effect of concentration on inhibition of the corrosion of iron by solutions of sodium benzoate, Short communication, Corrosion Science, 12, pp. 679-681.

Page C. L., 1975, Mechanism of corrosion protection in reinforced concrete marine structures, Nature, Vol. 258, pp. 514-515.

Page C. L. and Treadaway K. W. J., 1982, Aspects of the electrochemistry of steel in concrete, Nature, 297, pp. 105-115.

Page C. L. and Vennesland Φ., 1983, Pore solution composition and chloride binding capacity of silica-fume cement pastes, Materials and Structures, 16, No.91, pp. 19-25.

Page C. L., Yu S. W., and Bertolini L., 1994, Some potential side-effects of electrochemical chloride removal from reinforced concrete, Proceedings of UK Corrosion and Eurocorr 94, Vol. 3, The Institute of Materials, London, pp. 228-238.

Page C. L. and Yu S. W., 1995, Potential effects of electrochemical desalination of concrete on alkali-silica reaction, Magazine of Concrete Research, 47, pp. 23-31.

Page C. L., 1997, Cathodic protection of reinforced concrete: principles and applications, in Blankvoll A. (Ed.), Proc. Int. Conf. "Repair of Concrete Structures", Svolvaer, Norwegian Public Roads Administration, Oslo, pp. 123-131.

Page C. L., Ngala V. T., and Page M. M., 2000, Corrosion inhibitors in concrete repair systems, Magazine of Concrete Research, 52, No.1, pp. 25-37.

Page C. L., 2000, Aspects of the performance of corrosion inhibitors applied to reinforced concrete, Proceedings of 9th European Symposium on Corrosion Inhibitors, Ann. Univ. Ferrara, New Series, Sez. V., Suppl. N. 11, Vol. 1, pp. 261-276.

Page C. L., 2002, Application of electrochemical techniques for maintenance of corroding reinforced concrete structures, in: Proceedings of the first fib congress 2002 on Concrete Structures in the 21st Century, Osaka, Vol. 1, pp. 147-158.

Page M. M., Page C. L., Ngala V. T., and Anstice D. J., 2002, Ion chromatographic analysis of corrosion inhibitors in concrete, Construction and Building Materials, 16, pp. 73-81.

Page M. M., Page C. L., Shaw S., and Sawada S., 2005, Ion Chromatographic analysis of amines, alkanolamines, and associated anions in concrete, Journal of Separation Science, 28, pp.471-476.

Pagenkopf G. K., 1978, Introduction to Natural Water Chemistry, Dekker, New York, pp. 94-111.

Pajkossy T., 1994, Impedance of rough capacitive electrodes, Journal of Electrochemical Chemistry, 364, pp. 111-125.

Parrott L. J., 1987, A review of carbonation in reinforced concrete, British Cement Association Report C/1-0987.

Parrott L. J., 1994, A study of carbonation-induced corrosion, Magazine of Concrete Research, 46, pp. 23-28.

Parrott L. J., 1990, Damage caused by carbonation of reinforced concrete, Materials and Structures/ Materiaux et Constructions, 23, pp. 230-234.

Phanasgaonkar A., Cherry B., and Forsyth M., 1996, Corrosion inhibition properties of organic amines in a simulated concrete environment: Mechanism and time dependency of inhibition, Proceedings of the International Conference on Understanding Corrosion Mechanisms in Concrete – A Key to Improving Infrastructure Durability, Cambridge, MA, Section 6, p. 6.

Phanasgaonkar A., Cherry B., and Forsyth M., 1997, Organic corrosion inhibitors; How do they inhibit and can they really migrate through concrete?, in: Concrete & Prevention 1997, Paper No. 054, Brisbane.

Phanasgaonkar A., Cherry B., and Forsyth M., 2000, Protection of reinforcement in concrete by combining surface applied migratory corrosion inhibitors with electric field, in: Corrosion & Prevention, Paper No. 024, Auckland.

Ping G., Elliott S., Hristova R., Beaudoin J. J., Brousseau R., and Baldock B., 1997, A study of corrosion inhibitor performance in chloride contaminated concrete by electrochemical impedance spectroscopy, ACI Materials Journal, 94, pp. 385-395.

Pitzer K. S., 1987, A thermodynamic model for aqueous solutions of liquid-like density, Reviews in Mineralogy, 17, pp. 97-142.

Pitzer K. S., 1991, Activity Coefficients in Electrolyte Solutions, 2nd ed., Pitzer K. S., Ed., CRC Press, Boca Raton, FL, pp. 75-153.

Plummer L. N., Wigley T. M. L., and Parkhurst D. L., 1978, The kinetics of calcite dissolution in CO_2-water systems at 5°C to 60°C and 0.0 to 1.0 atm CO_2, American Journal of Science, 278, pp. 179-216.

Purnell P, Short N. R., and Page C. L., 2001, Super-critical carbonation of glass-fibre reinforced cement. Part 1: mechanical testing and chemical analysis, Composites Part A: applied science and manufacturing, 32, pp. 1777-1787.

Qian S. and Cusson D., 2004, Electrochemical evaluation of the performance of corrosion-inhibiting system in concrete bridges, Cement and Concrete Composites, 26, pp. 217-233.

Randles J. E. B., 1947, Kinetics of rapid electrode reactions, Discussions of the Faraday Society, No. 1, pp. 11-50.

Ravichandran R. and Rajendran N., 2005, Electrochemical behaviour of brass in artificial seawater: effect of organic inhibitors, Applied Surface Science, 241, pp. 449-458.

Richardson M. G., 2002, Fundamentals of Durable Reinforced Concrete, Spon, London, p. 84.

Robinson R. A. and Stokes R. H., 1965, Electrolyte Solutions, 2nd ed. (revised), Academic Press, Inc., New York, pp. 133-173.

Rozenfeld I. L., 1981, Corrosion inhibitors, McGraw-Hill International Book Company, pp. 133-138.

Sagoe-Crentsil K. K., Glasser F. P., and Irvine J. T. S., 1992, Electrochemical characteristics of reinforced concrete corrosion as determined by impedance spectroscopy, British Corrosion Journal, 27, pp. 113-119.

Samson E., Lemaire G., Marchand J., and Beaudoin J. J., 1999, Modeling chemical activity effects in strong ionic solutions, Computational Materials Science, 15, pp. 285-294.

Sanjuán M. A. and del Olmo C., 2001, Carbonation resistance of one industrial mortar used as a concrete coating, Building and Environment, 36, pp. 949-953.

Sawada S., 2005, Ionic Migration in Cement-based Materials, Ph.D. thesis, University of Leeds, Chapter 5.

Sawada S., Page C. L., and Page M. M., 2005, Electrochemical injection of organic corrosion inhibitors into concrete, Corrosion Science, 47, pp. 2063-2078.

Sawada S., Kubo J., Page C. L., and Page M. M., 2007, Electrochemical injection of organic corrosion inhibitors into carbonated cementitious materials: Part I – Effects on pore solution chemistry, Corrosion Science, 49, pp. 1186-1204.

Seki M., Chikuma S., Ito Y., Morikawa M., and Kubo J., 1999, Investigations on reinforcement corrosion in real concrete viaducts (Internal report, Japanese only), Central Japan Railway Company.

Seki M., Chikuma S., Morikawa M., Kubo J., and Naruse M., 2001, Investigations on long-term durability of coatings applied on concrete (Internal report supervised by Uomoto T. (Professor of Tokyo University), Japanese only), Central Japan Railway Company.

Seneviratne A. M. G., Sergi G., Maleki M. T., Sadegzadeh M., and Page C. L., 1996, Effect of surface treatment of concrete on reinforcement corrosion, In: Page C. L., Bamforth P. B., Figg J. (Eds.), Corrosion of reinforcement in concrete construction, Elsevier, London, pp. 567-576.

Seneviratne A. M. G., Sergi G., Maleki M. T., Sadegzadeh M., and Page C. L., 1999, Surface coatings for controlling reinforcement corrosion in carbonated concrete, In: Swamy R. N. (Ed.), Infrastructure regeneration and rehabilitation, improving the quality of life through better construction, a vision for the next millennium, Sheffield Academic Press, Sheffield, pp. 663-672.

Seneviratne A. M. G., Sergi G. and Page C. L., 2000, Performance characteristics of surface coatings applied to concrete for control of reinforcement corrosion, Construction and Building Materials, 14, pp. 55-59.

Sergi G., 1986, Corrosion of Steel in Concrete: Cement Matrix Variables, PhD. thesis, Aston University.

Sergi G., Lattey S. E., and Page C. L., 1990, Influence of surface treatments on corrosion rates of steel in carbonated concrete, Corrosion of Reinforcement in Concrete, Page C. L., Treadaway K., and Bamforth P. (Eds.), Elsevier, pp. 409-419.

Sergi G., Page C. L., and Thompson D. M., 1991, Electrochemical induction of alkali-silica reaction in concrete, Materials and Structures, Vol. 24, pp. 359-361.

Sergi G., Walker R. J., and Page C. L., 1996, Mechanism and criteria for the re-alkalisation of concrete, Corrosion of Reinforcement in concrete construction, Page C.L., Bamforth P.B. and Figg J.W. (Eds.), Royal Society of Chemistry, Cambridge, pp. 491-500.

Shaw S. J., 2002, Supercritically carbonated cement composites with controlled pore solution chemistry, MSc thesis, University of Leeds.

Short N. R., Purnell P., and Page C. L., 2001, Preliminary investigations into the supercritical carbonation of cement pastes, Journal of materials science, 36, pp. 35-41.

Silverman D. C. and Carrico J. E., 1988, Electrochemical impedance technique – A practical tool for corrosion prediction, Corrosion, 44, pp. 280-287.

Snedecor G. W. and Cochran W. G., 1967, Statistical methods, Iowa State University Press, pp. 83-106.

Stern M. and Geary A. L., 1957, Linear polarization, Journal of the Electrochemical Society, 104, pp. 56-63.

Swamy R. N. and Tanikawa S., 1989, Surface coatings to preserve concrete durability, Proceedings of International Conference on Protection of Concrete, Dhir R. K. and Green J. W. (Eds.), E & FN Spon. London, pp. 149-165.

Swamy R. N. and Tanikawa S., 1993, An external surface coating to protect concrete and steel from aggressive environments, Materials and Structures, 26, pp. 465-478.

Taylor H.F.W, 1987, A method for predicting alkali ion concentration in cement pore solutions, Advances in Cement Research, 1, No. 1, pp. 5-17.

Tan Y. J., Bailey S., and Kinseilla B., 1996, An investigation of the formation and destruction of corrosion inhibitor films using electrochemical impedance spectroscopy (EIS), Corrosion Science, 38, pp. 1545-1561.

Trabanelli G., Monticelli C., Grassi V., and Frignani A., 2005, Electrochemical study on inhibitors of rebar corrosion in carbonated concrete, Cement and Concrete Research, 35, pp. 1804-1813.

Truc O., Ollivier J. P., and Nilsson L. O., 2000, Numerical simulation of multi-species transport through saturated concrete during a migration test – *MsDiff* code, Cement and Concrete Research, 30, pp. 1581-1592.

Tsiatas G. and Robinson J., 2002, Durability evaluation of concrete crack repair systems, Transportation Research Record, No. 1795, pp. 82-87.

Tritthart J., 2003, Transport of a surface-applied corrosion inhibitor in cement paste and concrete, Cement and Concrete Research, 33, pp. 829-834.

Tuutti K., 1980, Service life of structures with regard to corrosion of embedded steel, in "Performance of concrete in marine environment", ACI SP-65, pp. 223-236.

Tuutti K., 1982, Corrosion of Steel in Concrete, Swedish Foundation for Concrete Research (CBI), Stockholm, 1982, S-100, p. 44.

Wang Y., Li L. Y., and Page C. L., 2001, A two-dimensional model of electrochemical chloride removal from concrete, Computational Materials Science, 20, pp. 196-212.

Wombacher F., Maeder U., and Marazzani B., 2004, Aminoalcohol based mixed corrosion inhibitors, Cement and Concrete Composites, 26, pp. 209-216.

Yu S. W. and Page C. L., 1996, Computer simulation of ionic migration during electrochemical chloride extraction from hardened concrete, British Corrosion Journal, 31, No. 1, pp. 73-75.

APPENDIX A:

THE CALCULATION OF CARBONATE AND BICARBONATE CONCENTRATIONS IN THE PORE SOLUTION CONTAINING ORGANIC CORROSION INHIBITORS

The procedures to calculate the concentrations of carbonate and bicarbonate ions in the pore solution containing organic corrosion inhibitors, ethanolamine, guanidine, and arginine, from the data obtained by titration are shown below.

A.1 Solutions containing ethanolamine or arginine

A.1.1 Premises

The series of equilibrium involved are assumed to be as follows;

$$RNH_3^+ \Leftrightarrow RNH_2 + H^+ \quad (pKa' 9.75 \text{ for ethanolamine and } pKa' 9.30 \text{ for arginine}) \qquad (A)$$

$$HCO_3^- \Leftrightarrow CO_3^{2-} + H^+ \quad (pK_2\ 10.34) \qquad (B)$$

$$H_2CO_3 \Leftrightarrow HCO_3^- + H^+ \quad (pK_1\ 6.38) \qquad (C)$$

where RNH_2 is the molecular form of ethanolamine or arginine, and RNH_3^+ is the cationic form. The concentration of cationic species and hydroxyl can be considered to be negligible at pH values of 7.0 and 4.0. Thus, hydrogen ions provided by nitric acid are assumed to have been consumed by carbonate, bicarbonate, inhibitor molecules, and hydroxyl when pH value is reduced to 7.0, as illustrated below. Subsequently hydrogen ions are assumed to have been consumed by bicarbonate when pH value is lowered to 4.0.

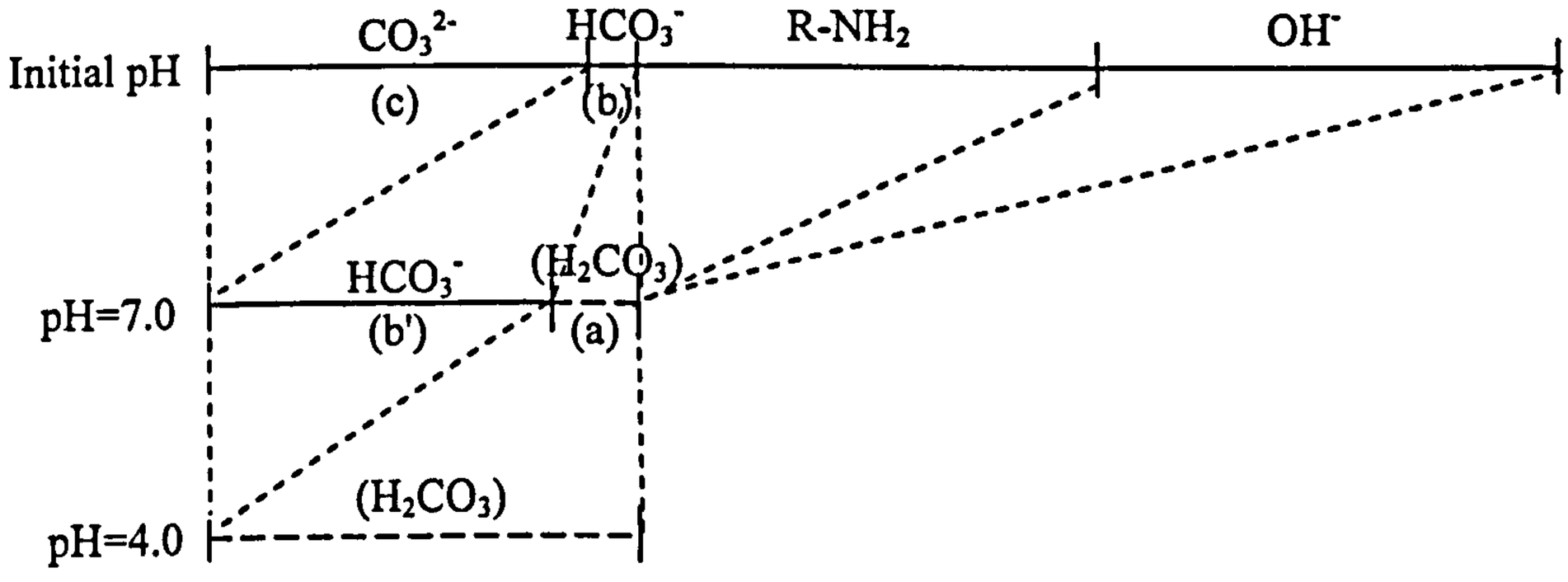

A.1.2 Experimental values

The initial values of pH_{init} are determined by means of a pH electrode and a pH digital meter described in section 2.5. The amounts of 10mM nitric acid required to lower the pH of 1ml sample solution down to 7.0 and 4.0, are obtained by titration.

A.1.3 Calculation

There are four unknowns to be solved: The total amount of carbonate (c) and bicarbonate (b) in the initial solution (mole), and the total amount of bicarbonate (b') and carbonic acid (a) in the pore solution of pH 7.0 (mole).

Mass balance is given by:

$$c + b = b' + a \tag{1}$$

The equilibria (B) and (C) are given by:

$$\log \frac{c}{b} = -pK_2 + pH_{init} \tag{2}$$

$$\log \frac{b'}{a} = -pK_1 + 7.0 \tag{3}$$

All the hydrogen ions (N, mole) consumed between pH 7.0 and 4.0 are used to convert (b') bicarbonate ions to carbonic acid:

$$N = b' \tag{4}$$

Above Eqs. (1)-(4) are the four simultaneous equations to be solved for the four unknowns, (c), (b), (b'), and (a). The initial concentrations of carbonate (c) and bicarbonate (b) present in the pore solution are finally obtained:

$$c = \frac{(1+10^{pK_1-7.0}) \cdot 10^{(pH_{init}-pK_2)}}{1+10^{(pH_{init}-pK_2)}} \cdot N \tag{5}$$

$$b = \frac{(1+10^{pK_1-7.0})}{1+10^{(pH_{init}-pK_2)}} \cdot N \tag{6}$$

A.2 Solutions containing guanidine

A.2.1 Premises

The series of equilibrium involved are assumed to be as follows;

$$RNH_3^+ \Leftrightarrow RNH_2 + H^+ \quad (pKa\ 13.6) \tag{D}$$

$$HCO_3^- \Leftrightarrow CO_3^{2-} + H^+ \quad (pK_2\ 10.34) \tag{B}$$

$$H_2CO_3 \Leftrightarrow HCO_3^- + H^+ \quad (pK_1\ 6.38) \tag{C}$$

where RNH_2 is the molecular form of guanidien and RNH_3^+ is the cationic form. The concentration of cationic species and hydroxyl can be considered to be negligible at pH values of 9.0 and 4.0. Thus, hydrogen ions provided by nitric acid are assumed to have been consumed by carbonate, bicarbonate, inhibitor molecules, and hydroxyl when pH value is reduced to 9.0, as illustrated below. Subsequently hydrogen ions are assumed to have been consumed by carbonate and bicarbonate when pH value is lowered to 4.0.

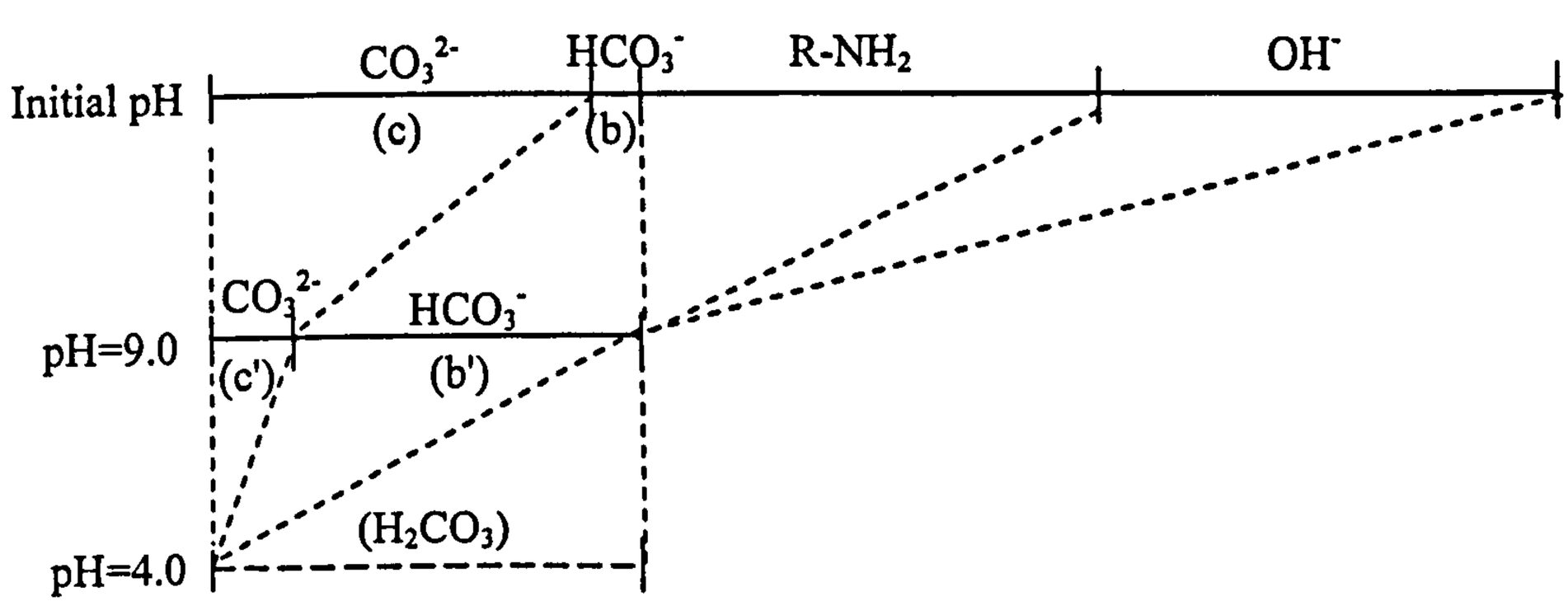

A.2.2 Experimental values

The initial values of pH_{init} are determined by means of a pH electrode and a pH digital meter described in section 2.5. The amounts of 10mM nitric acid required to lower the pH of 1ml sample solution down to 9.0 and 4.0, are obtained by titration.

A.2.3 Calculation

There are four unknowns to be solved: The total amount of carbonate (c) and bicarbonate (b) in the initial solution (mole), and the total amount of carbonate (c') and bicarbonate (b') in the pore solution of pH 9.0 (mole).

Mass balance is given by:

$$c + b = c' + b' \tag{7}$$

The equilibria (B) and (C) are given by:

$$\log\frac{c}{b} = -pK_2 + pH_{init} \tag{8}$$

$$\log\frac{c'}{b'} = -pK_2 + 9.0 \tag{9}$$

All the hydrogen ions (N, mole) consumed between pH 9.0 and 4.0 are used to convert (b') bicarbonate ions to carbonic acid:

$$N = 2 \cdot c' + b' \tag{10}$$

Above Eqs. (7)-(10) are the four simultaneous equations to be solved for the four unknowns, (c), (b), (c'), and (b'). The initial concentrations of carbonate (c) and bicarbonate (b) present in the pore solution are finally obtained:

$$c = \frac{(1+10^{9.0-pK_2}) \cdot 10^{(pH_{init}-pK_2)}}{(1+2\cdot 10^{9.0-pK_2}) \cdot (1+10^{(pH_{init}-pK_2)})} \cdot N \tag{11}$$

$$b = \frac{(1+10^{9.0-pK_2})}{(1+2\cdot 10^{9.0-pK_2}) \cdot (1+10^{(pH_{init}-pK_2)})} \cdot N \tag{12}$$

APPENDIX B:

THE COMPLETE LISTS OF CONCENTRATIONS OF SPECIES IN THE PORE SOLUTION AFTER INHIBITOR INJECTION TREATMENT TO UNIFORMLY CARBONATED MEDIUM

Table B.1 Concentrations of species in pore solution of carbonated cement paste after treatment of 1M ethanolamine nitrate at 0A/m^2 (Ethanolamine and cations)

Distance from surface (mm)	pH	Concentrations (mmol/l)						
		Organic inhibitors		Na^+	K^+	Mg^{2+}	Ca^{2+}	Sum of charge
		Total	Cations					
2.5	9.2	499.0	398.8	15.9	11.3	40.2	109.0	724.4
7.5	8.2	214.3	208.1	18.4	16.2	98.2	75.3	589.8
12.5	8.0	110.0	108.0	23.6	13.8	99.4	66.9	478.2
17.5	8.0	32.2	31.6	14.8	7.4	84.0	57.3	336.5
22.5	8.7	7.8	7.1	17.6	7.0	46.6	56.0	237.0
27.5	9.2	7.1	5.6	12.8	5.8	29.0	43.5	169.2
34.0	9.4	16.0	11.1	15.4	5.7	6.7	43.3	132.1
40.5	8.7	2.0	1.8	8.5	3.5	25.1	38.5	141.1

Table B.2 Concentrations of species in pore solution of carbonated cement paste after treatment of 1M ethanolamine nitrate at 0A/m^2 (Anions)

Distance from surface (mm)	pH	Concentrations (mmol/l)						
		OH^-	Cl^-	SO_4^{2-}	NO_3^-	CO_3^{2-}	HCO_3^-	Sum of charge
2.5	9.2	1.41E-2	10.0	25.2	840.4	0.8	12.0	914.3
7.5	8.2	1.66E-3	19.0	32.2	601.1	0.0	6.2	690.8
12.5	8.0	1.05E-3	24.6	30.4	398.7	0.0	8.5	492.7
17.5	8.0	9.12E-4	36.9	30.2	225.9	0.0	11.7	335.1
22.5	8.7	5.25E-3	30.8	26.3	112.2	0.1	4.9	200.9
27.5	9.2	1.48E-2	28.0	23.6	53.6	0.3	3.7	133.1
34.0	9.4	2.51E-2	24.6	17.2	45.7	0.5	4.2	109.9
40.5	8.7	4.79E-3	23.5	26.1	20.0	0.1	3.6	99.5

Table B.3 Concentrations of species in pore solution of carbonated cement paste after treatment of 1M ethanolamine nitrate at 1A/m^2 (Ethanolamine and cations)

Distance from surface (mm)	pH	Concentrations (mmol/l)						
		Organic inhibitors		Na^+	K^+	Mg^{2+}	Ca^{2+}	Sum of charge
		Total	Cations					
2.5	8.0	822.7	814.2	9.7	16.5	33.6	81.0	1069.6
7.5	9.3	410.7	308.5	7.9	10.2	22.3	48.8	468.9
12.5	9.3	156.8	117.1	3.5	5.7	11.7	27.7	205.2
17.5	9.5	104.9	68.8	9.7	6.6	8.5	22.0	146.2
22.5	9.4	37..9	26.5	10.3	5.8	13.4	23.3	116.1
27.5	9.5	20.7	13.0	23.6	8.8	6.9	19.0	97.2
34.0	10.9	19.1	1.4	21.0	7.8	2.6	11.4	58.2
40.5	9.5	4.8	3.2	15.7	5.9	11.9	29.6	107.8
45.5	8.1	4.4	4.3	10.8	3.3	24.8	25.6	119.2
50.5	7.8	4.8	4.7	10.8	4.7	23.1	26.2	118.7

Table B.4 Concentrations of species in pore solution of carbonated cement paste after treatment of 1M ethanolamine nitrate at 1A/m^2 (Anions)

Distance from surface (mm)	pH	Concentrations (mmol/l)						
		OH^-	Cl^-	SO_4^{2-}	NO_3^-	CO_3^{2-}	HCO_3^-	Sum of charge
2.5	8.0	9.33E-4	13.5	43.4	795.5	0.1	14.6	910.6
7.5	9.3	1.86E-2	14.9	111.8	193.6	1.1	13.1	447.6
12.5	9.3	1.91E-2	17.3	76.7	16.8	0.8	9.6	198.8
17.5	9.5	2.95E-2	5.8	44.4	9.7	0.6	4.8	110.4
22.5	9.4	2.40E-2	4.4	35.8	2.1	0.5	4.2	83.2
27.5	9.5	3.31E-2	2.3	18.4	3.0	0.7	4.5	47.9
34.0	10.9	7.08E-1	1.1	8.1	3.3	0.9	0.3	23.4
40.5	9.5	2.82E-1	10.7	24.6	1.2	0.4	3.1	64.9
45.5	8.1	1.23E-3	19.7	35.0	1.4	0.0	4.9	96.0
50.5	7.8	6.92E-4	22.6	32.5	2.2	0.0	2.9	92.7

Table B.5 Concentrations of species in pore solution of carbonated cement paste after treatment of 1M ethanolamine nitrate at 5A/m^2 (Ethanolamine and cations)

Distance from surface (mm)	pH	Concentrations (mmol/l)						
		Organic inhibitors		Na^+	K^+	Mg^{2+}	Ca^{2+}	Sum of charge
		Total	Cations					
2.5	7.8	556.6	551.0	16.8	7.3	18.3	100.9	813.5
7.5	10.0	225.2	82.2	13.6	7.9	1.7	7.9	123.0
12.5	10.3	222.6	47.2	10.6	4.4	1.2	6.4	77.4
17.5	10.5	292.3	43.3	4.3	5.6	1.1	1.9	59.2
22.5	10.7	477.6	50.2	5.2	14.2	1.5	2.7	77.9
27.5	11.1	1128.8	50.4	7.6	18.3	2.2	4.8	90.3
34.0	11.6	1157.8	15.4	27.2	28.8	2.3	6.1	88.2
40.5	10.0	108.6	39.1	22.5	13.6	8.6	22.7	137.7
45.5	9.5	36.0	23.6	10.4	4.4	13.7	26.8	119.5
50.5	9.9	15.1	6.6	30.0	7.9	17.3	26.9	132.7

Table B.6 Concentrations of species in pore solution of carbonated cement paste after treatment of 1M ethanolamine nitrate at 5A/m^2 (Anions)

Distance from surface (mm)	pH	Concentrations (mmol/l)						
		OH^-	Cl^-	SO_4^{2-}	NO_3^-	CO_3^{2-}	HCO_3^-	Sum of charge
2.5	7.8	5.75E-4	14.4	32.2	795.1	0.0	15.9	890.0
7.5	10.0	9.77E-2	4.8	60.5	17.0	13.7	30.6	200.8
12.5	10.3	2.09E-1	2.2	23.5	2.2	12.3	12.9	89.2
17.5	10.5	3.24E-1	2.2	13.1	0.5	18.4	12.4	78.4
22.5	10.7	4.79E-1	1.3	6.8	0.9	35.1	16.0	102.6
27.5	11.1	1.20E 0	3.0	5.6	1.7	57.8	10.5	143.0
34.0	11.6	4.17E 0	1.2	6.1	1.8	44.7	2.3	111.1
40.5	10.0	1.00E-1	9.6	46.1	0.0	2.6	5.8	113.0
45.5	9.5	2.95E-2	14.0	36.2	0.0	0.7	5.3	93.0
50.5	9.9	7.24E-2	16.4	33.6	0.0	1.9	5.7	93.2

Table B.7 Concentrations of species in pore solution of carbonated cement paste after treatment of 0.5M guanidine carbonate at $0A/m^2$ (Guanidine and cations)

Distance from surface (mm)	pH	Concentrations (mmol/l)						
		Organic inhibitors		Na^+	K^+	Mg^{2+}	Ca^{2+}	Sum of charge
		Total	Cations					
2.5	9.7	227.5	227.5	9.0	12.1	10.8	5.9	282.1
7.5	9.0	52.3	52.3	24.8	5.9	18.4	20.9	161.4
12.5	9.9	23.5	23.5	14.2	3.5	19.3	22.9	125.7
17.5	8.6	8.9	8.9	34.4	8.1	32.9	27.1	171.4
22.5	8.5	3.1	3.1	19.5	9.2	36.6	29.9	164.9
27.5	9.8	1.6	1.6	22.5	5.8	16.6	32.7	128.5
34.0	9.7	5.5	5.5	19.3	8.0	3.2	23.7	86.5
40.5	8.8	0.0	0.0	18.4	11.4	22.6	26.4	128.0

Table B.8 Concentrations of species in pore solution of carbonated cement paste after treatment of 0.5M guanidine carbonate at $0A/m^2$ (Anions)

Distance from surface (mm)	pH	Concentrations (mmol/l)						
		OH^-	Cl^-	SO_4^{2-}	NO_3^-	CO_3^{2-}	HCO_3^-	Sum of charge
2.5	9.7	5.25E-2	12.9	89.7	-	14.8	61.8	283.9
7.5	9.0	8.91E-3	22.3	51.3	-	0.4	9.2	134.8
12.5	9.9	7.41E-2	19.6	35.9	-	1.1	3.4	97.2
17.5	8.6	3.63E-3	30.7	42.0	-	0.4	7.7	123.1
22.5	8.5	2.95E-3	35.3	42.2	-	0.3	6.4	126.8
27.5	9.8	6.31E-2	27.1	25.7	-	0.8	2.8	83.1
34.0	9.7	5.01E-2	22.0	18.3	-	0.6	2.7	62.6
40.5	8.8	6.31E-3	26.1	30.2	-	0.2	4.5	91.4

Table B.9 Concentrations of species in pore solution of carbonated cement paste after treatment of 0.5M guanidine carbonate at 1A/m^2 (Guanidine and cations)

Distance from surface (mm)	pH	Concentrations (mmol/l)						
		Organic inhibitors		Na^+	K^+	Mg^{2+}	Ca^{2+}	Sum of charge
		Total	Cations					
2.5	9.4	458.0	458.	3.7	0.0	25.0	14.6	540.9
7.5	9.2	261.8	261.8	11.5	0.0	10.0	15.9	325.5
12.5	10.0	112.0	112.0	6.0	6.3	9.2	14.0	170.6
17.5	8.6	49.6	49.6	17.5	4.9	17.6	30.1	167.3
22.5	8.7	23.2	23.2	15.7	6.0	12.3	23.9	117.1
27.5	8.9	4.4	4.4	16.0	9.9	7.0	18.0	80.4
34.0	11.2	2.1	2.1	17.7	14.6	2.4	7.7	54.8
40.5	8.5	0.0	0.0	15.0	4.1	22.4	26.7	117.4
45.5	8.7	0.0	0.0	12.9	7.7	25.7	25.2	122.3
50.5	8.5	0.0	0.0	13.2	6.4	28.9	24.3	126.1

Table B.10 Concentrations of species in pore solution of carbonated cement paste after treatment of 0.5M guanidine carbonate at 1A/m^2 (Anions)

Distance from surface (mm)	pH	Concentrations (mmol/l)						
		OH^-	Cl^-	SO_4^{2-}	NO_3^-	CO_3^{2-}	HCO_3^-	Sum of charge
2.5	9.4	2.34E-2	23.6	168.6	-	10.3	96.5	477.9
7.5	9.2	1.70E-2	10.0	157.4	-	1.1	14.2	341.2
12.5	10.0	1.07E-1	6.9	74.4	-	1.6	3.2	162.2
17.5	8.6	4.27E-3	3.9	53.2	-	0.3	6.0	116.8
22.5	8.7	5.50E-3	4.0	33.7	-	0.3	6.9	78.8
27.5	8.9	7.41E-3	2.4	14.7	-	0.3	5.5	37.8
34.0	11.2	1.58E 0	1.7	8.0	-	2.5	0.3	24.6
40.5	8.5	3.16E-3	11.1	32.1	-	0.2	5.0	80.8
45.5	8.7	5.25E-3	18.9	32.9	-	0.3	5.5	90.8
50.5	8.5	3.16E-3	20.8	34.5	-	0.3	6.4	96.8

Table B.11 Concentrations of species in pore solution of carbonated cement paste after treatment of 0.5M guanidine carbonate at 5A/m^2 (Guanidine and cations)

Distance from surface (mm)	pH	Concentrations (mmol/l)						
		Organic inhibitors		Na^+	K^+	Mg^{2+}	Ca^{2+}	Sum of charge
		Total	Cations					
2.5	11.4	497.9	494.6	7.1	0.0	0.0	0.7	503.2
7.5	12.3	293.7	279.3	7.1	0.0	0.0	5.5	297.5
12.5	12.2	209.0	200.6	5.7	0.0	0.0	8.3	222.9
17.5	12.1	130.4	126.3	9.2	4.9	0.0	5.9	152.3
22.5	12.0	85.9	83.7	8.7	3.1	0.0	7.6	110.7
27.5	12.5	150.0	138.0	8.0	3.5	0.0	2.8	155.0
34.0	13.1	512.9	393.9	25.6	19.5	0.0	2.3	443.6
40.5	10.5	19.9	19.9	28.9	3.6	5.3	18.8	100.6
45.5	8.9	3.0	3.0	7.7	5.4	20.0	18.1	92.3
50.5	9.1	0.6	0.6	9.0	2.8	21.0	19.6	93.6

Table B.12 Concentrations of species in pore solution of carbonated cement paste after treatment of 0.5M guanidine carbonate at 5A/m^2 (Anions)

Distance from surface (mm)	pH	Concentrations (mmol/l)						
		OH^-	Cl^-	SO_4^{2-}	NO_3^-	CO_3^{2-}	HCO_3^-	Sum of charge
2.5	11.4	2.63E 0	9.8	127.5	-	96.1	44.7	504.3
7.5	12.3	2.04E+1	4.1	63.4	-	108.3	8.6	376.5
12.5	12.2	1.66E+1	4.6	57.7	-	38.9	0.4	214.8
17.5	12.1	1.29E+1	3.6	36.2	-	23.6	0.3	136.4
22.5	12.0	1.05E+1	2.2	16.8	-	23.6	0.3	93.8
27.5	12.5	3.47E+1	2.9	10.8	-	33.4	0.1	126.1
34.0	13.1	1.20E+2	2.7	12.7	-	156.9	0.3	462.4
40.5	10.5	3.16E-1	10.6	28.5	-	4.7	2.0	79.3
45.5	8.9	7.46E-3	15.5	32.1	-	0.3	6.4	86.8
50.5	9.1	1.23E-2	17.4	32.3	-	0.3	5.5	88.0

Table B.13 Concentrations of species in pore solution of carbonated cement paste after treatment of 0.5M arginine nitrate at $0A/m^2$ (Arginine and cations)

Distance from surface (mm)	pH	Concentrations (mmol/l)						
		Organic inhibitors		Na^+	K^+	Mg^{2+}	Ca^{2+}	Sum of charge
		Total	Cations					
2.5	8.5	300.9	262.2	9.5	2.9	34.4	68.6	480.5
7.5	8.8	61.2	45.7	16.5	2.9	41.1	69.1	285.6
12.5	9.0	20.0	13.7	17.3	3.7	41.1	45.5	208.0
17.5	9.5	4.6	1.9	14.2	2.6	20.4	40.0	139.5
22.5	8.5	2.0	1.8	15.4	2.5	32.5	29.1	142.8
27.5	8.2	0.0	0.0	16.6	2.4	30.8	30.6	141.7
34.0	8.3	0.0	0.0	10.9	1.5	27.2	36.2	139.3
40.5	8.6	0.0	0.0	14.1	1.8	27.2	25.0	120.4

Table B.14 Concentrations of species in pore solution of carbonated cement paste after treatment of 0.5M arginine nitrate at $0A/m^2$ (Anions)

Distance from surface (mm)	Concentrations (mmol/l)							
	Inhibitor anions	OH^-	Cl^-	SO_4^{2-}	NO_3^-	CO_3^{2-}	HCO_3^-	Sum of charge
2.5	0.0	2.95E-3	5.4	26.0	371.7	0.2	12.3	441.7
7.5	0.0	6.76E-3	27.3	17.8	192.5	0.1	3.7	259.3
12.5	0.0	9.12E-3	13.8	24.5	141.8	0.2	5.5	210.6
17.5	0.0	2.88E-2	20.0	18.7	69.2	0.5	3.9	131.6
22.5	0.0	3.24E-3	25.6	25.9	48.5	0.0	3.8	129.7
27.5	0.0	1.66E-3	25.2	31.8	30.0	0.0	4.7	123.5
34.0	0.0	2.29E-3	26.9	30.7	14.5	0.0	4.2	107.0
40.5	0.0	4.07E-3	26.9	32.6	9.8	0.0	4.6	106.5

Table B.15 Concentrations of species in pore solution of carbonated cement paste after treatment of 0.5M arginine nitrate at 1A/m^2 (Arginine and cations)

Distance from surface (mm)	pH	Concentrations (mmol/l)						
		Organic inhibitors		Na^+	K^+	Mg^{2+}	Ca^{2+}	Sum of charge
		Total	Cations					
2.5	8.7	303.4	247.9	10.7	4.3	6.0	48.7	372.3
7.5	9.2	189.8	103.6	3.1	1.2	1.5	29.1	169.1
12.5	10.0	103.0	16.2	5.6	1.5	0.8	8.9	42.7
17.5	10.1	56.2	8.2	2.5	1.0	0.8	5.7	24.6
22.5	9.9	22.5	4.9	2.4	1.7	0.5	7.9	25.9
27.5	9.6	3.3	1.1	2.6	1.5	0.7	5.7	18.1
34.0	10.2	0.0	0.0	15.0	4.1	0.4	3.9	27.6
40.5	9.5	0.0	0.0	5.0	1.7	2.2	8.1	27.3
45.5	9.2	0.0	0.0	3.8	1.4	2.3	10.6	30.9
50.5	9.2	0.0	0.0	5.7	2.2	4.2	16.0	48.3

Table B.16 Concentrations of species in pore solution of carbonated cement paste after treatment of 0.5M arginine nitrate at 1A/m^2 (Anions)

Distance from surface (mm)	Concentrations (mmol/l)							
	Inhibitor anions	OH^-	Cl^-	SO_4^{2-}	NO_3^-	CO_3^{2-}	HCO_3^-	Sum of charge
2.5	0.0	4.47E-2	10.4	21.0	310.7	1.3	20.8	386.6
7.5	0.0	1.66E-2	2.5	26.5	117.9	2.8	9.1	188.2
12.5	0.3	1.07E-1	2.0	9.0	20.3	2.9	5.9	52.5
17.5	0.2	1.17E-1	1.6	8.3	0.1	2.6	4.9	28.9
22.5	0.0	7.08E-2	2.2	8.3	0.3	1.9	5.7	28.5
27.5	0.0	4.07E-2	1.1	4.1	0.0	0.2	1.2	10.9
34.0	0.0	1.58E-1	1.0	10.7	0.2	0.6	0.8	24.7
40.5	0.0	3.24E-2	4.8	9.0	0.0	0.2	1.2	24.5
45.5	0.0	1.70E-2	5.9	9.4	0.0	0.0	1.3	25.9
50.5	0.0	1.62E-2	8.6	15.1	0.3	0.0	1.3	40.4

Table B.17 Concentrations of species in pore solution of carbonated cement paste after treatment of 0.5M arginine nitrate at 5A/m^2 (Arginine and cations)

Distance from surface (mm)	pH	Concentrations (mmol/l)						
		Organic inhibitors		Na^+	K^+	Mg^{2+}	Ca^{2+}	Sum of charge
		Total	Cations					
2.5	8.6	308.9	254.5	7.2	2.6	7.9	113.9	507.9
7.5	9.8	237.1	53.0	3.0	1.7	0.9	7.2	73.8
12.5	10.1	367.7	53.3	5.2	1.1	0.7	7.1	75.1
17.5	10.4	313.4	25.0	4.1	0.8	0.0	5.9	41.7
22.5	10.8	471.9	15.7	2.9	0.3	0.4	8.6	36.8
27.5	11.2	533.8	6.5	3.9	1.5	0.0	12.6	37.1
34.0	12.1	456.2	0.6	32.0	16.7	0.0	7.9	65.2
40.5	9.8	31.1	7.1	12.0	3.5	1.2	15.1	55.1
45.5	9.1	7.4	4.6	8.8	2.6	7.6	16.9	65.1
50.5	9.1	5.2	3.3	6.9	1.9	4.2	12.2	44.8

Table B.18 Concentrations of species in pore solution of carbonated cement paste after treatment of 0.5M arginine nitrate at 5A/m^2 (Anions)

Distance from surface (mm)	Concentrations (mmol/l)							
	Inhibitor anions	OH^-	Cl^-	SO_4^{2-}	NO_3^-	CO_3^{2-}	HCO_3^-	Sum of charge
2.5	0.0	4.27E-3	10.5	23.5	397.3	0.4	20.2	475.7
7.5	0.2	6.92E-2	1.3	9.2	8.6	4.7	14.8	52.9
12.5	0.6	1.17E-1	0.9	5.2	0.7	11.7	21.8	57.9
17.5	1.0	2.29E-1	2.6	4.5	0.8	14.7	14.1	57.2
22.5	4.1	5.75E-1	0.1	3.7	2.0	24.3	9.2	71.9
27.5	12.9	1.58E 0	1.0	3.2	1.6	26.2	5.0	80.9
34.0	72.9	1.20E+1	0.4	8.2	1.2	32.9	0.6	169.3
40.5	0.0	6.76E-2	7.9	14.5	3.8	1.3	4.3	47.8
45.5	0.0	1.23E-2	8.8	25.4	2.2	0.3	4.5	66.8
50.5	0.0	1.15E-2	10.5	14.4	1.6	0.2	4.6	46.0

APPENDIX C:

THE COMPLETE LISTS OF CONCENTRATIONS OF SPECIES IN THE PORE SOLUTION AFTER INHIBITOR INJECTION TREATMENT TO PARTIALLY CARBONATED MEDIUM

Table C.1 Concentrations of species in pore solution of partially carbonated cement paste after treatment of 1M ethanolamine nitrate (Ethanolamine and cations)

Distance from surface (mm)	pH	Concentrations (mmol/l)						
		Organic inhibitors		Na^+	K^+	Mg^{2+}	Ca^{2+}	Sum of charge
		Total	Cations					
[Left column]								
3.0	10.2	990.0	259.3	17.9	18.7	0.8	45.3	388.1
9.0	11.1	1420.1	58.1	10.2	15.8	3.3	11.4	113.5
15.0*	12.8	1161.8	1.0	83.3	86.7	3.9	0.2	179.3
21.0*	13.5	407.4	0.1	138.2	213.5	9.4	7.0	384.6
27.0*	13.3	154.2	0.0	114.8	127.3	0.0	2.7	247.5
[Centre column]								
3.0	10.4	947.3	190.2	1.8	11.2	1.0	47.3	299.8
9.0	11.2	981.0	30.7	33.8	21.6	0.0	2.1	90.3
15.0	11.0	1401.8	74.6	38.3	18.5	0.0	7.1	145.7
21.0	11.9	1157.4	9.1	63.7	43.5	0.0	8.0	132.5
27.0	10.0	84.7	31.4	25.1	19.1	3.2	15.3	112.5
[Right column]								
3.0	10.1	852.5	259.0	12.5	19.3	0.6	49.3	390.6
9.0	11.3	1466.6	42.0	11.7	15.7	6.9	9.3	102.0
15.0*	12.8	1205.9	1.0	75.7	93.9	0.0	2.0	174.6
21.0*	13.5	350.7	0.1	153.2	216.9	3.6	11.6	400.5
27.0*	13.3	173.6	0.1	120.9	108.5	0.0	2.6	234.7

*: initially non-carbonated

Table C.2 Concentrations of species in pore solution of carbonated cement paste after treatment of 1M ethanolamine nitrate (Anions)

Distance from surface (mm)	pH	Concentrations (mmol/l)						
		OH^-	Cl^-	SO_4^{2-}	NO_3^-	CO_3^{2-}	HCO_3^-	Sum of charge
[Left column]								
3.0	10.2	0.2	5.7	9.7	263.4	24.0	34.8	371.5
9.0	11.1	1.3	0.9	4.6	27.3	38.8	6.4	122.7
15.0*	12.8	67.6	1.1	0.9	8.8	53.6	0.2	186.6
21.0*	13.5	302.0	2.5	2.3	3.3	31.4	0.0	375.1
27.0*	13.3	218.8	1.5	0.8	0.5	23.8	0.0	270.1
[Centre column]								
3.0	10.4	0.2	4.5	6.1	223.4	24.5	24.4	313.8
9.0	11.2	1.7	1.0	5.1	11.5	40.4	5.1	110.4
15.0	11.0	1.0	0.8	15.5	7.1	52.2	11.4	155.7
21.0	11.9	7.1	3.1	13.5	4.9	60.0	11.7	173.6
27.0	10.0	0.1	1.9	49.6	6.6	2.4	5.4	117.9
[Right column]								
3.0	10.1	0.1	4.9	6.9	268.1	20.2	35.9	363.3
9.0	11.3	1.9	0.8	3.5	14.3	36.0	4.1	100.1
15.0*	12.8	69.2	1.1	0.9	4.7	50.5	0.2	178.0
21.0*	13.5	323.6	2.6	4.2	3.9	21.9	0.0	382.3
27.0*	13.3	177.8	2.1	1.1	2.6	31.7	0.0	248.2

*: initially non-carbonated

Table C.3 Concentrations of species in pore solution of partially carbonated cement paste after treatment of 0.5M guanidine carbonate (Guanidine and cations)

Distance from surface (mm)	pH	Concentrations (mmol/l)						
		Organic inhibitors		Na^+	K^+	Mg^{2+}	Ca^{2+}	Sum of charge
		Total	Cations					
[Left column]								
3.0	12.7	499.8	447.2	7.9	0.0	0.0	6.8	468.8
9.0	13.2	753.5	545.9	14.0	26.7	0.0	5.4	597.5
15.0*	13.6	845.7	442.3	17.4	28.1	0.0	6.8	501.5
21.0*	13.6	449.2	219.4	81.4	134.5	0.0	6.5	448.4
27.0*	13.3	55.3	36.0	69.4	105.2	1.1	9.1	230.9
[Centre column]								
3.0	11.7	497.1	491.4	7.4	0.0	0.8	7.2	514.8
9.0	12.9	338.1	287.0	11.5	11.6	0.6	8.5	328.5
15.0	12.5	217.2	201.2	18.7	16.5	1.1	5.2	249.1
21.0	12.9	255.8	212.4	40.8	35.8	2.9	8.2	311.2
27.0	10.8	10.0	10.0	16.2	13.3	6.1	22.4	96.4
[Right column]								
3.0	12.6	454.0	410.1	7.9	9.4	0.9	6.5	442.3
9.0	13.2	763.0	563.2	14.2	0.0	1.2	10.3	600.4
15.0*	13.6	781.4	413.2	17.1	28.1	0.5	6.4	472.3
21.0*	13.6	448.9	224.5	93.9	134.1	3.0	10.5	479.4
27.0*	13.3	38.9	25.1	67.0	109.3	1.5	14.9	234.1

*: initially non-carbonated

Table C.4 Concentrations of species in pore solution of carbonated cement paste after treatment of 0.5M guanidine carbonate (Anions)

Distance from surface (mm)	pH	Concentrations (mmol/l)						
		OH^-	Cl^-	SO_4^{2-}	NO_3^-	CO_3^{2-}	HCO_3^-	Sum of charge
[Left column]								
3.0	12.7	46.8	4.3	40.5	-	157.9	0.7	448.6
9.0	13.2	151.4	11.0	55.7	-	156.7	0.2	587.4
15.0*	13.6	363.1	2.7	6.9	-	37.4	0.0	454.3
21.0*	13.6	416.9	2.3	4.8	-	19.4	0.0	467.7
27.0*	13.3	213.8	2.3	1.3	-	16.4	0.0	251.5
[Centre column]								
3.0	11.7	4.6	5.0	92.7	-	134.1	6.3	469.5
9.0	12.9	70.8	7.2	62.0	-	56.4	0.2	314.9
15.0	12.5	31.6	3.9	37.1	-	62.4	0.4	235.0
21.0	12.9	81.3	2.6	40.0	-	68.1	0.0	300.0
27.0	10.8	0.6	5.7	40.9	-	4.3	1.5	98.2
[Right column]								
3.0	12.6	42.7	4.1	31.2	-	166.8	0.9	443.7
9.0	13.2	141.3	6.4	55.1	-	167.3	0.3	592.7
15.0*	13.6	354.8	3.4	23.5	-	43.2	0.0	491.5
21.0*	13.6	398.1	2.1	4.7	-	19.5	0.0	448.7
27.0*	13.3	218.8	2.1	0.8	-	12.9	0.0	248.4

*: initially non-carbonated

APPENDIX D:

THE DETAILED DERIVATION OF EQUATIONS

APPENDIX D-A

If the rate of reaction (5-A) from left to right is expressed as R_A, and so on, the reaction rate for each species can be written with $R_A \cdots R_E$, as follows:

$$R_{Ca} = R_A + R_B,\ R_{CO_3} = R_A + R_D,\ R_{SO_4} = R_B,\ R_I = -R_C,\ R_M = R_C,\ R_{HCO_3} = -R_D,$$
$$R_{OH} = -R_c - R_D + R_E,\ R_H = R_E.$$

where R_I and R_M represent the reaction rates for the ionic and molecular inhibitor species respectively. Eliminating $R_A \cdots R_E$ the following three independent equations are then obtained:

$$R_{Ca} - R_{CO_3} - R_{HCO_3} - R_{SO_4} = 0,\ R_I + R_M = 0,\ R_H - R_{OH} + R_I + R_{HCO_3} = 0.$$

If $\Lambda_I(x)$ is defined as $\Lambda_I = \frac{J_I(x)}{dx} - \frac{J_I(x+dx)}{dx}$ or $\Lambda_I = \left(\frac{J_I(x)}{dx} - \frac{J_I(x+dx)}{dx}\right) + \left(\frac{J_I(z)}{dz} - \frac{J_I(z+dz)}{dz}\right)$ for one-dimensional or two-dimensional models respectively, from Eq. (5-9) or (5-34) and the above three equations, the following may be derived:

$$\frac{\partial C_{Ca}}{\partial t} - \frac{\partial C_{HCO_3}}{\partial t} - \frac{\partial C_{CO_3}}{\partial t} - \frac{\partial C_{SO_4}}{\partial t} = \Lambda_{Ca} - \Lambda_{HCO_3} - \Lambda_{CO_3} - \Lambda_{SO_4} \quad \text{(A1)},\quad \frac{\partial C_I}{\partial t} + \frac{\partial C_M}{\partial t} = \Lambda_I + \Lambda_M \quad \text{(A2)},$$

$$\frac{\partial C_H}{\partial t} - \frac{\partial C_{OH}}{\partial t} + \frac{\partial C_I}{\partial t} + \frac{\partial C_{HCO_3}}{\partial t} = \Lambda_H - \Lambda_{OH} + \Lambda_I + \Lambda_{HCO_3} \quad \text{(A3)}$$

Solution equilibria involving water, calcium carbonate, and calcium sulphate are represented by: $C_H \cdot C_{OH} = K_w$, $C_{Ca} \cdot C_{CO_3} = K_{s1}$, $C_{Ca} \cdot C_{SO_4} = K_{s2}$, from which the following three equations are obtained by differentiating with respect to time:

$$\frac{\partial C_H}{\partial t} = -\frac{K_w}{C_{OH}^2}\frac{\partial C_{OH}}{\partial t} \quad \text{(A4)},\quad C_{CO_3} \cdot \frac{\partial C_{Ca}}{\partial t} + C_{Ca} \cdot \frac{\partial C_{CO_3}}{\partial t} = 0 \quad \text{(A5)},\quad C_{SO_4} \cdot \frac{\partial C_{Ca}}{\partial t} + C_{Ca} \cdot \frac{\partial C_{SO_4}}{\partial t} = 0 \quad \text{(A6)}$$

Similarly, equilibria involving the molecular and ionic inhibitor species, carbonate and bicarbonate are represented by: $\log(C_M/C_I) = -pK_a + pH$ and $\log(C_{CO_3}/C_{HCO_3}) = -pK_2 + pH$, from which the following expressions are derived by differentiation:

$$\frac{\partial C_I}{\partial t} C_{OH} + \frac{\partial C_{OH}}{\partial t} C_I - 10^{pK_a - pK_w} \cdot \frac{\partial C_M}{\partial t} = 0 \quad \text{(A7)},\quad \frac{\partial C_{HCO_3}}{\partial t} C_{OH} + \frac{\partial C_{OH}}{\partial t} C_{HCO_3} - 10^{pK_2 - pK_w} \cdot \frac{\partial C_{CO_3}}{\partial t} = 0 \quad \text{(A8)}$$

Since Λ_H is expressed in terms of Λ_{OH} as $\Lambda_H = -\frac{D_H}{D_{OH}}\frac{K_w}{C_{OH}^2}\Lambda_{OH}$ (see Eq. (G4) in Appendix D-G), Eq. (A3) can be written using (A4) as follows:

$$\left(1 + \frac{K_w}{C_{OH}^2}\right)\frac{\partial C_{OH}}{\partial t} - \frac{\partial C_{HCO_3}}{\partial t} - \frac{\partial C_I}{\partial t} = \left(1 + \frac{D_H}{D_{OH}}\frac{K_w}{C_{OH}^2}\right)\Lambda_{OH} - \Lambda_{HCO_3} - \Lambda_I \quad \text{(A9)}$$

APPENDIX D-B

If the rate of reaction (5-L), (5-M) from left to right is expressed as R_L and R_Z, the following equations may be simply derived:

$$R_{Ca} = R_A + R_B - R_L,\ R_{CO_3} = R_A + R_D,\ R_{SO_4} = R_B,\ R_I = -R_C,\ R_M = R_C - R_Z,$$
$$R_{RCOO^-} = -R_Z,\ R_{HCO_3} = -R_D,\ R_{OH} = -R_c - R_D + R_E - 2R_L - R_Z,\ R_H = R_E.$$

Eliminating $R_A \cdots R_E$, R_L and R_Z from the right hand side of the above equations, the following two independent equations are obtained:

$$R_{OH} - 2R_{Ca} + 2R_{CO_3} + R_{HCO_3} + 2R_{SO_4} - R_I - R_H + R_{RCOO^-} = 0,$$
$$R_I + R_M + R_{RCOO^-} = 0.$$

From Eq. (5-9) or (5-34) and the above two equations, the following are derived taking into consideration $\frac{\partial C_H}{\partial t} = -\frac{K_w}{C_{OH}^2}\frac{\partial C_{OH}}{\partial t}$ (A4) and $\Lambda_H = -\frac{D_H}{D_{OH}}\frac{K_w}{C_{OH}^2}\Lambda_{OH}$ (see Eq. (G4) in Appendix D-G),

$$\left(1+\frac{K_w}{C_{OH}^2}\right)\frac{\partial C_{OH}}{\partial t} - 2\frac{\partial C_{Ca}}{\partial t} + 2\frac{\partial C_{CO_3}}{\partial t} + \frac{\partial C_{HCO_3}}{\partial t} + 2\frac{\partial C_{SO_4}}{\partial t} - \frac{\partial C_I}{\partial t} + \frac{\partial C_{RCOO^-}}{\partial t}$$

$$= \left(1+\frac{D_H}{D_{OH}}\frac{K_w}{C_{OH}^2}\right)\Lambda_{OH} - 2\Lambda_{Ca} + 2\Lambda_{CO_3} + \Lambda_{HCO_3} + 2\Lambda_{SO_4} + \Lambda_{HCO_3} - \Lambda_I + \Lambda_{RCOO^-} \quad \text{(B1)},$$

$$\frac{\partial C_I}{\partial t} + \frac{\partial C_M}{\partial t} + \frac{\partial C_{RCOO^-}}{\partial t} = \Lambda_I + \Lambda_M + \Lambda_{RCOO^-} \quad \text{(B2)}$$

From the solubility equilibrium condition of calcium hydroxide: $C_{Ca} \cdot C_{OH}^2 = K_{s3}$, the following equation is obtained by differentiating with respect to time:

$$2C_{Ca} \cdot \frac{\partial C_{OH}}{\partial t} + C_{OH} \cdot \frac{\partial C_{Ca}}{\partial t} = 0 \quad \text{(B3)}$$

Similarly, equilibrium involving the molecular and anionic inhibitor is represented by:
$\log(C_{RCOO^-}/C_M) = -pK_{a3} + pH$, from which the following expression is derived by differentiation:

$$\frac{\partial C_M}{\partial t}C_{OH} + \frac{\partial C_{OH}}{\partial t}C_M - 10^{pK_{a3}-pK_w} \cdot \frac{\partial C_{RCOO^-}}{\partial t} = 0 \quad \text{(B4)}$$

APPENDIX D-C

The reaction rates have the following relationships:

$$R_{CO_3}^* = R_D^*,\ R_I^* = -R_C^*,\ R_M^* = R_C^*,\ R_{HCO_3}^* = -R_D^*,\ R_H^* = R_E^*,\ R_{OH}^* = -R_C^* - R_D^* + R_E^*.$$

Eliminating $R_A^* \cdots R_E^*$, the following three independent equations are obtained:

$$R_H^* - R_{OH}^* + R_{HCO_3}^* + R_I^* = 0,\ R_{CO_3}^* + R_{HCO_3}^* = 0,\ R_I^* + R_M^* = 0.$$

Since the total anodic current is the sum of two components ($i = i^H + i^{OH}$), for example in the case of one-dimensional model, the following is derived by subtraction of Eq. (5-12) from (5-11):

$$\left(\frac{\partial C_H}{\partial t} - \frac{\partial C_{OH}}{\partial t}\right)\Bigg|_{x=0} = \frac{-J_H^* + J_{OH}^* + i/F}{x_a} + R_H^* - R_{OH}^* \quad \text{(C1)}$$

Using $\frac{\partial C_H}{\partial t} = -\frac{K_w}{C_{OH}^2}\frac{\partial C_{OH}}{\partial t}$ (A4) and $J_H = -\frac{D_H}{D_{OH}}\frac{K_w}{C_{OH}^2}J_{OH}$ (see Eq. (G3) in Appendix D-G) and Eq. (C1), the first independent equation of the above three can be changed in form to give:

$$\left\{\left(1+\frac{K_w}{C_{OH}^{*2}}\right)\frac{\partial C_{OH}}{\partial t} - \frac{\partial C_{HCO_3}}{\partial t} - \frac{\partial C_I}{\partial t}\right\}\Bigg|_{x=0} = -\frac{\left(1+\frac{D_H}{D_{OH}}\frac{K_w}{C_{OH}^{*2}}\right)J_{OH}^* - J_{HCO_3}^* - J_I^* + i/F}{x_a} \quad \text{(C2)}$$

The other two equations yield,

$$\left(\frac{\partial C_{CO_3}}{\partial t} + \frac{\partial C_{HCO_3}}{\partial t}\right)\Bigg|_{x=0} = -\frac{J_{CO_3}^* + J_{HCO_3}^*}{x_a} \quad \text{(C3)} \quad \text{and} \quad \left(\frac{\partial C_I}{\partial t} + \frac{\partial C_M}{\partial t}\right)\Bigg|_{x=0} = -\frac{J_I^* + J_M^*}{x_a} \quad \text{(C4)}$$

APPENDIX D-D

The reaction rates have the following relationships:

$$R_{CO_3}^* = -R_{D'}^*,\ R_I^* = R_{C'}^*,\ R_M^* = -R_{C'}^*,\ R_{HCO_3}^* = R_{D'}^*,\ R_H^* = -R_{C'}^* - R_{D'}^* + R_E^*,\ R_{OH}^* = R_E^*.$$

Eliminating $R_A^* \cdots R_E^*$, the following three independent equations are obtained:

$$R_H^* - R_{OH}^* + R_{HCO_3}^* + R_I^* = 0,\ R_{CO_3}^* + R_{HCO_3}^* = 0,\ R_I^* + R_M^* = 0.$$

Using $\frac{\partial C_{OH}}{\partial t} = -\frac{K_w}{C_H^2}\frac{\partial C_H}{\partial t}$, $J_{OH} = -\frac{D_{OH}}{D_H}\frac{K_w}{C_H^2}J_H$ (see Eq. (G5) in Appendix D-G) and Eq. (C1), for one-dimensional model, the first independent equation of the above three can be changed in form to read:

$$\left\{\left(1+\frac{K_w}{C_H^{*2}}\right)\frac{\partial C_H}{\partial t}+\frac{\partial C_{HCO_3}}{\partial t}+\frac{\partial C_I}{\partial t}\right\}\Bigg|_{x=0}=-\frac{\left(1+\frac{D_{OH}}{D_H}\frac{K_w}{C_H^{*2}}\right)J_H^*+J_{HCO_3}^*+J_I^*-i/F}{x_a} \quad \text{(D1)}$$

The other two equations yield,

$$\left(\frac{\partial C_{CO_3}}{\partial t}+\frac{\partial C_{HCO_3}}{\partial t}\right)\Bigg|_{x=0}=-\frac{J_{CO_3}^*+J_{HCO_3}^*}{x_a} \quad \text{(D2)} \quad \text{and} \quad \left(\frac{\partial C_I}{\partial t}+\frac{\partial C_M}{\partial t}\right)\Bigg|_{x=0}=-\frac{J_I^*+J_M^*}{x_a} \quad \text{(D3)}$$

From the three equilibria $\log(C_M/C_I)=-pK_a+pH$, $\log(C_{HCO_3}/C_{CO_2(aq)})=-pK_1+pH$ and $\log(C_{CO_3}/C_{HCO_3})=-pK_2+pH$, the following expressions are derived by differentiation with respect to time:

$$C_H^*\cdot\frac{\partial C_M}{\partial t}\Bigg|_{x=0}+C_M^*\cdot\frac{\partial C_H}{\partial t}\Bigg|_{x=0}=10^{-pK_a}\frac{\partial C_I}{\partial t}\Bigg|_{x=0} \quad \text{(D4) and} \quad C_H^*\cdot\frac{\partial C_{CO_3}}{\partial t}\Bigg|_{x=0}+C_{CO_3}^*\cdot\frac{\partial C_H}{\partial t}\Bigg|_{x=0}=10^{-pK_2}\frac{\partial C_{HCO_3}}{\partial t}\Bigg|_{x=0} \quad \text{(D5)}$$

APPENDIX D-E

The reaction rates have following relationships (note that here the rate concerned with reaction (5-P) and (5-Q) is expressed as R_P^*, and R_Q^*):

$$R_{R(NH_3)_2}^*=R_Q^*,\ R_I^*=R_{C'}^*-R_Q^*,\ R_M^*=-R_{C'}^*,\ R_{CO_3}^*=-R_{D'}^*,\ R_{HCO_3}^*=R_{D'}^*-R_P^*,$$

$$R_{CO_2(aq)}^*=R_P^*,\ R_H^*=-R_{C'}^*-R_{D'}^*+R_E^*-R_P^*-R_Q^*,\ R_{OH}^*=R_E^*.$$

Eliminating, $R_{C'}^*$, $R_{D'}^*$, $R_{E'}^*$, R_P^*, and R_Q^*, the following three independent equations are obtained:

$$R_H^*-R_{OH}^*+R_{HCO_3}^*+2R_{CO_2(aq)}^*+R_I^*+R_{R(NH_3)_2}^*=0,\ R_I^*+R_M^*+R_{R(NH_3)_2}^*=0,$$

$$R_{CO_3}^*+R_{HCO_3}^*+R_{CO_2(aq)}^*=0.$$

For example in the case of one-dimensional model, from Eqs. (5-12) and (5-15), the following can be obtained paying attention to $i=i^H+i^{OH}$:

$$\left(\frac{\partial C_H}{\partial t}-\frac{\partial C_{OH}}{\partial t}\right)\Bigg|_{x=0}=\frac{-J_H^*+J_{OH}^*-k_1C_H^*+i/F}{x_a}+R_H^*-R_{OH}^* \quad \text{(E1)}$$

Similarly using Eq. (G5) and Eq. (E1), the first independent equation of above three can be changed as follows:

$$\left\{\left(1+\frac{K_w}{C_H^{*2}}\right)\frac{\partial C_H}{\partial t}+\frac{\partial C_{HCO_3}}{\partial t}+2\cdot\frac{\partial C_{CO_2(aq)}}{\partial t}+\frac{\partial C_I}{\partial t}+\frac{\partial C_{R(NH_3)_2}}{\partial t}\right\}\Bigg|_{x=0}=-\frac{\left(1+\frac{D_{OH}}{D_H}\frac{K_w}{C_H^{*2}}\right)J_H^*+J_{HCO_3}^*+2\cdot J_{CO_2(aq)}^*+J_I^*+J_{R(NH_3)_2}^*-i/F}{x_a} \quad \text{(E2)}$$

The other two equations yield,

$$\left(\frac{\partial C_{CO_3}}{\partial t}+\frac{\partial C_{HCO_3}}{\partial t}+\frac{\partial C_{CO_2(aq)}}{\partial t}\right)\Bigg|_{x=0}=-\frac{J_{CO_3}^*+J_{HCO_3}^*+J_{CO_2(aq)}^*-k_1C_H^*}{x_a} \quad \text{(E3)}$$

and

$$\left(\frac{\partial C_I}{\partial t}+\frac{\partial C_M}{\partial t}+\frac{\partial C_{R(NH_3)_2}}{\partial t}\right)\Bigg|_{x=0}=-\frac{J_I^*+J_M^*+J_{R(NH_3)_2}^*}{x_a} \quad \text{(E4)}$$

From the solution equilibrium $\log(C_{HCO_3}/C_{CO_2(aq)})=-pK_1+pH$ and $\log(C_I/C_{R(NH_3)_2})=-pK_{a1}+pH$, the following two equations are derived by differentiation with respect to time:

$$C_H^*\cdot\frac{\partial C_{HCO_3}}{\partial t}\Bigg|_{x=0}+C_{HCO_3}^*\cdot\frac{\partial C_H}{\partial t}\Bigg|_{x=0}=10^{-pK_1}\frac{\partial C_{CO_2(aq)}}{\partial t}\Bigg|_{x=0} \quad \text{(E5) and} \quad C_H^*\cdot\frac{\partial C_I}{\partial t}\Bigg|_{x=0}+C_I^*\cdot\frac{\partial C_H}{\partial t}\Bigg|_{x=0}=10^{-pK_{a1}}\frac{\partial C_{R(NH_3)_2}}{\partial t}\Bigg|_{x=0} \quad \text{(E6)}$$

APPENDIX D-F

If the rate of reaction (5-T) from left to right is expressed as R_T, and so on, the reaction rate for each species can be written with R_C and R_T, as follows:

$$R_{Ca}=R_T,\ R_I=-R_C,\ R_M=R_C,\ R_{OH}=2R_T-R_C.$$

Eliminating R_C and R_T from the right hand side of the above equations, the following two independent equations are obtained:

$$R_{OH}-2R_{Ca}-R_I=0,\ R_I+R_M=0.$$

From Eq. (5-9) or (5-34) and the above two equations, the following are derived:

$$\frac{\partial C_{OH}}{\partial t} - 2\frac{\partial C_{Ca}}{\partial t} - \frac{\partial C_I}{\partial t} = \Lambda_{OH} - 2\Lambda_{Ca} - \Lambda_I \quad \text{(F1)} \quad \text{and} \quad \frac{\partial C_I}{\partial t} + \frac{\partial C_M}{\partial t} = \Lambda_I + \Lambda_M \quad \text{(F2)}$$

From the solubility equilibrium condition of calcium hydroxide: $C_{Ca} \cdot C_{OH}^2 = K_{s3}$, the following equation is obtained by differentiating with respect to time:

$$2C_{Ca} \cdot \frac{\partial C_{OH}}{\partial t} + C_{OH} \cdot \frac{\partial C_{Ca}}{\partial t} = 0 \quad \text{(F3)}$$

Equilibria involving the molecular/ionic inhibitor species are represented by: $\log(C_M/C_I) = -pK_a + pH$, yields,

$$\frac{\partial C_I}{\partial t} C_{OH} + \frac{\partial C_{OH}}{\partial t} C_I - 10^{pK_a - pK_w} \cdot \frac{\partial C_M}{\partial t} = 0 \quad \text{(F4)}$$

APPENDIX D-G

Since J satisfies the flux equation (Eq. (5-2)), J_H can be written as follows using $C_H \cdot C_{OH} = K_w$ and $\frac{\partial C_H}{\partial t} = -\frac{K_w}{C_{OH}^2}\frac{\partial C_{OH}}{\partial t}$,

$$J_H = -D_H \nabla C_H - z_H D_H \left(\frac{F}{RT}\nabla\phi\right) C_H = D_H \frac{K_w}{C_{OH}^2} \nabla C_{OH} - z_H D_H \left(\frac{F}{RT}\nabla\phi\right)\frac{K_w}{C_{OH}} \quad \text{(G1)}$$

Note that, for one-dimensional model, $\nabla C_I = \frac{\partial C_I}{\partial x}$ and so on.

J_{OH} being expressed as Eq. (G2) below, Eq. (G1) is simplified as Eq. (G3) taking into account, z_{OH}=-1 and z_H=1,

$$J_{OH} = -D_{OH} \nabla C_{OH} - z_{OH} D_{OH} \left(\frac{F}{RT}\nabla\phi\right) C_{OH} \quad \text{(G2)}$$

$$J_H = D_H \frac{K_w}{C_{OH}^2} \nabla C_{OH} + z_{OH} D_H \left(\frac{F}{RT}\nabla\phi\right)\frac{K_w}{C_{OH}}$$

$$= -\frac{D_H}{D_{OH}}\frac{K_w}{C_{OH}^2}\left[-D_{OH}\nabla C_{OH} - z_{OH} D_{OH}\left(\frac{F}{RT}\nabla\phi\right) C_{OH}\right] = -\frac{D_H}{D_{OH}}\frac{K_w}{C_{OH}^2} J_{OH} \quad \text{(G3)}$$

Since the definition of $\Lambda_I(x)$ is $\Lambda_I = \frac{J_I(x)}{dx} - \frac{J_I(x+dx)}{dx}$ or $\Lambda_I = \left(\frac{J_I(x)}{dx} - \frac{J_I(x+dx)}{dx}\right) + \left(\frac{J_I(z)}{dz} - \frac{J_I(z+dz)}{dz}\right)$ for one-dimensional or two-dimensional models respectively (in Appendix D-A), the following is finally derived:

$$\Lambda_H = -\frac{D_H}{D_{OH}}\frac{K_w}{C_{OH}^2}\Lambda_{OH} \quad \text{(G4)}$$

When J_{OH} is associated with J_H, the following can be derived using $C_H \cdot C_{OH} = K_w$ and Eq. (G3):

$$J_{OH} = -\frac{D_{OH}}{D_H}\frac{K_w}{C_H^2} J_H \quad \text{(G5)}$$

APPENDIX D-H

When Vc litres of Cc mol/l inhibitor solution are titrated against C_N mol/l nitric acid, the pH of the mixed solution can be obtained as a function of the volume (V litres) of nitric acid added as follows:

Mass balance: $m_I + m_M = C_C \cdot V_C$ (H1)

Equilibrium: $\frac{\gamma_m m_M/(V_c+V)\cdot\gamma_1 C_H}{\gamma_1 m_I/(V_c+V)} = 10^{-pKa}$, thus $m_M/m_I = 10^{-pKa'+pH}$ (H2)

Electroneutrality: $C_I + C_H = C_{NO_3} + C_{OH}$, thus $C_I/(V_c+V) = C_N \cdot V/(V_c+V) + 10^{pH-14}$ (H3)

where m_I, m_M are number of moles of inhibitor ions and molecules in the solution, and $10^{-pKa'} = \gamma_m 10^{-pKa}$. The concentration of hydrogen ion is neglected in Eq. (H3) since it is not significant in an alkaline solution. $m_I = C_c V_c/(10^{-pKa'+pH} + 1)$ is obtained from (H1) and (H2), and substituting this into (H3), the following is obtained using $K_a' = 10^{-pKa'}$,

$$10^{pH} = \frac{10^{14} Ka' C_N V + V_C + V}{2(V_c+V)Ka'}\left(-1 + \sqrt{1 - \frac{4\cdot 10^{14} Ka'(V_C+V)(C_N V - C_C V_C)}{(10^{14} Ka' C_N V + V_C + V)^2}}\right) \quad \text{(H4)}$$

Since $4\cdot10^{14}Ka'(V_C+V)(C_NV-C_CV_C)/(10^{14}Ka'C_NV+V_C+V)^2 << 1$, Eq. (H4) can be approximated as follows:

$$pH(V) \approx 14 + \log\frac{C_CV_C - C_NV}{10^{14}Ka'C_NV + V_C} \qquad \text{(H5)}$$

where V in the term $(10^{14}Ka'C_NV+V_C+V)$ is neglected since it is insignificant in comparison with $10^{14}Ka'C_NV$. If pH(V) in (H5) is differentiated twice with respect to V, the point of inflexion can be obtained as follows,

$$\frac{d^2(pH(V))}{dV^2} = 0 \Leftrightarrow V = \frac{10^{14}Ka'C_C - 1}{2\cdot10^{14}Ka'C_N}\cdot V_C \qquad \text{(H6)}$$

Then the pH at the point of inflexion is finally obtained by substituting (H6) into (H5), thus,

$$pH = pKa' \qquad \text{(H7)}$$

APPENDIX E:

THE COMPLETE LISTS OF WEIGHT LOSSES OF BARS EMBEDDED IN ELECTROCHEMICALLY TREATED SPECIMENS

Table E.1 Guanidine-treated specimens (NG); Total average: 2.29, variance: 2.26

Sample No.	Weight loss at each section No. (mg/cm^2)							
	1	2	3	4	5	6	7	8
1	0.35	0.59	1.25	1.48	2.75	1.91	1.61	1.12
2	0.99	1.38	2.89	1.33	2.44	2.22	2.47	4.12
3	1.35	1.66	7.52	2.55	3.08	4.10	2.24	3.55

Table E.2 Ethanolamine N.-treated specimens (NEn); Total average: 1.20, variance: 0.58

Sample No.	Weight loss at each section No. (mg/cm^2)							
	1	2	3	4	5	6	7	8
1	1.44	1.02	0.62	0.71	0.67	1.84	1.09	0.98
2	0.80	0.57	0.13	0.64	0.43	0.88	0.72	0.20
3	2.01	1.33	1.64	2.33	2.80	2.68	2.19	1.12

Table E.3 Ethanolamine C.-treated specimens (NEc); Total average: 1.15, variance: 0.35

Sample No.	Weight loss at each section No. (mg/cm^2)							
	1	2	3	4	5	6	7	8
1	0.30	0.65	0.42	0.42	0.31	0.96	0.50	0.48
2	1.13	1.98	1.67	1.60	2.13	2.36	1.79	1.23
3	1.44	1.09	0.97	1.56	1.43	0.88	1.34	1.06

Table E.4 Arginine-treated specimens (NA); Total average: 2.72, variance: 2.16

Sample No.	Weight loss at each section No. (mg/cm^2)							
	1	2	3	4	5	6	7	8
1	1.86	0.28	1.80	3.87	4.41	1.73	2.39	2.11
2	1.36	0.52	2.98	2.64	3.15	2.22	2.13	4.12
3	2.38	1.12	3.54	3.67	6.65	2.41	2.55	5.43

Table E.5 Electrochemically re-alkalised specimens (NR); Total average: 5.79, variance: 12.15

Sample No.	Weight loss at each section No. (mg/cm^2)							
	1	2	3	4	5	6	7	8
1	6.54	5.47	12.38	15.98	13.33	6.81	8.21	6.69
2	2.85	2.88	4.24	4.71	4.29	4.12	3.49	2.67
3	3.37	2.67	5.11	5.10	5.80	4.74	4.48	3.14

Table E.6 Control specimens (NC); Total average: 4.17, variance: 4.02

Sample No.	Weight loss at each section No. (mg/cm^2)							
	1	2	3	4	5	6	7	8
1	7.42	3.51	7.99	7.40	4.15	6.70	6.12	8.37
2	2.67	2.35	3.67	3.12	2.42	2.45	2.76	2.19
3	3.48	2.99	4.53	3.75	3.60	2.19	2.41	3.78

[Keys] N.: nitrate, C.: carbonate for ethanolamine-treated specimens

APPENDIX F:

THE STABILITY OF THE NUMERICAL SOLUTION

The number of elements and the time steps required to obtain results with good accuracy and to ensure convergence of the numerical solutions were investigated. Figure (A) below shows the accuracy of the solution with increasing number of elements (N). The "error" in the Figure is concerned with the ratio of the concentration of the injected inhibitor at the cathode calculated when a certain number of elements was used, to that calculated when N=1,000 was used (Error(%)=$(C_N-C_{1,000})/C_{1,000}\times100$). The Figure also describes the time step threshold at which divergence occurs. The value of "error" did not significantly depend on dt as long as the solution yielded convergence under the same element number. It can be seen from this Figure that the calculated condition employed in the present report (N=500 and dt=10 or 60) has good accuracy and ensures convergence. Figure (B) below shows the divergence-convergence threshold relationship between dx (element length) and dt (time step), which can be approximated by the theoretical divergence-convergence parabolic curve ($dt/(dx)^2$=const.) (Noye 1982).

Figure (A)

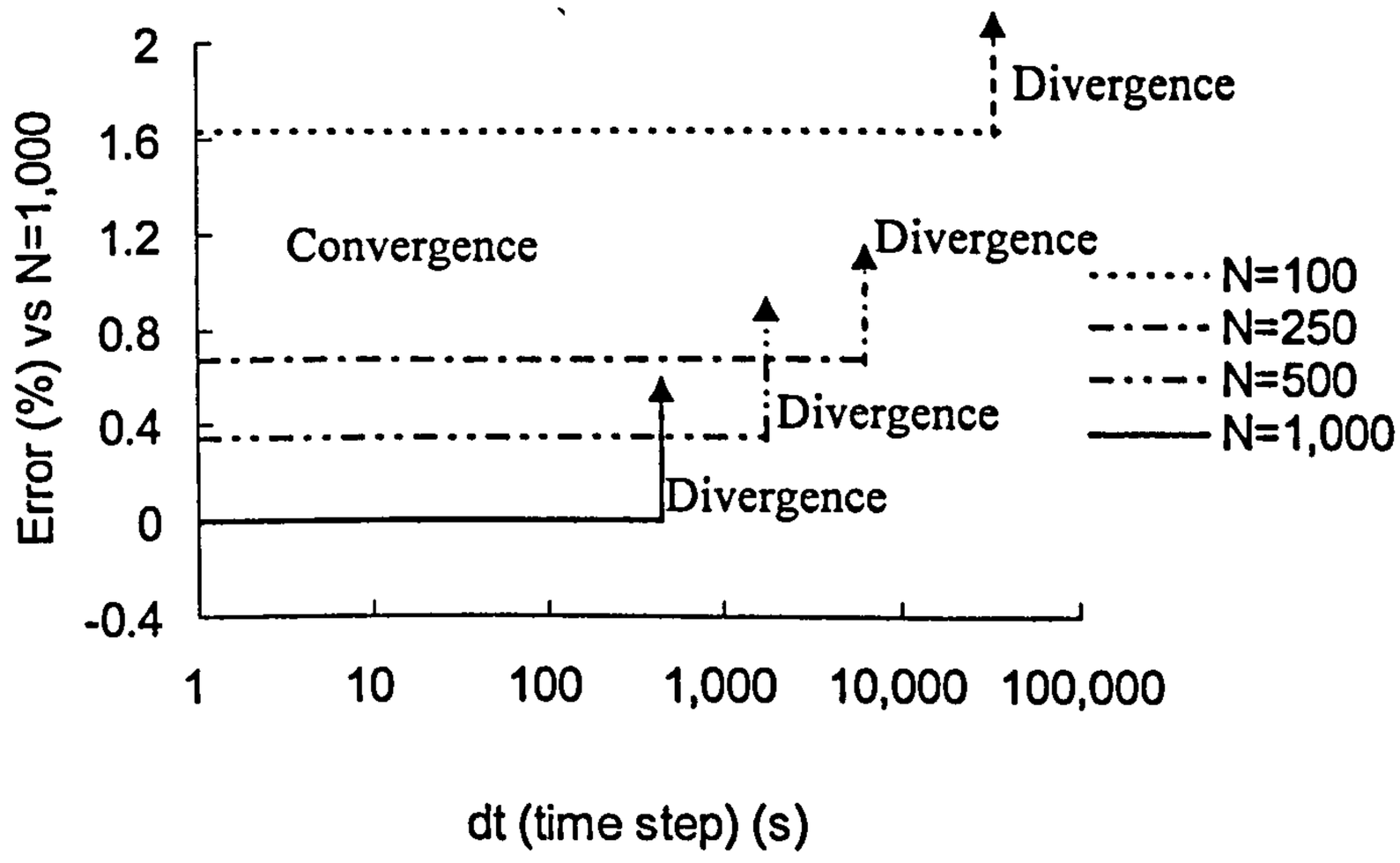

Figure (B)

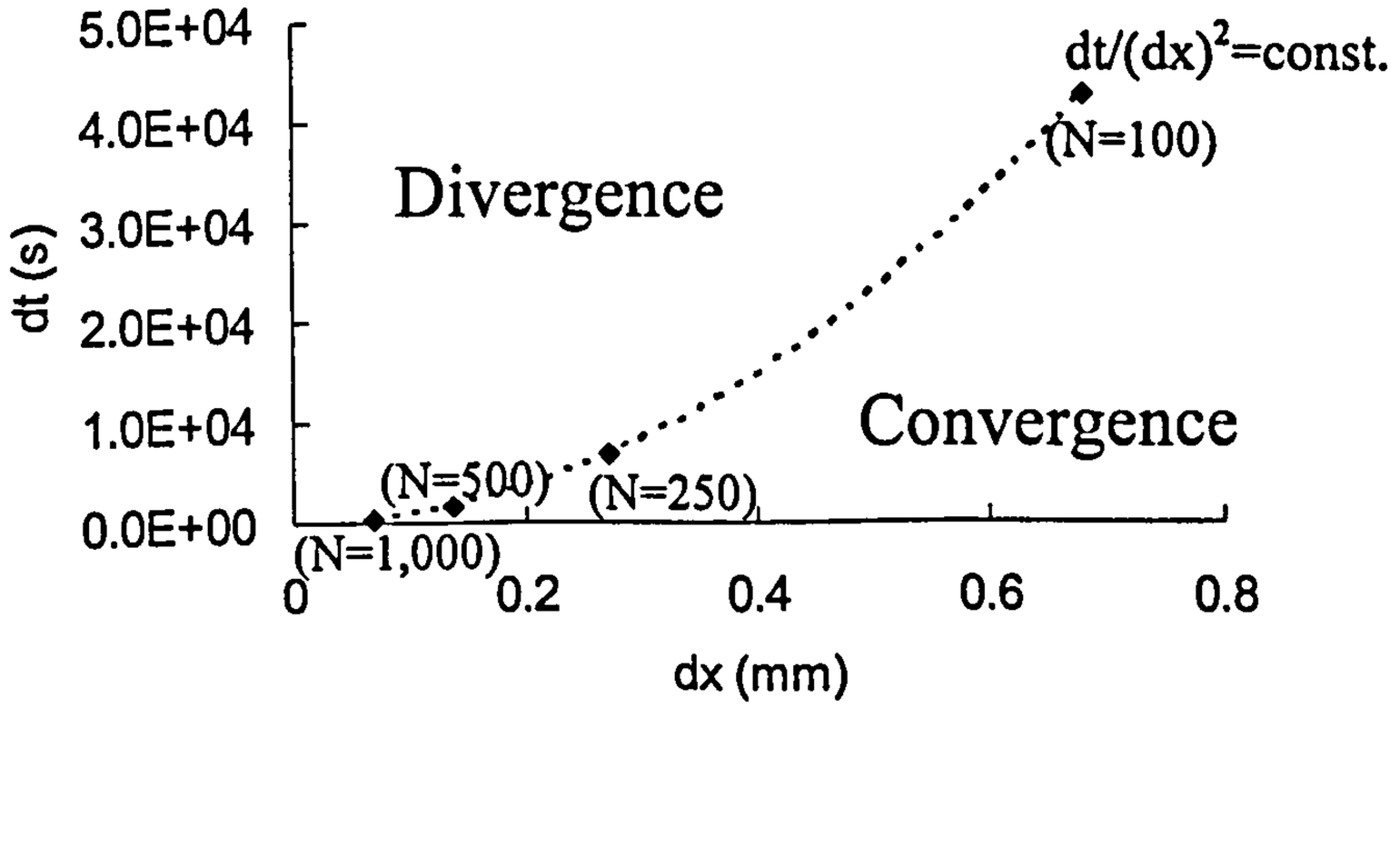

APPENDIX G:

PUBLISHED WORK

1. J. Kubo, S. Sawada, C. L. Page, and M. M. Page, 2007, Electrochemical injection of organic corrosion inhibitors into carbonated cementitious materials: Part 2. Mathematical modelling, Corrosion Science, 49, pp. 1205-1227.

2. S. Sawada, J. Kubo, C. L. Page, and M. M. Page, 2007, Electrochemical injection of organic corrosion inhibitors into carbonated cementitious materials: Part 1. Effects on pore solution chemistry, Corrosion Science, 49, pp. 1186-1204.

Available online at www.sciencedirect.com
ScienceDirect
Corrosion Science 49 (2007) 1205–1227
CORROSION SCIENCE
www.elsevier.com/locate/corsci

Electrochemical injection of organic corrosion inhibitors into carbonated cementitious materials: Part 2. Mathematical modelling

J. Kubo, S. Sawada [1], C.L. Page *, M.M. Page

School of Civil Engineering, University of Leeds, Leeds LS2 9JT, UK

Received 29 November 2005; accepted 8 June 2006
Available online 28 August 2006

Abstract

A mathematical model is presented for simulation of changes in the pore solution phase chemistry of carbonated hardened cement paste when aqueous solutions of organic base corrosion inhibitors are applied to the surface of the material and constant current densities in the range of 1–5 A/m^2 are passed between anodes placed within the inhibitor solutions and steel mesh cathodes embedded within the paste. The model, based on the Nernst–Planck equation, is used to predict the concentration profiles of electrochemically injected inhibitors and the major ionic species present within the pore electrolyte. For two specific organic base inhibitors with widely different pK_a values, viz. ethanolamine (pK_a 9.5) and guanidine (pK_a 13.6), the model predictions are compared with experimental results described in Part 1 of the investigations.

Keywords: A. Cement; A. Organic corrosion inhibitors; B. Electrochemical injection; B. Mathematical modelling; C. Carbonation

* Corresponding author. Tel.: +44 113 343 2283; fax: +44 113 343 2243.
E-mail address: c.l.page@leeds.ac.uk (C.L. Page).
[1] Present address: Nuclear Power Department, Kajima Corporation, 5-30 Akasaka 6-Chome, Minato-ku, Tokyo 107-8502, Japan.

0010-938X/$ - see front matter © 2006 Elsevier Ltd. All rights reserved.
doi:10.1016/j.corsci.2006.06.015

1. Introduction

The aim of this study was to establish a mathematical model for simulation of changes in the pore solution phase chemistry of carbonated hardened cement paste when basic organic corrosion inhibitors of the types investigated in Part 1 [1] are electrochemically injected under the influence of an applied current. Several researches on the modelling of migration of ions in concrete or related porous media have been reported, most of which are concerned with electrochemical chloride extraction. In some of these models, the transport of only a single ionic species, namely chloride ion, has been considered [2–4]. In others, however, the involvement of the various ions in the pore solution phase of the hydrated cement matrix within concrete has been accounted for and, in some cases, binding interactions at pore surfaces have also been included [5–10].

In the present work, two organic base corrosion inhibitors, ethanolamine ($HO–CH_2–CH_2–NH_2$) and guanidine ($HN=C(NH_2)_2$) with pK_a values of 9.5 and 13.6, respectively [11], were studied. To elucidate their migration in carbonated cementitious materials, it was necessary to examine the interactions of various ions in the pore solution phase, taking account of acid/base dissociation equilibria and the solubility products of relevant species, such as calcium carbonate, calcium sulfate and calcium hydroxide. The results derived from modelling are compared with the experimental data published in Part 1 of the investigations [1].

2. Transport of ions in porous media

It is well known that the transport of ions in an ideal electrolyte can be described by the equations of mass balance, ionic flux (Nernst–Planck), current conservation and electroneutrality in one dimension as follows [12,13]:

$$\frac{\partial C_i}{\partial t} = -\frac{\partial J_i}{\partial x} \tag{1}$$

$$J_i = -D_i \frac{\partial C_i}{\partial x} - z_i D_i \left(\frac{F}{RT}\frac{\partial \phi}{\partial x}\right) C_i \tag{2}$$

$$i = F\sum_{i=1}^{n} z_i J_i \tag{3}$$

$$\sum_{i=1}^{n} z_i C_i = 0 \tag{4}$$

where C_i is the concentration (mol/m^3), J_i is the flux (mol/m^2/s), D_i is the diffusion coefficient (m^2/s), z_i is the charge number of the ionic species i, F is the Faraday constant (9.64846×10^4 C/mol), R is the gas constant (8.3143 J/mol K), T is the temperature (K), ϕ is the potential (V), i is the current density applied to the pore solution (A/m^2), t is the time (s), and x is the position coordinate (m). Convection is assumed to be negligible in this model. Substituting Eq. (2) into (3), then into (1), we have

$$\frac{\partial C_i}{\partial t} = \frac{\partial}{\partial x}\left[D_i \frac{\partial C_i}{\partial x} - z_i D_i \frac{i/F + \sum z_i D_i \frac{\partial C_i}{\partial x}}{\sum z_i^2 D_i C_i} C_i\right] \tag{5}$$

Eq. (5) fully describes the transport behaviour of ions in an ideal electrolyte and gives the concentration profile of every ionic species for given initial and boundary conditions. The

fact that electro-neutrality (Eq. (4)) is maintained in the case of constant externally applied current is shown by multiplying the valence numbers by Eq. (1) and summing both sides for all species

$$\frac{\partial}{\partial t}\left(\sum_{i=1}^{n} z_i C_i\right) = -\frac{\partial}{\partial x}\left(\sum_{i=1}^{n} z_i J_i\right) = -\frac{1}{F}\frac{\partial i}{\partial x} \tag{6}$$

For a porous medium, such as concrete or a hydrated cement paste, the porosity and tortuosity need to be taken into account, leading to the following:

$$\tau^2 \frac{\partial C_i}{\partial t} = \frac{\partial}{\partial x}\left[D_i \frac{\partial C_i}{\partial x} - z_i D_i \frac{(\tau i)/(\varepsilon^2 F) + \sum z_i D_i \frac{\partial C_i}{\partial x}}{\sum z_i^2 D_i C_i} C_i\right] \tag{7}$$

where τ is the tortuosity of the pore structure and ε is the volume fraction of porosity.

3. Physical model

The physical system to which the above model is applied is shown in Fig. 1. It is assumed that an aqueous solution of the relevant corrosion inhibitor is applied to the surface of the carbonated cement paste and constant current density is passed between an anode placed in the inhibitor solution and a steel mesh cathode embedded within the cement paste. To simulate the dimensions of the specimens used in the experiments detailed in Part 1 [1], the cover depth and the thickness of the medium behind the steel cathode are set as $x_1 = 34$ mm and $x_2 = 16$ mm, respectively. In this model, the species in the pore solution taken into consideration are the same as in Part 1 [1] except for magnesium since its concentration was insignificant. It is also assumed that, in carbonated cement pastes, the only solid phases with solubility products that have to be taken into account are calcite and gypsum; all other solid carbonation products at the surfaces of the pores (such as hydrated silica and alumina gels) are simply regarded as insoluble, non-reacting components, which have negligible influence on the pore solution composition. The tortuosity τ is assumed to be 2 [8] and the porosity to be 0.34, the latter value being calculated from experimental data shown in Part 1 [1].

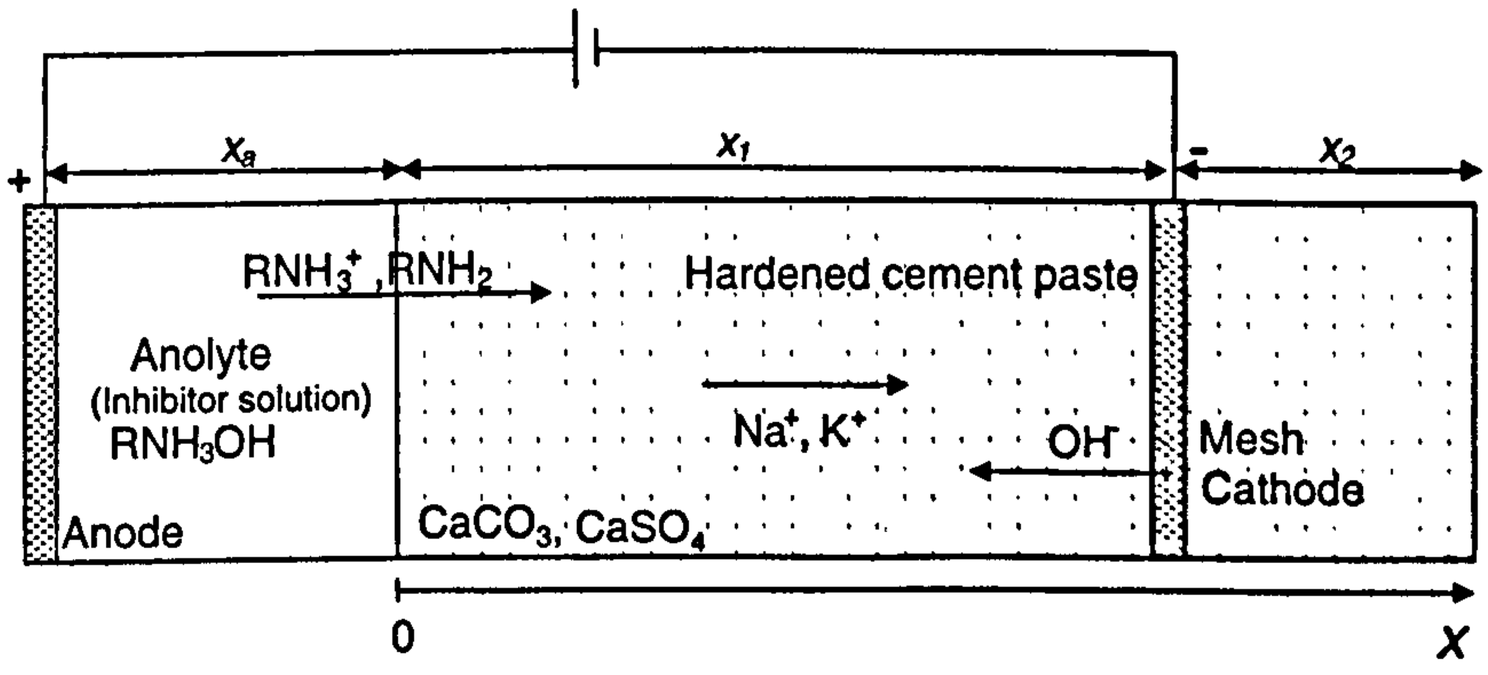

Fig. 1. Physical system of transport in hardened cement.

4. General and boundary conditions

4.1. General conditions in the pore solution

When an amine or alkanolamine-based corrosion inhibitor penetrates into an idealised carbonated cementitious material of the above type, the following chemical equilibria are assumed to be involved:

$$CaCO_3 \Longleftrightarrow Ca^{2+} + CO_3^{2-} \quad (A)$$

$$CaSO_4 \Longleftrightarrow Ca^{2+} + SO_4^{2-} \quad (B)$$

$$RNH_3^+ + OH^- \Longleftrightarrow RNH_2 + H_2O \quad (C)$$

$$HCO_3^- + OH^- \Longleftrightarrow CO_3^{2-} + H_2O \quad (D)$$

$$H_2O \Longleftrightarrow H^+ + OH^- \quad (E)$$

Since the pH of the pore solution within carbonated cementitious media is usually near 9.0 and the pK_a for the reaction

$$CO_2(aq) + H_2O \Longleftrightarrow HCO_3^- + H^+$$

is 6.35 [11], the concentration of carbonic acid is negligible. The formation of carbamate by the following reaction (F) [14] is also assumed to be insignificant since the concentration of $CO_2(aq)$ is very low

$$CO_2(aq) + 2RNH_2 \Longleftrightarrow RNH_3^+ + RNHCOO^- \quad (F)$$

If we consider an infinitesimal element of length, dx, the rates of change of concentration for each species i (caused by the inward and outward fluxes and the rates R_i of chemical reactions that produce species within the domain) can be expressed as follows:

$$\frac{\partial C_i}{\partial t} = \frac{J_i(x)}{dx} - \frac{J_i(x+dx)}{dx} + R_i \quad (8)$$

Note: $R_i = 0$ for ions such as sodium, potassium, chloride, and nitrate that are assumed not to react chemically with other species in the domain. For these species, the time derivatives of concentration are obtained from this equation. For other species, after each R_i term is eliminated by the procedures shown in Appendix A, Eqs. (A.1), (A.2), (A.5), (A.6)–(A.9) are obtained, which are the seven simultaneous equations to be solved to obtain time derivatives of concentration.

4.2. Boundary conditions at the cathode

At the steel cathode, there are two reactions generating hydroxyl ions due to water electrolysis:

$$2H_2O + 2e^- \rightarrow 2OH^- + H_2 \quad (G)$$

$$2H_2O + O_2 + 4e^- \rightarrow 4OH^- \quad (H)$$

Thus the boundary condition for hydroxyl ions at the cathode is simply expressed as follows:

$$J_{OH} = \frac{i}{z_{OH}F} = -\frac{i}{F} \quad (9)$$

Since (G) and (H) are the only reactions considered to take place at the cathode surface, it is assumed that the fluxes of other ion species are not affected by the existence of the steel.

4.3. Boundary conditions in the cathode region at a high pH

As shown in Part 1 [1] and in previous investigations [15], the concentration of calcium ions present in the pore solution phase of carbonated cement pastes is typically >20 mmol/l. Since the concentration of hydroxyl ions near the cathode is raised by reactions (G) and (H), it is to be expected that calcium hydroxide precipitation will occur locally when the concentrations of Ca^{2+} and OH^- ions exceed the solubility product for the reaction:

$$Ca^{2+} + 2OH^- \Rightarrow Ca(OH)_2 \quad (I)$$

After the system reaches this stage, the calcium ions consumed by reaction (I) are assumed to be replenished by reactions (A) and (B) so that the equilibrium saturation conditions for $CaSO_4$, $CaCO_3$ and $Ca(OH)_2$ are maintained. Thus at this stage the boundary condition must take into consideration the reactions (A)–(E) and (I). In this case, for the species that are assumed to react chemically with other species in the domain, after each R_i term in Eq. (8) is eliminated by the procedures shown in Appendix B, Eqs. (A.5)–(A.8) and (B.1)–(B.3) are obtained as the seven simultaneous equations to be solved for the time derivatives of concentration.

4.4. Boundary conditions at the anolyte interface

The pH of the external anolyte is assumed to be lowered by the following two reactions taking place at the anode:

$$4OH^- \Rightarrow 2H_2O + O_2 + 4e^- \quad (J)$$

$$2H_2O \Rightarrow O_2 + 4H^+ + 4e^- \quad (K)$$

If the current density consumed by each of the above reactions at the anode can be expressed as i^{OH} and i^{H}, respectively, the boundary conditions for each ionic species are described as follows:

$$\left.\frac{\partial C_H}{\partial t}\right|_{x=0} = \frac{i^H/F}{x_a} - \frac{J^*_H}{x_a} + R^*_H \quad (10)$$

$$\left.\frac{\partial C_{OH}}{\partial t}\right|_{x=0} = -\frac{i^{OH}/F}{x_a} - \frac{J^*_{OH}}{x_a} + R^*_{OH} \quad (11)$$

$$\left.\frac{\partial C_i}{\partial t}\right|_{x=0} = -\frac{J^*_i}{x_a} + R^*_i \quad (i \neq H \text{ and } i \neq OH) \quad (12)$$

where * denotes the values defined at the interface and R^*_H and R^*_{OH} are the reaction rates of other chemical reactions at the interface involving H^+ and OH^- ions. It is also assumed that the concentrations of all species in the anolyte are uniform since the transport of ions in the external electrolyte is much faster than in the internal pore solution.

4.4.1. Anolyte with alkaline pH

Before the anolyte solution is neutralised by reactions (J) and (K), it is assumed that the three reactions (C)–(E) take place. For the species that are assumed to react chemically

with other species in the anolyte, after each R_i term in Eqs. (10)–(12) is eliminated by the procedures shown in Appendix C, Eqs. (A.7), (A.8) and (C.2)–(C.4) are obtained as the five simultaneous equations to be solved for the time derivatives of concentration.

4.4.2. Anolyte with neutral pH

As the pH value of the anolyte is lowered to the near-neutral region, but before it becomes low enough to start dissolving significant quantities of solid material from the surface of the carbonated cement paste, it is assumed that the following reactions occur as well as reaction (E):

$$RNH_2 + H^+ \Longleftrightarrow RNH_3^+ \tag{C'}$$

$$CO_3^{2-} + H^+ \Longleftrightarrow HCO_3^- \tag{D'}$$

For the species that are assumed to react chemically with other species in the anolyte, after each R_i term in Eqs. (10)–(12) is eliminated by the procedures shown in Appendix D, Eqs. (D.1)–(D.5) are obtained as the five simultaneous equations to be solved for the time derivatives of concentration.

4.4.3. Anolyte with acidic pH

The enhancement in concentration of hydrogen ion at the anode eventually causes dissolution of calcium carbonate (assumed to be in the form of calcite) from the surface of the carbonated cement paste. In this process, the following reaction is dominant under acidic conditions (pH < 4) [16]:

$$CaCO_3 + H^+ \Rightarrow Ca^{2+} + HCO_3^- \tag{L}$$

the dissolution flux J_{Diss} being given by:

$$J_{Diss} = k_1[H^+] = k_1 C_H^* \tag{13}$$

where k_1 is a dissolution rate constant. *Note*: J_{Diss} has a positive value if the flux goes in the negative x-direction. Therefore the boundary conditions for hydrogen, calcium, and bicarbonate are changed from Eqs. (10) and (12) as follows:

$$\left.\frac{\partial C_H}{\partial t}\right|_{x=0} = \frac{i^H/F}{x_a} - \frac{J_H^*}{x_a} - \frac{J_{Diss}}{x_a} + R_H^* = \frac{i^H/F}{x_a} - \frac{J_H^*}{x_a} - \frac{k_1 C_H^*}{x_a} + R_H^* \tag{14}$$

$$\left.\frac{\partial C_{Ca}}{\partial t}\right|_{x=0} = -\frac{J_{Ca}^*}{x_a} + \frac{J_{Diss}}{x_a} = -\frac{J_{Ca}^*}{x_a} + \frac{k_1 C_H^*}{x_a} \tag{15}$$

$$\left.\frac{\partial C_{HCO_3}}{\partial t}\right|_{x=0} = -\frac{J_{HCO_3}^*}{x_a} + \frac{J_{Diss}}{x_a} + R_{HCO_3}^* = -\frac{J_{HCO_3}^*}{x_a} + \frac{k_1 C_H^*}{x_a} + R_{HCO_3}^* \tag{16}$$

Here the equilibrium between bicarbonate and hydrated carbon dioxide, for the equation shown below, needs to be introduced since pK_1 for the following reaction is 6.35 [11]:

$$HCO_3^- + H^+ \Longleftrightarrow CO_2(aq) + H_2O \tag{M}$$

For the species that are assumed to react chemically with other species in the anolyte, after each R_i term in Eqs. (11), (12), (14)–(16) is eliminated by the procedures shown in Appendix E, Eqs. (D.4), (D.5) and (E.2)–(E.5) are obtained as the six simultaneous equations whose solutions yield the time derivatives of concentration for each species. This condition is taken into account in the modelling to be described only when the pH of the anolyte is

below 4.0. In this model, $k_l = 1.65 \times 10^{-5}$ cm/s is derived from the average dissolution rate under non-stirring conditions, as reported elsewhere [17].

5. Activity coefficients

To account for the non-idealised behaviour of concentrated electrolytes, it is necessary to consider how to model the activity coefficients of the various ionic species [18]. These may be treated in several ways, as discussed elsewhere in relation to modelling of electrochemical chloride extraction from concrete [6]. In the present contribution, however, a modified Davies equation [19] (Eq. (17)) is used as this has been claimed to be usually fairly accurate over a range of ionic strengths up to 1200 mmol/l:

$$\ln \gamma_z = -\frac{Az^2\sqrt{I}}{1 + Ba\sqrt{I}} + \frac{((-4.17 \times 10^{-5})I + C)Az^2 I}{\sqrt{1000}} \tag{17}$$

where γ_z is the activity coefficient for the ionic species with a charge number of z, I is the ionic strength of the solution defined by $I = 0.5\sum_{j=1}^{n} z_j^2 C_j$ (mmol/l), A and B are the Debye–Hückel constant and extended Debye–Hückel constant, respectively, as shown in [19], C is 0.2 and a is the mean radius of all ions, which is assumed to be 0.3 nm in this model. The values of the equilibrium constants appearing in the previous sections are shown in Table 1 along with the corrections that need to be applied to them, taking into account the activity coefficients.

Whilst the activity coefficients of the ionic species referred to in Table 1 can be estimated by means of Eq. (17), those of the uncharged molecular species require further consideration. Thus the activity coefficient for hydrated carbon dioxide molecules, $CO_2(aq)$, is assumed to be 1.0 since their concentration in solution is quite low. Similarly, for guanidine solutions, the high pK_a value (13.6) implies that the proportion of guanidine existing in the molecular form is generally small enough for its activity coefficient to be assumed to be 1.0. In the case of ethanolamine solutions, however, the much lower pK_a value (9.5) means that the assumption would be invalid because a substantial proportion of the inhibitor exists as the molecular species in carbonated cement pore solutions. Thus for ethanolamine, a molecular activity coefficient, γ_m, must be introduced which can be incorporated into an apparent dissociation constant for the inhibitor, K'_a, expressed as follows:

Table 1
Equilibrium constants used in the model and their corrections

Species	Equilibrium constant	$-\log K$ [11]	Corrections (K')
RNH_2	$Ka = \gamma_m[RNH_2]\gamma_1[H^+]/\gamma_1[RNH_3^+]$	9.5 (Ethanolamine) 13.6 (Guanidine)	Ka/γ_m
HCO_3^-	$K_1 = \gamma_1[HCO_3^-]\gamma_1[H^+]/[CO_2(aq)]$	6.35	K_1/γ_1^2
CO_3^{2-}	$K_2 = \gamma_2[CO_3^{2-}]\gamma_1[H^+]/\gamma_1[HCO_3^-]$	10.33	K_2/γ_2
$CaCO_3$	$K_{s1} = \gamma_2[Ca^{2+}]\gamma_2[CO_3^{2-}]$	8.47	K_{s1}/γ_2^2
$CaSO_4$	$K_{s2} = \gamma_2[Ca^{2+}]\gamma_2[SO_4^{2-}]$	4.31	K_{s2}/γ_2^2
$Ca(OH)_2$	$K_{s3} = \gamma_2[Ca^{2+}]\gamma_1^2[OH^-]^2$	5.30	$K_{s3}/\gamma_1^2\gamma_2$
H_2O	$K_w = \gamma_1[H^+]\gamma_1[OH^-]$	14.0	K_w/γ_1^2

$$pK'_a = -\log\frac{[RNH_2]\cdot[H^+]}{[RNH_3^+]} = -\log\frac{\gamma_m\cdot[RNH_2]\cdot\gamma_1\cdot[H^+]}{\gamma_1\cdot[RNH_3^+]} + \log\gamma_m$$
$$= pK_a + \log\gamma_m \quad (18)$$

The activity coefficient of a neutral solute in an electrolyte solution may be estimated by means of the Pitzer model [20,21], from which the molecular activity coefficient, γ_m, of a species such as RNH_2 can be represented as follows:

$$\log\gamma_m \approx 2\left(\lambda_{RNH_2\cdot RNH_2}C_{RNH_2} + \sum_{i\neq RNH_2}\lambda_{RNH_2\cdot i}C_i\right) \quad (19)$$

where λ_{ij} are binary interaction parameters representing the short range interactions between the species i and j in the solution. This equation indicates that the activity coefficient is affected by the self-interaction between the inhibitor molecules and by the inhibitor molecule–ion interactions. Unfortunately, however, published λ_{ij} values relating to ethanolamine are not available. Thus, to provide some indication of the likely contributions to γ_m of the two different interactions, ethanolamine solutions at concentrations of 0.01, 0.1, 0.5 and 1.0 M were titrated against 1.0 M nitric acid. The solutions also contained Na_2SO_4 at concentrations of 0.0, 0.01, and 0.05 M because the two ions (Na^+ and SO_4^{2-}) are important constituents of the pore solution phase of carbonated cement pastes and they have been found to exhibit relatively large λ_{ij} values in aqueous ammonia solutions [22]. The titration curves are shown in Fig. 2 for the cases of 0.01 M, 0.1 M, 1.0 M ethanolamine without Na_2SO_4. The total number of moles was kept as 0.005 by adjusting the volume of the ethanolamine solutions. Since the point of inflexion of a titration curve indicates the pK'_a value of the initial solution, as shown in Appendix G, the pK'_a values were estimated from the zero points of the second derivatives of the titration curves, the latter being interpolated with a third order polynomial function. The results obtained for pK'_a and γ_m are shown in Table 2, from which the molecular self-interaction appeared to be dominant and the pK'_a value was approximately constant for ethanolamine solutions at concentrations >0.1 M. For the sake of simplicity, a constant pK'_a value of 9.75 was therefore assumed in the modelling reported below.

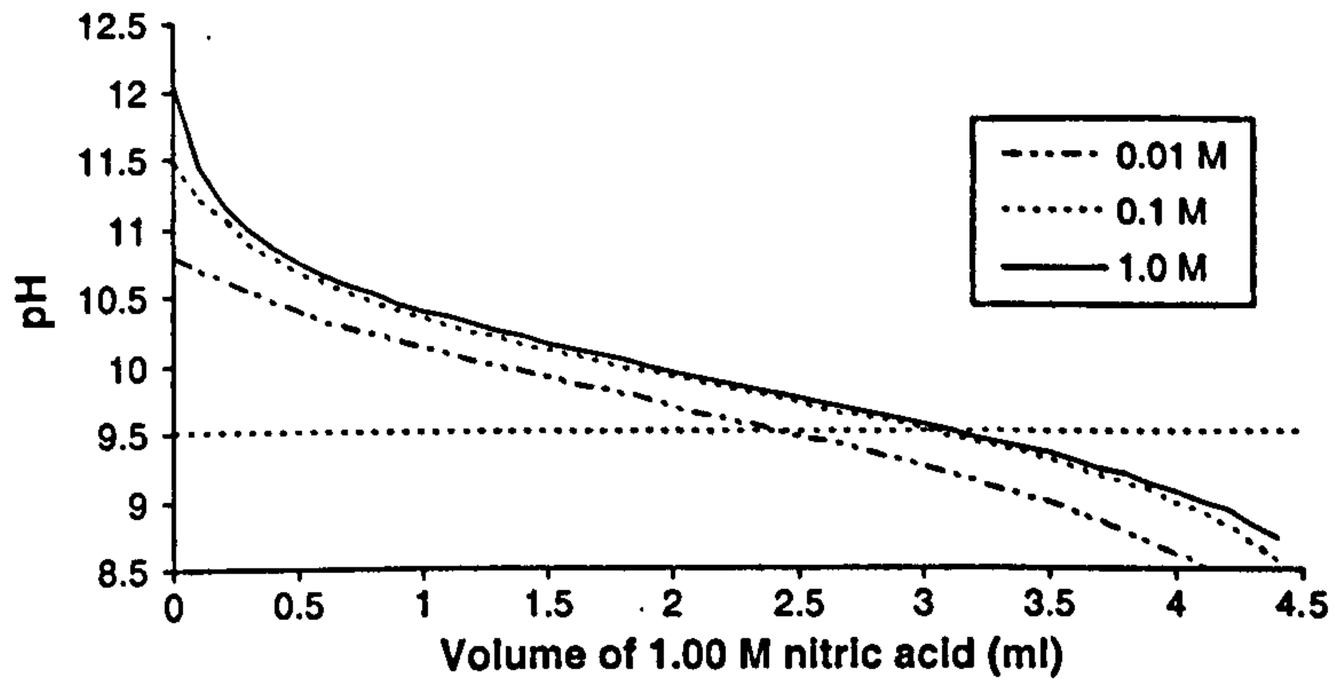

Fig. 2. Titration curves for 0.01 M, 0.1 M and 1.0 M ethanolamine solutions against 1 M nitric acid.

Table 2
pK'_a values of ethanolamine obtained from titrations

Concentration of inhibitor (mol/l)	Without Na_2SO_4		0.01 M Na_2SO_4		0.05 M Na_2SO_4	
	pK'_a	γ_m	pK'_a	γ_m	pK'_a	γ_m
Dilute solution	9.5 [11]	1.000	–	–	–	–
0.01	9.65	1.412	9.65	1.412	9.67	1.480
0.10	9.76	1.819	9.75	1.778	9.79	1.950
0.50	9.75	1.778	9.75	1.778	9.78	1.905
1.00	9.75	1.778	9.75	1.778	9.78	1.905

6. The application of the model

A finite difference method [23] was used to compute the concentration profiles through the domain that is assumed to consist of infinitesimal elements with a length of dx. It was also assumed that each element has a representative value at its central node, $x = x_j$, where j is the number of the discrete area, thus the concentration of the species i in a certain element j can be represented as follows:

$$C_i(x_j) \approx \int_{x_j-\frac{1}{2}dx}^{x_j+\frac{1}{2}dx} C_i(x)dx/dx \tag{20}$$

For example, the second derivative of the concentration with respect to x is given at the element as follows:

$$\left.\frac{\partial^2 C_i(x)}{\partial x^2}\right|_{x=x_j} \approx \frac{C_i(x_{j+1}) - 2C_i(x_j) + C_i(x_{j-1})}{dx^2} \tag{21}$$

In this paper, the fourth order Runge Kutta method [24] was applied for the integration of Eq. (7). The system of equations was solved with a FORTRAN 95 programme [25], the algorithm of which is described as follows:

1. The initial concentrations of each species ($C_i(x)$ at $t = 0$) are given at each element as described in the following section.
2. Activity coefficients γ_i are calculated for each species and the values of the equilibrium constants are corrected as shown in Table 1.
3. The time derivatives of concentration for each species are calculated by the procedures already mentioned in the general or boundary conditions section above based on Eq. (8).
4. The concentrations of each species at the next time step are obtained by the integration of Eq. (7) at all nodes.
5. The routines of 2–4 above are repeated for the time steps required after which the final concentrations of each species are obtained.

The numbers of elements and the time steps required to obtain results with good accuracy and to ensure convergence of the numerical solutions were investigated until a stable solution was obtained, from which the computations were performed with 500 elements and with a constant time step of 0.1 s for the first 10,000 loops and then a time step of 10 s.

When the pH of the anolyte is reduced below pH 4, the generation of carbon dioxide gas may need to be taken into account. According to Henry's law, the partial pressure of carbon dioxide (P_{CO_2}) is related to the concentration of (CO_2(aq)) as follows:

$$CO_2(g) + H_2O \Longleftrightarrow CO_2(aq) \quad \text{(N)}$$

$$K_H = [CO_2(aq)]/P_{CO_2} \quad (22)$$

where K_H is Henry's constant. The naturally occurring partial pressure of CO_2(g) is $10^{-3.5}$ atm at 1 atm total pressure. With $K_H = 10^{-1.42}$ M/atm at 25 °C [26], the saturation concentration of CO_2(aq) is assumed to be $10^{-4.92}$ M. In the computation, after CO_2(aq) reaches this value, the excess of this species is assumed to be converted to carbon dioxide gas due to the reaction (N) from the right to the left hand side. Since CO_2(aq) is not electrically charged, this conversion does not affect the overall charge balance among the species at the interface.

7. Initial conditions

Anolyte solutions of volume 120 ml containing 1.0 M ethanolamine nitrate at pH 8.0 (produced by mixing equal volumes of 2 M ethanolamine and 1.97 M nitric acid) and

Table 3
Initial conditions of species in pore and external solutions

	Charge number (z_i)	In pore solution (mol/l) [pH = 9.0]	Diffusion coefficient (D_i) (m^2/s)	In external solution (mol/l)	
				Ethanolamine nitrate [pH = 8.0]	Guanidine carbonate [pH = 11.74]
OH^-	−1	1.00×10^{-5} [a]	5.3×10^{-10} [g]	1.00×10^{-6} [a]	5.50×10^{-3} [a]
Na^+	+1	9.00×10^{-3} [b]	2.8×10^{-11} [g]	–	–
K^+	+1	6.00×10^{-3} [b]	4.0×10^{-11} [g]	–	–
Ca^{2+}	+2	7.43×10^{-3} [c]	1.6×10^{-11} [g]	–	–
RNH_3^+	+1	–	6.0×10^{-11} (for ethanolamine) [h] 3.0×10^{-11} (for guanidine) [h]	9.83×10^{-1} [c]	9.86×10^{-1} [c]
RNH_2	0	–	–	1.75×10^{-2} [e]	1.36×10^{-2} [e]
CO_3^{2-}	−2	6.68×10^{-7} [d]	9.2×10^{-11} [i]	–	4.81×10^{-1} [e]
HCO_3^-	−1	1.43×10^{-5} [e]	1.2×10^{-10} [i]	–	1.87×10^{-2} [e]
CO_2(aq)	0	3.42×10^{-8} [e]	–	–	7.61×10^{-8} [e]
SO_4^{2-}	−2	9.56×10^{-3} [c]	1.1×10^{-10} [i]	–	–
Cl^-	−1	1.07×10^{-2} [f]	1.0×10^{-10} [g]	–	–
NO_3^-	−1	–	1.9×10^{-10} [i]	9.83×10^{-1}	–
H^+	+1	1.00×10^{-9} [a]	9.3×10^{-10} [i]	1.00×10^{-8} [a]	1.82×10^{-12} [a]

[a] Determined from pH of electrolyte.
[b] Experimental data [1].
[c] Calculated by adjusting experimental data taking solubility product of $CaSO_4$ into account.
[d] Calculated from solubility product of $CaCO_3$.
[e] Calculated from dissociation constants of relevant species at each pH.
[f] Set to maintain charge balance.
[g] Li and Page [8].
[h] Calculated from model applied to diffusion specimens.
[i] Estimated by dividing diffusion coefficient of species in dilute solution [11] by ratio of diffusion coefficient of hydroxyl ion in dilute solution [11] to that in porous medium [8].

0.5 M guanidine carbonate (1 M with respect to guanidine) were used, as detailed in Part 1 [1]. The assumed initial concentrations of the internal and external solutions as well as the diffusion coefficients and the charge numbers of the various ions are given in Table 3. The pH values and the concentrations of sodium and potassium ions in the pore solution and initial anolyte solution were based on experimental measurements recorded in Part 1 [1]. Experimentally determined calcium and sulfate ion concentrations, which exceeded the solubility product of calcium sulfate recorded in Table 1, were adjusted by dilution to yield the assumed equilibrium values. The concentrations of carbonate species were then calculated from the solubility product of calcium carbonate and the other relevant equilibrium constants shown in Table 1.

8. Results and discussion

8.1. Organic corrosion inhibitors in the pore solution

The computed concentration profiles of both inhibitors after treatments at 1 A/m^2 and 5 A/m^2 for 7 days are plotted in Fig. 3 along with the corresponding experimental data. It may be seen that the results from modelling are in general agreement with those obtained from experiment, showing that both inhibitors penetrate into the carbonated medium progressively with increase in current density and that they attain a significant concentration at the cathode ($x = 34$ mm) when a current density of 5 A/m^2 is applied for seven days. This supports the observations reported in Part 1 [1] and confirms that the intensity

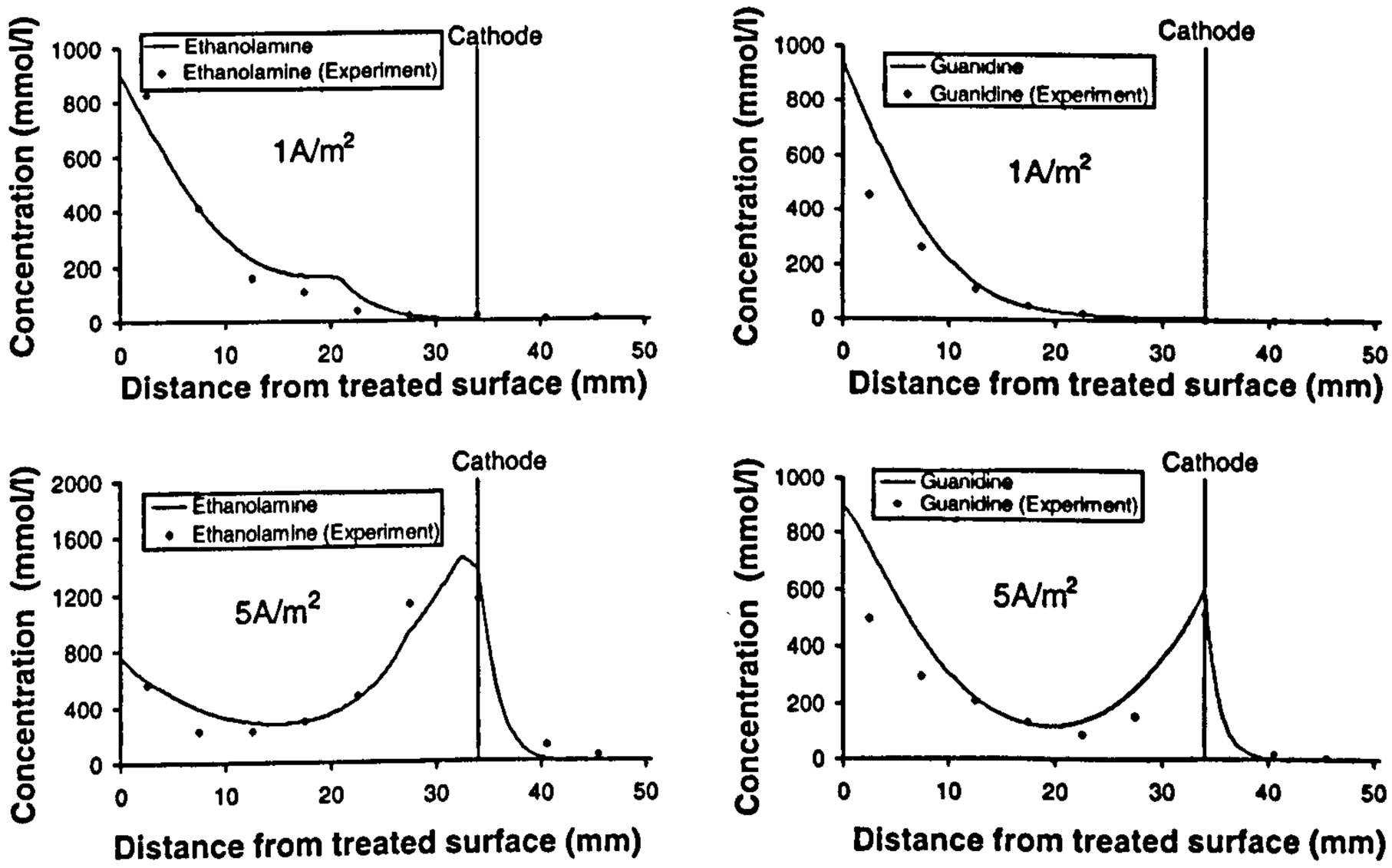

Fig. 3. Computed and experimental concentration profiles for both inhibitors after galvanostatic treatments (1 A/m^2, 5 A/m^2) applied for 7 days.

and duration of the required treatment are similar to those used for electrochemical realkalisation of carbonated concrete [27].

The computed pH profiles and the concentration profiles of ionic and molecular species of the inhibitors are shown in Fig. 4 along with the values of pH obtained from experiment. In the case of ethanolamine at a current density of 5 A/m^2, it is clear that the predominant form of the inhibitor at the cathode is molecular and that the highest concentration is observed just a few millimetres from the cathode where the concentration of ethanolamine cations approaches zero. In contrast for the case of guanidine at a current density of 5 A/m^2, the peak concentration occurs at the cathode where almost half of the inhibitor exists in the cationic form. The difference in pH profiles recorded for the two inhibitors is simply due to the lower pK_a value of ethanolamine, which results in its consuming more of the migrating hydroxyl ions generated at the cathode. The pH values are in agreement with those obtained in the experiments in the case of the applied current density of 5 A/m^2. However, there are some unexplained discrepancies near the cathode at the current density of 1 A/m^2 in the cases of both inhibitors.

The concentrations of both inhibitors remaining in the anolyte at each current density are shown in Table 4 along with the concentrations of other cationic species while the concentrations of the anions are shown in Table 5. The reason for the substantial difference in the concentration of guanidine measured experimentally after treatment for 7 days at 5 A/m^2, compared with that predicted by the model, is unclear but might be attributable to anodic oxidation and/or evaporation losses.

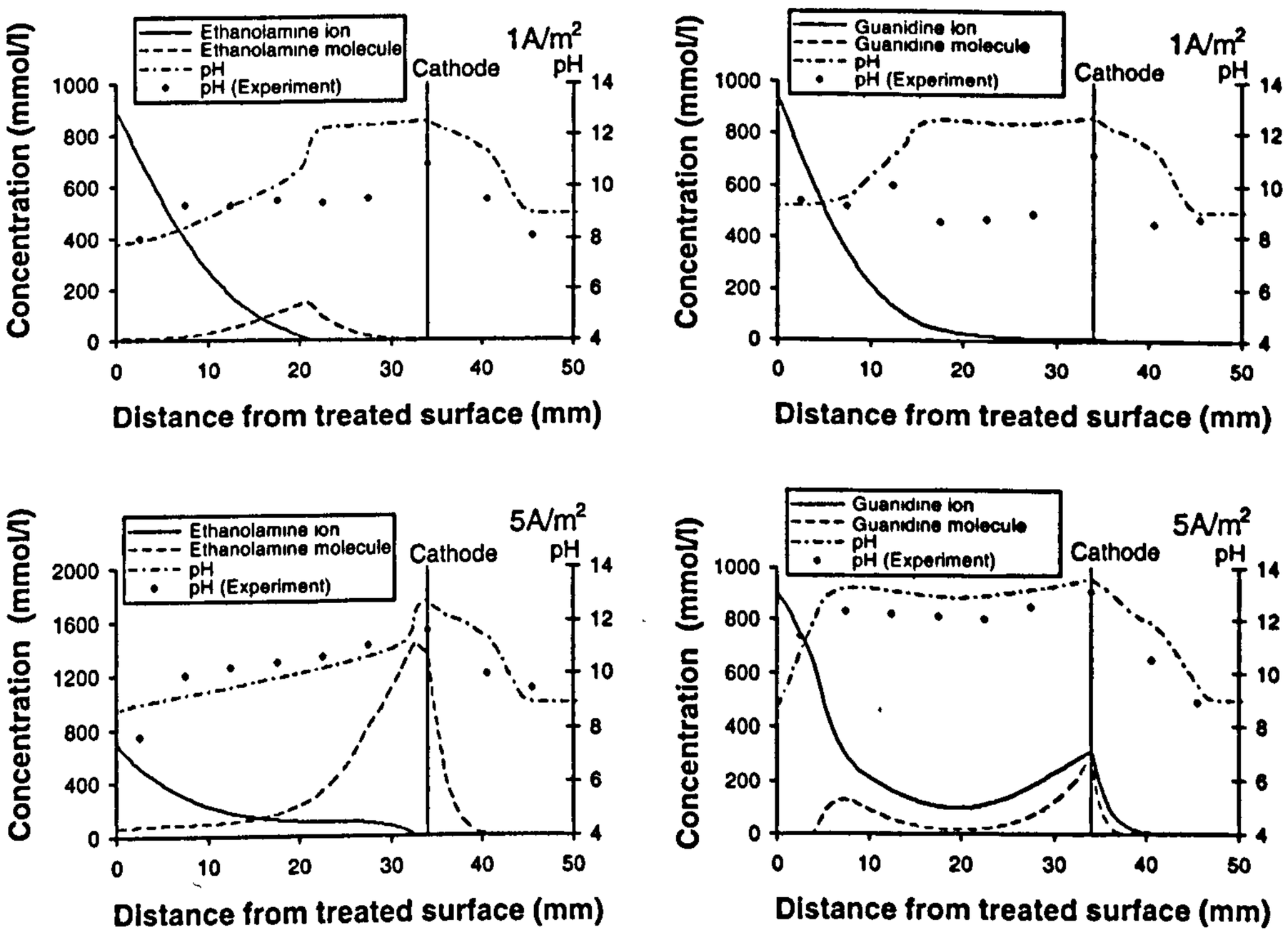

Fig. 4. Computed and experimental pH profiles and concentration profiles for inhibitor ions and molecules after galvanostatic treatments applied for 7 days (top: 1 A/m^2, bottom: 5 A/m^2).

Table 4
Concentration of inhibitors and cations in anolytes after 7 days of treatment

Anolyte	Current density (A/m^2)	Method	Concentrations (mmol/l)							
			Inhibitors		Na^+	K^+	Mg^{2+}	Ca^{2+}	H^+	Sum of charge
			Total	Cationic						
1 M ethanolamine nitrate	1	Modelling	912.9	912.9	0.6	0.4	–	3.6	9.7	930.8
	1	Experiment	970.8	970.8	2.1	N/D	5.7	38.5	9.5	1071.0
	5	Modelling	808.6	808.6	0.3	0.2	–	31.3	110.4	982.2
	5	Experiment	856.2	856.2	10.5	12.4	16.6	168.4	61.7	1310.7
0.5 M guanidine carbonate	1	Modelling	957.6	955.1	0.3	0.2	–	0.0	0.0	955.6
	1	Experiment	912.1	912.0	3.8	N/D	3.0	2.5	0.0	926.8
	5	Modelling	922.5	922.4	0.1	0.1	–	0.0	0.0	922.7
	5	Experiment	651.1	651.1	5.0	N/D	0.0	1.5	0.0	659.0

Table 5
Concentration of anions in anolytes after 7 days of treatment

Anolyte	Current density (A/m^2)	Method	pH	Concentrations (mmol/l)						
				OH^-	Cl^-	SO_4^{2-}	NO_3^-	CO_3^{2-}	HCO_3^-	Sum of charge
1 M ethanolamine nitrate	1	Modelling	2.01	0.0	1.8	0.7	927.4	0.0	0.0	930.8
	1	Experiment	2.01	0.0	6.5	6.9	971.9	0.0	0.0	992.3
	5	Modelling	0.96	0.0	3.2	0.1	978.8	0.0	0.0	982.2
	5	Experiment	1.21	0.0	9.8	26.8	1092.7	0.0	0.0	1156.1
0.5 M guanidine carbonate	1	Modelling	10.92	0.8	1.0	52.0	–	385.1	79.7	955.6
	1	Experiment	9.7	0.1	5.6	11.1	–	284.9	299.6	897.3
	5	Modelling	9.25	0.0	2.8	181.3	–	38.8	480.0	922.7
	5	Experiment	8.8	0.0	6.6	57.0	–	23.6	516.8	684.5

8.2. The environment near the cathode

Fig. 5 shows the computed changes in pH at the cathode at a current density of 5 A/m^2 for both inhibitors and the result of similar computations made, for the case of guanidine, without taking into consideration the precipitation of calcium hydroxide at the cathode. It is clear that the pH of the initially near-neutral pore solution is raised at almost the same rate to just over 12.5 at the cathode during the first day of treatment in all three cases. Thereafter, for ethanolamine, the pH value tends to decrease slowly owing to the consumption of hydroxyl ions that occurs when the inhibitor arrives in the vicinity of the steel. In contrast, for guanidine, the pH progressively rises towards about 13.5 if calcium hydroxide precipitation is considered and to somewhat higher values if this process is not taken into account. This implies that, in the cases of both inhibitors, calcium hydroxide precipitated at the cathode functions as a buffer of moderate alkalinity. This may be considered a beneficial phenomenon, providing enhanced corrosion protection to the steel, as discussed in Part 1 [1].

8.3. Effect of molecular interactions

As noted in Section 5, in the case of ethanolamine, the effects of molecular interactions cannot be ignored but may be simply offset by replacing the thermodynamic pK_a value

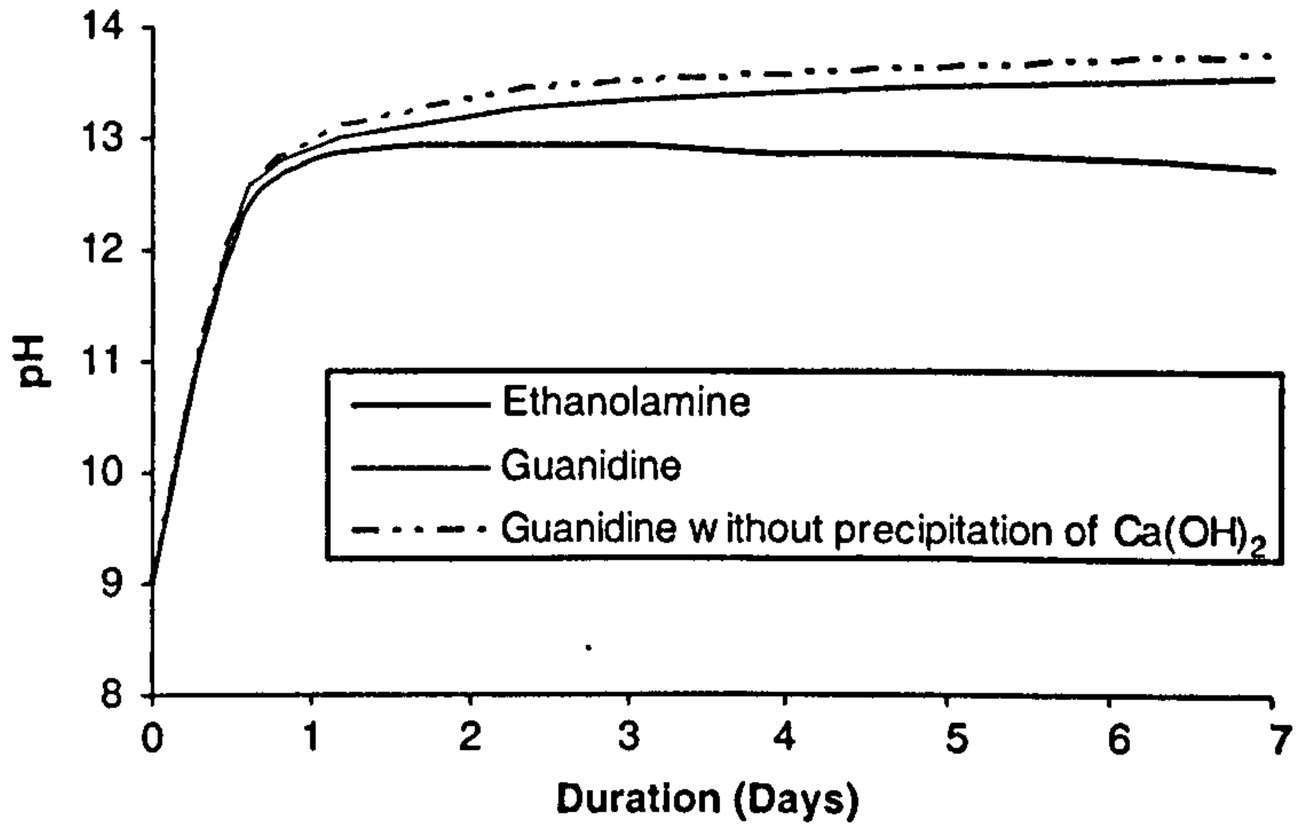

Fig. 5. Evolution of pH at cathode at current density of 5 A/m^2 for both inhibitors and, for guanidine, without considering precipitation of calcium hydroxide.

(=9.5) with a higher apparent pK'_a value (=9.75). This tends to reduce the discrepancies in charge balance (30–100 mmol/l) that were found in the experimental data for specimens treated at a current density of 5 A/m^2 [1] to more reasonable values (10–70 mmol/l) and also results in a slightly modified form of the inhibitor penetration profile. Fig. 6 shows the concentration profiles of ethanolamine calculated with and without consideration of molecular interactions; from this it appears that the use of the pK'_a value results in a somewhat better fit to the experimental data.

8.4. Effect of the solubility product of calcium carbonate

The concentrations of alkali metal ions predicted by the model are similar to those determined experimentally and are insignificant in comparison with the inhibitor

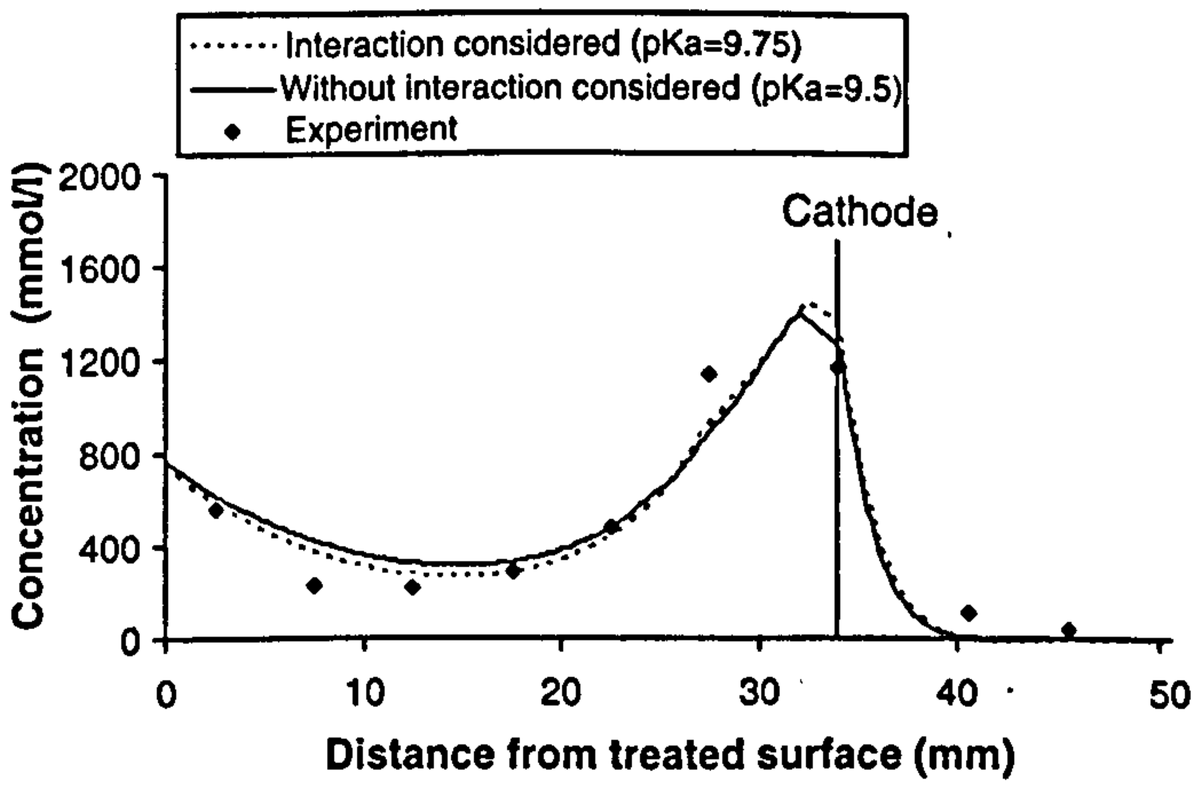

Fig. 6. Computed concentration profile of ethanolamine with and without consideration of molecular activity coefficient.

concentrations; thus they are not shown or discussed further here. The concentration profiles of carbonate and bicarbonate ions (as well as those of sulfate), however, are represented in Fig. 7 for the case of guanidine, from which it is apparent that the computed concentrations of carbonate and bicarbonate are generally about two orders of magnitude smaller than the corresponding experimental values. These discrepancies may be attributable to supersaturation of the pore solutions with calcium carbonate. If it is arbitrarily assumed that the solubility of calcium carbonate is governed by an apparent solubility product ($K'_{s1} = 3.36 \times 10^{-5}$ mol^2/l^2) which is 10^4 times greater than the normal value reported in the literature [11], the computed concentration profiles of CO_3^{2-}, HCO_3^- and SO_4^{2-} at a current density of 5 A/m^2 in the case of guanidine are as shown in Fig. 8. It can be seen from these results that a much better fit to the experimental data is thus obtained and a peak of carbonate concentration at the cathode is simulated. This peak is caused by the displacement of calcium ions from $CaCO_3$ to $Ca(OH)_2$ which precipitates at the cathode owing to the high pH. A further significant finding here is that the large change in the assumed value for the apparent solubility product of calcium carbonate has relatively little effect on the computed concentration profiles of the two corrosion inhibitors, as shown in Fig. 9. This is because the calculated contributions to the ionic

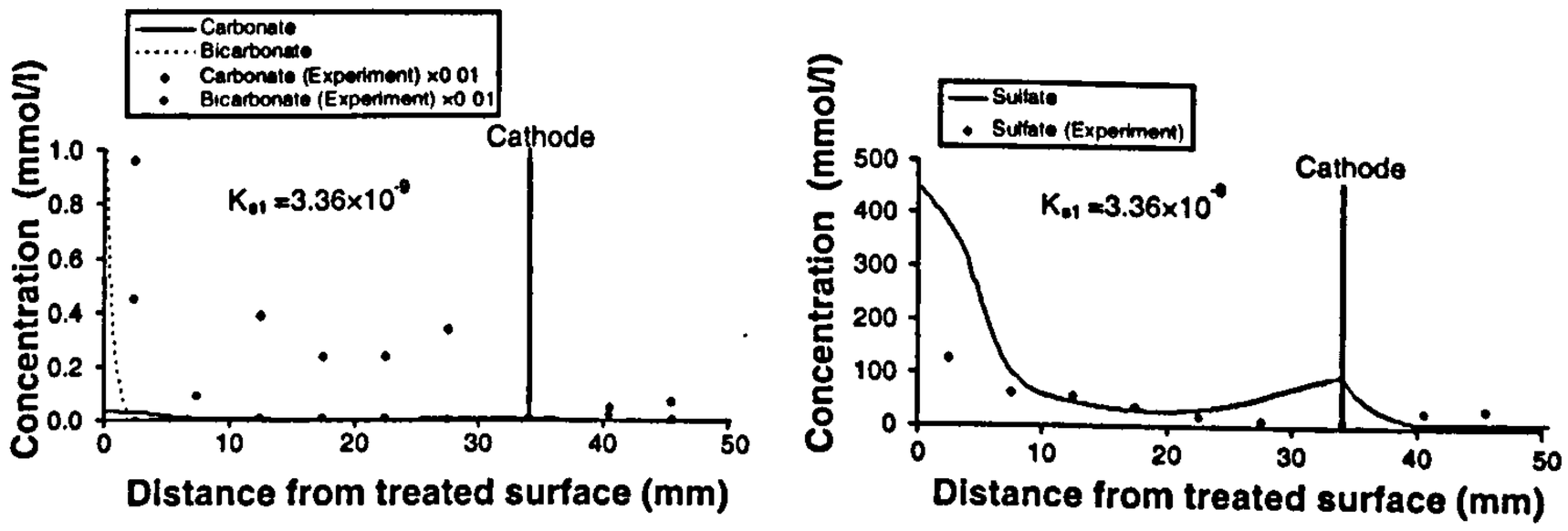

Fig. 7. Computed concentration profiles of carbonate, bicarbonate and sulfate ions after guanidine treatment at 5 A/m^2 for 7 days.

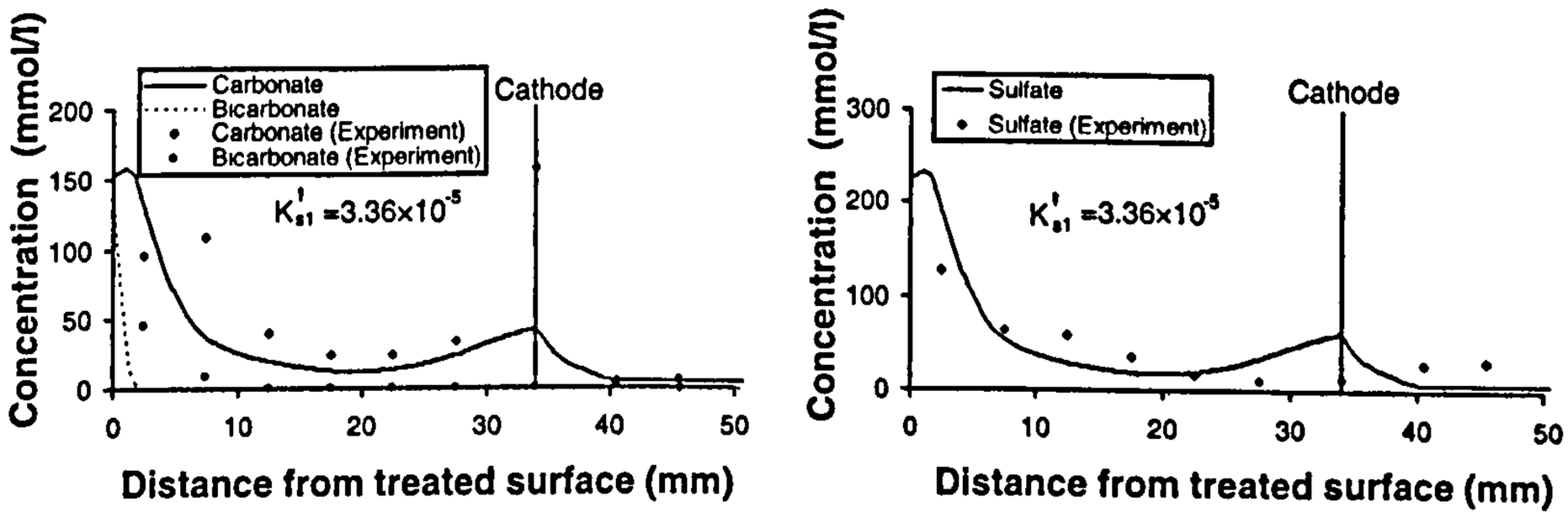

Fig. 8. Computed concentration profiles of carbonate, bicarbonate and sulfate ions, assuming 3.36×10^{-5} mol^2/l^2 as solubility product of calcium carbonate, after guanidine treatment at 5 A/m^2 for 7 days.

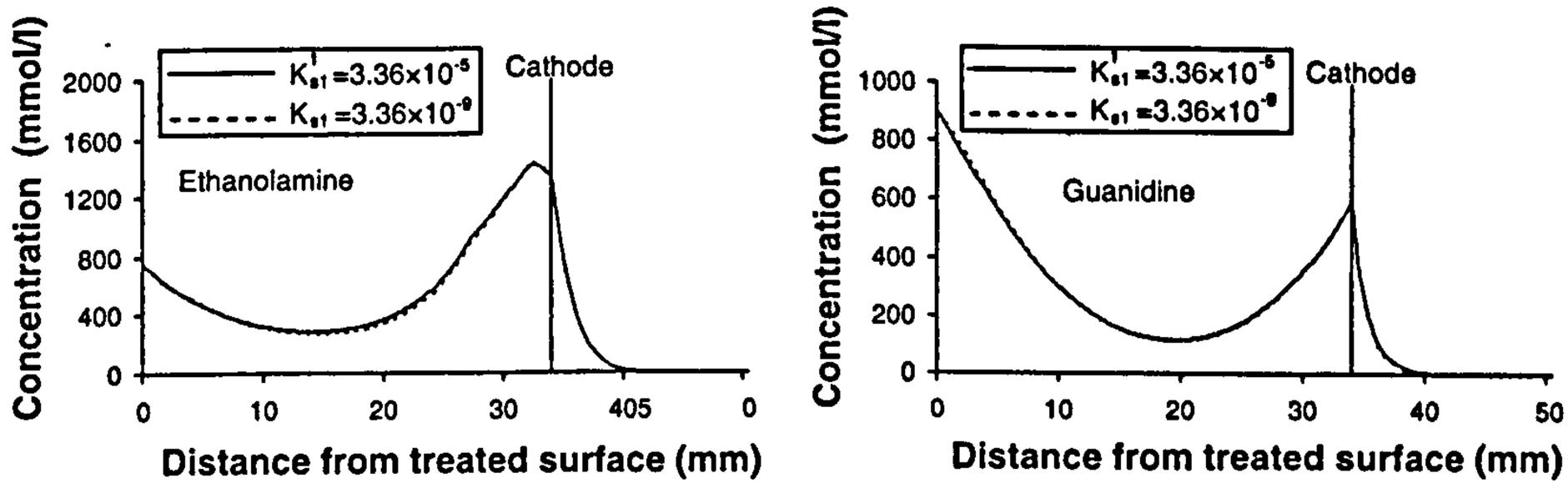

Fig. 9. Computed concentration profiles of inhibitors, assuming 3.36×10^{-5} mol^2/l^2 as the solubility product of calcium carbonate, after treatments at 5 A/m^2 for 7 days (left: ethanolamine, right: guanidine).

strength of CO_3^{2-}, HCO_3^- and SO_4^{2-} are almost unchanged and hence have little effect on the potential gradient in the pore solution, as defined by the following equation:

$$\frac{\partial \phi}{\partial x} = -\frac{RT}{F} \cdot \frac{i/F + \sum z_i D_i \partial C_i / \partial x}{\sum z_i^2 D_i C_i} \tag{23}$$

Thus changes in the assumed value of the solubility product of calcium carbonate have little influence on the concentration of other ions involved.

9. Conclusions

The main conclusions of this part of the investigations may be summarised as follows.

(1) The proposed model yields reasonable general agreement with experimentally determined concentration profiles for two organic base inhibitors of widely varying pK_a values that were subjected to electrochemical injection into carbonated cement paste.
(2) In the case of ethanolamine (pK_a 9.5), improved agreement between modelling and experiment was obtained when molecular interactions were represented by the introduction of an activity coefficient, γ_m, which raised the apparent pK'_a value of the inhibitor to 9.75; for guanidine (pK_a 13.6), no such modification was required.
(3) In the cases of both inhibitor injection treatments, calcium hydroxide precipitation at the cathode was shown to affect the evolution of pH in the vicinity of the embedded steel as a function of current density and time, the precipitated calcium hydroxide functioning as a buffer of moderate alkalinity.
(4) To obtain reasonable correspondence between modelling predictions and experimental concentration profiles determined for carbonate, bicarbonate and sulfate ions, it was necessary to assume a much larger apparent solubility product for calcium carbonate than that reported in the literature; this had only minor influence on the computed concentration profiles of the two corrosion inhibitors.
(5) Further development of the model described may lead to improved understanding of the rates of dispersion of electrochemically injected corrosion inhibitors on cessation of treatments of the sort employed in this research; this should allow the long-term effectiveness of the corrosion inhibition conferred on embedded steel to be predicted quantitatively.

Acknowledgements

We wish to thank Dr. L.Y. Li for helpful discussions. We are also grateful to the Central Japan Railway Company for providing funds to support the first-named author and to the Kajima Corporation, Japan, for providing funds to support the second-named author.

Appendix A

If the rate of reaction (A) from left to right is expressed as R_A, and so on, the reaction rate for each species can be written with $R_A \ldots R_E$, as follows:

$$R_{Ca} = R_A + R_B, \quad R_{CO_3} = R_A + R_D, \quad R_{SO_4} = R_B, \quad R_I = -R_C, \quad R_M = R_C,$$
$$R_{HCO_3} = -R_D, \quad R_{OH} = -R_C - R_D + R_E, \quad R_H = R_E$$

where R_I and R_M represent the rates of production for the ionic and molecular inhibitor species, respectively. Eliminating $R_A \ldots R_E$, the following three independent equations are then obtained:

$$R_{Ca} - R_{CO_3} - R_{HCO_3} - R_{SO_4} = 0, \quad R_I + R_M = 0, \quad R_H - R_{OH} + R_I + R_{HCO_3} = 0$$

If $\Lambda_i(x)$ is defined as $\Lambda_i = \frac{J_i(x)}{dx} - \frac{J_i(x+dx)}{dx}$, from Eq. (8) and the above three equations, the following may be derived:

$$\frac{\partial C_{Ca}}{\partial t} - \frac{\partial C_{HCO_3}}{\partial t} - \frac{\partial C_{CO_3}}{\partial t} - \frac{\partial C_{SO_4}}{\partial t} = \Lambda_{Ca} - \Lambda_{HCO_3} - \Lambda_{CO_3} - \Lambda_{SO_4} \tag{A.1}$$

$$\frac{\partial C_I}{\partial t} + \frac{\partial C_M}{\partial t} = \Lambda_I + \Lambda_M \tag{A.2}$$

$$\frac{\partial C_H}{\partial t} - \frac{\partial C_{OH}}{\partial t} + \frac{\partial C_I}{\partial t} + \frac{\partial C_{HCO_3}}{\partial t} = \Lambda_H - \Lambda_{OH} + \Lambda_I + \Lambda_{HCO_3} \tag{A.3}$$

Solution equilibria involving water, calcium carbonate, and calcium sulfate are represented by: $C_H \cdot C_{OH} = K_w$, $C_{Ca} \cdot C_{CO_3} = K_{s1}$, $C_{Ca} \cdot C_{SO_4} = K_{s2}$, from which the following three equations are obtained by differentiating with respect to time:

$$\frac{\partial C_H}{\partial t} = -\frac{K_w}{C_{OH}^2} \frac{\partial C_{OH}}{\partial t} \tag{A.4}$$

$$C_{CO_3} \cdot \frac{\partial C_{Ca}}{\partial t} + C_{Ca} \cdot \frac{\partial C_{CO_3}}{\partial t} = 0 \tag{A.5}$$

$$C_{SO_4} \cdot \frac{\partial C_{Ca}}{\partial t} + C_{Ca} \cdot \frac{\partial C_{SO_4}}{\partial t} = 0 \tag{A.6}$$

Similarly, equilibria involving the molecular and ionic inhibitor species, carbonate and bicarbonate are represented by: $\log(C_M/C_I) = -pK_a + pH$ and $\log(C_{CO_3}/C_{HCO_3}) = -pK_2 + pH$, from which the following expressions are derived by differentiation:

$$\frac{\partial C_I}{\partial t} C_{OH} + \frac{\partial C_{OH}}{\partial t} C_I - 10^{pK_a - pK_w} \cdot \frac{\partial C_M}{\partial t} = 0 \tag{A.7}$$

$$\frac{\partial C_{HCO_3}}{\partial t} C_{OH} + \frac{\partial C_{OH}}{\partial t} C_{HCO_3} - 10^{pK_2 - pK_w} \cdot \frac{\partial C_{CO_3}}{\partial t} = 0 \tag{A.8}$$

Since Λ_H is expressed in terms of Λ_{OH} as $\Lambda_H = -\frac{D_H}{D_{OH}}\frac{K_w}{C_{OH}^2}\Lambda_{OH}$ (see Eq. (F.4) in Appendix F), Eq. (A.3) can be written using (A.4) as follows:

$$\left(1+\frac{K_w}{C_{OH}^2}\right)\frac{\partial C_{OH}}{\partial t}-\frac{\partial C_{HCO_3}}{\partial t}-\frac{\partial C_I}{\partial t}=\left(1+\frac{D_H}{D_{OH}}\frac{K_w}{C_{OH}^2}\right)\Lambda_{OH}-\Lambda_{HCO_3}-\Lambda_I \tag{A.9}$$

Appendix B

If the rate of reaction (I) from left to right is expressed as R_X, the following equations may be simply derived:

$$R_{Ca}=R_A+R_B-R_X,\quad R_{CO_3}=R_A+R_D,\quad R_{SO_4}=R_B,\quad R_I=-R_C,\quad R_M=R_C,$$
$$R_{HCO_3}=-R_D,\quad R_{OH}=-R_C-R_D+R_E-2R_X,\quad R_H=R_E$$

Eliminating $R_A\cdots R_E$, and R_X from the right hand side of the above equations, the following two independent equations are obtained:

$$R_{OH}-2R_{Ca}+2R_{CO_3}+R_{HCO_3}+2R_{SO_4}-R_I-R_H=0,\quad R_I+R_M=0$$

From Eq. (8) and the above two equations, the following are derived taking into consideration $\frac{\partial C_H}{\partial t}=-\frac{K_w}{C_{OH}^2}\frac{\partial C_{OH}}{\partial t}$ (A.4) and $\Lambda_H=-\frac{D_H}{D_{OH}}\frac{K_w}{C_{OH}^2}\Lambda_{OH}$ (see Eq. (F.4) in Appendix F),

$$\left(1+\frac{K_w}{C_{OH}^2}\right)\frac{\partial C_{OH}}{\partial t}-2\frac{\partial C_{Ca}}{\partial t}+2\frac{\partial C_{CO_3}}{\partial t}+\frac{\partial C_{HCO_3}}{\partial t}+2\frac{\partial C_{SO_4}}{\partial t}-\frac{\partial C_I}{\partial t}$$
$$=\left(1+\frac{D_H}{D_{OH}}\frac{K_w}{C_{OH}^2}\right)\Lambda_{OH}-2\Lambda_{Ca}+2\Lambda_{CO_3}+\Lambda_{HCO_3}+2\Lambda_{SO_4}-\Lambda_I, \tag{B.1}$$

$$\frac{\partial C_I}{\partial t}+\frac{\partial C_M}{\partial t}=\Lambda_I+\Lambda_M \tag{B.2}$$

From the solubility equilibrium condition of calcium hydroxide: $C_{Ca}\cdot C_{OH}^2=K_{s3}$, the following equation is obtained by differentiating with respect to time:

$$2C_{Ca}\cdot\frac{\partial C_{OH}}{\partial t}+C_{OH}^2\cdot\frac{\partial C_{Ca}}{\partial t}=0 \tag{B.3}$$

Appendix C

The rates of production have the following relationships:

$$R_{CO_3}^*=R_D^*,\quad R_I^*=-R_C^*,\quad R_M^*=R_C^*,\quad R_{HCO_3}^*=-R_D^*,\quad R_H^*=R_E^*,$$
$$R_{OH}^*=-R_C^*-R_D^*+R_E^*$$

Eliminating $R_A^*\cdots R_E^*$, the following three independent equations are obtained:

$$R_H^*-R_{OH}^*+R_{HCO_3}^*+R_I^*=0,\quad R_{CO_3}^*+R_{HCO_3}^*=0,\quad R_I^*+R_M^*=0$$

Since the total anodic current is the sum of two components ($i=i^H+i^{OH}$), the following is derived by subtraction of Eq. (11) from (10):

$$\left(\frac{\partial C_H}{\partial t}-\frac{\partial C_{OH}}{\partial t}\right)\Big|_{x=0}=\frac{-J_H^*+J_{OH}^*+i/F}{x_a}+R_H^*-R_{OH}^* \tag{C.1}$$

Using $\frac{\partial C_H}{\partial t} = -\frac{K_w}{C_{OH}^2}\frac{\partial C_{OH}}{\partial t}$ (A.4) and $J_H = -\frac{D_H}{D_{OH}}\frac{K_w}{C_{OH}^2}J_{OH}$ (see Eq. (F.3) in Appendix F) and Eq. (C.1), the first independent equation of the above three can be changed in form to give:

$$\left(1+\frac{K_w}{C_{OH}^{*2}}\right)\frac{\partial C_{OH}}{\partial t} - \frac{\partial C_{HCO_3}}{\partial t} - \frac{\partial C_I}{\partial t} = -\frac{\left(1+\frac{D_H}{D_{OH}}\frac{K_w}{C_{OH}^{*2}}\right)J_{OH}^* - J_{HCO_3}^* - J_I^* + i/F}{x_a} \tag{C.2}$$

The other two equations yield,

$$\left(\frac{\partial C_{CO_3}}{\partial t} + \frac{\partial C_{HCO_3}}{\partial t}\right)\Big|_{x=0} = -\frac{J_{CO_3}^* + J_{HCO_3}^*}{x_a} \tag{C.3}$$

and

$$\left(\frac{\partial C_I}{\partial t} + \frac{\partial C_M}{\partial t}\right)\Big|_{x=0} = -\frac{J_I^* + J_M^*}{x_a} \tag{C.4}$$

Appendix D

The rates of production have the following relationships:

$$R_{CO_3}^* = -R_{D'}^*, \quad R_I^* = R_{C'}^*, \quad R_M^* = -R_{C'}^*, \quad R_{HCO_3}^* = R_{D'}^*,$$
$$R_H^* = -R_{C'}^* - R_{D'}^* + R_E^*, \quad R_{OH}^* = R_E^*$$

Eliminating $R_A^* \ldots R_E^*$, the following three independent equations are obtained:

$$R_H^* - R_{OH}^* + R_{HCO_3}^* + R_I^* = 0, \quad R_{CO_3}^* + R_{HCO_3}^* = 0, \quad R_I^* + R_M^* = 0$$

Using $\frac{\partial C_{OH}}{\partial t} = -\frac{K_w}{C_H^2}\frac{\partial C_H}{\partial t}$, $J_{OH} = -\frac{D_{OH}}{D_H}\frac{K_w}{C_H^2}J_H$ (see Eq. (F.5) in Appendix F) and Eq. (C.1), the first independent equation of the above three can be changed in form to read:

$$\left\{\left(1+\frac{K_w}{C_H^{*2}}\right)\frac{\partial C_H}{\partial t} + \frac{\partial C_{HCO_3}}{\partial t} + \frac{\partial C_I}{\partial t}\right\}\Big|_{x=0} = -\frac{\left(1+\frac{D_{OH}}{D_H}\frac{K_w}{C_H^{*2}}\right)J_H^* + J_{HCO_3}^* + J_I^* - i/F}{x_a} \tag{D.1}$$

The other two equations yield,

$$\left(\frac{\partial C_{CO_3}}{\partial t} + \frac{\partial C_{HCO_3}}{\partial t}\right)\Big|_{x=0} = -\frac{J_{CO_3}^* + J_{HCO_3}^*}{x_a} \tag{D.2}$$

and

$$\left(\frac{\partial C_I}{\partial t} + \frac{\partial C_M}{\partial t}\right)\Big|_{x=0} = -\frac{J_I^* + J_M^*}{x_a} \tag{D.3}$$

From the three equilibria $\log(C_M/C_I) = -pK_a + pH$, $\log(C_{HCO_3}/C_{CO_{2(aq)}}) = -pK_1 + pH$ and $\log(C_{CO_3}/C_{HCO_3}) = -pK_2 + pH$, the following expressions are derived by differentiation with respect to time:

$$C_H^* \cdot \frac{\partial C_M}{\partial t}\Big|_{x=0} + C_M^* \cdot \frac{\partial C_H}{\partial t}\Big|_{x=0} = 10^{-pK_a}\frac{\partial C_I}{\partial t}\Big|_{x=0} \tag{D.4}$$

and

$$C^*_{\mathrm{H}} \cdot \left.\frac{\partial C_{\mathrm{CO_3}}}{\partial t}\right|_{x=0} + C^*_{\mathrm{CO_3}} \cdot \left.\frac{\partial C_{\mathrm{H}}}{\partial t}\right|_{x=0} = 10^{-\mathrm{p}K_2} \left.\frac{\partial C_{\mathrm{HCO_3}}}{\partial t}\right|_{x=0} \tag{D.5}$$

Appendix E

The production rates have the following relationships (note that here the rate concerned with reaction (M) is expressed as R^*_{m} to avoid confusion with R^*_{M}):

$$R^*_{\mathrm{I}} = R^*_{C'}, \quad R^*_{\mathrm{M}} = -R^*_{C'}, \quad R^*_{\mathrm{CO_3}} = -R^*_{D'}, \quad R^*_{\mathrm{HCO_3}} = R^*_{D'} - R^*_{\mathrm{m}}, \quad R^*_{\mathrm{CO_2(aq)}} = R^*_{\mathrm{m}},$$

$$R^*_{\mathrm{H}} = -R^*_{C'} - R^*_{D'} + R^*_{\mathrm{E}} - R^*_{\mathrm{m}}, \quad R^*_{\mathrm{OH}} = R^*_{\mathrm{E}}$$

Eliminating, $R^*_{C'}$, $R^*_{D'}$, R^*_{E}, and R^*_{m}, the following three independent equations are obtained:

$$R^*_{\mathrm{H}} - R^*_{\mathrm{OH}} + R^*_{\mathrm{HCO_3}} + 2R^*_{\mathrm{CO_2(aq)}} + R^*_{\mathrm{I}} = 0, \quad R^*_{\mathrm{I}} + R^*_{\mathrm{M}} = 0, \quad R^*_{\mathrm{CO_3}} + R^*_{\mathrm{HCO_3}} + R^*_{\mathrm{CO_2(aq)}} = 0$$

From Eqs. (11) and (14), the following can be obtained paying attention to $i = i^{\mathrm{H}} + i^{\mathrm{OH}}$:

$$\left.\left(\frac{\partial C_{\mathrm{H}}}{\partial t} - \frac{\partial C_{\mathrm{OH}}}{\partial t}\right)\right|_{x=0} = \frac{-J^*_{\mathrm{H}} + J^*_{\mathrm{OH}} - k_1 C^*_{\mathrm{H}} + i/F}{x_{\mathrm{a}}} + R^*_{\mathrm{H}} - R^*_{\mathrm{OH}} \tag{E.1}$$

Similarly using Eq. (F.5) in Appendix F and Eq. (E.1), the first independent equation of the above three can be changed as follows:

$$\left.\left\{\left(1 + \frac{K_{\mathrm{w}}}{C^{*2}_{\mathrm{H}}}\right)\frac{\partial C_{\mathrm{H}}}{\partial t} + \frac{\partial C_{\mathrm{HCO_3}}}{\partial t} + 2 \cdot \frac{\partial C_{\mathrm{CO_2(aq)}}}{\partial t} + \frac{\partial C_{\mathrm{I}}}{\partial t}\right\}\right|_{x=0}$$

$$= -\frac{\left(1 + \frac{D_{\mathrm{OH}}}{D_{\mathrm{H}}}\frac{K_{\mathrm{w}}}{C^{*2}_{\mathrm{H}}}\right)J^*_{\mathrm{H}} + J^*_{\mathrm{HCO_3}} + 2 \cdot J^*_{\mathrm{CO_2(aq)}} + J^*_{\mathrm{I}} - i/F}{x_{\mathrm{a}}} \tag{E.2}$$

The other two equations yield,

$$\left.\left(\frac{\partial C_{\mathrm{CO_3}}}{\partial t} + \frac{\partial C_{\mathrm{HCO_3}}}{\partial t} + \frac{\partial C_{\mathrm{CO_2(aq)}}}{\partial t}\right)\right|_{x=0} = -\frac{J^*_{\mathrm{CO_3}} + J^*_{\mathrm{HCO_3}} + J^*_{\mathrm{CO_2(aq)}} - k_1 C^*_{\mathrm{H}}}{x_{\mathrm{a}}} \tag{E.3}$$

and

$$\left.\left(\frac{\partial C_{\mathrm{I}}}{\partial t} + \frac{\partial C_{\mathrm{M}}}{\partial t}\right)\right|_{x=0} = -\frac{J^*_{\mathrm{I}} + J^*_{\mathrm{M}}}{x_{\mathrm{a}}} \tag{E.4}$$

From the solution equilibrium $\log(C_{\mathrm{HCO_3}}/C_{\mathrm{CO_2(aq)}}) = -\mathrm{p}K_1 + \mathrm{pH}$, the following equation is derived by differentiation with respect to time:

$$C^*_{\mathrm{H}} \cdot \left.\frac{\partial C_{\mathrm{HCO_3}}}{\partial t}\right|_{x=0} + C^*_{\mathrm{HCO_3}} \cdot \left.\frac{\partial C_{\mathrm{H}}}{\partial t}\right|_{x=0} = 10^{-\mathrm{p}K_1} \left.\frac{\partial C_{\mathrm{CO_2(aq)}}}{\partial t}\right|_{x=0} \tag{E.5}$$

Appendix F

Since J satisfies the flux equation (Eq. (2)), J_{H} can be written as follows using $C_{\mathrm{H}} \cdot C_{\mathrm{OH}} = K_{\mathrm{w}}$ and $\frac{\partial C_{\mathrm{H}}}{\partial t} = -\frac{K_{\mathrm{w}}}{C^2_{\mathrm{OH}}}\frac{\partial C_{\mathrm{OH}}}{\partial t}$,

$$J_{\mathrm{H}} = -D_{\mathrm{H}}\frac{\partial C_{\mathrm{H}}}{\partial x} - z_{\mathrm{H}}D_{\mathrm{H}}\left(\frac{F}{RT}\frac{\partial \phi}{\partial x}\right)C_{\mathrm{H}} = D_{\mathrm{H}}\frac{K_{\mathrm{w}}}{C^2_{\mathrm{OH}}}\frac{\partial C_{\mathrm{OH}}}{\partial x} - z_{\mathrm{H}}D_{\mathrm{H}}\left(\frac{F}{RT}\frac{\partial \phi}{\partial x}\right)\frac{K_{\mathrm{w}}}{C_{\mathrm{OH}}} \tag{F.1}$$

J_{OH} being expressed as Eq. (F.2) below, the above Eq. (F.1) is simplified as Eq. (F.3) taking into account, $z_{OH} = -1$ and $z_H = 1$,

$$J_{OH} = -D_{OH}\frac{\partial C_{OH}}{\partial x} - z_{OH}D_{OH}\left(\frac{F}{RT}\frac{\partial \phi}{\partial x}\right)C_{OH} \tag{F.2}$$

$$J_H = D_H\frac{K_w}{C_{OH}^2}\frac{\partial C_{OH}}{\partial x} + z_{OH}D_H\left(\frac{F}{RT}\frac{\partial \phi}{\partial x}\right)\frac{K_w}{C_{OH}}$$

$$= -\frac{D_H}{D_{OH}}\frac{K_w}{C_{OH}^2}\left[-D_{OH}\frac{\partial C_{OH}}{\partial x} - z_{OH}D_{OH}\left(\frac{F}{RT}\frac{\partial \phi}{\partial x}\right)C_{OH}\right] = -\frac{D_H}{D_{OH}}\frac{K_w}{C_{OH}^2}J_{OH} \tag{F.3}$$

Since the definition of $\Lambda_i(x)$ is $\Lambda_i = \frac{J_i(x)}{dx} - \frac{J_i(x+dx)}{dx}$ (in Appendix A), the following is finally derived:

$$\Lambda_H = -\frac{D_H}{D_{OH}}\frac{K_w}{C_{OH}^2}\Lambda_{OH} \tag{F.4}$$

When J_{OH} is associated with J_H, the following can be derived using $C_H \cdot C_{OH} = K_w$ and Eq. (F.3):

$$J_{OH} = -\frac{D_{OH}}{D_H}\frac{K_w}{C_H^2}J_H \tag{F.5}$$

Appendix G

When V_c l of C_c mol/l inhibitor solution are titrated against C_N mol/l nitric acid, the pH of the mixed solution can be obtained as a function of the volume (V l) of nitric acid added as follows:

Mass balance: $m_I + m_M = C_C \cdot V_C$ (G.1)

Equilibrium: $\frac{\gamma_m m_M/(V_c+V)\cdot \gamma_I C_H}{\gamma_I m_I/(V_c+V)} = 10^{-pK_a}$, thus $m_M/m_I = 10^{-pK_a'+pH}$ (G.2)

Electroneutrality: $C_I + C_H = C_{NO_3} + C_{OH}$, thus $C_I/(V_c+V) = C_N \cdot V/(V_c+V) + 10^{pH-14}$ (G.3)

where m_I, m_M are number of moles of inhibitor ions and molecules in the solution, and $10^{-pK_a'} = \gamma_m 10^{-pK_a}$. The concentration of hydrogen ion is neglected in Eq. (G.3) since it is not significant in an alkaline solution. $m_I = C_c V_c/(10^{-pK_a'+pH} + 1)$ is obtained from (G.1) and (G.2), and substituting this into (G.3), the following is obtained using $Ka' = 10^{-pK_a'}$,

$$10^{pH} = \frac{10^{14}Ka'C_NV + V_C + V}{2(V_c+V)Ka'}\left(-1 + \sqrt{1 - \frac{4\cdot 10^{14}Ka'(V_C+V)(C_NV - C_CV_C)}{(10^{14}Ka'C_NV + V_C + V)^2}}\right) \tag{G.4}$$

Since $4\times 10^{14}\,Ka'(V_C+V)(C_NV - C_CV_C)/(10^{14}\,Ka'C_NV + V_C + V)^2 \ll 1$, Eq. (G.4) can be approximated as follows:

$$pH(V) \approx 14 + \log\frac{C_CV_C - C_NV}{10^{14}Ka'C_NV + V_C} \tag{G.5}$$

where V in the term $(10^{14}\,Ka'C_N V + V_C + V)$ is neglected since it is insignificant in comparison with $10^{14}\,Ka'C_N V$. If pH(V) in (G.5) is differentiated twice with respect to V, the point of inflexion can be obtained as follows:

$$\frac{d^2(pH(V))}{dV^2} = 0 \Longleftrightarrow V = \frac{10^{14}Ka'C_C - 1}{2 \times 10^{14}Ka'C_N} \cdot V_C \tag{G.6}$$

Then the pH at the point of inflexion is finally obtained by substituting (G.6) into (G.5), thus,

$$pH = pK'_a \tag{G.7}$$

References

[1] S. Sawada, J. Kubo, C.L. Page, M.M. Page, Electrochemical injection of organic corrosion inhibitors into carbonated cementitious materials: Part I – Effects on pore solution chemistry, Corros. Sci., in press, doi:10.1016/j.corsci.2006.06.020.

[2] C. Andrade, J.M. Diez, A. Alamaan, C. Alonso, Mathematical modelling of electrochemical chloride extraction from concrete, Cem. Concr. Res. 25 (1995) 727–740.

[3] A.M. Hassanein, G.K. Glass, N.R. Buenfeld, A mathematical model for electrochemical removal of chloride from concrete structures, Corrosion 54 (1998) 323–332.

[4] N.R. Buenfeld, G.K. Glass, A.M. Hassanein, J-Z. Zhang, Chloride transport in concrete subjected to an electric field, J. Mater. Civ. Engrg. 10 (1998) 220–228.

[5] S.W. Yu, C.L. Page, Computer simulation of ionic migration during electrochemical chloride extraction from hardened concrete, Br. Corros. J. 31 (1996) 73–75.

[6] L.Y. Li, C.L. Page, Modelling of chloride extraction from concrete: influence of ionic activity coefficients, Comput. Mater. Sci. 9 (1998) 303–308.

[7] L.Y. Li, C.L. Page, Mathematical modelling of electrochemical chloride removal from concrete, in: R. de Borst et al. (Eds.), Computational Modelling of Concrete Structures, Balkema, Rotterdam/Brookfield, 1998, pp. 497–503.

[8] L.Y. Li, C.L. Page, Finite element modelling of chloride removal from concrete by an electrochemical method, Corros. Sci. 42 (2000) 2145–2165.

[9] O. Truc, J.P. Ollivier, L.O. Nilsson, Numerical simulation of multi-species transport through saturated concrete during a migration test – *MsDiff* code, Cem. Concr. Res. 30 (2000) 1581–1592.

[10] Y. Wang, L.Y. Li, C.L. Page, A two-dimensional model of electrochemical chloride removal from concrete, Comput. Mater. Sci. 20 (2001) 196–212.

[11] D.R. Lide (Ed.), Handbook of Chemistry and Physics, 85th ed., CRC Press, Boca Raton, FL, 2004.

[12] A.J. Bard, L.R. Faulkner, Electrochemical Methods: Fundamentals and Applications, Wiley, New York, 1980.

[13] J.S. Newman, Electrochemical Systems, Prentice-Hall, Englewood Cliffs, NJ, 1973.

[14] P.M.M. Blauwhoff, G.F. Versteeg, W.P.M. van Swaaij, A study on the reaction between CO_2 and alkanolamines in aqueous solutions, Chem. Eng. Sci. 39 (1984) 207–225.

[15] D.J. Anstice, C.L. Page, M.M. Page, The pore solution phase of carbonated cement pastes, Cem. Concr. Res. 35 (2005) 377–383.

[16] L.N. Plummer, T.M.L. Wigley, D.L. Parkhurst, The kinetics of calcite dissolution in CO_2–water systems at 5 °C to 60 °C and 0.0 to 1.0 atm CO_2, Am. J. Sci. 278 (1978) 179–216.

[17] J.G. Brown, P.D. Glynn, Kinetic dissolution of carbonates and Mn oxides in acidic water: measurement of in situ field rates and reactive transport modeling, Appl. Geochim. 18 (2003) 1225–1239.

[18] C.W. Davies, Ion Association, Butterworth, London, 1962.

[19] E. Samson, G. Lemaire, J. Marchand, J.J. Beaudoin, Modeling chemical activity effects in strong ionic solutions, Comput. Mater. Sci. 15 (1999) 285–294.

[20] K.S. Pitzer, A thermodynamic model for aqueous solutions of liquid-like density, Rev. Mineral. 17 (1987) 97–142.

[21] K.S. Pitzer, in: K.S. Pitzer (Ed.), Activity Coefficients in Electrolyte Solutions, second ed., CRC Press, Boca Raton, FL, 1991, pp. 75–153.

[22] S.L. Clegg, P. Brimblecombe, Solubility of ammonia in pure aqueous and multicomponent solutions, J. Phys. Chem. 93 (1989) 7237–7248.
[23] J. Noye, in: J. Noye (Ed.), Numerical Solutions of Partial Differential Equations, Elsevier/North-Holland, 1982.
[24] W.H. Hundsdorfer, in: W.H. Hundsdorfer, J. Verwer (Eds.), Numerical Solution of Time-dependent Advection–Diffusion–Reaction Equations, Springer, London, 2003.
[25] H.J. Lee, in: H.J. Lee, W.E. Schiesser (Eds.), Ordinary and Partial Difference Equation Routines in C, C++, Fortran, Java, Maple, and MATLAB, CRC Press, Boca Raton, FL, 2003 (Chapter 4).
[26] G.K. Pagenkopf, Introduction to Natural Water Chemistry, Dekker, New York, 1978.
[27] J. Mietz (Ed.), Electrochemical Rehabilitation Methods for Reinforced Concrete Structures – A State of the Art Report, European Federation of Corrosion Publications, vol. 24, The Institute of Materials, London, 1998.

Available online at www.sciencedirect.com
ScienceDirect
Corrosion Science 49 (2007) 1186–1204
CORROSION SCIENCE
www.elsevier.com/locate/corsci

Electrochemical injection of organic corrosion inhibitors into carbonated cementitious materials: Part 1. Effects on pore solution chemistry

S. Sawada [1], J. Kubo, C.L. Page *, M.M. Page

School of Civil Engineering, University of Leeds, Leeds LS2 9JT, UK

Received 29 November 2005; accepted 8 June 2006
Available online 25 September 2006

Abstract

This series of investigations was intended to clarify phenomena associated with electrochemical injection of the organic base corrosion inhibitors, ethanolamine and guanidine, into carbonated concrete. In Part 1, experiments were conducted with laminated specimens of carbonated cement paste, that were specially designed to facilitate analysis with adequate spatial resolution to assess changes in their pore solution phase chemistry after they had been subjected to constant current electrolysis between embedded cathodes and external anodes. The anolyte solutions provided sources of ethanolamine or guanidine in contact with the exterior specimen surfaces. Effects of variations in the applied current density and duration of electrolysis on the concentration profiles of the two inhibitors and the other main constituents of the pore solution phase were determined. The results have been used to underpin the development of a mathematical model, which is described in Part 2.

Keywords: A. Cement; A. Organic corrosion inhibitors; C. Carbonation; C. Dissociation constant; C. Migration

* Corresponding author. Tel.: +44 113 343 2283; fax: +44 113 343 2243.
E-mail address: c.l.page@leeds.ac.uk (C.L. Page).
[1] Present address: Nuclear Power Department, Kajima Corporation, 5-30 Akasaka 6-Chome, Minato-ku, Tokyo 107-8502, Japan.

0010-938X/$ - see front matter © 2006 Elsevier Ltd. All rights reserved.
doi:10.1016/j.corsci.2006.06.020

1. Introduction

The possibility of using electrochemical treatments of limited duration to promote the injection of certain types of corrosion inhibitor into reinforced concrete has been proposed by several researchers with the aim of controlling the corrosion rate of embedded steel reinforcement [1–4]. In a previous investigation by some of the present authors [4], it was shown that rates of injection into carbonated concrete of the organic base corrosion inhibitors, ethanolamine and guanidine, could be greatly enhanced by applying constant current densities (in the range of 1–5 A/m^2) for several days between an embedded steel cathode and an external surface anode placed in an aqueous solution containing the relevant inhibitor. Several aspects of the inhibitor transport mechanism and its relationship to compositional features of the pore solution phase of the carbonated concrete remained unresolved although it was clear that the evolution of the pH profile within the pore solution and the magnitudes of the dissociation constants of the organic base inhibitors concerned played a dominant role.

To obtain a deeper understanding of phenomena underlying the electrochemical injection of ethanolamine and guanidine into carbonated concrete, it was necessary to devise a means of performing detailed pore solution analyses of material sampled at closely spaced intervals along the migration path between the anode and cathode. The use of concrete specimens with coarse aggregates was considered unsuitable for this purpose because of the spatial resolution limitations imposed by the presence of the aggregates on sampling and analysis of the pore solution. It was therefore decided to undertake the experiments to be described in this paper with laminated specimens of carbonated cement pastes. These could be readily sectioned after inhibitor injection to provide appropriately sized samples for pore solution expression and analysis by means of techniques that have recently been developed to evaluate features of the pore solution chemistry of carbonated cement pastes [5].

2. Experimental details

2.1. Specimen preparation

2.1.1. Carbonated cement pastes

Ordinary Portland cement (OPC), for which chemical analysis data are shown in Table 1, was used to manufacture carbonated cement paste specimens. The cement pastes were made by hand mixing with distilled water for about 5 min to produce mixtures with a water/cement ratio (w/c) of 0.6. The mixtures were poured into cylindrical PVC containers (49 mm in diameter by 75 mm in height), which were vibrated for 2–4 min to get rid of trapped air bubbles. The cylinders were sealed and rotated end-over-end at a speed of about 8 rpm for at least 24 h in order to minimise segregation and bleeding. They were then stored in a high humidity curing room at a temperature of 22 ± 2 °C for 2 weeks.

Table 1
Chemical analysis of OPC (% by mass)

CaO	SiO_2	Al_2O_3	Fe_2O_3	SO_3	MgO	Na_2O	K_2O	LOI
63.76	20.69	4.72	3.06	2.92	2.08	0.26	0.61	0.87

After demoulding, the specimens were immersed in 35 mM NaOH solution to minimise leaching of calcium hydroxide and other cement hydration products. They were then stored in another curing room at a temperature of 38 ± 2 °C for 8 weeks to accelerate cement hydration.

When the cylindrical samples had been cured they were cut into discs, approximately 5 mm in thickness, by means of a diamond saw with distilled water as lubricant. The discs were placed upright in a sealed tank, in which the atmosphere was conditioned at 75% RH over saturated sodium chloride solution. Pure CO_2 gas was passed through this tank for about 30 min every day and the depths of carbonation of the specimens were monitored by removing individual discs from the tank, fracturing them and spraying their freshly exposed surfaces with phenolphthalein solution. After about three months of this treatment, the phenolphthalein test confirmed that the specimens were fully carbonated throughout their thickness. They were then kept at 75% RH in air for a further period of 6–7 months.

2.1.2. Fabrication of embedded cathodes

Carbonated cement paste discs containing stainless steel meshes, which were to be used as the cathodes in subsequent experiments, were fabricated by a more rapid technique utilising super-critical carbon dioxide ($scCO_2$) [6–8]. Cement paste mixtures with w/c of 0.6 were made in a similar manner to those described in Section 2.1.1. They were cast into containers (49 mm in diameter and 8 mm in thickness) containing Type 316 stainless steel mesh and vibrated for 1 min to get rid of entrapped air bubbles. After the surfaces had been finished with a trowel, the discs were cured for 1 day in sealed boxes in which the atmosphere was kept at 100% RH. The discs were demoulded and then conditioned by placing them in an oven at 45 °C until their moisture content corresponded to a degree of drying of about 70% [7]. The conditioned samples were exposed to water-saturated $scCO_2$ in a stainless steel pressure vessel for 12 h at just over 71 bar and 31 °C, as described elsewhere [8]. After removal from the vessel, they were kept in air at 75% RH until required.

2.2. Organic corrosion inhibitors

The two organic corrosion inhibitors studied, ethanolamine ($HO \cdot CH_2 \cdot CH_2 \cdot NH_2$) and guanidine ($HN{=}C(NH_2)_2$), were bases of widely differing strengths, the pK_a values of their cationic conjugate acids, $HO \cdot CH_2 \cdot CH_2 \cdot NH_3^+$ and $(NH_2)_3C^+$, being 9.5 and 13.6, respectively [9]. All the chemicals employed were of analytical reagent grade with the exception of guanidine carbonate which was >98% pure. The electrolyte solutions used were 1 M ethanolamine nitrate at pH 8.0 (produced by mixing equal volumes of 2 M ethanolamine and 1.97 M nitric acid) and 0.5 M guanidine carbonate at pH 11.7 (1 M with respect to guanidine).

2.3. Treatment of specimens with corrosion inhibitors

Before being subjected to the electrochemical treatments, carbonated cement paste discs were converted to a saturated surface-dry condition by procedures designed to minimise the leaching of ions from the pore solutions [5]. The discs were placed horizontally on glass plates, and distilled water was added dropwise to each disc until excess water was observable. The excess water was carefully removed by means of cotton wool, and the discs were placed in an upright position on platforms above distilled water in sealed tanks. After being stored

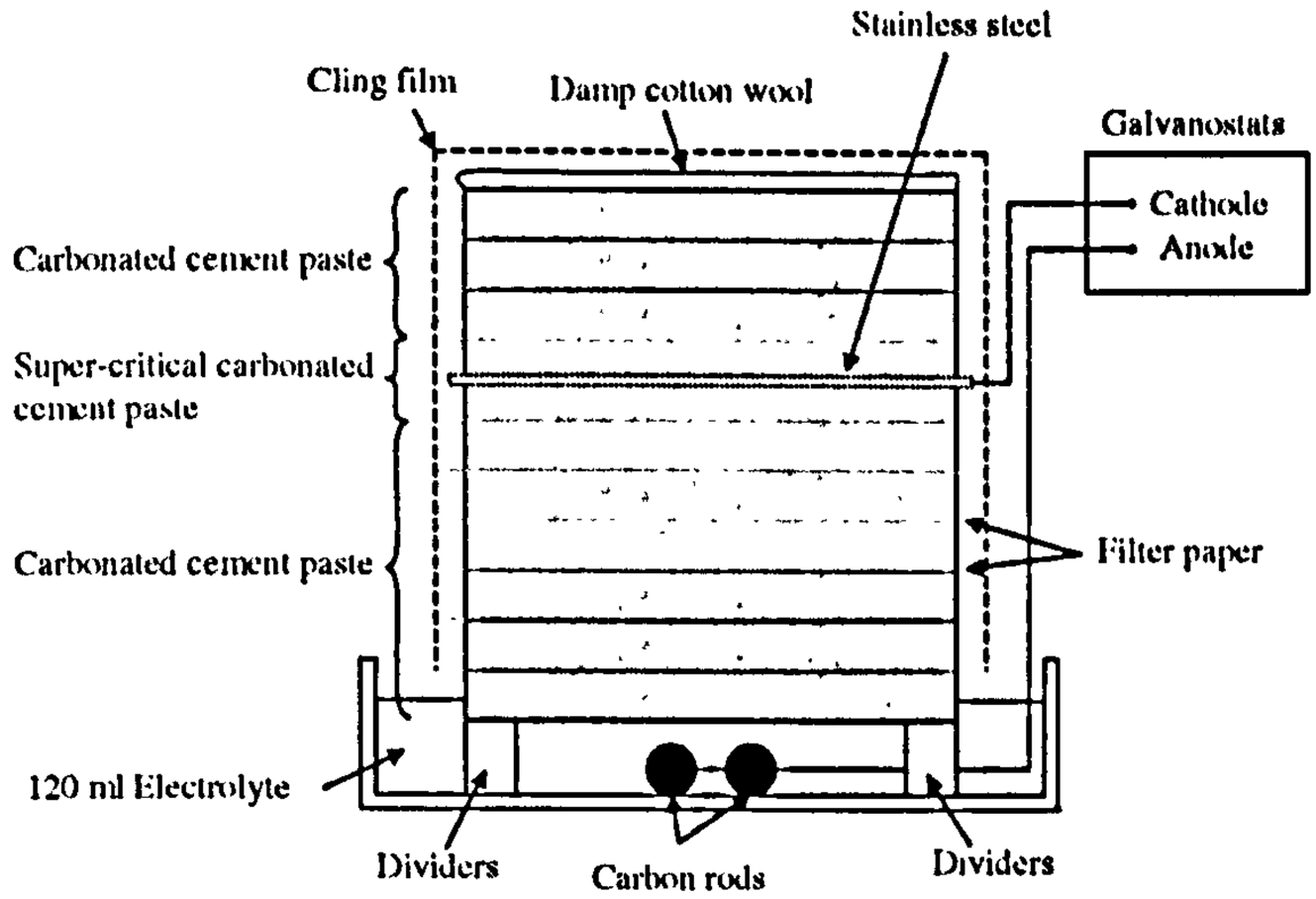

Fig. 1. Experimental arrangement.

for 1 h, the discs were removed from the tanks, and distilled water was added to the opposite side of each disc by the same technique as previously described. The discs were then put back into the tanks and, after being stored over distilled water for another hour, their weights were measured. These procedures were carried out once per day and were continued until practically constant weights were achieved, indicating that a saturated surface-dry condition had been attained. After final weighing, some of the discs were placed in an oven at 105 °C for 24 h and then reweighed to determine the evaporable water content. The other saturated-surface dry discs were stacked together with damp filter papers sandwiched between them to promote good electrolytic contact, as illustrated in Fig. 1. The side surfaces of the laminated specimens thus formed were then wrapped with 'cling-film' to prevent moisture losses resulting from resistive heating during subsequent electrochemical treatment applied to the material.

Four identical laminated specimens were set up for each experiment in which constant current electrolysis was applied by means of the arrangement illustrated in Fig. 1. Each electrolytic treatment was performed in a container in which the atmosphere was kept at about 100% RH. Two carbon rods serving as anodes were contained in a shallow dish filled with 120 ml of one of the electrolytes, described in Section 2.2. The concentrations of inhibitors and associated anions in the anolytes and their initial pH values were measured before the specimens were immersed in them to a depth of 2 mm. The circuits were then completed and current densities were galvanostatically controlled at either 1 or 5 A/m^2 of the disc surface area, the periods of treatment being 7 days in all cases. Control specimens were also immersed for 7 days to a depth of 2 mm in the various electrolytes without application of a current. In this case, only one disc (instead of three) was placed above the super-critically carbonated cement paste disc containing the stainless steel mesh.

2.4. Ionic distributions in the pore solution

After electrolytic treatments had been applied, the four identical specimens used were delaminated and the discs at given positions within them (i.e. corresponding to fixed

distances from the surface in contact with the anolyte) were stacked together to form cylinders (each approximately 20 mm in height). These cylinders were then subjected to pore solution expression at applied pressures of up to 350 MPa in a device of the type described elsewhere [10]. The volume of expressed pore solution thus obtained from each cylinder was typically of the order of 2 ml, which was sufficient to permit analysis of the various dissolved ionic species. In order to characterise the initial pore solution compositions of the carbonated and the super-critically carbonated cement pastes, disc specimens which had not been exposed to electrolytic treatment were also subjected to pore solution expression after being brought to a saturated, surface-dry condition using similar procedures to those described previously [5].

Within 30 min of collecting pore solutions, pH measurements were conducted with a combined glass and reference electrode. Concentrations of carbonate and bicarbonate ions were also determined by monitoring the evolution of pH during titration of a 1.0 ml sample of the pore solution against 10 mM nitric acid. Full details of the procedures and calculations are presented elsewhere [11]. Concentrations of the corrosion inhibitors (ethanolamine and guanidine) and those of all other significant cations (Na^+, K^+, Mg^{2+}, Ca^{2+}) and anions (Cl^-, SO_4^{2-}, NO_3^-) in the pore solutions were determined by means of a Dionex DX500 ion chromatography system, operated as described elsewhere [12,13].

The anolyte solutions were also collected immediately after the electrolytic treatments had been completed and concentrations of their major dissolved ions and pH values were determined as described above.

3. Results

The ionic concentrations and pH values of the pore solution of cement pastes subjected to the carbonation procedures described in Sections 2.1.1 and 2.1.2 are shown in Table 2. Evaporable water contents, which were calculated from the loss of weight at 105 °C, were 0.18 and 0.22 g/g dry weight of sample for carbonated cement paste and for super-critically carbonated cement paste respectively. Both carbonation procedures effectively neutralised the hydrated cement pastes as indicated by the pH values of about 9.0 which are far below the typical values (>13) found for non-carbonated specimens [14]. The concentrations of other ions in the pore solution were also of similar magnitudes to those reported in a previous study of carbonated cements [5].

Complete sets of analytical data obtained for the pore solution constituents after inhibitor injection treatments had been performed are presented in Tables 3–8. Here it should

Table 2
Ionic concentrations and pH values in the pore solution of carbonated cement pastes before treatment with inhibitors

Method	pH	Concentrations (mmol/l)									Sum of charge	
		Na^+	K^+	Mg^{2+}	Ca^{2+}	OH^-	Cl^-	SO_4^{2-}	CO_3^{2-}	HCO_3^-	Cation	Anion
Accelerated carbonation	9.0	9.0	6.3	18.8	23.4	0.01	37.4	30.1	0.3	6.0	99.7	104.2
Super-critical carbonation	9.7	5.1	6.0	1.5	22.6	0.05	33.1	17.4	1.0	4.4	59.3	74.5

Table 3
Ionic concentrations and pH values in the pore solution of carbonated cement paste treated with 1.0 M ethanolamine nitrate at current density of 0 A/m^2

Distance from surface (mm)	Concentrations (mmol/l)											Sum of charge	
	Ethanolamine cation	Na^+	K^+	Mg^{2+}	Ca^{2+}	OH^-	Cl^-	SO_4^{2-}	NO_3^-	CO_3^{2-}	HCO_3^-	Cation	Anion
2.5	344.9	15.9	11.3	40.2	109.0	1.41×10^{-2}	10.0	25.2	840.4	0.8	12.0	670.5	914.3
7.5	203.6	18.4	16.2	98.2	75.3	1.66×10^{-3}	19.0	32.2	601.1	0.0	6.2	585.3	690.8
12.5	106.5	23.6	13.8	99.4	66.9	1.05×10^{-3}	24.6	30.4	398.7	0.0	8.5	476.7	492.7
17.5	31.2	14.8	7.4	84.0	57.3	9.12×10^{-4}	36.9	30.2	225.9	0.0	11.7	336.0	335.1
22.5	6.7	17.6	7.0	46.6	56.0	5.25×10^{-3}	30.8	26.3	112.2	0.1	4.9	236.5	200.9
27.5	4.8	12.8	5.8	29.0	43.5	1.48×10^{-2}	28.0	23.6	53.6	0.3	3.7	168.4	133.1
34.0	8.9	15.4	5.7	6.7	43.3	2.51×10^{-2}	24.6	17.2	45.7	0.5	4.2	129.9	109.9
40.5	1.7	8.5	3.5	25.1	38.5	4.79×10^{-3}	23.5	26.1	20.0	0.1	3.6	141.0	99.5

Table 4
Ionic concentrations and pH values in the pore solution of carbonated cement paste treated with 1.0 M ethanolamine nitrate at current density of 1 A/m^2

Distance from surface (mm)	Concentrations (mmol/l)											Sum of charge	
	Ethanolamine cation	Na^+	K^+	Mg^{2+}	Ca^{2+}	OH^-	Cl^-	SO_4^{2-}	NO_3^-	CO_3^{2-}	HCO_3^-	Cation	Anion
2.5	804.0	9.7	16.5	33.6	81.0	9.33×10^{-4}	13.5	43.4	795.5	0.1	14.6	1059.4	910.6
7.5	258.5	7.9	10.2	22.3	48.8	1.86×10^{-2}	14.9	111.8	193.6	1.1	13.1	418.8	447.6
12.5	97.8	3.5	5.7	11.7	27.7	1.91×10^{-2}	17.3	76.7	16.8	0.8	9.6	186.0	198.8
17.5	54.2	9.7	6.6	8.5	22.0	2.95×10^{-2}	5.8	44.4	9.7	0.6	4.8	131.6	110.4
22.5	21.5	10.3	5.8	13.4	23.3	2.40×10^{-2}	4.4	35.8	2.1	0.5	4.2	111.1	83.2
27.5	10.1	23.6	8.8	6.9	19.0	3.31×10^{-2}	2.3	18.4	3.0	0.7	4.5	94.3	47.9
34.0	0.8	21.0	7.8	2.6	11.4	7.08×10^{-1}	1.1	8.1	3.3	0.9	0.3	57.6	23.4
40.5	2.5	15.7	5.9	11.9	29.6	2.82×10^{-2}	10.7	24.6	1.2	0.4	3.1	107.2	64.9
45.5	4.3	10.8	3.3	24.8	25.6	1.23×10^{-3}	19.7	35.0	1.4	0.0	4.9	119.1	96.0
50.5	4.7	10.8	4.7	23.1	26.2	6.92×10^{-4}	22.6	32.5	2.2	0.0	2.9	118.7	92.7

Table 5
Ionic concentrations and pH values in the pore solution of carbonated cement paste treated with 1.0 M ethanolamine nitrate at current density of 5 A/m^2

Distance from surface (mm)	Concentrations (mmol/l)											Sum of charge	
	Ethanolamine cation	Na^+	K^+	Mg^{2+}	Ca^{2+}	OH^-	Cl^-	SO_4^{2-}	NO_3^-	CO_3^{2-}	HCO_3^-	Cation	Anion
2.5	546.7	16.8	7.3	18.3	100.9	5.75×10^{-4}	14.4	32.2	795.1	0.0	15.9	809.1	890.0
7.5	55.0	13.6	7.9	1.7	7.9	9.77×10^{-2}	4.8	60.5	17.0	13.7	30.6	95.8	200.8
12.5	29.3	10.6	4.4	1.2	6.4	2.09×10^{-1}	2.2	23.5	2.2	12.3	12.9	59.5	89.2
17.5	26.0	4.3	5.6	1.1	1.9	3.24×10^{-1}	2.2	13.1	0.5	18.4	12.4	42.0	78.4
22.5	29.6	5.2	14.2	1.5	2.7	4.79×10^{-1}	1.3	6.8	0.9	35.1	16.0	57.3	102.6
27.5	28.9	7.6	18.3	2.2	4.8	1.20×10^{0}	3.0	5.6	1.7	57.8	10.5	68.7	143.0
34.0	8.7	27.2	28.8	2.3	6.1	4.17×10^{0}	1.2	6.1	1.8	44.7	2.3	81.5	111.1
40.5	26.1	22.5	13.6	8.6	22.7	1.00×10^{-1}	9.6	46.1	0.0	2.6	5.8	124.7	113.0
45.5	18.6	10.4	4.4	13.7	26.8	2.95×10^{-2}	14.0	36.2	0.0	0.7	5.3	114.5	93.0
50.5	4.6	30.0	7.9	17.3	26.9	7.24×10^{-2}	16.4	33.6	0.0	1.9	5.7	130.7	93.2

Table 6
Ionic concentrations and pH values in the pore solution of carbonated cement paste treated with 0.5 M guanidine carbonate at current density of 0 A/m^2

Distance from surface (mm)	Concentrations (mmol/l)											Sum of charge	
	Guanidine cation	Na^+	K^+	Mg^{2+}	Ca^{2+}	OH^-	Cl^-	SO_4^{2-}	NO_3^-	CO_3^{2-}	HCO_3^-	Cation	Anion
2.5	227.5	9.0	12.1	10.8	5.9	5.25×10^{-2}	12.9	89.7	–	14.8	61.8	282.1	283.9
7.5	52.3	24.8	5.9	18.4	20.9	8.91×10^{-3}	22.3	51.3	–	0.4	9.2	161.4	134.8
12.5	23.5	14.2	3.5	19.3	22.9	7.41×10^{-2}	19.6	35.9	–	1.1	3.4	125.7	97.2
17.5	8.9	34.4	8.1	32.9	27.1	3.63×10^{-3}	30.7	42.0	–	0.4	7.7	171.4	123.1
22.5	3.1	19.5	9.2	36.6	29.9	2.95×10^{-3}	35.3	42.2	–	0.3	6.4	164.9	126.8
27.5	1.6	22.5	5.8	16.6	32.7	6.31×10^{-2}	27.1	25.7	–	0.8	2.8	128.5	83.1
34.0	5.5	19.3	8.0	3.2	23.7	5.01×10^{-2}	22.0	18.3	–	0.6	2.7	86.5	62.6
40.5	0.0	18.4	11.4	22.6	26.4	6.31×10^{-3}	26.1	30.2	–	0.2	4.5	128.0	91.4

Table 7
Ionic concentrations and pH values in the pore solution of carbonated cement paste treated with 0.5 M guanidine carbonate at current density of 1 A/m^2

Distance from surface (mm)	Concentrations (mmol/l)											Sum of charge	
	Guanidine cation	Na^+	K^+	Mg^{2+}	Ca^{2+}	OH^-	Cl^-	SO_4^{2-}	NO_3^-	CO_3^{2-}	HCO_3^-	Cation	Anion
2.5	458.0	3.7	0.0	25.0	14.6	2.34×10^{-2}	23.6	168.6	–	10.3	96.5	540.9	477.9
7.5	261.8	11.5	0.0	10.0	15.9	1.70×10^{-2}	10.0	157.4	–	1.1	14.2	325.2	341.2
12.5	112.0	6.0	6.3	9.2	14.0	1.07×10^{-1}	6.9	74.4	–	1.6	3.2	170.6	162.2
17.5	49.6	17.5	4.9	17.6	30.1	4.27×10^{-3}	3.9	53.2	–	0.3	6.0	167.3	116.8
22.5	23.2	15.7	6.0	12.3	23.9	5.50×10^{-3}	4.0	33.7	–	0.3	6.9	117.1	78.8
27.5	4.4	16.0	9.9	7.0	18.0	7.41×10^{-3}	2.4	14.7	–	0.3	5.5	80.4	37.8
34.0	2.1	17.7	14.6	2.4	7.7	1.58×10^{0}	1.7	8.0	–	2.5	0.3	54.8	24.6
40.5	0.0	15.0	4.1	22.4	26.7	3.16×10^{-3}	11.1	32.1	–	0.2	5.0	117.4	80.8
45.5	0.0	12.9	7.7	25.7	25.2	5.25×10^{-3}	18.9	32.9	–	0.3	5.5	122.3	90.8
50.5	0.0	13.2	6.4	28.9	24.3	3.16×10^{-3}	20.8	34.5	–	0.3	6.4	126.1	96.8

Table 8
Ionic concentrations and pH values in the pore solution of carbonated cement paste treated with 0.5 M guanidine carbonate at current density of 5 A/m^2

Distance from surface (mm)	Concentrations (mmol/l)											Sum of charge	
	Guanidine cation	Na^+	K^+	Mg^{2+}	Ca^{2+}	OH^-	Cl^-	SO_4^{2-}	NO_3^-	CO_3^{2-}	HCO_3^-	Cation	Anion
2.5	494.6	7.1	0.0	0.0	0.7	2.63×10^{0}	9.8	127.5	–	96.1	44.7	503.2	504.3
7.5	279.3	7.1	0.0	0.0	5.5	2.04×10^{1}	4.1	63.4	–	108.3	8.6	297.5	376.5
12.5	200.6	5.7	0.0	0.0	8.3	1.66×10^{1}	4.6	57.7	–	38.9	0.4	222.9	214.8
17.5	126.3	9.2	4.9	0.0	5.9	1.29×10^{1}	3.6	36.2	–	23.6	0.3	152.3	136.4
22.5	83.7	8.7	3.1	0.0	7.6	1.05×10^{1}	2.2	16.8	–	23.6	0.3	110.7	93.8
27.5	138.0	8.0	3.5	0.0	2.8	3.47×10^{1}	2.9	10.8	–	33.4	0.1	155.0	126.1
34.0	393.9	25.6	19.5	0.0	2.3	1.20×10^{2}	2.7	12.7	–	156.9	0.3	443.6	462.4
40.5	19.9	28.9	3.6	5.3	18.8	3.16×10^{-1}	10.6	28.5	–	4.7	2.0	100.6	79.3
45.5	3.0	7.7	5.4	20.0	18.1	7.46×10^{-3}	15.5	32.1	–	0.3	6.4	92.3	86.8
50.5	0.6	9.0	2.8	21.0	19.6	1.23×10^{-2}	17.4	32.3	–	0.3	5.5	93.6	88.0

Table 9
Ionic concentrations and pH values in the anolyte after treatment with inhibitors

Anolyte	Current density (A/m^2)	pH	Concentrations (mmol/l)														Sum of charge	
			Organic inhibitors		Na^+	K^+	Mg^{2+}	Ca^{2+}	H^+	OH^-	Cl^-	SO_4^{2-}	NO_3^-	CO_3^{2-}	HCO_3^-		Cation	Anion
			Total	Cationic														
1 M Ethanolamine Nitrate	0	7.9	979.2	955.2	9.5	17.7	5.2	12.1	1.3×10^{-5}	7.9×10^{-4}	2.4	1.9	961.5	0.0	13.5		1016.9	981.1
	1	2.0	970.8	970.8	2.1	N/D	5.7	38.5	9.5	1.0×10^{-9}	6.5	6.9	971.9	0.0	0.0		1071.0	992.3
	5	1.2	856.2	856.2	10.5	12.4	16.6	168.4	61.7	1.6×10^{-10}	9.8	26.8	1092.7	0.0	0.0		1310.7	1156.1
	Initial	8.0	1090.1	1060.0	–	–	–	–	1.1×10^{-5}	8.9×10^{-4}	–	–	974.9	–	–		1060.0	974.9
0.5 M Guanidine Carbonate	0	9.9	954.9	954.7	8.9	N/D	2.7	2.8	1.1×10^{-7}	8.7×10^{-2}	1.6	0.8	–	364.3	220.1		974.6	952.0
	1	9.7	912.1	912.0	3.8	N/D	3.0	2.5	2.0×10^{-7}	5.0×10^{-2}	5.6	11.1	–	284.9	299.6		926.8	897.3
	5	8.8	651.1	651.1	5.0	N/D	0.0	1.5	1.6×10^{-6}	6.3×10^{-3}	6.6	57.0	–	23.6	516.8		659.1	684.5
	Initial	11.7	985.3	971.9	–	–	–	–	1.8×10^{-9}	5.5	–	–	–	481.3	18.7		971.9	986.8

be emphasised that the concentrations of cationic conjugate acids of the two organic bases were calculated directly from their pK_a values and the hydroxyl ion concentrations of the pore solutions concerned. In some cases, in spite of the fact that all of the major ionic species expected to be present were accounted for, fairly large apparent charge imbalances were observed, especially in the cases of the specimens containing ethanolamine. These discrepancies may be attributable partly to accumulated analytical errors but another significant factor is likely to be the errors arising from the assumption that the concentrations of cationic conjugate acids of weak organic bases such as ethanolamine may be estimated simply from their pK_a values in pore solutions of measured pH. Thermodynamic data such as pK_a values are applicable to ideal dilute aqueous solutions [9], whereas the pore solutions analysed in the present research contained widely varying concentrations of their dissolved ions and molecules. This causes complications that will be discussed further in Part 2 of the investigations [15].

The pH values and chemical compositions of the anolytes after the electrolytic treatments were completed are presented in Table 9, together with initial data for these solutions. The pH of ethanolamine nitrate solutions was found to have significantly decreased at the high current density (5 A/m^2) and the surface of the cement paste specimens immersed in these solutions, was visibly deteriorated. The guanidine carbonate solutions remained slightly alkaline (pH ~ 9), however, even after the passage of 5 A/m^2 for 7 days.

4. Discussion

4.1. Organic corrosion inhibitors

Figs. 2 and 3 show the overall penetration profiles of ethanolamine and guanidine, respectively. They indicate that injection of both inhibitors within the pore solution phase of the carbonated cement pastes was promoted by the electrochemical treatments, particularly at the higher of the two applied current densities, findings that are consistent with

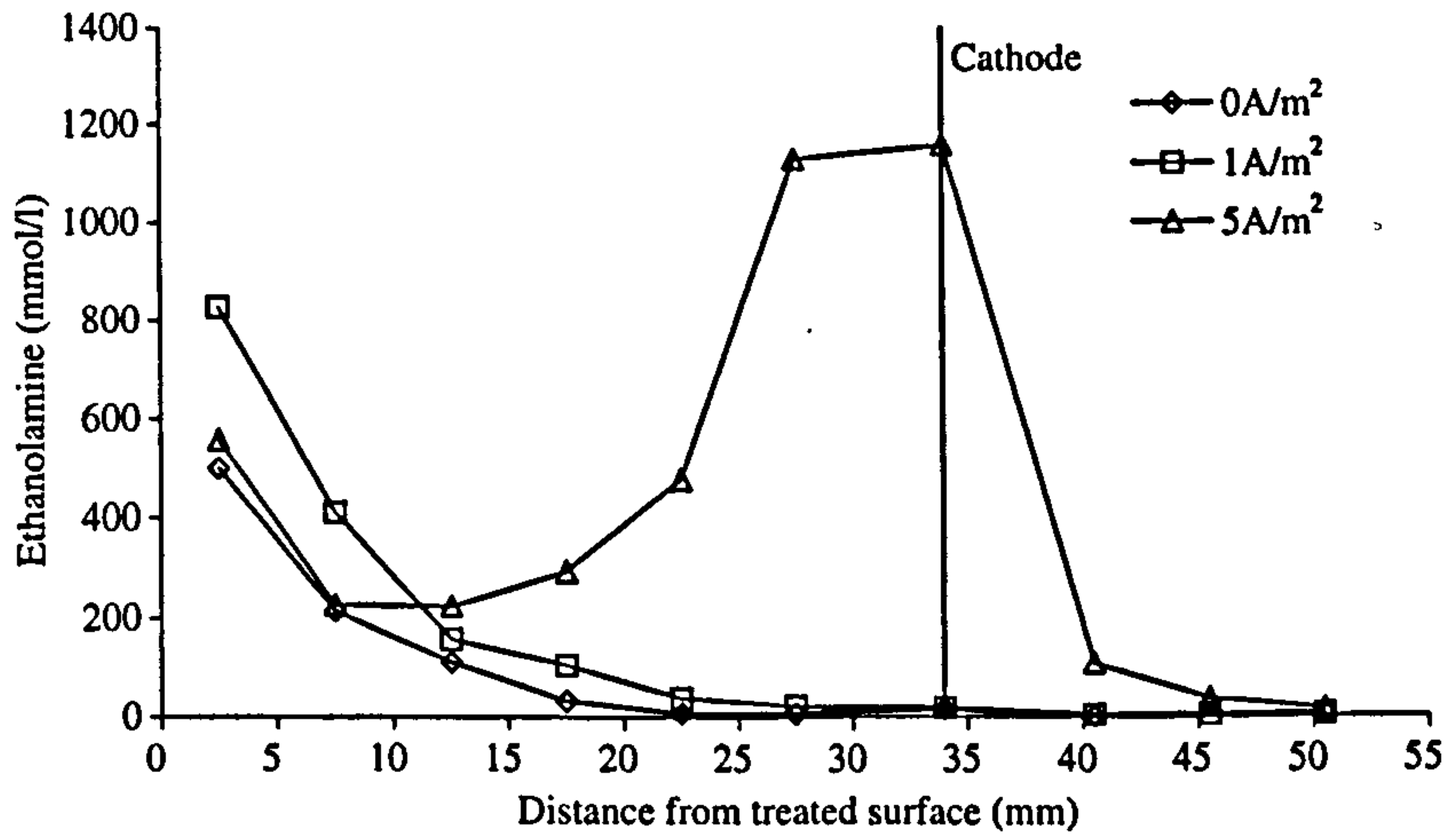

Fig. 2. Concentration profile of ethanolamine in carbonated cement pastes of w/c 0.6 applied as 1.0 M ethanolamine nitrate.

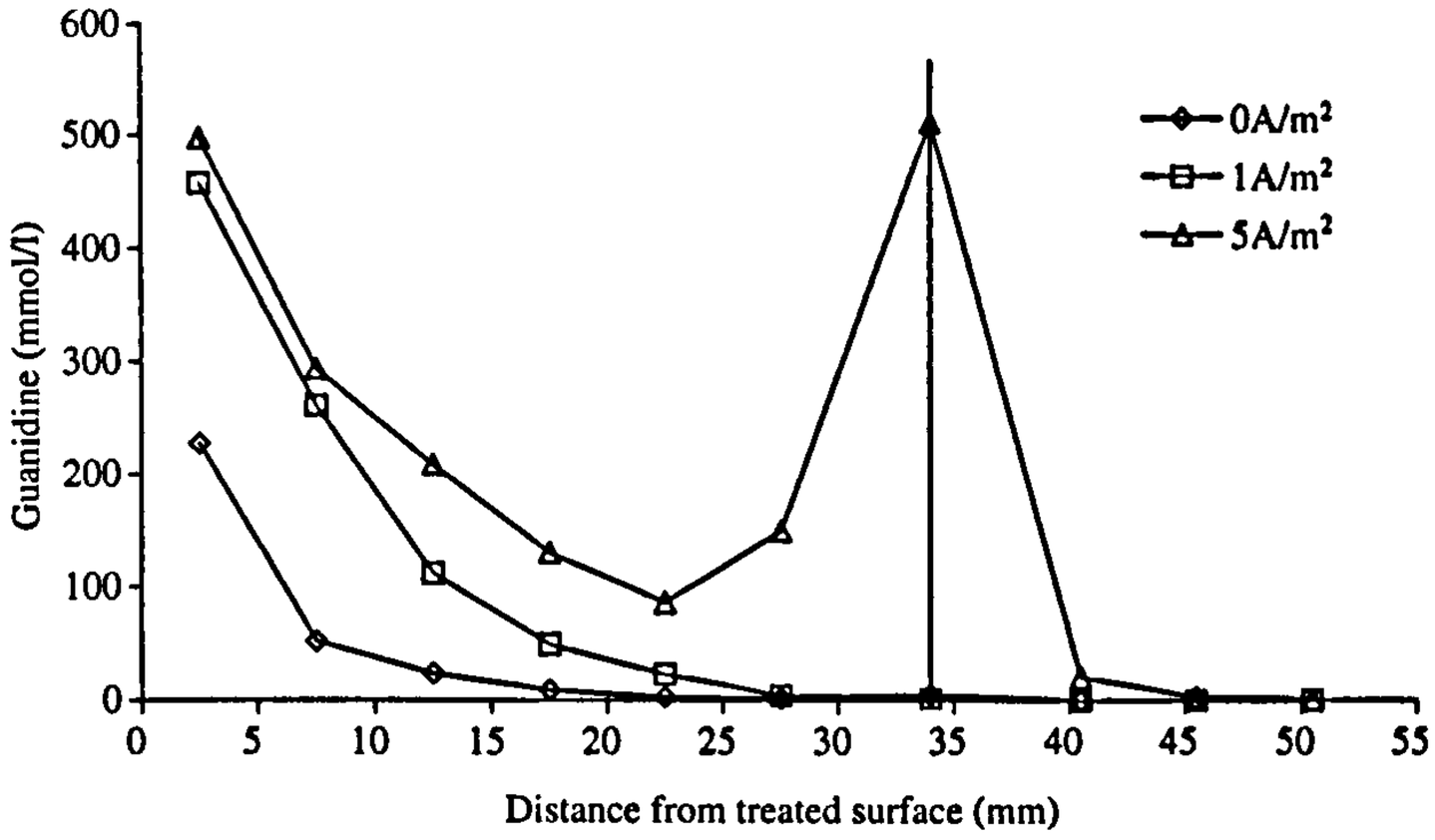

Fig. 3. Concentration profile of guanidine in carbonated cement pastes of w/c 0.6 applied as 0.5 M guanidine carbonate.

the results obtained for carbonated concrete specimens in a previous investigation [4]. The highest concentration of guanidine was observed at the position of the cathode, whereas the profiles for ethanolamine had plateaux of high concentrations in the region a few millimetres from the cathode. Again this is very similar to what was found previously and is explicable in terms of the different degrees of ionisation of the two inhibitors, particularly in the zone near the cathode where hydroxyl ions are generated. As shown in Tables 5 and 8, at the higher applied current density of 5 A/m^2, the apparent concentrations of the cationic conjugate acid of ethanolamine were relatively small except near the anode, whereas fairly high concentrations of guanidine cations were found in the cathode zone since the pK_a value of these cations was still greater than the pH values of the pore solution near the cathode.

The concentrations of both inhibitors remaining in the anolyte decreased with the progress of the electrochemical treatments as shown in Table 9 and the quantities of ethanolamine and guanidine lost from the anolytes are plotted against the quantities injected into the carbonated cement pastes specimens in Fig. 4. The latter were calculated from the inhibitor concentrations in the pore solution and the evaporable water content of the specimens, based on the assumption that the evaporable water content provides a reasonable estimate of the pore water that was available to support ionic migration. It is clear from Fig. 4 that the amounts of inhibitor lost from the anolytes were significantly higher than those penetrating into the cement matrix, especially in the case of guanidine carbonate. This difference is probably attributable largely to side-effects of the electrochemical treatment, such as anodic oxidation and/or evaporation of the organic bases, as previously suggested [4].

4.2. pH values

The distributions of pH recorded for the various specimens are illustrated in Fig. 5. In the case of those specimens treated with ethanolamine, the pH values tended to rise

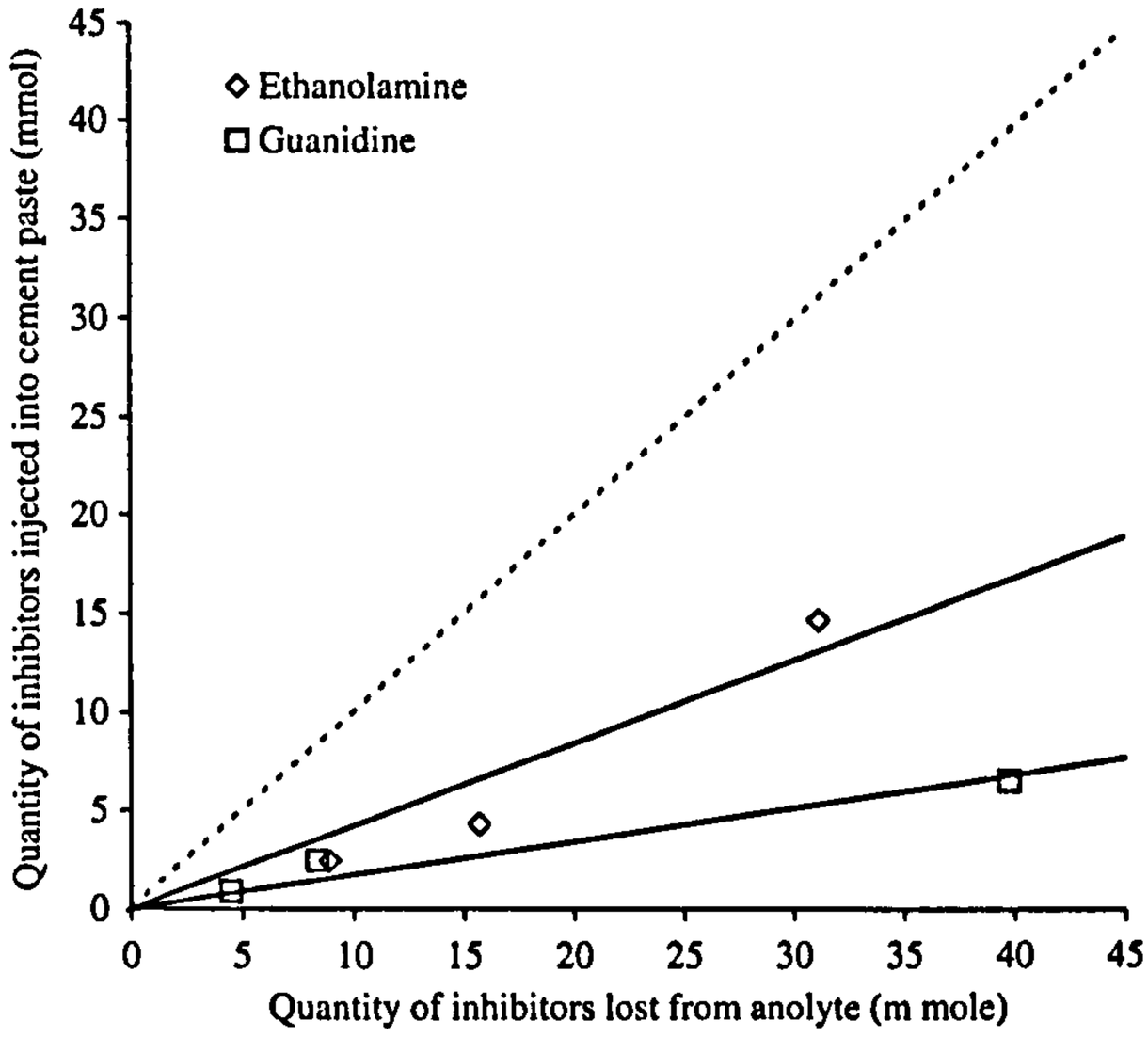

Fig. 4. Comparison of quantity of corrosion inhibitors injected into carbonated cement paste of w/c 0.6 with that decreasing in anolyte (original content of inhibitors in anolyte was 120 m mole).

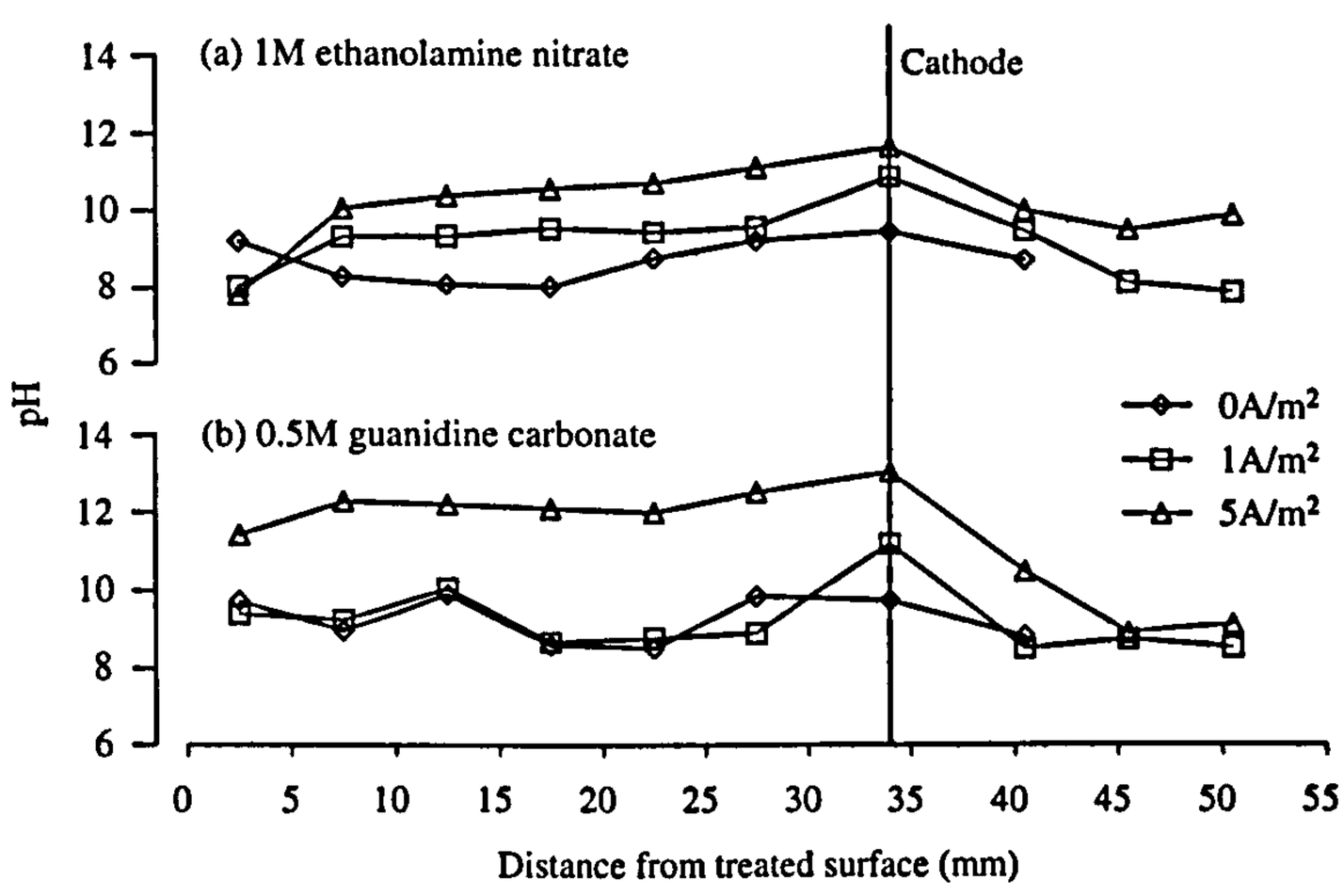

Fig. 5. Distributions of pH values in carbonated cement pastes of w/c 0.6 treated with inhibitors.

throughout the material progressively with the increase of circulated charge, except in the regions near the external anodes. The low pH values recorded near the anodes clearly resulted from acidification of the anolyte due to generation of hydrogen ions by the anodic reaction. In the case of specimens treated with guanidine, sharp increases in pH were noted

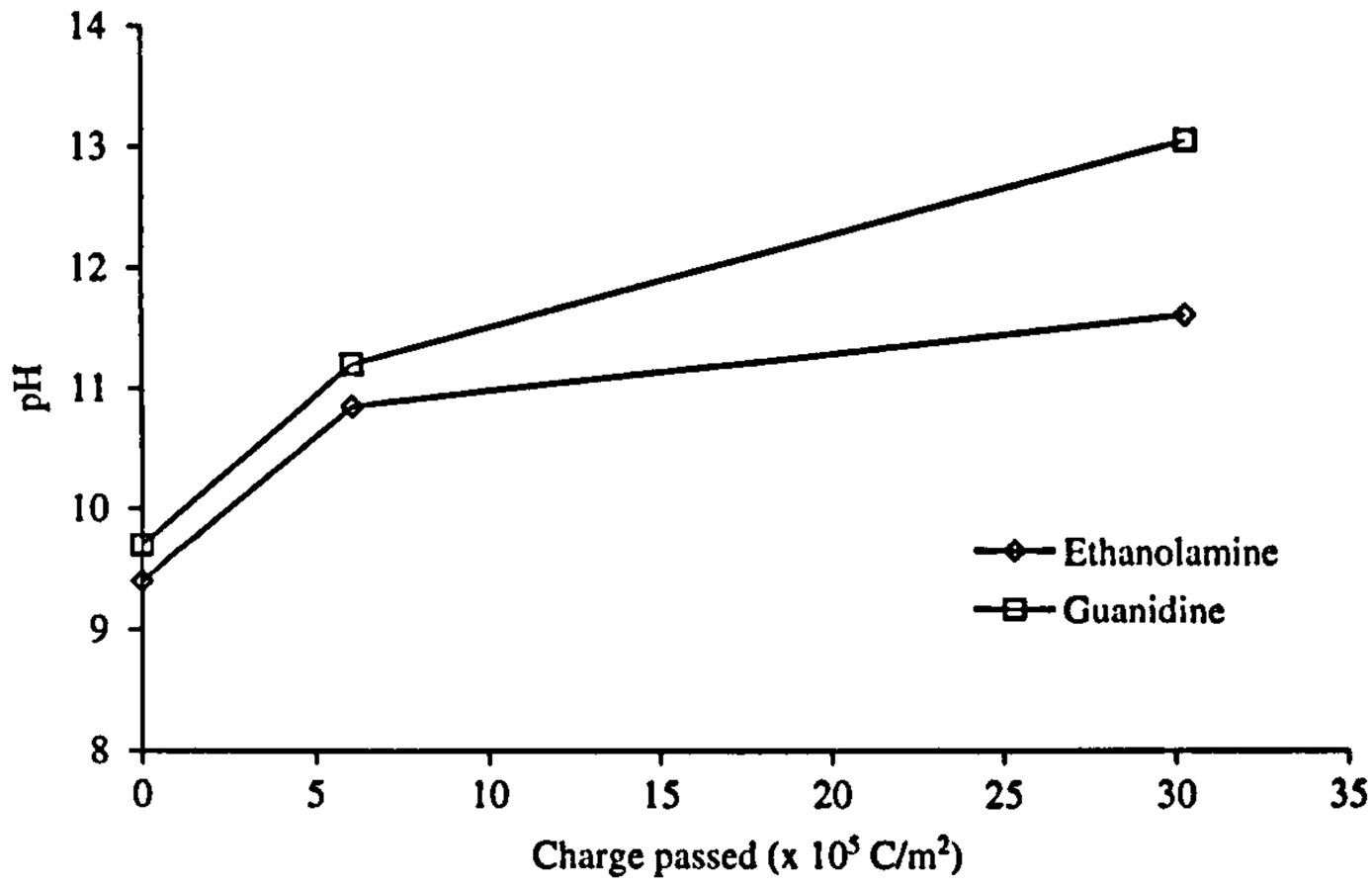

Fig. 6. pH values at the cathode as a function of circulated charge.

only in the vicinity of the cathode at the lower applied current density of 1 A/m^2, but the pore solution pH values were raised above 12 over almost the entire lengths of the specimens by the treatment at 5 A/m^2.

Fig. 6 shows the pH values in the cathodic region as a function of circulated charge. The pH values observed for both inhibitors appeared to follow a similar rising trend until 6×10^5 C/m^2 had been passed but, beyond that point, the pH increase for ethanolamine was much smaller than that for guanidine. At a current density of 1 A/m^2 (6×10^5 C/m^2 charge passed in 7 days), neither of the inhibitors was found to have reached the cathode region at significant concentrations (see Figs. 2 and 3) and thus the increase in pH there was simply caused by water electrolysis. At a current density of 5 A/m^2 (30×10^5 C/m^2 charge passed in 7 days), however, significant concentrations of the inhibitors had penetrated to the cathode and therefore influenced the fate of cathodically generated hydroxyl ions to very different extents. Thus ethanolamine (with a pK_a value of 9.5) consumed hydroxyl ions more extensively than guanidine (with a pK_a value of 13.6) and so led to the observed pH values of the cathodic regions of <12 (ethanolamine) and >13 (guanidine).

This more modest rise in pH at the cathode in the case of ethanolamine might be considered advantageous if electrochemical injection of inhibitors were to be applied to concrete containing aggregates that are susceptible to the alkali-silica reaction. The latter phenomenon, which can cause local expansion and cracking of concrete, has been shown to be induced in the vicinity of embedded steel cathodes polarised at high current densities in non-carbonated concrete with certain types of potentially reactive siliceous aggregate [16,17]. It remains uncertain whether this might also pose similar risks for fully or partially-carbonated concrete with potentially reactive aggregates if subjected to electrochemical treatments that restore very high internal pH values in the material adjacent to the cathode.

4.3. Sulfate ions

As shown in Tables 4, 5, 7 and 8, the concentrations of dissolved sulfate ions increased markedly, particularly near the anodes, when electrolytic treatments were applied.

Moreover, in the case of guanidine even without applied current, an increase in sulfate ion concentration near the external surface was also observed (see Table 6). These effects cannot be explained in terms of redistribution of sulfate ions originally present in the initial pore solution and they indicate that dissolution of sulfate ions from the solid cement carbonation products must have occurred during the treatments. Since there was no significant variation in the concentration profile of sulfate ions in the case of ethanolamine treatment without current (see Table 3) and no significant increase in sulfate ions near the cathode at the current density of 5 A/m^2 in the case of guanidine despite its high concentration (see Table 8), it would seem that the organic inhibitors had no direct role in promoting the dissolution of sulfate ions.

A tentative explanation of the observed sulfate ion concentrations in the cases where specimens were exposed to the inhibitor solutions without applied current may be given in terms of solubility equilibria involving calcium sulfate, which is expected to be present as gypsum in carbonated cement pastes, produced by carbonation of calcium sulfoaluminate hydrate phases in the cement [18,19]. Thus for the specimens exposed to guanidine carbonate solution, calcium ions decreased in concentration near the external surface due to precipitation of $CaCO_3$ (see Tables 6–8) and correspondingly the concentration of sulfate ions increased to satisfy the solubility product of $CaSO_4$, as shown in the same tables. In contrast, for the specimens exposed to ethanolamine nitrate solution, the near-surface concentration of calcium ions increased in the pore solution of reduced pH value and the corresponding sulfate concentrations were therefore small (see Table 3). However, the significant changes in sulfate ion concentration associated with the application of the electrolytic treatments cannot be readily explained without resort to mathematical modelling of the type proposed in Part 2 of this investigation [15].

4.4. Carbonate and bicarbonate ions

Substantial increases in the concentrations of carbonate ions at the cathode were observed when 5 A/m^2 had been applied for 7 days, especially so in the case of specimens treated with guanidine carbonate solution (compare Tables 3 and 5 with Tables 6 and 8). As there was no external source of carbonate ions in the case of ethanolamine and it was difficult to imagine how carbonate ions could have moved from the anolyte to the cathode against the action of an electrical field in the case of guanidine, this local increase of carbonate ions is regarded as clear evidence of the dissolution of calcium carbonate in the vicinity of the stainless steel cathode. This may be explained simply in terms of the effect of cathodically generated hydroxyl ions on the solubility equilibria of $Ca(OH)_2$ and $CaCO_3$ thus favouring the following reaction in the cathodic region:

$$CaCO_3 + 2OH^- \rightarrow Ca(OH)_2 + CO_3^{2-}$$

Support for this hypothesis is provided by the findings of Konno et al. [20] who observed that saturated calcium carbonate was easily converted to calcium hydroxide in a high pH environment.

From the experimental results obtained in this study, it may therefore be inferred that precipitation of calcium hydroxide can occur in the vicinity of the cathode as a consequence of the electrochemical treatments applied at high current density to carbonated concrete or similar carbonated cement-based materials. This is expected to re-create a lime-rich layer of

solid portlandite (and/or its reaction products with hydrous silica gel) in the interfacial zone between the steel and the carbonated cement matrix. The presence of a lime-rich interfacial transition zone at the steel/concrete interface is believed to have a significant role in stabilising the passive condition of the steel and thus in reducing the risk of corrosion in certain conditions [21]. This could be practically relevant, particularly in cases where carbonated concrete is subject to chloride contamination. A related phenomenon, the induced precipitation of portlandite at cathodically polarised steel surfaces in non-carbonated mortars subjected to electrochemical chloride extraction treatments, has been observed previously by others [22] and it has been suggested that this may significantly enhance the threshold level of chloride contamination for corrosion of steel in concrete [23].

5. Conclusions

The following conclusions may be drawn from this part of the investigations:

(1) In confirmation of the findings previously recorded from experiments with carbonated concrete specimens (w/c 0.86), the organic base corrosion inhibitors, ethanolamine and guanidine, were both effectively injected into carbonated cement paste (w/c 0.6) at depths corresponding to normal cover thicknesses to reinforcing steel when temporary electrochemical treatments of the types investigated were applied for up to a week at high current density (5 A/m^2). The inhibitor penetration profiles observed were explicable in terms of the degrees of ionisation of ethanolamine (pK_a 9.5) and guanidine (pK_a 13.6) in carbonated cement paste.
(2) The hydroxyl ion concentration of the pore solution near the embedded cathode was restored to a high value (pH > 13) in the case of treatment for a week at 5 A/m^2 with guanidine carbonate solution. The restoration of alkalinity near the cathode was more moderate in the case of similar treatment with ethanolamine nitrate solution (pH < 12).
(3) The distribution of the concentrations of a number of anions in the pore solution, notably sulfate and carbonate/bicarbonate, were significantly altered as a result of the electrochemical injection treatments applied and it appeared that the effects observed involved dissolution of these anions from solid phases present in the carbonated cement pastes.
(4) Quantitative explanation of the above effects and of significant apparent anomalies in the sums of anionic and cationic charges detected in certain regions of specimens into which ethanolamine had been injected has required the development of a mathematical model that is to be described in Part 2 of the investigations [15].
(5) Mechanistic features and factors influencing the effectiveness of corrosion inhibition induced on pre-corroded steel in carbonated concrete by electrochemically injected ethanolamine and guanidine require further investigation; these matters are currently being studied in comparison with related aspects of conventional electrochemical realkalisation treatments [24] as part of the PhD project of one of the authors (J.K.).

Acknowledgements

We are grateful to the Kajima Corporation, Japan, for providing funds to support the first-named author and to the Central Japan Railway Company, Japan, for providing

funds to support the second-named author. We also wish to express our thanks to Mr. Stuart Shaw and Ms. Karen Stevens for their experimental assistance.

References

[1] M.F. Asaro, A.T. Gaynor, S. Hettiarachchi, Electrochemical removal and protection of concrete bridge components: injection of synergistic corrosion inhibitors, Report SHRP-S/FR-90-02, Strategic Highway Research Program, National Research Council, Washington, DC, 1990.
[2] A. Phanasgaonkar, B. Cherry, M. Forsyth, Corrosion inhibition properties of organic amines in a simulated concrete environment: mechanism and time dependency of inhibition, in: Proceedings of the International Conference on 'Understanding Corrosion Mechanisms in Concrete – A Key to Improving Infrastructure Durability', Cambridge, MA, 1996, Section 6, pp. 1–6.
[3] C.L. Page, V.T. Ngala, M.M. Page, Corrosion inhibitors in concrete repair systems, Mag. Concr. Res. 52 (2000) 25–37.
[4] S. Sawada, C.L. Page, M.M. Page, Electrochemical injection of organic corrosion inhibitors into concrete, Corros. Sci. 47 (2005) 2063–2078.
[5] D.J. Anstice, C.L. Page, M.M. Page, The pore solution phase of carbonated cement pastes, Cem. Concr. Res. 35 (2005) 377–383.
[6] N.R. Short, P. Purnell, C.L. Page, Preliminary investigations into the supercritical carbonation of cement pastes, J. Mater. Sci. 36 (2000) 35–41.
[7] P. Purnell, N.R. Short, C.L. Page, Super-critical carbonation of glass-fibre reinforced cement. Part 1: Mechanical testing and chemical analysis, Composites Part A 32 (2001) 1777–1787.
[8] S.J. Shaw, Supercritical carbonated cement composites with controlled pore solution chemistry, MSc Thesis, University of Leeds, 2002.
[9] D.R. Lide (Ed.), Handbook of Chemistry and Physics, 84th ed., CRC Press, Boca Raton, Florida, 2003.
[10] C.L. Page, Ø. Vennesland, Pore solution composition and chloride binding capacity of silica-fume cement pastes, Mater. Struct. 16 (1983) 19–25.
[11] S. Sawada, Ionic migration in cement-based materials, PhD Thesis, University of Leeds, 2005.
[12] M.M. Page, C.L. Page, V.T. Ngala, D.J. Anstice, Ion chromatographic analysis of corrosion inhibitors in concrete, Constr. Build. Mater. 16 (2002) 73–81.
[13] M.M. Page, C.L. Page, S. Shaw, S. Sawada, Ion chromatographic analysis of amines, alkanolamines, and associated anions in concrete, J. Sep. Sci. 28 (2005) 471–476.
[14] P. Nixon, C.L. Page, Pore solution chemistry and alkali aggregate reaction, in: J.M. Scanlon (Ed.), ACI Special Publication: 'Concrete Durability', American Concrete Institute, Detroit, SP-100, vol. 2, 1987, pp. 1833–1862.
[15] J. Kubo, S. Sawada, C.L. Page, M.M. Page, Electrochemical injection of organic corrosion inhibitors into carbonated cementitious materials. Part 2: Mathematical modelling, Corros. Sci., submitted for publication.
[16] G. Sergi, C.L. Page, D.M. Thompson, Electrochemical induction of alkali-silica reaction in concrete, Mater. Struct. 24 (1991) 359–361.
[17] C.L. Page, S.W. Yu, Potential effects of electrochemical desalination of concrete on alkali-silica reaction, Mag. Concr. Res. 47 (1995) 23–31.
[18] T. Grounds, H.G. Midgley, D.V. Nowell, Carbonation of ettringite by atmospheric carbon dioxide, Thermochim. Acta 135 (1988) 347–352.
[19] T. Nishikawa, K. Suzuki, S. Ito, Decomposition of synthesized ettringite by carbonation, Cem. Concr. Res. 22 (1992) 6–14.
[20] H. Konno, Y. Nanri, M. Kitamura, Crystallization of aragonite in the causticizing reaction, Powder Technol. 123 (2002) 33–39.
[21] C.L. Page, Mechanism of corrosion protection in reinforced concrete marine structures, Nature 258 (1975) 514–515.
[22] T.D. Marcotte, C.M. Hansson, B.B. Hope, The effect of electrochemical chloride extraction treatment on steel-reinforced mortar: Part 2 – Microstructural characterisation, Cem. Concr. Res. 29 (1999) 1561–1568.
[23] G.K. Glass, N.R. Buenfeld, The inhibitive effects of electrochemical treatment applied to steel in concrete, Corros. Sci. 42 (2000) 923–927.
[24] J. Mietz (Ed.), Electrochemical rehabilitation methods for reinforced concrete structures – a state of the art report, European Federation of Corrosion Publications, vol. 24, The Institute of Materials, London, 1998.